Rapid Synthesis by Rational Design: An Ion-Templated Macrocyclooligomerization-Based Approach to Prepare Collections of Natural Product-Like Cyclodepsipeptides, Leading to the Discovery of a New Antiarrhythmic Small Molecule

By

Suzanne M. Batiste

Dissertation

Submitted to the Faculty of the

Graduate School of Vanderbilt University

in partial fulfillment of the requirements

for the degree of

DOCTOR OF PHILOSOPHY

in

Chemistry

May 11, 2018

Nashville, Tennessee

Approved:

Jeffrey N. Johnston, Ph.D.
Brian O. Bachmann, Ph.D.
David W. Wright, Ph.D.
Björn C. Knollmann, M.D., Ph.D.

Acknowledgments

There have been a number of people throughout my academic career who have helped and encouraged me in significant ways. Without these individuals, this dissertation would probably not exist, and I am forever thankful for all of their support and guidance.

I would not be the scientist I am today without guidance and support from my advisor, Prof. Jeff Johnston. I could not have asked for a better mentor. After observing Jeff's unwavering passion for chemistry in class, I was eager to rotate in his lab, and later officially join. Over the past five years, Jeff granted me intellectual freedom in my studies, which has allowed my passion for chemistry to flourish, and has resulted in scientific problem solving abilities I didn't know I was capable of. Jeff has also facilitated numerous opportunities for me to grow as a scientist within and outside of Vanderbilt, and for those I am forever grateful.

Along those lines, I am grateful for the opportunity to participate in a chemical biology collaboration over the course of my PhD, and would like to thank Prof. Bjorn Knollmann for facilitating the biology portion of this collaboration, and for serving as the fourth member of my PhD committee. I would like to thank Knollmann lab post-doc, Dr. Daniel J. Blackwell, for conducting the spark experiments, Ca^{2+}-binding experiments, and *in vivo* studies that will be discussed later in this document—additional thank you is in order for taking the time to answer my questions with very clear explanations of concepts, allowing me to observe some experiments, and for entertaining my desire to inject a cockroach with *nat*-(-)-verticilide when I showed up to lab with one. I am also thankful to Dr. Robyn Rebbeck and Dr. Razvan Cornea for help with the [^{3}H]ryanodine binding experiments, Dr. Kyungsoo Kim for the intact myocyte experiments, and Dr. Nieves Gomez-Hurtado for preliminary screening in permeabilized myocytes.

Thank you to my committee members, Prof. Brian Bachmann, Prof. David Wright, and Prof. Bjorn Knollmann, for taking time out of their schedules to be a significant part of my educational career, and for all of their advice, helpful project discussions, and guidance on proposal writing that they have provided. I'd like to thank Dr. Steve Townsend for providing me numerous opportunities to attend lunch with visiting speakers. Thank you to Dr. Nathan Schley and Dr. Alissa Hare for providing good advice when I was searching for postdoc positions, and also for advice on proposal writing. Thank you to Dr. Don Stec and Dr. Markus Voehler for their upkeep of the Vanderbilt NMR facilities, and for being more than willing to teach me new NMR techniques.

I would like to thank all the members of the Johnston group, past and present, for all of the "good discussions", advice, comic relief, and friendship over the years. One of the main reasons I joined the Johnston group was because of everyone's positive energy, excitement, and passion for chemistry—so thank you for creating a work environment where there was continual interest to learn, regardless if it was 9am or 9pm. Dr. Amanda Doody and Dr. Ki Bum Hong helped me get started in lab—thank you for teaching me everything from setting up reactions, to putting together a properly formatted subgroup report. Post-docs Dr. Sergey Tsukanov and Dr. Yasunori Toda showed me the rigor it takes to be successful in organic chemistry research, and were always willing to help me work through problems. Dr. Mike Danneman gave me ample practice working through mechanisms on the board, was a great role model on how to give an excellent research presentation, and made me laugh almost every day with his jokes and impersonations. Dr. Brandon Vara always answered my questions (no matter how crazy), and was the epitome of a graduate student who was truly passionate about chemistry. Additional thanks to Mike and Brandon for all of the advice over the years (chemistry, life, career, etc.). Dr. Dan Sprague taught me the joys of obscure chemical literature and craft beer, and has also been a great nocturnal lab-mate and friend

during my time at Vanderbilt. Dr. Ken Schwieter taught me efficiency in lab, everything I know about formatting manuscripts for publication, and was an excellent song writer—thank you for the musical entertainment while we ran columns. I would also like to thank Michael Crocker for super fun NMR discussions, and for a common appreciation of cats and unicorns. I'd especially like to thank Jade Bing who has been a voice of reason in lab (and outside of lab), close friend, and roommate—thank you for all the feedback on my presentations, for tolerating my cat when he steals your food, and for many fun times outside of lab. Finally, I'd like to thank Abby Smith for working very hard with me over the past year in preparation to continue/expand on my projects after I graduate.

Finally, I'd like to thank my family. I'd like to thank my sister, Jeannette, for supporting my love for science, and for her efforts to keep me updated with the latest fashion trends. Major thanks are owed to my mom and dad. My parents have always supported my interests in science, from wanting to "find a cure" for anthrax infections as a child, to pursuing an advanced degree in organic chemistry. The encouragement, love, and support that I have received from my parents over the last 27 years has been invaluable. I am forever grateful to them.

“Sometimes the questions are complicated and the answers are simple.”

- Dr. Seuss

TABLE OF CONTENTS

LIST OF TABLES

LIST OF FIGURES

Figures Page

LIST OF SCHEMES

Chapter I

I. An UmAS-based approach to the total synthesis of (-)-verticilide

1.1 Introduction to cyclic peptides and depsipeptides

Natural products and their derivatives are a major source of approved pharmaceuticals.[1] Over the past three decades, about 80% of chemotherapeutic agents are classified as natural products or mimic natural products.[2] Of these different natural product-based drugs, many are cyclic peptides and depsipeptides (Figure 1). For example, cyclic peptide cyclosporin A,[3] which was isolated from *Tolypocladium,* was found to be a powerful immunosuppressant. Romidepsin,[4] a cyclic depsipeptide that was isolated from terrestrial bacterium *Chromobacterium violaceum,* induces tumor cell death by chelating Zn-dependent histone deacetylase. Another cyclic depsipeptide, emodepside,[5] is a natural product-inspired anthelmintic.

Figure 1. FDA approved cyclic peptide and depsipeptide drugs

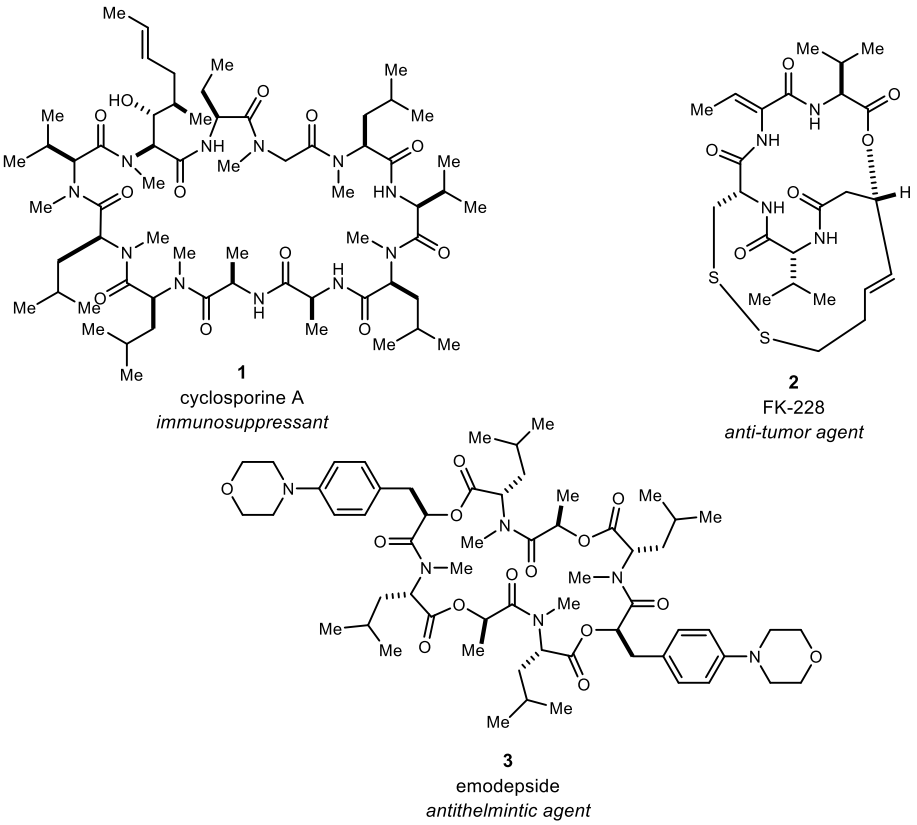

[1] Newman, D. J.; Cragg, G. M. *J. Nat. Prod.* **2012**, *75*, 311.
[2] Kitagaki, J.; Shi, G.; Miyauchi, S.; Murakami, S.; Yang, Y. *Anticancer Drugs* **2015**, *26*, 259.
[3] Wenger, R. M. *Angew. Chem. Int. Ed.* **1985**, *24*, 77.
[4] VanderMolen, K. M.; McCulloch, W.; Pearce, C. J.; Oberlies, N. H. *J. Antibiot.* **2011**, *64*, 525.
[5] Crisford, A.; Murray, C.; O'Connor, V.; Edwards, R. J.; Kruger, N.; Welz, C.; von Samson-Himmelstjerna, G.; Harder, A.; Walker, R. J.; Holden-Dye, L. *Mol. Pharmacol.* **2011**, *79*, 1031.

Cyclic peptide and depsipeptide natural products have a number of structural and chemical properties that make them inspiring scaffolds for inhibition of non-conventionally 'druggable' targets such as protein-protein interfaces (PPIs).[6] This interest was initially sparked by the observation that natural product-derived drugs often violate Lipinski's Rule of Five[7] criteria for conventional drug-likeness (Figure 2), suggesting that they occupy an area of chemical space that represents an alternative solution to achieving both potency and good pharmaceutical properties.[8]

Figure 2. Depsipeptide macrocycles violate Lipinski's rule of five

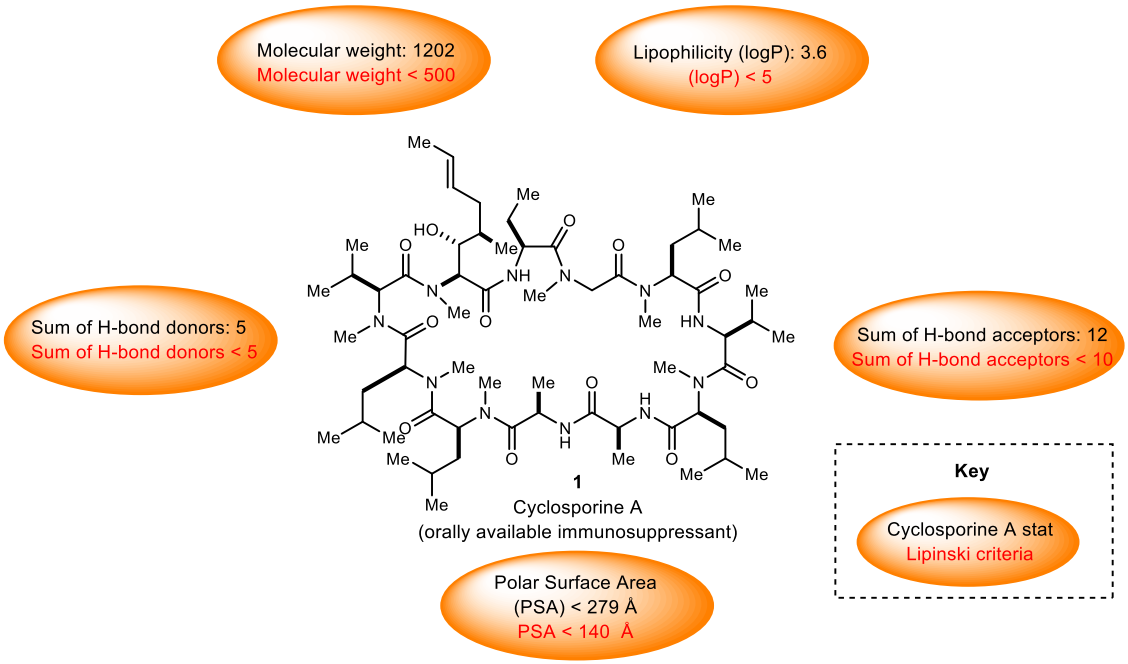

The high prevalence of macrocycles among these "beyond-Rule-of-Five" molecules suggests that their cyclic structure is important for favorable pharmaceutical properties. Studies have speculated that the well-defined conformation of the macrocyclic structure increases binding affinity to a target by eliminating unproductive conformations that would be observed in its linear counterpart.[6] The constrained conformation of macrocycles also contributes to increased resistance to degradation by proteases because there are no N- or C-termini, and increased permeation through cell membranes,[9] and thus improved bioavailability.

The relationship between structure and membrane permeability is an important determinant of whether a "beyond-Rule-of-5" target will be orally bioavailable. Despite their number of favorable pharmaceutical properties, most cyclic peptides have less than 1% oral bioavailability and are therefore delivered through injection. There are a few exceptions, mainly cyclic peptides

[6] Villar, E. A.; Beglov, D.; Chennamadhavuni, S.; Porco, J. A., Jr.; Kozakov, D.; Vajda, S.; Whitty, A. *Nat. Chem. Biol.* **2014**, *10*, 723.
[7] Leeson, P. *Nature* **2012**, *481*, 455.
[8] Ganesan, A. *Curr. Opin. Chem. Biol.* **2008**, *12*, 306.
[9] Bockus, A. T.; McEwen, C. M.; Lokey, R. S. *Curr. Top. Med. Chem.* **2013**, *13*, 821.

containing *N*-methyl amides, such as cyclosporine A (oral bioavailability 22%).[10] Lokey and coworkers examined the relationship between structure and membrane permeability (Figure 3) in a library of natural-product derived hexapeptides and found that conformation of the peptide backbone is key to the molecule's ability to passively diffuse through the cell membrane.[10,11] The stable conformation of these cyclic peptides, dependent on the stereochemistry of amino acid residues, allows them to intramolecularly hydrogen bond in order to bury polar groups during passive diffusion through the cell membrane, as observed with peptides **4** and **5**. It was also found that *N*-methylated derivatives (**6**) had significantly better membrane permeability, and thus have an increased chance of oral bioavailability.

Figure 3. Stereochemistry and *N*-methylation heavily influence membrane permeability[11]

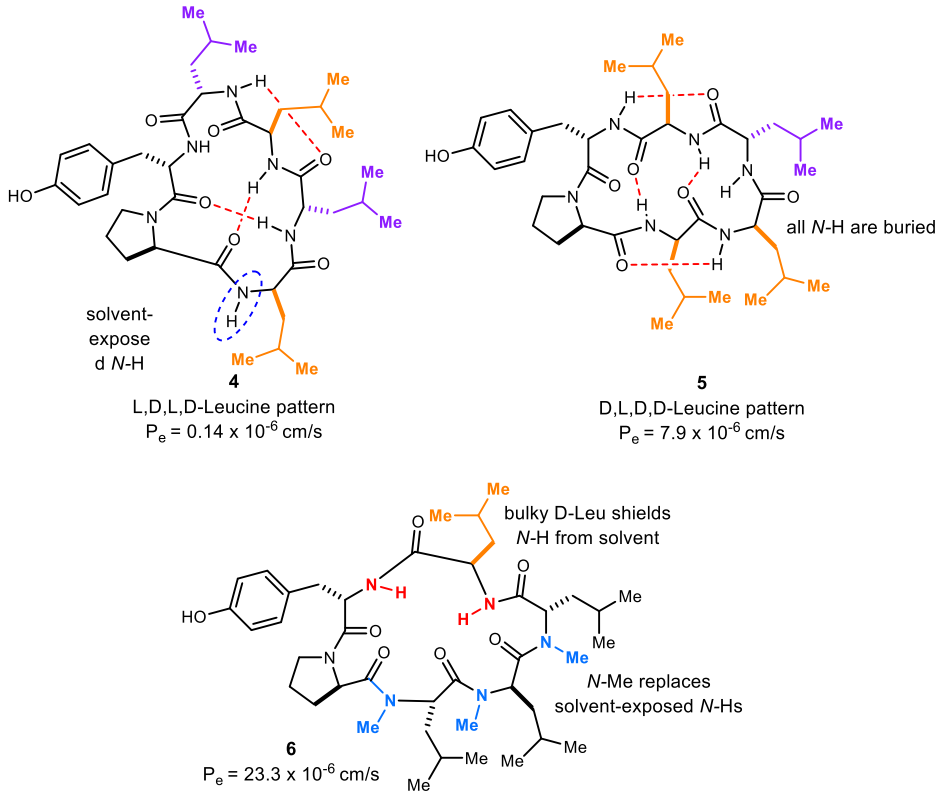

Although cyclic peptide and depsipeptide drugs can be synthesized by enzymes in nature, synthetic methods using coupling reagents have been developed to produce these molecules and their derivatives on large enough scale to sell. While these methods are widely used and quite effective for some substrates, using them to create *N*-methylated cyclic peptides and depsipeptides still poses a problem.

[10] Hill, T. A.; Lohman, R. J.; Hoang, H. N.; Nielsen, D. S.; Scully, C. C.; Kok, W. M.; Liu, L.; Lucke, A. J.; Stoermer, M. J.; Schroeder, C. I.; Chaousis, S.; Colless, B.; Bernhardt, P. V.; Edmonds, D. J.; Griffith, D. A.; Rotter, C. J.; Ruggeri, R. B.; Price, D. A.; Liras, S.; Craik, D. J.; Fairlie, D. P. *ACS Med. Chem. Lett.* **2014**, *5*, 1148..
[11] Hewitt, W. M.; Leung, S. S.; Pye, C. R.; Ponkey, A. R.; Bednarek, M.; Jacobson, M. P.; Lokey, R. S. *J. Am. Chem. Soc.* **2015**, *137*, 715.

1.2 Chemical synthesis of *N*-methyl peptides and depsipeptides

1.2.1 Traditional methods

N-Methyl peptides and depsipeptides are commonly synthesized through a dehydrative method in which the amide or ester linkage is formed through condensation of an amine or alcohol with a carboxylic acid. As shown in Scheme 1, one of the most frequently used dehydrative methods to form *N*-methyl amide bonds is traditional solution phase peptide synthesis in which the carboxylic acid and amine are coupled in the presence of an electrophilic coupling reagent.[12] In this method, the carboxylic acid (**7**) is activated by the coupling reagent to form an active ester

Scheme 1. Traditional solution phase coupling

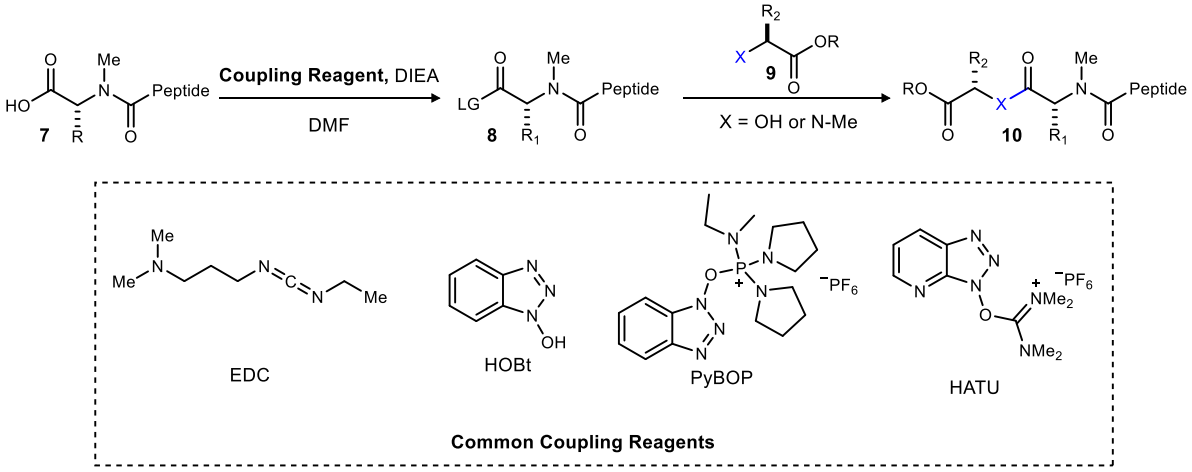

species (**8**) which undergoes attack of the nucleophilic amine (**9**, X=NHMe) to form the coupled product (**10**). However, when this method is used to form *N*-methyl amide or ester linkages the reaction is often slow and low yielding due to the sterically hindered and weakly nucleophilic *N*-methyl amine and alcohol nucleophiles, respectively. Additionally, when this reaction is slow, epimerization through intramolecular oxazolone formation[12] is likely to occur (Scheme 2).

Scheme 2. Epimerization through oxazolone formation

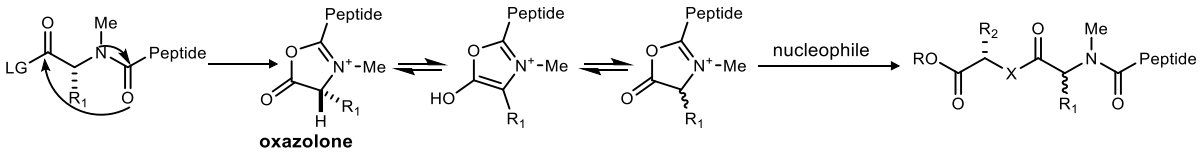

Solid phase peptide synthesis (SPPS) is another method used to form *N*-methyl amide or ester linkages (Scheme 3). In this method, a hydroxyl/amine protected amino acid is bound to a resin, deprotected, and then allowed to react with the solution-phase active ester species to form

[12] Montalbetti, C. A. G. N.; Falque, V. *Tetrahedron* **2005**, *61*, 10827.

the ester or amide linkage.[12] In SPPS, the peptide chain is synthesized from C-terminus to N-terminus. This ensures that the active ester species is not connected to the peptide chain,

Scheme 3. Solid phase peptide synthesis

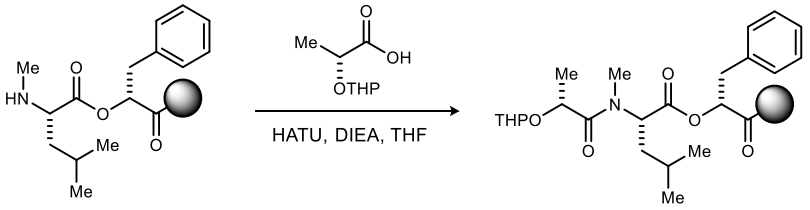

therefore avoiding epimerization through intramolecular oxazolone formation. However, SPPS is considerably more difficult than solution phase peptide synthesis in the case of *N*-methyl depsipeptide synthesis.[13] This is due to further decreased reactivity of resin-bound *N*-methyl amine nucleophiles toward the active ester species in addition to low yielding ester-formation reactions. *N*-Methyl substituents are also much bulkier than non-methylated amides and cause

Scheme 4. Diketomorpholine formation

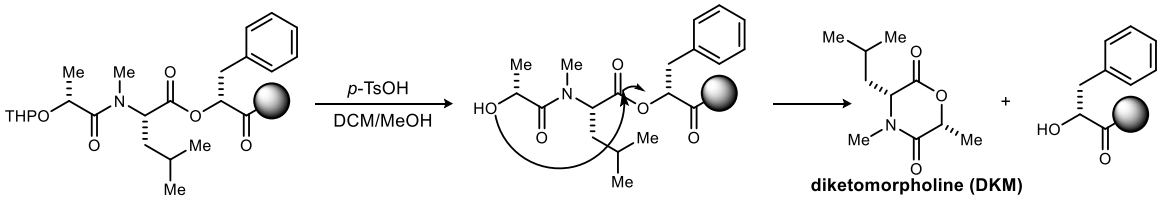

the linear depsipeptide chain to be conformationally strained.[14] Thus, Thorpe-Ingold induced diketomorpholine formation and cleavage from the resin (Scheme 4) is a common side reaction upon deprotection of the resin-bound hydroxyl group.[14,15] Additionally, epimerization through ketene formation (Scheme 5) of the activated ester species is a common issue with solid phase *N*-methyl depsipeptide synthesis.[12]

Scheme 5. Epimerization through ketene formation

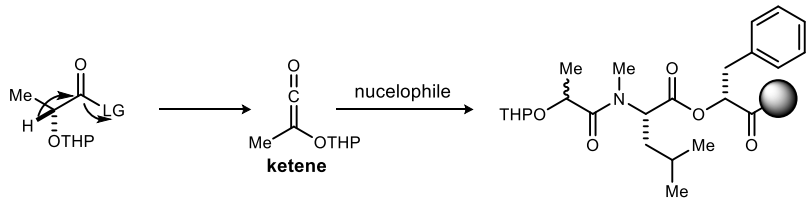

[13] Scherkenbeck, J.; Lüttenberg, S.; Ludwig, M.; Brücher, K.; Kotthaus, A. *Eur. J. Org. Chem.* **2012**, *2012*, 1546.
[14] Kaneti, J.; Kirby, A. J.; Koedjikov, A. H.; Pojarlieff, I. G. *Org. Biomol. Chem.* **2004**, *2*, 1098.
[15] Coin, I. *J. Pept. Sci.* **2010**, *16*, 223.

1.2.2 UmAS as a new method to prepare depsipeptides

Umpolung Amide Synthesis (UmAS) is a new route to the preparation of amides that was discovered[16] by Shen and Makley of the Johnston group. Unlike conventional condensative amide synthesis where the nucleophile is an amine and the electrophile is an active ester

Figure 4. Condensative amide synthesis vs UmAS

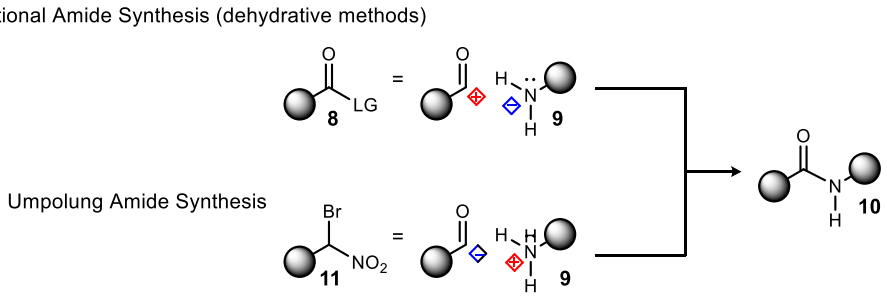

derivative (**8**), this method uses a bromonitroalkane (**11**) as an acyl donor for the amine (**9**). An iodonium ion source is used to activate the amine and potassium carbonate is added as a stoichiometric base. These conditions allow for a reversal of polarity (umpolung)[17] in that the acyl donor is the nucleophile and the amine is the electrophile (Figure 4).

Scheme 6. Speculated UmAS mechanism

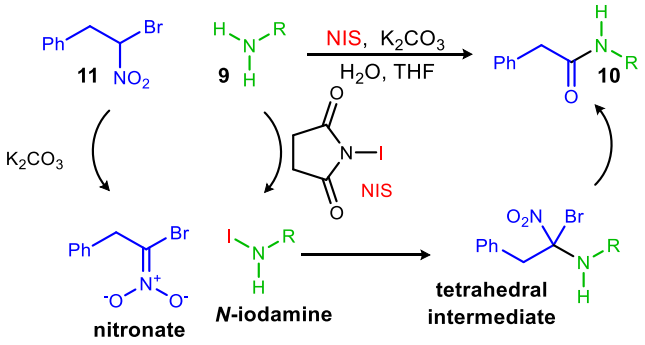

The general mechanism of UmAS is shown in Scheme 6. First, the amine (**9**) is activated by NIS to form an *N*-halamine, and the bromonitroalkane (**11**) is deprotonated to form a nitronate species. Then, the nitronate attacks the *N*-halamine to form a tetrahedral intermediate which is then hydrolyzed to form the amide product (**10**). UmAS mechanistically does not allow for epimerization due to the absence of an active ester intermediate, which is present in traditional amide coupling.

[16] Shen, B.; Makley, D. M.; Johnston, J. N. *Nature* **2010**, *465*, 1027.
[17] umpolung: Seebach, D.; Corey, E. J. *J. Org. Chem.* **1975**, *40*, 231.

Scheme 7. α-Hydroxy amides in depsipeptide synthesis via UmAS & SPPS

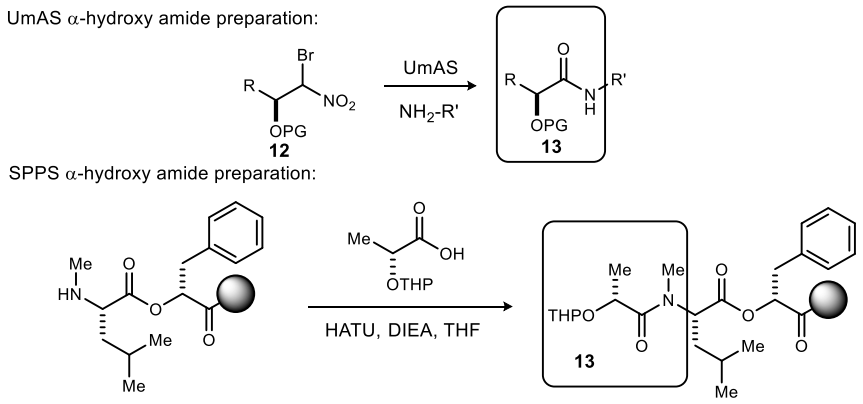

UmAS can be applied to depsipeptide synthesis through coupling an α-hydroxy bromonitroalkane (**12**) with an amine to form α-hydroxy amide (**13**) intermediates.[18] Alternatively, these are formed in solid phase depsipeptide synthesis as shown in Scheme 7.

Other common pathways to prepare α-hydroxy amides (Scheme 8) include enantioselective formation of cyanohydrins (**14**)[19] followed by hydrolysis and

Scheme 8. Enantioselective α-hydroxy amide preparations

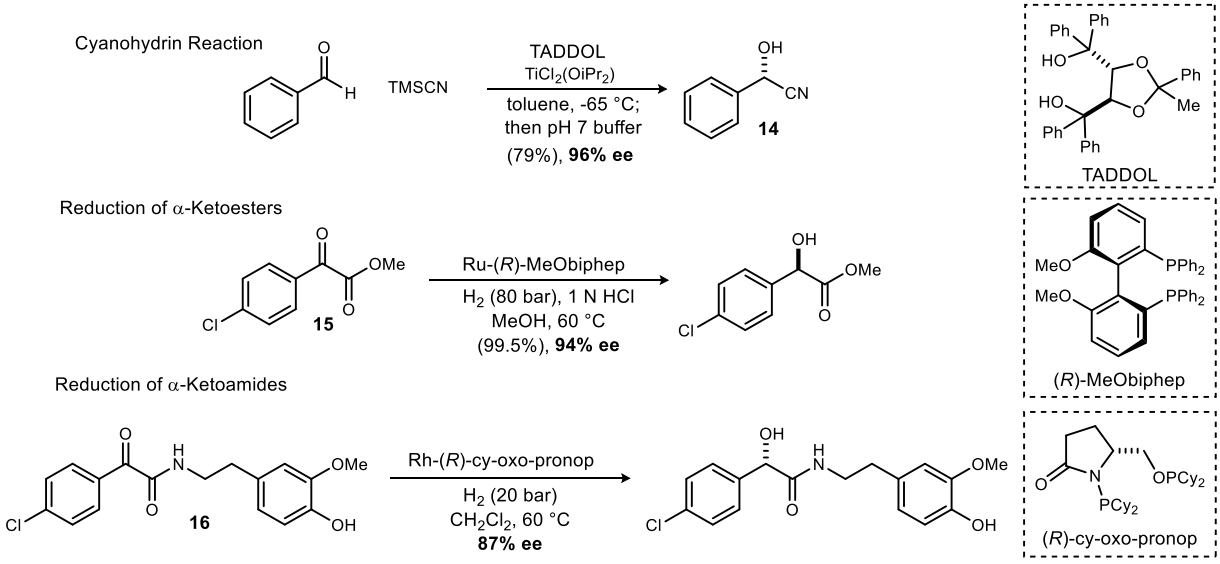

traditional coupling with an amine, and enantioselective reduction of an α-ketoester (**15**) or α-ketoamide (**16**).[20] Although cyanohydrin and α-ketoester reduction give the α-hydroxy product in high enantioenrichment, problems with epimerization of the α-hydroxy carbon have been reported

[18] Leighty, M. W.; Shen, B.; Johnston, J. N. *J. Am. Chem. Soc.* **2012**, *134*, 15233.
[19] North, M.; Usanov, D. L.; Young, C. *Chem. Rev.* **2008**, *108*, 5146..
[20] Cederbaum, F.; Lamberth, C.; Malan, C.; Naud, F.; Spindler, F.; Studer, M.; Blaser, H.-U. *Adv. Synth. Catal.* **2004**, *346*, 842..

when the hydrolyzed adducts are coupled with an amine. This epimerization occurs due to deprotonation and reprotonation of the α-hydroxy center by the organic base used in traditional amide coupling. In α-hydroxy acid derivatives, the α-hydrogen is further acidified by the hydroxyl group during active ester formation, thus making its deprotonation more favorable.

Scheme 9. Epimerization of the α-hydroxy carbon

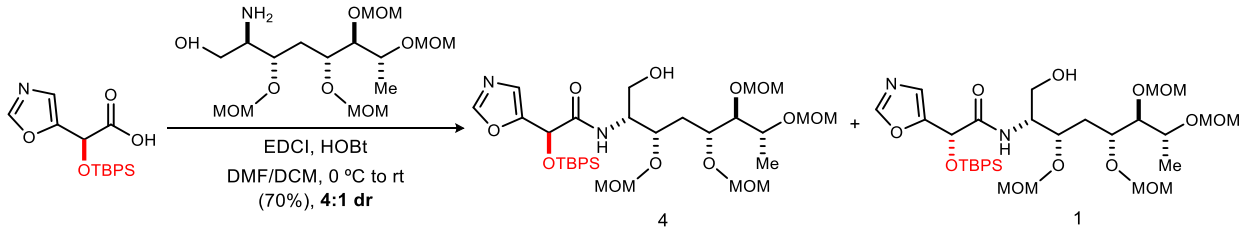

Chandrasekhar's synthesis of bengazole A[21] illustrates this effect. A reaction that should have led to a single diastereomer instead produced a 4:1 ratio of diastereomers, due to epimerization of the α-hydroxy carbon (Scheme 9).

Figure 5. Conventional α-hydroxy amide synthesis vs Henry/UmAS sequence[18]

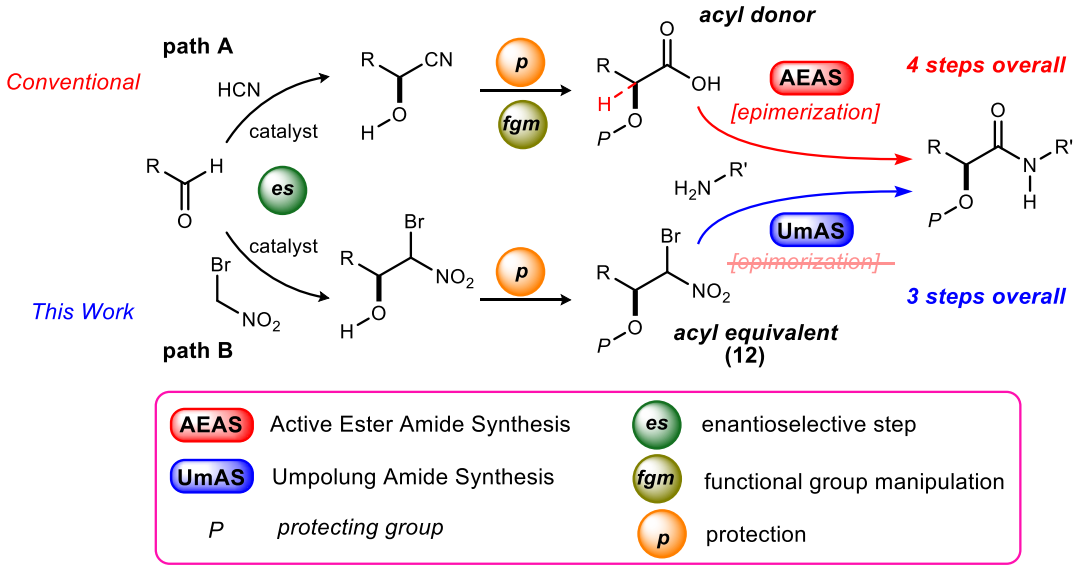

In order to avoid the problem of epimerization, Leighty and Shen developed a new strategy using an enantioselective Henry addition and protection, followed by UmAS to prepare α-hydroxy amides[18] (Figure 5). UmAS mechanistically avoids epimerization of the α-hydroxy carbon, and it also eliminates the functional group manipulation step that is common to carboxylic acid intermediates. Furthermore, the enantioselective Henry is just one method to prepare donors (**12**).

[21] Chandrasekhar, S.; Sudhakar, A. *Org. Lett.* **2010**, *12*, 236.

Leighty and Shen examined copper acetate bis(oxazoline)[22] chemistry for the Henry addition, but found that these methods only gave the desired product in moderate enantiomeric excess.[18] It is hypothesized that the copper counterion may affect the structure of the substrate-bound catalyst (Figure 6).[23] By increasing the sterics on one face of the Cu(II) complex, Leighty and Shen hypothesized that the aldehyde would have an increased chance of coordinating in the desired position of the complex. Different bis(oxazoline) ligands were tried with various copper(II) salts, and *tert*-butyl bis(oxazoline) (**17**) complexed with copper(II) *ortho*-iodo benzoate was found to give the highest ee. Leighty and Shen also found that MOM-protection of the crude alcohol prevented their *retro*-Henry decomposition.

Figure 6. Hypothesized conformation of the Cu(II) complex[23]

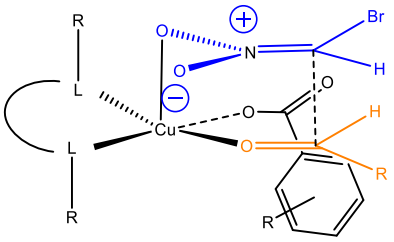

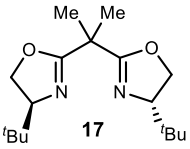

A scope of 19 different MOM-protected bromonitroalkanes (**18**) (82-99% ee) were then coupled to α-methyl benzyl amine (**19**) (Scheme 10) to confirm conservation of configuration during the coupling. In each case, the coupling provided the desired amide (**20**) as a single diastereomer in moderate to good yield, confirming that the α-oxy center did not epimerize during UmAS.

Scheme 10. Enantioselective synthesis of MOM-protected α-oxy bromonitroalkanes and their use in UmAS[18]

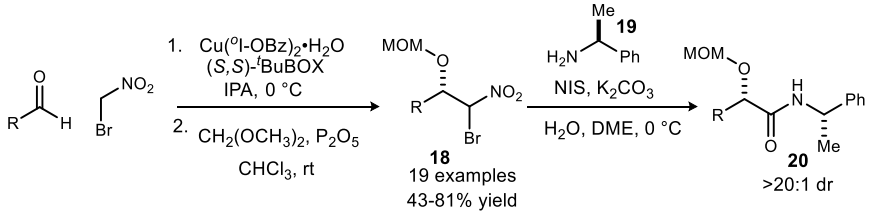

[22] Evans, D. A.; Seidel, D.; Rueping, M.; Lam, H. W.; Shaw, J. T.; Downey, C. W. *J. Am. Chem. Soc.* **2003**, *125*, 12692.

[23] Leighty, M. W.; Shen, B.; Johnston, J. N. Enantioselective synthesis of α-hydroxy amides via umpolung amide synthesis. Presented at 243rd ACS National Meeting & Exposition, San Diego, CA, United States, March 25-29, 2012; ORGN.

1.3 Isolation and prior synthesis of (-)-verticilide

Ryanodine, a plant alkaloid, is an agonist of ryanodine receptor (RyR). RyR is a Ca^{2+}-release channel of the sarcoplasmic reticulum which plays key roles in muscle and neuronal function. Inhibition of this receptor would disrupt the release of calcium, thus disturbing cellular function and ultimately killing the organism.[24] Three types of RyR exist in mammalian cells, but insects have a distinct RyR, thereby making it a potential target for new insecticides.

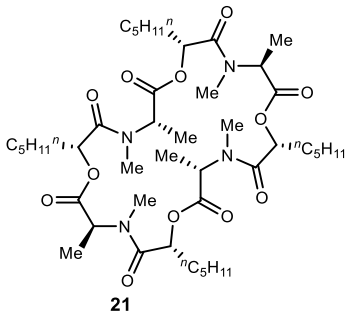

(-)-Verticilide (**21**) was first isolated from a culture broth of *Verticillium* sp. FKI-1033[25] by Ōmura and coworkers in the course of screening for potential insecticides. (-)-Verticilide is a 24-membered depsipeptide that selectively inhibits ryanodine binding to insect RyR with an IC_{50} value of 4.2 μM, making it a potential lead compound for new insecticides.[26]

Scheme 11. Ōmura's preparation of 2-hydroxyhepanoic acid benzyl ester for structure elucidation[26]

Note: The (-) ester was synthesized the same way, but starting from L-malic acid

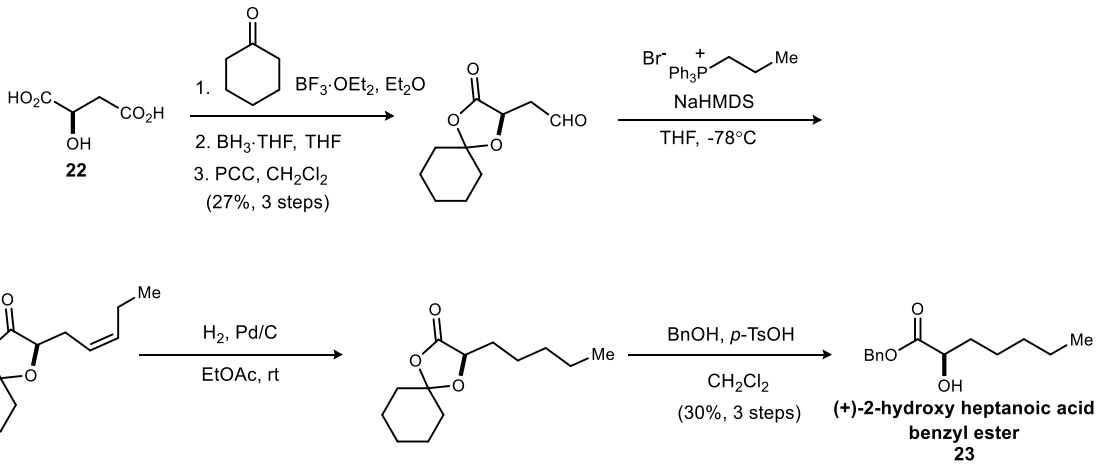

Ōmura and coworkers synthesized (-)-verticilide and elucidated its structure in 2006.[26] The depsipeptide consists of four 2-hydroxyheptanoic acid residues and four *N*-methyl-L-alanine residues. In order to determine the absolute stereochemistry of the α-hydroxy center, Ōmura and coworkers degraded biologically synthesized (-)-verticilide with 6 M HCl to afford 2-hydroxyheptanoic acid and *N*-methyl-L-alanine, which was determined by amino acid analysis. Then, the 2-hydroxyheptanoic acid was treated with cesium carbonate and benzyl bromide to provide the benzyl ester. ^{1}H NMR, ^{13}C NMR, and MS confirmed that the data from the natural product matched the data from esters that were synthesized using malic acid as a chiral auxiliary (Scheme 11). Each enantiomer of synthetic ester was then mixed in a 1:1 ratio with the natural ester and examined by HPLC. The natural ester and (+)-2-hydroxyheptanoic acid (**23**) had identical

[24] Sattelle, D. B.; Cordova, D.; Cheek, T. R. *Invert. Neurosci.* **2008**, *8*, 107.
[25] Ōmura, S,;, K.; Masuma, R. Patent PCT WO2004044214, 2004.
[26] Monma, S.; Sunazuka, T.; Nagai, K.; Arai, T.; Shiomi, K.; Matsui, R.; Omura, S. *Org. Lett.* **2006**, *8*, 5601.

HPLC retention times, which confirmed the *R*-configuration of the natural residue. However, the route shown in Scheme 11 was impractical for the (+)-enantiomer due to the expense of D-malic acid (**22**). Thus, a new synthetic route using a chiral auxiliary was conducted (Scheme 12). (*R*)-Oxazolidinone **24** and heptanoyl chloride were condensed (**25**) followed by diastereoselective α-oxidation with the Davis reagent to give the α-oxy product (**26**) as a single diastereomer. Then, TBDMS protection of the hydroxyl group followed by transesterification, and finally deprotection gave the α-hydroxy ester (**26**) in excellent yield.

Scheme 12. Preparation of *R*-2-hydroxyheptanoic acid benzyl ester[26]

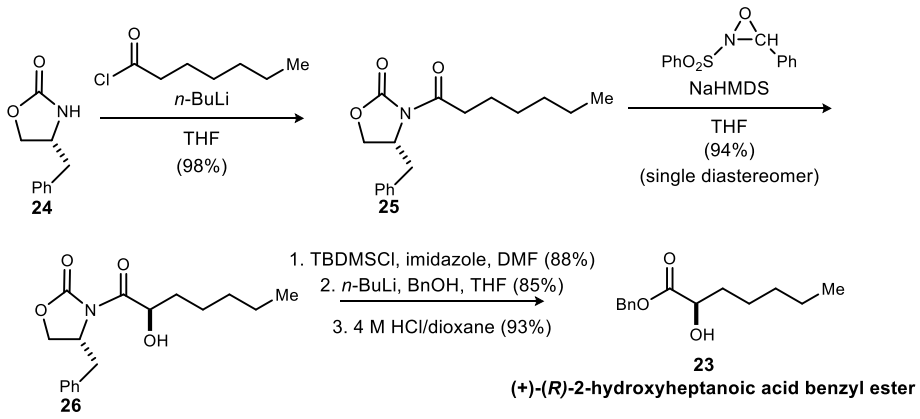

The final steps of Ōmura's synthesis of (-)-verticilide (Scheme 13) include a series of convergent deprotections and standard peptide couplings, the final being a ring-closing macrolactamization. Ōmura and coworkers were able to synthesize (-)-verticilide in 66% overall yield with a 13 step longest linear sequence.

Scheme 13. Final steps in Ōmura's synthesis of (-)-verticilide[26]

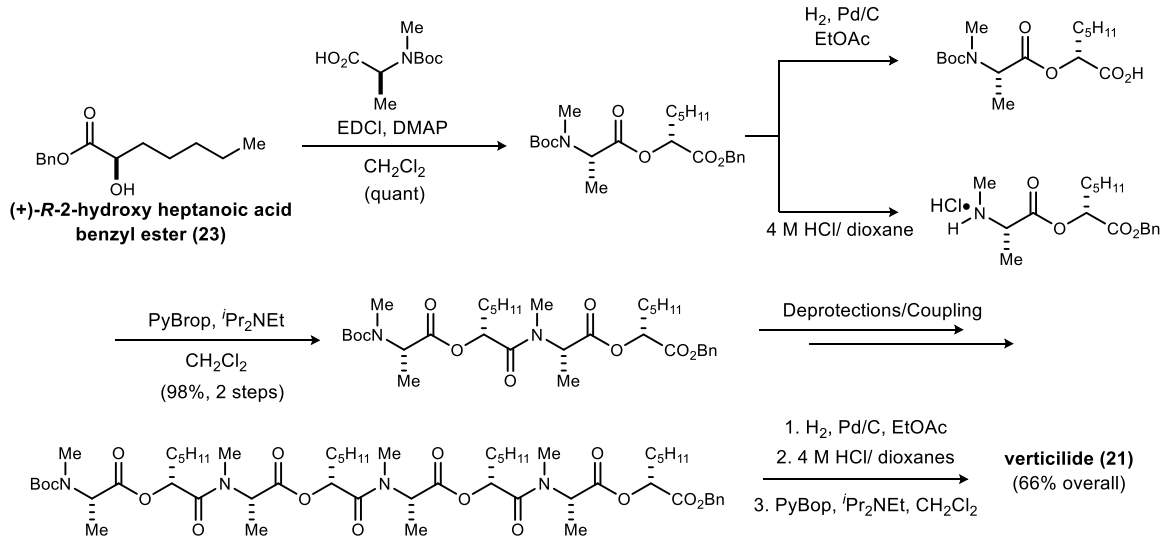

1.4. First generation endeavors toward an UmAS-based approach to (-)-verticilide

Ōmura's synthesis[26] provides an example of an excellent contemporary route to (-)-verticilide, by which to benchmark alternatives. Like Ōmura, this route to (-)-verticilide (Scheme 14) sets the stereochemistry of the α-hydroxy center early in the synthesis, but instead of using chiral auxiliaries, we explored the enantioselective Henry route to α-hydroxy amides. Utilizing the enantioselective Henry and MOM-protection sequence to create our chiral starting material is much more efficient, requiring only two steps, instead of six, to establish the chiral center. The α-oxy bromonitroalkane can then be coupled to *N*-methyl alanine under UmAS conditions to afford an α-hydroxy amide, which can undergo a series of convergent deprotections, Mitsunobu couplings, and a final macrolactonization to afford (-)-verticilide. The use of UmAS and Mitsunobu reactions is beneficial in that neither coupling reaction involves formation of an active ester intermediate, thus epimerization will be mechanistically avoided.

Scheme 14. Proposed synthesis of (-)-verticilide incorporating the enantioselective Henry and UmAS sequence

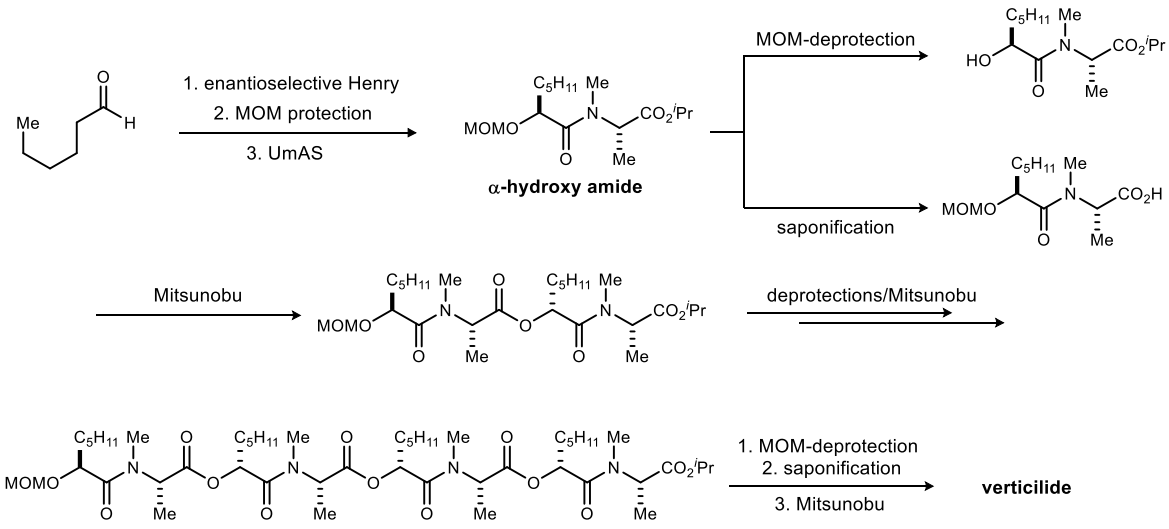

As mentioned earlier, enantioselective Henry conditions developed by Leighty and Shen delivered bromonitroalkanes from 82-99% ee utilizing Evans' bis(oxazoline) catalyst. Although the optimized conditions delivered products in high ee, the reaction yield (52%) was too low for use in this synthesis. As a replacement, Blay's camphor-derived ligand[27] (**27**) was used.

[27] Blay, G.; Climent, E.; Fernández, I.; Hernández-Olmos, V.; Pedro, J. R. *Tetrahedron: Asymmetry* **2007**, *18*, 1603.

Table 1. Enantioselective Henry temperature & bromonitromethane addition screen

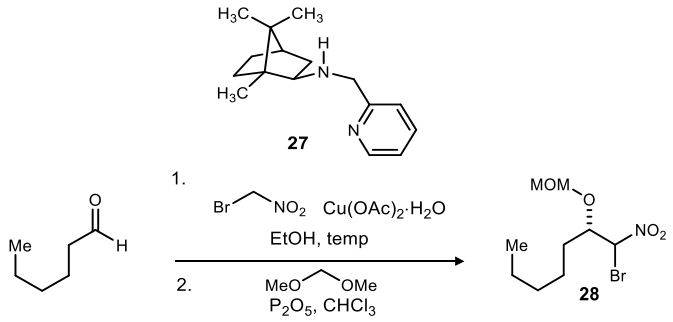

entry	bromonitromethane addn. method (10 equiv)	temperature (°C)	time (days)	yield[a] (%)	ee major/minor[b] (%)
1	all at once	0	2	96	65/81
2	all at once	-20	2	54	71/85
3	all at once	-50	4	12	85/91
4	2.5 equiv/day	-20	4	75	50/80
5	2.5 equiv/day	-50	4	N/A	N/A

[a]Isolated yield. [b]Enantiomeric excess determined by HPLC using an OZ-H column.

In order to obtain **28** with the best possible enantioselection, a number of different Henry conditions were tried on a 1.63 mmol scale (Table 1). Since the BOX chemistry was done at 0 °C,[18] hexanal was first subjected to the Blay conditions at that temperature. As the temperature was lowered, enantioselection increased, but yield greatly suffered. The reaction was suspected to be sluggish at lower temperatures, so reaction time was increased. This still gave no improvement in yield. Another hypothesis was that bromonitromethane was decomposing during the long reaction times, therefore addition of bromonitromethane in aliquots over 4 days was attempted. Adding 2.5 equivalents of bromonitromethane per day improved the yield in the -20 °C case, but enantioselection dropped significantly. Ultimately, the 0 °C conditions were chosen to scale up because they gave the highest yield, and enantioselection was not significantly lower than the -20 °C trials. When scaled up to 6.5 mmol at 0 °C, neither the yield nor ee were consistent after repeating this reaction many times. The yields ranged from 42-95% and the ee ranged from 70-80%. More consistent ee was observed when the workup of this reaction was modified in that the 1 N HCl was pre-chilled and added dropwise. However, the yield of bromonitroalkane **28** continued to vary due to formation of a dibromonitroalkane side product (**29**). This product was not observed in the crude NMR of the Henry, thus was hypothesized to be forming during the MOM-protection step. Slowly quenching the MOM-protection at 0 °C allowed for more consistent yields and formation of little to no dibromonitroalkane side product. After observing consistent yields and enantioselection (90% yield and 70/75% ee), the reaction was cooled to -20 °C for 4 days and subjected to the new workup to afford

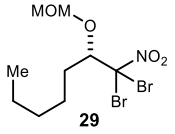

the desired product (**28**) in 95-99% yield and 84/85% ee. This material was then carried on to the UmAS step.

Umpolung Amide Synthesis with *N*-methyl amino esters (*N*,*N*-disubstituted amines) has been attempted in our group previously by Shackleford. Her results showed that the coupling works, but only in low yield (30-40%).[28] In order for the proposed (-)-verticilide synthesis to be just as efficient as Ōmura's, the yield of the UmAS with the disubstituted amine step needed to be raised significantly. Table 2 shows the first series of experiments to raise the yield of the reaction. Initially, the MOM-protected bromonitroalkane (**28**) and *N*-methyl alanine ester (**30**) were subjected to stoichiometric (1.0 equiv NIS) and catalytic (0.1 equiv NIS) UmAS conditions at 0 °C. Unsurprisingly, product (**31**) was produced in very low yield. Increasing the amount of amine improved the yield slightly, but not enough to be significant.

Table 2. UmAS with *N*-methyl alanine isopropyl ester halogen source screen

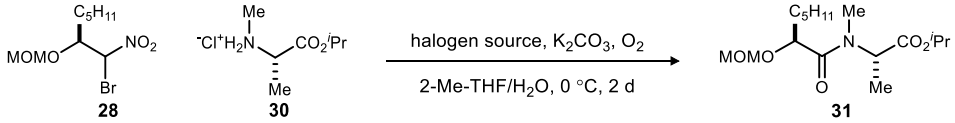

entry	amine (equiv)	halogen source (equiv)	yield[a] (%)
1	1.5	NIS (1.0)	7
2	2.0	NIS (1.0)	8
3	1.5	NIS (0.1)	12
4	1.5	NBS (1.0)	N/A
5	1.5	NCS (1.0)	N/A

[a]Isolated yield.

Since proline methyl ester is a reasonable substrate for UmAS, we hypothesize that acyclic *N*,*N*-disubstituted amines are on the margins of reactivity since a small amount of product can be isolated. Our mechanistic picture for UmAS involves *N*-halamine formation. Since the *N*-methyl alanine ester seemed to be decomposing faster than it was reacting, it was hypothesized that changing the halogen source might slow its decomposition pathway. When NBS and NCS were added to the reaction, very little conversion to product was observed. These findings show that the most reactive halogen source is needed for these challenging substrates, but somehow must be stabilized to prevent decomposition of the amine.

[28] Shackleford, J.P., *Masters Thesis* **2012**.

Table 3. *N*-Chloramine in UmAS optimization attempts

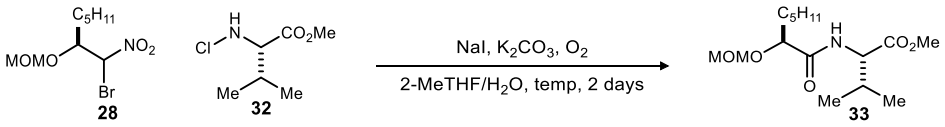

entry	NaI (equiv)	temperature (°C)	yield[a] (%)
1	0	0	N/A
2	0.1	0	17
3	0.5	0	34
4	1.0	0	30
5	1.0	RT	24
6	1.0	60	13

[a]Isolated yield.

Wang and coworkers had similar problems with highly reactive *N*-iodamines when developing their aminocyclization methodology.[29] To solve their problem, they catalytically generated the *N*-iodamine in situ from a more stable *N*-chloramine source. Wang's method of catalytically generating an *N*-iodamine was first tested in UmAS using a known *N*-chlorovaline methyl ester (**32**).[30] After confirmation by NMR that the *N*-chloramine was successfully synthesized, it was subjected to standard UmAS conditions (Table 3), but with NaI as the iodine source. The yield of the initial trial was still low, but the reaction was much cleaner. The crude NMR showed mainly starting material (bromonitroalkane **28**), a carboxylic acid derivative of the bromonitroalkane (**34**), and the desired amide (**33**, Figure 7). However, analogous amine decomposition products to those previously observed with *N*-methyl alanine ester were not found.

Figure 7. Major products of UmAS with *N*-chlorovaline

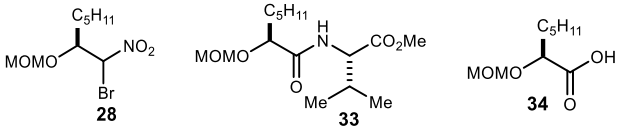

In attempts to increase the rate of amide-bond formation, the reaction was conducted at room temperature and at 60 °C. Heating the reaction did consume all of the starting material, but it was converted mostly to carboxylic acid **34** (Figure 7) rather than the desired amide. Because the reaction went so cleanly to carboxylic acid and amide when heated, those conditions were applied to UmAS with *N*-methyl alanine ester (Table 4). As expected, the products of the reaction were carboxylic acid **34** and amide **31** (1:1 ratio). Surprisingly, the yield (34%) was much higher than when the reaction was conducted at 0 °C. These results suggest that heating the reaction favors the pathway to the carboxylic acid and the UmAS pathway over the many decomposition pathways

[29] Huang, H. T.; Lacy, T. C.; Blachut, B.; Ortiz, G. X., Jr.; Wang, Q. *Org. Lett.* **2013**, *15*, 1818.
[30] Lu, S. P.; Lewin, A. H. *Tetrahedron* **1998**, *54*, 15097.

observed at 0 °C. Unfortunately, a reaction with 34% yield was too low to use in the synthesis of (-)-verticilide, so UmAS with alanine isopropyl ester (monosubstituted amine) followed by *N*-methylation was attempted in order to obtain **31a** in a more efficient manner (Scheme 15).

Table 4. UmAS with *N*-methyl alanine isopropyl ester temperature study

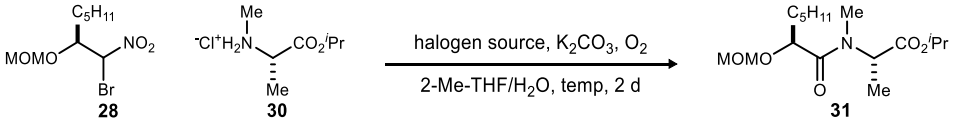

28 **30** **31**

entry	halogen source (equiv)	temperature (°C)	yield[a] (%)
1	NIS (1.0)	0	7
2	NIS (0.1)	0	12
3	NaI (1.0)	60	34
4	NaI (0.1)	60	25

[a]Isolated yield.

UmAS with the free base of alanine isopropyl ester (**35**) gave the desired amide (**36a**) in 80% yield under standard stoichiometric conditions. Unlike the amide products of *N*-methyl alanine isopropyl ester (**31a**, **31b**), the diastereomers (**36a**, **36b**) were separable by flash column chromatography, providing another compelling reason to pursue the alternative procedure. After UmAS, the single diastereomer (**36a**) was *N*-methylated using sodium hydride and methyl iodide to afford **31a** in 78% yield. Initially, problems with epimerization of the α-oxy center arose during *N*-methylation, presumably due to the deprotonation of the amide product. Since the N-H bond is more polarized than the α-C-H bond, deprotonation of the nitrogen should proceed faster. Because of this, the epimerization problem was solved by simply decreasing the reaction temperature from ambient to 0 °C and the equivalents of NaH from four to two.

Scheme 15. New strategy to obtain the *N*-methyl amide: sequential UmAS and methylation steps

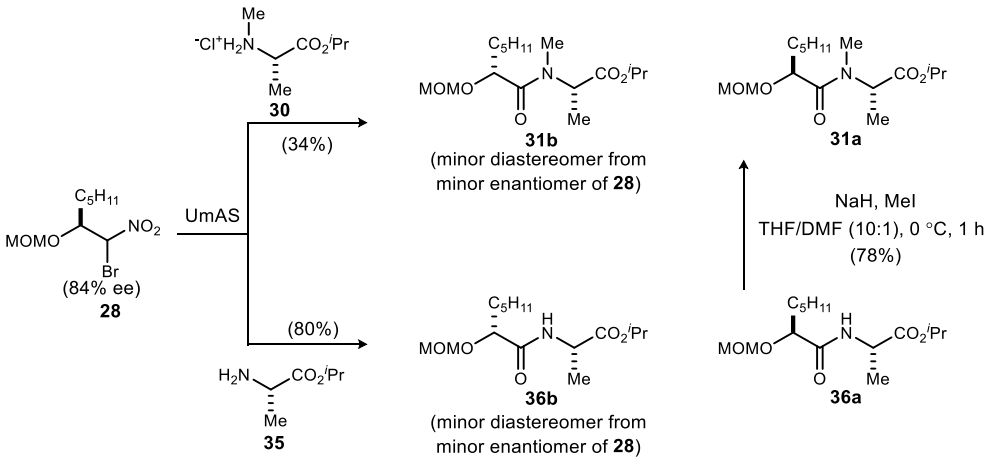

The next steps in the route to (-)-verticilide were to divide **31a** into two portions and remove the MOM-group from one portion, and saponify the ester of the other. Table 5 shows the series of conditions that were tried in order to obtain the desired alcohol (**37**).

Table 5. MOM-deprotection optimization

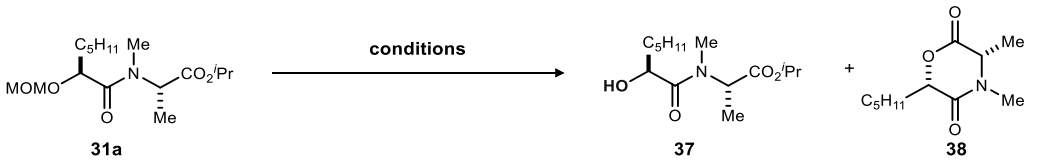

31a **37** **38**

entry	conditions	resulting products[a]
1	TFA/CH_2Cl_2 (1:1), rt, 1h	**37**, **38** (1:1)[a]
2	TFA/CH_2Cl_2 (1:1), 0 °C, 1 h	**37**, **38** (1:1)[a]
3	conc. HCl (10 equiv)/MeOH, rt, 1 h	**37**, **38** (1:1)[a]
4	BBr_3/CH_2Cl_2, -78 °C to rt, 3 h	**38** only
5	BF_3•Et_2O, PhSH/CH_2Cl_2, rt, 1 h	**37** only

[a]Ratios of products are representative of what was isolated from the crude reaction mixture

Initially, **31a** was subjected to standard Brønsted acid-based MOM-deprotection conditions [trifluoroacetic acid in dichloromethane at ambient temperature]. Surprisingly, these conditions not only resulted in MOM-deprotection, but also cyclization to form diketomorpholine **37**. When the reaction was stopped after only 30 minutes, an equal ratio of **31a** to **37** to **38** was observed, which indicates that cyclization was occurring very quickly after the hydroxyl group was deprotected. However, cyclization to **38** was not immediate, meaning that there was a glimmer of hope that this deprotection could be optimized to favor formation of **37** only. The fast intramolecular cyclization of **37** to **38** can be explained by ground state destabilization effects. In this case, entropic strain from the *N*-methyl amide[14] and activation of the isopropyl ester in the acidic reaction conditions raised the ground state energy of the free alcohol (**37**), and thereby decreased the energy barrier of its intramolecular cyclization to **38**. Because **37** didn't immediately convert to **38** in the reaction, it was hypothesized that intramolecular cyclization to **38** could be minimized in less activating deprotection conditions. Unfortunately decreasing the temperature and using a different Brønsted acid did not improve the reaction, so boron reagents were then tried. BBr_3 was too aggressive and resulted in complete lactonization of the molecule. Milder conditions (BF_3•OEt_2 and thiophenol) that were effective in the late stages of the total synthesis of (+)-brefeldin A[31] were then tried, and successfully provided alcohol **37** in 75% yield without formation of **38.** Saponification of **31a** following the Evans protocol[32] went smoothly as predicted to give acid **39** (Scheme 16).

[31] Kim, D.; Lee, J.; Shim, P. J.; Lim, J. I.; Jo, H.; Kim, S. *J. Org. Chem.* **2002**, *67*, 764.
[32] Evans, D. A.; Wu, L. D.; Wiener, J. J. M.; Johnson, J. S.; Ripin, D. H. B.; Tedrow, J. S. *J. Org. Chem.* **1999**, *64*, 6411.

Scheme 16. Ester saponification

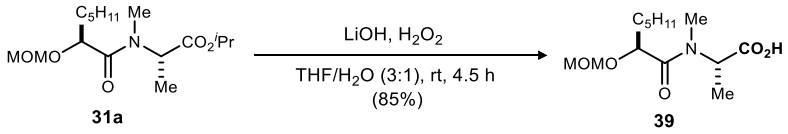

Alcohol **37** and acid **39** were then subjected to Mitsunobu conditions to form tetradepsipeptide **40** with inverted stereochemistry at the α-hydroxy center of the alcohol (Scheme 18). Initial Mitsunobu conditions were taken from Martin's synthesis of macbecin I and herbimycin A[33] because sterics around the alcohol in Martin's synthesis were similar to those of the desired tetradepsipeptide. Although using DEAD in the conditions produced the tetradepsipeptide in moderate (63%) yield, separating DEAD byproducts from the desired product proved to be extremely difficult. However, DIAD byproducts were much more easily separated, so DIAD was used instead.

Scheme 18. Mitsunobu conditions to form the tetradepsipeptide

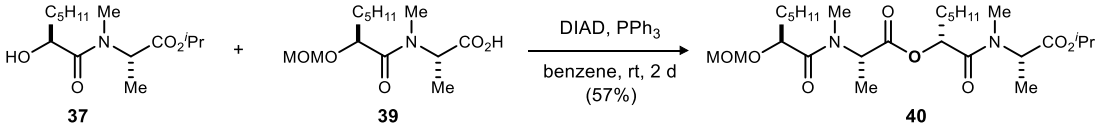

Following the first Mitsunobu reaction, **40** was divided into two portions to be saponified and MOM-deprotected, respectively. By this point, my dad's favorite saying, "expect the unexpected" had been fully ingrained in daily lab practices, so it was unsurprising that product **41** was not observed upon attempted saponification of **40**. Instead, carboxylic acid **39** and diketomorpholines **42** and **43** were the major products (Scheme 17). Further attempts to saponify tetradepsipeptide **40** are summarized in Table 6.

Scheme 17. Tetradepsipeptide saponification conditions

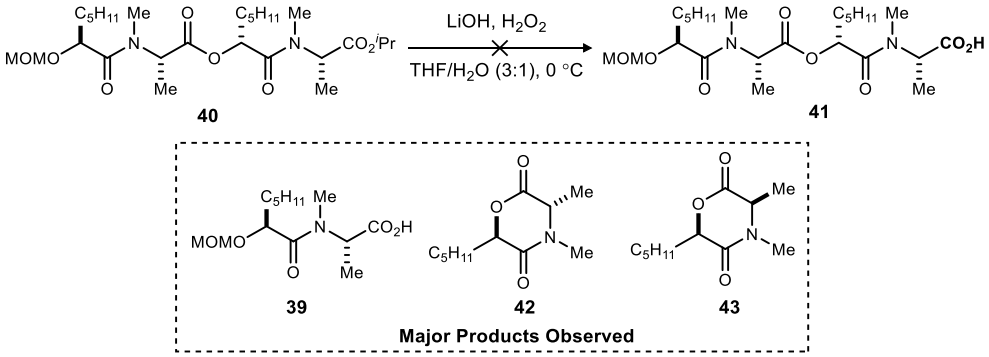

[33] Martin, S. F.; Dodge, J. A.; Burgess, L. E.; Limberakis, C.; Hartmann, M. *Tetrahedron* **1996**, *52*, 3229.

Table 6. Tetradepsipeptide saponification attempts

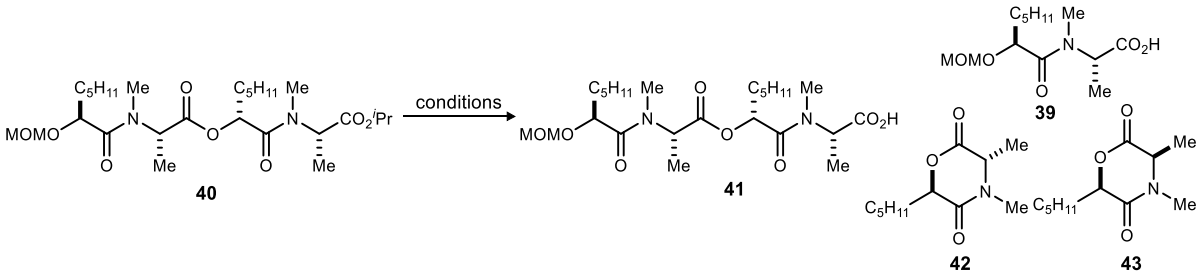

entry	conditions	temperature (°C)	time (hours)	NMR time after rxn (hours)	formation of **41**[a] (Y/N)	ratio of **39**:**42**&**43**[b]	ratio of **42**:**43**[c]
1	$LiOH/H_2O_2$	0	2	<1	N	1:3.5	1:1
2	$LiOH/H_2O_2$	0	0.17	<1	N	7.4:1	1:1
3	LiOH	0	0.17	<1	N	8:1	2:1
4	Me_3SnOH	90	18	<1	Y	5:1	1:1
5	Me_3SnOH	90	18	4	Y	2.5:1	1.8:1
6	Me_3SnOH	90	18	2	Y	3.5:1	1.4:1
7	PhSeNa, 18-C-6	50	24	<1	N	5.2:1	1:2
8	KO_2, 18-C-6	rt	6	<1	Y	5:1	1:2
9	KO_2, 18-C-6	rt	6	18	Y	1.3:1	1:1.6

[a]Determined by LCMS. [b,c]Ratios are of the crude reaction mixture and were determined using ^1H NMR

Since the major products of entry 1 are acid **39** and diketomorpholines **42** and **43**, it was hypothesized that the central ester bond of tetradepsipeptide **40** was cleaving faster than the isopropyl ester. When the reaction was repeated and stopped after ten minutes to examine the relative rates of the two possible saponifications, formation of **41** was not observed. Formation of only **39**, **42**, and **43** confirmed that the center ester linkage of **40** is cleaved much faster than the isopropyl ester in the presence of lithium hydroxide and hydrogen peroxide. The peroxide anion is a small nucleophile, so a larger nucleophile (hydroxide) was thought to be necessary in order to selectively saponify the terminal isopropyl ester. Hydroxide conditions unfortunately gave the same result, so some alternative saponification methods were considered. Literature examples that employed tin reagents showed that tributyltin oxide selectively cleaved an ethyl ester in the presence of a lactone,[34] but that trimethyltin hydroxide was a much better reagent to cleave isopropyl esters.[35] When trimethyltin hydroxide was used on **40**, **41** was initially observed by NMR and LCMS, but when checked four hours later showed only **39** and increased amounts of **42**. The reaction was repeated, and the same decomposition was observed. Attempts to cleave the isopropyl ester in an S_N2-like fashion using sodium phenyl selenide[36] were unsuccessful as well. Finally, conditions with potassium superoxide and 18-crown-16[37] were tried as another saponification attempt with a bulky nucleophile. The superoxide conditions afforded results similar to the

[34] Salomon, C. J.; Mata, E. G.; Mascaretti, O. A. *J. Org. Chem.* **1994**, *59*, 7259.
[35] Furlán, R. L. E.; Mata, E. G.; Mascaretti, O. A. *Tetrahedron Lett.* **1996**, *37*, 5229.
[36] Liotta, D.; Sunay, U.; Santiesteban, H.; Markiewicz, W. *J. Org. Chem.* **1981**, *46*, 2605.
[37] San Filippo, J., Jr.; Chern, C. I.; Valentine, J. S. *J. Org. Chem.* **1976**, *41*, 1076.

trimethyltin hydroxide conditions: initial observation of **41** by LCMS with increased amounts of **42** over time.

Scheme 19. Proposed tetradepsipeptide acid decomposition mechanism

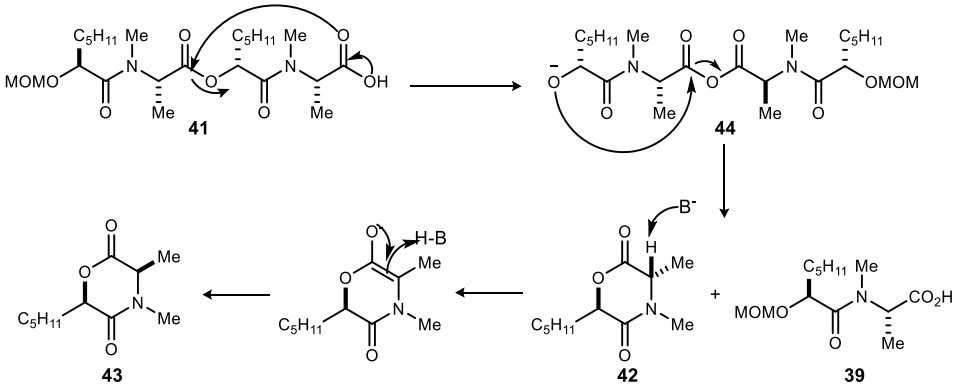

In both of the conditions where tetradepsipeptide carboxylic acid **41** was formed, the amount of diketomorpholine **42** appeared to increase over time by NMR. This observation confirmed the instability of **41** because it was decomposing not only in the basic reaction conditions, but also on standing after work up. The postulated mechanism of decomposition (Scheme 19) is through an intramolecular acyl transfer to form mixed anhydride **44**, followed by cyclization and cleavage to form acid **39** and diketomorpholine **42**. Diketomorpholine **43** can be formed through epimerization of **42** in basic reaction conditions. Because tetradepsipeptide carboxylic acid **41** proved too unstable to use in the next convergent Mitsunobu coupling, this proposed route to (-)-verticilide was no longer viable and was revised.

1.5 UmAS-based approach to (-)-verticilide: revised route

Due to the instability of the deprotected *N*-methylated intermediates, this route was revised (Scheme 20) in that the depsipeptide intermediates were carried through without methylation. In this route, the α-oxy bromonitroalkane can be coupled to free base alanine benzyl ester under UmAS conditions to afford α-hydroxy amide intermediate **45** which can be convergently coupled and ultimately cyclized in a series of Mitsunobu reactions to afford *N*-H macrocycle **53**. Then, **53** can be transformed to the natural product (-)-verticilide through a final tetra-*N*-methylation reaction. In this synthesis, the use of a benzyl ester instead of an isopropyl ester avoids basic deprotection conditions which may lead to cleavage or epimerization of linear depsipeptide intermediates. The benzyl ester can also be removed in strongly Lewis acidic conditions,[38] such as $AlCl_3$, which sets the stage for a one-step global deprotection of **51**, as opposed to the two-step MOM-deprotection/saponification in the previous route.

[38] Tsuji, T.; Kataoka, T.; Yoshioka, M.; Sendo, Y.; Nishitani, Y.; Hirai, S.; Maeda, T.; Nagata, W. *Tetrahedron Lett.* **1979**, *20*, 2793.

Scheme 20. Revised route to (-)-verticilide

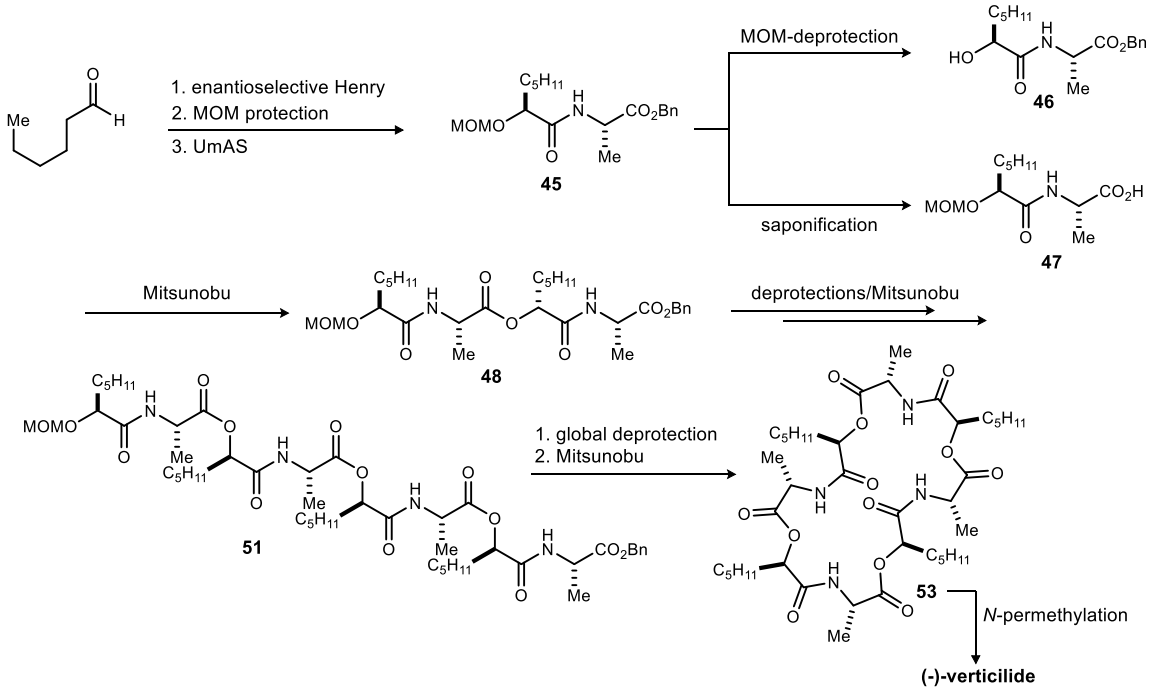

In the revised route, steps toward tetradepsipeptide synthesis went smoothly (Scheme 21). UmAS coupling of **28** and the free base of alanine benzyl ester proceeded smoothly to afford α-hydroxy amide **45** in 80% yield. Ester **45** was then divided into two portions for convergent MOM

Scheme 21. Revised route: tetradepsipeptide formation

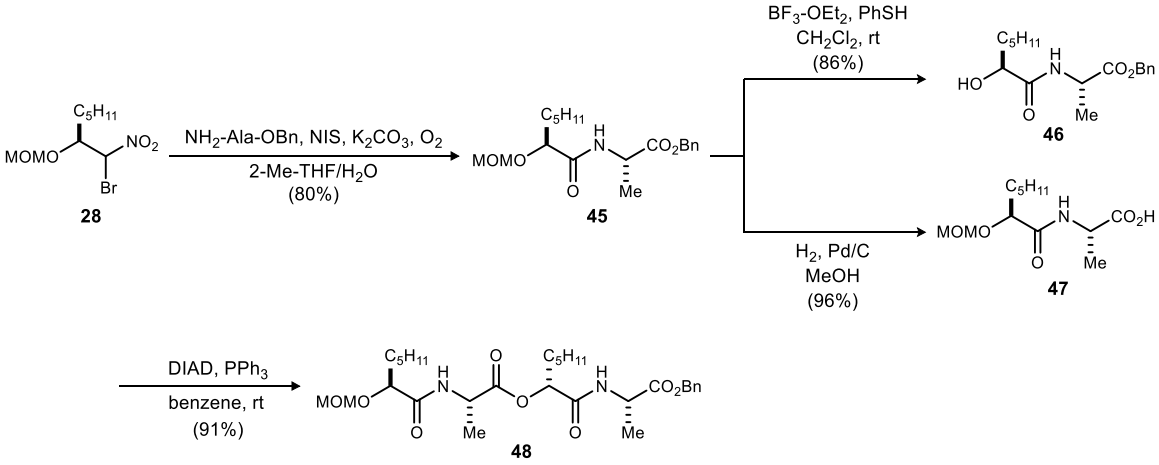

and benzyl deprotections. MOM-deprotection of **45** with BF_3•OEt_2 and thiophenol afforded alcohol **46** in 86% yield without observable formation of diketomorpholine side products. However, the order of reagent addition in these conditions was vital for selective MOM-deprotection. If BF_3•OEt_2 was added to the reaction before thiophenol, a large amount of benzyl-deprotection was observed. Because **46** appeared to be much more stable than its *N*-methyl analog,

Scheme 23. Revised route: octadepsipeptide formation

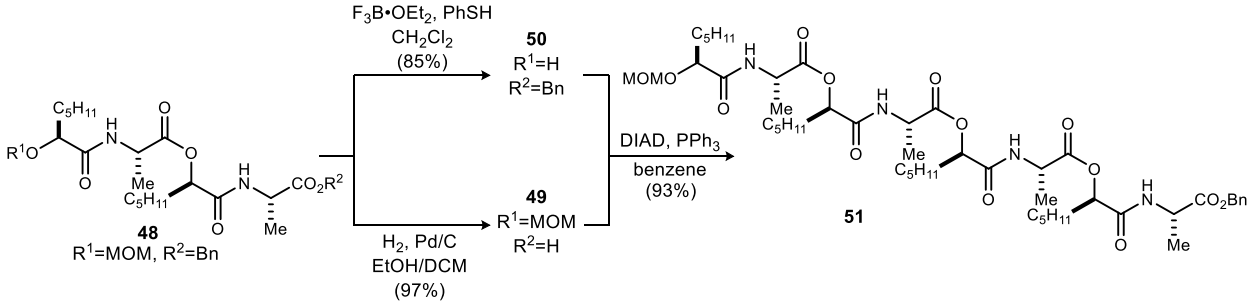

harsher conditions using trifluoroacetic acid were attempted, but did not have any effect on the substrate. Benzyl-deprotection of **45** using palladium on carbon afforded the acid (**47**) in 96% yield. Alcohol **46** and acid **47** were then coupled in a Mitsunobu reaction using DIAD and PPh_3 to afford tetradepsipeptide **48** in 91% yield. Substrate **48** was then divided into two portions for the second round of convergent MOM and benzyl deprotections in preparation for octadepsipeptide formation (Scheme 23). Tetradepsipeptide **48** is the only true solid thus far in the synthesis, *and* it is insoluble in most solvents (methanol, ethanol, ethyl acetate, ether, hexanes, benzene, toluene), aside from dichloromethane, chloroform, and DMSO. Because of its insolubility, the conditions to benzyl-deprotect **48** were adjusted to a 10:1 mixture of ethanol and dichloromethane instead of methanol, affording tetradepsipeptide acid **49** in quantitative yield. Unlike its *N*-methyl analog, **49** was bench stable. MOM ether **48** was deprotected with BF_3•OEt_2 and thiophenol to afford tetradepsipeptide alcohol **50** in 86% yield without formation of diketomorpholine decomposition products. Acid **49** and alcohol **50** were then coupled in the same Mitsunobu reaction conditions used for tetradepsipeptide formation, to provide octadepsipeptide **51** in 93% yield. Octadepsipeptide **51** was then globally deprotected with $AlCl_3$ in nitromethane to afford *seco*-acid **52** in 97% yield (Scheme 22). Despite the strongly Lewis acidic conditions, no cleavage or cyclized products were observed in this reaction.

Scheme 22. Revised route: *seco*-acid formation

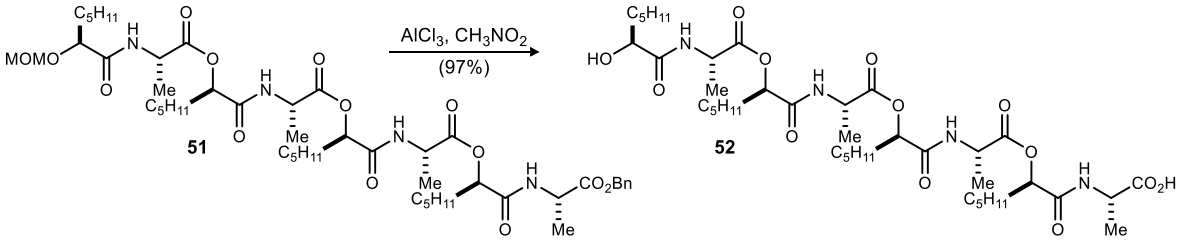

In the literature, depsipeptide macrolactonization tends to exhibit low to moderate yield due to the tendency of the alcohol to eliminate, and the sterically hindered nature of the carboxylic acid. Macrolactamization is therefore generally favored for the macrocyclization step in cyclodepsipeptide synthesis.[39] For example, macrolactonization of depsipeptide FK228[40] proved difficult as most conditions yielded only recovered starting material or alcohol-elimination side products. Extensive optimization of Mitsunobu conditions to suppress elimination of the alcohol

[39] Wen, S.; Packham, G.; Ganesan, A. *J. Org. Chem.* **2008**, *73*, 9353.
[40] Li, K. W.; Wu, J.; Xing, W.; Simon, J. A. *J. Am. Chem. Soc.* **1996**, *118*, 7237.

afforded the macrocycle in 64% yield, but unfortunately used a vast excess of Mitsunobu reagents. When Mitsunobu conditions were tried in order to cyclize alternating cyclodepsipeptide bacillistatin 2,[41] the product was formed in only trace amounts. However, when conditions with 2-methyl-6-nitrobenzoic anhydride (MNBA) were used, bacillistatin 2 was cyclized in 88% yield, demonstrating that macrolactonization is not necessarily an inefficient route for depsipeptide cyclization. In both cases, optimized macrolactonization conditions involved slow addition of coupling reagents to avoid unwanted side product formation or dimerization.

Scheme 24. Macrolactonization of octadepsipeptide *seco*-acid 52

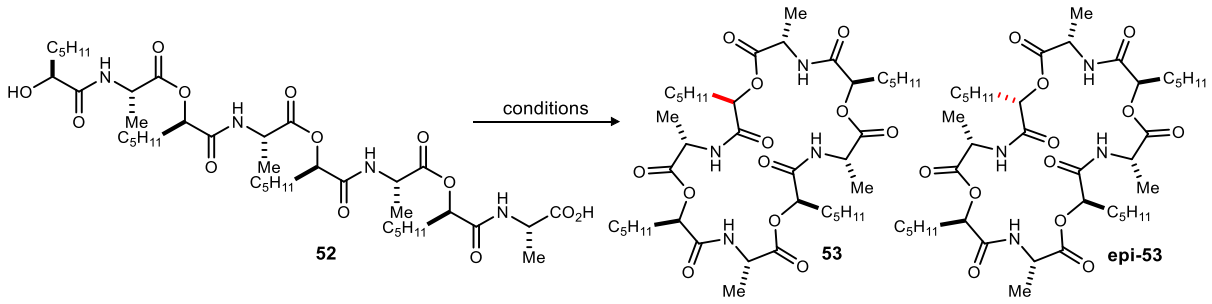

entry	conditions	product	yield[a]
1	Mitsunobu	**53**	79%
2	Yamaguchi	*epi*-**53**	51%

[a]Isolated yield.

In this synthesis, optimized Mitsunobu macrolactonization conditions of **52** only use 5 equivalents of DIAD and 6 equivalents of PPh_3, less than half the amount used in the precedents followed. In order to avoid acylated side products, DIAD was added to the reaction slowly over 40 minutes, affording symmetrical cyclodepsipeptide **53** in 79% yield (Scheme 24). Additionally, **52** was cyclized without inverting the stereocenter in Yamaguchi macrolactonization conditions to afford non-symmetrical macrocycle *epi*-**53** in 51% yield.

N-Permethylation of cyclic peptides and depsipeptides is relatively rare in the literature. As previously mentioned, the most common way to make *N*-methylated cyclic peptides and depsipeptides is through coupling *N*-methyl amino acids in solution or solid phase peptide synthesis. Known methods to *N*-methylate macrocyclic peptides and depsipeptides are summarized in Scheme 25. The first example in Scheme 25 involves *N*-methylation of a resin-bound cyclic hexapeptide scaffold (**54**) to create a diverse library of *N*-methylated cyclic peptides for discovery of orally bioavailable scaffolds.[42] The *N*-methylation conditions involve treatment of the cyclic peptide scaffold with lithium *tert*-butoxide in THF followed by draining the base solution and addition of methyl iodide in DMSO to selectively afford a trimethylated product (**55**). Other scaffolds with the same amino acid sequence but varied stereochemistry were synthesized and *N*-methylated. Six scaffolds selectively afforded either a tri or tetramethylated product.

[41] Pettit, G. R.; Hu, S.; Knight, J. C.; Chapuis, J.-C. *J. Nat. Prod.* **2009**, *72*, 372.
[42] White, T. R.; Renzelman, C. M.; Rand, A. C.; Rezai, T.; McEwen, C. M.; Gelev, V. M.; Turner, R. A.; Linington, R. G.; Leung, S. S.; Kalgutkar, A. S.; Bauman, J. N.; Zhang, Y.; Liras, S.; Price, D. A.; Mathiowetz, A. M.; Jacobson, M. P.; Lokey, R. S. *Nat. Chem. Biol.* **2011**, *7*, 810.

However, the other 26 hexapeptide scaffolds either gave a mixture of products or no reaction due to the conformational nature of the cyclic peptide.

Scheme 25. Known methods of *N*-methylation applied to macrocyclic peptides and depsipeptides

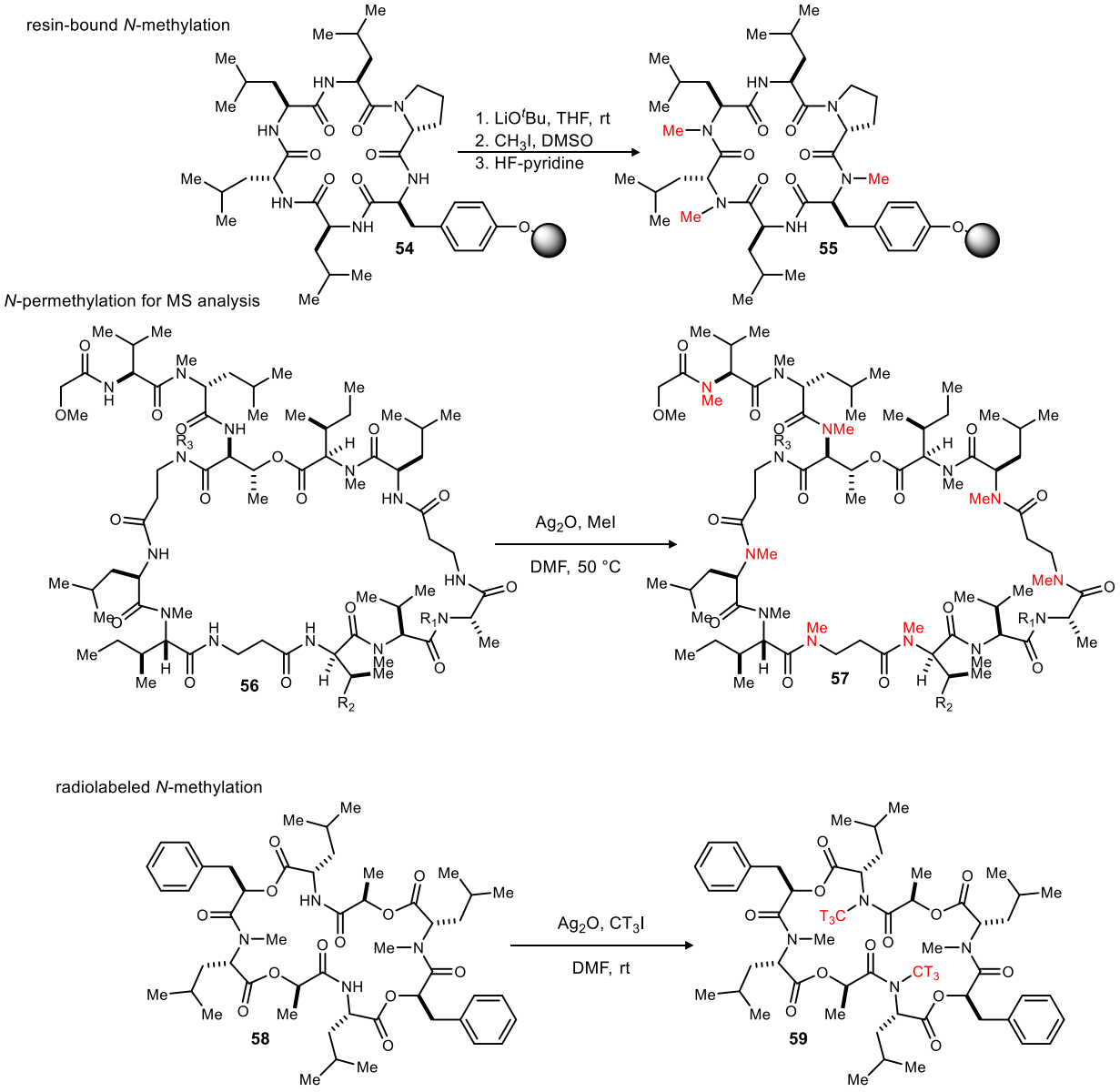

A second example is *N*-permethylation of theonallapeptolide natural products[43] in an effort to elucidate their structure. MS analysis of the theonallapeptolides was impossible because of all of the fragment ions of the same molecular weights, such as Ala and β-Ala; Leu, *allo*-Ile, and Me-Val; Me-Leu, Me-Ile, and Me-*allo*-Ile. In order to confirm their structure, the theonallapeptolides (**56**) were *N*-methylated with Ag_2O in DMF to yield a permethylated compound (**57**) that was

[43] Roy, M. C.; Ohtani, I. I.; Ichiba, T.; Tanaka, J.; Satari, R.; Higa, T. *Tetrahedron* **2000**, *56*, 9079.

subsequently hydrolyzed to its *N*-methyl amino acid subunits. Use of Marfey's reagent and ^{1}H NMR analysis of the *N*-methyl amino acids confirmed their structure and stereochemistry, allowing for non-ambiguous structure elucidation.

Table 7. *N*-Methylation optimization attempts: round 1

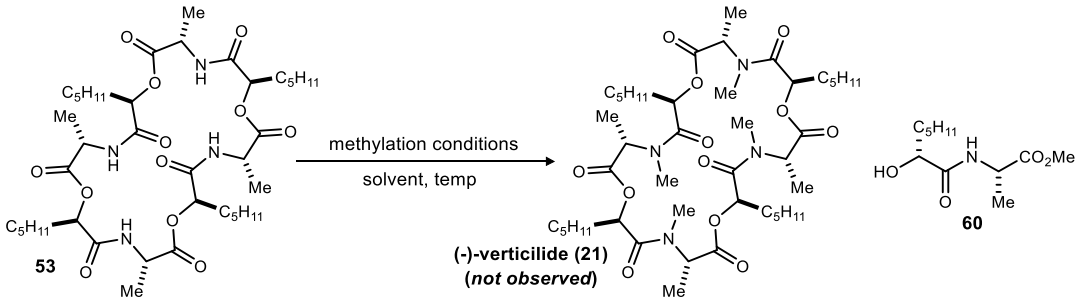

entry	methylation conditions	solvent	temp (°C)
1	NaH, MeI	THF/DMF (10:1)	0 to rt
2	Ag_2O, MeI	DMF	50
3	Ag_2O, MeI	THF	rt
4	DIAD, PPh_3, MeOH	THF	rt

The last example in Scheme 25 is *N*-dimethylation with CT_3I for receptor binding studies of the natural product PF1022A[44] (**58**). After over 70 different experiments, optimized conditions use a vast excess of CT_3I and Ag_2O in DMF to afford the radiolabeled product (**59**) in 7% yield. PF1022A is a depsipeptide with alternating *N*-methyl amino acid and hydroxy acid residues, similar to (-)-verticilide. The difficulty to *N*-methylate dimethyl PF1022A precursor was accurate foreshadowing to optimization of the last *N*-tetramethylation step in this route to (-)-verticilide.

Figure 8. Hypothesized solvent-dependent conformations of 53

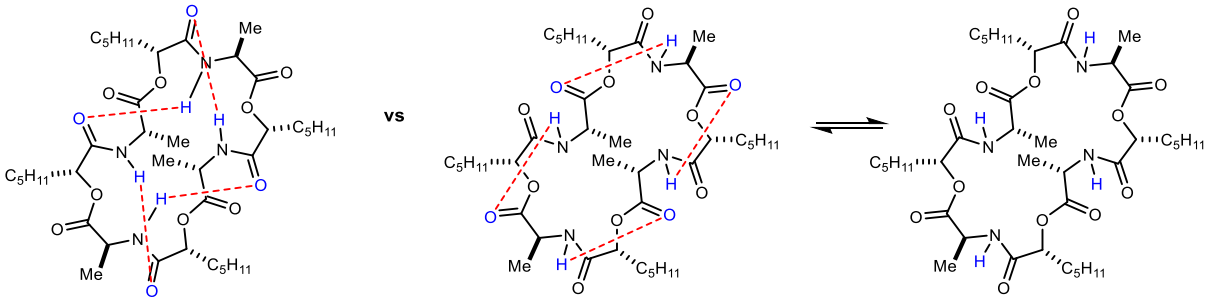

[44] Pleiss, U.; Harder, A.; Turberg, A.; Londershausen, M.; Iinuma, K.; Mencke, N.; Jeschke, P.; Bonse, G. *J. Label. Compd. Radiopharm.* **1996**, *38*, 61.

Initial attempts to *N*-methylate **53** were largely unsuccessful (Table 7), affording alcohol **60** as the major product. The same Ag_2O conditions that successfully methylated the theonallapeptidolides[43] and dimethyl PF1022A[44] afforded **60** as the major product as well. What was most surprising about these trials is that the major product (**60**) was not *N*-methylated or epimerized, despite the large amount of methylating reagents used. It is hypothesized that *N*-methylation was not occurring in these reactions because of the conformation of **53** in solution (Figure 8).

Several literature examples,[45,46,47,48] have demonstrated how cyclodepsipeptides have solvent-dependent conformations due to intramolecular hydrogen bonding. In-depth studies on the conformation of valinomycin,[45,46] a cyclododecadepsipeptide natural product, in solution found that the depsipeptide exhibits a strong network of 4→1 intramolecular hydrogen bonds in non-polar to medium polar solvents (cyclic ether, hydrocarbon, DMSO, DMF), shielding the amide protons from the outside environment. In polar solvents (water, alcohols, DMF), the depsipeptide amide protons are exposed to the outside environment in a fast equilibrium between weak 3→1 intramolecular hydrogen bonds and hydrogen bonding with the solvent environment. With this

Figure 9. Hypothesized shift of hydrogen bond network in free and ion coordinated 53

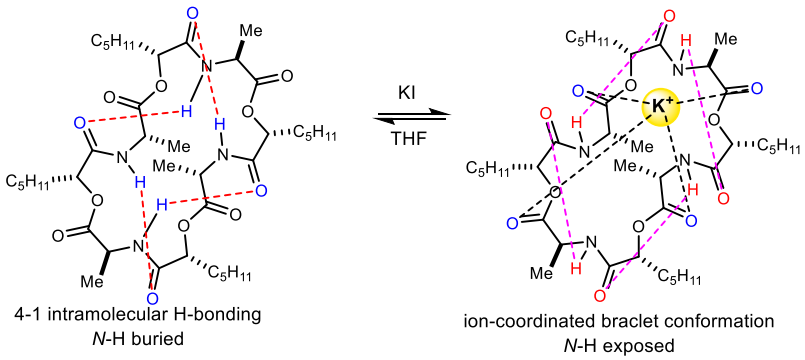

information, the lack of *N*-methylation in the initial attempts to methylate **53** makes sense because the solvents used were moderately polar, thus the amide hydrogens would be engaged in 4→1 intramolecular hydrogen bonding and less reactive (Figure 8). Unfortunately, polar solvents such as alcohols and water are not suitable to use in the basic conditions required for *N*-methylation. However, according to several references,[47,49,50,51,52,53] cyclic peptides and depsipeptides have the ability to coordinate ions in solution. The cyclic antibiotic, valinomycin, has been heavily studied in this field due to its ability act as a selective potassium ion carrier in biological membrane systems. X-ray crystal stuctures[53] and NMR studies[51,52] of the potassium ion-valinomycin complex have shown that the depsipeptide is in a bracelet-like structure: its ester carbonyls are coordinated

[45] Patel, D. J.; Tonelli, A. E. *Biochemistry* **1973**, *12*, 486.
[46] Grochulski, P.; Smith, G. D.; Langs, D. A.; Duax, W. L.; Pletnev, V. Z.; Ivanov, V. T. *Biopolymers* **1992**, *32*, 757.
[47] Heitz, F.; Kaddari, F.; Heitz, A.; Raniriseheno, H.; Lazaro, R. *Int. J. Pept. Protein Res.* **1989**, *34*, 387.
[48] Kato, T.; Mizuno, H.; Lee, S.; Aoyagi, H.; Kodama, H.; Go, N.; Kato, T. *Int. J. Pept. Protein Res.* **1992**, *39*, 485.
[49] Pitchayawasin, S.; Kuse, M.; Koga, K.; Isobe, M.; Agata, N.; Ohta, M. *Bioorg. Med. Chem. Lett.* **2003**, *13*, 3507..
[50] Kimura, S.; Imanishi, Y. *Biopolymers* **1983**, *22*, 2383.
[51] Grell, E.; Funck, T. *Eur. J. Biochem.* **1973**, *34*, 415.
[52] Patel, D. J. *Biochemistry* **1973**, *12*, 496.
[53] Ovchinnikov, Y. A. *FEBS Lett.* **1974**, *44*, 1.

to the ion and the amide protons are exposed to the outside environment, partaking in weak H-bonding with the non-ion coordinated carbonyls. This bracelet-like conformation is extremely similar to valinomycin's polar solvent conformation, but can be achieved in a non-polar solvent. In order to achieve a "polar conformation" so that the amide protons would be reactive in *N*-methylation conditions, **53** was pre-stirred with KI in hopes that the cyclic substrate would coordinate to the potassium ion (Figure 9).

N-Methylation trials using an ion source to coordinate **53** are summarized in Table 8. Initial results of *N*-methylation using either KI or NaI as the ion source and NaH as the base in THF were slightly more promising in that the major products were *N*-methylated, but no desired *N*-methylated macrocyclic products were observed. Changing the base to Li_2CO_3 or K_2CO_3 did not produce any *N*-methylated side products. However, LiHMDS and Cs_2CO_3 did afford ring-opened and cleaved *N*-methylated side products; reactivity also appeared diminished relative to NaH. Changing the solvent from THF to 2-Me-THF, MeCN, or DCM did not improve this. In fact, in

Table 8. *N*-Methylation of ion-coordinated *N*-H 24-membered ring

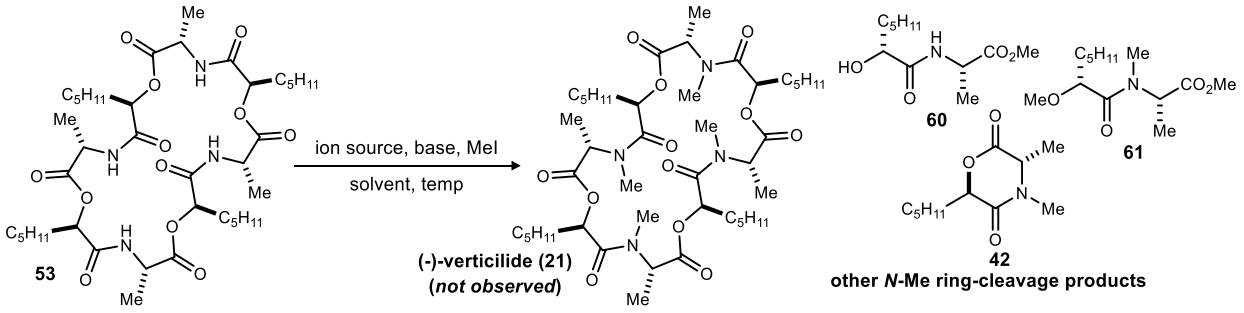

entry	ion source	base	solvent	temp (°C)	*N*-methylation?	major products[a]
1	KI	NaH	THF	rt	Yes	**42**, **61**, + *N*-Me cleavage pdts
2	KI	NaH	THF	0	Yes	**42**, **61**, + *N*-Me cleavage pdts
3	NaI	NaH	THF	0	Yes	**42**, **61**, + *N*-Me cleavage pdts
4	KI	NaH	2-Me THF	0	Yes	**42**, **61**, + *N*-Me cleavage pdts
5	NaI	NaH	2-Me THF	0	Yes	**42**, **61**, + *N*-Me cleavage pdts
6	KI	K_2CO_3	THF	rt	No	**60**
7	KI	K_2CO_3	MeCN	rt	No	**60**
8	KI	Cs_2CO_3	THF	rt	Yes	**60**, **42**, **61**, + *N*-Me cleavage pdts
9	KI	Cs_2CO_3 + $Sc(OTf)_3$	THF	rt	No	**53** + ring opened **53**
10	KI	Li_2CO_3	THF	rt	No	**53**
11	KI	LiHMDS	DCM	0	No	mostly **53**
12	KI	LiHMDS	THF	0	Yes	**60**, **61**, **42** + *N*-Me cleavage pdts
13	KI	Ag_2O + $CaSO_4$	THF	rt	Yes	**61**

[a]Major products were determined from the ^{1}H NMR spectrum of the crude reaction mixture by comparison to ^{1}H NMR spectra from authentic samples, and verified by LCMS

entry 11 (Table 8), LiHMDS in DCM did not react, but when the solvent was changed to THF in

entry 12 (Table 8), *N*-methylation and cleavage of the macrocycle occurred. This may indicate that solvent has an effect on the stability of the potassium coordination complex.

In reviewing all trials to *N*-methylate **53**, it is apparent that **53** must be in a "polar conformation" in order for *N*-methylation to occur. Although the valinomycin-potassium complex is very stable, valinomycin and **53** are structurally quite different. Valinomycin is a cyclododecadepsipeptide of $[L\text{-}D\text{-}D\text{-}L]_3$ repeating units and **53** is a 24-membered depsipeptide of $[L\text{-}D\text{-}L\text{-}D]_2$ repeating units. Cyclooctadepsipeptide valinomycin $[L\text{-}D\text{-}D\text{-}L]_2$ ion complexes have been analyzed,[53] but were found to be strained and unstable. Based on this, we can conclude that the ion complex of **53** did form in solution, but is too unstable for *N*-permethylation to go to completion. Additionally, solvent conformation studies of cyclooctadepsipeptide valinomycin analogs in DMF demonstrated that the macrocycles exhibited a more "polar conformation" consisting of only two weak 3→4 H-bonds,[50] unlike the cyclododecadepsipeptide natural product which exhibits a "nonpolar conformation" of four 4→1 H-bonds.[52] With the hope that **53** would exhibit a similar "polar conformation" as the valinomycin analogs, *N*-methylation was attempted in DMF with NaH as the base. Much to our delight, these conditions successfully provided (-)-verticilide in 78% yield, and the total synthesis was completed in a 10-step longest linear sequence. Furthermore, variation of the base and reaction time of the NaH/DMF methylation conditions afforded desmethyl analogs **62** and **63** in moderate selectivity (Table 9).

Table 9. *N*-Methylation conditions to afford (-)-verticilide and derivatives

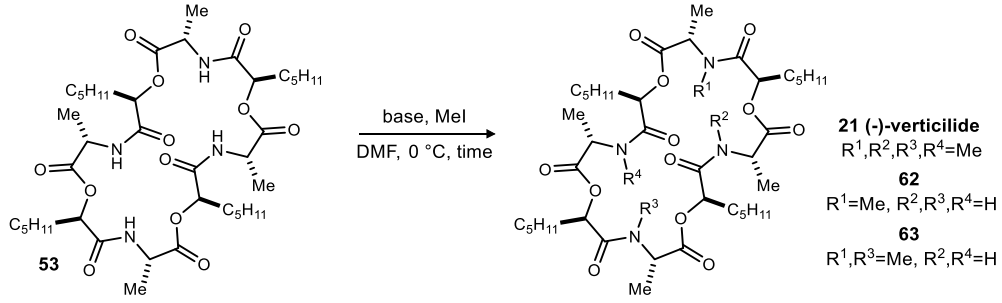

entry	base	time	major product	yield[a]
1	NaH	25 m	**21**	78%
2	NaH	13 m	**63**	31%
3	LiHMDS	15 m	**62**	35%

[a]Isolated yield.

1.6 Conclusion

In summary, our UmAS-based approach has successfully been applied to the total synthesis of (-)-verticilide, providing the natural product in a 10-step longest linear sequence and 29% overall yield (Scheme 26). Unique features of this synthesis include: 1. an enantioselective Henry, MOM-protection, and then UmAS methodology to make the key α-hydroxy amides; 2. high-yielding, convergent Mitsunobu couplings and macrolactonization; 3. a final *N*-permethylation on an alternating amino acid-hydroxy acid macrocyclic substrate. Racemization, a common challenge of *N*-methyl depsipeptide synthesis, is avoided because an active ester intermediate is not formed in the UmAS and Mitsunobu coupling reactions. This route provides a platform for convenient access of a structurally diverse array of cyclic depsipeptide derivatives with the use of enantioselective methods, which provide broad access to α-hydroxy amide side chains, and the final *N*-methylation reaction, which can be tailored to afford different *N*-methylated derivatives.

Scheme 26. Total synthesis of (-)-verticilide summary

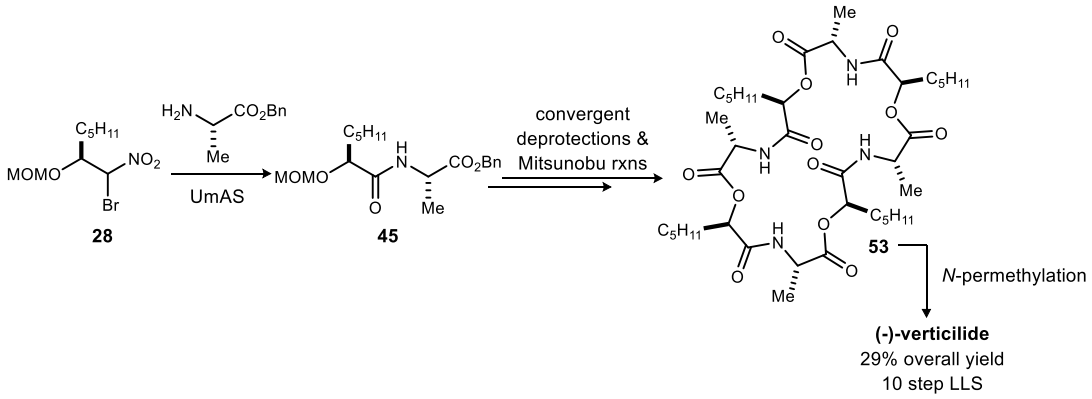

Chapter II

II. Synthesis of size-diverse collections of cyclodepsipeptides via an ion-templated Mitsunobu cyclooligomerization

2.1 Background and importance of macrocycle size

The ring size of macrocyclic natural products plays an important role in their biological activity because large and small macrocycles exhibit different protein binding modes.[6] As shown in Figure 10, large macrocycles, like cyclosporin (**1**) and pectenotoxin-2 (**64**), tend to bind in an edge-on or face-on mode. In the edge on mode, the macrocycle (**1**) is perpendicular to the protein surface with one edge of the ring interacting with the cleft of the binding pocket and substituents interacting with adjacent binding pockets. The outer edge of the ring is exposed to the outside environment in this case. In face-on mode, the macrocycle (**64**) lies flat across a large area of the protein surface, therefore interacting with multiple pockets on the protein. Small macrocycles, such as macbecin (**65**), tend to exhibit compact binding where the macrocycle is in a compact globular conformation, almost completely buried in the pocket. With this information, different sized natural product inspired macrocycles can be designed to fit differently shaped protein binding sites in a fragment-based drug discovery fashion.

Figure 10. Macrocycle binding modes.[6] Figure adapted from *Nat. Chem. Biol.* 2014, *10*, 723.

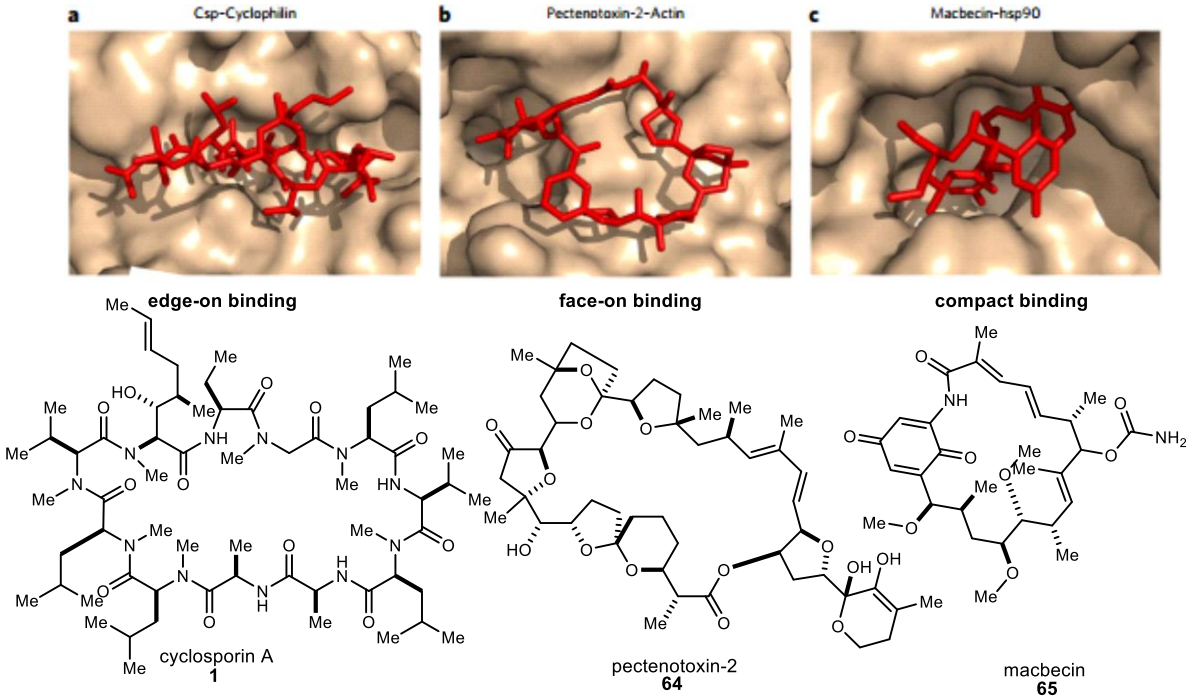

The unique binding modes of large macrocycles are especially interesting in drug discovery because the macrocycles are able to interact with a larger number of hot spots on the protein surface.[6] FTMap analysis is a computational method to reliably identify the locations of binding energy hot spots that are exploited by known ligands. FTMap analysis involves placing probe

molecules on a dense region of the protein, energy minimization, and finally overlaying the results to find the significant binding energy 'hot spots' on the protein.[54] Then, analogous FTMap analysis is conducted on various macrocyclic ligands and other "conventional" small molecule ligands to identify which 'hot spots' each type of molecule occupies. From these analyses, the number of 'hot spots' each drug can access can be quantitatively determined. On average, macrocyclic ligands were found to occupy significantly more 'hot spots' than small molecule ligands (5.2 vs 3.6),[6] which further reinforces their significance in drug discovery.

2.2 Cyclooligomerization: a rapid method to synthesize complex macrocycles

As introduced in Chapter 1, (–)-verticilide (**21**) is a fungal cyclooligomeric depsipeptide (COD) natural product, derived from alternating α-hydroxy acid and α-amino acid monomers. Fungal CODs (Figure 11) are structurally privileged natural products as demonstrated by their broad spectrum of biological activities, including antibiotic, insecticidal, and antitumor activities.[55] In nature, their synthesis is mediated by fungal-COD-producing nonribosomal peptide synthetases (NRPSs), which recursively condense and then cyclize a series of peptidol monomer units. The number of ligations during cyclooligomerization is determined by the shape and size of the reaction chamber within the NRPSs, thus resulting in size-selective production of each COD natural product. As convenient and selective as this reaction is in nature, its application to the chemical synthesis of oligomeric natural-product like molecules is limited because of its difficulty to control.

Figure 11. Cyclooligomeric depsipeptide (COD) natural products

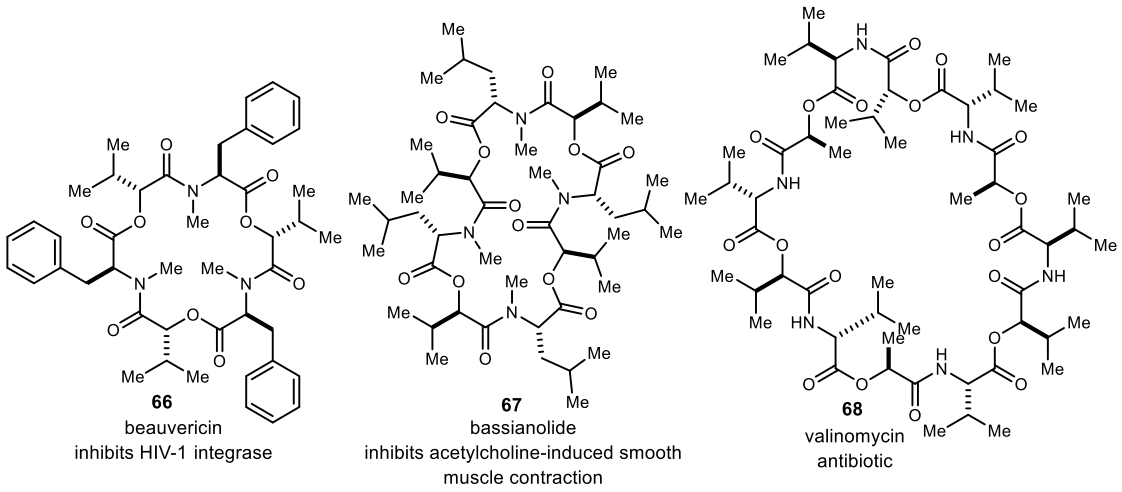

[54] Brenke, R.; Kozakov, D.; Chuang, G.-Y.; Beglov, D.; Hall, D.; Landon, M. R.; Mattos, C.; Vajda, S. *Bioinformatics* **2009**, *25*, 621.
[55] Sussmuth, R.; Muller, J.; von Dohren, H.; Molnar, I. *Nat. Prod. Rep.* **2011**, *28*, 99..

Because of their biomedical applications, interest in the preparation of peptidic macrocycles is growing at a tremendous pace, driving the development of new approaches, and the underlying chemistry to support them. Inspired by nature, condensative amidation based-oligomerization strategies have been implemented to synthesize cyclooligomeric peptide natural products, and natural product-like macrocycles (Scheme 27). Rothe[56,57] used *o*-phenylene chlorophosphite to trimerize and cyclize a tetradepsipeptide fragment to form 36-membered depsipeptide valinomycin (**68**). Conducting the reaction at 100 °C was necessary due to the sterically hindered cyclization, and a non-polar solvent (toluene, 50 mM) was necessary in order to promote oligomerization over monocyclization, ultimately isolating valinomycin in 7% yield. Wipf[58,59] used a similar method for his total synthesis of westiellamide (**69**). Diphenylphosphoryl azide (DPPA) was chosen as the optimal coupling reagent because other reagents, such as HATU, and FDPP provided lower yields of cyclic peptides and larger amounts of linear oligomers. Additionally, epimerization was observed at both chiral centers on the oxazoline in basic reaction conditions, so the opposite enantiomer of threonine was used to make the oxazoline in order to account for this. The optimized reaction conditions using DPPA in DMF (15 mM) afforded the desired cyclotrimerized natural product in 20% yield along with the cyclotetramer in 25% yield.

Scheme 27. Cyclooligomerization methods to synthesize oligomeric peptide and depsipeptide macrocycles

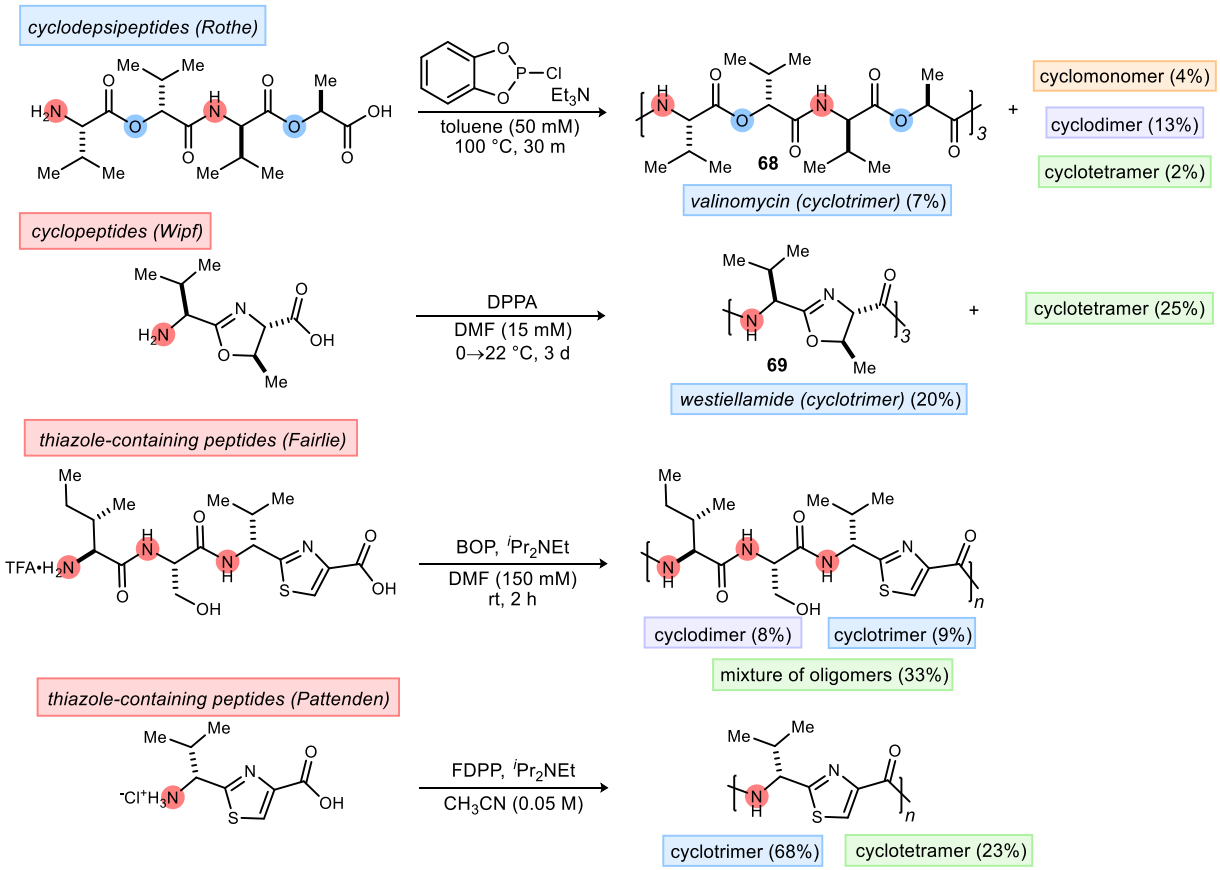

[56] Rothe, M.; Kreiss, W. *Angew. Chem. Int. Ed.* **1973**, *12*, 1012.
[57] Rothe, M.; Kreiss, W. *Angew. Chem. Int. Ed.* **1977**, *16*, 113.
[58] Wipf, P.; Miller, C. P.; Grant, C. M. *Tetrahedron* **2000**, *56*, 9143.
[59] Wipf, P.; Miller, C. P. *J. Am. Chem. Soc.* **1992**, *114*, 10975.

Fairlie[60] and Pattenden[61] developed amidation-based cyclooligomerization strategies to access a variety of thiazole-containing peptidic macrocycles for conformational studies. In both examples optimization of overall yield and size diversity was the focus, as opposed to targeting a particular ring size. Both groups faced difficulties with the formation of insoluble linear polymers, as opposed to cyclized products. In optimal conditions, Fairlie isolated 8% cyclodimer, 9% cyclotrimer, and 33% mixture of oligocycles composed of 4 monomers or greater. Pattenden was able to obtain high yields of macrocyclic products, but only observed two ring sizes cyclotrimer and cyclotetramer.

To best of our knowledge, there are no examples of a controlled oligomerization/macrocyclization to produce collections of macrocyclic depsipeptides. The impact of such an approach would be further magnified by the ability to manipulate the size distributions of products within collections, or even selectively favor a particular ring size.

2.3 Initial discovery of a Mitsunobu cyclooligomerization (MCO)

Chemical synthesis of macrocyclic peptides and depsipeptides typically suffers from the disadvantages associated with the preparation of their linear precursors. In order to overcome the tedium associated with a linear approach and solid-phase synthesis, a **M**acro**C**yclo**O**ligomerization (MCO) approach is a possible solution to reduce linear step-count. However, as explained in the previous section, this approach tends to be quite non-selective in terms of ring size. It is often more efficient in terms of yield to synthesize the desired depsipeptide chain length and then cyclize in a stepwise fashion. I could say that we were looking to streamline our first generation synthesis of (-)-verticilide when a Mitsunobu MCO approach was implemented, but like many super cool findings in chemistry, it was discovered by accident.

Scheme 28. Discovery of a Mitsunobu cyclooligomerization reaction

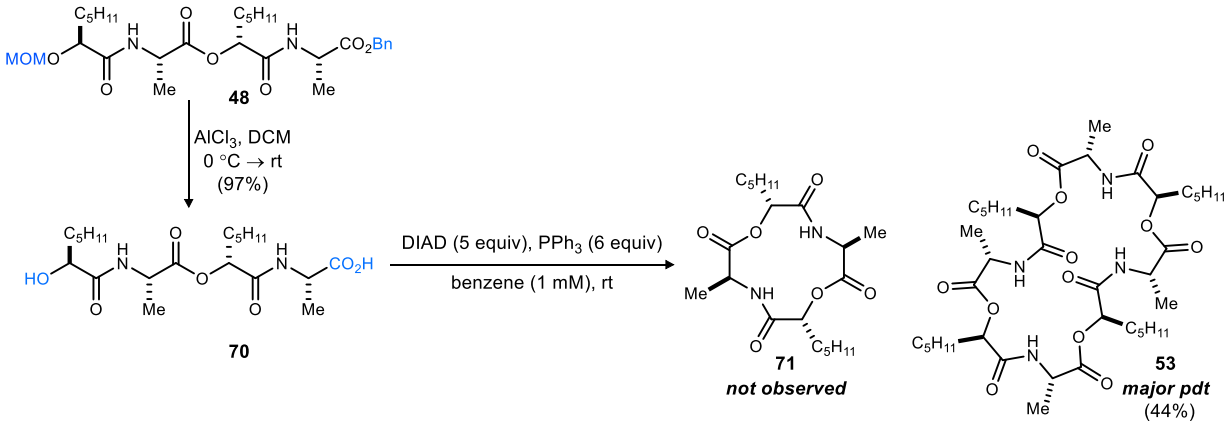

Cyclooligomerization of tetradepsipeptide subunit **70** was discovered during attempts to create a 12-membered derivative of (-)-verticilide (**71**, Scheme 28). When **70** was subjected to our optimized Mitsunobu macrolactonization conditions, 12-membered macrocycle **71** was not observed, but instead the 24-membered *N*-H precursor (**53**) to (-)-verticilide that we made earlier

[60] Sokolenko, N.; Abbenante, G.; Scanlon, M. J.; Jones, A.; Gahan, L. R.; Hanson, G. R.; Fairlie, D. P. *J. Am. Chem. Soc.* **1999**, *121*, 2603.
[61] Bertram, A.; Hannam, J. S.; Jolliffe, K. A.; González-López de Turiso, F.; Pattenden, G. *Synlett* **1999**, *1999*, 1723.

was isolated in 44% yield. With this result, it was apparent that an MCO approach could provide N-H macrocycle **53** in two fewer steps than our first generation route to (-)-verticilide. Additionally, this result was particularly exciting because previously reported cyclooligomerizations of large monomers faced significant challenges with direct monomer cyclization. Thus began the quest to develop reaction conditions for efficient production of cyclized products.

First, the equivalents of Mitsunobu reagents were adjusted to half the amount as the original conditions. Careful analysis and purification of the reaction mixture provided the 24-membered ring (**53**) to 63%, and small amounts of two other cyclodepsipeptide oligomers. ^{1}H NMR analysis of these cyclooligomers revealed very similar spectra, differing primarily in the chemical shift rather than the coupling pattern of each proton, reinforcing the expectation these products are constitutionally identical. Analysis by LCMS confirmed that these products were indeed size-distinct molecules, isolated in pure form. The two new macrocycles were determined to be a 36-membered ring (**72**) and 60-membered ring (**73**) in 16 and 5% respective yields. Then, the effects of concentration were examined (Figure 12), as literature examples[56,57,58] found that concentration greatly affected the cyclization efficiency of the overall reaction and the product size distribution. In the most dilute concentration (0.5 mM), little overall reactivity or selectivity was observed, affording the 24-membered ring (**53**) and 36-membered ring (**72**) in 18 and 21% respective yields. Increasing the concentration to 5 mM produced around the same results as 1 mM, but increasing the concentration another 10 fold to 50 mM decreased the yield of **53** (54%). In the most concentrated reaction conditions, more polymerized linear chains were observed, thereby confirming that more dilute conditions were necessary for efficient cyclization. Because product formation was essentially the same at 1 and 5 mM and the use of less solvent in a reaction is preferred, the more concentrated conditions (5 mM) were used in subsequent experiments.

Figure 12. MCO concentration studies

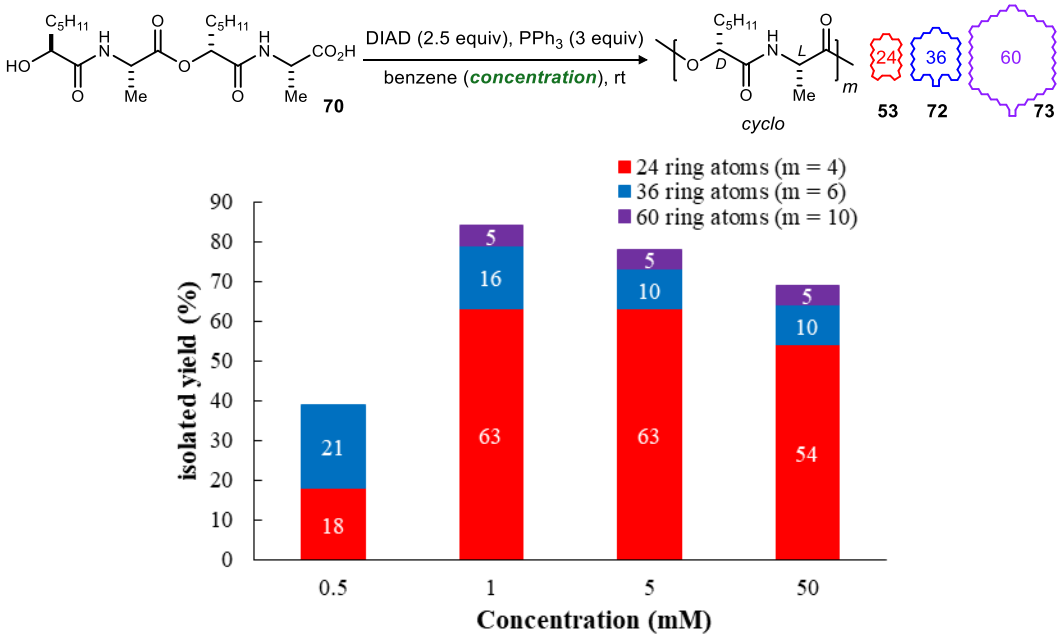

2.4 Ion-templated Mitsunobu cyclooligomerization

Scheme 29. Ion-templated cyclization reactions

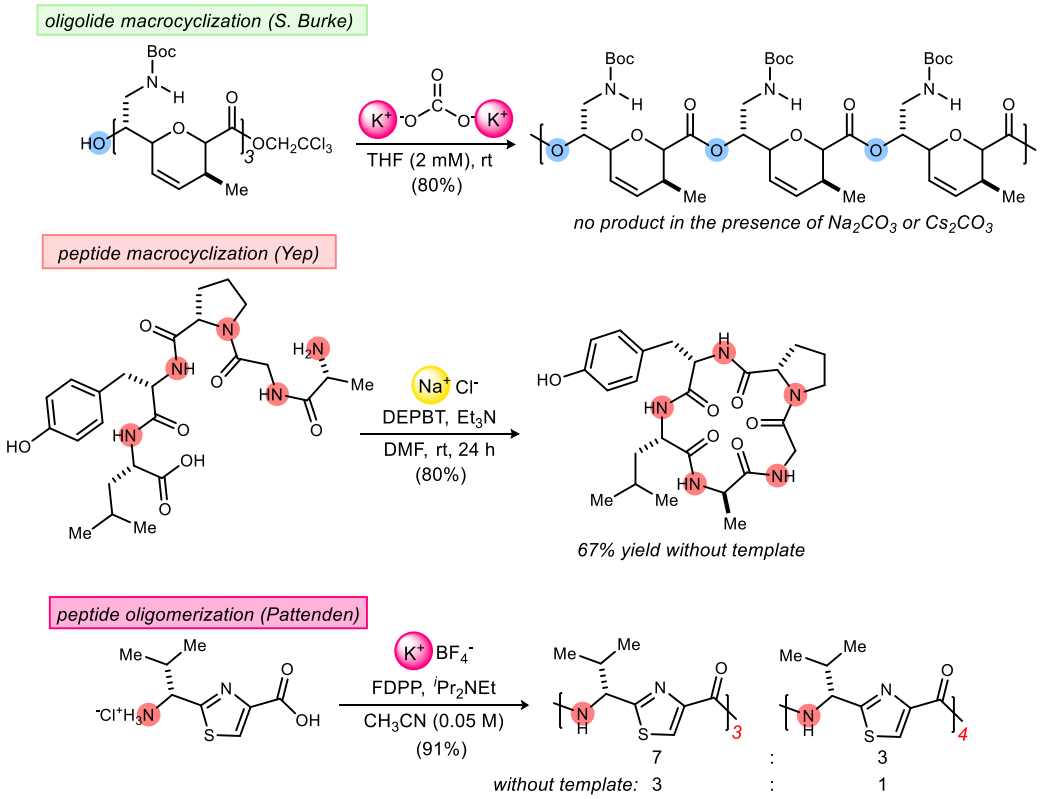

Because cyclic peptides and depsipeptides tend to be ionophoric in nature,[47,49,51] metal salt templates have been added to macrocyclization reactions (Scheme 29) based on the hypothesis that the salts can bind their linear precursors and cause a conformationally enhanced rate of cyclization of one product over the other.[62,63,64] Burke has shown that the efficiency of an 18-membered oligolide macrocyclization can be enhanced by templation effects by means of K^+ ions,[63] and Yep observed a 13% increase in yield of a cyclic pentapeptide upon addition of NaCl.[64] Pattenden extended this hypothesis to cyclooligomerization reactions in order to favor different size-distributions of cyclic peptides,[65] and observed a difference in cyclotrimer to cyclotetramer product ratio when KBF_4 was added.

Motivated by the success of these examples, an improved yield of (-)-verticilide by MCO was sought based on the hypothesis that the growing depsipeptide oligomers might bind to salt additives, which in turn might lead to depsipeptide-salt complexes with a conformationally-enhanced rate of macrocyclization relative to chain elongation. However, our basis for this hypothesis is by no means a direct comparison, as known applications of this phenomenon are amidation reactions, which are conducted in a polar solvent that can readily solubilize the salt

[62] Marti-Centelles, V.; Pandey, M. D.; Burguete, M. I.; Luis, S. V. *Chem. Rev.* **2015**, *115*, 8736.
[63] Burke, S. D.; McDermott, T. S.; O'Donnell, C. J. *J. Org. Chem.* **1998**, *63*, 2715.
[64] Liu, M.; Tang, Y. C.; Fan, K. Q.; Jiang, X.; Lai, L. H.; Ye, Y. H. *J. Pept. Res.* **2005**, *65*, 55.
[65] Blake, A. J.; Hannam, J. S.; Jolliffe, K. A.; Pattenden, G. *Synlett* **2000**, *2000*, 1515.

additive. The use of polar solvents and salt additives is contraindicated in a Mitsunobu reaction due to their ability to disrupt the reactive ion pairs,[66,67,68] potentially slowing or stopping the coupling reaction entirely. Therefore, the unprecedented reactivity we observed with the addition of various alkali metal salts (5 equiv.) to the reaction conditions is hypothesized to be due to an ion-templating effect between the linear depsipeptide chain and the metal ions in solution.

Figure 13. MCO of tetradepsipeptide 70: effect of salt additives on size distribution of products

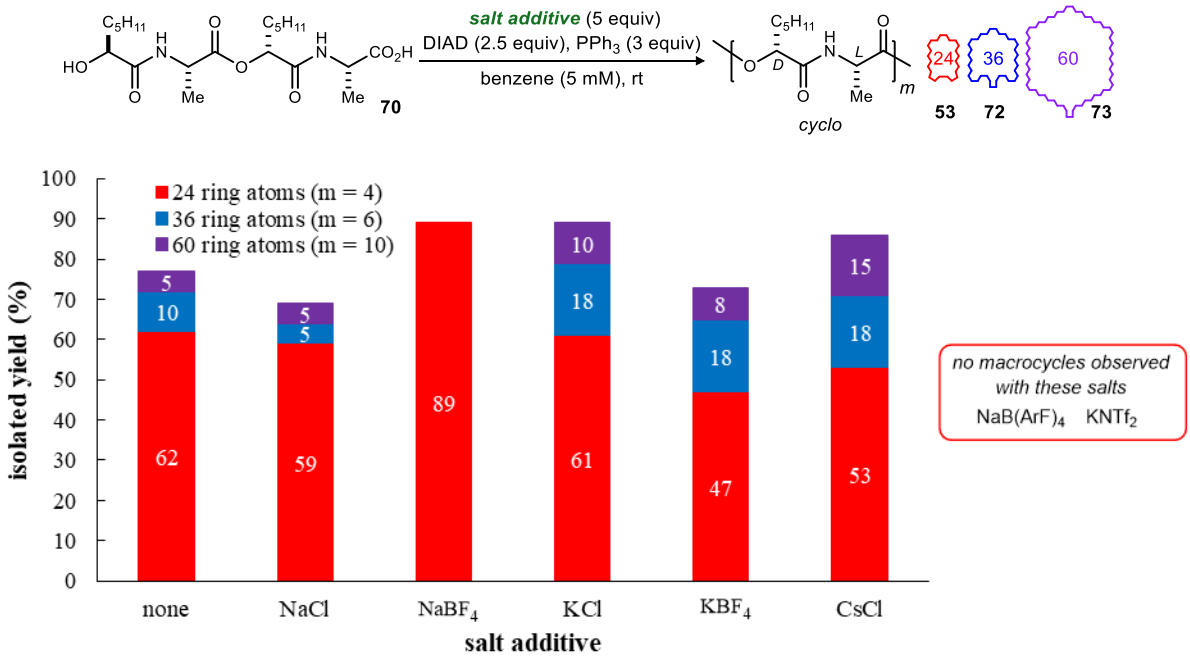

Figure 13 summarizes the subset of alkali metal salts that were examined with tetradepsipeptide **70**. Compared to conditions without a salt additive, addition of NaCl, KCl, or CsCl did not increase the yield of 24-membered ring **53**. However, with increasing metal cation size, the amounts of 36- and 60-membered rings were increased. Most notably, CsCl tripled the yield of the 60-membered ring and nearly 40% of total isolated macrocycles were larger than 24-ring atoms—results much different than salt-free conditions where only 20% of total isolated macrocycles were greater than 24-ring atoms. An interesting property of this reaction is that neither the *seco*-acid nor the salt is readily soluble in benzene, but after all reaction components are added, the reaction is homogeneous. However, when NaCl was used, the reaction never became completely homogeneous, most likely because sodium is too tightly associated to its counter anion in the nonpolar reaction conditions to be sufficiently reactive. In attempts to gain more cation-substrate interaction, salts with more dissociated counterions were examined. Some non-coordinating counterions, such as PF_6^- and ClO_4^-, are known to form stable and insoluble complexes with arylphosphonium cations,[69] which is likely why an insoluble precipitate formed when $NaB(ArF)_4$ and $KNTf_2$ were added, and no macrocyclic products were observed. However, $NaBF_4$ remained inert in the reaction, and promoted exclusive formation of the 24-membered ring

[66] Hughes, D. L.; Reamer, R. A.; Bergan, J. J.; Grabowski, E. J. J. *J. Am. Chem. Soc.* **1988**, *110*, 6487.
[67] Elson, K. E.; Jenkins, I. D.; Loughlin, W. A. *Org. Biomol. Chem.* **2003**, *1*, 2958.
[68] But, T. Y. S.; Toy, P. H. *Chem. Asian J.* **2007**, *2*, 1340.
[69] Poupon, J.-C.; Boezio, A. A.; Charette, A. B. *Angew. Chem. Int. Ed.* **2006**, *45*, 1415.

(**53**) in 89% yield. Here, an ion template would allow the linear chain to reside in a conformation that increases the rate of cyclization to the 24-membered ring relative to continued oligomerization. This supports the hypothesis that enhanced ring size-selection is occurring through an ion-templating effect. More notably, this documents the unprecedented ability of alkali metal salts to enhance formation of macrocycles in Mitsunobu macrocyclooligomerization conditions.

Scheme 30. Synthesis and early investigation of Mitsunobu MCO with a didepsipeptide monomer

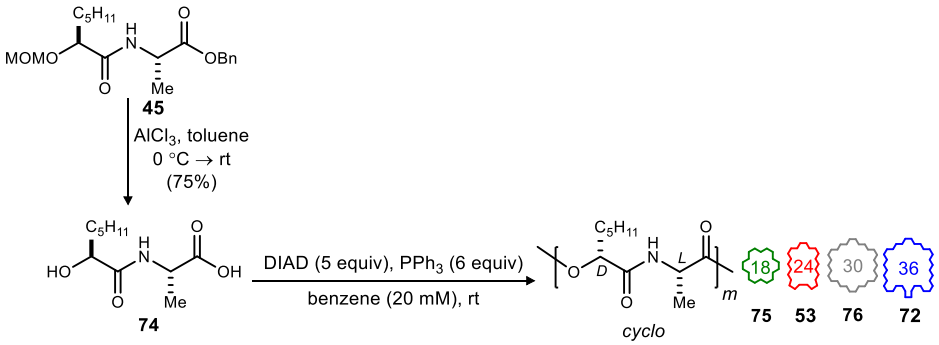

We were then curious about how a monomer half the size of **70** would fare in this reaction. While tetradepsipeptide **70** limits the possibilities of oligomers to multiples of 12 atom lengths, didepsipeptide **74** broadens the scope of potential products by providing access to oligomers that are multiples of 6. Didepsipeptide **74** was prepared by global deprotection of **45**, just as tetradepsipeptide **70** was prepared from **48** (Scheme 30). Use of a similar oligomerization protocol led to a very different profile of macrocyclic oligomers. Analysis and purification of the crude reaction mixture identified four different cyclodepsipeptide oligomers ranging in yield from 9-24%. The major product this time was the 36-membered ring (**72**), while the 24-membered ring (**53**) was formed in only 15% yield. Two new macrocycles, identified as 18-membered (**75**) and 30-membered (**76**) rings, were formed in 9% and 16% yields, respectively.

A similar exploration of salt effects was pursued as shown in Figure 14. Compared to the standard conditions, use of $LiBF_4$ and LiBr additives arrested the production of any cyclodepsipeptide products. Lithium salts are known chaotropes, so they may be binding too tightly to the ionic Mitsunobu intermediates at such a level that no reactivity is observed. However, a shift in the size-distribution of macrocyclic products was observed in the presence of $NaBF_4$, KBF_4, and CsCl. In the presence of any of these three salts, production of 18-membered ring **75** was completely suppressed. These three salts also provided increased amounts of 24-membered ring (**53**) relative to 30-membered ring (**76**), compared to providing them in nearly equal amounts without a salt additive. This effect was most significant with $NaBF_4$, which provided the 24-membered ring (**53**) in 25% yield, as opposed to only 15% without the salt. Ring-size enhancement in the presence of a salt additive was most significant for the 36-membered ring (**72**), which was isolated in 44% yield with KBF_4, nearly double the yield of salt-free conditions. Additionally, KBF_4 increased the overall isolated yield of macrocycles from 64% to 81%, along with evidence that less material was converted into linear DIAD-substrate acylation byproducts. This type of

byproduct is common[70,71,72] in Mitsunobu reactions, especially in the presence of excess coupling reagents, which are generally required for a macrolactonization to occur. However, an ion template would allow the linear chain to reside in a conformation that increases the rate of cyclization relative to acylation.

Figure 14. Effect of salt additives on size distribution of products from MCO with a didepsipeptide monomer

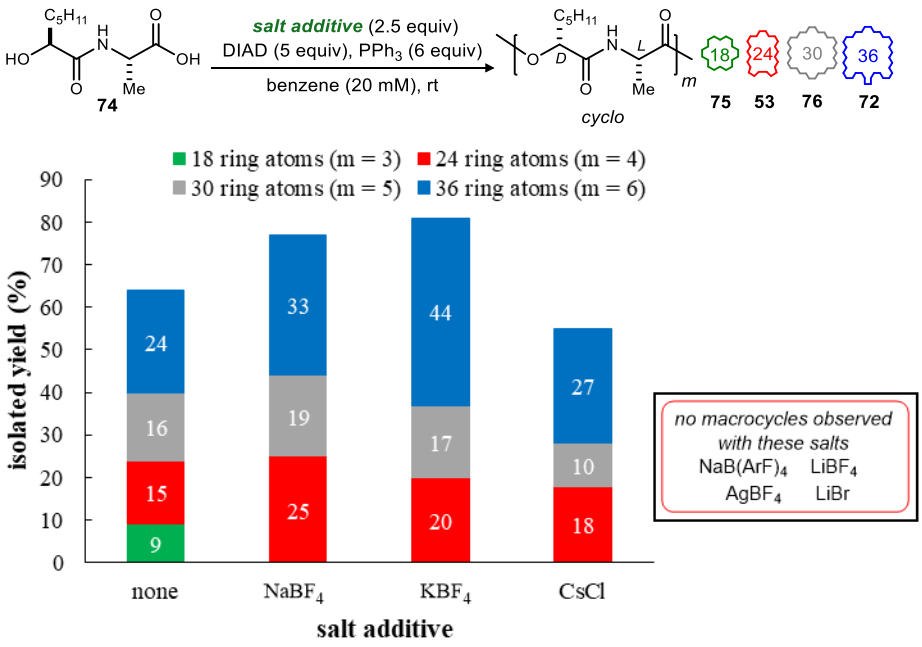

Collectively, these additive effects provide a range of control that either enhances the formation of one macrocycle size relative to others, or enhances diversity of oligomer size in a single reaction. In terms of concise preparations of (-)-verticilide, both approaches result in the same 24-membered *N*-H macrocycle (**53**), which upon *N*-permethylation provides the natural product. Contrasting approaches, the shorter preparation of (-)-verticilide (6 steps, 15% yield) using didepsipeptide **74** results in several cyclooligomers; use of tetradepsipeptide **70** and a salt effect that favors dimerization/macrocyclization to **53** is only slightly longer (8 steps, 36% yield), but is more efficient when targeting a specific natural product.

2.5 Examination of stereochemical effects

Thus far we have studied the effects of monomer size on macrocyclic product size distribution, and how the distributions shift in the presence of different alkali metal templates. Because enantioselective catalysis is the basis for our depsipeptide monomer synthesis, precursors with varying α-hydroxy acid or α-amino acid stereochemistry can be readily prepared. Thus, we prepared the D-Ala epimer of **77**, to synthesize collections of homochiral D,D-cyclodepsipeptides and study the effects of monomer stereochemistry on product size distribution. As shown in Figure 15, the behaviors of **77** generally paralleled its diastereomer (**74**), but some differences in the

[70] Evans, D. A.; Ratz, A. M.; Huff, B. E.; Sheppard, G. S. *J. Am. Chem. Soc.* **1995**, *117*, 3448.
[71] Nicolaou, K. C.; Sun, Y.-P.; Guduru, R.; Banerji, B.; Chen, D. Y. K. *J. Am. Chem. Soc.* **2008**, *130*, 3633.
[72] Mukherjee, S.; Bordawekar, S.; Nere, N. *Ind. Eng. Chem. Res.* **2016**, *55*, 4867.

cyclization of diastereomers **77** and **74** were apparent in salt-free MCO conditions. First, direct cyclization to the 6-membered diketomorpholine product (**78**) was dominant (38% yield) in the additive-free MCO, as opposed to the formation of larger oligomers with **74**. In general, the smaller ring sizes were most favored, forming the 18-membered macrocycle (**79**) in 14% yield, and the 24-membered macrocycle (**80**) in 11% yield. Added salts again modified both size-distribution and efficiency of macrocyclooligomerization. $NaBF_4$ enhanced the production of the 18- and 24-membered rings at the expense of direct cyclization to the 6-membered ring. Interestingly, KBF_4, which significantly increased product formation with monomer **74**, seemed to decrease the overall yield of macrocycles produced with monomer **77**. The effect of CsCl was also notable, as it produced a rather even distribution of the original three ring sizes, plus a 30-membered macrocycle (**81**) which was not observed in salt-free conditions, in a combined isolated yield of 93%.

Figure 15. MCO of didepsipeptide 77: effect of salt additives on size distribution of products

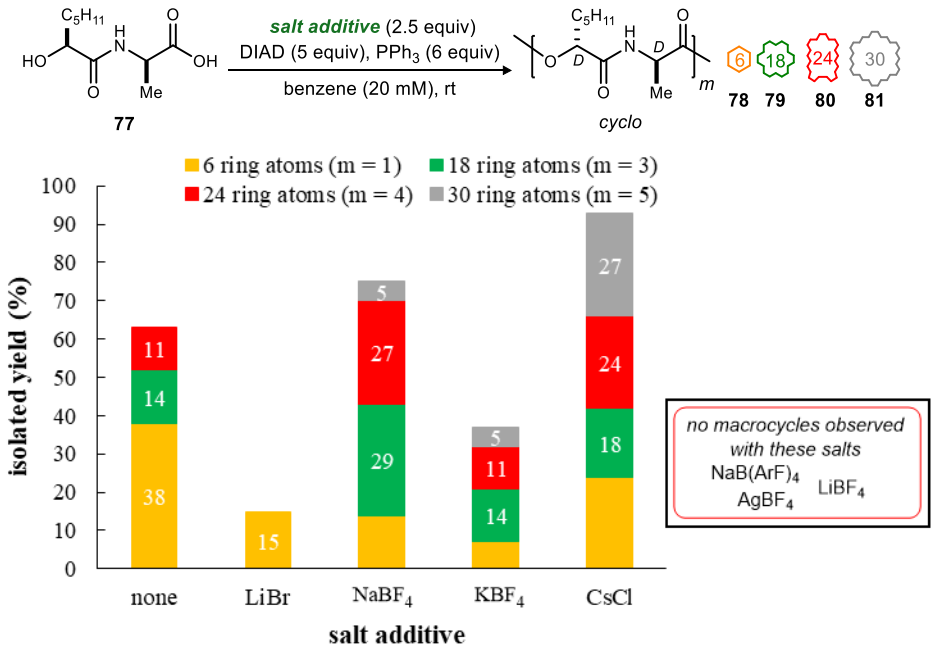

2.6 Examination of structural effects with the total synthesis of (-)-bassianolide

From these studies, we have established a methodology to rapidly synthesize collections of CODs with unprecedented ease, and we have found that the relative distributions of products in each collection can be modulated in the presence of an alkali metal salt. This method was successfully used to synthesize the natural product (-)-verticilide, and several stereochemically and ring size-diverse analogs. However, the monomers studied up to this point were composed of alternating α-hydroxyheptanoic acid and alanine building blocks. We were interested in investigating the level of generality that might be inherent to the method. Confident that the Mitsunobu MCO could be used to synthesize any 24-membered COD natural product, attention turned to the most sterically hindered of them all, (-)-bassianolide (**67**), to test the generality of our method.

2.6.1 Introduction: (-)-bassianolide and its previous synthesis

(-)-Bassianolide (**67**) was first isolated from an entomopathogenic fungus, *Beauveria bassiana*, found on the corpses of silk worms by Suzuki and coworkers[73] in the course of screening for insecticidal metabolites. (-)-Bassianolide is a 24-membered depsipeptide that is lethal to silkworm larvae at a dosage greater than 8 ppm.[74] At a lower dose, this depsipeptide was found to cause atony, a symptom of muscular relaxation. Additionally, (-)-bassianolide was screened for ability to inhibit acetylcholine (ACh)-induced muscle contractions and was found to inhibit smooth muscle contractions in guinea pig intestinal cells at a concentration of 10 μM.[75] Its mechanism of inhibition was found to be different than known ACh-induced muscle contraction inhibitors, papaverine (**83**) and verapamil (**84**), in that does not appear to involve changes in the binding activity of ACh to the muscarinic receptor, the membrane potential, or the contractile machinery of the intestinal wall. Because (-)-bassianolide did not change the permeability of mono or divalent cations through cell membranes during the membrane potential experiments, (-)-bassianolide most likely does not have any ionophoric properties *in vivo*, unlike its 18-membered analog enniantin C (**82**).[55]

Figure 16. (-)-Bassianolide's structure leads to unique biological activity

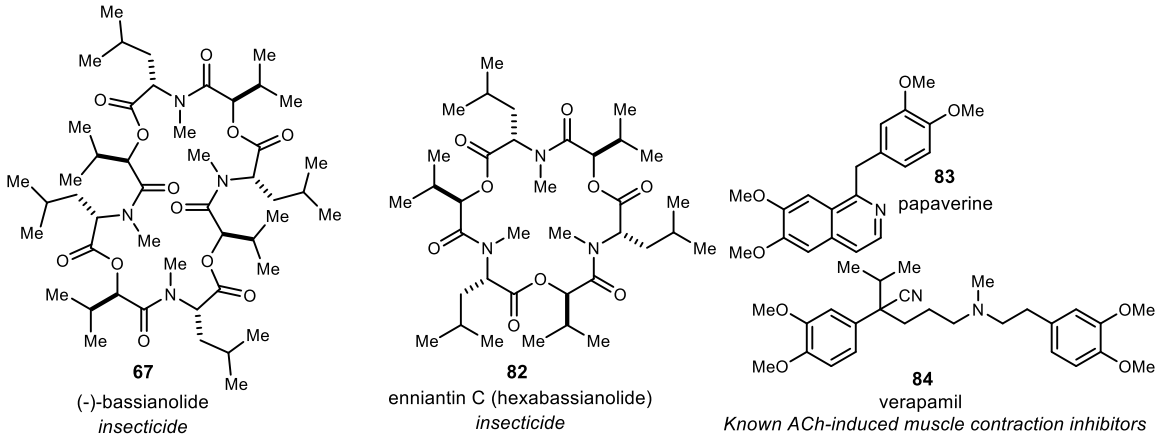

Suzuki and coworkers synthesized (-)-bassianolide[76] and elucidated its structure[73] in 1977. Acid hydrolysis of the natural product and comparison with an authentic amino acid sample identified *N*-methyl-L-leucine as the only amino acid residue, and an ether extract of the hydrolysate yielded solely α-hydroxyisovaleric acid. The stereochemistry of the hydroxy acid was identified by reducing (-)-bassianolide with $LiBH_4$ to didepsipeptide **85**, and comparing its R_f, ^1H NMR, and ^{13}C NMR spectra to synthetic didepsipeptides **85a** and **85b** (Scheme 31). The didepsipeptide from the natural product (**85**) was identical to **85a**, thus the acid in the natural product was identified as D-α-hydroxyisovaleric acid. ^1H NMR analysis revealed five *N*-methyl signals, but FD- and EI mass spectra indicated a molecular formula that was in accordance with

[73] Suzuki, A.; Kanaoka, M.; Isogai, A.; Tamura, S.; Murakoshi, S.; Ichinoe, M. *Tetrahedron Lett.* **1977**, *18*, 2167..
[74] Kanaoka, M.; Isogai, A.; Murakoshi, S.; Ichinoe, M.; Suzuki, A.; Tamura, S. *Agric. Biol. Chem.* **1978**, *42*, 629.
[75] Nakajyo, S.; Shimizu, K.; Kometani, A.; Suzuki, A.; Ozaki, H.; Urakawa, N. *Jpn. J. Pharmacol.* **1983**, *33*, 573..
[76] Kanaoka, M.; Isogai, A.; Suzuki, A. *Tetrahedron Lett.* **1977**, *18*, 4049.

four *N*-methyl amino acid and four hydroxy acid residues, so the cyclooctadepsipeptide and cyclodecadepsipeptide were synthesized to confirm the structure.

Scheme 31. (-)-Bassianolide structure elucidation

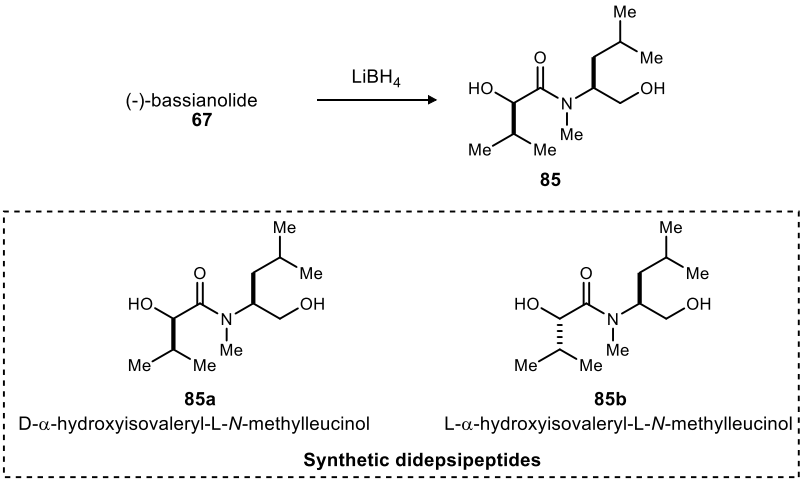

As shown in Scheme 32, the chiral D-α-hydroxy ester starting material was synthesized in three steps from D-valine.[77] In this sequence, D-valine was diazotized in the presence of sodium acetate and acetic acid to afford the α-acetoxy acid (**86**) with retention of stereochemistry. Then, *tert*-butyl ester formation was followed by deacetylation to afford the D-α-hydroxyisovaleric ester starting material (**87**).

Scheme 32. Suzuki's starting material preparation

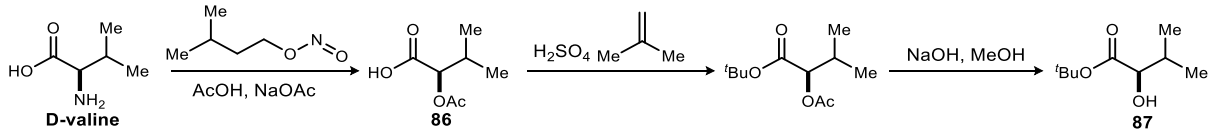

The D-ester was then coupled to *N*-Cbz-*N*-methyl-L-leucine using PCl_5 to form a depsipeptide species, which was then subjected to a series of convergent deprotections, traditional peptide couplings, and a final macrolactamization using the same acid chloride method (Scheme 33). With this method, Suzuki and coworkers were able to synthesize (-)-bassianolide in a 10-step longest linear sequence and 9% yield over the last 7 steps.[78] The synthetic cyclooctadepsipeptide data was in agreement with that of the natural product, thus successfully verifying its structure.

[77] Plattner, P. A.; Vogler, K.; Studer, R. O.; Quitt, P.; Keller-Schierlein, W. *Experientia* **1963**, *19*, 71.
[78] Yields to make the hydroxy acid and amino acid starting materials were not reported.

Scheme 33. Suzuki's synthesis of (-)-bassianolide

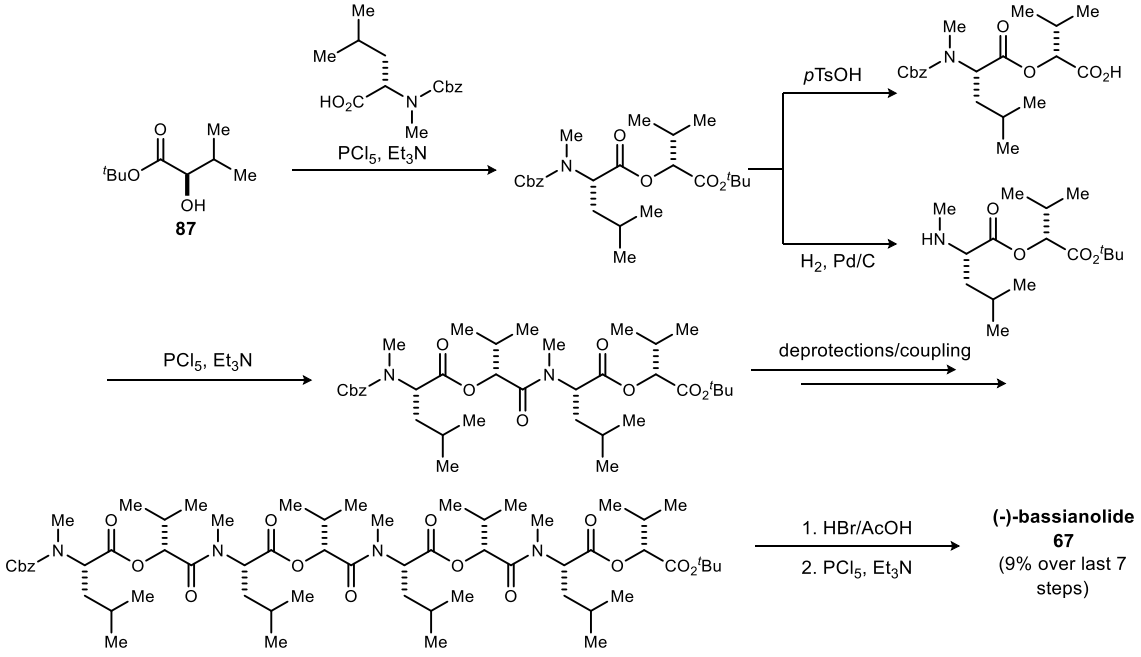

Using the same acid chloride method, (-)-bassianolide's cyclohexadepsipeptide analog, enniantin C (**82**), and desmethylbassianolide derivatives were synthesized[79] to investigate the relationship between structure and biological activity, as well as structure and conformation. ^{1}H NMR temperature studies showed that that (-)-bassianolide exists in two conformers in solution: one symmetrical and one asymmetrical. The presence of two conformers in solution explains why five *N*-methyl signals were observed in the initial proton NMR spectrum. This phenomenon was not seen in *N*-permethylated hexadepsipeptide enniantin C or any of the *N*-desmethyl derivatives. Suzuki and coworkers also observed increasing difficulty in cyclization of the *N*-methylated derivatives that was directly proportional to the amount of non *N*-methylated leucine residues (Figure 17). This difficulty was proposed to be due to helical intramolecular hydrogen bonding (Figure 18). If the linear peptide were to exist in a hydrogen bond-mediated helical conformation, the terminal functional groups may not be in an ideal position to react, thus explaining the observed low yielding macrolactamizations.

[79] Isogai, A.; Kanaoka, M.; Suzuki, A. *Pept. Chem.* **1979**, *16*, 165.

Figure 17. Comparison of macrolactamization yields to afford (-)-bassianolide and its *N*-desmethyl analogs

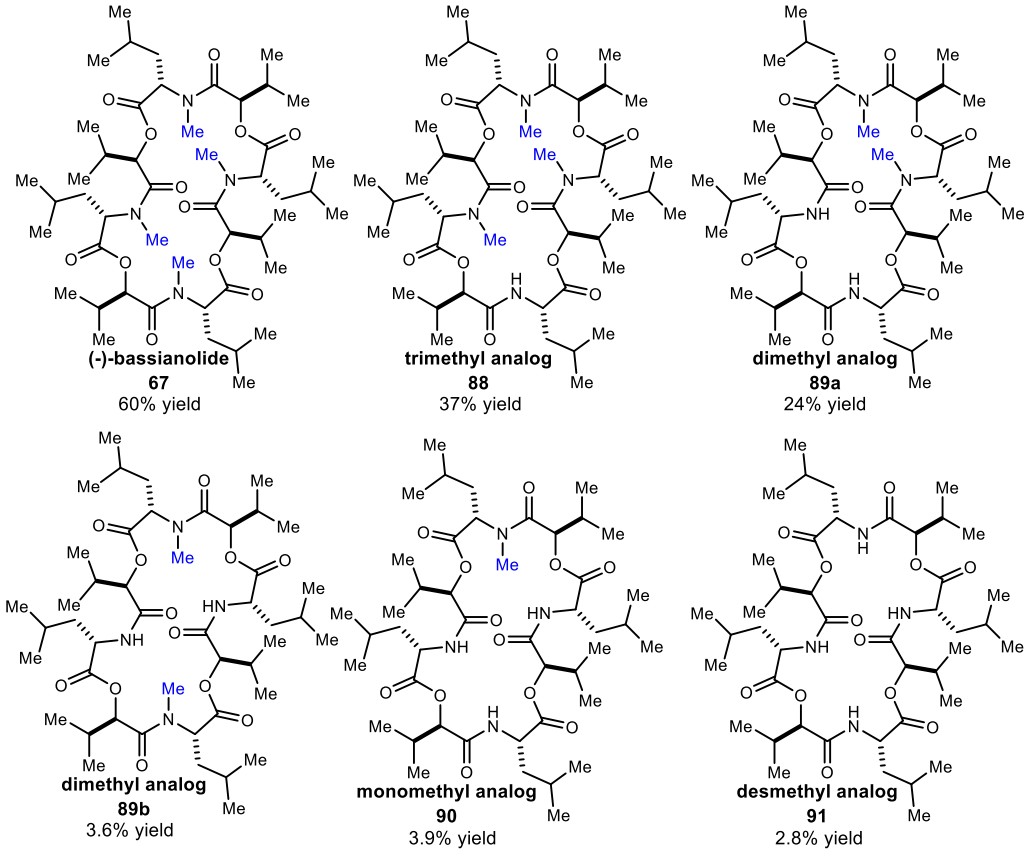

Figure 18. Helical hydrogen bonding conformation of *N*-desmethyl analogs

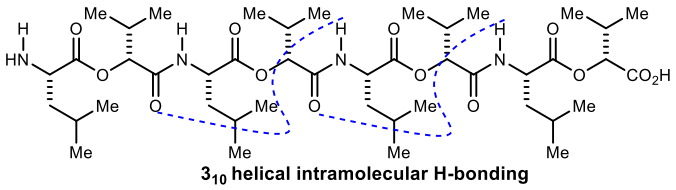

2.6.2 Overview of the proposed Mitsunobu MCO-based approach

Like Ōmura's synthesis of (-)-verticilide,[26] Suzuki's synthesis provides an excellent example of a contemporary route to (-)-bassianolide using starting materials from the chiral pool. Similar to Suzuki's route, our synthesis (Scheme 34) will use L-leucine as the amino acid starting material, but an *S*-α-hydroxy acid surrogate will be used instead of D-α-hydroxyisovaleric acid. The α-oxy bromonitroalkane will be coupled to *L*-leucine in an UmAS reaction to provide an α-hydroxy amide, which will then be convergently deprotected and coupled in a Mitsunobu reaction to ultimately afford a tetradepsipeptide *seco*-acid monomer. Based on previous selectivity and reactivity patterns with larger monomers, we predict that the tetradepsipeptide *seco*-acid will be able to favorably undergo cyclodimerization to the 24-membered ring in a Mitsunobu MCO. Finally, the *N*-H 24-membered ring will be permethylated to afford the natural product. This synthesis will test the limits of reactivity of our route by incorporating more hindered substrates. Branched amino and α-hydroxy acid residues may make the Mitsunobu couplings more difficult, thus creating the opportunity to modify the route and broaden its utility for more challenging cyclodepsipeptides.

Scheme 34. Proposed MCO-based synthesis of (-)-bassianolide

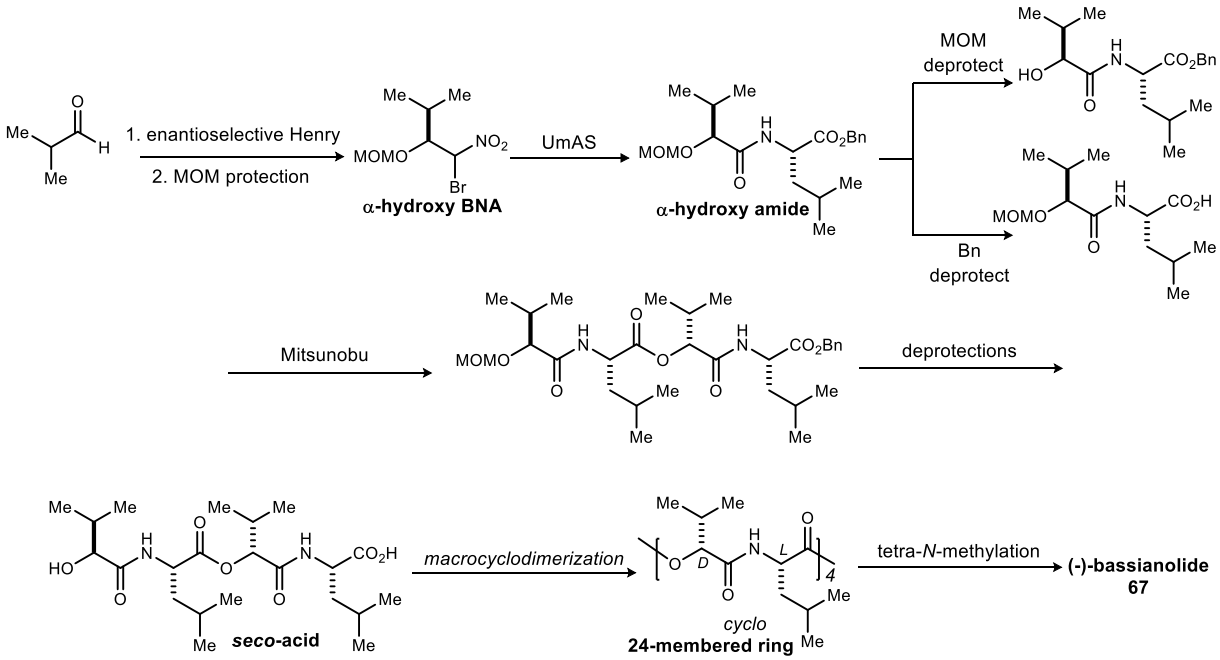

2.6.3 Development of a Mitsunobu MCO-based synthesis of (-)-bassianolide

Challenges with the intermediates in this route began in the first step. Our optimized enantioselective Henry conditions (Blay catalyst **27** at -20°C) that provided high yields in our total synthesis of (-)-verticilide proved to be much less effective when isobutyraldehyde was used in

Table 10. Enantioselective bromonitromethane addition into isobutyraldehyde

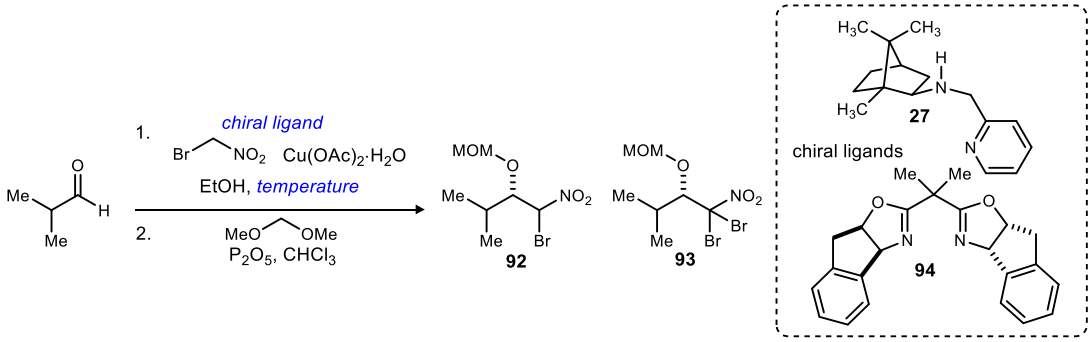

entry	chiral ligand	temperature (°C)	yield[a] of **92** (%)	yield[a] of **93** (%)	ee[b] (%)
1	**27**	-20	30	-	81/84
2	**27**	0	43	-	69/71
3	**94**	0	-	15	93

[a]Isolated yield. [b]Enantiomeric excess was determined by chiral HPLC using an OZ-H column.

the reaction conditions (Table 10). The apparent reactivity was much lower. We revisited Blay's work,[80] only to find that α-substituted aldehydes were not reported in their substrate scope. Raising the temperature of the reaction only slightly increased the yield (from 30 to 43%), at the expense of enantioselection. Extending the reaction time reaction time from three to four days did not make a significant difference in yield or ee. Thus, we hypothesized that the Blay ligand (**27**) may be too bulky to effectively catalyze bromonitromethane addition into α-substituted aldehydes. Evans' Inda-BOX ligand (**94**) with copper(II)acetate was reported to efficiently catalyze nitromethane addition into bulky aldehydes,[22] and therefore it seemed like a promising ligand to catalyze our targeted bromonitromethane addition. However, using **94** did not provide improved results—formation of bromonitroalkane **92** was not observed. Instead dibromonitroalkane **93** was isolated in 15% yield, albeit with high enantioselection (93% ee).

[80] Blay, G.; Hernandez-Olmos, V.; Pedro, J. R. *Chem. Commun.* **2008**, 4840.

Scheme 35. Enantioselective synthesis of a nitroalkane donor for one-pot UmAS

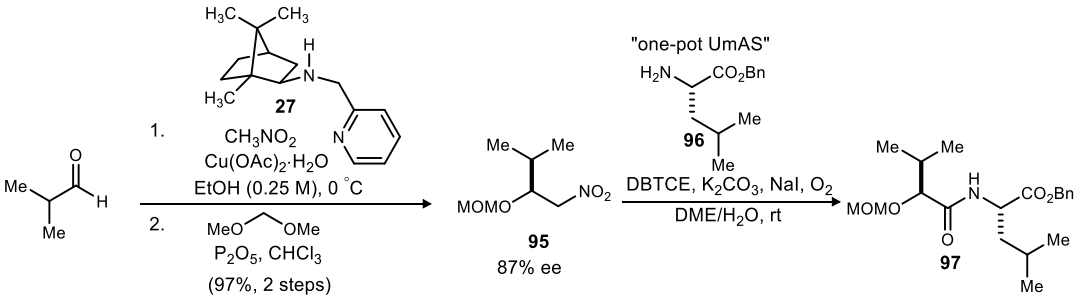

Around the time that our targeted bromonitromethane addition was in development, Schwieter discovered that a *nitroalkane* can be subjected to UmAS conditions in the presence of a bromonium source to afford amide products in similar yields to the original conditions from a bromonitroalkane starting material.[81] Because of the apparent challenges faced in the synthesis of bromonitroalkane **92**, nitroalkane **95** was synthesized, and a one-pot bromination/UmAS approach to synthesize α-hydroxy amide **97** was pursued instead (Scheme 35).

Table 11. Optimization of one-pot bromination/amidation UmAS to afford α-hydroxy amide 97

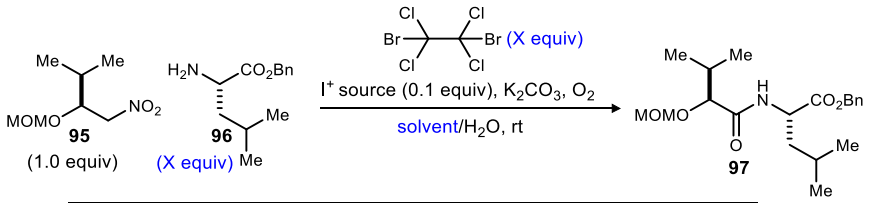

entry	amine (equiv)	DBTCE (equiv)	iodine source (0.1 equiv)	solvent (0.2 M)	yield[a] (%)
1	2.0	1.0	NaI	DME	61
2	1.2	1.0	NaI	DME	65
3	1.2	1.0	NaI	2-Me THF	33
4	**1.2**	**1.2**	**NaI**	**DME**	**73**
5	1.2	1.2	NIS	DME	57

[a]Isolated yield.

One factor to consider when implementing the one-pot UmAS amidation strategy (Table 11) is that the reaction is considerably more heterogeneous than a standard UmAS reaction. In order to achieve a high yield in a standard UmAS reaction, extremely vigorous and uniform mixing is required in order to prevent the reagents from clumping and sticking to the side of the flask. In attempts to avoid clumping, NaI was used instead of NIS, as it is soluble in water and does not produce succinimide as an insoluble byproduct. Initial results from subjecting nitroalkane **95** to one-pot bromination/amidation conditions were promising, providing amide **97** in 61% yield. However, this yield was substantially lower than what was observed in standard UmAS conditions using bromonitroalkane **92** (78% yield). A major

Scheme 36. Oxime byproduct

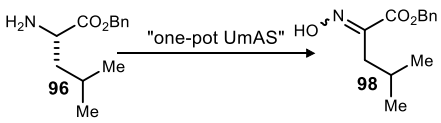

[81] Schwieter, K. E.; Johnston, J. N. *Chem. Commun.* **2016**, *52*, 152.

byproduct that formed from the excess amine (**96**) in oxidizing conditions was oxime[82,83] **98** (Scheme 36). This particular byproduct presented a purification challenge, as it could not be washed away in the acidic workup, and it elutes near the product during flash column purification. For the sake of convenience, the equivalents of amine were reduced to 1.2, which resulted in significantly less oxime byproduct **98** and a slightly higher yield of **97**. Changing the solvent to 2-Me THF resulted in poor conversion due to insolubility of the reagents, and using NIS instead of NaI resulted in diminished yields due to reagent clumping and the formation of a strange paste. However, adding slightly more DBTCE (1.2 equiv) increased the yield to 73%, which is more comparable to the yield observed in traditional UmAS conditions (Scheme 37).

Scheme 37. Traditional UmAS approach vs one-pot UmAS approach summary

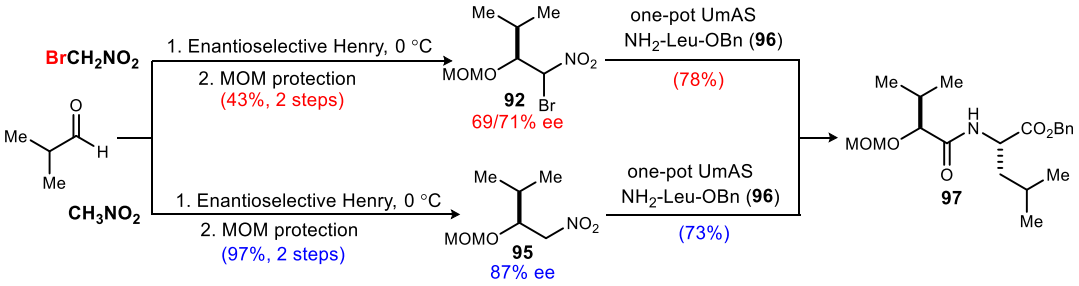

Although the UmAS step was optimized to afford **97** in good yield and fewer quantities of byproducts, this reaction remained a challenge to purify. The diastereomers[84] of amide **97** proved extremely difficult to separate using flash column chromatography, as their R_f values overlap. Because of this, major byproducts of the reaction were removed by FCC, and the diastereomers of **97** were separated using preparatory HPLC. Following separation of diastereomers, **97** was convergently deprotected to afford alcohol **99** and acid **100** in good yields. As predicted, the

Scheme 38. Synthesis of the tetradepsipeptide monomer en route to (-)-bassianolide

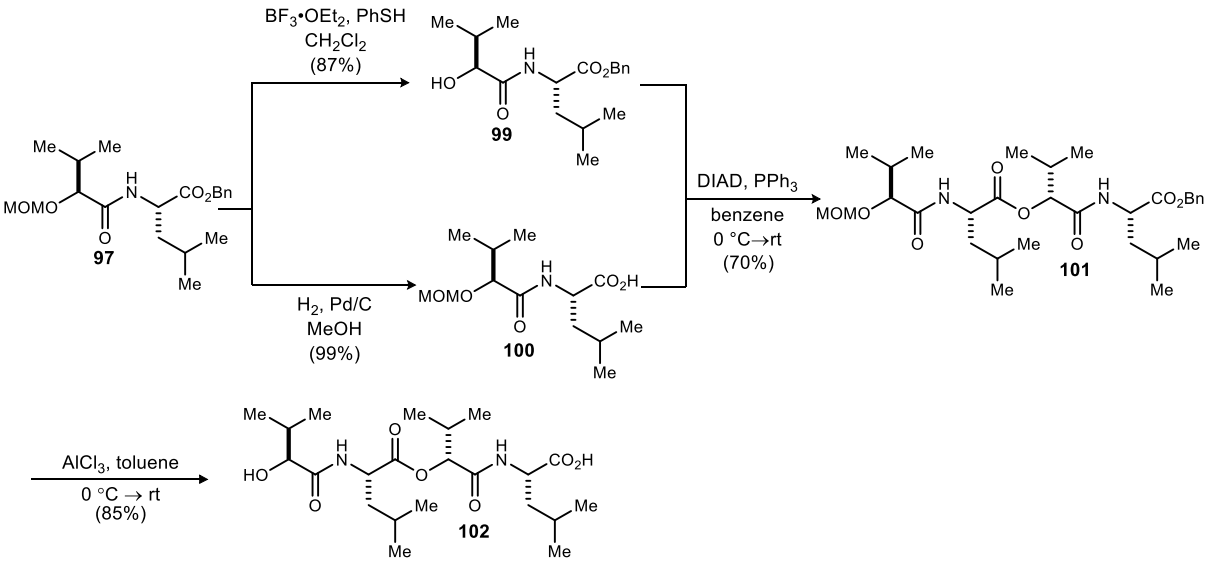

[82] Wu, L. Y.; Choi, J. K.; Hatton, K. Y.; Berkman, C. E. *Tetrahedron Lett.* **2010**, *51*, 402.
[83] Koji, K.; Teruaki, M. *Bull. Chem. Soc. Jpn.* **1991**, *64*, 2948.
[84] The starting nitroalkane was only 87% ee, so the minor enantiomer reacted to form some amount of D,L-epimer of **97**.

Mitsunobu coupling of more hindered substrates (**99** and **100**) was significantly more difficult than coupling the analogous adducts in the total synthesis of (-)-verticilide, initially affording tetradepsipeptide **101** in 35% yield. In order to slow the formation of acylated DIAD, the major byproduct, acid **100** was slowly added to the reaction at 0 °C to prevent it from warming up and causing excess side reactions to occur. This small change in procedure provided **101** in 70% yield, a modest result compared to the 91% yield observed in the analogous route to (-)-verticilide. (Scheme 38). Unfortunately, tetradepsipeptide **101** and reduced DIAD have overlapping R_f values, so **101** was also purified using preparatory HPLC. Finally, global deprotection of **101** afforded the linear cyclooligomerization precursor (**102**) in 85% yield (Scheme 38).

Figure 19. Structural comparison of tetradepsipeptide monomers 102 and 48

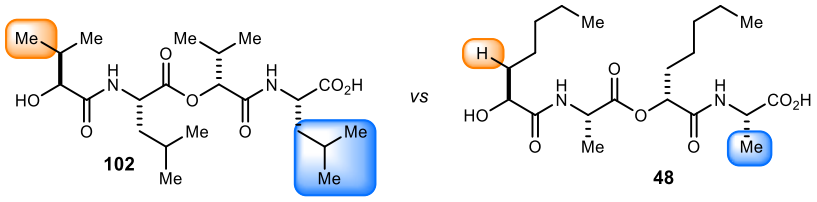

Compared to the tetradepsipeptide monomer (**48**) used to synthesize (-)-verticilide, the tetradepsipeptide monomer (**102**) for (-)-bassianolide is much more sterically hindered (Figure 19). Therefore, it was unsurprising that **102** was much less reactive in the Mitsunobu MCO. When subjected to our previously optimized conditions with 5 equivalents of $NaBF_4$ at 5 mM concentration, **102** provided the 24-membered macrocycle (**91**) in 21% yield, nearly double the yield than without the salt additive (Table 12). Additionally, the physical appearance of the reaction with **102** and a salt additive was much different than the reaction without a salt additive prior to work up. The reaction without the salt was mostly homogeneous, unlike the reaction with $NaBF_4$ which had a considerable amount of white precipitate. The reaction with $NaBF_4$ was initially homogeneous, and seemed to produce this white precipitate over the course of the reaction time. At first glance, the white solid was thought to be precipitated $NaBF_4$, but when the crude reaction without salt was concentrated a similar-looking white solid was observed. When both crude reactions were dissolved in DMSO-d_6 and analyzed by ^{1}H NMR, it was apparent that much more product had formed in the reaction with $NaBF_4$, indicating that the white precipitate was the desired product. Both reactions selectively produced the same 24-membered ring as the major product. No other macrocyclic products were found when each reaction was subjected to preparatory HPLC purification, but some starting material was recovered.

The observed difficulty in cyclodimerization of **102** was expected based on Suzuki's cyclization[79] attempt of an analogous amino-acid linear precursor, which afforded the cyclized product in only 2.8% yield. They attributed this difficulty to an intramolecular hydrogen bonding-induced helical conformation[79] that made cyclization unfavorable to occur. This would not only explain the diminished overall yield, but also why the yield with the salt additive is significantly higher: the sodium ions may interrupt intramolecular hydrogen bonding, which in turn causes the linear chain to change conformation, making cyclization more favorable. In order to further examine the role of $NaBF_4$ in this reaction, monomer **102** was subjected to cyclodimerization conditions with varying amounts of the salt additive (Table 12). The amount of $NaBF_4$ in solution was found to be crucial to overall reactivity. When the amount of $NaBF_4$ in the reaction was less than or greater than five equivalents, little cyclized product was formed. Interestingly, this reaction is also not dependent on a certain concentration of $NaBF_4$ in solution. **91** did not form with *2.5*

equivalents of $NaBF_4$ in a reaction *twice as concentrated* (10 mM) as standard conditions (5 mM), but **91** was isolated in 31% yield in the presence of *5 equivalents* of $NaBF_4$ at standard 5 mM concentration. Additionally, **91** was retrieved in 24% yield from a reaction with *5 equivalents* of $NaBF_4$ and *double* the standard reaction concentration (10 mM).

Table 12. Investigation of the role of $NaBF_4$ in cyclodimerization to *N*-H bassianolide

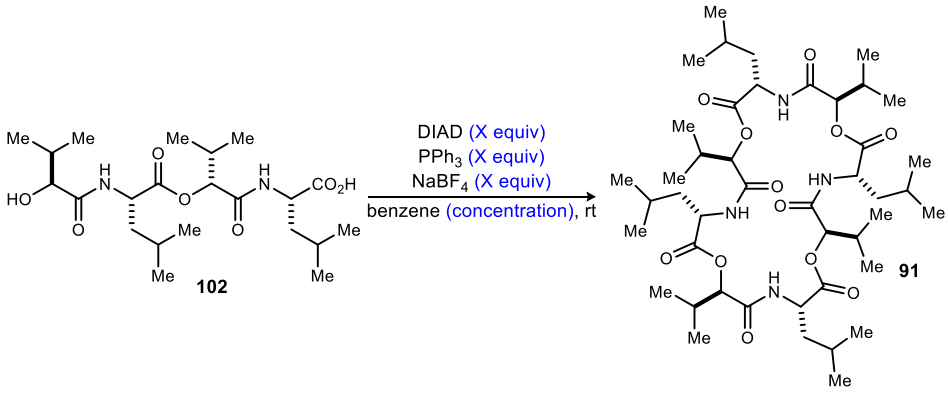

entry	$NaBF_4$ (equiv)	DIAD, PPh_3 (equiv, equiv)	concentration (mM)	yield[a] (%)
1	none	(2.5, 3.0)	5.0	11%
2	5.0	(2.5, 3.0)	5.0	21%[b]
3	3.0	(2.5, 3.0)	5.0	8%
4	10	(2.5, 3.0)	5.0	-
5	5.0	(5.0, 6.0)	5.0	31%
6	2.5	(5.0, 6.0)	10	-
7	5.0	(5.0, 6.0)	10	24%

[a]Isolated yield. [b]Repeated 1x to confirm result.

As summarized in Table 13, the effects of other chaotropic[85] salts ($LiBF_4$, LiBr) or solvents (DMF, THF, EtOAc), changing the solvent entirely (THF, benzene/THF), or heating the reaction did not improve the yield of the 24-membered ring or other cyclized products. Instead these additives appeared to shut the oligomerization/cyclization reaction down completely, but some starting material could be recovered. The lack of reactivity observed here may be attributed to the chaotropic additives interacting with the ionic Mitsunobu intermediates more than the substrate itself.

[85] Thakkar, A.; Trinh, T. B.; Pei, D. *ACS Comb. Sci.* **2013**, *15*, 120.

Table 13. Investigation of other chaotropes and solvents

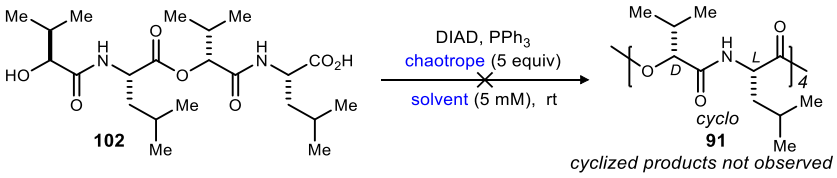

entry	chaotrope (5 equiv)	solvent (5 mM)
1	$NaBF_4$[a]	benzene
2	LiBr	benzene
3	LiCl	benzene
4	$LiBF_4$	benzene
5	DMF	benzene
6	EtOAc	benzene
7	none	benzene/THF
8	LiBr	benzene/THF
9	none	THF
10	LiBr	THF

[a]Reaction conducted at 60 °C.

Furthermore, synthesis of (-)-bassianolide using our first generation approach was not feasible because alcohol **103** and acid **104** were unable to undergo Mitsunobu coupling to form octadepsipeptide **105** (Scheme 39). Despite its modest yield, Mitsunobu cyclooligomerization has shown to be a more effective method to synthesize **91** than Suzuki's linear macrolactamization approach. Our best conditions provided the desired 24-membered ring in 31% yield, a significant improvement on the 2.8% yield[79] achieved by Suzuki.

Scheme 39. Attempted octadepsipeptide synthesis

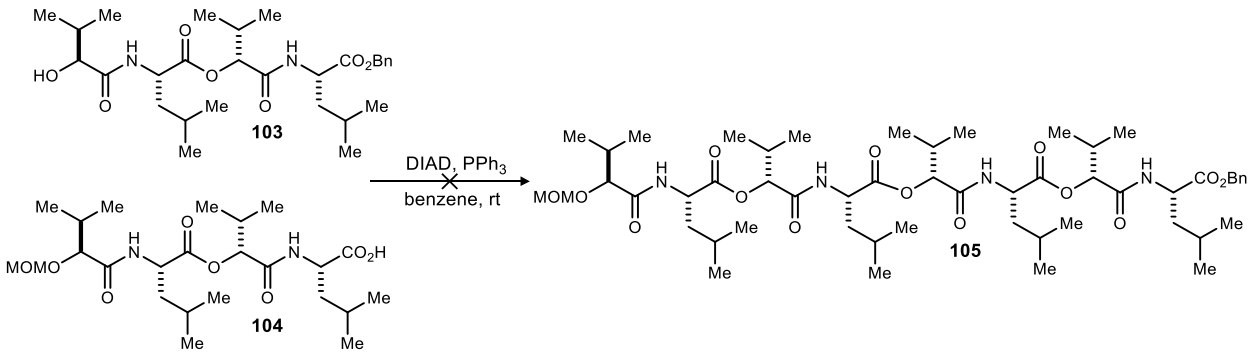

Finally, permethylation of **91** (Scheme 40) provided (-)-bassianolide in 9% overall yield, with an 8-step longest linear sequence. Although this synthesis is lower yielding than our original synthesis of (-)-verticilide, it is fewer steps than Suzuki's route and provides the natural product in similar yield. This synthesis also demonstrates that our route to cyclic *N*-methylated depsipeptides can be applied to substrates that are inherently difficult to make.

Scheme 40. *N*-Permethylation of *N*-H bassianolide 91

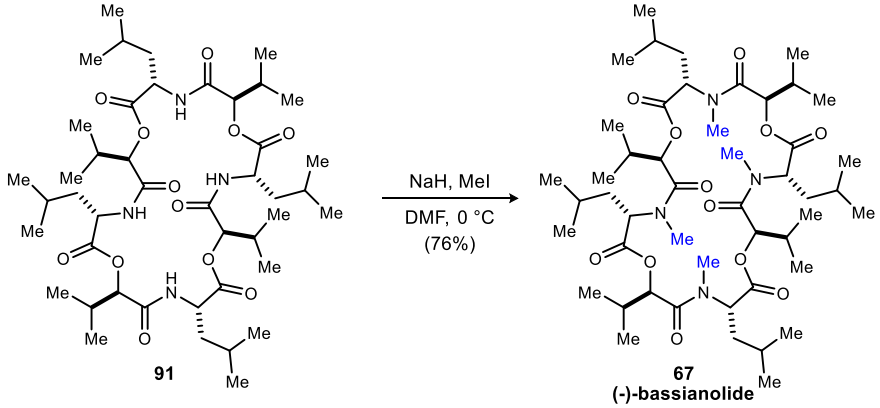

2.7 Conclusion

In summary, a combination of enantioselective α-oxy amide synthesis and Mitsunobu-based depsipeptide synthesis provides rapid access to macrocyclic depsipeptides. The use of salt additives in the Mitsunobu macrocyclooligomerization can enhance the selectivity for a single macrocycle size, or formation of size-diverse collections of macrocycles. A concise synthesis of the natural product (-)-verticilide grounds the work in a biologically active natural product, while providing equally straightforward access to its unnatural macrocyclic oligomers. Finally, (-)-bassianolide was prepared in 8 steps to establish the generality of approach while highlighting the advantage of a Mitsunobu reaction-based synthesis. Furthermore, the hybridization of enantioselective methods and UmAS provides broad access to α-oxy amide side chains without risk of epimerization during amide synthesis. The salt additive effects we describe illustrate the potential for achieving orthogonal aims of diversity and selectivity in separate experiments, and evidence of reagent control over oligomerization/cyclization. Our Mitsunobu-based MCO strategy also provides the ability to frame-shift macrocycle size-distribution by the judicious choice of monomer size (tetradepsipeptide vs didepsipeptide), thereby allowing large macrocycles to be synthesized with unprecedented ease. In this vein, the existence of large macrocyclic natural products is notable,[86,87] as is the dearth of methods that provide rapid access to this size regime.

[86] Onodera, K.-i.; Nakamura, H.; Oba, Y.; Ohizumi, Y.; Ojika, M. *J. Am. Chem. Soc.* **2005**, *127*, 10406.
[87] Ványolós, A.; Dékány, M.; Kovács, B.; Krámos, B.; Bérdi, P.; Zupkó, I.; Hohmann, J.; Béni, Z. *Org. Lett.* **2016**, *18*, 2688.

Chapter III

III. Evidence for ion-templation during Mitsunobu cyclooligomerization

As discussed in Chapter 2, we have developed an ion-mediated Mitsunobu MacroCycloOligomerization (MCO) reaction of hydroxy acid depsipeptides which provides small collections of cyclic depsipeptides in good overall yield.[88] The approach can produce a single macrocycle, or provide rapid access to multiple macrocyclic oligomers in good overall yield. Because cyclic peptides and depsipeptides tend to be ionophoric in nature, alkali metal salts were added to the MCO based on the hypothesis that the salts might bind the growing depsipeptide oligomer and cause a conformationally enhanced rate of cyclization of one product over the other. This hypothesis has been extended to other cyclooligomerization reactions in order to favor different size-distributions of cyclic peptide[65,89] products, but absent from the field is a broadly effective and rational approach, coupled to a rigorous analytical platform that might rationalize the product size-distributions. The ultimate goal would be development of a tool to predictably select a template for a particular size-regime (Figure 20).

Figure 20. Mitsunobu MCO strategy for measurement-based macrocycle synthesis

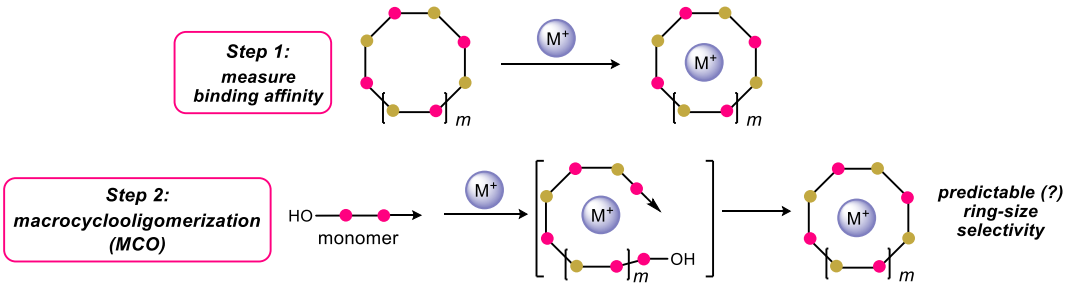

3.1 Introduction

3.1.1 Classification of templated oligomerization reactions

The relation between amplification and template-binding is commonly explored in thermodynamically controlled macrocyclooligomerization for the creation of dynamic

[88] Batiste, S. M.; Johnston, J. N. *Proc. Natl. Acad. Sci. U. S. A.* **2016**, *113*, 14893.
[89] Marti-Centelles, V.; Burguete, M. I.; Luis, S. V. *J. Org. Chem.* **2016**, *81*, 2143.

combinatorial libraries (DCLs).[90,91,92,93,94,95,96,97] In a thermodynamically-driven[98] templated oligomerization, the product distribution depends on the relative stabilities of the product-template complexes. A template that selectively binds one product can shift the equilibrium toward that species in high yields. However, optimization of an irreversible (kinetic) templated oligomerization reaction is quite different because the product distribution is dependent on multiple rates, including the template's role in transition state stabilization leading to each product.[99,100,101] A kinetic template could bind early intermediates (lower oligomers) to slow their cyclization, while binding later intermediates (higher oligomers) to favor a conformation that undergoes more rapid cyclization. The driving-force behind faster cyclization to a select product in a kinetic templating reaction is that the template almost invariably binds the product more tightly than the precursor-template complex.[102] Therefore, the product is also favored thermodynamically. Therefore, studying the relative binding properties of a range of templates to the products of a reaction is a practical way to infer their templating behavior.[102,103]

3.1.2 Isothermal titration calorimetry (ITC)

Several methods are commonly used to elucidate the behavior of a metal complex in solution, such as UV-Vis spectroscopy, NMR spectroscopy, soft-ionization MS spectrometry, and CD spectroscopy. However, these analytical methods are not always applicable, especially in the analysis of complexes that are disordered, fragile, insoluble, paramagnetic, and/or have multiple binding modes.[104] In contrast, isothermal titration calorimetry (ITC) is a very powerful tool for studying the thermodynamics of a binding event. The endothermic or exothermic heat is directly measured from the reaction between a titrant (metal ion) and chelating ligand (macrocycle), thus enabling elucidation of the enthalpy (ΔH) of the reaction and an association constant (K_a). The reaction enthalpy, or energy of binding, gives insight on the mechanism of binding. For example, a negative enthalpy parameter may indicate a strong H-bonding interaction between the metal and ligand, or a positive enthalpy may indicate that the binding event is accompanied by an unfavorable conformational change at the expense of H-bonding. The association constant (K_a) is an equilibrium constant defined by the ratio of ion-macrocycle complex to unbound species in solution. A large K_a ($> 10^4\ M^{-1}$) is indicative of strong binding. Additionally, the ion to macrocycle

[90] Corbett, P. T.; Leclaire, J.; Vial, L.; West, K. R.; Wietor, J. L.; Sanders, J. K.; Otto, S. *Chem. Rev.* **2006**, *106*, 3652.
[91] Ludlow, R. F.; Liu, J.; Li, H.; Roberts, S. L.; Sanders, J. K.; Otto, S. *Angew. Chem. Int. Ed. Engl.* **2007**, *46*, 5762.
[92] Roberts, S. L.; Furlan, R. L.; Otto, S.; Sanders, J. K. *Org. Biomol. Chem.* **2003**, *1*, 1625.
[93] Corbett, P. T.; Sanders, J. K.; Otto, S. *J. Am. Chem. Soc.* **2005**, *127*, 9390.
[94] Corbett, P. T.; Sanders, J. K.; Otto, S. *Chem. Eur. J.* **2008**, *14*, 2153.
[95] Furlan, R. L.; Ng, Y. F.; Otto, S.; Sanders, J. K. *J. Am. Chem. Soc.* **2001**, *123*, 8876.
[96] Di Stefano, S. *J. Phys. Org. Chem.* **2010**, *23*, 797.
[97] Berrocal, J. A.; Cacciapaglia, R.; Stefano, S. D.; Mandolini, L. *New J. Chem.* **2012**, *36*, 40.
[98] Furlan, R. L.; Otto, S.; Sanders, J. K. *Proc. Natl. Acad. Sci. U. S. A.* **2002**, *99*, 4801.
[99] Anderson, S.; Anderson, H. L.; Sanders, J. K. M. *Acc. Chem. Res.* **2002**, *26*, 469.
[100] Fahrenbach Albert, C. In *Pure Appl. Chem.* 2015; Vol. 87, p 205.
[101] Lucas, D.; Minami, T.; Iannuzzi, G.; Cao, L.; Wittenberg, J. B.; Anzenbacher, P., Jr.; Isaacs, L. *J. Am. Chem. Soc.* **2011**, *133*, 17966.
[102] Anderson, H. L.; Sanders, J. K. M. *J. Chem. Soc., Chem. Commun.* **1989**, 1714.
[103] Anderson, H. L.; Sanders, J. K. M. *Angew. Chem. Int. Ed.* **1990**, *29*, 1400.
[104] Kano, K.; Kondo, M.; Inoue, H.; Kitagishi, H.; Colasson, B.; Reinaud, O. *Inorg. Chem.* **2011**, *50*, 6353.

stoichiometry of complexation (N) is determined by the inflection point of the resulting titration curve (Figure 21).

Figure 21. Schematic of an ITC microcalorimeter and sample ITC thermogram

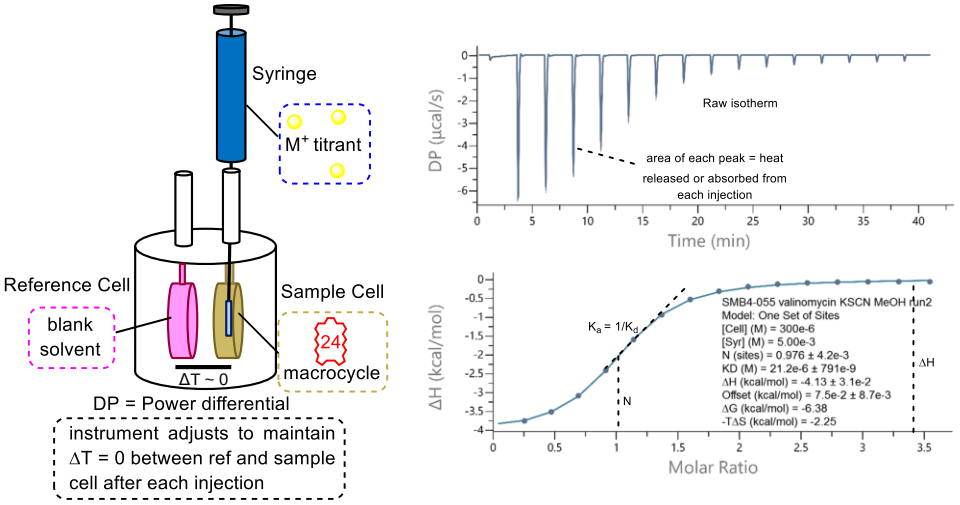

The main principle of ITC is to monitor the change in heat associated with a binding event brought on by titrating one solution into another. A schematic diagram of a typical ITC is shown in Figure 21. An ITC instrument has a pair of identical coin-shaped cells, denoted as sample and reference cells surrounded by an adiabatic jacket. The metal ion solution (syringe) is titrated into the macrocycle solution (sample cell) in small aliquots over time, and the ITC has a feedback mechanism where it measures the heat released or absorbed by the sample cell. During the titration, the temperature difference between the reference and the sample cell is monitored and power is supplied to both cells to maintain a constant temperature difference. The power that is needed to maintain constant temperature after each injection translates to the signal that appears on the raw thermogram. Exothermic reactions require a decrease in feedback power, whereas endothermic reactions will require an increased power feedback. The adiabatic jacket surrounding the sample and reference cells acts as a large thermal reservoir so that the power required to maintain the steady temperature after each injection quickly returns to baseline.[105]

Once the titration is completed, ΔH can be determined by integrating the raw heat peaks, as it is directly proportional to the raw heat generated or absorbed with each injection. Then, an appropriate binding model is selected, and the data is fitted by the instrument software to yield the final thermodynamic parameters.

3.2 Experimental design to determine template effects in the Mitsunobu MCO

The development of a rapid synthesis[88] of collections of natural product-like cyclodepsipeptides, particularly one that includes a means to manipulate complex structural elements (i.e. substituents and configuration) could be a powerful platform to explore chemical

[105] Salim, N. N.; Feig, A. L. *Methods* **2009**, *47*, 198.

diversity for a broad range of specific applications.[11,106,107,108,109] Our contribution to this effort includes a hybridization of enantioselective synthesis, Umpolung Amide Synthesis (UmAS), and an ion-templated Mitsunobu macrocyclooligomerization (MCO). A Mitsunobu reaction was adopted as the key transform for both oligomerization and macrocyclization processes. In a Mitsunobu reaction, the stereospecific nucleophilic displacement of an alcohol electrophile with a carboxylic acid nucleophile is irreversible, and is therefore inherently kinetically governed. Additionally, a key feature of this discovery, albeit unprecedented, was that ionic salts affect the overall production efficiency of the MCO, as well as the ring-size selectivity for arrays of macrocyclic products. We wondered whether the nature of the salt could be the basis for predicting how the size distribution of macrocycles will change as an ion templates the process. The notable amplification of various ring sizes discussed in Chapter 2, led to the hypothesis that size selectivity could be correlated to macrocycle-metal binding interactions measured using isothermal titration calorimetry (ITC).

3.2.1 Analysis of macrocycle-ion binding interactions with ITC measurements

The ion-templated Mitsunobu MCO is performed in benzene, but the ITC experiments described here were conducted in methanol. Attempts to prepare ITC runs in other organic solvents and solvent mixtures, such as benzene, dichloromethane/acetonitrile (3:7), or acetonitrile, led to the observation that the salts alone and/or salt-macrocycle complex were not sufficiently soluble. As a result, consistent ITC data could not be obtained. Methanol is starkly different in polarity to benzene (solvent for MCO), and it is known that solvent does affect binding affinity.[104,110,111] However, several accounts have shown that although binding constants do vary with solvent, the trend of their relative binding is consistent.[112,113,114,115] Our goal was to observe, if possible, *trends in binding interactions as a function of macrocycle and cation size* in an attempt to rationalize the apparent ion-templating effect. Therefore, the determination of absolute binding constants in the reaction solvent (benzene) was deemed less important.

ITC measurements were performed using a MicroCal PEAQ-ITC instrument (MicroCal Inc., Northampton, MA). All experiments were performed at 25 °C *in anhydrous methanol*. Optimal instrument settings for consistent results *in methanol* include: reference power set to 5 µcal/mol, stir speed set to 1000 rpm, and instrument feedback set to low. These settings are extremely important when conducting experiments in methanol in order to avoid instrumental overcompensation for measured heats (resulting in oscillating raw heats). See Experimental

---

[106] Beeler, A. B.; Acquilano, D. E.; Su, Q.; Yan, F.; Roth, B. L.; Panek, J. S.; Porco, J. A., Jr. *J. Comb. Chem.* **2005**, *7*, 673.
[107] Liu, S.; Gu, W.; Lo, D.; Ding, X. Z.; Ujiki, M.; Adrian, T. E.; Soff, G. A.; Silverman, R. B. *J. Med. Chem.* **2005**, *48*, 3630.
[108] Chen, Y.; Bilban, M.; Foster, C. A.; Boger, D. L. *J. Am. Chem. Soc.* **2002**, *124*, 5431.
[109] Garcia-Martin, F.; Cruz, L. J.; Rodriguez-Mias, R. A.; Giralt, E.; Albericio, F. *J. Med. Chem.* **2008**, *51*, 3194.
[110] Cougnon, F. B.; Au-Yeung, H. Y.; Pantos, G. D.; Sanders, J. K. *J. Am. Chem. Soc.* **2011**, *133*, 3198.
[111] Sessler, J. L.; Gross, D. E.; Cho, W. S.; Lynch, V. M.; Schmidtchen, F. P.; Bates, G. W.; Light, M. E.; Gale, P. A. *J. Am. Chem. Soc.* **2006**, *128*, 12281.
[112] Amini, M. K.; Shamsipur, M. *J. Phys. Chem.* **1991**, *95*, 9601.
[113] Shamsipur, M.; Irandoust, M. *J. Solution Chem.* **2008**, *37*, 657.
[114] Izatt, R. M.; Pawlak, K.; Bradshaw, J. S.; Bruening, R. L. *Chem. Rev.* **1991**, *91*, 1721.
[115] Danil de Namor, A. F.; Matsufuji-Yasuda, T. T.; Zegarra-Fernandez, K.; Webb, O. A.; El Gamouz, A. *Croat. Chem. Acta* **2013**, *86*, 1.

Section for important instructions regarding ITC experiment set up, data processing, and cleaning the instrument.

3.2.2 Normalized amplification factor analysis: a measure of significance in template effect

In order to correlate trends in binding interactions with changes in macrocycle size distribution, we sought a term to determine which template-induced changes are significant. As mentioned in the Introduction section, templates are commonly used to shift the size distribution of macrocycles in dynamic combinatorial library (DCL) to favor a thermodynamic product. The response of a DCL to a template is routinely analyzed in terms of the amplification factors (AFs) of the individual macrocycles. AFs are defined as the concentration of the macrocycle formed in the presence of the template over the concentration of macrocycle in the absence of the template, as defined by equation (1):

$$[A_T]/[A_0] \quad (1)$$

However, comparing the AFs of macrocycles in a library, which are initially formed in very different amounts without a template, is not very meaningful. For example, a macrocycle that initially makes up half the contents of the library cannot have an AF larger than 2 if a template causes that product to form selectively. On the other hand, a macrocycle that initially makes up 2% of the same untemplated library can have an AF up to 50 if that product is formed selectively in the presence of a template. In this case, AFs of 2 and 50 are both representative of a single macrocycle being formed selectively, but cannot be compared to each other in a straightforward fashion. However, normalized amplification factor (AF_n) is a unitless value between -1 (complete disappearance of product) and 1 (maximum possible product) to determine significance of increase in yield of individual products in the presence of a template, relative to the control and others formed in the reaction.[116,117,118] To compare amplification factors between different products, the concentrations of the products are normalized on the basis of the maximum concentration of available monomers. Because AF_n is based on available monomer concentration, the term can be applied to ion-templated MCO when the available monomer concentration is normalized to represent the isolated yield of macrocycles in the reaction,[96,97] defined by equation (2):

$$\frac{[A_T]-[A_0]}{[A_{max}]-[A_0]} \quad (2)$$

[116] Hamieh, S.; Saggiomo, V.; Nowak, P.; Mattia, E.; Ludlow, R. F.; Otto, S. *Angew. Chem. Int. Ed. Engl.* **2013**, *52*, 12368.
[117] Ulatowski, F.; Sadowska-Kuziola, A.; Jurczak, J. *J. Org. Chem.* **2014**, *79*, 9762.
[118] Ulatowski, F.; Dąbrowa, K.; Jurczak, J. *Tetrahedron Lett.* **2016**, *57*, 1820.

Here, $[A_T]$ and $[A_0]$ are the respective concentrations of a given product formed with and without a template, and $[A_{max}]$ represents the maximum possible concentration of that product, based on the amount of available monomers. In order to account for experimental variance, the literature-accepted value for a significant template-induced change is when $|AF_n| > 0.09$.[116] Because this parameter has never been used for a kinetic templating reaction, it was necessary to verify that the variance within control reactions was less than 0.09, or adjust the value for a significant change in library composition accordingly.

Figure 22. Determination of variance within untemplated reactions

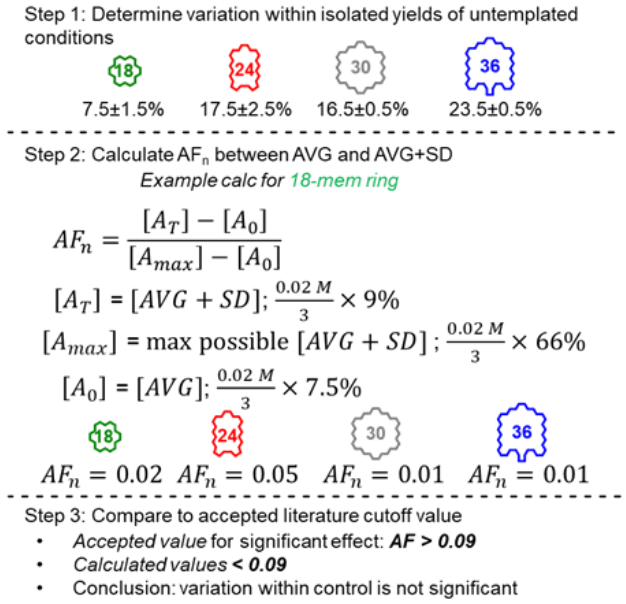

Figure 22 outlines an example calculation for the collection of macrocycles resulting from untemplated MCO runs from didepsipeptide monomer **74**. Based on these results, the AF_n within untemplated control experiments is less than 0.09 across the board, averaging out to be 0.02. This calculation was also done within multiple runs of templated MCO, and as expected, there was little to no variation between repeated runs. Therefore, $|AF_n| > 0.09$ represents a template-induced change more than double what is observed within repeated sets of identical experiments, and is therefore able to represent the cutoff value between experimental error and a significant template-induced change for the MCO experiments. Amplification factor analysis allows us to have quantitative grounds to determine which macrocyclic products are significantly increased, decreased, or not affected in the presence of a salt added to an MCO reaction. The AF_n values for all collections of macrocycles discussed later in this chapter have been calculated, and are referenced as a guideline to determine if the yield of a product has changed beyond the margin of experimental error in the presence of an ion template. With these calculations in hand, we are now able to correlate significant template effects with thermodynamic parameters obtained from ITC measurements.

3.3 Correlation of ITC Measurements with MCO salt effects

3.3.1 Patterns between monomer size and salt effects explained by ITC measurements

A key factor that effected the size distribution of products formed in the ion-templated MCO was the size of the monomer starting material. For example, tetradepsipeptide **70** and didepsipeptide **74** ultimately afford structurally identical D,L-24- and 36-membered rings, but their relative yields formed from each monomer are quite different. To better understand this difference in behavior, salt-macrocycle binding interactions of MCO products formed from tetradepsipeptide **70** and didepsipeptide **74** were determined by ITC (Figure 24 and Figure 23). The data from ITC can be used to rationalize why different amounts of 24- and 36-membered rings are produced from tetradepsipeptide monomer **70** and didepsipeptide monomer **74** in the presence of the same ion

templates. Under salt-free conditions, tetradepsipeptide **70** inherently produces cyclodimer **53** as the major product, along with 36-membered ring **72** and 60-membered ring **73** in minor amounts. However, in the presence of $NaBF_4$, **53** is formed exclusively. As expected, **53** strongly and favorably binds Na^+ in a 1:1 stoichiometry. However, **72** and **73** also bind Na^+, but in 2:1 ion to macrocycle ratios. The selectivity observed in the reaction despite the measured Na^+ binding ability of the other two potential products can be explained by a *positive templating effect*:[103,99] Na^+ promotes the preorganization[62,92] of two tetradepsipeptide building blocks (**72**), driven by favorable binding to the linear precursor to **53** in a conformation that accelerates an inherently favorable ring-closure.

Figure 23. Correlation of ITC data with salt effects on collections of macrocycles formed using 70[a]

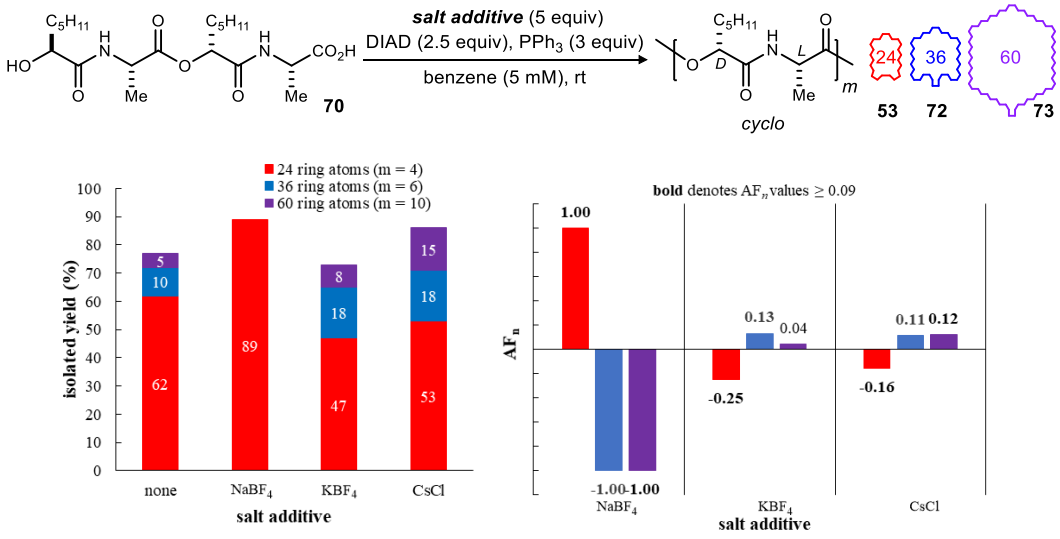

template	*24-mem ring* (**53**)			*36-mem ring* (**72**)			*60-mem ring* (**73**)		
	K_a (M^{-1})	ΔH	N	K_a (M^{-1})	ΔH	N	K_a (M^{-1})	ΔH	N
Na^+	$3.18x10^4$	–	1:1	$1.56x10^4$	–	2:1	$7.04x10^3$	+	2:1
K^+	$2.67x10^3$	–	1:1	$2.06x10^4$	–	1:1	$2.97x10^3$	+	3:1
Cs^+	$<1.00x10^3$			$5.95x10^3$	–	1:1	$4.27x10^3$	+	3:1

[a]ITC binding affinities $<1x10^3$ M^{-1} are not detected

Additionally, a combination of the inherently slow oligomerization of **70** and preorganization of a two-Na^+ ion cyclization template, can explain why cyclotrimerization to provide **72** is much slower than cyclodimerization to form **53**. Similar logic can be applied to arrive at a reason why didepsipeptide **74** did not provide the same results with Na^+: the rate of intermolecular (Mitsunobu) coupling of **74** is much faster than that for **70**, so although the yield of the 24-membered ring (**53**) is greater than observed in salt-free conditions, the concentrated reaction conditions and more reactive monomer (**74**) renders intermolecular coupling a more competitive process than in the former example. Additionally, 18-membered ring **75** and 30-membered ring **76** were found to exist in an equilibrium of 1:2 Na^+ to macrocycle aggregates and 2:1 Na^+ to macrocycle complexes, averaging 1.5 bound ions.[119,120] The observation of a 1:2 binding

[119] Both macrocycles gave atypical sigmoidal ITC thermograms with inflection points at 0.5 and 1.5.
[120] Darby, S. J.; Platts, L.; Daniel, M. S.; Cowieson, A. J.; Falconer, R. J. *J. Therm. Anal. Calorim.* **2016**, *127*, 1201.

pattern with **75** can imply that Na^+ promotes the preorganization of two linear-precursors, which then rapidly undergo cyclodimerization to the 36-membered ring (**72**) with the help of a second Na^+ ion. Because **76** is substantially larger than **75**, formation of a 1:2 metal-linear peptide complex is more likely to result in stable aggregates, as opposed to the precursor of a cyclodimerization reaction. Thus, the ITC binding pattern observed with **75**, which has the strongest 2-Na^+ binding constant, can imply that cyclization of the linear precursor is slowed by the formation of aggregates, but is then accelerated when the complex gains an additional Na^+ ion.

Figure 24. Correlation of ITC data with salt effects on collections of macrocycles formed using 74[a]

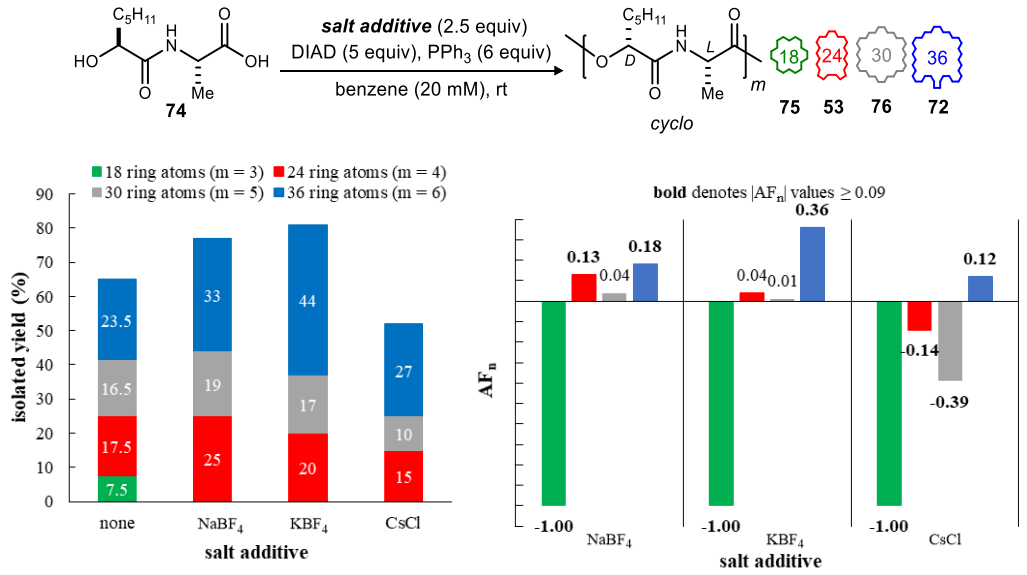

template	*18-mem ring* (75)			*24-mem ring* (53)			*30-mem ring* (76)			*36-mem ring* (72)		
	K_a (M^{-1})	ΔH	N	K_a (M^{-1})	ΔH	N	K_a (M^{-1})	ΔH	N	K_a (M^{-1})	ΔH	N
Na^+	$8.33x10^4$	–	1:2 *then* 2:1	$3.18x10^4$	–	1:1	$3.44x10^4$	–	1:2 *then* 2:1	$1.56x10^4$	–	2:1
K^+	$<1x10^3$			$2.67x10^3$	–	1:1	$<1x10^3$			$2.06x10^4$	–	1:1
Cs^+	$<1x10^3$			$<1x10^3$			$<1x10^3$			$5.95x10^3$	–	1:1

[a]ITC binding affinities $<1x10^3$ M^{-1} are not detected

In the presence of a slightly larger cation, K^+, with tetradepsipeptide **70**, the 36-membered ring (**72**) is significantly increased relative to the control, while the 24-membered ring (**53**) is decreased. The 36-membered ring has the greatest enthalpically favorable 1:1 binding to K^+, but is not produced selectively, unlike what was observed with the 24-membered ring and Na^+. This can be explained by the overall efficacy of K^+ as a cyclization template. An effective template must have the capacity to bind early linear intermediates in the oligomerization reaction, but also prevent them from competitively cyclizing.[99,103] In this case, the untemplated cyclodimerization reaction is very fast, and addition of K^+ slows it, but not enough to selectively favor formation of the cyclotrimer (**72**). However, addition of K^+ to the MCO with didepsipeptide monomer **74** produces the 36-membered ring in nearly double its original amount. In conjunction with the inherent fast intermolecular oligomerization of monomer **1**, and strong binding to K^+, the rate of 36-membered ring cyclization can be selectively increased. ITC indicates that the other ring sizes either weakly

bind (K_a < 1x10^4 M^{-1}),[118] or do not bind K^+ at detectable levels (K_a < 1x10^3 M^{-1}), so their cyclization rates and respective yields are minimally affected.

The largest cation (Cs^+) with tetradepsipeptide **70** significantly amplified both of the larger ring sizes relative to the control, but did not favor them substantially as observed with **53** and Na^+. ITC data shows that **72** and **73** have similar, but weak, binding affinities to Cs^+ (Figure 23). However, Cs^+ with didepsipeptide monomer **74** does not result in significant amplification of macrocycles relative to the salt-free control. In these two examples, the modest change in size distribution can largely be attributed to the lack of a driving force from formation of a strong Cs^+-binding product.

3.3.2 Use of ITC measurements to explain MCO salt effects with D,D-macrocycles

The use of enantioselective catalysis to prepare depsipeptide monomers provided a synthesis platform to investigate a broad scope of precursors that might exhibit a more diverse range of behaviors in the MCO reaction. Therefore, we wondered whether the trends observed with monomers **70** and **74** might also apply to monomers with different stereochemistry (Figure 25). Unlike its L,L-analog (**74**), L,D-monomer (**77**) inherently favored direct cyclization to the 6-membered ring (**78**), in addition to producing small amounts of 18-membered (**79**) and 24-membered (**80**) rings in salt-free conditions. However, addition of Na^+ doubled the amounts of both **79** and **80**, while the 6-membered ring (**78**) was significantly decreased. Additionally, a small amount of a 30-membered ring (**81**), which was not observed in salt-free conditions, was formed. Macrocycles **79**, **80**, and **81** strongly bind Na^+, while **78** does not at detectable levels, which can explain why the rate of direct cyclization to **78** was so greatly decreased. Additionally, the binding affinities of **79** and **80** to Na^+ are strong enough to drive preorganization of their linear precursors and subsequent cyclization at a rate much faster than intermolecular oligomerization and cyclization to **81,** despite its slightly stronger binding affinity to Na^+. Additionally, **81** displays a positive enthalpy of binding, suggesting that the binding is accompanied by unfavorable conformational change[92,121,122] as opposed to hydrogen bonding. Because binding interactions of cyclized products are known to reflect their respective linear precursors, it can be inferred that the transition state leading to **81** binds Na^+ in a conformation that does not promote cyclization (*negative templating effect)*,[99] which can explain why the rate of cyclization to **81** is not more competitive with **79** and **80.**

[121] Kandeel, M.; Al-Taher, A.; Nakashima, R.; Sakaguchi, T.; Kandeel, A.; Nagaya, Y.; Kitamura, Y.; Kitade, Y. *PLoS One* **2014**, *9*, e94538.
[122] Otto, S.; Engberts, J. B. *Org. Biomol. Chem.* **2003**, *1*, 2809.

Figure 25. Correlation of ITC data with salt effects on collections of macrocycles formed using 77[a]

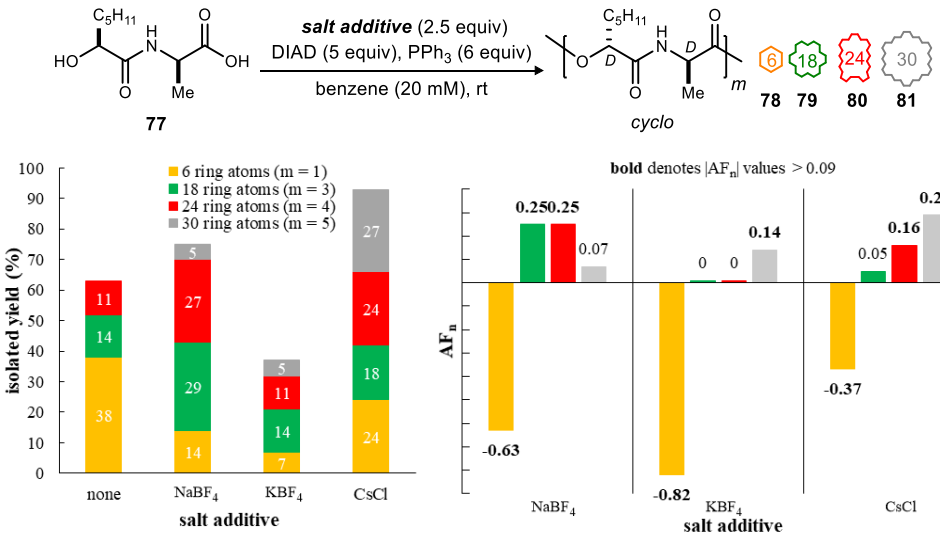

template	*6-mem ring* (**78**)			*18-mem ring* (**79**)			*24-mem ring* (**80**)			*30-mem ring* (**81**)		
	K_a (M^{-1})	ΔH	N	K_a (M^{-1})	ΔH	N	K_a (M^{-1})	ΔH	N	K_a (M^{-1})	ΔH	N
Na^+	<$1.00x10^3$			$2.52x10^4$	–	1:1	$7.75x10^4$	–	2:1	$9.09x10^4$	+	1:1
K^+	<$1.00x10^3$			<$1.00x10^3$			$8.55x10^3$	–	1:1	<$1.00x10^3$		1:1
Cs^+	<$1.00x10^3$			<$1.00x10^3$			$4.33x10^3$	–	1:1	$1.20x10^4$	–	1:1

[a]ITC binding affinities <$1x10^3$ M^{-1} are not detected

Addition of K^+ to monomer **77** decreased production of the monocyclized product, but only modestly increased the 30-membered ring (**81**) relative to the control and the other macrocyclic products. ITC data shows that **80** weakly binds K^+ and that macrocycles **78**, **79**, and **81** do not bind at detectable levels. In this example, the modest change in size distribution can be attributed to the lack of a driving force from formation of a strong K^+-binding product. The most notable results of this series were observed when Cs^+ was used as an additive: the 30-membered ring (**81**) was isolated as the major product, when it was not originally observed in salt-free conditions. The 30-membered ring (**81**) is the strongest 1:1 Cs^+-binder, followed by the 24-membered ring (**80**), while **78** and **79** do not have detectable binding. Here, Cs^+ effectively accelerates the rate of cyclization to the two Cs^+-binding macrocycles, which resulted in their increased production.

3.3.3 Analysis of structural and thermodynamic trends

From the results obtained thus far, we were able to see clear correlation between ITC measurements of macrocycle-salt binding interactions and the changes in size distribution of MCO products with salt additives. The correlations we made from each experiment were compiled and then used to extrapolate general structural and thermodynamic trends for cyclodepsipeptide synthesis via ion-templated MCO (Figure 26).

The ITC data generally indicates that there is a trend where macrocycles with a strong template binding affinity ($K_a > 1x10^4$) will be formed in substantially greater amounts in the presence of that template. The stoichiometry and enthalpy parameters from the ITC data, in combination with relative binding affinities, provide us with a full picture for how the ion template will affect the size distribution of products in a collection of macrocycles. A 1:1 metal ion to macrocycle complex observed by ITC indicates a faster rate of formation than what would be observed with a 2:1 complex, simply because preorganization of a 1-ion cyclization complex is faster than one that requires 2 ions. 1:2 Complexes have been observed by ITC, and were found to correlate with inhibited monocyclization of smaller rings, and increased formation of their corresponding cyclodimer in the presence of the salt additive. However, when observed with larger rings, 1:2 complexes correlate with overall slowed cyclization. The enthalpy parameter serves as a good indicator for whether or not cyclization to a particular ring size would be favorable in the presence of a given template. This parameter is especially important as a predictive measure if multiple macrocycles in a series have strong binding to a particular ion. In general, negative binding enthalpy with strong ion-affinity resulted in an increased rate of cyclization, and positive binding enthalpy with strong ion-affinity resulted in a slowed rate of cyclization.

Figure 26. Structural and thermodynamic trends for depsipeptide synthesis via ion-templated MCO

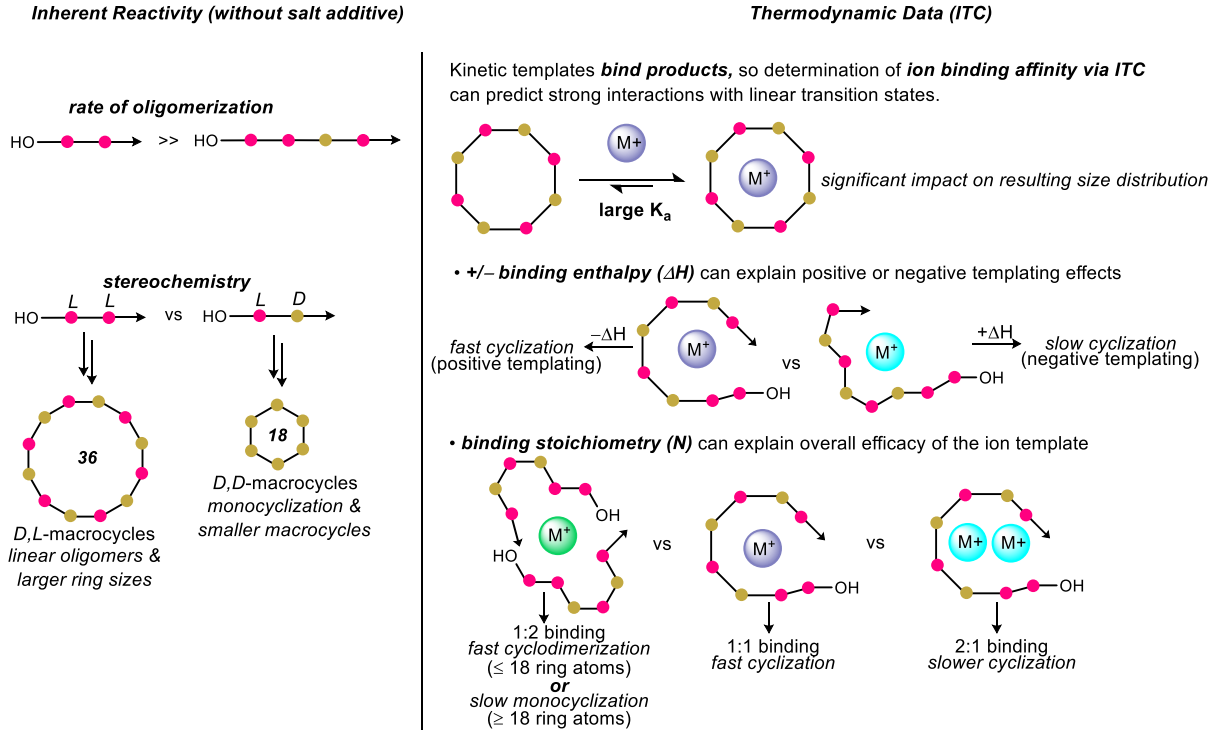

3.3.4 A test of generality: correlation of trends in binding with a new D,L monomer

The long-term goal of this strategy is the prediction of size-selectivity for macrocyclic products for various salt additives. On the basis of the trends described in the previous section, we propose that the distribution of macrocycles using salt additives as a variable suggests that inherent structure-based reactivity can be inferred from ITC-analysis of macrocycle-salt binding. However, all of the monomers studied until this point were composed of alternating α-hydroxyheptanoic acid

and alanine residues. Therefore we were motivated to test the generality of this approach by using our newly established analytical method to roughly predict the template-induced changes in size distribution of macrocycles from a new monomer (Scheme 41).

Scheme 41. Synthesis of a new monomer to test our hypothesis

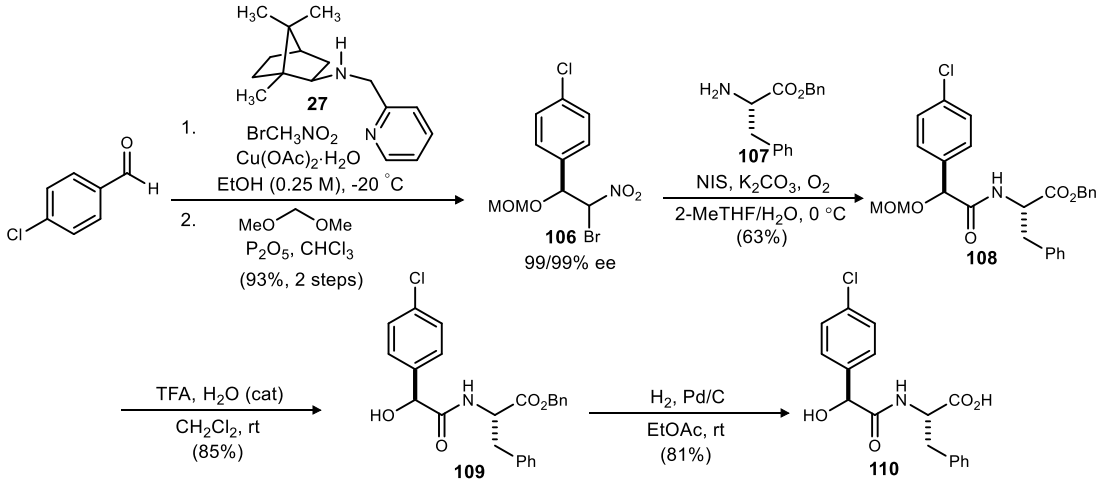

4-Chloro mandelic acid-containing monomer **110** was targeted for the synthesis of macrocycles that could be rapidly identified by mass spectrometry. The aryl rings were predicted to improve overall ionization efficiency, and the chlorine isotopes have a very distinctive 3:1 mass abundance, which could serve as a reliable marker to rapidly identify the sizes of macrocycles formed in a crude reaction mixture. Our optimized enantioselective Henry conditions (Blay catalyst **27** at -20°C), followed by MOM protection provided bromonitroalkane **106** in high yield and enantioselection. Contrary to previous literature reports,[18] **106** is a solid and could be recrystallized to furnish enantiopure material. Donor **106** was then coupled to L-phenylalanine benzyl ester (**107**) under UmAS conditions to afford α-hydroxy amide **108**. The MOM-ether was then deprotected using TFA, and the benzyl ester was then removed via hydrogenolysis with palladium on carbon in ethyl acetate to afford the didepsipeptide *seco*-acid monomer **110**. Interestingly, when EtOAc was used as the solvent for the benzyl deprotection, dehalogenation of the aryl ring did not occur. However, when previously optimized benzyl deprotection conditions were attempted, which use methanol as the solvent, the aryl ring was rapidly dehalogenated.

Didepsipeptide **110** was then subjected to untemplated MCO conditions, and its products were analyzed by ITC *before* running the MCOs with salts added. Without salt, didepsipeptide **110** provided 18-, 24-, and 36-membered rings, as determined by mass spec (Figure 27).

Figure 27. Chlorine isotopes are a helpful tool to identify new macrocyclic products

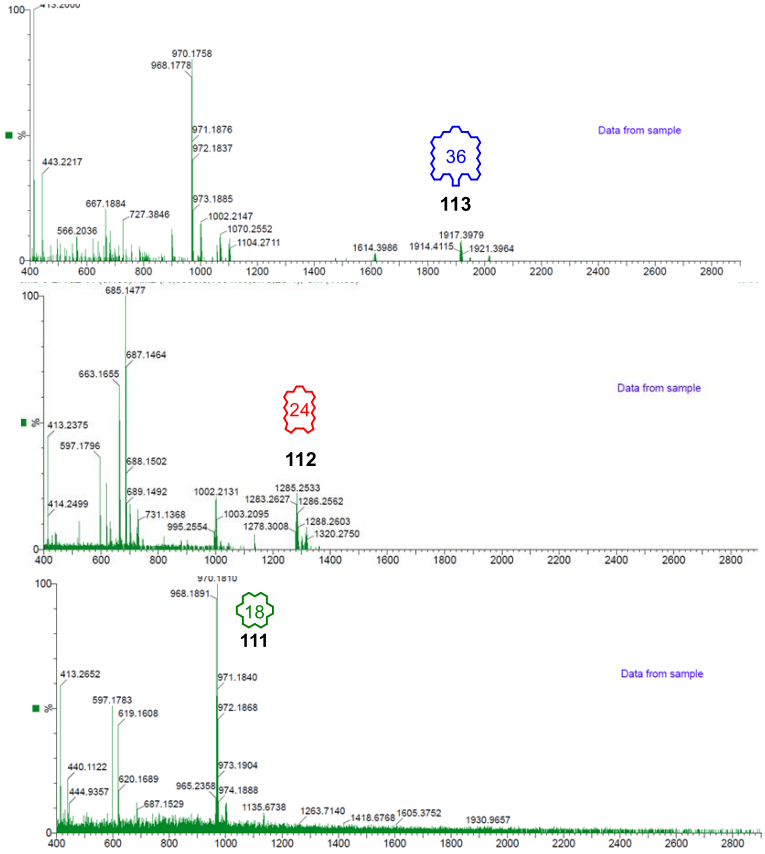

The overall yield of the untemplated MCO using **110** was quite low (47%), likely due to the steric effect of $A^{1,3}$-strain (from the 4-chloro mandelic acid residue) on the Mitsunobu reaction. The low initial efficiency provided a workable starting point to study the effects of salts, especially those that might induce more reactive conformations by templation. The thermodynamic interactions of **111**, **112**, and **113** with various salts were measured by ITC (Figure 28), and predictions for how the size distribution might change in the presence of salts were made based on the structural and thermodynamic trends observed in previous examples. With sodium, the 24-membered ring (**112**) has an order of magnitude stronger 1:1 binding affinity than the other two macrocycles, and thus, it should be amplified the most. Macrocycles **111** and **113** also have strong binding affinities to Na^+, but are not expected to be greatly increased. Preorganization to form **112** will likely be faster than cyclization to **111**, and **113** requires a double-ion template, which will form more slowly than the single-ion template required for **112**. In general, **111**, **112**, and **113** have fairly weak binding affinities to the larger metal cations (K^+ and Cs^+), compared to the previously described examples. Macrocycles **111** and **113** both have enthalpically favorable, weak 1:1 binding affinities for K^+, and **112** has a strong, enthalpically disfavored 2:1 binding affinity. The thermodynamically disfavored double-ion binding of the 24-membered ring may result in a diminished rate of cyclization, and potentially promote the formation of a 30-membered ring, which is *not* formed in the untemplated oligomerization. Lastly, **112** and **113** weakly bind Cs^+, while **111** does not, which is hypothesized to result in modest amplification of both of the former.

Figure 28. Use of ITC to predict changes in product size distribution from 110[a]

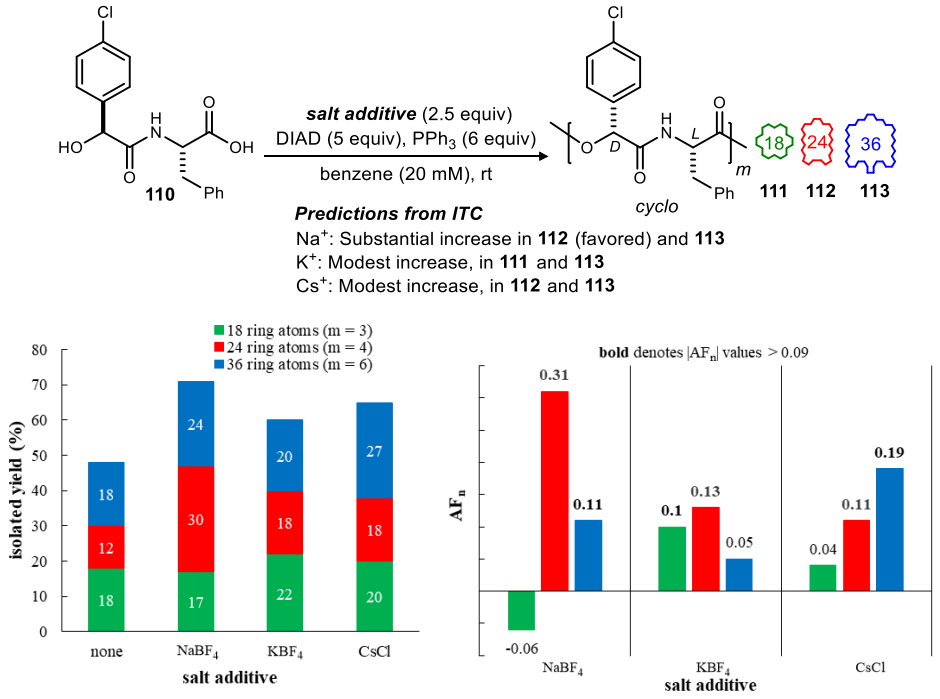

template	*18-mem ring* (111)			*24-mem ring* (112)			*36-mem ring* (113)		
	K_a (M^{-1})	ΔH	N	K_a (M^{-1})	ΔH	N	K_a (M^{-1})	ΔH	N
Na^+	$3.79x10^4$	–	1:1	$1.21x10^5$	–	1:1	$4.13x10^4$	+	2:1
K^+	$7.58x10^3$	–	1:1	$1.75x10^4$	+	2:1	$4.88x10^3$	+	1:1
Cs^+	$<1.00x10^3$			$5.65x10^3$	–	1:1	$6.54x10^3$	+	1:1

[a]ITC binding affinities $<1x10^3$ M^{-1} are not detected

Next, these predictions were compared to the outcomes when **110** was subjected to MCO conditions using the various ion templates. As shown in Figure 28 the size-distributions of macrocycles formed in the presence of salts are largely aligned with the predictions made from ITC measurements. Out of the three salt additives, Na^+ and Cs^+ provided size-distributions that most closely resembled the predictions. The addition of Na^+ substantially amplified the strongest-binding macrocycle (**112**), and modestly increased **113**, while Cs^+ significantly increased **112** and **113**, relative to the control, in modest amounts as predicted. The template effect of K^+ was more difficult to predict because a 30-membered ring was not isolated from the salt-free conditions; hence, its binding affinity to K^+ is unknown, and the binding affinities of all three isolated macrocycles were weak. The significant, yet modest amplification of the 24-membered ring (**112**), concomitant with little amplification of the other two ring sizes may be due to K^+ causing the reaction to stall at the 24-membered linear precursor. The 24-membered ring (**112**) has an enthalpically unfavorable double-ion binding to K^+, which could mean that its linear precursor's rate of inter- and intramolecular coupling are both slowed, resulting in the reaction to stall at this intermediate. Because ion binding is a reversible process, the amplification of **112** could be due to untemplated cyclization of some of its accumulated linear precursor.

3.4 Conclusion

In summary, we have implemented ITC as a tool to study macrocycle-template binding interactions, and show that these measurements can be correlated to size-distributions of depsipeptides formed during Mitsunobu-based MCOs. These studies have identified key trends (summarized in section 3.3.3, Figure 26) in quantitative metal ion-cyclic depsipeptide binding interactions across discrete collections of macrocycles. Importantly, these behaviors can be elucidated across collections of macrocycles formed from monomers of different sizes (didepsipeptide vs tetradepsipeptide), stereochemistry (D,L vs D,D macrocycle precursor), and side-chains (aliphatic, aryl). The thermodynamic trends highlighted in this chapter provide the first analytical platform to rationally select a template for a targeted size-regime of cyclodepsipeptides. Our current efforts are directed at broadening the synthetic impact of this method by continuing to expand our scope of cyclodepsipeptides, while uncovering more structure-related trends with ITC measurements. Future studies will explore this tool further, perhaps as a measure to correlate antibiotic activity of cyclodepsipeptides with ion-binding selectivity.[53]

Chapter IV

IV. Trends in monomer stereochemistry & sterics with MCO size distribution

4.1 Introduction

We have established a methodology to rapidly synthesize collections of CODs with unprecedented ease, and have found that the relative distributions of products in each collection can be modulated in the presence of an alkali metal salt. We then implemented ITC as a tool to study macrocycle-template binding interactions, and showed that these measurements can be correlated to size-distributions of depsipeptides formed during Mitsunobu-based MCOs. These studies have identified key trends in quantitative metal ion-cyclic depsipeptide binding interactions across discrete collections of macrocycles. MCO results from $[HyHept\text{-}Ala]_n$ monomers of different sizes (didepsipeptide vs tetradepsipeptide) and stereochemistry (L,L or L,D), ground the basis of these trends. Efforts to extend the generality of these trends were described using results generated from a new L,L-monomer with aryl residues.

Figure 29. HyIv-containing COD natural products

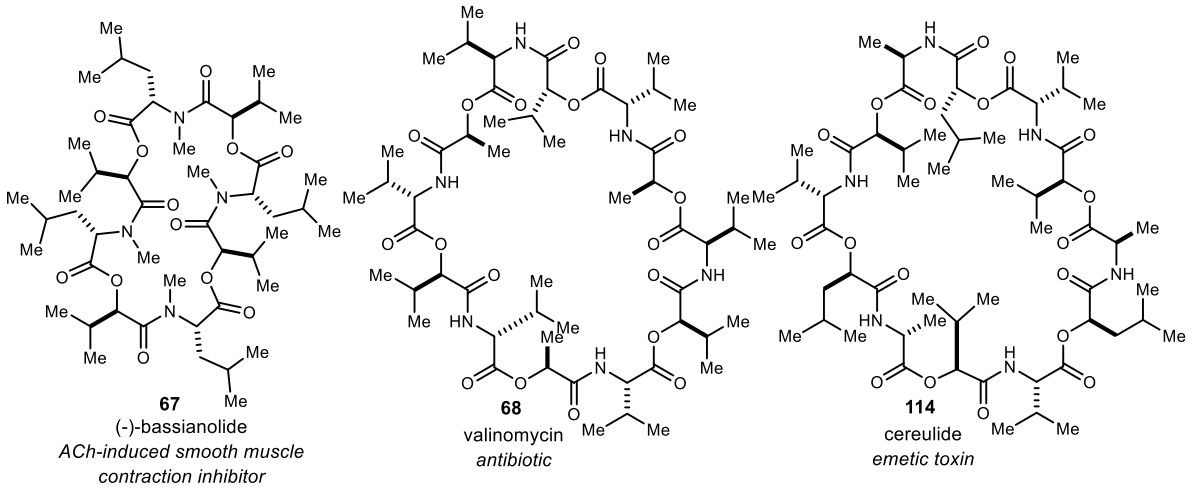

Another important stereochemical pattern that we have yet to investigate, and that is found in COD natural products is a repeating subunit of D,D,L,L-hydroxy and amino acids. Valinomycin[123] (**68**) and cereulide[124] (**114**) are two important members of this class, both of which contain D-α-hydroxyisovaleric acid (HyIv) residues (Figure 29)—a hydroxy acid found in a number of COD natural products, including (-)-bassianolide (**67**). However, our synthesis of (-)-bassianolide (Chapter 2) revealed that steric hindrance plays a significant role in the overall efficacy of our method, in addition to the size distribution of products formed. Therefore, we wondered if the steric effects from HyIv residues could be overcome by the stereochemical pattern of the monomer.

[123] Brockmann, H.; Schmidt-Kastner, G. *Chem. Ber.* **1955**, *88*, 57.
[124] Suwan, S.; Isobe, M.; Ohtani, I.; Agata, N.; Mori, M.; Ohta, M. *J. Chem. Soc., Perkin Trans. 1* **1995**, 765.

As our ultimate goal for this methodology is to develop a tool to predictably synthesize a particular size regime of macrocycles, we extended our studies to understand the effects of stereochemistry and steric hindrance on the resulting size-distribution of macrocycles.

4.2 Correlation of stereochemistry and sterics: D,L-macrocycles

4.2.1 MCO-based synthesis of (-)-bassianolide: A case study

In Chapter 2, we established that the synthesis of (-)-bassianolide using our first generation modular-convergent route was not feasible because alcohol **103** and acid **104** were unable to undergo Mitsunobu coupling to form octadepsipeptide **105** (Scheme 39). This dearth of reactivity in a straightforward Mitsunobu coupling motivated us to determine whether sterics around the hydroxyl group or carboxylic acid had a greater effect on product formation relative to the other.

Steric effects of the branched hydroxyl and amino acids were further investigated in coupling the hindered substrates (**99** and **100**) with the analogous substrates from our (-)-verticilide synthesis (Scheme 42). As we suspected, the β,β-disubstituted α-hydroxy residue is the most likely cause of the diminished yields in our route to (-)-bassianolide, affording mixed depsipeptide **115** in only 42% yield. The branched leucine residue adjacent to the carboxylic acid (**100**) did not seem to affect the reaction, affording mixed depsipeptide **116** in 86% yield.

Scheme 42. Investigation of steric hindrance, independently in α-oxy and carboxylic acid Mitsunobu reactants

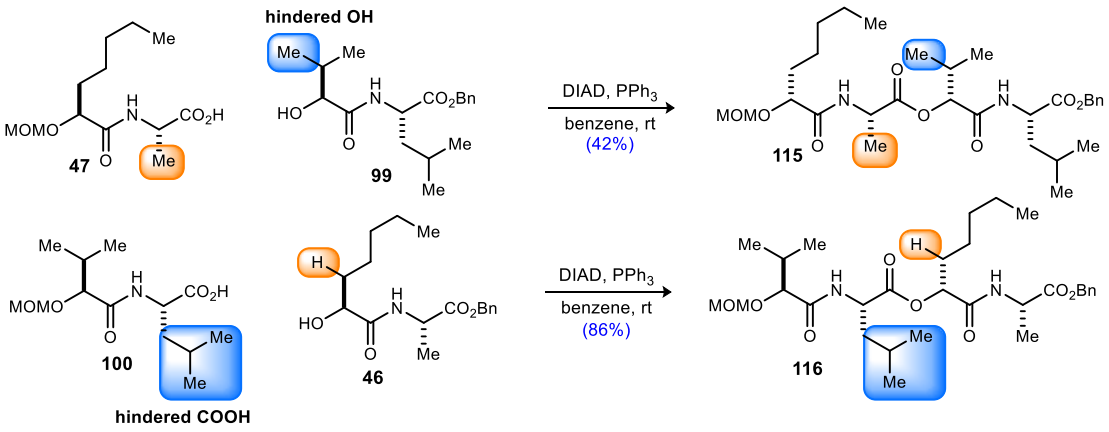

In addition to steric hindrance, α-helical conformation of the depsipeptide chain has been reported as a major contributing factor to difficult macrocyclizations.[79,125] In general peptide chains that contain alternating D and L stereochemistry,[126] and those with bulky residues (valine, isoleucine) alternating with leucine, phenylalanine, or alanine[127] tend to favor a helical conformation. For depsipeptides, however, the ester oxygens tend to work as a β-sheet breakers, and hence promote α-helical structure.[128] This structural phenomenon is caused by electronic

[125] Naganawa, H.; Takita, T.; Suzuki, A.; Tamura, S.; Lee, S.; Izumiya, N. *Agric. Biol. Chem.* **1976**, *40*, 2223.
[126] Jourdan, F.; Lazzaroni, S.; Méndez, B. L.; Lo Cantore, P.; de Julio, M.; Amodeo, P.; Iacobellis, N. S.; Evidente, A.; Motta, A. *Proteins: Struct., Funct., Bioinf.* **2003**, *52*, 534.
[127] Levitt, M. *Biochemistry* **1978**, *17*, 4277.
[128] Oku, H.; Yamada, K.; Katakai, R. *Biopolymers* **2008**, *89*, 270.

repulsion between amide carbonyl groups and ester oxygen groups, which becomes more significant with increased chain length.

Based on these reports, the substrates used in our synthesis of (-)-bassianolide, which are alternating amide and ester, containing helix-promoting building-blocks, should prefer to reside in an α-helical conformation which deters cyclization. However, tetradepsipeptide (**117**) also fits the criteria for a preferred helical conformation, but when subjected to our optimized MCO conditions, was able to provide 24-membered ring **118** in 74% yield (Scheme 43). Interestingly, the 24-membered ring was the only ring size isolated from the reaction, just as the 24-membered ring was the only ring size formed with the tetradepsipeptide precursors to (-)-bassianolide and (-)-verticilide. This outcome supports our hypothesis that $NaBF_4$ promotes preorganization of the didepsipeptide to form the 24-membered ring, and suggests that the diminished reactivity observed in the MCO with **102** is likely caused by intramolecular hydrogen bonding interactions which stabilize a conformation where the hydroxyl group is largely shielded by the bulky α-hydroxy sidechain.

Scheme 43. MCO of mixed L,L,D,L-tetradepsipeptide 117

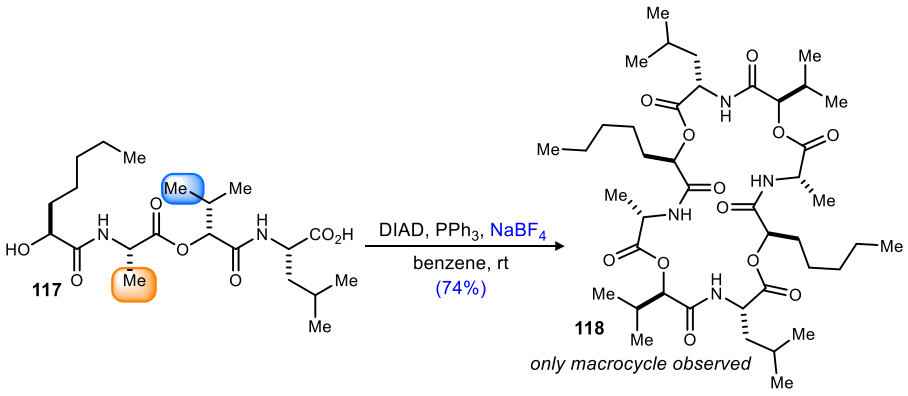

4.2.2 Comparison of steric effects with L,L-didepsipeptides

In our studies with (-)-verticilide we observed that didepsipeptide monomer **74** had an inherently fast rate of intramolecular coupling, and good overall yield of macrocyclic products without a salt additive (65%). We therefore hypothesized that the use of **119** would be a more reactive replacement for **102,** and potentially allow for a larger size distribution of rings to form in addition to forming the 24-membered ring (**91**) in higher yield. Unfortunately, **119** did not provide any additional macrocyclic products relative to its original tetradepsipeptide congener—the monomer was mostly converted to linear acylated DIAD derivatives and 5% yield of the 24-membered ring was observed. However, when the L-HyIv and L-Leu residues were exchanged for planar analogs, reactivity is restored and didepsipeptide **110** provided cyclized products in an overall 48% yield. Compared to didepsipeptide **74** the yield of macrocycles from **110** is substantially lower due to $A^{1,3}$-strain from the phenyl rings. Additionally the conformational rigidity that results from sterically hindered residues has a direct effect on the range of ring sizes that will be formed in the MCO[129,130] —the least number of products is observed with our most

[129] Huang, F.; Nau, W. M. *Angew. Chem. Int. Ed. Engl.* **2003**, *42*, 2269.
[130] Al Toma, R. S.; Brieke, C.; Cryle, M. J.; Sussmuth, R. D. *Nat. Prod. Rep.* **2015**, *32*, 1207.

hindered monomer (**119**), and the most with the least hindered monomer (**74**), as summarized in Figure 30.

Figure 30. Relationship between steric hindrance and MCO product size distribution without salt

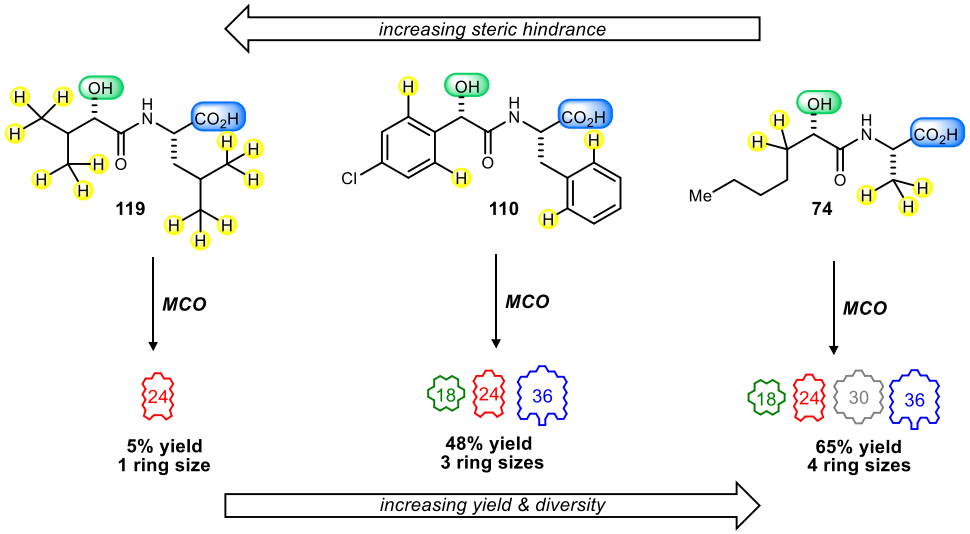

4.2.3 Mandelic acid residues violate the expected C_n-symmetry of D,L macrocycles

Mandelic acid-derived chiral auxiliaries are well established reagents used to derivatize chiral compounds to determine their absolute stereochemical configuration by ^{1}H NMR. The structure of the chiral auxiliary is important for this purpose because it must be able to fix a particular conformation (rigidity) and contain a group that is able to produce a consistent space-oriented anisotropic effect (aromatic ring) that selectively shields or deshields substituents on the attached substrate.[131] Anisotropic effects of functional groups in ^{1}H NMR spectra have been reported to occur with aryl residue-containing peptide and depsipeptide macrocycles. However, this phenomenon is more common when there is an aryl moiety within the ring.[132] A more common cause of shifted peaks in ^{1}H NMR spectra with aryl residue-containing depsipeptides result from the rigid nature of the aryl group and the flexibility of the ester linkages. Depsipeptide natural products triostin C (**120**) and echinomycin (**121**) appear as unsymmetrical molecules by NMR, despite their apparent C_2-symmetry (Figure 31). X-ray crystal structures reveal that their effective C_2-symmetry is prevented by the twisting (ca 50°) of one of the quinoxaline rings in echinomycin (**121**) and by a rotation of one of the ester linkages with the formation of an intramolecular hydrogen bond in triostin C (**120**).[133]

[131] Seco, J. M.; Quiñoá, E.; Riguera, R. *Chem. Rev.* **2004**, *104*, 17.
[132] Morais, M.; Zamora-Carreras, H.; Raposinho, P.; Oliveira, M.; Pantoja-Uceda, D.; Correia, J.; Jiménez, M. *Molecules* **2017**, *22*, 1189.
[133] Sheldrick, G. M.; Heine, A.; Schmidt-Base, K.; Pohl, E.; Jones, P. G.; Paulus, E.; Waring, M. J. *Acta Crystallogr. B.* **1995**, *51 (Pt 6)*, 987.

Figure 31. Conformation-induced symmetry-breaking effects in C_2-symmetric depsipeptides

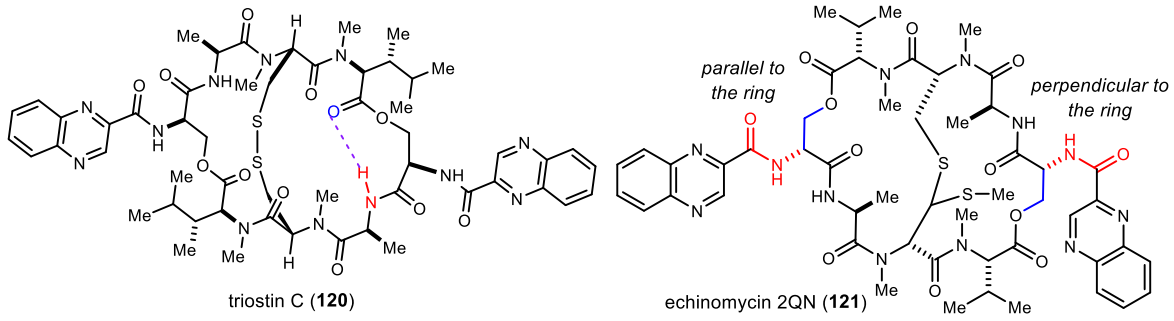

Interestingly, the depsipeptide macrocycles with 4-ClMan residues from this work appeared as either a single asymmetric conformer (**111**), or a symmetric conformer with apparent minor asymmetric conformers present (**112** and **113**), whereas those with aliphatic residues only appear as a single symmetric conformer. This phenomenon was especially apparent with the 18-membered ring (**111**)—the most sterically congested of the three sizes formed from the MCO, and therefore it's most likely to contain a twisted aryl ring or rotated ester linkage to relieve ring strain. 2D-NOESY experiments on **111** showed NOEs between Phe-2 aryl ring and Phe-1 N-H, and 4-ClMan-1 C-H (Figure 32, highlighted in red), which explains why the macrocycle's expected C_3-symmetry is broken. In order to accommodate these NOEs, the ester linkage between Phe-2 and 4-ClMan-3 is likely rotated so that Phe-2 can rest under the macrocycle instead of around the

Figure 32. Relevant NOE correlations for 18-membered ring 111 in CD_3CN

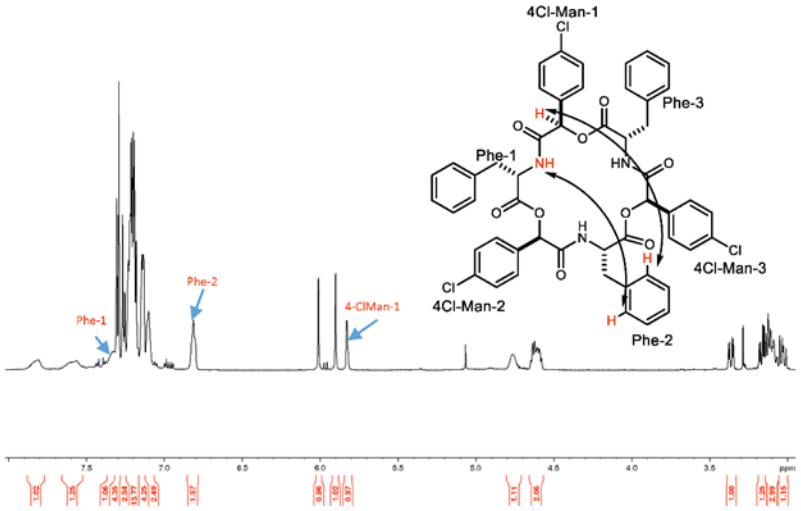

around the outside. The 18-membered ring was also found to prefer different conformations when it was analyzed by ^{1}H NMR in various solvents. For example, **111** was completely asymmetric in DMSO and MeCN, and a very broad, nearly symmetric conformer in $CDCl_3$. This shift in peak ratios confirms that the unusual absence of symmetric that we initially observed by ^{1}H NMR was a result of solvent-dependent conformation, and not epimerization of a stereocenter.

4.3 Correlation of stereochemistry and sterics: D,D,L,L-macrocycles

From the trends observed with L,L-didepsipeptide *seco*-acid monomers, we were able to see a clear correlation between sterics around the hydroxyl group and the overall yield of macrocycles formed in the initial MCO without a salt additive. Furthermore, we observed that the range of ring sizes formed in the MCO correlate to steric hindrance, where the least hindered monomer will form the widest range of ring sizes and the most hindered will provide the narrowest distribution. With broadening our scope of monomer stereochemistry in mind, we then shifted our studies to L,D,L,L-tetradepsipeptide monomers to synthesize collections of valinomycin-like macrocycles with D,D,L,L repeating units. Here, we are interested in determining if the trends with stereochemistry follow suit with the previous example, and what new behaviors will occur in the MCO by changing the tetradepsipeptide monomer stereochemistry.

4.3.1 Introduction to valinomycin & synthetic derivatives

Valinomycin (**68**, Figure 29) is a cyclic depsipeptide natural product that was first isolated in 1955 from *Streptomyces*.[123] This depsipeptide antibiotic which is composed of three (D-HyIv-D-Val-L-Lac-L-Val) tetradepsipeptide subunits, has been heavily studied in this field due to its ability to act as a selective potassium ion carrier in biological membrane systems. In fact, it displays the best potassium to sodium selectivity of all known potassium ionophores.[134] This favorable selectivity offers important advantages in the use of valinomycin with potassium selective electrodes.[135] Because of its high ion selectivity, it is a desirable scaffold to create new ionophoric depsipeptides with sidechains that can be tethered to a membrane (e.g. lysine) or residues that carry chromophores that are sensitive to a particular bound ion.[136] However, there are very few studies with modified valinomycins due to synthetic limitations. As mentioned in Chapter 1, synthesis of alternating amide-ester depsipeptides is highly challenging on solid phase, so solution phase synthesis is preferred. In that regard, condensative amidation approaches have been developed in solution,[136,137,138] but they suffer from disadvantages such as 24-hour addition time of coupling reagent for the final macrolactonization, and having to handle and purify large depsipeptide intermediates. Rothe developed a cyclooligomerization approach,[56,57] which had the advantage of fewer steps, but at the expense of yield (7%). Therefore, an approach which can rapidly provide valinomycin-inspired cyclodepsipeptides in good yield would be a valuable contribution to the field.

[134] Ivanov, V. T.; Laine, I. A.; Ryabova, I. D.; Ovchinnikov, Y. A. *Chem. Nat. Compd.* **1970**, *6*, 753.
[135] Armstrong, R. D. *Electrochim. Acta* **1987**, *32*, 1549.
[136] Dawson, J. R.; Dory, Y. L.; Mellor, J. M.; McAleer, J. F. *Tetrahedron* **1996**, *52*, 1361.
[137] Dory, Y. L.; Mellor, J. M.; McAleer, J. F. *Tetrahedron Lett.* **1989**, *30*, 1695.
[138] Kuisle, O.; Quiñoá, E.; Riguera, R. *J. Org. Chem.* **1999**, *64*, 8063.

4.3.2 MCO-based synthesis of 4-FMan-valinomycins

Our quest to synthesize modified valinomycins began with the synthesis of tetradepsipeptide monomer **122**. In **122**, the HyIv residue that is present in the analogous tetradepsipeptide monomer for *nat*-(+)-valinomycin (**123**) is replaced with a more planar substitute in the form of 4-fluoro mandelic acid (4-FMan) because of the low reactivity that was previously observed with tetradepsipeptide **102** (Figure 33). A fluorinated aryl ring was designed to endow the products with a unique NMR-active nucleus. ^{19}F NMR could therefore be leveraged to measure yields from crude reaction mixtures, since ^{1}H NMR has thus far not been a viable option due to overlapping peaks.

Figure 33. Steric comparison between monomers 122 and 123

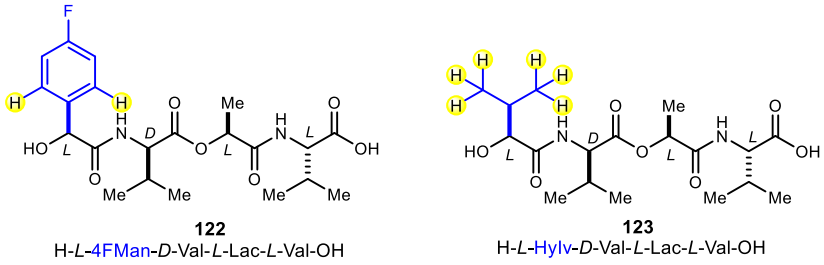

Our route to **122** began with the synthesis of tridepsipeptide amine **128** (Scheme 44). The strategy here was to synthesize an amine with 3 of the common residues of valinomycin, so that tetradepsipeptide derivatives that vary at the hydroxyl terminus could be readily synthesized in UmAS. DEPBT-mediated coupling between D-lactic acid sodium salt (**124**) with L-valine benzyl ester (**125**) provided didepsipeptide alcohol (**126**), which underwent a Mitsunobu reaction with Boc-D-valine (**127**) to afford the Boc-protected tridepsipeptide. Boc-Deprotection with 4 M HCl/dioxanes afforded the amine hydrochloride salt (**128**), which was triturated with diethyl ether, and then used in subsequent reactions without further purification.

Scheme 44. Synthesis of tridepsipeptide amine 128

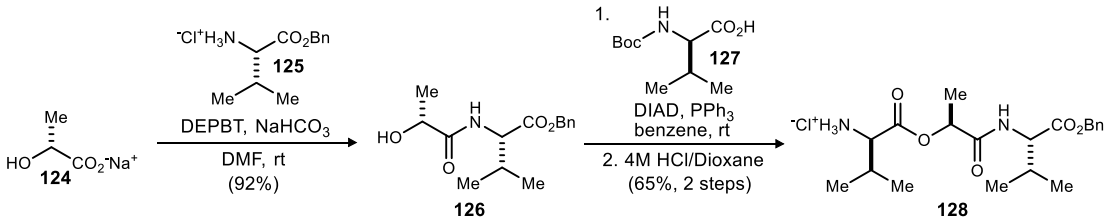

With amine **128** in hand, the usual sequence for MCO monomer synthesis was followed (Scheme 45). Our optimized enantioselective Henry conditions (Blay catalyst **27** at -20 °C), followed by MOM protection provided bromonitroalkane **129** in high yield and enantioselection. Once again, contrary to previous literature reports,[18] **129** is a solid and could be recrystallized to furnish enantiopure material. Donor **129** was coupled to amine HCl salt **128** under UmAS conditions to afford tetradepsipeptide **130**. The MOM-ether was then deprotected using BF_3•OEt_2

and thiophenol, and the benzyl ester was removed via hydrogenolysis with palladium on carbon in ethyl acetate to afford the tetradepsipeptide *seco*-acid monomer **122**.

Scheme 45. Synthesis of tetradepsipeptide 122

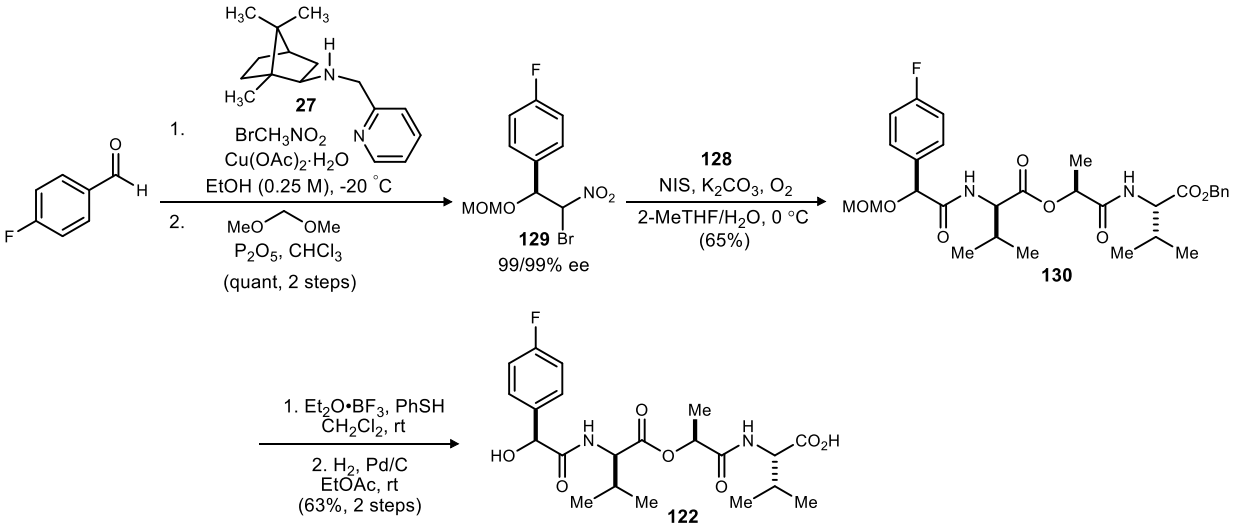

Hydroxy acid **122** was then subjected to our optimized MCO conditions without salt for tetradepsipeptide monomers, and the crude reaction mixture was analyzed by ^{1}H NMR and ^{19}F NMR. As observed in previous examples, the ^{1}H NMR spectrum had many overlapping peaks, and thus was a poor tool to gauge ratios of products. The ^{19}F NMR spectrum clearly indicated that starting material was consumed, and there were several peaks in the region expected for macrocyclic products, many of which were overlapping. Although ^{19}F NMR would not be a viable tool to determine NMR yields of products, it is a much more straightforward tool to match isolated

Figure 34. Stacked ^{19}F NMR comparison of macrocycles from 122

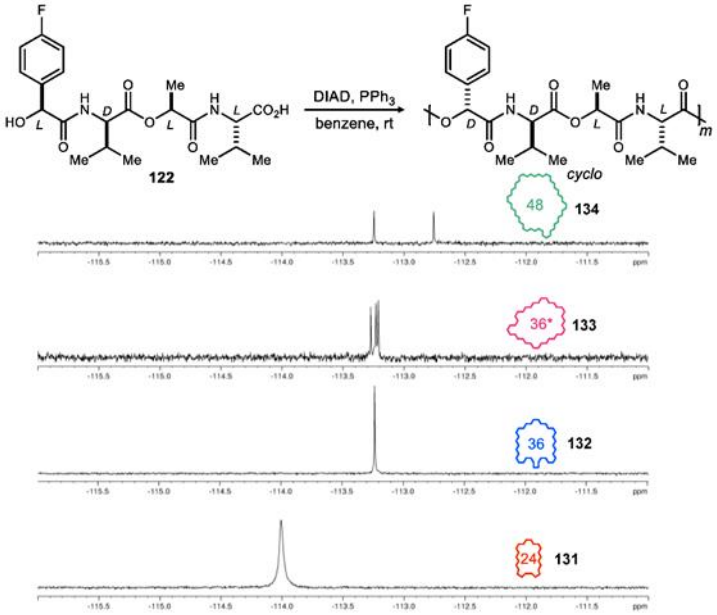

products with the original contents of the crude reaction mixture. As observed with the 4-ClMan hydroxy acid (**110**), the overall yield of the untemplated MCO was not as high as observed with our (-)-verticilide tetradepsipeptide (**70**), likely due to $A^{1,3}$ strain from the aryl ring. However, it was much higher than observed with **110** and a collection of 24-, 36-, and 48- membered rings were isolated in 63% overall yield (Figure 34).

Figure 35. Relevant NOE correlations for asymmetric 36-membered ring 133 in DMSO-d_6

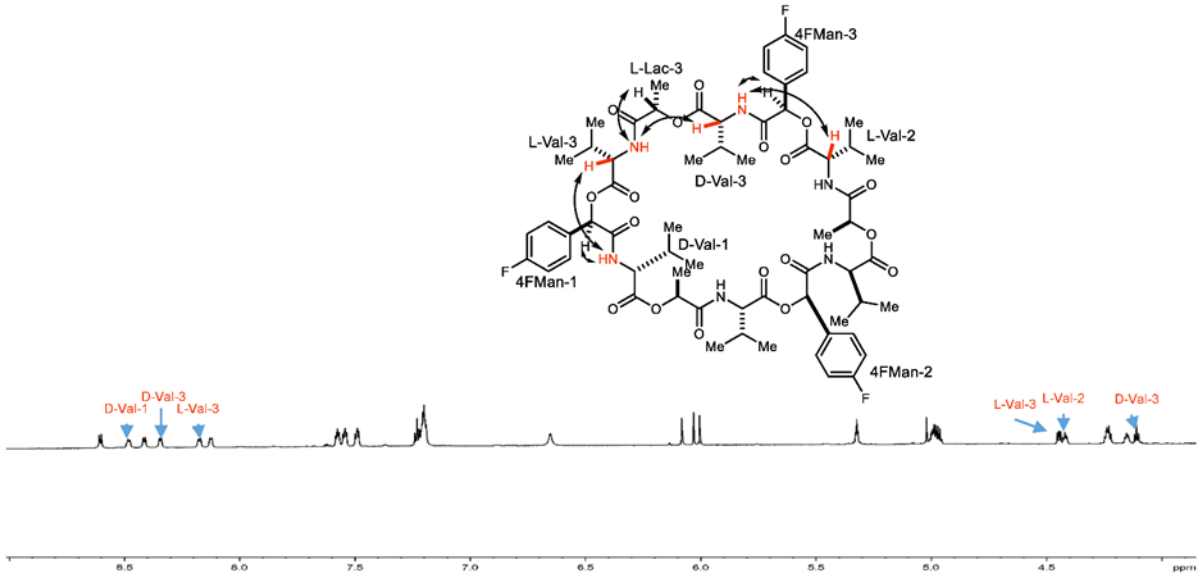

The 24 membered ring (**131**) was isolated in 35% yield as a single symmetrical conformer. The 36-membered ring however, was slightly more complex—it was isolated in 13% yield as a symmetric conformer (**132**), but another macrocycle (**133**) that had identical molecular weight (as per LCMS analysis) and eluted approximately 3 minutes before it on preparatory HPLC, was isolated in 6% yield. Further TOF and MS/MS analysis revealed that this macrocycle had a similar time of flight and MS/MS fragmentation pattern as the 36-membered ring, which indicates that it is, indeed, the same size. However, its ^{1}H NMR spectrum (Figure 35) has 3x the amount of peaks that it should have, in addition to 3 distinct fluorine peaks by ^{19}F NMR (Figure 34). 2D-NMR experiments were conducted on **133** to learn more about its structure: HMBC confirmed it is one continuous macrocycle, and not two interlinked. However, 2D-NOESY showed long range cross-peaks (highlighted in red) which indicate that two 4-FMan ester linkages and one L-lac ester linkage were twisted, giving rise to an asymmetric conformation (Figure 35). This macrocycle did not appear be converting to a symmetrical conformer by ^{1}H NMR in DMSO-d_6. However, further spectral comparison between **133** and **132** revealed that the central fluorine peak of **133** overlapped with the symmetrical conformer (**132**). Additionally, there are some peaks that are identical between the two compounds by ^{1}H NMR. Therefore, **133** is likely a stable and separable asymmetric conformer of **132**. This type of stability between conformers has not been reported for any cyclooligodepsipeptides, to date. However, there are reports of other types of depsipeptide and

peptide macrocycles that exist in two separable conformers.[139,140,141,142] Depsipeptide macrocycle triostin A is a good example of this—its activation energy for conformational interconversion is reported to be >22 kcal/mol, which results in two stable and separable conformers.[133] X-Ray crystal structures of the conformers revealed that the large energy barrier between the two conformers likely exists because a conformational change would involve breaking hydrogen bonds on each side of the molecule, and disrupting π-stacking interactions.[133]

Valinomycin is known to reside in a bracelet-like conformation, which is highly stabilized by H-bonds between the amide *N*-H's and ester carbonyls.[143] Therefore, the high energy barrier between **132** and **133** is likely due to the activation energy necessary to break a stable H-bonded network. The amounts of **132** and **133** that were isolated in the reaction, relative to what was present by crude ^{19}F NMR indicates that **132** is not converting to **133** over time, and must be formed from a specific conformation of the linear precursor in the MCO.

The last macrocycle (**134**) isolated from the reaction also had an interesting asymmetric conformation (Figure 36). Its ^{1}H NMR spectrum revealed twice the number of peaks as expected, and ^{19}F NMR showed two very distinct fluorine resonances. None of these resonances overlapped at all with the 24-membered ring, and TOF and MS/MS analysis confirmed that this macrocycle

Figure 36. Relevant NOE correlations for 48-membered ring 134 in DMSO-*d*$_6$

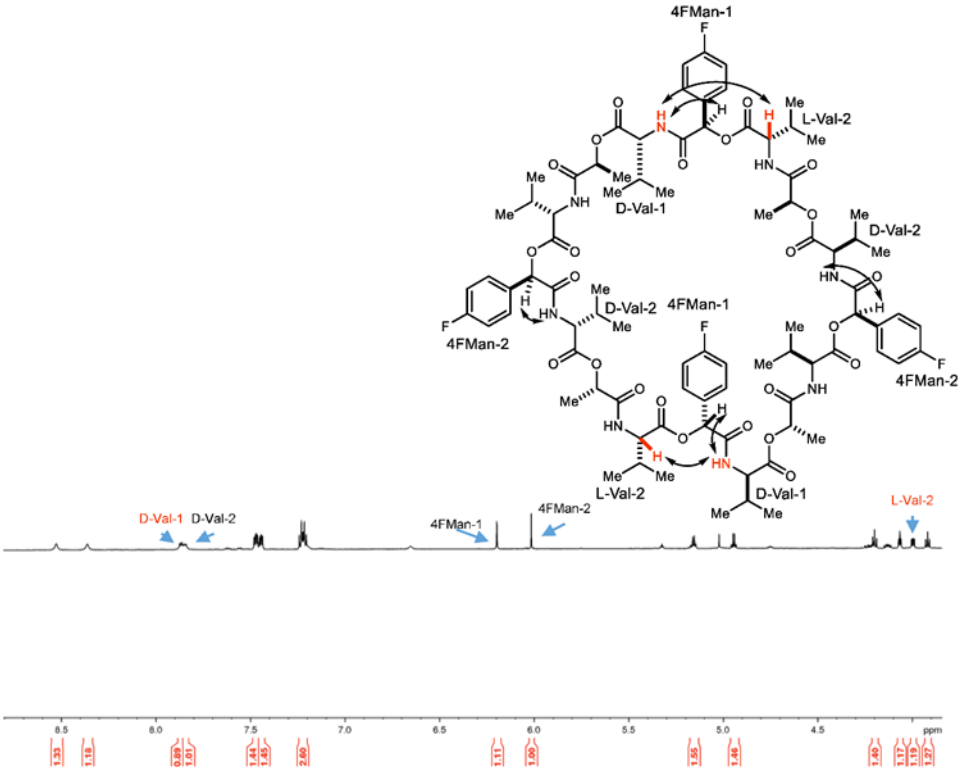

[139] Steinmetz, H.; Gerth, K.; Jansen, R.; Schläger, N.; Dehn, R.; Reinecke, S.; Kirschning, A.; Müller, R. *Angew. Chem. Int. Ed.* **2011**, *50*, 532.
[140] Tomooka, K.; Uehara, K.; Nishikawa, R.; Suzuki, M.; Igawa, K. *J. Am. Chem. Soc.* **2010**, *132*, 9232.
[141] Denekamp, C.; Gottlieb, L.; Tamiri, T.; Tsoglin, A.; Shilav, R.; Kapon, M. *Org. Lett.* **2005**, *7*, 2461.
[142] Tabudravu, J. N.; Jaspars, M.; Morris, L. A.; Kettenes-van den Bosch, J. J.; Smith, N. *J. Org. Chem.* **2002**, *67*, 8593.
[143] Bystrov, V. F.; Gavrilov, Y. D.; Ivanov, V. T.; Ovchinnikov, Y. A. *Eur. J. Biochem.* **1977**, *78*, 63.

was not a conformer of the 24-membered ring, but instead our first 48-membered ring, isolated in 8% yield. HMBC confirmed that **134** was a continuous 48-membered macrocycle, and 2D-NOESY revealed that its expected C_4-symmetry was broken by 2 twisted ester linkages (highlighted in red) to afford ^{1}H NMR (Figure 36) and ^{19}F NMR (Figure 34) spectra with apparent C_2-symmetry.

Having established the structures of our new macrocycles formed without templation, tetradepsipeptide **122** was subjected to templated MCO conditions. The results of the templated experiments are summarized in Figure 37 . Overall, the collection of ring sizes seemed to be less promiscuously affected by the addition of a metal ion template. This is not terribly surprising because valinomycin's rigid and hollow cylindrical structure is what gives it such specific potassium ion affinity. The D,L-macrocycles that we have analyzed previously have much more inherent conformational freedom to interact with a wider range of ion sizes. The D,D,L,L-stereochemical pattern allows the macrocycles in this collection to adopt more rigid, "valinomycin-like" conformations. Therefore, matching ion binding site size with cation size will be more necessary for a significant templating effect in the MCO.

Figure 37. Examination of stereochemical effects in the MCO by synthesis of D,D,L,L-macrocycles from 122[a]

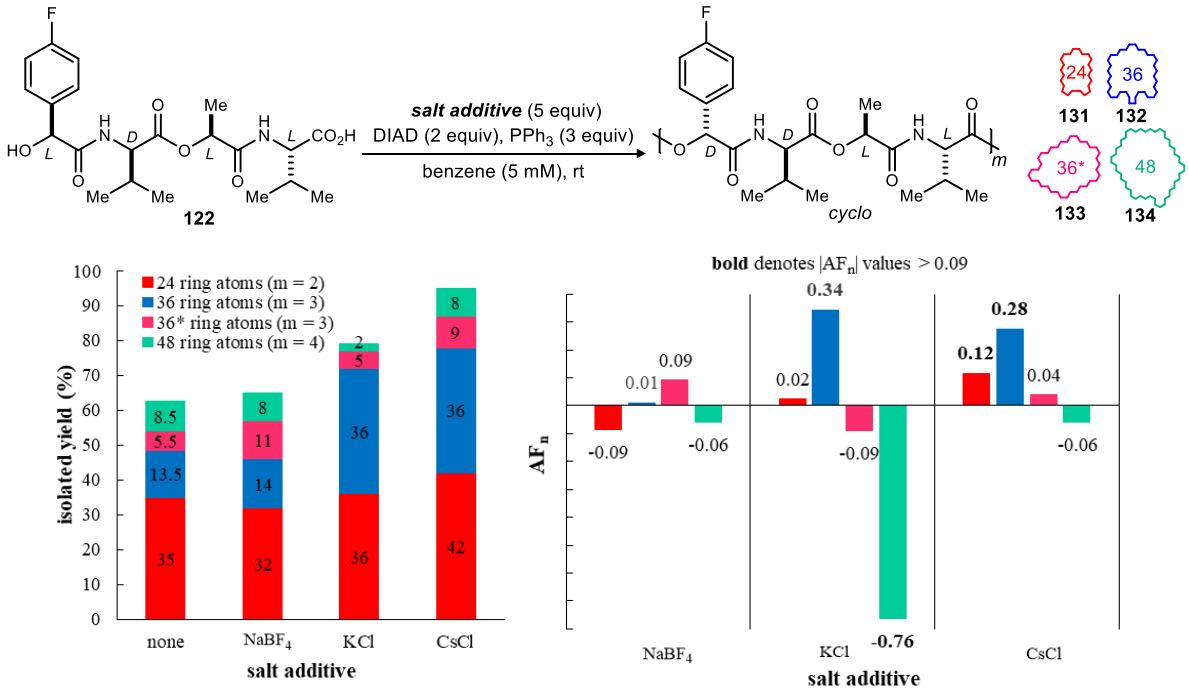

template	*24-mem ring* (**131**)			*36-mem ring* (**132**)		
	K_a (M^{-1})	ΔH	N	K_a (M^{-1})	ΔH	N
Na^+	<1.00x10^3			<1.00x10^3		
K^+	<1.00x10^3			8.85x10^3	–	1:1

[a]ITC binding affinities <1x10^3 M^{-1} are not detected

In this example, **131** and **132** were the only ring sizes that were substantially affected by the presence of an alkali metal salt template. However, no significant changes were observed with Na^+, which has largely been the metal cation with the most substantial effect on D,L-macrocycles. The D,D,L,L-macrocycles appeared to be more substantially influenced by larger ion templates.

Most notably, the 36-membered ring was formed in nearly 3x its original amount in the presence of K^+. The largest cation (Cs^+) significantly amplified both the 24- and 36-membered rings, and provided a 95% isolated yield of macrocycles overall.

As mentioned earlier in this chapter, valinomycin had the best K^+/Na^+ selectivity of all known potassium complexones.[53] In methanol, it is reported to have a binding affinity for K^+ that is >10,000x stronger than Na^+. Valinomycin can also strongly bind Cs^+,[144] but its affinity for K^+ in methanol is still 3x greater. As valinomycin's claim-to-fame is its incredible K^+/Na^+ selectivity, ITC data was obtained to measure Na^+ and K^+ binding affinities with **131** and **132** (Figure 37).[145] Neither macrocycle has affinity for Na^+, and only the 36-membered ring (**132**) binds K^+, albeit more weakly than that observed in previous examples of depsipeptides with potassium ion-affinity. The limit of accurate detection on our ITC instrument is $1x10^3$ M^{-1}, so if **132** bound sodium ions with similar affinity as valinomycin (around $4x10^0$ M^{-1}), it would not be detected.

However, the K^+-selective binding here allows the 36-membered ring (**132**) to be increased substantially because its rate of formation can be increased selectively over the 24-membered ring. The 36-membered ring is not formed as the only product due to the lack of a strong driving force from formation of a strong K^+-binding product. Nonetheless, this example marks the most substantially increased example of a cyclotrimerization that we have observed from a tetradepsipeptide monomer thus far.

4.3.3 MCO-based synthesis of the natural valinomycins

The promising results we obtained from tetradepsipeptide **122**, despite $A^{1,3}$ strain from the α-hydroxyl aryl groups gave us incentive to synthesize the tetradepsipeptide precursor to the natural product valinomycin, as outlined in Scheme 46.

Scheme 46. Synthesis of tetradepsipeptide *seco*-acid 123

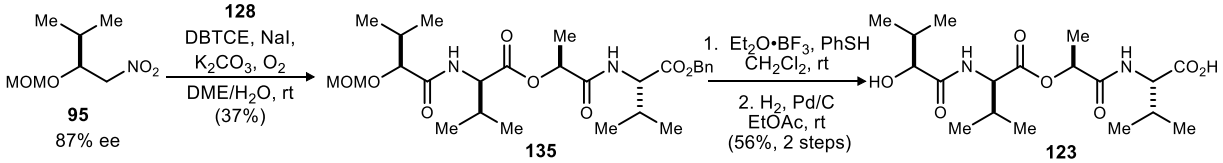

MCO of **123** (Scheme 47) provided two main compounds, both of which happen to be natural products: montanastatin (**136**, 24-membered ring), and valinomycin (**68**, 36-membered ring). These two products were retrieved in 15% and 8% yields, respectively, and 23% yield overall. Unlike our MCO with **102** for (-)-bassianolide, starting material (**123**) was not recovered, nor observed when the crude reaction mixture was analyzed by LCMS. *seco*-Acid **123** is clearly reactive in MCO conditions, despite containing an L-HyIv residue at the hydroxy terminus, but its intramolecular cyclization proves difficult. The behavior of **123** in the MCO is interesting, because if we compare **123** and **102** (Figure 38), both are sterically hindered monomers around the hydroxy terminus, and therefore both are relatively unreactive in MCO conditions. Their distinct behavior

[144] Valinomycin's binding affinity to cesium ions in methanol was reported to be around $2x10^4$ M^{-1}, and in the same article its affinity to potassium ions in methanol was reported to be around $6x10^4$ M^{-1} (ref 146).

[145] **131** and **132** were the only macrocycles analyzed by ITC because the other two were not substantially affected by ions, and therefore are predicted to not have significant binding affinity. I didn't measure their affinities to Cs^+. This was also before I ran the reaction with CsCl, so that data will be obtained before I leave Vanderbilt. (Or it will be the pilot ITC measurement to train Michael Crocker and Abby on the ITC).

Scheme 47. MCO with 123 to synthesize montanastatin and valinomycin

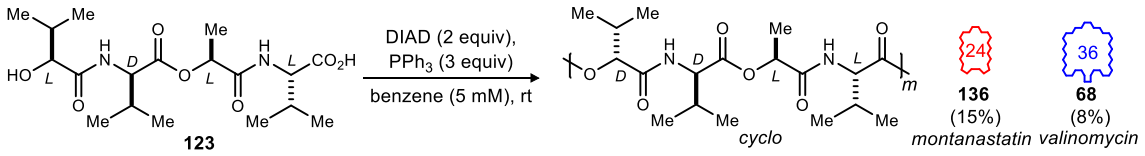

in the MCO is likely due to their differing stereochemical patterns. Precipitation and aggregation was not observed with **123**, as it was with **102** in MCO conditions, which can be explained by each monomers unique stereochemical sequence.

Figure 38. Comparison of MCO with HyIv-containing monomers 123 and 102

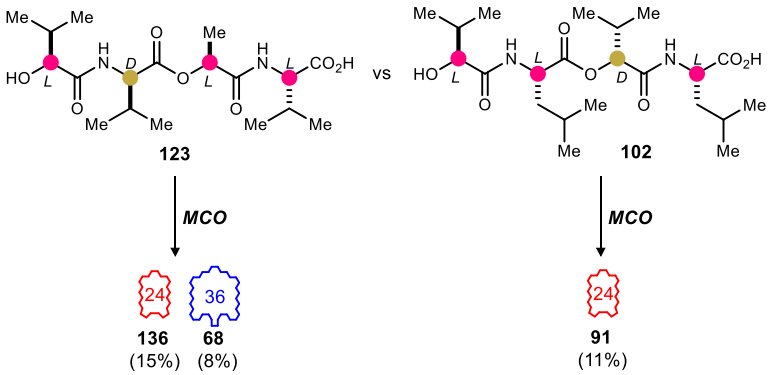

The binding affinity of valinomycin to K^+ was measured to be $5x10^4$ M^{-1}, which is in agreement with literature values.[146,147] Montanastatin was not analyzed by ITC because it does not bind Na^+, K^+, or Cs^+ at a level that would be detected with our instrument.[148] Valinomycin's ionophoric properties are what is responsible for its broad spectrum cytotoxicity. Montanastatin, on the other hand, is not known to be particularly ionophoric, and is also magnitudes less cytotoxic than valinomycin.[149] Perhaps these properties are foreshadowing for a potassium-spiked MCO: valinomycin's strong and selective driving force to complex with K^+ may drive the MCO to provide the 36-membered ring selectively. Results for the potassium-spiked MCO are on the horizon.[150]

4.4 Analysis of steric and stereochemical trends

From these studies, we are now able to elucidate trends which correlate steric hindrance around the hydroxy terminus and monomer stereochemistry to the size distribution of macrocycles that will be obtained from the MCO (Figure 39). In general, larger substituents adjacent to the hydroxy-terminus will generate narrower size distributions of macrocycles and lower overall

[146] Ehala, S.; Kasicka, V.; Makrlik, E. *Electrophoresis* **2008**, *29*, 652.
[147] Rose, M. C.; Henkens, R. W. *Biochim. Biophys. Acta, Gen. Subj.* **1974**, *372*, 426.
[148] Montanastatin, or "octa-valinomycin" was has affinities of 40 and 10 M^{-1} to Na^+ and K^+, respectively, in EtOH. Binding at this level is considered negligible for our purposes (ref 53)
[149] Pettit, G. R.; Tan, R.; Melody, N.; Kielty, J. M.; Pettit, R. K.; Herald, D. L.; Tucker, B. E.; Mallavia, L. P.; Doubek, D. L.; Schmidt, J. M. *Bioorg. Med. Chem.* **1999**, *7*, 895.
[150] Our prep-HPLC is broken. Crude K^+-spiked valinomycin MCO reaction is currently stored at -20 °C waiting to be purified

yields in the untemplated MCO. A clear example of this was presented in our studies with L,L-monomers to provide D,L-macrocycles, where the least hindered monomer (**74**) provided a collection of 4 different macrocycles, and the most hindered monomer (**119**) only provided one. This trend also exists with larger monomers (**70** and **102**), and with different stereochemical sequences (**122** vs **123**).

Our investigation of monomers with new stereochemical patterns revealed that L,D,L,L-monomers provide macrocycles with more specific ion interactions, and therefore have more selective amplification in the ion-templated MCO. A notable example of this was observed with 36-membered ring **131**, which selectively binds potassium and was amplified nearly 3x in the presence of a K^+-salt, while other macrocycles in the collection were not affected. Additionally, the conformation of L,D,L,L-monomers enables good reactivity in the untemplated MCO, despite sterics around the hydroxyl group. This conformational distinction allowed tetradepsipeptide **123** to undergo both cyclodimerization and trimerization in the untemplated MCO to provide montanastatin and valinomycin in a combined 23% yield, which is double the amount of 24-membered ring (**91**) isolated from the tetradepsipeptide precursor for (-)-bassianolide (**102**). Additionally, **123** was fully consumed at the end of the reaction, unlike with **102**, where starting material was recovered.

Figure 39. Steric and stereochemical trends for depsipeptide synthesis via Mitsunobu MCO

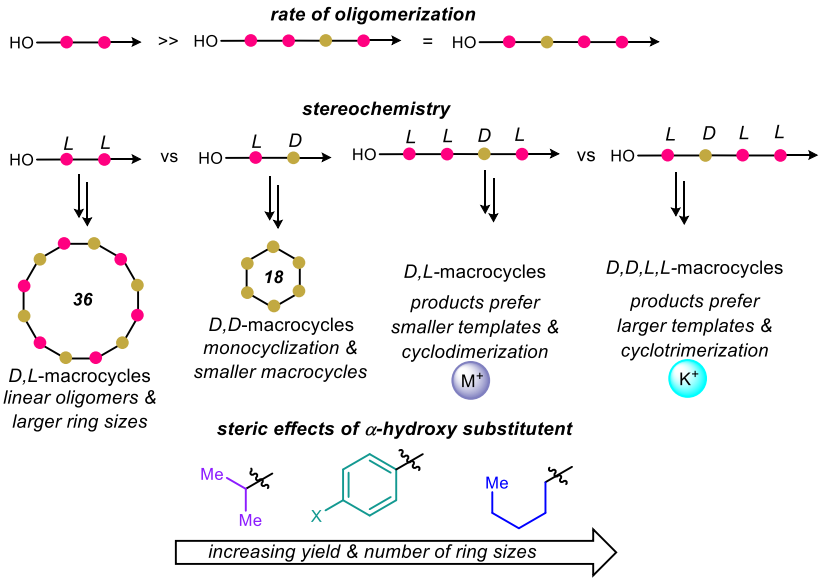

4.5 Conclusion

In summary, we have studied a scope of *seco*-acid monomers varying in size and steric hindrance to uncover more structure-related behavioral trends in the Mitsunobu MCO, and their impact on the resulting size distribution of products. These studies have identified key trends (summarized in section 4.3.3, Figure 39) that relate the variety of macrocycles formed in each collection to the steric hindrance surrounding the hydroxy terminus. Synthesis of new valinomycin-like tetradepsipeptide monomers revealed that amplification of macrocycles in the presence of a particular template can be tuned to be more selective with more conformationally rigid D,D,L,L macrocycles. These discoveries provide a useful addition to our previously

established trends (Chapter 3), and a valuable step toward our goal of broadening the synthetic impact of this method. Future studies will be directed at expanding the scope of templates used in the MCO for the synthesis of D,D,L,L macrocycles. Templates that previously shut down the MCO through excessive interaction with the Mitsunobu reagents may become viable options due to selective driving forces from formation of a strong template-binding product.

Chapter V

V. Illuminating the dark side of natural products

A longstanding driver for total chemical synthesis of natural products stems from nature's production of complex biologically active small molecules, and their limited accessibility in the chemistry world. As chemists, we are continuously aspiring to reach nature's synthetic efficiency with our own hands by filling our synthetic toolbox with new methodologies. Up until this point, my dissertation has detailed key aspects of a well-established pragmatic approach (Figure 20): development of new reactions/methods (MCO) to ultimately synthesize a complex biologically active target (verticilide). However, this program would not be complete without assaying the natural product and its natural product-like congeners for new, but also known, biological activity.

Figure 40. Overview of the relationship between new method development and therapeutic development

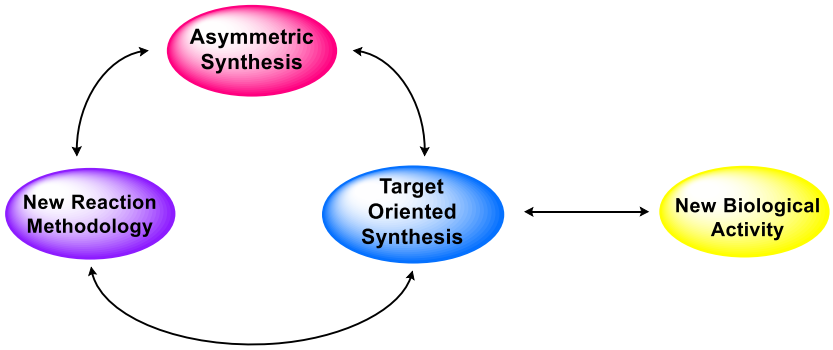

As discussed previously, (-)-verticilide was found to be a potent insect ryanodine receptor (RyR) agonist. Given its known RyR binding abilities, we hypothesized that verticilide may also act on the mammalian cardiac ryanodine receptor (RyR2). Hence, we began a collaboration with Dr. Björn Knollmann's laboratory, where the mechanistic contribution of RyR2 to potentially fatal arrhythmia syndromes is a main research focus. During this collaboration, I had the opportunity to work with two postdocs in the Knollmann lab: Dr. Nieves Gomez-Hurtado, and then Dr. Daniel J. Blackwell, who conducted the majority of the experiments that will be discussed here. This chapter will detail the biological studies (conducted by Dan and other collaborators) of (-)-verticilide and its unnatural enantiomer (synthesized by me), and the resulting discovery of a new antiarrhythmic small molecule.

5.1 Introduction

5.1.1 Ryanodine receptor 2 (RyR2) as a target for disease cures

Ryanodine receptors (RyR) are intracellular Ca^{2+} release channels that play a critical role in excitable tissue. Located in the endoplasmic or sarcoplasmic reticulum (ER, SR) membrane, RyRs are the largest known ion channels with a molecular mass of greater than 2 megadaltons. Cryogenic electron microscopy (cryo-EM) has been the primary tool for structural elucidation of RyRs, and it has gradually unveiled fine architectural details with increasing resolutions from

below 20 to 3.8 Å.[151,152,153] Ryanodine receptors are tetrameric in structure—composed of four identical protomers. Each protomer consists of a cytoplasmic region of over 4500 residues and a carboxyl terminal transmembrane (TM) domain. The four identical TM segments enclose a central ion-conducting pore, whereas the cytoplasmic regions serve as a scaffold for interactions with a diverse array of ligands and protein modulators, such as FKBP and calmodulin (CaM).[153] The large cytoplasmic region of RyR associates tightly with FKBP12 (RyR1) and FKBP12.6 (RyR2). These accessory proteins stabilize the RyR complex and enable the four subunits to open and close in a coordinated manner.[154] Calmodulin is a ubiquitous Ca^{2+}-binding protein that that serves as an intracellular Ca^{2+} sensor, and plays an important role in Ca^{2+} signaling. Calmodulin binds to and regulates RyR in a Ca^{2+}-dependent manner: at submicromolar Ca^{2+} concentrations CaM activates RyR1 and 3, but inhibits RyR2, and at micromolar Ca^{2+} concentrations CaM inhibits all RyR isoforms (reducing opening of the channel).[154] RyR are also controlled luminally through interactions with calsequestrin, junctin, and triadin. Calsequestrin (CASQ) is a polymeric Ca^{2+}-binding protein that resides in the junctional SR near the luminal opening of RyR. Polymerized CASQ can bind 40-50 mol of Ca^{2+}/mol of CASQ, and is responsible for fast Ca^{2+} binding and release from the junctional SR via its association with junctin and triadin.[155] RyR activity is also modulated by PKA-dependent and CaMKII-dependent phosphorylation of at least three reported sites.[156] RyR phosphorylation increases sensitivity of RyRs to cytosolic Ca^{2+}, leading to increased RyR Ca^{2+} release.[156]

Mammals have three RyR isoforms: RyR1 and RyR2, which are abundantly expressed in skeletal and cardiac muscle, respectively, and RyR3, which has a broad expression profile, usually co-expressing with RyR1 or RyR2. Neuronal expression of RyR varies, but RyR2 is most abundant. RyR2 is activated by Ca^{2+} influx by a mechanism known as calcium-induced calcium release, which is fundamental to cellular processes ranging from muscle contraction to learning and memory. To date, more than 150 RyR2 mutations have been identified that lead to dysregulated RyR2-mediated calcium release, and are associated with a variety of neuropathies and cardiovascular diseases.[157,158] In the brain, spontaneous Ca^{2+} leak via RyR2 is implicated in a number of diseases, including Alzheimer's disease (AD), memory loss,[159] neurodegeneration, and seizures.[160,161] Increased neuronal RyR2 mRNA and protein expression have been found in patients

[151] Zalk, R.; Clarke, O. B.; des Georges, A.; Grassucci, R. A.; Reiken, S.; Mancia, F.; Hendrickson, W. A.; Frank, J.; Marks, A. R. *Nature* **2015**, *517*, 44.
[152] Yan, Z.; Bai, X.-c.; Yan, C.; Wu, J.; Li, Z.; Xie, T.; Peng, W.; Yin, C.-c.; Li, X.; Scheres, S. H. W.; Shi, Y.; Yan, N. *Nature* **2014**, *517*, 50.
[153] Peng, W.; Shen, H.; Wu, J.; Guo, W.; Pan, X.; Wang, R.; Chen, S. R.; Yan, N. *Science* **2016**, *354*.
[154] Divet, A.; Paesante, S.; Bleunven, C.; Anderson, A.; Treves, S.; Zorzato, F. *J. Muscle Res. Cell Motil.* **2005**, *26*, 7.
[155] Handhle, A.; Ormonde, C. E.; Thomas, N. L.; Bralesford, C.; Williams, A. J.; Lai, F. A.; Zissimopoulos, S. *J. Cell Sci.* **2016**, *129*, 3983.
[156] Li, Y.; Sirenko, S.; Riordon, D. R.; Yang, D.; Spurgeon, H.; Lakatta, E. G.; Vinogradova, T. M. *Am. J. Physiol. Heart Circ. Physiol.* **2016**, *311*, H532.
[157] Fill, M.; Copello, J. A. *Physiol. Rev.* **2002**, *82*, 893.
[158] Venetucci, L.; Denegri, M.; Napolitano, C.; Priori, S. G. *Nat. Rev. Cardiol.* **2012**, *9*, 561.
[159] Yuan, Q.; Deng, K. Y.; Sun, L.; Chi, S.; Yang, Z.; Wang, J.; Xin, H. B.; Wang, X.; Ji, G. *Sci. Rep.* **2016**, *6*, 21087.
[160] Johnson, J. N.; Tester, D. J.; Bass, N. E.; Ackerman, M. J. *J. Child Neurol.* **2010**, *25*, 916.
[161] Lehnart, S. E.; Mongillo, M.; Bellinger, A.; Lindegger, N.; Chen, B. X.; Hsueh, W.; Reiken, S.; Wronska, A.; Drew, L. J.; Ward, C. W.; Lederer, W. J.; Kass, R. S.; Morley, G.; Marks, A. R. *J. Clin. Invest.* **2008**, *118*, 2230.

with mild cognitive impairment and AD.[162,163] Patients with AD have a variety of posttranslational modifications that increase RyR2-mediated Ca^{2+} leak and accelerate the development of symptoms.[164] Other neuropathies are associated with specific point mutations in RyR2 or its regulatory partners. Therapies aimed at stabilizing RyR2 and reducing Ca^{2+} leak support the hypothesis that this protein complex is involved in a diverse range of neuropathies. Genetic ablation of the RyR2 PKA-mediated phosphorylation site reduced Ca^{2+} leak and ameliorated AD symptoms and disease progression in an AD mouse model.[164] The pan-RyR inhibitor, dandrolene (Figure 41), has been shown to be neuroprotective in mouse models of Huntington's disease,[165] cerebral ischemia,[166] and spinocerebellar ataxia type 2 and 3,[167,168] suggesting a direct role for RyR2-mediated Ca^{2+} leak.

Figure 41. RyR-modulating small molecules

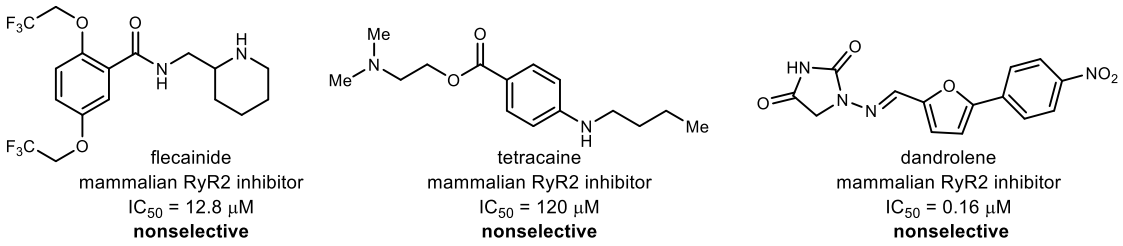

In the heart, RyR2 mediated excitation-contraction (EC) coupling and opening of RyR2 channels is tightly regulated.[169] Abnormally high RyR2 activity during diastole causes EC-coupling-independent spontaneous intracellular Ca^{2+} release from the sarcoplasmic reticulum (SR) and has been documented in human heart diseases associated with both atrial and ventricular arrhythmia (i.e., heart failure, atrial fibrillation).[170,171,172,173] Mutations in RyR2 and its binding partners that increase SR Ca^{2+} leak cause primary atrial and ventricular arrhythmia syndromes such as catecholaminergic polymorphic ventricular tachycardia (CPVT), providing strong evidence for

[162] Bruno, A. M.; Huang, J. Y.; Bennett, D. A.; Marr, R. A.; Hastings, M. L.; Stutzmann, G. E. *Neurobiol. Aging* **2012**, *33*, 1001 e1.
[163] Kelliher, M.; Fastbom, J.; Cowburn, R. F.; Bonkale, W.; Ohm, T. G.; Ravid, R.; Sorrentino, V.; O'Neill, C. *Neuroscience* **1999**, *92*, 499.
[164] Lacampagne, A.; Liu, X.; Reiken, S.; Bussiere, R.; Meli, A. C.; Lauritzen, I.; Teich, A. F.; Zalk, R.; Saint, N.; Arancio, O.; Bauer, C.; Duprat, F.; Briggs, C. A.; Chakroborty, S.; Stutzmann, G. E.; Shelanski, M. L.; Checler, F.; Chami, M.; Marks, A. R. *Acta Neuropathol.* **2017**, *134*, 749.
[165] Chen, X.; Wu, J.; Lvovskaya, S.; Herndon, E.; Supnet, C.; Bezprozvanny, I. *Mol. Neurodegener.* **2011**, *6*, 81.
[166] Wei, H.; Perry, D. C. *J. Neurochem.* **2002**, *67*, 2390.
[167] Liu, J.; Tang, T. S.; Tu, H.; Nelson, O.; Herndon, E.; Huynh, D. P.; Pulst, S. M.; Bezprozvanny, I. *J. Neurosci.* **2009**, *29*, 9148.
[168] Chen, X.; Tang, T. S.; Tu, H.; Nelson, O.; Pook, M.; Hammer, R.; Nukina, N.; Bezprozvanny, I. *J. Neurosci.* **2008**, *28*, 12713.
[169] Bers, D. M. *Nature* **2002**, *415*, 198.
[170] Wehrens, X. H.; Marks, A. R. *Nat. Rev. Drug Discov.* **2004**, *3*, 565.
[171] Marks, A. R. *J. Clin. Invest.* **2013**, *123*, 46.
[172] Dobrev, D.; Carlsson, L.; Nattel, S. *Nat. Rev. Drug Discov.* **2012**, *11*, 275.
[173] Nattel, S.; Burstein, B.; Dobrev, D. *Circ. Arrhythm. Electrophysiol.* **2008**, *1*, 62.

the mechanistic contribution of RyR2 to arrhythmia risk in humans.[174] Further support comes from gene-targeted mouse models of CPVT, where catecholamine-induced spontaneous Ca^{2+} release from the sarcoplasmic reticulum (SR) via RyR2 generates potentially fatal cardiac arrhythmias.[175,176] Previously, the Knollmann lab discovered that an antiarrhythmic small molecule drug currently in clinical use, flecainide (Figure 41), reduced CPVT episodes both in CPVT patients and in a calsequestrin knockout (*Casq2*$^{-/-}$) mouse model of CPVT.[177] Although flecainide effectively suppresses spontaneous Ca^{2+} release in CPVT cardiomyocytes,[177,178] recent work suggests that the flecainide mode of action is unrelated to direct RyR2 inhibition.[179] Furthermore, flecainide is only 30% effective in suppressing spontaneous Ca^{2+} waves at 10 μM concentration.[178] Currently, an RyR2-selective probe does not exist. Therefore, new small molecule tool-compounds that selectively modulate RyR2 are needed to understand regulation of cellular Ca^{2+} flux and its potential as a pharmacologic target for the prevention of cardiac arrhythmias triggered by untimely Ca^{2+} release through RyR2 channels.

5.1.2 Uncover novel biological functions with unnatural enantiomers of natural products

Natural products often serve as an excellent discovery platform to uncover new chemical tools, as they can provide diverse molecular architectures and immediate accessibility in amounts sufficient to examine initial biological activity.[180] In most cases, chiral natural products are produced biosynthetically as a single enantiomer, but in rare cases can be produced as both enantiomers in a racemic mixture or as the opposite enantiomer from a different species.[181] The two mirror image isomers have identical chemical properties, but often exhibit different biological functions or activities,[182,183] which makes them discovery tools to study stereodifferentiated interactions between these complex small molecules and a targeted biomolecule (Figure 42).

Because many natural products are only available as a single enantiomer biosynthetically, chemical synthesis must be used in order to access the unnatural enantiomer for further biological studies. The importance of screening the unnatural enantiomer of natural products has been confirmed by the discovery of more potent cytotoxic agents (*ent*-(-)-roseophilin[184] and *ent*-(+)-

[174] Knollmann, B. C.; Chopra, N.; Hlaing, T.; Akin, B.; Yang, T.; Ettensohn, K.; Knollmann, B. E.; Horton, K. D.; Weissman, N. J.; Holinstat, I.; Zhang, W.; Roden, D. M.; Jones, L. R.; Franzini-Armstrong, C.; Pfeifer, K. *J. Clin. Invest.* **2006**, *116*, 2510.
[175] Loaiza, R.; Benkusky, N. A.; Powers, P. P.; Hacker, T.; Noujaim, S.; Ackerman, M. J.; Jalife, J.; Valdivia, H. H. *Circ. Res.* **2013**, *112*, 298.
[176] Kannankeril, P. J.; Mitchell, B. M.; Goonasekera, S. A.; Chelu, M. G.; Zhang, W.; Sood, S.; Kearney, D. L.; Danila, C. I.; De Biasi, M.; Wehrens, X. H.; Pautler, R. G.; Roden, D. M.; Taffet, G. E.; Dirksen, R. T.; Anderson, M. E.; Hamilton, S. L. *Proc. Natl. Acad. Sci. U. S. A.* **2006**, *103*, 12179.
[177] Watanabe, H.; Chopra, N.; Laver, D.; Hwang, H. S.; Davies, S. S.; Roach, D. E.; Duff, H. J.; Roden, D. M.; Wilde, A. A.; Knollmann, B. C. *Nat. Med.* **2009**, *15*, 380.
[178] Galimberti, E. S.; Knollmann, B. C. *J. Mol. Cell. Cardiol.* **2011**, *51*, 760.
[179] Bannister, M. L.; Thomas, N. L.; Sikkel, M. B.; Mukherjee, S.; Maxwell, C.; MacLeod, K. T.; George, C. H.; Williams, A. J. *Circ. Res.* **2015**, *116*, 1324.
[180] Newman, D. J.; Cragg, G. M. *J. Nat. Prod.* **2016**, *79*, 629.
[181] Finefield, J. M.; Sherman, D. H.; Kreitman, M.; Williams, R. M. *Angew. Chem. Int. Ed. Engl.* **2012**, *51*, 4802.
[182] Noguchi, T.; Oishi, S.; Honda, K.; Kondoh, Y.; Saito, T.; Ohno, H.; Osada, H.; Fujii, N. *Chem. Commun.* **2016**, *52*, 7653.
[183] Felicio, M. R.; Silva, O. N.; Goncalves, S.; Santos, N. C.; Franco, O. L. *Front. Chem.* **2017**, *5*, 5.
[184] Boger, D. L.; Hong, J. *J. Am. Chem. Soc.* **2001**, *123*, 8515.

deguelin[185]), and new biological activity with *ent*-(+)-batrachotoxin[186] (Figure 42). However, due to synthetic barriers, there are few instances where the biological activity of an unnatural enantiomer can be studied in comparison to its naturally occurring enantiomer. As a consequence, *ent*-natural products that can only be accessed by chemical synthesis represent underexplored leads, occupying "dark chemical space."[182,187]

Figure 42. Biological relevance of unnatural mirror image isomers of natural products

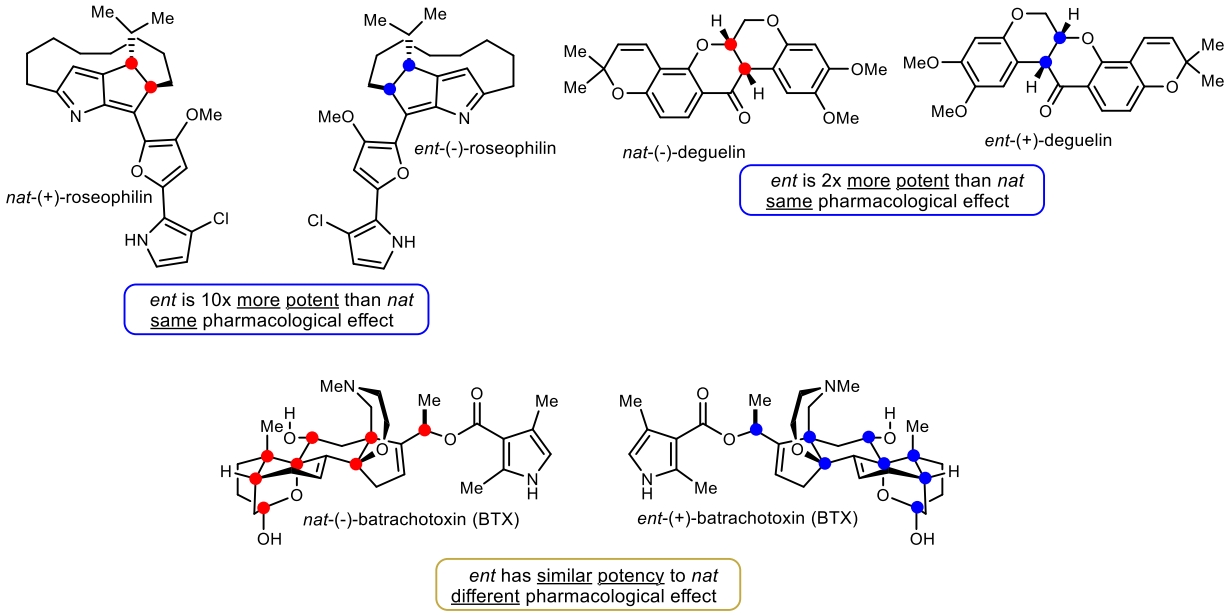

As expected from a privileged class of natural products, fungal CODs, such as (-)-verticilide, are only available as a single enantiomer biosynthetically. Fungal COD-producing nonribosomal peptide synthetases (NRPSs) selectively activate a specific enantiomer in the condensation domain from a racemic mixture to be coupled with the next in the sequence;[188,189] therefore, stereochemical variation does not occur naturally. Unlike terpene or polyketide natural products which can be found in nature as the racemate or as the opposite enantiomer from another organism,[181] the opposite enantiomer of fungal COD natural products can only be accessed by chemical synthesis. Unfortunately, traditional chemical synthesis of CODs is a notoriously challenging, slow process in many cases.[55] Consequently, the biological relevance of *ent*-COD natural products and other derivatives is largely under explored. The robust methodology that we have developed to synthesize COD natural products renders both enantiomers readily accessible by simply changing the catalyst in the Henry addition, and changing the amino acid in the UmAS step (Scheme 48), and the Mitsunobu MCO enables their rapid synthesis.

[185] Farmer, R. L.; Scheidt, K. A. *Chem. Sci.* **2013**, *4*, 3304.
[186] Logan, M. M.; Toma, T.; Thomas-Tran, R.; Du Bois, J. *Science* **2016**, *354*, 865.
[187] Wassermann, A. M.; Lounkine, E.; Hoepfner, D.; Le Goff, G.; King, F. J.; Studer, C.; Peltier, J. M.; Grippo, M. L.; Prindle, V.; Tao, J.; Schuffenhauer, A.; Wallace, I. M.; Chen, S.; Krastel, P.; Cobos-Correa, A.; Parker, C. N.; Davies, J. W.; Glick, M. *Nat. Chem. Biol.* **2015**, *11*, 958.
[188] Pieper, R.; Haese, A.; Schroder, W.; Zocher, R. *Eur. J. Biochem.* **1995**, *230*, 119.
[189] Xu, Y.; Zhan, J.; Wijeratne, E. M.; Burns, A. M.; Gunatilaka, A. A.; Molnar, I. *J. Nat. Prod.* **2007**, *70*, 1467.

Scheme 48. Enantioselective synthesis of COD natural products

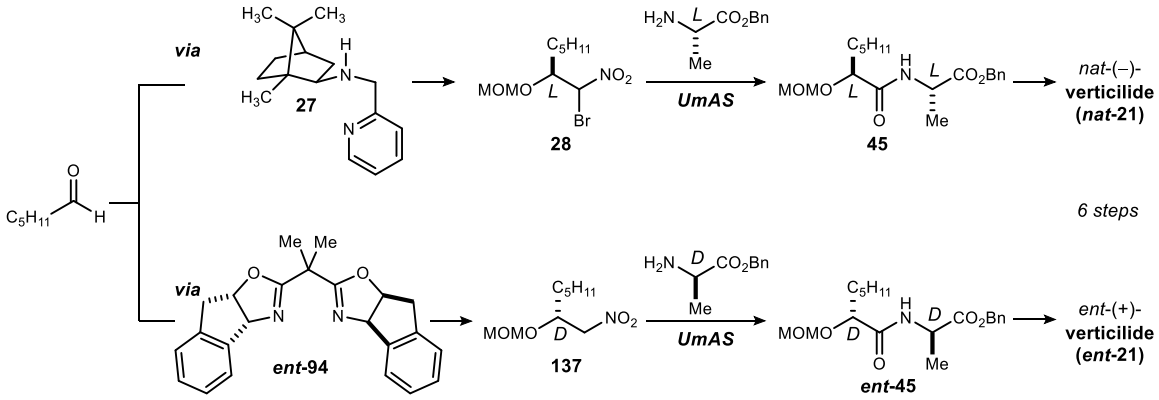

The pathological implications of Ca^{2+} leak via ryanodine receptor type 2 (RyR2) make RyR2 an attractive therapeutic target for drug development, and sparked the beginning of our collaboration with the Knollmann lab. Here, we used our straightforward synthetic approach to synthesize the fungal COD natural product and known insect RyR agonist (-)-verticilide, and several congeners to determine their activity against mammalian RyR2 spontaneous Ca^{2+} leak for the prevention of cardiac arrhythmias.

5.2 The discovery of a novel potent inhibitor of RyR2-mediated Ca^{2+} leak

Upon its isolation in 2006, (-)-verticilide was found to be an RyR agonist, selectively binding insect RyR with an IC_{50} value of 4.2 μM.[26] Because insects have only one RyR isoform, (-)-verticilide is a promising lead for developing new insecticides. (-)-Verticilide weakly binds mouse RyR1 with an IC_{50} value of 53.9 μM,[190] but its affinity to mammalian RyR2 or RyR3 is unknown. Given its known RyR binding abilities, we hypothesized that verticilide may also act on mammalian RyR2. Herein we compared the biological activity of *nat*-(-)-verticilide, its enantiomer (*ent*-(+)-verticilide), and both of their synthetic precursors on RyR2-mediated Ca^{2+} release in single cardiomyocytes isolated from wild-type mice and a mouse model of human CPVT.

[190] Shiomi, K.; Matsui, R.; Kakei, A.; Yamaguchi, Y.; Masuma, R.; Hatano, H.; Arai, N.; Isozaki, M.; Tanaka, H.; Kobayashi, S.; Turberg, A.; Omura, S. *J. Antibiot.* **2010**, *63*, 77.

Scheme 49. Macrocyclooligomerization (MCO) and modular convergent routes to verticilide

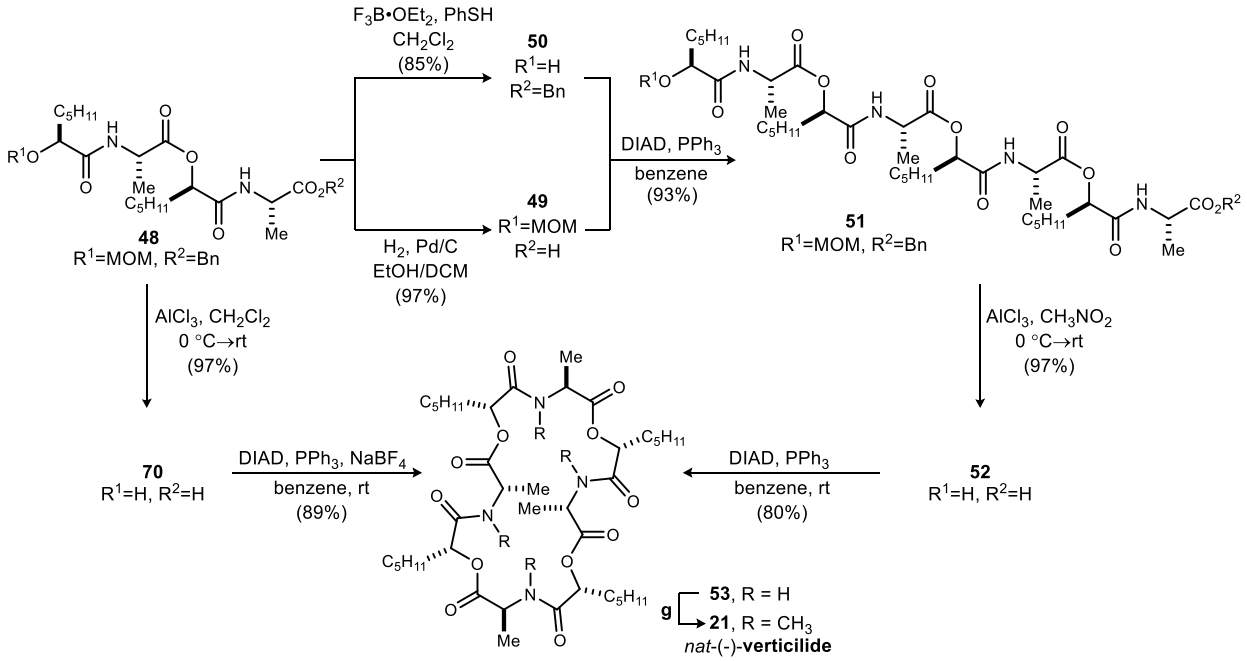

In order to get a sense of structure-activity relationship of any observed activity, we wanted to test the desmethyl macrocyclic precursor (**53**) to verticilide, and the linear macrocyclization precursor to **53**. These two synthetic precursors were selected to inform us if cyclic structure and *N*-methylation are structural features important for resulting bioactivity. Additionally, the enantiomer of verticilide (*ent*-**21**) and both synthetic precursors were synthesized in order to determine if bioactivity was due to specific chiral receptor-ligand interactions. Thus, two approaches to the synthesis of verticilide were leveraged in order to obtain the verticilide congeners needed to investigate activity against RyR2. First, *nat*-(-)-verticilide was synthesized using our Mitsunobu MCO approach from tetradepsipeptide *seco*-acid **70** in an 8-step longest linear sequence.[88] To obtain the linear precursor to verticilide, the synthesis was diverted from common tetradepsipeptide intermediate **48** to ultimately access **52** through a series of convergent deprotection and coupling steps (Scheme 49). Finally, **52** was subjected to Mitsunobu macrocyclization conditions to afford the 24-membered N-H precursor **53**, which was transformed to *nat*-(-)-verticilide by per-*N*-methylation.[88]

Scheme 50. Synthetic sequence to access *ent*-(+)-verticilide

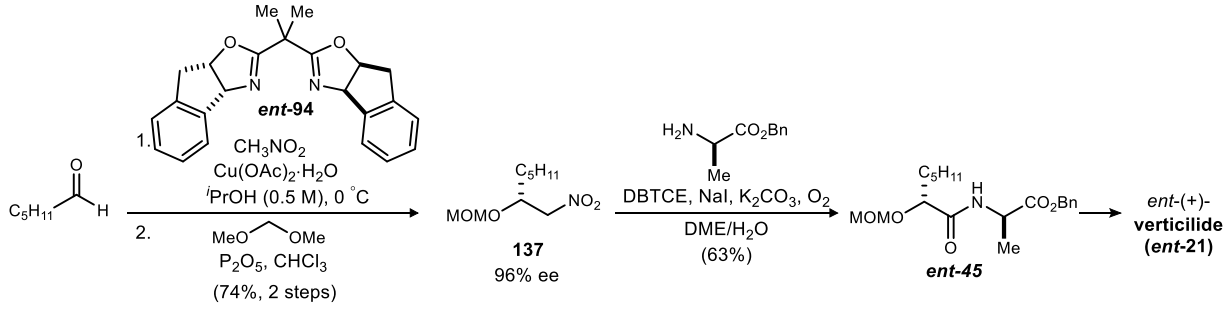

Additionally, this simple, rapidly executed platform was used to prepare mirror image isomers *ent*-**52**, *ent*-**53**, and *ent*-(+)-verticilide (*ent*-**21**), by simply changing the catalyst from **27** to *ent*-**94** in the Henry addition, and using D-alanine benzyl ester instead of the L-enantiomer in the UmAS step (Scheme 50). Then, *ent*-**45** was used in the same series of steps as *nat* to arrive at the desired mirror image compounds in pure form.

Figure 43. Ca^{2+} spark measurements of RyR activity in $Casq2^{-/-}$ cardiomyocytes

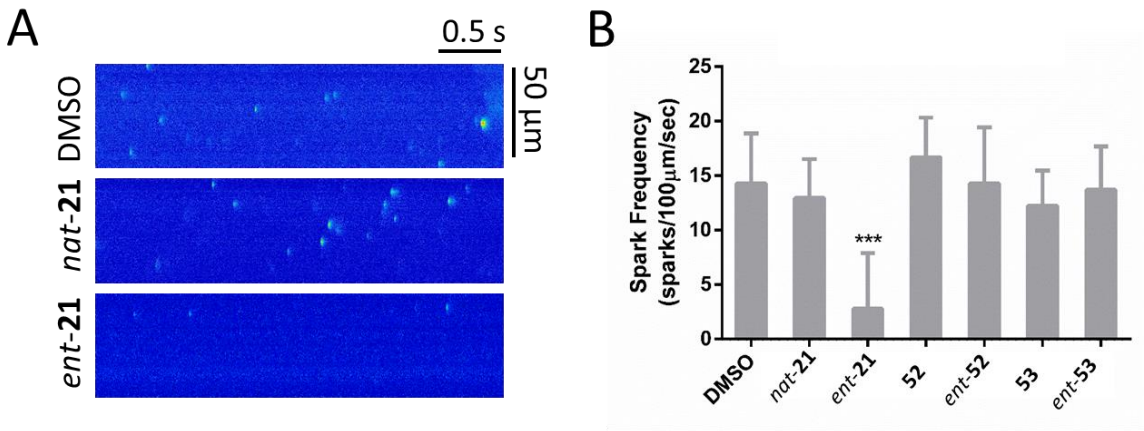

A) Representative confocal line scans of Ca^{2+} sparks in the absence (DMSO) or presence of 25 µM *nat*-**21** or *ent*-**21** in permeabilized $Casq2^{-/-}$ cardiomyocytes. **B)** Ca^{2+} spark frequency in $Casq2^{-/-}$ cardiomyocytes treated with 25 µM nat-**21**, **52**, **53**, and their respective enantiomers. Data are presented as mean ± SEM. N ≥ 30 cells per group. *** $p < 0.001$ vs DMSO by 1-way ANOVA with Tukey's post-hoc test. Data and figure produced by Dan Blackwell (Knollmann lab).

The functional effects of *nat*-(-)- and *ent*-(+)-verticilide and their *N*-H congeners on RyR2 activity were investigated using *Casq*2 gene knockout (*Casq2*$^{-/-}$) mice developed from a C57BL/6J strain, a validated model of human CPVT that exhibits pathologically-increased RyR2 activity.[174] Ventricular mouse myocytes were isolated, permeabilized with saponin to enable equivalent access of the compounds to the SR membrane, and incubated with DMSO or 25 µM *nat*- and *ent*-**21, 52**, **53**. RyR2 activity was measured in the form of Ca^{2+} sparks, which are elementary Ca^{2+} release events generated by spontaneous openings of intracellular RyR2 Ca^{2+} release channels.[191] Figure 43A shows representative confocal line scans illustrating spontaneous Ca^{2+} sparks in cells treated with DMSO, *nat*-**21**, or *ent*-**21**. Interestingly, we found that, whereas *nat*-**21** and the synthetic precursors had no effect on Ca^{2+} sparks, *ent*-**21** significantly reduced spark frequency (Figure 43B), indicating that *ent*-**21** inhibits RyR2-mediated Ca^{2+} release, but *nat*-**21** does not.

RyR2-mediated SR Ca^{2+} release is sensitive to the Ca^{2+} concentration present at the cytosolic face of RyR2.[192] To confirm that $[Ca^{2+}]_{free}$ was not altered by any of the compounds, Fluo-4 fluorescence was measured under spark assay conditions. The internal spark solution was incubated with DMSO or 25 µM *nat*-**21**, **52**, **53**, and their respective enantiomers for 10 minutes and $[Ca^{2+}]_{free}$ was calculated from a set of Ca^{2+} standards. None of the compounds altered $[Ca^{2+}]_{free}$ (Figure 44), confirming that the observed activity, or lack thereof, is not an artifact of Ca^{2+} chelation.

[191] Cheng, H.; Lederer, W. J.; Cannell, M. B. *Science* **1993**, *262*, 740.
[192] Meissner, G. *Annu. Rev. Physiol.* **1994**, *56*, 485.

Figure 44. Free Ca^{2+} measurements in spark assay conditions

Data are presented as mean ± SD from 5 replicates; not significant by one-way ANOVA. Data and figure produced by Dan Blackwell (Knollmann lab).

Our finding that *ent*-**21** significantly decreases RyR2-dependent spontaneous Ca^{2+} leak but *nat*-**21** does not, suggests that there is a specific ligand-receptor interaction between *ent*-**21** and a chiral binding site in the cell. Enantiomer-dependent inhibition of RyR2-mediated Ca^{2+} release has also been reported for the drug propafenone, which has antiarrhythmic properties similar to flecainide and is clinically used in racemic form.[193] Compared to *S*-propafenone, *R*-propafenone is a significantly more potent inhibitor of RyR2 single channels in artificial bilayers[193] and Ca^{2+} sparks in cardiomyocytes[178] (Figure 45). Similar to *nat*-**21**, the linear congeners and their enantiomers did not exhibit an inhibitory effect. Hence, the cyclic form of *ent*-**21** is also essential for activity.

Figure 45. Enantiomer-dependent inhibition of RyR2-mediated Ca^{2+} release with propafenone

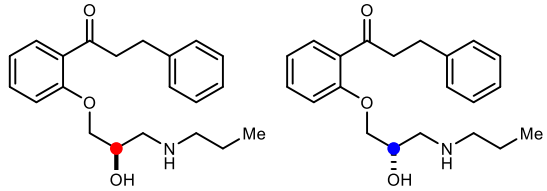

To test whether *ent*-**21** directly inhibits RyR, we measured [^{3}H]ryanodine binding — an index of RyR activity[194] — to skeletal (RyR1) and cardiac (RyR2) porcine muscle SR preparations. Skeletal and cardiac SR were incubated with 50 μM *nat*-**21**, *ent*-**21**, and tetracaine for three hours. *Nat*-**21** increased RyR1 activity, but had no effect on RyR2 (Figure 46A). Conversely, *ent*-**21** inhibited RyR2, but had no effect on RyR1. The experimentally-used RyR inhibitor, tetracaine, inhibited both isoforms. *Ent*-**21** was selected to generate full dose response curves for both cardiac

[193] Hwang, H. S.; Hasdemir, C.; Laver, D.; Mehra, D.; Turhan, K.; Faggioni, M.; Yin, H.; Knollmann, B. C. *Circ. Arrhythm. Electrophysiol.* **2011**, *4*, 128.
[194] Rebbeck, R. T.; Nitu, F. R.; Rohde, D.; Most, P.; Bers, D. M.; Thomas, D. D.; Cornea, R. L. *J. Biol. Chem.* **2016**, *291*, 15896.

and skeletal SR. *Ent*-**21** inhibited RyR2 in a concentration-dependent manner with an apparent IC_{50} of approximately 0.1 µM and maximal inhibition of approximately 20% (Figure 46B), but had no effect on RyR1 up to 50 µM (Figure 46C). *ent*-**21** was a significantly more potent RyR2 inhibitor than the previously studied RyR inhibitors flecainide or tetracaine.

Figure 46. [^{3}H]Ryanodine binding assays to measure RyR activity

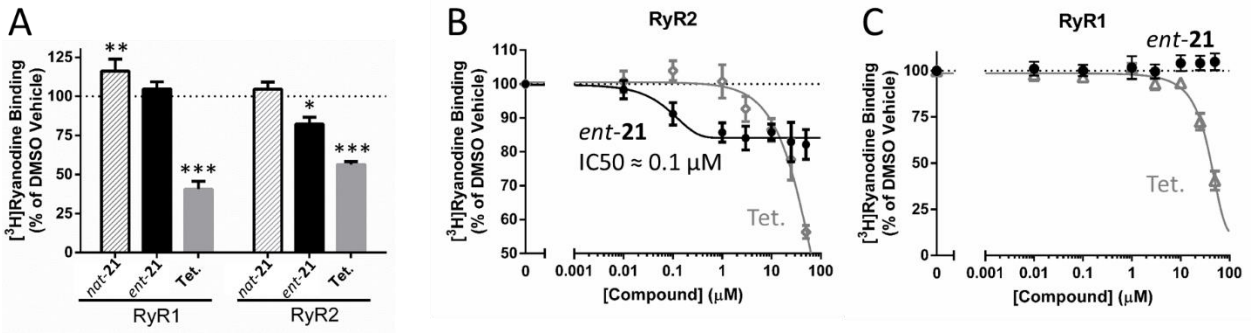

A) Comparison of [^{3}H]ryanodine binding to SR isolated from porcine longissimus dorsi (RyR1) or cardiac ventricle (RyR2) in the presence of 50 µM *nat*-**21**, *ent*-**21**, or tetracaine (tet). **B)** Dose response curves for *ent*-**21** and tet inhibition of [^{3}H]ryanodine binding to RyR2. **C)** Dose response curves for *ent*-**21** and tet inhibition of [^{3}H]ryanodine binding to RyR1. N = 4 replicates for each concentration tested. * $p < 0.05$ vs DMSO, ** $p < 0.01$ vs DMSO, *** $p < 0.001$ vs DMSO by t-test. Data produced by Robyn Rebbeck (Cornea lab), and figure produced by Dan Blackwell (Knollmann lab).

The dearth of RyR2 activity observed with *nat*-**21**, a known insect RyR agonist, can be explained by the differences in structural homology between insect RyR and mammalian RyR2. The amino acid sequence of insect RyR only shares about 45% homology with the mammalian isoforms.[195] The carboxy-terminal portion of insect RyR, which forms the pore region of the Ca^{2+}

Figure 47. Comparison of Ca^{2+} release inhibition by *ent*-21 with classical inhibitors in WT cardiomyocytes

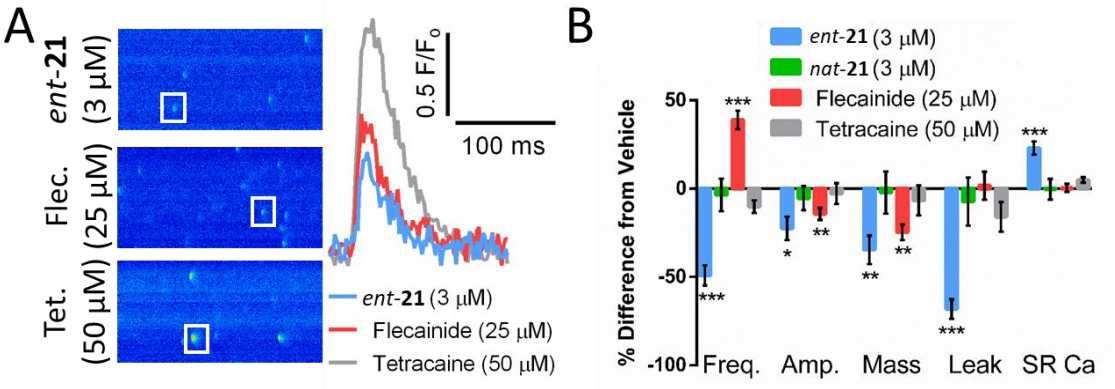

A) Representative Ca^{2+} sparks from permeabilized wild-type cardiomyocytes treated with 3 µM *ent*-**21**, 25 µM flecainide, or 50 µM tetracaine. Graph indicates amplitude of Ca^{2+} release of the selected representative sparks over time. **B)** Percent change in spark frequency, amplitude, mass, leak, and SR Ca^{2+} content relative to vehicle (DMSO), obtained from wild-type myocytes (N ≥ 30 cells per group). SR Ca^{2+} content was measured as the Ca^{2+} transient amplitude elicited by application of 10 mM caffeine (n ≥ 5 cells per group). Data are presented as mean ± SEM. * $p < 0.05$ vs DMSO, ** $p < 0.01$ vs DMSO, *** $p < 0.001$ vs DMSO by t-test. Data and figure produced by Dan Blackwell (Knollmann lab).

[195] Xu, X.; Bhat, M. B.; Nishi, M.; Takeshima, H.; Ma, J. *Biophys. J.* **2000**, *78*, 1270.

release channel, is highly conserved with over 90% homology with the corresponding region of the mammalian isoforms.[195] However, insect and mammalian RyR isoforms differ greatly in the large amino-terminal portion of the channel, which extends into the cytosol and contains multiple binding sites for Ca^{2+} release channel modulators.[195] These regions of high divergence are possible candidates for *ent*-(+)-verticilide interaction with mammalian RyR2, but are not amenable for interaction with *nat*-**21**. It is unknown whether *ent*-(+)-**21** binds to insect RyR, however the lack of effect of *nat*-(-)-verticilide on mammalian RyR2 is reassuring for developing it and its congeners as insecticides.[26]

To further characterize the Ca^{2+} release inhibition by *ent*-**21**, we applied a lower concentration (3 µM) to wild-type mouse cardiomyocytes and compared results to two other classical Ca^{2+} release inhibitors, flecainide and tetracaine (representative line scans and sparks are shown in Figure 47A). 3 µM *ent*-**21** exhibited a dual effect on Ca^{2+} sparks: a significant reduction in the rate of spontaneous Ca^{2+} sparks (measured as spark frequency) and the amount of Ca^{2+} released during each Ca^{2+} spark (measured as spark amplitude and spark mass) (Figure 47B). As a result, Ca^{2+} spark-mediated SR Ca^{2+} leak was drastically reduced and, importantly, was not a result of reduced SR Ca^{2+} load (Figure 47B). Interestingly, the effect of *ent*-**21** on spark mass was analogous to flecainide, whereas the experimental RyR2 inhibitor tetracaine did not reduce spark mass. The effects of *ent*-**21** on Ca^{2+} spark frequency were similar to the RyR2 inhibitor tetracaine, but different from flecainide, which caused a paradoxical increase in spark frequency, in keeping with previous findings.[196] *ent*-**21** significantly reduced Ca^{2+} leak, whereas flecainide is a leak-neutral blocker.[196] Taken together, our results demonstrate that *ent*-**21** is not only significantly more potent, but also a more effective Ca^{2+} release inhibitor than flecainide and tetracaine and exhibits a different mechanism of action than other RyR inhibitors.

Figure 48. *ent*-21 inhibits spontaneous Ca^{2+} release (SCR) in isolated intact Casq2$^{-/-}$ cardiomyocytes

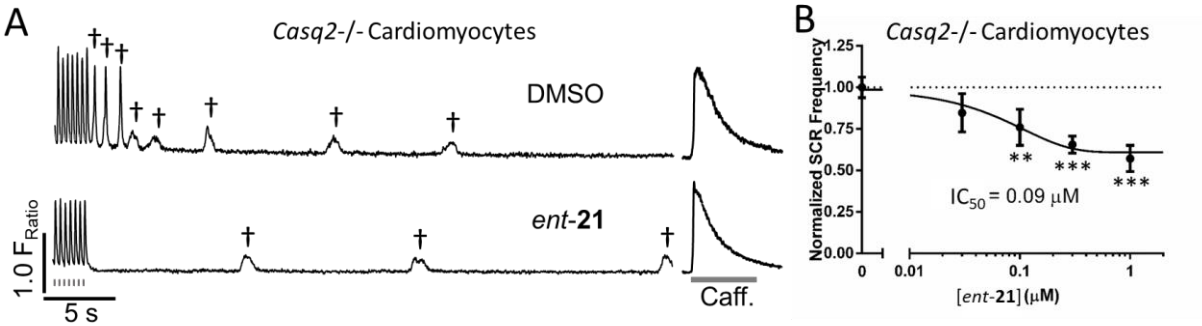

A) Isolated cardiomyocytes were field stimulated at 3 Hz for 20 seconds followed by 40 seconds recording of SCR events (†). Application of 10 mM caffeine (caff) was used to measure SR Ca^{2+} content. **B)** SCR frequency following cessation of pacing. N = 63, 27, 31, 63, 30, and 27 cells for 0, 0.03, 0.1, 0.3, and 1.0 µM *ent*-**21**, respectively. ** $p < 0.01$, *** $p < 0.001$ vs DMSO by t-test. Data produced by Kyungsoo Kim (Knollmann lab), and figure produced by Dan Blackwell (Knollmann lab).

nat-**21** is capable of crossing cellular membranes based on its documented insecticidal activity and insect RyR inhibition. To test whether *ent*-**21** crosses the cell membrane, we measured spontaneous Ca^{2+} release in intact *Casq*$2^{-/-}$ cardiomyocytes. Isolated cardiomyocytes were incubated for 3 hours with 0, 0.03, 0.1, 0.3, and 1.0 µM *ent*-**21** and electrically paced at 3 Hz for

[196] Hilliard, F. A.; Steele, D. S.; Laver, D.; Yang, Z.; Le Marchand, S. J.; Chopra, N.; Piston, D. W.; Huke, S.; Knollmann, B. C. *J. Mol. Cell. Cardiol.* **2010**, *48*, 293.

20 seconds with 1.0 µM isoproterenol to stimulate adrenergic activation and a CPVT-like cellular phenotype consisting of spontaneous Ca^{2+} release events (Figure 48A). Spontaneous Ca^{2+} release can produce triggered beats that evoke ventricular ectopy and are the cellular source of arrhythmogenesis.[197] *ent*-**21** significantly reduced the frequency of spontaneous Ca^{2+} release (Figure 48B), suggesting that *ent*-**21** is able to transverse the cell membrane and exert biological activity. Inhibition of spontaneous Ca^{2+} release mirrored the potency and dose dependence observed in the [^{3}H]ryanodine binding assay, but with a greater biological efficacy. Consistent with inhibition of RyR2-mediated Ca^{2+} release, *ent*-**21** reduced diastolic Ca^{2+} levels, decreased Ca^{2+} transient amplitude, and delayed time to peak of paced transients. *ent*-**21** did not alter SR Ca^{2+} content or Ca^{2+} decay kinetics, indicating that reduced SR load or impaired Ca^{2+} reuptake do not account for the reduction in spontaneous Ca^{2+} release (Figure 49).

Figure 49. Intracellular Ca^{2+} handling in intact $Casq2^{-/-}$ cardiomyocytes

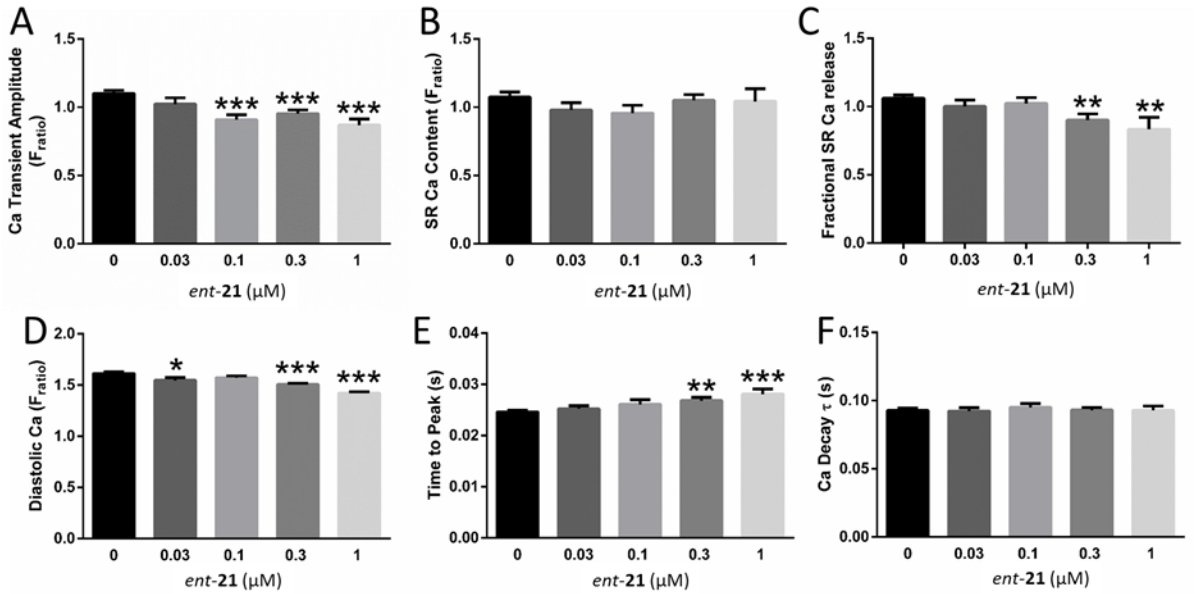

A) Paced Ca^{2+} transient amplitudes. **B)** Caffeine-induced Ca^{2+} transient amplitude. **C)** Fractional SR Ca^{2+} release (paced transient amplitude/SR Ca^{2+} content). **D)** Diastolic Ca^{2+} measurements during field stimulation. **E)** Time to peak and **F)** Ca^{2+} decay kinetics of paced transients. Data presented as mean ± SEM, ** $p < 0.01$, *** $p < 0.001$ vs DMSO by t-test. N = 63, 27, 31, 63, 30, and 27 cells for 0, 0.03, 0.1, 0.3, and 1.0 µM *ent*-**21**, respectively. Data produced by Kyungsoo Kim (Knollmann lab), and figure produced by Dan Blackwell (Knollmann lab).

To determine whether *ent*-**21** inhibition of Ca^{2+} release in cardiomyocytes *in vitro* translates into activity against ventricular arrhythmia *in vivo*, $Casq2^{-/-}$ mice were injected intraperitoneally (i.p.) with 30 mg/kg *nat*-**21**, *ent*-**21**, or DMSO of equivalent volume. After 30 minutes, mice were anesthetized with inhaled isoflurane and electrocardiogram recordings were made during i.p. injection of 3.0 mg/kg isoproterenol to induce CPVT. Figure 50A (first panel) illustrates the HR response to isoproterenol injection (0 s) and subsequent development of ventricular arrhythmias. *ent*-**21** significantly reduced the number of ventricular ectopic beats (Figure 50A, B), primarily in the form of premature ventricular complexes (PVCs). *ent*-**21** also

[197] Schlotthauer, K.; Bers, D. M. *Circ. Res.* **2000**, *87*, 774.

reduced the incidence of ventricular tachycardia (Figure 50C), an established risk factor for sudden cardiac death.[198]

Figure 50. *ent*-21 inhibits ventricular arrhythmia in Casq2$^{-/-}$ mice

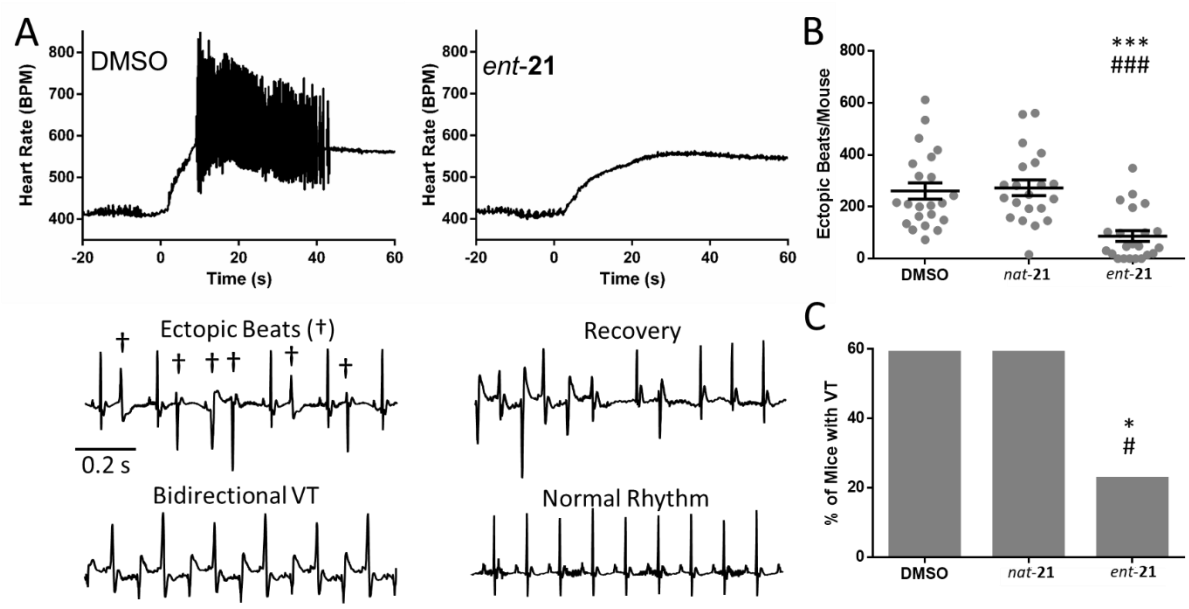

A) Representative heart rate traces in Casq2$^{-/-}$ mice treated with DMSO or *ent*-**21**. Isoproterenol (3.0 mg/kg i.p.) was injected at 0 s. Rhythm strips show arrhythmia features. Ectopic beats (†) produce a variable HR in the traces. **B)** Quantification of catecholamine-induced ectopic beats by surface electrocardiogram in Casq2$^{-/-}$ mice injected intraperitoneally with 30 mg/kg (drug/body weight) *nat*-**21** or *ent*-**21** or DMSO of equivalent volume 30 minutes prior to recordings. *** $p < 0.001$ vs DMSO or ### $p < 0.001$ vs *nat*-**21** by Mann-Whitney U-test. Data presented as mean ± SEM. **C)** Incidence of ventricular tachycardia (VT). $p = 0.0305$ for *ent*-**21** vs DMSO (*) or *ent*-**21** vs *nat*-**21** (#) by Fisher's exact test. N = 22 mice per group. Data and figure produced by Dan Blackwell (Knollmann lab).

There were no differences in baseline heart rate (HR) prior to isoproterenol; however, there was a significant reduction in peak HR and, consequently, ΔHR after isoproterenol injection in the *ent*-**21** group (Figure 51). The HR reduction by *ent*-**21** is consistent with its block of RyR2 channels in the sinoatrial node and hence the intracellular Ca^{2+} clock responsible for HR acceleration in response to catecholamines.[199] To exclude the possibility that the reduction in peak HR was responsible for the arrhythmia reduction by *ent*-**21**, we used a linear regression model to assess whether lower peak HR or ΔHR confer protection from ectopic beats. No association was found between peak or ΔHR and the number of ectopic beats in the DMSO and *nat*-**21** groups (Figure 51). Hence, RyR2 inhibition by *ent*-**21**, rather than reduced peak HR or ΔHR, is responsible for the reduction in ectopic beats evinced by *ent*-**21**.

Drugs that block cell membrane Na^+ or L-type Ca^{2+} channels can prevent CPVT in mouse models and humans.[200,201] To assess whether *ent*-**21** *in vivo* efficacy was a result of Na^+ channel

[198] Knollmann, B. C.; Roden, D. M. *Nature* **2008**, *451*, 929.
[199] Lakatta, E. G.; Maltsev, V. A.; Vinogradova, T. M. *Circ. Res.* **2010**, *106*, 659.
[200] Katz, G.; Khoury, A.; Kurtzwald, E.; Hochhauser, E.; Porat, E.; Shainberg, A.; Seidman, J. G.; Seidman, C. E.; Lorber, A.; Eldar, M.; Arad, M. *Heart Rhythm* **2010**, *7*, 1676.
[201] Khoury, A.; Marai, I.; Suleiman, M.; Blich, M.; Lorber, A.; Gepstein, L.; Boulos, M. *Heart Rhythm* **2013**, *10*, 1671.

or Ca^{2+} channel block, we measured the ECG QRS duration (prolonged by Na^{+} channel blockers) and the PR interval (prolonged by Ca^{2+} channel blockers). *ent*-**21** had no significant effect on QRS (Figure 52A) or PR interval (Figure 52B), indicating that Na^{+} or Ca^{2+} channel block by *ent*-**21** does not contribute to its antiarrhythmic activity *in vivo*.

Figure 51. Heart rate (HR) response in Casq2$^{-/-}$ mice

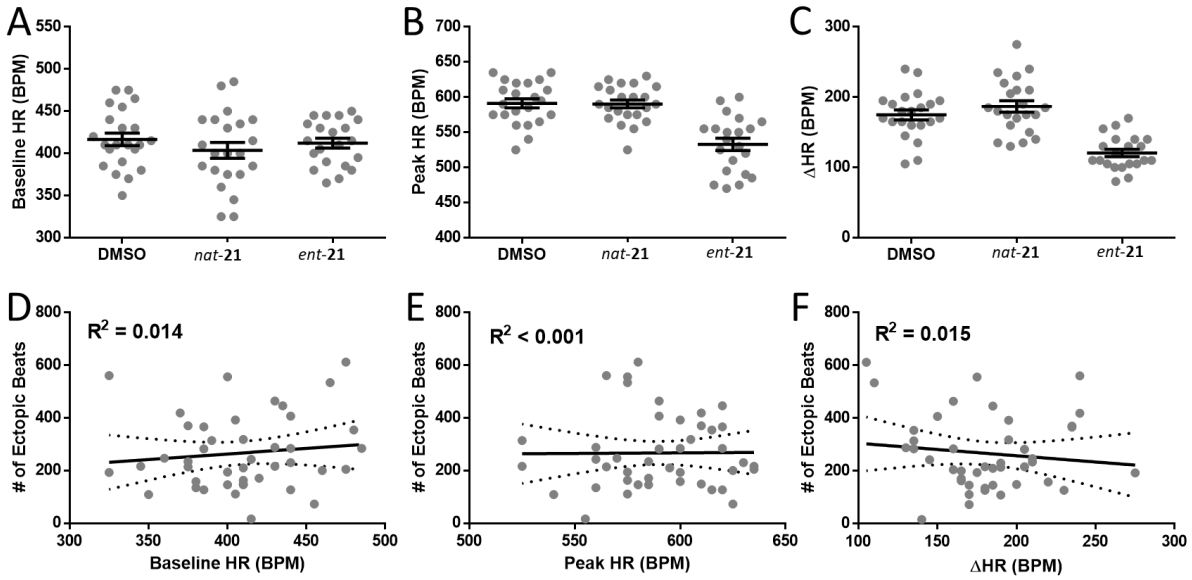

A) Baseline, **B)** peak, and **C)** ΔHR (n = 22 mice per group). **D, E, F)** Linear regression models (shown with 95% confidence interval) of combined DMSO and *nat*-**21** treatment (n = 44 mice). Bars in A, B, and C are mean ± SEM. Data and figure produced by Dan Blackwell (Knollmann lab).

Figure 52. Surface electrocardiogram parameters from recordings in Casq2$^{-/-}$ mice

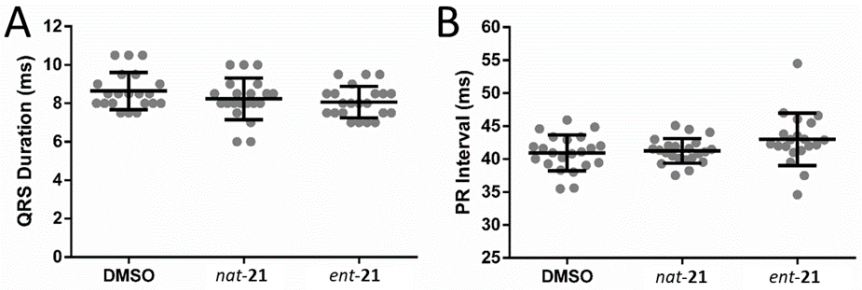

A) QRS duration. **B)** PR interval. N = 22 mice per group, data shown as mean ± SD. Not significant by one-way ANOVA. Data and figure produced by Dan Blackwell (Knollmann lab).

5.3 Conclusion

In the heart, RyR2-mediated Ca^{2+} release plays a critical role in linking electrical excitation to mechanical contraction, a process known as EC coupling. Inappropriately timed Ca^{2+} release can trigger arrhythmogenic events such as atrial or ventricular tachycardia and sudden death. Current therapeutic interventions with flecainide are capable of at least partially inhibiting Ca^{2+}

release mediated arrhythmias;[178] however, new small-molecule tools are needed to further understand the role of Ca^{2+} flux regulators and their relevance for preventing arrhythmias, especially since flecainide is contraindicated in patients with structural heart disease and heart failure.[202] In the brain, inhibition of RyR2-mediated Ca^{2+} leak has proven beneficial in preventing or delaying the onset of neuropathological symptoms in a variety of diseases. Our current investigation led us to examine the effects of a known insect RyR modulator, *nat*-(-)-verticilide, two synthetic precursors, and their mirror image isomers (*ent*). Whereas natural verticilide had no effect on mammalian RyR2, remarkably, we found that its enantiomer significantly inhibited RyR2-mediated Ca^{2+} leak by a distinct mechanism of action compared to other RyR2 inhibitors (Figure 53).

Figure 53. Summary of our discovery of a novel inhibitor of RyR2-mediated Ca^{2+} leak

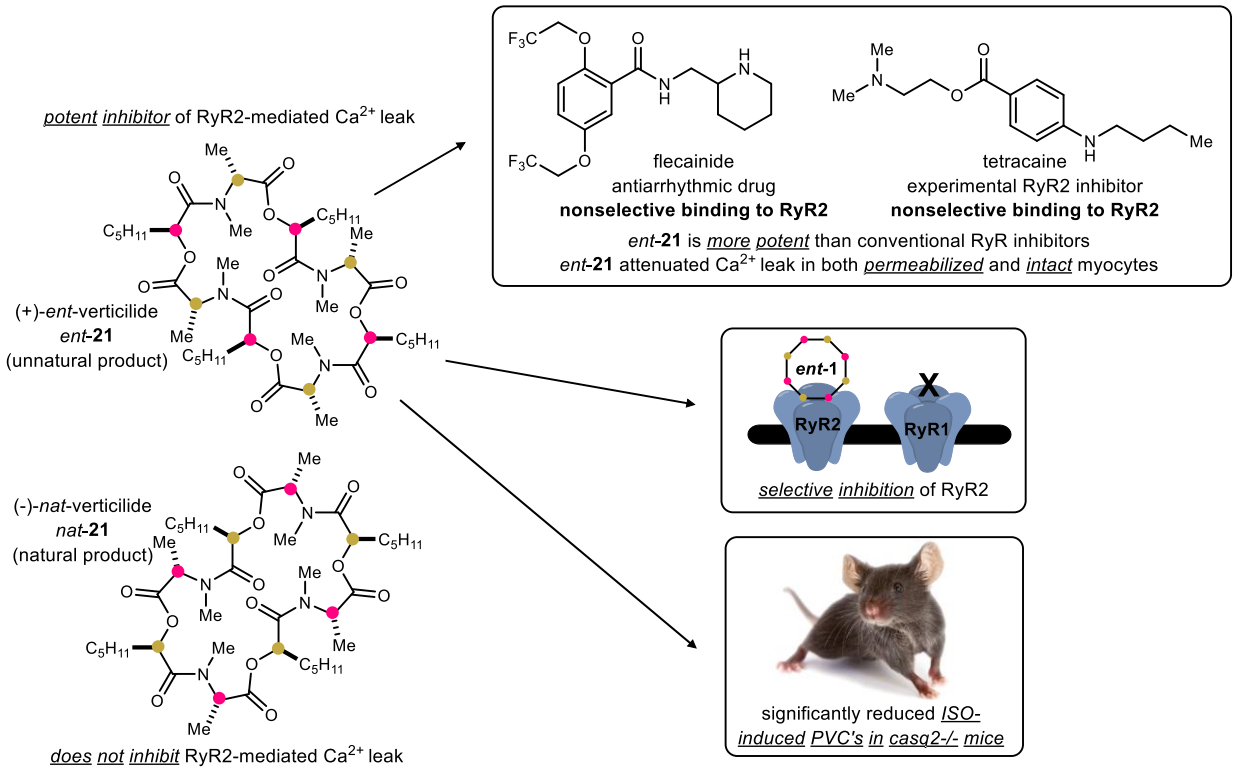

ent-(+)-Verticilide significantly attenuated spontaneous Ca^{2+} release in myocytes isolated from both a CPVT mouse model and wild-type mice. Importantly, *nat*-**21**, **52**, **53**, and their respective enantiomers did not bind to Ca^{2+}. The combined reduction of Ca^{2+} spark frequency, amplitude, and mass resulted in a drastic reduction of Ca^{2+} leak in the presence of *ent*-(+)-verticilide, which is a different mode of action than the prototype compounds tetracaine and flecainide. Additionally, [^{3}H]ryanodine binding experiments revealed that *ent*-(+)-verticilide selectively acts on RyR2, and not RyR1. This finding is significant because current RyR probes (e.g. flecainide and tetracaine) block all RyR subtypes, making them inadequate tools to study the role of RyR2-mediated Ca^{2+} leak in various diseases. *ent*-(+)-Verticilide inhibited spontaneous Ca^{2+} release in intact cardiomyocytes (as opposed to only permeabilized), and therefore

[202] Echt, D. S.; Liebson, P. R.; Mitchell, L. B.; Peters, R. W.; Obias-Manno, D.; Barker, A. H.; Arensberg, D.; Baker, A.; Friedman, L.; Greene, H. L.; et al. *N. Engl. J. Med.* **1991**, *324*, 781.

demonstrated ability to effectively permeate a cell membrane. Furthermore, the activity observed *in vitro* translated to *in vivo* studies, where *ent*-(+)-verticilide significantly reduced isoproterenol-induced PVCs in *Casq2*$^{-/-}$ mice. These data suggest that we have discovered a novel potent inhibitor of intracellular Ca^{2+} leak, and a potentially promising lead compound for drug discovery platforms aimed at developing therapeutics for heart failure, atrial fibrillation, and CPVT, and neurological diseases such as Alzheimer's disease, seizures, and neurodegenerative disorders.

However, a definite molecular mechanism for inhibition of spontaneous Ca^{2+} release by *ent*-(+)-verticilide remains unknown, as verticilide does not resemble any other known Ca^{2+} release inhibitors. The observed decrease in spontaneous Ca^{2+} release by *ent*-(+)-verticilide may be due to direct binding to RyR2, or it may indirectly regulate RyR2 opening via accessory proteins. Previous studies have shown that calmodulin (CaM),[203] Ca^{2+}-CaM Kinase II,[204] and FK 506 proteins,[205] among others,[206] are all important regulators of RyR2 function. It is possible that *ent*-(+)-verticilide suppresses Ca^{2+} leak by indirectly inhibiting RyR2 via one of these mechanisms. Future studies are needed to establish the precise molecular mechanism(s) responsible for *ent*-(+)-verticilide-induced Ca^{2+} spark suppression.

At this time, however, our report highlights a rare and exciting discovery of an unnatural enantiomer that potently suppresses RyR2-mediated Ca^{2+} leak, while the natural product is completely inactive. Due to synthetic barriers, there are few instances where the biological activity of an unnatural enantiomer can be studied in comparison to its naturally occurring analogue[184,185,186,207,208,209,210,211,212,213] Within these instances, the unnatural enantiomer is generally found to be comparably potent to the natural product,[186,209-213] and there are a select few examples where the unnatural enantiomer is greater than 3x more potent than the natural product.[184,185] However, our discovery is unique since, to the best of our knowledge, there are no examples where the unnatural enantiomer of a natural product is highly potent in a biological system while the natural enantiomer is completely inactive. Our ability to access the unnatural – or "dark" –enantiomer and discovery of its activity raises the question whether similar dark chemical space holds generally untapped potential. In the case of verticilide, the unnatural enantiomer induces a pharmacological behavior similar, but mechanistically orthogonal to existing Ca^{2+} release inhibitors flecainide and tetracaine, while the natural product is inactive. This discovery not only confirms the importance of developing straightforward synthetic methods toward natural products and their derivatives, but also contributes to the ongoing excitement to explore 'dark chemical space'[182,187] for chemical biology.

---

[203] Balshaw, D. M.; Xu, L.; Yamaguchi, N.; Pasek, D. A.; Meissner, G. *J. Biol. Chem.* **2001**, *276*, 20144.
[204] Wehrens, X. H.; Lehnart, S. E.; Reiken, S. R.; Marks, A. R. *Circ. Res.* **2004**, *94*, e61.
[205] Chelu, M. G.; Danila, C. I.; Gilman, C. P.; Hamilton, S. L. *Trends Cardiovasc. Med.* **2004**, *14*, 227.
[206] Van Petegem, F. *J. Biol. Chem.* **2012**, *287*, 31624.
[207] Hung, D. T.; Nerenberg, J. B.; Schreiber, S. L. *Chem. Biol.* **1994**, *1*, 67.
[208] Siddiqi, S. M.; Chen, X.; Schneller, S. W.; Ikeda, S.; Snoeck, R.; Andrei, G.; Balzarini, J.; De Clercq, E. *J. Med. Chem.* **1994**, *37*, 551.
[209] Wade, D.; Boman, A.; Wahlin, B.; Drain, C. M.; Andreu, D.; Boman, H. G.; Merrifield, R. B. *Proc. Natl. Acad. Sci. U. S. A.* **1990**, *87*, 4761.
[210] Tichenor, M. S.; Trzupek, J. D.; Kastrinsky, D. B.; Shiga, F.; Hwang, I.; Boger, D. L. *J. Am. Chem. Soc.* **2006**, *128*, 15683.
[211] Iwasa, E.; Hamashima, Y.; Fujishiro, S.; Higuchi, E.; Ito, A.; Yoshida, M.; Sodeoka, M. *J. Am. Chem. Soc.* **2010**, *132*, 4078.
[212] Sando, L.; Henriques, S. T.; Foley, F.; Simonsen, S. M.; Daly, N. L.; Hall, K. N.; Gustafson, K. R.; Aguilar, M. I.; Craik, D. J. *ChemBioChem* **2011**, *12*, 2456.
[213] Boger, D. L.; Johnson, D. S. *Proc. Natl. Acad. Sci. U. S. A.* **1995**, *92*, 3642.

Chapter VI

VI. Conclusion and outlook

6.1 Conclusion

The work presented here began as an effort to develop an UmAS-based synthesis of the bioactive natural product, (-)-verticilide. Over the course of this document, the original synthesis was streamlined to a platform that enables the rapid synthesis of collections of natural product-like cyclodepsipeptides through a hybridization of enantioselective catalysis, Umpolung Amide Synthesis (UmAS), and a Mitsunobu macrocyclooligomerization (MCO).[88] The efficiency and simplicity of this approach was illustrated by the shortest synthesis of cyclodepsipeptide natural products (-)-verticilide, (-)-bassianolide, (+)-montanastatin,[214] and (+)-valinomycin,[214] in addition to several other structural, stereochemical, and ring size-diverse analogs. A key feature of this discovery, however, was that ionic salts, which are normally contraindicated in Mitsunobu conditions, can enhance the formation of size-diverse collections of macrocycles or selectivity for a single macrocycle size through an ion-templating effect. This led us to implement isothermal titration calorimetry (ITC) as a tool to study macrocycle-template binding interactions, and show that these measurements can be correlated to size-distributions of depsipeptides formed during Mitsunobu-based MCOs.[215] These studies identified key trends in quantitative metal ion-cyclic depsipeptide binding interactions across discrete collections of macrocycles, which we demonstrated can be used to predict the effects of salts in new examples. Finally, the newly accessible area of chemical space that resulted from the rational synthesis of unnatural products led to the discovery of a new inhibitor of ryanodine receptor (RyR2)-mediated calcium leak in a collaborative effort with the Knollmann lab.[216]

Many directions and applications of this work remain, some known, many waiting to be revealed by new discoveries or creative disruptions. The remainder of this chapter briefly outlines a few of many possible project ideas that would be interesting to develop in the future, some of which have some supporting preliminary data.

6.2 Outlook

6.2.1 Hetero-MCO for the synthesis of collections RGD-containing macrocycles

As discussed in previous chapters, traditional synthesis of cyclodepsipeptides using active ester-forming reagents in both solution and solid phase is inherently challenging, especially with increasing ring-size. All bioactive depsipeptides of interest do not consist of one repeating unit, and ring-size is an important structural feature to screen in medicinal chemistry. Therefore, an impactful extension of this approach would be to develop a controlled polymerization targeting the synthesis of ring-size congeners of a bioactive peptide sequence, expanded by a smaller linker sequence (Scheme 51).

---

[214] Batiste, S. M.; Johnston, J. N. *unpublished results*.
[215] Batiste, S. M.; Johnston, J. N. *J. Am. Chem. Soc.* **2018**, *in press*.
[216] Batiste, S. M.[+]; Blackwell, D. J.[+]; Kim, K.; Gomez-Hurtado, N.; Rebbeck, R. T.; Cornea, R. L.; Johnston, J. N.*; Knollmann, B. C.*; *submitted*.

Scheme 51. Hetero-MCO synthesis of collections of RGD macrocycles

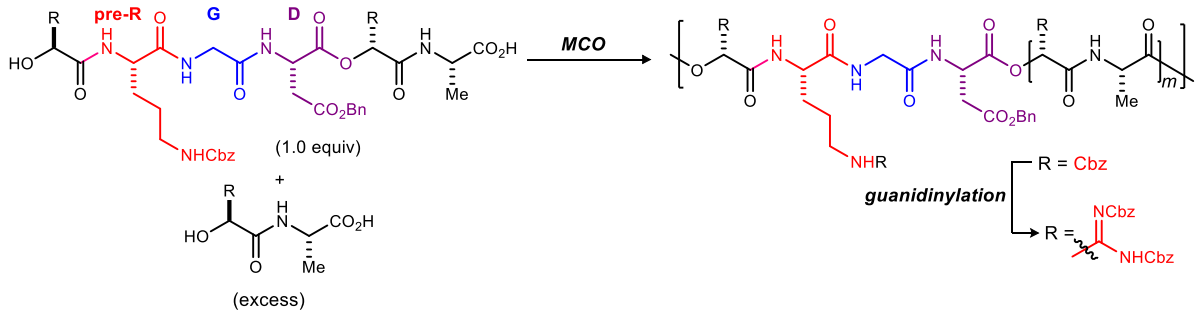

With the goal to develop a hetero-MCO in mind, we have begun to develop an approach around the incorporation of the tripeptide Arginine-Glycine-Aspartic Acid (RGD), also known as the universal cell recognition sequence.[217] The RGD sequence is the cell attachment site of a large number of adhesive extracellular matrix (ECM), blood, and cell surface proteins, and nearly half of the over 20 known integrins recognize the RGD sequence in their adhesion protein binding sites.[217] As the integrin-mediated cell attachment influences and regulates cell migration, growth, differentiation, and apoptosis, synthetic RGD-containing small molecules can be used to probe integrin functions in various biological systems, and provide a basis for drug design targeting diseases such as cancer and thrombosis.[218] Additionally, specific integrins are overexpressed in diseased cells, making the RGD-binding site a direct target for drug design. For example, $\alpha_v\beta_3$ and $\alpha_v\beta_5$ integrins mediate the binding of endothelial cells during tumor angiogenesis, and are overexpressed in solid tumors.[219] Merck used this receptor specificity to their advantage to design a more specific and less toxic chemotherapeutic. The resulting lead compound, Cilengitide©,[220] was an RGD-containing cyclic pentapeptide, which made it to Phase III clinical trials[221] before it was discontinued. The rigid structure of cyclic RGD-containing peptides[222] has proven useful in the development of Cilengitide© and other analogs. Furthermore, studies that examine the effects of amide to ester substitution resulted in an analog three times as potent,[223] which highlights the importance of RGD-containing depsipeptides to medicinal chemistry.

In addition to the usual challenges associated with traditional depsipeptide synthesis, there are a number of challenges associated with the incorporation of arginine into a peptide sequence. The two main challenges are unwanted deprotection of the delta N-protecting group under basic conditions, and deamidation via nucleophilic attack on the guanidine.[224] These two challenges occur more when Cbz protecting groups are used, and can potentially be avoided with the use of Boc protecting groups.[224] However, the harsh acidic conditions necessary to remove Boc-groups at the end of the synthesis would likely result in decomposition of the macrocyclic products. In

[217] Ruoslahti, E. *Annu. Rev. Cell Dev. Biol.* **1996**, *12*, 697.
[218] Thundimadathil, J. *J. Amino Acids* **2012**, *2012*, 967347.
[219] Chen, Z.; Deng, J.; Zhao, Y.; Tao, T. *Int. J. Nanomedicine* **2012**, *7*, 3803.
[220] Dechantsreiter, M. A.; Planker, E.; Mathä, B.; Lohof, E.; Hölzemann, G.; Jonczyk, A.; Goodman, S. L.; Kessler, H. *J. Med. Chem.* **1999**, *42*, 3033.
[221] Carlos, M.-M.; Florian, R.; Horst, K. *Anti-Cancer Agents Med. Chem.* **2010**, *10*, 753.
[222] Haubner, R.; Schmitt, W.; Hölzemann, G.; Goodman, S. L.; Jonczyk, A.; Kessler, H. *J. Am. Chem. Soc.* **1996**, *118*, 7881.
[223] Cupido, T.; Spengler, J.; Ruiz-Rodriguez, J.; Adan, J.; Mitjans, F.; Piulats, J.; Albericio, F. *Angew. Chem. Int. Ed.* **2010**, *49*, 2732.
[224] Bastiaans, H. M. M.; van der Baan, J. L.; Ottenheijm, H. C. J. *J. Org. Chem.* **1997**, *62*, 3880.

this work, the challenges associated with Cbz-Arginine incorporation were avoided with the use of a truncated ornithine (Orn)-containing monomer, which can undergo a late-stage guanidinylation to provide the desired arginine.[225]

Scheme 52. Preliminary RGD macrocycle synthesis results: homo-MCO vs hetero-MCO

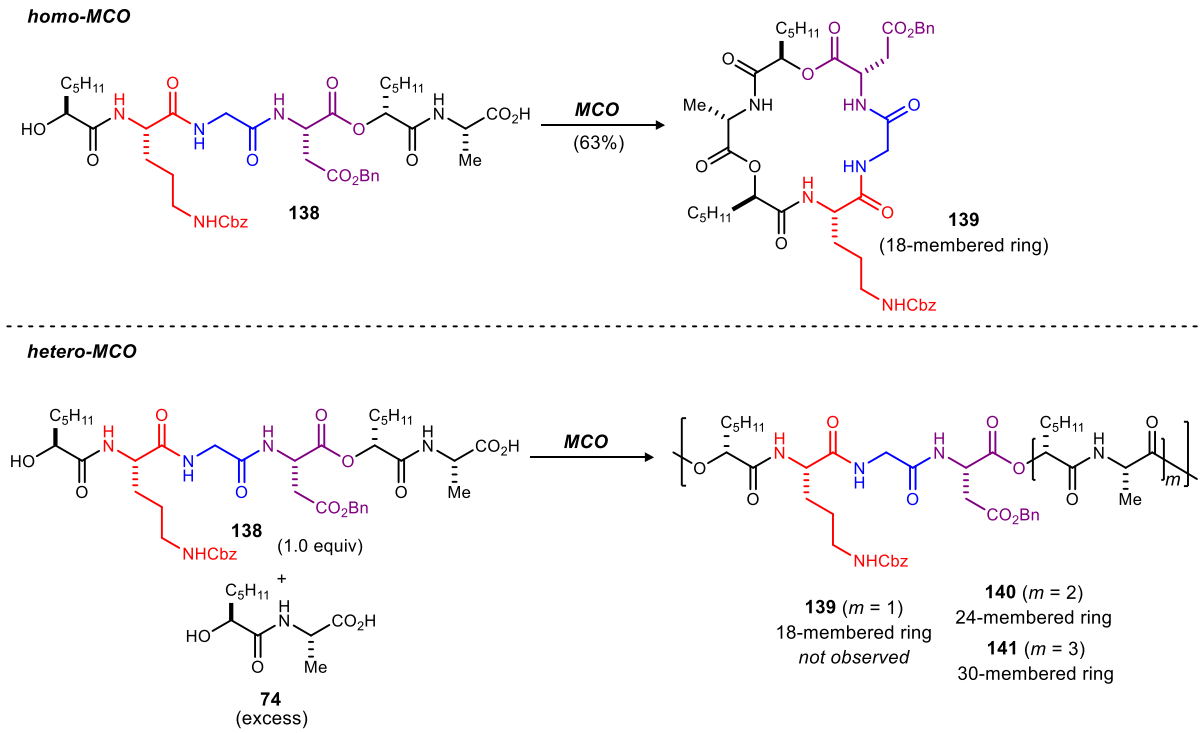

Monomer **138**, alone, rapidly undergoes macrolactonization when subjected to standard Mitsunobu MCO conditions. However, when subjected to MCO conditions in the presence of excess **74**, 18-membered ring **139** was not observed. Instead, formation of RGD-containing oligomers with mono (**140**) and di-incorporation (**141**) of **74** were identified by LCMS.[226] This preliminary result is promising for our goal of developing a controlled hetero-MCO. Further optimization of conditions, screening of templates, and ITC analysis, is necessary to develop this reaction to its full potential.

[225] Wohlrab, A.; Lamer, R.; VanNieuwenhze, M. S. *J. Am. Chem. Soc.* **2007**, *129*, 4175.

[226] 1H NMR spectra of **140** and **141** were very broad, so LCMS is the basis for proposed ring sizes. This reaction was run with 7.0 mg of **138** and 3.6 mg of **74**. Isolated approximately 1-2 mgs of **140** and **141**.

Table 14. Global deprotection attempts

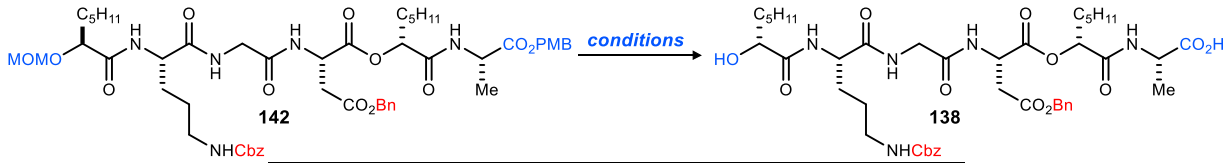

entry	conditions	isolated yield (%)
1	TFA, CH_2Cl_2, rt, 20 m	27
2	TFA, anisole, CH_2Cl_2 rt, 2 h	50
3	$ZrCl_4$, rt, 20 m	42
4	1. ^{p}TsOH/anisole , dioxane 0°C, 2. TFA/DCM, rt	8

A major barrier to this project is the current synthesis of RGD-containing monomer **138**, and challenges associated with the compatibility of sidechain protecting groups with the hydroxy terminal-MOM group. The acidic conditions required to remove the MOM group, also result in partial removal of the Orn-Cbz group. Despite much effort in attempting to develop new MOM-deprotection conditions, the yield of the final deprotection step remains low. Therefore, attempting the synthesis with a different hydroxyl protecting group may be the best option, since the Bn and Cbz sidechain protecting groups are necessary to ensure that the macrocyclic products remain intact upon their deprotection.

The MOM group is used in our synthesis of α-oxy bromonitroalkanes because it is easily installed under mild acidic conditions (dimethoxymethane, P_2O_5). The use of basic conditions to install the hydroxyl protecting group are not tolerated, and result in decomposition through a retro-Henry pathway. However, a cursory protecting group screen revealed that the MOM-group is not the only viable hydroxy protecting group, especially because nitroalkanes are viable donors in UmAS. Bromonitroalkanes bearing 1-ethoxyethyl (EE) or 2-methoxy-2-propyl (MOP) groups spontaneously deprotect/decompose (in my hands). However, nitroalkanes bearing EE or MOP protecting groups can be installed without decomposition, but only EE survived UmAS reasonably well. The EE group can be removed using PPTS (1 equiv), which will not deprotect the Cbz, Bn, or even the highly acid-labile PMB ester. The downside of using the EE group is that it adds a chiral center to all of the EE-containing intermediates, and therefore adds a significant element of complexity[227] to reaction monitoring by TLC, purification steps, and subsequent characterization by NMR spectroscopy.

6.2.2 Development of improved MCO purification

A major challenge with the Mitsunobu MCO, and with Mitsunobu chemistry in general, is purification, especially on scale. When the MCO is run on small scale, the usual silica plug is sufficient to separate the bulk of the reagent byproducts from the material that will be subjected to

[227] Disclaimer: your TLC plate and ^{1}H NMR spectra will look terrible if your starting nitroalkane is not enantiopure (or close to it). I suggest using the IndaBOX catalyst (we have materials to make both enantiomers of catalyst to afford either *R* or *S*-nitroalkane) because the ee of the products with IndaBOX (96% ee) is much higher than with the Blay catalyst (87% ee)

prep HPLC purification. However, upon scale-up, the excess reagents become magnitudes more difficult to remove. Additionally, with interests to expand our scope of macrocycles to include variants with polar sidechains on the horizon, prep HPLC purification will soon become much more challenging. Preliminary results with polar sidechain-containing macrocycles revealed that the product retention times are very, very close to, and some overlapping, with triphenylphosphine oxide (TPPO) and DIAD-derived hydrazine. Therefore, it is worth investigating new MCO conditions that enable clean and fast removal of reagent byproducts.

Protocols to precipitate DIAD hydrazine and TPPO usually involve nonpolar solvents, which in this case will result in precipitation of products as well. However, a protocol using $ZnCl_2$ to precipitate TPPO from polar solvents was recently published,[228] and was attempted with the MCO from ethyl acetate.[229] Although $ZnCl_2$ did successfully precipitate the majority of the TPPO from the crude reaction mixture, the protocol resulted in diminished yields compared to usual.

A promising alternative to traditional Mitsunobu reagents (DIAD and PPh_3) are fluorinated variants developed by Curran and coworkers.[230,231] The use of ^{F}DEAD and $^{F}PPh_3$ enables separation of reagent byproducts from desired products by fluorous solid phase extraction (FSPE) with a fluorous silica plug. Elution with 80% MeOH provides the non-fluorinated desired products, and a final Et_2O flush elutes the fluorinated reagent byproducts. Additionally, the use of these fluorinated reagents has been shown to substantially improve purification without sacrificing yield.

6.2.3 Drug delivery depsipeptides

Nuclear delivery of cell-impermeable and water insoluble small molecules is a major challenge to overcome in drug-delivery vehicle design. Cellular uptake of drug-delivery vehicles occurs predominantly through endocytosis, which is problematic if the compound remains trapped in the endosomes and cannot reach the target in the nucleus. Thus, drug-delivery strategies that promote endosomal escape or avoid the pathway all together are in high-demand. Parang and coworkers have designed a library of amphiphilic, homochiral cyclic peptides as nuclear transporters that enter the cell through a non-endocytotic pathway.[232] A library of different ring sizes (12 to 30 ring atoms) with charged amino acids were synthesized using Fmoc-based solid phase peptide synthesis. These cyclic peptides were then linked to a fluorophore in order to examine cellular uptake, nuclear localization, and small molecule transport abilities. The cyclic peptide with the best of all three properties is a 24-membered macrocycle with alternating L-Trp and L-Arg residues (**142**). Examining cellular uptake of **142** in the presence of endocytotic inhibitors did not change its ability to permeate the cell membrane, thus Parang and coworkers hypothesize that the cyclic peptide enters the membrane through direct membrane transduction, rather than endocytosis. This is proposed to occur through a combination of positively charged arginine interactions with the negatively charged phospholipids, and hydrophobic interactions between tryptophan and hydrophobic residues in the lipid bilayer.[233]

---

[228] Batesky, D. C.; Goldfogel, M. J.; Weix, D. J. *J. Org. Chem.* **2017**, *82*, 9931.
[229] $ZnCl_2$ protocol was attempted by Abby Smith.
[230] Dandapani, S.; Curran, D. P. *Tetrahedron* **2002**, *58*, 3855.
[231] Dandapani, S.; Curran, D. P. *J. Org. Chem.* **2004**, *69*, 8751.
[232] Mandal, D.; Nasrolahi Shirazi, A.; Parang, K. *Angew. Chem. Int. Ed. Engl.* **2011**, *50*, 9633.
[233] Nasrolahi Shirazi, A.; Tiwari, R. K.; Oh, D.; Banerjee, A.; Yadav, A.; Parang, K. *Mol. Pharm.* **2013**, *10*, 2008.

Peptides consisting entirely of L-amino acids are potential immunogens, causing a hypersensitivity reaction *in vivo*.[234] Additionally, cyclic charged polypeptide vehicles are notorious for either extreme stability, retaining their contents for days at a time, or for rapid clearance from blood circulation without any delivery to the cells.[235] Thus, peptidomimetics have been designed in attempts to afford better pharmacological properties *in vivo*.[236] Polymeric micelles have been of increasing interest over the past two decades as drug delivery vehicles for poorly water soluble drugs.[237] Polymeric micelles have a number of useful properties for drug delivery such as water solubility, biodegradability, and a stable micellar structure with a hydrophobic core that can physically entrap hydrophobic drugs. However, achieving high drug loading in these micelles is often difficult because interactions of the drug with the core of the micelle are variable.[237] Polydepsipeptides possess degradability of polyesters and functionality of polypeptides, thus are a convenient material to tailor intermolecular interactions with a drug of choice.

Figure 54. Amphiphilic polypeptide vehicle

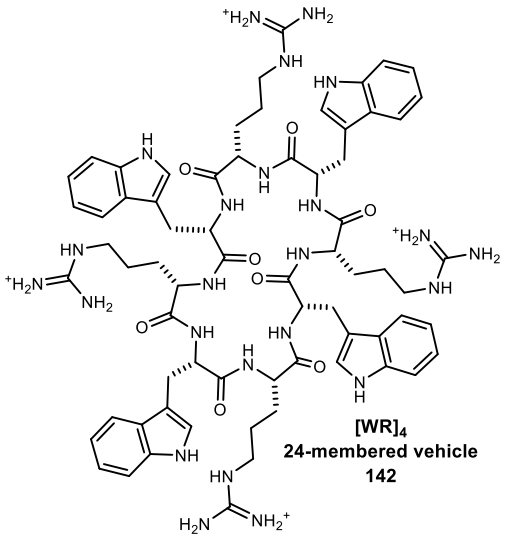

Our Mitsunobu MCO can be applied to drug delivery vehicle design to create cyclodepsipeptide vehicles with charged residues (such as ornithine, lysine, and arginine). Although polar side chain-containing substrates were not detailed in this dissertation, promising results were observed with **143**, which contains a D-Lac-L-Orn-Gly sequence. Unlike the alternating amide-ester depsipeptides discussed in this document, this monomer will create macrocycles with a repeating amide-amide-ester sequence. This sequence may be more ideal than the former for drug delivery purposes because the resulting depsipeptide products will likely be less sensitive to hydrolysis, but also more lipophilic than purely amide-containing macrocycles. Replacing amide bonds with ester linkages has been shown to increase conformational flexibility and amphiphilicity, two properties that are favorable for cell membrane penetration.[238] Additionally, removal of amide protons reduces intramolecular hydrogen bonding,[239] which is beneficial when the macrocycle needs to intermolecularly hydrogen bond with the drug and the phospholipid bilayer in order to successfully enter the cell.

[234] Lien, S.; Lowman, H. B. *Trends Biotechnol.* **2003**, *21*, 556.
[235] Tian, B.; Tao, X.; Ren, T.; Weng, Y.; Lin, X.; Zhang, Y.; Tang, X. *J. Mater. Chem.* **2012**, *22*, 17404.
[236] Avan, I.; Hall, C. D.; Katritzky, A. R. *Chem. Soc. Rev.* **2014**, *43*, 3575.
[237] Takahashi, A.; Ozaki, Y.; Kuzuya, A.; Ohya, Y. *Biomed Res. Int.* **2014**, *2014*, 579212.
[238] Bionda, N.; Stawikowski, M.; Stawikowska, R.; Cudic, M.; Lopez-Vallejo, F.; Treitl, D.; Medina-Franco, J.; Cudic, P. *ChemMedChem* **2012**, *7*, 871.
[239] Scheike, J. A.; Baldauf, C.; Spengler, J.; Albericio, F.; Pisabarro, M. T.; Koksch, B. *Angew. Chem. Int. Ed. Engl.* **2007**, *46*, 7766.

Figure 55. MCO with polar side chain-containing monomer 143

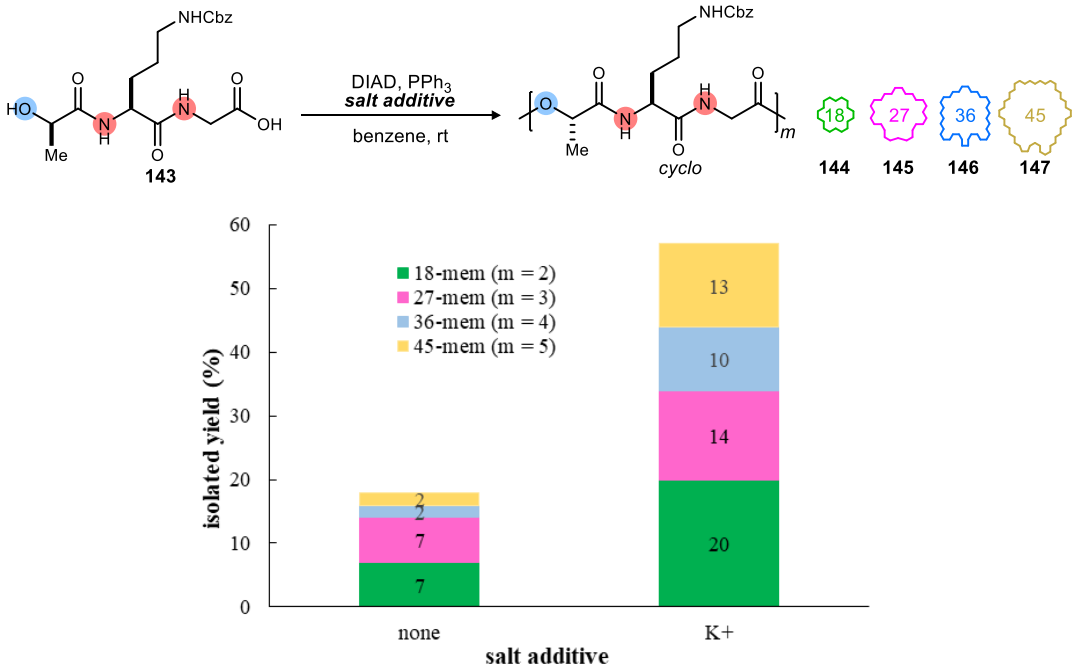

Following preparation of **143**, it was subjected to standard Mitsunobu-MCO conditions [DIAD (2.5 equiv), PPh_3 (3.0 equiv), benzene (5 mM)] with and without salt additive. Potassium chloride (5.0 equiv) was selected as the templating salt. The D-Lac-L-Orn-Gly monomer creates macrocycle sizes in multiples of 9, with an ester-amide-amide backbone sequence. In addition to the polar side chain, the dipeptide character of the monomer renders it substantially more polar than depsipeptides studied in this document, so the usual prep HPLC assay was adjusted in order to purify the products. The preliminary results are shown in Figure 55.

This monomer was not very reactive in the MCO without salt, providing total macrocycle product in 18% overall yield. The addition of a potassium salt increased the total yield of these same macrocyclic products to 57% yield. Our hypothesis is that potassium enhances the formation of each of the four macrocycles, roughly 2-5x. Despite the polar side chain, the Mitsunobu-MCO delivers synthetically useful amounts of depsipeptide macrocycles. The longer, more polar tripeptide monomer behaves similarly to the didepsipeptide monomers we have studied. The effect of salt on the Mitsunobu-MCO of **143** is clearly enhancing. In this case, all four macrocycles are enhanced in amount. Further interpretation of this result would require the same thorough experimentation provided for those cases described in previous chapters. This success with a very different, more polar monomer suggests broader application.

6.2.4 Discovery of new compatible Lewis acidic templates in the MCO

An area of our Mitsunobu-MCO that has yet to be fully explored and understood in detail is the scope of templates that are compatible with the reaction. We are faced with the challenge that the basis of the process is Mitsunobu chemistry, which is inherently incompatible with the addition of excess electrolytes. However, if the ions that are added interact with the substrates more than the Mitsunobu reagents, a templating effect is observed without loss of overall

reactivity. Therefore, it is possible that there are more effective templates that have yet to be discovered.

The basis of the work outlined in this document provides the protocols necessary to discover new templates that are compatible with Mitsunobu MCO conditions in a rapid manner. The use of a chlorine or bromine-containing monomer, such as didepsipeptide **110**, will produce products with very distinctive LCMS fragmentation patterns due to Cl and Br isotope abundances, which serve as a reliable marker to rapidly identify the sizes of new macrocycles formed in a crude reaction mixture. Some interesting new templates to investigate are NH_4^+X, quaternary ammonium salts, guanidinium salts, other metals that might be inert to the reagents (Mg^{2+}, Cs^{2+}, Sr^{2+}, Ba^{2+}, Rb^+). Chloride is generally a safe counteranion if the BF_4^- salt is not commercially available, but Br^- and I^- counterions can potentially undergo Appel chemistry in Mitsunobu conditions. Alkali metal salts with $^-PF_6$, $^-$BARF, and $^-NTf_2$ form insoluble complexes with Mitsunobu reagents. Transition metal salts may be considered, however metals such as Ag, Pd, Ni, Pt, Au, Cu, Ir, Zn, Co, Rh, Ru will rapidly react with PPh_3, and should probably be avoided.

MCO reactions with the new templates can be screened for products on small scale using LCMS. This approach will generate results quickly without wasting time interpreting potentially complex crude NMR spectra. Note: these steps are not quantitative measures of products—reactions where products are detected by LCMS, should be repeated on larger scale (minimum 15 mg of starting material), in order to obtain isolated yields (as per the MCO protocol listed in the supporting information). Finally, ITC can be used to measure binding affinities of macrocycles to any new MCO-compatible templates. The thermodynamic trends we have elucidated from this method provide the first analytical platform to rationally select a template for a targeted size-regime of cyclodepsipeptides. Continuing to reveal new template and substrate-related trends will continue to broaden the synthetic impact of this method.

Appendix 7.1 Synthesis & characterization of organic molecules

Glassware was flame-dried under vacuum for all non-aqueous reactions. All reagents and solvents were commercial grade and purified prior to use when necessary. Benzene and dichloromethane (CH_2Cl_2) were dried by passage through a column of activated alumina as described by Grubbs.[1] Blay[2,3] ligand was prepared according to literature procedures. Bromonitromethane (90% technical grade) was used as received. NIS was recrystallized from dioxane/CCl_4. Flash column chromatography was performed using Sorbent Technologies 230-400 mesh silica gel with solvent systems indicated. Analytical thin layer column chromatography was performed using Sorbent Technologies 250 µm glass-backed UV254 silica gel plates, and was visualized by fluorescence upon 250 nm radiation and/or the by use of ceric ammonium molybdate (CAM), phosphomolybdic acid (PMA), or potassium permanganate ($KMnO_4$). Solvent removal was effected by rotary evaporation under vacuum (~ 25-40 mm Hg). All extracts were dried with $MgSO_4$ unless otherwise noted.

Preparative HPLC was performed on an Agilent 1260 system (column: Zorbax Eclipse XDB-C18; 21.2 mm x 150 mm, 5 µm, flow rate 8 mL/min) with 210 nm monitoring wavelength and water/acetonitrile (+0.1% TFA) gradient as indicated.

Nuclear magnetic resonance spectra (NMR) were acquired on a Bruker AV-400 (400 MHz), Bruker DRX-400 (400 MHz), Bruker DRX-500 (500 MHz), Bruker AV-II-600 (600 MHz), Bruker AV-III-800 (800 MHz), or Bruker AV-III-900 (900 MHz) instrument. Chemical shifts are measured relative to residual solvent peaks as an internal standard set to δ 7.26 and δ 77.0 ($CDCl_3$), δ 2.50 and δ 39.5 (DMSO-d_6), δ 1.94 and δ 118.3 (CD_3CN), unless otherwise specified. Ratios of diastereomers and isomeric products were measured directly from integration of ^1H NMR absorptions of protons common to the components. Reported chemical shifts and integrations for macrocycles resulting from macrocyclooligomerization (MCO) correspond to only the major conformer. Mass spectra were recorded on a Thermo Electron Corporation MAT 95XP-Trap mass spectrometer by use of the ionization method noted by the Indiana University Mass Spectrometry Facility. IR spectra were recorded on a Nicolet Avatar 360 spectrophotometer and are reported in wavenumbers (cm^{-1}) as neat films on a NaCl plate (transmission). Melting points were obtained using a Meltemp melting point apparatus and are not corrected, or an OptiMelt automated melting point system available (Stanford Research Systems). Optical rotations were measured on a Perkin Elmer-341 polarimeter.

7.1.1 General procedures

Umpolung Amide Synthesis (UmAS): A round-bottom flask was charged with bromonitroalkane (1 equiv, 0.2 M), amine (1.2 equiv), 2-Me-THF, and H_2O (5 equiv). The mixture was cooled to 0 °C and treated with NIS (1 equiv) followed by K_2CO_3 (2 equiv) and an O_2 balloon. The heterogeneous solution was stirred for 2 days at 0 °C, and then treated at 0 °C with 1 N HCl and poured into CH_2Cl_2. The aqueous layer was extracted with CH_2Cl_2, and the combined organic layers were washed with satd aq $Na_2S_2O_3$, dried, and concentrated. The crude residue was subjected to flash column chromatography to afford the amide.

One-Pot UmAS: A round-bottom flask was charged with nitroalkane (1 equiv, 0.2 M), amine (2.0 equiv), DME, and H_2O (5 equiv). The mixture was then treated with DBTCE (1.2 equiv) followed by NaI (0.1 equiv), K_2CO_3 (2 equiv) and an O_2 balloon. The heterogeneous solution was vigorously stirred for 1-2 days at ambient temperature, and then treated at 0 °C with 1 N HCl and poured into CH_2Cl_2. The aqueous layer was extracted with CH_2Cl_2, and the combined organic layers were washed with satd aq $Na_2S_2O_3$, dried, and concentrated. The crude residue was subjected to flash column chromatography to afford the amide.

[1] A. B. Pangborn, M. A. Giardello, R. H. Grubbs, R. K. Rosen, F. J. Timmers, *Organometallics* **1996**, *15*, 1518.
[2] Blay, G.; Climent, E.; Fernández, I.; Hernández-Olmos, V.; Pedro, J. R. *Tetrahedron: Asymmetry* **2007**, *18*, 1603.
[3] Blay, G.; Domingo, L. R.; Hernández-Olmos, V.; Pedro, J. R. *Chem. Eur. J.* **2008**, *14*, 4725.

Methoxymethylene ether (MOM) Deprotection I: A flame-dried round-bottom flask under argon atmosphere was charged with MOM-protected amide (1 equiv, 0.05 M) in CH_2Cl_2. Thiophenol (5 equiv) was added to the solution, followed by $Et_2O{\bullet}BF_3$ (5 equiv). The reaction was allowed to stir for 1 h at room temperature and then poured into CH_2Cl_2. The organic solution was washed twice with satd aq $NaHCO_3$, followed by brine, and then dried and concentrated. The residue was subjected to flash column chromatography to furnish the alcohol.

Methoxymethylene Ether (MOM) Deprotection II: A round-bottom flask was charged with MOM-protected amide (1 equiv, 0.1 M), TFA/CH_2Cl_2 solution (50% v/v), and a drop of water (approx. 10 µL). The reaction was allowed to stir overnight at room temperature and then concentrated. The crude residue was dissolved in EtOAc, washed twice with satd aq $NaHCO_3$, followed by brine, and then dried and concentrated. The residue was subjected to flash column chromatography to furnish the alcohol.

Benzyl Deprotection I: A round-bottom flask was charged with benzyl ester (1 equiv, 0.1 M) in MeOH. 10% Pd/C (0.2 equiv) was added to the stirring solution and a light vacuum (60 Torr) was applied, followed by backflush using a hydrogen balloon. The reaction was allowed to stir for 1 h and then filtered through Celite and concentrated to furnish the carboxylic acid.

Benzyl Deprotection II: A round-bottom flask was charged with benzyl ester (1 equiv, 0.05 M) in EtOAc. 10% Pd/C (0.2 equiv) was added to the stirring solution and a light vacuum (60 Torr) was applied, followed by backflush using a hydrogen balloon. The reaction was allowed to stir for 25 min and then filtered through Celite and concentrated to a residue that was subjected to preparative HPLC. Preparative HPLC was performed on an Agilent 1260 system (column: Zorbax Eclipse XDB-C18; 21.2 mm x 150 mm, 5 µm, flow rate 20 mL/min) with 210 nm monitoring wavelength and gradient of 5 to 95% acetonitrile in water (+0.1% TFA) over 30 min. The desired fractions were then diluted with EtOAc, washed with water (three times), followed by brine, and then dried and concentrated.[4]

Global Deprotection: A flame-dried round-bottomed flask under inert atmosphere was charged with $AlCl_3$ (10 equiv), and toluene (0.05 M relative to amide) at 0 °C. Then MOM and benzyl-protected depsipeptide (1.0 equiv) were dissolved in a small amount of toluene and added dropwise to the stirring solution. The reaction was allowed to slowly warm to ambient temperature and stir until starting material was no longer present by TLC. The mixture was then cooled to 0 °C and quenched with satd aq Rochelle's salt. The heterogeneous solution was stirred at ambient temperature until two distinct layers were apparent, and then diluted with EtOAc and water. The aqueous layer was extracted with EtOAc, and the combined organic layers were washed with brine, dried, and concentrated to a residue that was subjected to preparative HPLC. Preparative HPLC was performed on an Agilent 1260 system (column: Zorbax Eclipse XDB-C18; 21.2 mm x 150 mm, 5 µm, flow rate 8 mL/min) with 210 nm monitoring wavelength and gradient of 5 to 95% acetonitrile in water (+0.1% TFA) over 30 min. The desired fractions were then diluted with EtOAc, washed with water (three times), followed by brine, and then dried and concentrated.[4]

Mitsunobu: A flame-dried round-bottom flask under inert atmosphere was charged with PPh_3 (2 equiv), DIAD (2 equiv), and benzene, and was stirred at ambient temperature for 30 m. The alcohol (1 equiv, 0.05 M) was added to the solution, followed by the carboxylic acid (1.1 equiv). The reaction was stirred for 24 h, and then concentrated to afford a residue that was subjected to flash column chromatography.

[4] Unless otherwise specified, preparatory HPLC fractions containing depsipeptides (macrocyclic or linear) were subjected to extractive workup. These compounds are sensitive to cleavage under the high-heat conditions necessary to remove the acidic water-acetonitrile solvent system via rotary evaporation. Additionally, these compounds retain polar solvents & TFA, so the washes (water for acidic depsipeptides, satd aq $NaHCO_3$ for non-acidic depsipeptides) are necessary for complete removal.

Tetradepsipeptide MCO: A flame-dried round-bottomed flask under inert atmosphere was charged with a salt additive (5 equiv), *seco*-acid (1 equiv in CH_2Cl_2, 0.38 M), PPh_3 (3 equiv), and benzene to bring the final concentration of *seco*-acid to 0.005 M. DIAD (2.5 equiv) was then added to the stirred solution in 5 aliquots over 40 minutes. The reaction was allowed to stir at ambient temperature for 24 h, and then concentrated to afford a residue that was subjected to the MCO purification protocol.

Didepsipeptide MCO: A flame-dried round-bottomed flask under inert atmosphere was charged with a salt additive (2.5 equiv), *seco*-acid (1 equiv), PPh_3 (6 equiv), and benzene to bring the final concentration of *seco*-acid to 0.02 M. DIAD (5.0 equiv) was then added to the stirred solution in 15 aliquots over 120 minutes. The reaction was allowed to stir at ambient temperature for 24 h, and then concentrated to afford a residue that was subjected to the MCO Purification Protocol.

7.1.2. General MCO purification tutorial

MCO Purification Protocol: The crude residue was filtered through a plug (1.9 cm x 8.2 cm) of silica gel to remove excess Mitsunobu reagents, and to roughly separate macrocyclic products into two fractions prior to separation using preparatory HPLC. [Some macrocycles exhibited similar R_f by prep-HPLC, but very different R_f when using normal phase silica gel; see figures below.] A stepwise MeOH/DCM gradient allowed the crude mixture to be separated into three fractions (Fraction 1: 0.5-1% MeOH/DCM; Fraction 2: 2-3% MeOH/DCM; Fraction 3: 20% MeOH DCM) prior to prep HPLC purification. The contents of Fraction 1 (Mitsunobu reagent byproducts only) were discarded, and Fractions 2 & 3 were dissolved (separately) in DMSO and subjected to prep HPLC purification. Preparative HPLC was performed on an Agilent 1260 system (column: Zorbax Eclipse XDB-C18; 21.2 mm x 150 mm, 5 µm, flow rate 8 mL/min) with 210 nm monitoring wavelength and gradient of 5 to 95% acetonitrile in water (+0.1% TFA) over 40 min. Fractions containing macrocyclic products were then diluted with EtOAc and washed twice with satd aq $NaHCO_3$, followed by brine, and then dried and concentrated.[4]

Sample prep HPLC traces from MCO of didepsipeptide **74**:

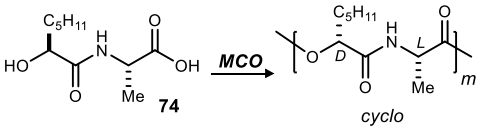

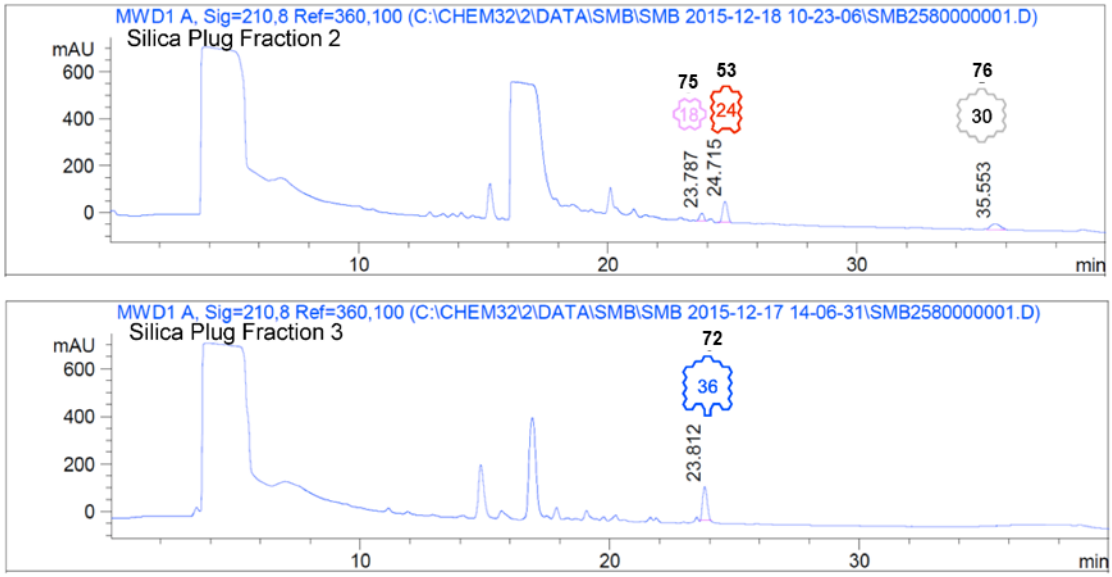

Sample prep HPLC traces from MCO of didepsipeptide **77**:

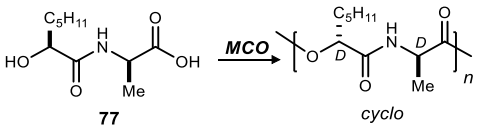

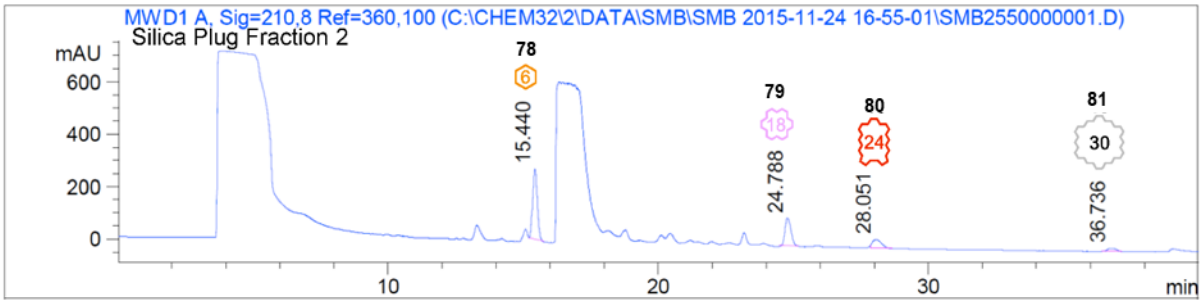

Sample prep HPLC traces from MCO of tetradepsipeptide **70**:

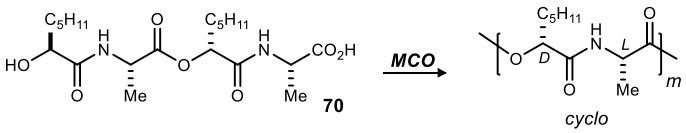

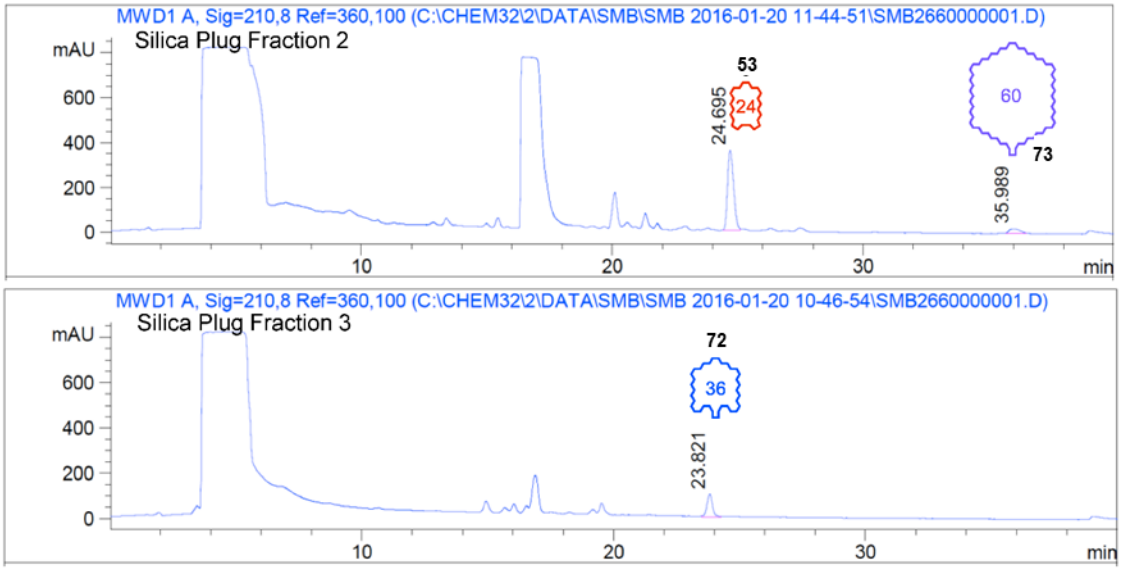

Sample prep HPLC trace from MCO of didepsipeptide **110**:

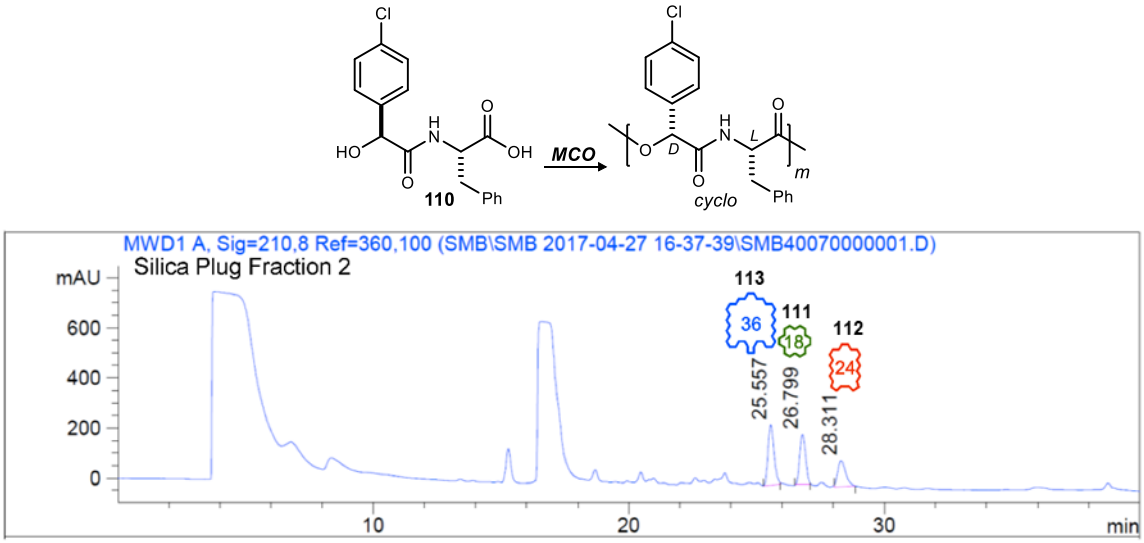

7.1.3. Characterization data for reported compounds

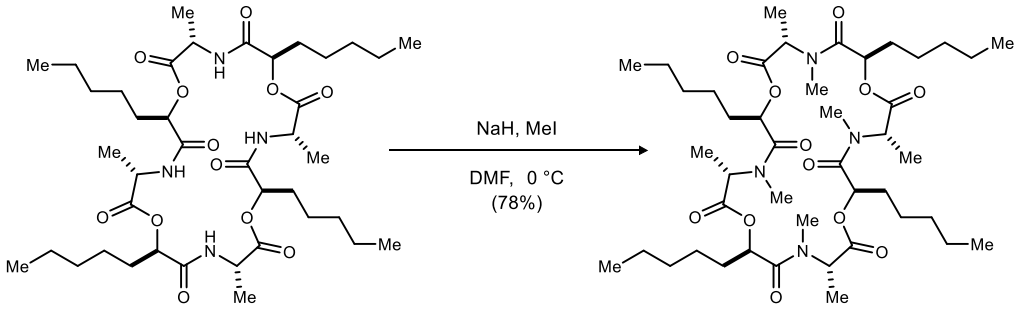

(–)-Verticilide (*nat*-21). A flame-dried round-bottom flask was charged with *N*-H depsipeptide **6** (20.0 mg, 25.1 μmol) and dry DMF (500 μL) at 0 °C. Methyl iodide (62.5 μL, 1.00 mmol) was then added to the reaction mixture, and NaH (6.0 mg, 251 μmol in DMF (250 μL)) was added slowly to the reaction mixture in 50 μL aliquots over 15 minutes. The reaction was allowed to stir at 0 °C for 25 m, and it was then quenched by the dropwise addition of satd aq NH_4Cl. The aqueous layer was extracted with EtOAc, and the combined organic layers were washed with satd aq $NaHCO_3$, satd aq $Na_2S_2O_3$, water and brine, and then dried and concentrated to afford a residue that was subjected to flash column chromatography (SiO_2, 1-5% methanol in dichloromethane) to afford (-)-verticilide (16.7 mg, 78%) as a colorless oil. $[\alpha]_D^{20}$ -47 (*c* 0.21, MeOH)[5]; R_f = 0.21 (5% MeOH/DCM); IR (film) 2955, 2920, 2851, 1746, 1667, 1539, 1466, 1378, 1199, 1019 cm^{-1}; HRMS (ESI): Exact mass calcd for $C_{44}H_{76}N_4NaO_{12}$ $[M+Na]^+$ 875.5357, found 875.5341.

[5] Lit value: $[\alpha]_D^{25}$ -53 (*c* 0.20, MeOH). Shiomi, K.; Matsui, R.; Kakei, A.; Yamaguchi, Y.; Masuma, R.; Hatano, H.; Arai, N.; Isozaki, M.; Tanaka, H.; Kobayashi, S.; Turberg, A.; Omura, S. *J. Antibiot.* **2010**, *63*, 77.

Comparison of prepared (-)-verticilide and literature values:[5]

^{1}H δ Literature	Mult, *J* values	^{1}H δ Synthesis	Mult, *J* values
0.52	d, *J* = 7.0 Hz	0.55	d, *J* = 6.8 Hz
0.63	d, *J* = 7.0 Hz	0.67	d, *J* = 7.6 Hz
0.83-1.00	m	0.84-1.04	m
1.28	m	1.28-1.51	s of m
1.39	m		
1.51	m		
1.58	m	1.58	m
1.68-1.85	m	1.68-1.88	m
2.07	m	2.00-2.25	br m
2.15-2.22	m		
2.82	s	2.89	s
2.85	s	3.01	s
2.98	s	3.04	s
3.01	s	3.1	s
3.22	s	3.25	s
4.39	dd, *J* = 11.6, 4.0 Hz	4.43	dd, *J* = 10.6, 4.4 Hz
4.96	d, *J* = 2.3 Hz	4.99	d, *J* = 2.8 Hz
5.15	d, *J* = 7.7 Hz	5.16	br m
5.25	d, *J* = 6.9 Hz	5.28	d, *J* = 6.8 Hz
5.41	d, *J* = 7.9 Hz	5.45	d, *J* = 8.0 Hz
5.41	dd, J = 12.1, 4.2 Hz	5.45	dd, J = 11.8, 4.3 Hz
5.48	d, *J* = 2.2 Hz	5.5	d, *J* = 2.0 Hz
5.59	dd, J = 12.2, 4.6 Hz	5.62	dd, J = 12.3, 4.4 Hz
5.62	dd, *J* = 12.2, 4.3 Hz	5.65	dd, *J* = 12.3, 4.2 Hz

^{13}C Literature values	^{13}C Synthesis values	Difference	^{13}C Literature values	^{13}C Synthesis values	Difference
14.7	14.7	0	30.5	30.5	0
15.7	15.7	0	30.7	30.8	0.1
17.8	17.9	0.1	30.9	30.9	0
18.1	18	0.1	31	31.2	0.2
18.2	18.2	0	31.6	31.6	0
18.4	18.4	0	36.7	36.74	0.04
18.5	18.44	0.06	36.7	36.78	0.08
18.6	18.6	0	37.6	37.6	0
18.7	18.7	0	37.9	37.9	0
20.2	20.1	0.1	38.5	38.5	0
20.6	20.6	0	53.3	53.2	0.1
20.8	20.7	0.1	54.2	54.2	0
20.8	20.8	0	54.3	54.23	0.07
21	21	0	57.5	57.5	0
21.3	21.2	0.1	74.2	74.2	0
23.4	23.3	0.1	74.3	74.3	0
23.5	23.4	0.1	75.2	75.2	0
23.5	23.5	0	76.8	76.8	0
23.6	23.6	0	168.7	168.6	0.1
23.7	23.7	0	169.1	169.1	0
24.7	24.7	0	169.4	169.4	0
24.9	24.8	0.1	170.2	170.2	0
24.9	24.9	0	170.3	170.24	0.06
25.2	25.2	0	170.5	170.5	0
25.4	25.4	0	170.8	170.8	0
28.2	28.2	0	171	171	0
29.6	29.55	0.05	171.4	171.3	0.1
29.7	29.58	0.12	171.5	171.5	0
30.2	30.2	0			

(+)-Verticilide (*ent*-21) was prepared following an identical procedure. Preparative HPLC (5-95% aqueous acetonitrile, 210 nm, flow rate: 8 mL/min, R_t = 25.2 m) afforded (+)-verticilide with spectroscopic data identical to its enantiomer, except $[\alpha]_D^{20}$ +48 (*c* 0.16, MeOH).

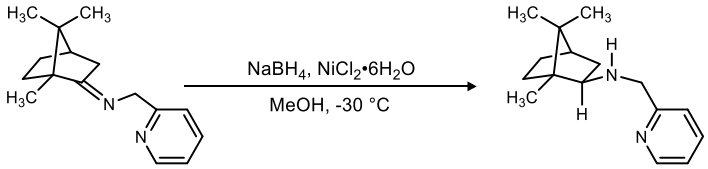

Blay Ligand (27). $NaBH_4$ (3.28 g, 86.6 mmol) was added in three portions to a stirred solution of imino pyridine[6] (2.10 g, 8.66 mmol) and $NiCl_2$•$6H_2O$ (2.27 g, 9.53 mmol) in MeOH (124 mL) at -30 °C under inert atmosphere over a 1 h period. The black heterogeneous solution continued to stir at -30 °C for an additional 2 h, and was then concentrated under reduced pressure. The black residue was dissolved in 1 N HCl and was extracted with CH_2Cl_2. The aqueous layer was then adjusted to pH 10 with 1 N NH_4OH, and was extracted with CH_2Cl_2. The combined organic extracts were washed with brine, dried, and concentrated to an oil that was subjected to flash column chromatography (SiO_2, 30-100% ethyl acetate in hexanes) to afford the title compound as a yellow oil (1.08 g, 51%). R_f = 0.1 (50% EtOAc/hexanes); spectroscopic data (^{1}H NMR) was in complete accord with that previously reported.[7]

[6] Blay, G.; Climent, E.; Fernández, I.; Hernández-Olmos, V.; Pedro, J. R. *Tetrahedron: Asymmetry* **2007**, *18*, 1603.
[7] Blay, G.; Domingo, L. R.; Hernández-Olmos, V.; Pedro, J. R. *Chem. Eur. J.* **2008**, *14*, 4725.

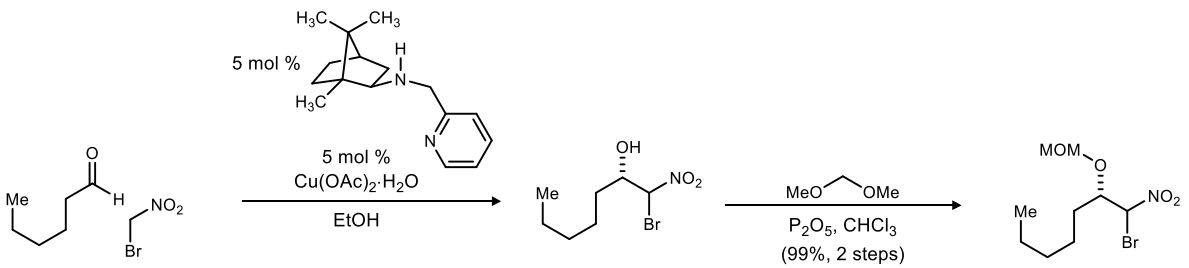

(2*S*)-1-Bromo-2-(methoxymethoxy)-1-nitroheptane (28). Following the Blay[3] enantioselective Henry procedure, Blay ligand (79.5 mg, 326 µmol) and $Cu(OAc)_2$•H_2O (65.0 mg, 326 µmol) stirred at ambient temperature in EtOH (26 mL) for 1 h. The royal blue solution was then cooled to -20 °C and hexanal (800 µL, 6.51 mmol) was added and allowed to stir for 10 m before bromonitromethane (4.54 mL, 65.1 mmol) addition. After stirring for 5 days at -20 °C, the reaction was quenched dropwise at -20 °C with pre-chilled 1 N HCl and the aqueous layer was extracted with CH_2Cl_2. Following drying and concentration under reduced pressure, the crude alcohol was dissolved in $CHCl_3$ (33 mL), treated with P_2O_5 (9.24 g, 65.1 mmol) and dimethoxymethane (11.5 mL, 76.1 mmol), and stirred at ambient temperature overnight. The reaction was cooled to 0 °C, quenched slowly with satd aq $NaHCO_3$, and then poured into CH_2Cl_2. The aqueous layer was extracted with CH_2Cl_2. The organic layers were dried and concentrated to an oil that was subjected to flash column chromatography (SiO_2, 0.5-5% diethyl ether in hexanes) to afford the title compound in 2:1 d.r. as a pale yellow oil (1.84 g, 99%, 2 steps). The diastereomers were determined to be 84% ee by chiral HPLC analysis (Chiralcel OZ-H, 2% ^{i}PrOH /hexanes, 0.4 mL/min, t_r(d_1e_1, minor) = 11.3 min, t_r(d_1e_2, major) = 12.3 min, t_r(d_2e_1, minor) = 13.2 min, t_r(d_2e_2, major) = 13.8 min). R_f = 0.52 (10% EtOAc/hexanes); IR (film) 2956, 2929, 2863, 1575, 1462, 1328, 1156, 1104, 1010, 923 cm^{-1}; ^{1}H NMR (600 MHz, $CDCl_3$) δ 6.12 (d, *J* = 3.4 Hz, 1H), 5.92 (d, *J* = 8.2 Hz, 1H), 4.70 (d, *J* = 7.1 Hz, 1H), 4.67 (d, *J* = 7.1 Hz, 1H), 4.65 (d, *J* = 7.0 Hz, 1H), 4.63 (d, *J* = 7.0 Hz, 1H), 4.25 (ddd, *J* = 8.2, 5.6, 4.0 Hz, 1H), 4.16 (ddd, *J* = 7.6, 5.4, 3.4 Hz, 1H), 3.39 (s, 3H), 3.36 (s, 3H), 1.82-1.66 (series of m, 4H), 1.48-1.26 (series of m, 12H), 0.91-0.88 (m, 6H); ^{13}C NMR (150 MHz, $CDCl_3$) ppm 97.3, 97.0, 84.0, 80.8, 79.3, 79.2, 56.4 (2C), 31.6, 31.43, 31.39, 30.2, 24.8, 23.1, 22.4 (2C), 13.92, 13.91; HRMS (CI): Exact mass calcd for $C_9H_{17}BrNO_4$ [M-H]$^+$ 282.0335, found 282.0331.

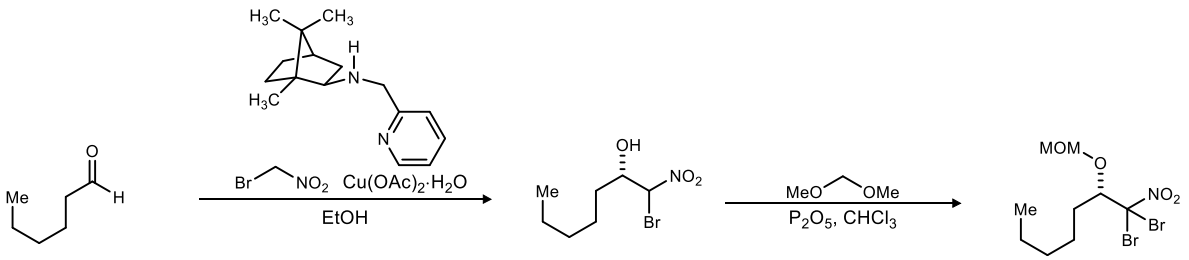

(*S*)-1,1-Dibromo-2-(methoxymethoxy)-1-nitroheptane (29). This dibromonitroalkane is isolated as a co-product from the Henry and MOM protection sequence as a colorless oil. R_f = 0.60 (10% EtOAc/hexanes); ^{1}H NMR (600 MHz, $CDCl_3$) δ 4.69 (d, *J* = 6.9 Hz, 1H), 4.65 (d, *J* = 6.9 Hz, 1H), 4.33 (dd, *J* = 8.3, 2.3 Hz, 1H), 3.36 (s, 3H), 2.01-1.96 (m, 1H), 1.82-1.75 (m, 1H), 1.67-1.61 (m, 1H), 1.52-1.48 (m, 1H), 1.41-1.30 (m, 4H), 0.92 (t, *J* = 7.0 Hz, 3H); ^{13}C NMR (150 MHz, $CDCl_3$) ppm 98.2, 93.9, 85.8, 56.7, 33.6, 31.5, 25.7, 22.4, 13.9; HRMS (CI): Exact mass calcd for $C_9H_{16}N^{79}Br^{81}Br$ [M-H]$^+$ 361.9420, found 361.9413.

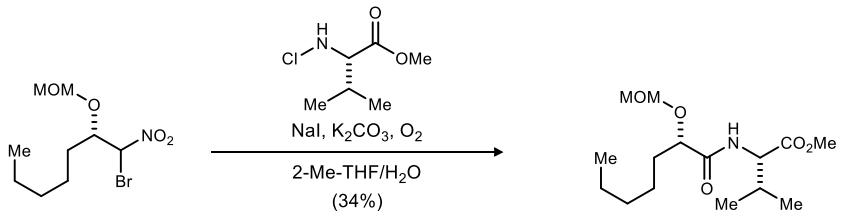

Methyl ((*S*)-2-(methoxymethoxy)heptanoyl)-L-valinate (33). Following the standard UmAS procedure, nitroalkane (50.0 mg, 176 μmol) and amine[8] (35.0 mg, 211 μmol) at 0 °C over 2 d afforded a crude yellow oil. Flash column chromatography (SiO_2, 10-20% ethyl acetate in hexanes) afforded the pure amide as a colorless oil (18 mg, 34% yield). $[a]_D^{25}$ +77 (*c* 0.13, $CHCl_3$); R_f = 0.42 (30% EtOAc/hexanes); IR (film) 3423, 2962, 2873, 1746, 1683, 1517, 1384, 1209, 1156, 1102, 1034 cm^{-1}; ^1H NMR (600 MHz, $CDCl_3$) δ 6.98 (d, *J* = 8.8 Hz, 1H), 4.69 (s, 2H), 4.55 (dd, *J* = 9.1, 5.0 Hz, 1H), 4.11 (dd, *J* = 6.7, 4.6 Hz, 1H), 3.74 (s, 3H), 3.42 (s, 3H), 2.23-2.18 (m, 1H), 1.81-1.72 (m, 2H), 1.42-1.26 (series of m, 6H), 0.95 (d, *J* = 6.8 Hz, 3H), 0.91 (d, *J* = 6.9 Hz, 3H), 0.89-0.86 (m, 3H); ^{13}C NMR (150 MHz, $CDCl_3$) ppm 172.5, 172.1, 96.1, 77.9, 56.6, 56.1, 52.1, 32.7, 31.5, 31.1, 24.3, 22.5, 19.0, 17.8, 14.0; HRMS (ESI): Exact mass calcd for $C_{15}H_{29}NNaO_5$ $[M+Na]^+$ 326.1943, found 326.1930.

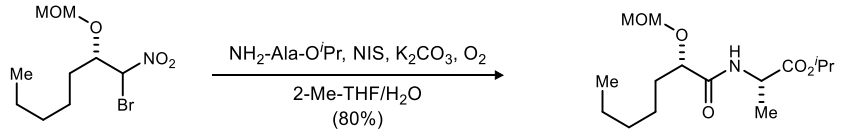

(***S*)-Isopropyl 2-((*S*)-2-(methoxymethoxy)heptanamido)propanoate (36a).** Following the UmAS general procedure, nitroalkane (1.40 g, 4.93 mmol) and amine (775 mg, 5.91 mmol) at 0 °C over 2 days afforded a mahogany colored oil. The residue was subjected to flash column chromatography (SiO_2, 15-20% ethyl acetate in hexanes) to afford the major diastereomer as a pale yellow solid (1.20 g, 80% yield). Mp = 30 °C; $[a]_D^{25}$ -26 (*c*, 0.12, $CHCl_3$); R_f = 0.43 (30% ethyl acetate/hexanes); IR (film) 3310, 2955, 2874, 1734, 1669, 1532, 1456, 1378, 1341, 1212, 1157, 1106, 1039, 921 cm^{-1}; ^1H NMR (500 MHz, $CDCl_3$) δ 7.09 (d, *J* = 7.4 Hz, 1H), 5.03 (qqd, *J* = 6.2, 6.2, 6.2 Hz, 1H), 4.70 (d, *J* = 6.6 Hz, 1H), 4.68 (d, *J* = 6.7 Hz, 1H), 4.57 (dq, *J* = 7.3, 7.3 Hz, 1H), 4.07 (dd, *J* = 5.7, 5.7 Hz, 1H), 3.42 (s, 3H), 1.79-1.68 (m, 2H), 1.39 (d, *J* = 7.1 Hz, 3H), 1.37-1.27 (series of m, 6H), 1.25 (d, *J* = 6.2 Hz, 3H), 1.24 (d, *J* = 6.1 Hz, 3H), 0.87 (m, 3H); ^{13}C NMR (125 MHz, $CDCl_3$) ppm 172.4, 173.0, 96.0, 77.4, 69.1, 56.2, 47.6, 32.8, 31.5, 24.3, 22.5, 21.7, 21.6, 18.6, 13.9; HRMS (ESI): Exact mass calcd for $C_{15}H_{30}NO_5$ $[M+H]^+$ 304.2124, found 304.2131.

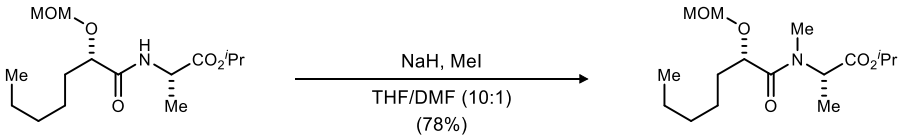

Isopropyl *N*-((*S*)-2-(methoxymethoxy)heptanoyl)-*N*-methyl-L-alaninate (31a). NaH (135 mg, 5.60 mmol) was obtained from the glove box and added to a flame-dried round bottom flask under inert atmosphere, followed by THF (12.8 mL) and DMF (1.25 mL). The solution was chilled to 0 °C and the amide (850 mg, 2.80 mmol)

[8] Huang, H. T.; Lacy, T. C.; Blachut, B.; Ortiz, G. X., Jr.; Wang, Q. *Org. Lett.* **2013**, *15*, 1818.

was slowly added. The reaction was stirred for 10-15 minutes until bubbling stopped. Methyl iodide (872 μL, 14.0 mmol) was then added dropwise over 20-30 minutes. The heterogeneous solution was warmed to ambient temperature and stirred for 1.0 h. At 0 °C, the reaction was slowly quenched with satd aq NH_4Cl and poured into EtOAc. The ethyl acetate extracted were washed with satd aq $NaHCO_3$ and brine, and then dried and concentrated. The burnt orange-colored residue was subjected to flash column chromatography (SiO_2, 15-30% ethyl acetate in hexanes) to afford the *N*-methyl amide as a yellow oil (693 mg, 78%). $[a]_D^{25}$ -81 (*c* 0.26, $CHCl_3$); R_f = 0.28 (30% EtOAc/hexanes); IR (film) 2936, 1734, 1657, 1467, 1403, 1376, 1215, 1156, 1106, 1040, 920 cm^{-1}; ^1H NMR (500 MHz, toluene-d_8)[9] δ 5.22 (q, *J* = 7.3 Hz, 1H), 4.91 (qqd, *J* = 6.2, 6.2, 6.2 Hz, 1H), 4.69 (d, *J* = 6.8 Hz, 1H), 4.53 (d, *J* = 6.8 Hz, 1H), 4.42 (dd, *J* = 6.8, 6.8 Hz, 1H), 3.23 (s, 3H), 2.72 (s, 3H), 1.86-1.82 (m, 2H), 1.51-1.21 (series of m, 9H), 1.02-0.99 (m, 6H), 0.92-0.89 (m, 3H); ^{13}C NMR (125 MHz, toluene-d_8) ppm 171.1, 170.6, 95.3, 74.5, 67.8, 55.1, 52.7, 32.3, 31.63, 31.58, 30.3, 25.2, 22.6, 21.2, 13.8, 13.6; HRMS (ESI): Exact mass calcd for $C_{16}H_{31}NNaO_5$ $[M+Na]^+$ 340.2100, found 340.2100.

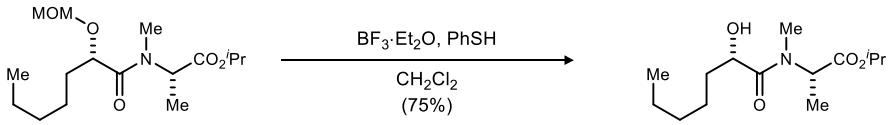

Isopropyl *N*-((*S*)-2-hydroxyheptanoyl)-*N*-methyl-L-alaninate (37). Following general MOM deprotection procedure I, *N*-methyl amide (320 mg, 1.01 mmol) at ambient temperature for 1 h afforded a crude pale yellow oil. Flash column chromatography (SiO_2, 20-40% ethyl acetate in hexanes) afforded the alcohol (208 mg, 75%) as a colorless oil. $[a]_D^{25}$-42 (*c* 0.63, $CHCl_3$); R_f = 0.21 (30% EtOAc/hexanes); IR (film) 3445, 2937, 2860, 1735, 1645, 1467, 1379, 1319, 1208, 1146, 1109, 1079 cm^{-1}; ^1H NMR (600 MHz, $CDCl_3$)[10] δ 5.24 (q, *J* = 7.3 Hz, 1H), 5.02 (qqd, *J* = 6.3, 6.3, 6.3 Hz, 1H), 4.38-4.34 (m, 1H), 2.90 (s, 3H), 1.71-1.45 (series of m, 4H), 1.40 (d, *J* = 7.4 Hz, 3H), 1.34-1.29 (m, 4H), 1.23, (d, *J* = 6.3 Hz, 6H), 0.91-0.88 (m, 3H), O-*H* not observed; ^{13}C NMR (150 MHz, $CDCl_3$) ppm 175.0, 170.8, 68.9, 68.3, 52.7, 34.4, 31.6, 30.3, 24.6, 22.6, 21.75, 21.74, 14.0, 13.94; HRMS (ESI): Exact mass calcd for $C_{14}H_{27}NNaO_4$ $[M+Na]^+$ 296.1838, found 296.1825.

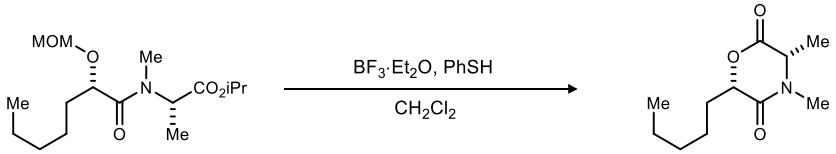

(3*S*,6*S*)-3,4-Dimethyl-6-pentylmorpholine-2,5-dione (38). This lactone is isolated as a side product from the MOM-deprotection procedure as a colorless oil. $[a]_D^{25}$ +2.5 (*c* 0.16, $CHCl_3$); R_f = 0.11 (30% EtOAc/hexanes); IR (film) 2958, 2871, 1756, 1679, 1458, 1382, 1319, 1244, 1061 cm^{-1}; ^1H NMR (600 MHz, $CDCl_3$) δ 4.77 (dd, *J* = 9.1, 4.1 Hz, 1H), 4.14 (q, *J* = 7.1 Hz, 1H), 2.98 (s, 3H), 2.06-2.01 (m, 1H), 1.85-1.78 (m, 1H), 1.62 (d, *J* = 7.2 Hz, 3H), 1.59-1.44 (series of m, 3H), 1.34-1.31 (m, 3H), 0.91-0.88 (m, 3H); ^{13}C NMR (150 MHz, $CDCl_3$) ppm 167.5, 165.5, 79.1, 55.5, 34.3, 31.4, 31.1, 24.8, 22.4, 18.3, 13.9; HRMS (CI): Exact mass calcd for $C_{11}H_{20}NO_3$ $[M+H]^+$ 214.1438, found 214.1430.

[9] Rotamers were observed by NMR, and confirmed by variable temperature NMR analysis. Data for the major rotamer is listed.
[10] Rotamers were observed by NMR, and confirmed by variable temperature NMR analysis. Data for the major rotamer is listed.

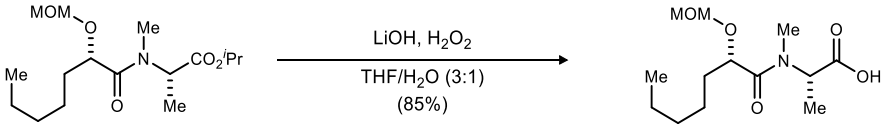

***N*-((S)-2-(methoxymethoxy)heptanoyl)-*N*-methyl-L-alanine (39).** Following the Evans protocol[10], the *N*-methyl amide (345 mg, 1.09 mmol) provided the acid (255 mg, 85% yield) as an analytically pure colorless oil.$[\alpha]_D^{25}$ -81 (*c* 0.63, $CHCl_3$); R_f = 0.33 (10% MeOH/CH_2Cl_2); IR (film) 2955, 1743, 1622, 1466, 1407, 1379, 1305, 1210, 1156, 1102, 1037, 920 cm^{-1}; ^1H NMR (600 MHz, $CDCl_3$)[11] δ 5.17 (q, *J* = 7.3 Hz, 1H), 4.66-4.63 (m, 2H), 4.40 (dd, *J* = 8.5, 4.8 Hz, 1H), 3.37 (s, 3H), 3.04 (s, 3H), 1.81-1.67 (m, 2H), 1.46 (d, *J* = 7.3 Hz, 3H), 1.41-1.28 (m, 6H), 0.90-0.88 (m, 3H), COO*H* not observed ; ^{13}C NMR (150 MHz, $CDCl_3$) ppm 174.8, 173.2, 95.9, 74.5, 56.0, 53.2, 32.2, 31.6, 31.5, 25.1, 22.5, 14.0, 13.9; HRMS (ESI): Exact mass calcd for $C_{13}H_{25}NNaO_5$ $[M+Na]^+$ 298.1630, found 298.1617.

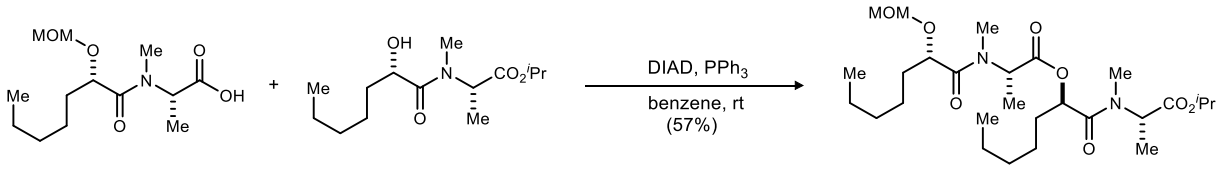

(*R*)-1-(((*S*)-1-isopropoxy-1-oxopropan-2-yl)(methyl)amino)-1-oxoheptan-2-yl *N*-((*S*)-2-(methoxymethoxy)heptanoyl)-*N*-methyl-L-alaninate (40). Following the Mitsunobu general procedure, alcohol (268 mg, 980 μmol) and acid (351 mg, 1.27 mmol) at ambient temperature for 36 h afforded a crude brown oil. Flash column chromatography (SiO_2, 20-50% ethyl acetate in hexanes) provided the tetradepsipeptide (294 mg, 57%) as a colorless oil.$[\alpha]_D^{25}$-65 (*c* 0.12, $CHCl_3$); R_f = 0.04 (30% EtOAc/hexanes); IR (film) 2955, 2872, 1738, 1659, 1467, 1408, 1377, 1308, 1217, 1147, 1102, 1039, 920 cm^{-1}; ^1H NMR (600 MHz, $CDCl_3$)[12] δ 5.48 (q, *J* = 7.2 Hz, 1H), 5.20 (dd, *J* = 8.5, 4.7 Hz, 1H), 5.03 (qqd, *J* = 6.3, 6.3, 6.3 Hz, 1H), 4.91 (q, *J* = 7.3 Hz, 1H), 4.65 (d, *J* = 7.0 Hz, 1H), 4.62 (d, *J* = 7.0 Hz, 1H), 4.45 (m, 1H), 3.38 (s, 3H), 3.03 (s, 3H), 3.02 (s, 3H), 1.79-1.69 (m, 4H), 1.45-1.41 (m, 2H), 1.37 (d, *J* = 7.3 Hz, 6H), 1.33-1.30 (m, 8H), 1.27-1.22 (m, 8H), 0.90-0.87 (m, 6H); ^{13}C NMR (150 MHz, $CDCl_3$) ppm 172.3, 171.3, 170.6, 170.0, 95.6, 73.4, 71.4, 68.7, 55.9, 53.5, 51.6, 32.2, 31.8, 31.6, 31.4, 31.0, 30.9, 25.3, 24.8, 22.5, 22.4, 21.7, 15.4, 14.2, 14.0, 13.97, 13.91; HRMS (ESI): Exact mass calcd for $C_{27}H_{51}N_2O_8$ [M+H] 531.3645, found 531.3638.

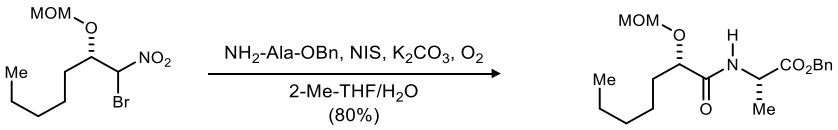

Benzyl ((*S*)-2-(methoxymethoxy)heptanoyl)-*L*-alaninate (45). Following the UmAS general procedure, bromonitroalkane (1400 mg, 4.927 mmol) and amine (1060 mg, 5.912 mmol) afforded a mahogany colored oil. The residue was subjected to flash column chromatography (SiO_2, 10-20% ethyl acetate in hexanes) to afford the major diastereomer as a waxy yellow solid (1380 mg, 80%). Mp = 44-47 °C; $[\alpha]_D^{20}$ -71 (*c* 0.13, $CHCl_3$); R_f = 0.41 (30% EtOAc/hexanes); IR (film) 3263, 2953, 1741, 1652, 1533, 1458, 1220, 1156, 1126, 1099, 1067, 1018, 753, 700 cm^{-1}; ^1H NMR (400 MHz, $CDCl_3$) δ 7.39-7.32 (m, 5H), 7.08 (br d, *J* = 7.6 Hz, 1H), 5.20 (d, *J* = 12.2 Hz, 1H), 5.15 (d, *J* = 12.2 Hz, 1H), 4.69 (dq, *J* = 7.3, 7.3 Hz, 1H), 4.67 (d, *J* = 6.7 Hz, 1H), 4.65 (d, *J* = 6.7 Hz,

[11] Rotamers were observed by NMR, and confirmed by variable temperature NMR analysis. Data for the major rotamer is listed.
[12] Rotamers were observed by NMR, and confirmed by variable temperature NMR analysis. Data for the major rotamer is listed.

1H), 4.07 (dd, *J* = 6.2, 4.9 Hz, 1H), 3.38 (s, 3H), 1.80-1.70 (m, 2H), 1.43 (d, *J* = 7.2 Hz, 3H), 1.41-1.26 (br m, 6H), 0.88 (t, *J* = 6.9 Hz, 3H); ^{13}C NMR (150 MHz, $CDCl_3$) ppm 172.7, 172.1, 135.3, 128.6, 128.5, 128.2, 96.1, 77.4, 67.2, 56.2, 47.5, 32.8, 31.6, 24.3, 22.5, 18.6, 14.0; HRMS (ESI): Exact mass calcd for $C_{19}H_{29}NNaO_5$ $[M+Na]^+$ 374.1943, found 374.1936.

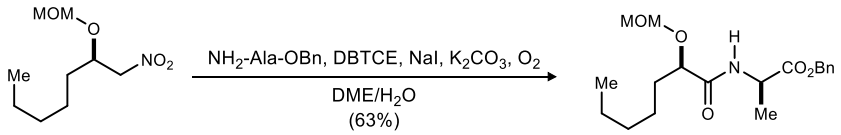

Benzyl ((*R*)-2-(methoxymethoxy)heptanoyl)-*D*-alaninate (*ent*-45). Following the One-Pot UmAS general procedure, nitroalkane (940 mg, 4.58 mmol) and amine (1.64 g, 9.16 mmol) afforded an orange oil. The residue was subjected to flash column chromatography (SiO_2, 10-30% ethyl acetate in hexanes) to afford the major diastereomer as a waxy yellow solid (1.02 g, 63%), with spectroscopic data identical to its enantiomer, except $[\alpha]_D^{20}$ +70 (*c* 0.12, $CHCl_3$).

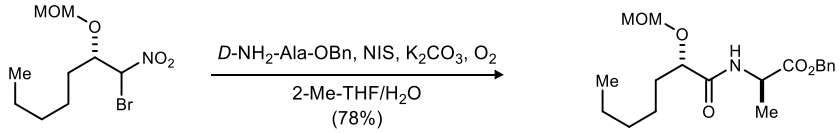

Benzyl ((*S*)-2-(methoxymethoxy)heptanoyl)-D-alaninate (*epi*-45). Following the UmAS general procedure, bromonitroalkane (980 mg, 5.45 mmol) and amine (721 mg, 4.02 mmol) afforded an orange oil. The residue was subjected to flash column chromatography (SiO_2, 10-20% ethyl acetate in hexanes) to afford the major diastereomer as a waxy yellow solid (943 mg, 78%). Mp = 42-44 °C; $[\alpha]_D^{20}$ -24 (*c* 0.25, $CHCl_3$); R_f = 0.30 (30% EtOAc/hexanes); IR (film) 3257, 2950, 2857, 1741, 1655, 1543, 1455, 1278, 1227, 1155, 1131, 1116, 1103, 1064, 1029 cm^{-1}; ^{1}H NMR (400 MHz, $CDCl_3$) δ 7.38-7.31 (m, 5H), 7.02 (br d, *J* = 7.3 Hz, 1H), 5.21 (d, *J* = 12.3 Hz, 1H), 5.15 (d, *J* = 12.3 Hz, 1H), 4.68 (d, *J* = 6.8 Hz, 1H), 4.66 (d, *J* = 6.8 Hz, 1H), 4.65 (dq, *J* = 7.3, 7.2 Hz, 1H), 4.06 (dd, *J* = 6.5, 4.8 Hz, 1H), 3.40 (s, 3H), 1.81-1.69 (m, 2H), 1.44 (d, *J* = 7.2 Hz, 3H), 1.41-1.24 (br m, 6H), 0.88 (t, *J* = 6.8 Hz, 3H); ^{13}C NMR (100 MHz, $CDCl_3$) ppm 172.5, 172.2, 135.3, 128.6, 128.4, 128.1, 96.3, 78.0, 67.1, 56.2, 47.6, 32.7, 31.6, 24.3, 22.5, 18.4, 14.0; HRMS (ESI): Exact mass calcd for $C_{19}H_{29}NNaO_5$ $[M+Na]^+$ 374.1943, found 374.1927.

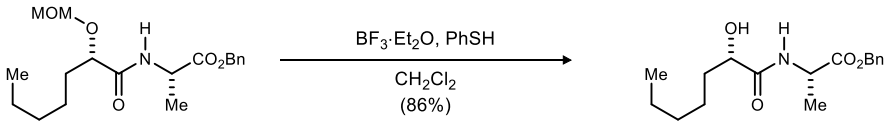

Benzyl ((*S*)-2-hydroxyheptanoyl)-*L*-alaninate (46). Following general MOM deprotection procedure I, the amide (434 mg, 1.23 mmol) afforded a crude pale yellow oil. Flash column chromatography (SiO_2, 20-40% ethyl acetate in hexanes) afforded the alcohol (325 mg, 86%) as a pale yellow oil. $[\alpha]_D^{20}$ -23 (*c* 0.43, $CHCl_3$); R_f = 0.25 (30% EtOAc/hexanes); IR (film) 3393, 3034, 2955, 2929, 2859, 1743, 1655, 1524, 1455, 1386, 1307, 1200, 1155, 1083, 1058 cm^{-1}; ^{1}H NMR (400 MHz, $CDCl_3$) δ 7.39-7.32 (m, 5H), 6.94 (br d, *J* = 7.1 Hz, 1H), 5.21 (d, *J* = 12.3 Hz, 1H), 5.16 (d, *J* = 12.3 Hz, 1H), 4.66 (dq, *J* = 7.2, 7.2 Hz, 1H), 4.13 (ddd, *J* = 8.3, 4.7, 3.6 Hz, 1H), 2.56 (br d, *J* = 5.0 Hz, 1H), 1.86-1.77 (m, 1H), 1.67-1.57 (m, 1H), 1.44 (d, *J* = 7.2 Hz, 3H), 1.40-1.25 (br m, 6H), 0.89 (t, *J* = 6.8 Hz, 3H); ^{13}C NMR (125 MHz, $CDCl_3$) ppm 173.4, 172.8, 135.3, 128.6, 128.5, 128.1, 72.1, 67.2, 47.8, 34.8,

31.5, 24.5, 22.5, 18.4, 14.0; HRMS (ESI): Exact mass calcd for $C_{17}H_{25}NNaO_4$ $[M+Na]^+$ 330.1681, found 330.1667.

Benzyl ((*R*)-2-hydroxyheptanoyl)-*D*-alaninate (*ent*-46) was prepared following an identical procedure from *ent*-4. Flash column chromatography (SiO_2, 20-40% ethyl acetate in hexanes) afforded the alcohol with spectroscopic data identical to its enantiomer, except $[\alpha]_D^{20}$ +31 (*c* 0.72, $CHCl_3$).

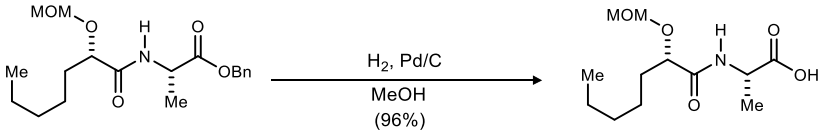

((*S*)-2-(Methoxymethoxy)heptanoyl)-*L*-alanine (47). Following general benzyl-deprotection procedure I, the amide (492 mg, 1.40 mmol) afforded the acid (351 mg, 96%) as an analytically pure orange oil. $[\alpha]_D^{20}$ -39 (*c* 0.26, $CHCl_3$); R_f = 0.28 (20% MeOH/DCM); IR (film) 3407, 2955, 2932, 2860, 1733, 1657, 1531, 1457, 1216, 1155, 1101, 1037 cm^{-1}; ^1H NMR (400 MHz, $CDCl_3$) δ 7.04 (br d, *J* = 7.0 Hz, 1H), 4.71 (s, 2H), 4.60 (dq, *J* = 7.2, 7.2 Hz, 1H), 4.10 (dd, *J* = 6.2, 4.8 Hz, 1H), 3.41 (s, 3H), 1.80-1.70 (m, 2H), 1.48 (d, *J* = 7.0 Hz, 3H), 1.42-1.26 (br m, 6H) 0.88 (t, *J* = 6.6 Hz, 3H), COO*H* not observed; ^{13}C NMR (125 MHz, $CDCl_3$) ppm 175.5, 173.2, 96.3, 77.5, 56.2, 47.8, 32.7, 31.5, 24.3, 22.5, 17.9, 14.0; HRMS (ESI): Exact mass calcd for $C_{12}H_{23}NNaO_5$ $[M+Na]^+$ 284.1474, found 284.1478.

((*R*)-2-(Methoxymethoxy)heptanoyl)-*D*-alanine (*ent*-47) was prepared following an identical procedure from *ent*-4, affording the acid with spectroscopic data identical to its enantiomer, except $[\alpha]_D^{20}$ +41 (*c* 0.20, $CHCl_3$).

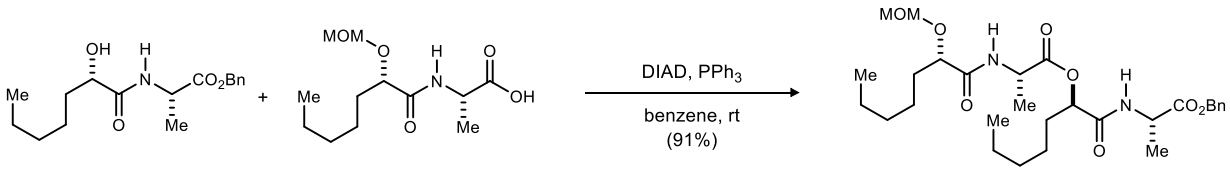

Benzyl ((R)-2-((((S)-2-(methoxymethoxy)heptanoyl)-L-alanyl)oxy)heptanoyl)-L-alaninate (48). Following the Mitsunobu general procedure, alcohol (340 mg, 1.11 mmol) and acid (310 mg, 1.19 mmol) were reacted at ambient temperature for 24 h to afford a crude brown oil. Flash column chromatography (SiO_2, 15-35% ethyl acetate in hexanes) provided the tetradepsipeptide (550 mg, 91%) as a white solid. Mp = 114 °C; $[\alpha]_D^{25}$ -17 (*c* 0.27, $CHCl_3$); R_f = 0.22 (30% EtOAc/hexanes); IR (film) 3310, 2955, 2930, 2859, 1747, 1657, 1535, 1456, 1378, 1344, 1201, 1156, 1104, 1059, 1032 cm^{-1}; ^1H NMR (400 MHz, $CDCl_3$) δ 7.38-7.30 (m, 5H), 7.10 (br d, *J* = 7.2 Hz, 1H), 6.98 (br d, *J* = 6.8 Hz, 1H), 5.21 (d, *J* = 12.2 Hz, 1H), 5.19 (dd, *J* = 7.8, 4.1 Hz, 1H), 5.13 (d, *J* = 12.2 Hz, 1H), 4.68 (s, 2H), 4.59 (dq, *J* = 7.3, 7.2 Hz, 1H), 4.45 (dq, *J* = 7.0, 6.8 Hz, 1H), 4.03 (dd, *J* = 6.3, 4.8 Hz, 1H), 3.41 (s, 3H), 1.93-1.68 (series of m, 4H), 1.47 (d, *J* = 7.2 Hz, 3H), 1.43 (d, *J* = 7.3 Hz 3H), 1.38-1.26 (br m, 12H), 0.89-0.85 (m, 6H); ^{13}C NMR (125 MHz, $CDCl_3$) ppm 173.0, 172.4, 172.2, 169.3, 135.6, 128.5, 128.3, 128.1, 96.3, 77.5, 74.7, 66.9, 56.3, 48.4, 48.0, 32.6, 31.6, 31.5, 31.2, 24.5, 24.3, 22.5, 22.4, 17.5, 17.3, 14.0, 13.9; HRMS (ESI): Exact mass calcd for $C_{29}H_{46}N_2NaO_8$ $[M+Na]^+$ 573.3152, found 573.3126.

Benzyl ((S)-2-((((R)-2-(methoxymethoxy)heptanoyl)-D-alanyl)oxy)heptanoyl)-D-alaninate (*ent*-48) was prepared following an identical procedure, but using *ent*-10 and *ent*-11. Flash column chromatography (SiO_2, 15-35% ethyl acetate in hexanes) afforded the tetradepsipeptide with spectroscopic data identical to its enantiomer, except $[\alpha]_D^{20}$ +12 (*c* 0.10, $CHCl_3$).

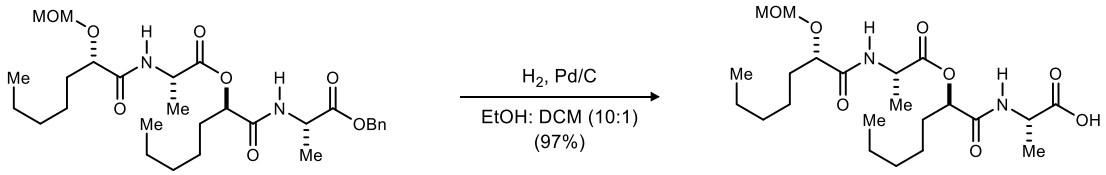

((*R*)-2-((((*S*)-2-(methoxymethoxy)heptanoyl)-L-alanyl)oxy)heptanoyl)-L-alanine (49). Following general benzyl deprotection procedure I, the amide[13] (275 mg, 499 μmol) afforded the acid (222 mg, 97%) as an analytically pure pale yellow oil. $[\alpha]_D^{20}$ -23 (*c* 0.12, $CHCl_3$); R_f = 0.56 (20% MeOH/DCM); IR (film) 3230, 2956, 2931, 2860, 1747, 1657, 1535, 1457, 1214, 1156, 1103, 1037 cm^{-1}; ^1H NMR (400 MHz, $CDCl_3$) δ 7.36 (br d, *J* = 7.0 Hz, 1H), 7.11 (br d, *J* = 6.9 Hz, 1H), 5.16 (dd, *J* = 8.2, 4.0 Hz, 1H), 4.68 (s, 2H), 4.57 (dq, *J* = 7.1, 7.1 Hz, 1H), 4.50 (dq, *J* = 7.2, 6.9 Hz, 1H), 4.06 (dd, *J* = 5.9, 5.1 Hz, 1H), 3.41 (s, 3H), 1.96-1.66 (series of m, 4H), 1.46 (d, *J* = 7.1 Hz, 3H), 1.41 (d, *J* = 7.2 Hz, 3H), 1.38-1.25 (br m, 12H), 0.89-0.85 (m, 6H), COO*H* not observed; ^{13}C NMR (125 MHz, $CDCl_3$) ppm 173.4, 172.2, 170.0, 169.8, 96.2, 77.4, 74.7, 56.3, 48.4, 48.2, 32.6, 31.6, 31.5, 31.2, 24.6, 24.3, 22.5, 22.4, 17.4, 17.3, 13.96, 13.91; HRMS (ESI): Exact mass calcd for $C_{22}H_{40}N_2NaO_8$ $[M+Na]^+$ 483.2682, found 483.2675.

((*S*)-2-((((*R*)-2-(methoxymethoxy)heptanoyl)-D-alanyl)oxy)heptanoyl)-D-alanine (*ent*-49) was prepared following an identical procedure from *ent*-**2**, affording the acid with spectroscopic data identical to its enantiomer, except $[\alpha]_D^{20}$ +20 (*c* 0.10, $CHCl_3$).

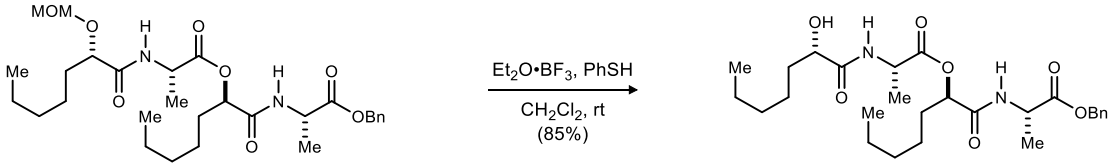

Benzyl ((*R*)-2-((((*S*)-2-hydroxyheptanoyl)-L-alanyl)oxy)heptanoyl)-L-alaninate (50). Following general MOM deprotection procedure I, the amide[13] (413 mg, 750 μmol) afforded a crude pale yellow oil. Flash column chromatography (SiO_2, 20-50% ethyl acetate in hexanes) afforded the alcohol (322 mg, 85%) as a pale yellow oil. $[\alpha]_D^{20}$ -14 (*c* 0.25, $CHCl_3$); R_f = 0.14 (30% EtOAc/hexanes); IR (film) 3314, 3068, 2955, 2928, 2858, 1747, 1654, 1534, 1456, 1380, 1199, 1155, 1061 cm^{-1}; ^1H NMR (400 MHz, $CDCl_3$) δ 7.38-7.30 (m, 5H), 7.14 (br d, *J* = 7.2 Hz, 1H), 6.96 (br d, *J* = 6.4 Hz, 1H), 5.21 (d, *J* = 12.2 Hz, 1H), 5.19 (dd, *J* = 7.3, 4.2 Hz, 1H), 5.14 (d, *J* = 12.2 Hz, 1H), 4.59 (dq, *J* = 7.2, 7.2 Hz, 1H), 4.47 (dq, 7.0, 6.9 Hz, 1H), 4.11 (ddd, *J* = 7.7, 4.1, 3.3 Hz, 1H), 2.68 (br d, *J* = 5.2 Hz, 1H), 1.96-1.77 (series of m, 3H), 1.66-1.56 (m, 1H), 1.47 (d, *J* = 7.2 Hz, 3H), 1.43 (d, *J* = 7.2 Hz, 3H), 1.40-1.25 (br m, 12H), 0.90-0.85 (m, 6H); ^{13}C NMR (125 MHz, $CDCl_3$) ppm 174.3, 172.7, 172.2, 169.3, 131.0, 128.6, 128.3, 128.1, 74.7, 72.0, 67.1, 48.4, 48.1, 34.5, 31.5, 31.45, 31.2, 24.6, 24.4, 22.5, 22.4, 17.6, 17.1, 13.97, 13.92; HRMS (ESI): Exact mass calcd for $C_{27}H_{42}N_2NaO_7$ $[M+Na]^+$ 529.2890, found 529.2868.

Benzyl ((*S*)-2-((((*R*)-2-hydroxyheptanoyl)-D-alanyl)oxy)heptanoyl)-D-alaninate (*ent*-50) was prepared following an identical procedure, but from *ent*-**2**. Flash column chromatography (SiO_2, 20-50% ethyl acetate in hexanes) afforded the alcohol with spectroscopic data identical to its enantiomer, except $[\alpha]_D^{20}$ +16 (*c* 0.10, $CHCl_3$).

[13] Batiste, S. M.; Johnston, J. N. *Proc. Natl. Acad. Sci. U. S. A.* **2016**, *113*, 14893.

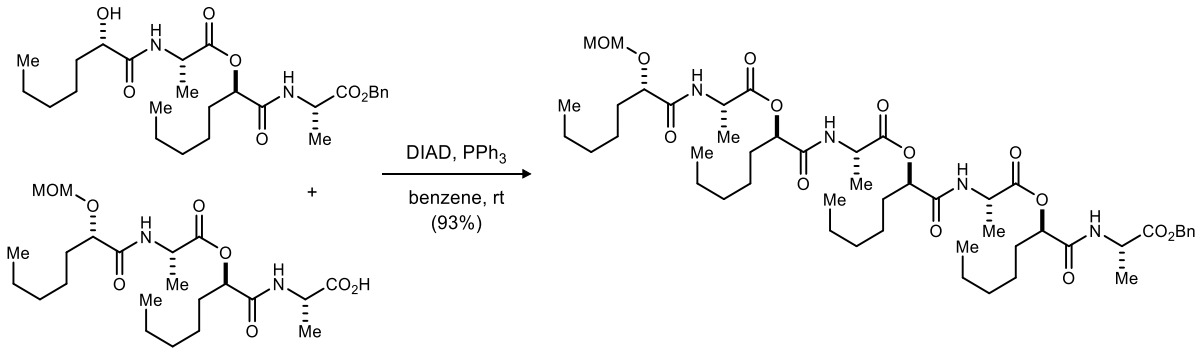

Benzyl ((*R*)-2-((((*R*)-2-((((*R*)-2-((((*S*)-2-(methoxymethoxy)heptanoyl)-L-alanyl)oxy)heptanoyl)-L-alanyl)oxy)heptanoyl)-L-alanyl)oxy)heptanoyl)-L-alaninate (51). Following the Mitsunobu general procedure, alcohol (210 mg, 415 μmol) and acid (222 mg, 482 μmol) were reacted at ambient temperature for 24 h to afford a crude pale yellow oil. Flash column chromatography (SiO_2, 10-40% ethyl acetate in hexanes) provided the tetramer (366 mg, 93%) as a pale yellow oil. $[\alpha]_D^{20}$ +12 (*c* 0.51, $CHCl_3$); R_f = 0.08 (30% EtOAc/hexanes); IR (film) 3307, 2955, 2930, 2860, 1750, 1655, 1536, 1456, 1382, 1334, 1196, 1154, 1115, 1061 cm^{-1}; ^1H NMR (400 MHz, $CDCl_3$) δ 7.64 (br d, *J* = 4.4 Hz, 1H), 7.59 (br d, *J* = 5.0 Hz, 1H), 7.36-7.28 (m, 6H), 6.99 (br d, *J* = 5.4 Hz, 1H), 5.19 (d, *J* = 12.3 Hz, 1H), 5.19 (dd, *J* = 8.4, 3.2 Hz, 3H), 5.13 (d, *J* = 12.4 Hz, 1H), 4.69 (d, *J* = 7.1 Hz, 1H), 4.68 (d, *J* = 7.1 Hz, 1H), 4.63 (dq, *J* = 7.3, 7.3 Hz, 1H), 4.32 (qd, *J* = 7.1, 5.2 Hz, 1H), 4.29 (qd, *J* = 7.1, 5.5 Hz, 1H), 4.24 (qd, *J* = 7.1, 4.4 Hz, 1H), 4.03 (dd, *J* = 7.6, 5.9 Hz, 1H), 3.42 (s, 3H), 1.97-1.67 (m, 8H), 1.48 (d, *J* = 7.1 Hz, 9H), 1.44 (d, *J* = 7.3 Hz, 3H), 1.40-1.21 (br m, 24H), 0.90-0.84 (m, 12H); ^{13}C NMR (125 MHz, $CDCl_3$) ppm 173.6, 172.5, 172.4, 172.3, 172.2, 170.7, 170.5, 169.7, 135.7, 128.5, 128.2, 128.0, 96.4, 77.5, 74.2, 73.9, 73.7, 66.8, 56.3, 49.5, 49.2, 48.9, 48.0, 32.6, 31.6, 31.5, 31.32, 31.28, 31.23, 31.21 (2C), 24.5, 24.4, 24.34, 24.25, 22.5, 22.4, 22.3 (2C), 17.4, 16.6, 16.3, 16.0, 13.97, 13.95, 13.90, 13.89; HRMS (ESI): Exact mass calcd for $C_{49}H_{80}N_4NaO_{14}$ $[M+Na]^+$ 971.5569, found 971.5551.

Benzyl ((*S*)-2-((((*S*)-2-((((*S*)-2-((((*R*)-2-(methoxymethoxy)heptanoyl)-D-alanyl)oxy)heptanoyl)-D-alanyl)oxy)heptanoyl)-D-alanyl)oxy)heptanoyl)-D-alaninate (*ent*-51) was prepared following an identical procedure, but using *ent*-49 and *ent*-50. Flash column chromatography (SiO_2, 10-40% ethyl acetate in hexanes) afforded the octadepsipeptide with spectroscopic data identical to its enantiomer, except $[\alpha]_D^{20}$ -15 (*c* 0.24, $CHCl_3$).

((*R*)-2-

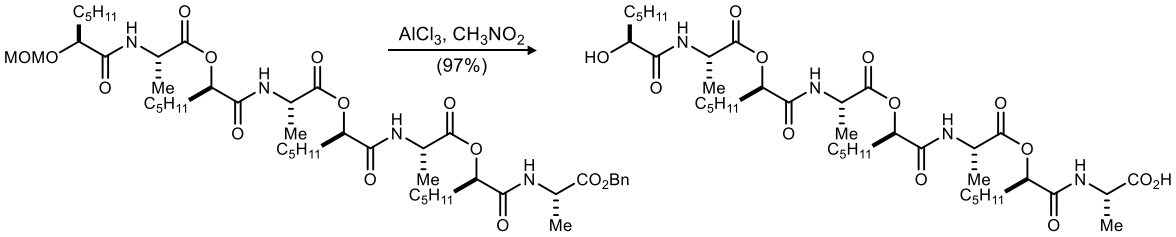

((((*R*)-2-((((*R*)-2-((((*S*)-2-hydroxyheptanoyl)-L-alanyl)oxy)heptanoyl)-L-alanyl)oxy)heptanoyl)-L-alanyl)oxy)heptanoyl)-L-alanine (52). A flame-dried round-bottomed flask under inert atmosphere was charged with $AlCl_3$ (209 mg, 1.59 mmol) and CH_3NO_2 (890 μL) at 0 °C. The MOM and benzyl-protected depsipeptide (151 mg, 159 μmol) was dissolved in CH_3NO_2 (700 μL) and added dropwise to the stirring solution. The reaction was allowed to slowly warm to ambient temperature and stir for 10 m, and then poured into ice water. The aqueous layer was extracted with EtOAc, and the combined organic layers were washed with water and brine, dried, and

concentrated to provide the *seco*-acid (125 mg, 97%) as an analytically pure pale yellow oil. $[\alpha]_D^{20}$ +16 (*c* 0.21, $CHCl_3$); R_f = 0.24 (10% MeOH/DCM); IR (film) 3316, 2956, 2930, 2861, 1750, 1656, 1537, 1456, 1382, 1198, 1154, 1063 cm^{-1}; ^1H NMR (400 MHz, $CDCl_3$) δ 7.65 (br d, *J* = 4.8 Hz, 1H), 7.60 (br d, *J* = 6.3 Hz, 1H), 7.35 (br d, *J* = 7.1 Hz, 1H), 7.15 (br d, *J* = 5.4 Hz, 1H), 5.22 (dd, *J* = 8.4, 4.1 Hz, 1H), 5.20 (dd, *J* = 8.5, 3.8 Hz, 1H), 5.15 (dd, *J* = 7.7, 4.3 Hz, 1H), 4.54 (dq, *J* = 7.2, 7.2 Hz, 1H), 4.45 (dq, *J* = 6.8, 6.7 Hz, 1H), 4.34 (qd, *J* = 6.7, 4.8 Hz, 1H), 4.32 (qd, *J* = 7.2, 5.3 Hz, 1H) 4.12 (dd, *J* = 7.8, 3.8 Hz, 1H), 2.44 (br s, 2H), 1.96-1.75 (br series of m, 7H), 1.67-1.58 (m, 1H), 1.50-1.45 (m, 12H), 1.42-1.24 (br m, 24H), 0.91-0.86 (m, 12H); ^{13}C NMR (125 MHz, $CDCl_3$) ppm 174.3, 173.9, 172.5, 172.3, 171.9, 171.0, 170.4, 169.1, 74.2, 74.1, 73.8, 72.0, 49.4, 48.95, 48.91, 48.3, 34.4, 31.43 (2C), 31.41, 31.3, 31.21, 31.19 (2C), 24.6, 24.41, 24.38, 24.32, 22.5, 22.40, 22.36, 22.33, 17.0, 16.6, 16.5, 16.1, 13.96, 13.92 (2C), 13.88; HRMS (ESI): Exact mass calcd for $C_{40}H_{71}N_4O_{13}$ $[M+H]^+$ 815.5018, found 815.4986.

((*S*)-2-((((*S*)-2-((((*S*)-2-((((*R*)-2-hydroxyheptanoyl)-D-alanyl)oxy)heptanoyl)-D-alanyl)oxy)heptanoyl)-D-alanyl)oxy)heptanoyl)-D-alanine (*ent*-52) was prepared following an identical procedure from *ent*-6, affording the *seco*-acid with spectroscopic data identical to its enantiomer, except $[\alpha]_D^{20}$ -13 (*c* 0.08, $CHCl_3$).

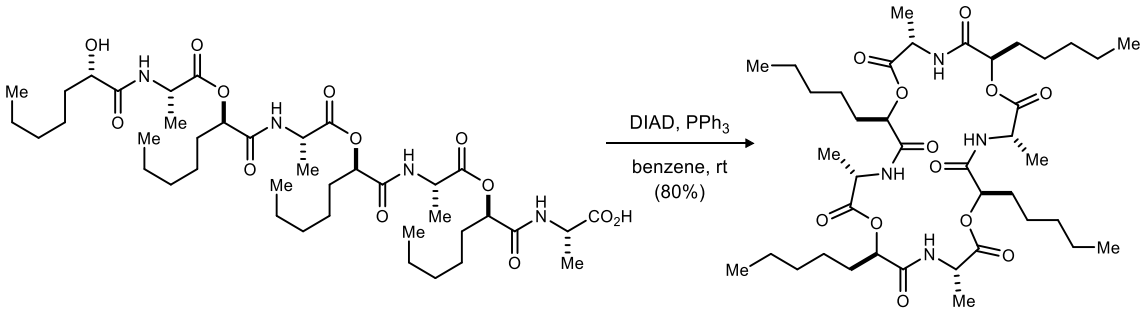

(3*S*,6*R*,9*S*,12*R*,15*S*,18*R*,21*S*,24*R*)-3,9,15,21-Tetramethyl-6,12,18,24-tetrapentyl-1,7,13,19-tetraoxa-4,10,16,22-tetraazacyclotetracosan-2,5,8,11,14,17,20,23-octaone (53). A flame-dried round-bottomed flask under inert atmosphere was charged with the *seco*-acid (232 mg, 285 μmol), PPh_3 (448 mg, 1.71 mmol) and benzene (285 mL). DIAD (280 μL, 1.43 mmol) was then added to the stirred solution in 5 x 56 μL aliquots over 40 minutes. The reaction was allowed to stir at ambient temperature for 18 h, and then was concentrated to afford an orange oil that was subjected to flash column chromatography (SiO_2, 0.5-5% methanol in dichloromethane) to afford the macrocycle (179 mg, 80%) as a white solid. Mp = 205-207 °C; $[\alpha]_D^{20}$ -6.3 (*c* 0.13, $CHCl_3$); R_f = 0.21 (50% EtOAc/Hexanes); IR (film) 3275, 2956, 2929, 2860, 1746, 1657, 1458, 1377, 1247, 1159, 1065 cm^{-1}; ^1H NMR (400 MHz, $CDCl_3$) δ 7.21 (br d, *J* = 7.2 Hz, 1H), 5.10 (dd, *J* = 7.4, 5.2 Hz, 1H), 4.23 (dq, *J* = 7.2, 7.0 Hz, 1H), 1.91-1.86 (m, 1H), 1.70-1.60 (m, 1H) 1.46 (d, *J* = 7.0 Hz, 3H), 1.36-1.25 (br m, 6H), 0.89-0.85 (m, 3H); ^{13}C NMR (125 MHz, $CDCl_3$) ppm 170.94, 170.87, 74.2, 48.5, 31.34, 31.27, 24.8, 22.4, 15.9, 13.8; HRMS (ESI): Exact mass calcd for $C_{40}H_{69}N_4O_{12}$ $[M+H]^+$ 797.4912, found 797.4877.

(3*R*,6*S*,9*R*,12*S*,15*R*,18*S*,21*R*,24*S*)-3,9,15,21-Tetramethyl-6,12,18,24-tetrapentyl-1,7,13,19-tetraoxa-4,10,16,22-tetraazacyclotetracosan-2,5,8,11,14,17,20,23-octaone (*ent*-53). Prepared following an identical procedure from *ent*-52. Flash column chromatography (SiO_2, 0.5-5% methanol in dichloromethane) provided the 24-membered macrocycle with spectroscopic data identical to its enantiomer, except $[\alpha]_D^{20}$ +6.4 (*c* 0.25, $CHCl_3$).

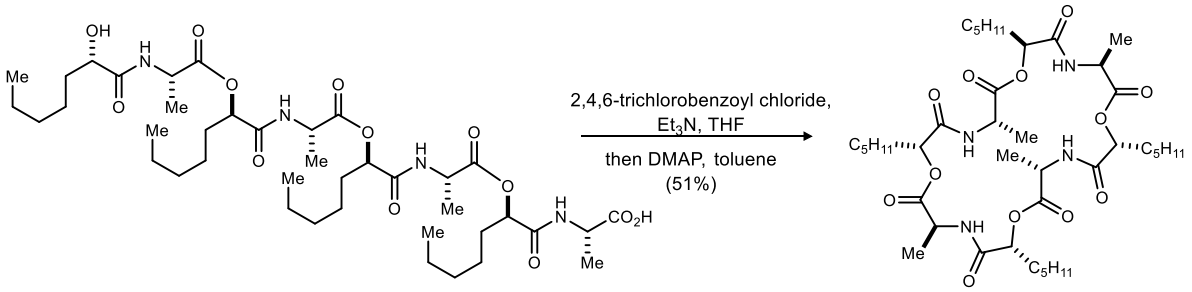

(3*S*,6*R*,9*S*,12*R*,18*R*,21*S*,24*S*)-3,9,15,21-tetramethyl-6,12,18,24-tetrapentyl-1,7,13,19-tetraoxa-4,10,16,22-tetraazacyclotetracosan-2,5,8,11,14,17,20,23-octaone (epi-53). A flame-dried round-bottom flask under inert atmosphere was charged with the seco-acid (20.0 mg, 24.5 μmol) in THF (2.88 mL). Et_3N (68.3 μL, 490 μmol) followed by 2,4,6-trichlorobenzoyl chloride (57.4 μL, 368 μmol) were then added. The solution was allowed to stir at ambient temperature for 15 minutes while a white precipitate formed. Then, a solution of DMAP (24.0 mg, 200 μmol) in toluene (5.00 mL) was added to the reaction over the span of 20 minutes. The heterogeneous reaction mixture continued to stir for an additional 15 m and was subsequently quenched with satd aq NH_4Cl. The aqueous layer was extracted with EtOAc, and the combined organic layers were washed with brine, and then dried and concentrated to afford a peach colored residue that was subjected to flash column chromatography (SiO_2, 15-50% ethyl acetate in hexanes) to afford the macrocycle (10.0 mg, 51%) as a colorless oil. $[\alpha]_D^{25}$ -9.0 (*c* 0.40, $CHCl_3$); R_f = 0.24 (3% MeOH/DCM); IR (film) 3285, 2956, 2927, 2858, 1749, 1656, 1548, 1457, 1379, 1209, 1158, 1116, 1064 cm^{-1}; ^1H NMR (400 MHz, $CDCl_3$) δ 7.11 (br s, 3H), 6.32 (br s, 1H), 5.13-5.01 (br m, 3H), 4.87 (br m, 1H), 4.64 (br dq, *J* = 6.8, 6.8 Hz, 1H), 4.42 (br m, 3H), 1.88-1.79 (m, 8H), 1.51-1.46 (m, 12H), 1.37-1.34 (br m, 24H), 0.89-0.86 (m, 12H); ^{13}C NMR (125 MHz, $CDCl_3$) ppm 172.0, 170.1, 170.0, 169.95, 169.9, 169.86, 169.7 (2C), 75.3 (br 4C), 48.9, 48.4, 47.8 (2C), 31.6, 31.3, 31.28, 31.22 (2C), 31.17, 31.15, 31.1, 24.60, 24.55, 24.5, 24.2, 22.32 (3C), 22.27, 17.1, 16.8, 16.6 (2C), 13.86 (2C), 13.82 (2C); HRMS (ESI): Exact mass calcd for $C_{40}H_{68}N_4NaO_{12}$ $[M+Na]^+$ 819.4731, found 819.4701.

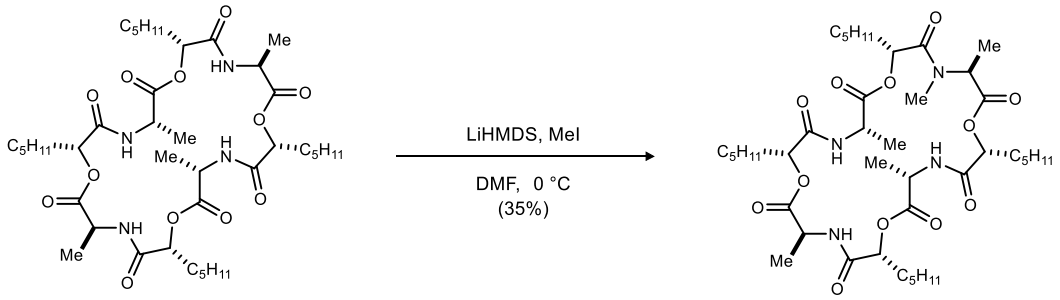

(3*S*,6*R*,9*S*,12*R*,15*S*,18*R*,21*S*,24*R*)-3,4,9,10,15,21-pentamethyl-6,12,18,24-tetrapentyl-1,7,13,19-tetraoxa-4,10,16,22-tetraazacyclotetracosan-2,5,8,11,14,17,20,23-octaone (62). A flame-dried round-bottom flask was charged with the *N*-H depsipeptide (10.0 mg, 12.5 μmol) and dry DMF (250 μL) at 0 °C. Methyl iodide (31.3 μL, 500 μmol) was added to the reaction mixture, and LiHMDS (5.23 mg, 31.2 μmol in DMF (50 μL)) was then added dropwise. The reaction was allowed to stir at 0 °C for 15 m, and it was then quenched by the dropwise addition of satd aq NH_4Cl. The aqueous layer was extracted with EtOAc, and the combined organic layers were washed with satd aq $NaHCO_3$, satd aq $Na_2S_2O_3$, water and brine, and then dried and concentrated to afford a residue that was subjected to preparative HPLC (5-95% aqueous acetonitrile, 210 nm, flow rate: 8 mL/min, R_t = 26.2 m) to afford monomethylated verticilide (3.5 mg, 35%) as a white solid. Mp = 153-155 °C; $[\alpha]_D^{25}$ -12 (*c* 0.13, $CHCl_3$); R_f = 0.26 (3% MeOH/DCM); IR (film) 3280, 2956, 2926, 2858, 1738, 1680, 1649, 1557, 1502, 1451, 1374, 1258,

1217, 1163, 1063 cm^{-1}; ^1H NMR (500 MHz, $CDCl_3$) δ 7.68 (br d, *J* = 7.1 Hz, 1H), 7.18 (br m, 2H), 5.20 (br m, 2H), 5.03 (br dd, *J* = 7.7, 6.0 Hz, 1H), 4.89 (br dd, *J* = 5.5, 5.5 Hz, 1H), 4.60 (br m, 2H), 4.09 (br m, 1H), 3.84 (br m, 1H), 3.17 (s, 3H), 2.04-1.72 (s of m, 8H), 1.51 (d, *J* = 7.4 Hz, 3H), 1.49 (d, *J* = 7.9 Hz, 3H), 1.47 (d, *J* = 7.3 Hz, 3H), 1.42 (d, *J* = 7.1 Hz, 3H), 1.37-1.25 (br m, 24H), 0.90-0.85 (m, 12H); ^{13}C NMR (125 MHz, $CDCl_3$) ppm 171.9, 170.52, 170.49, 170.4, 170.37, 170.08 (2C), 169.2, 74.36 (2C), 74.33, 74.27, 49.1 (2C), 48.0 (2C), 47.7, 31.7 (2C), 31.45, 31.40, 31.23, 31.15 (2C), 30.3, 25.2, 25.0, 24.95, 24.4, 22.5, 22.44 (2C), 22.41, 17.6, 16.7, 14.0, 13.94 (3C), 13.92, 13.6; HRMS (ESI): Exact mass calcd for $C_{41}H_{70}N_4NaO_{12}$ $[M+Na]^+$ 833.4888, found 833.4862.

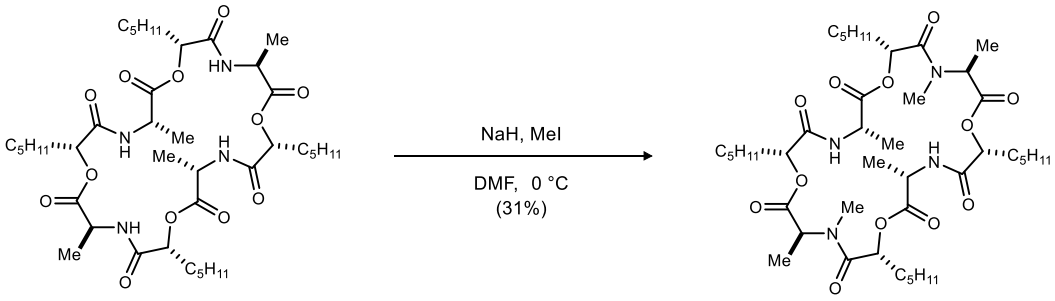

(3*S*,6*R*,9*S*,12*R*,15*S*,18*R*,21*S*,24*R*)-3,4,9,15,16,21-hexamethyl-6,12,18,24-tetrapentyl-1,7,13,19-tetraoxa-4,10,16,22-tetraazacyclotetracosan-2,5,8,11,14,17,20,23-octaone (63). A flame-dried round-bottom flask was charged with the *N*-H depsipeptide (10.0 mg, 12.5 μmol) and dry DMF (250 μL) at 0 °C. Methyl iodide (31.3 μL, 500 μmol) was added to the reaction mixture, and NaH (3.00 mg, 125 μmol in DMF (50.0 μL)) was then added dropwise. The reaction was allowed to stir at 0 °C for 15 m, and it was then quenched by the dropwise addition of satd aq NH_4Cl. The aqueous layer was extracted with EtOAc, and the combined organic layers were washed with satd aq $NaHCO_3$, satd aq $Na_2S_2O_3$, water and brine, and then dried and concentrated to afford a residue that was subjected to preparative HPLC (5-95% aqueous acetonitrile, 210 nm, flow rate: 8 mL/min, R_t = 27.2 m) to afford dimethylated verticilide (3.20 mg, 31%) as an opaque film. $[\alpha]_D^{25}$ -16 (*c* 0.13, $CHCl_3$); R_f = 0.31 (3% MeOH/DCM); IR (film) 3282, 2957, 2925, 2855, 1738, 1667, 1646, 1553, 1501, 1456, 1340, 1258, 1267, 1216, 1163, 1063 cm^{-1}; ^1H NMR (400 MHz, $CDCl_3$) δ 7.76 (br d, *J* = 8.7 Hz, 1H), 5.05 (dd, *J* = 10.2, 3.0 Hz, 1H), 4.87 (dd, *J* = 9.5, 3.6 Hz, 1H), 4.74 (dq, *J* = 7.9, 7.6 Hz, 1H), 3.82 (q, *J* = 7.0 Hz, 1H), 3.16 (s, 3H), 1.96-1.80 (s of m, 2H), 1.76-1.62 (s of m, 2H), 1.53 (d, *J* = 7.0 Hz, 3H), 1.45 (d, *J* = 7.4 Hz, 3H), 1.39-1.25 (br m, 12H), 0.92-0.87 (m, 6H); ^{13}C NMR (125 MHz, $CDCl_3$) ppm 172.5, 170.3, 169.8, 169.7, 76.2, 71.0, 59.1, 47.8, 36.1, 32.0, 31.4, 31.3, 30.2, 25.6, 25.4, 22.6, 22.4, 17.9, 14.0, 13.95, 13.89; HRMS (ESI): Exact mass calcd for $C_{42}H_{72}N_4NaO_{12}$ $[M+Na]^+$ 847.5044, 847.5040.

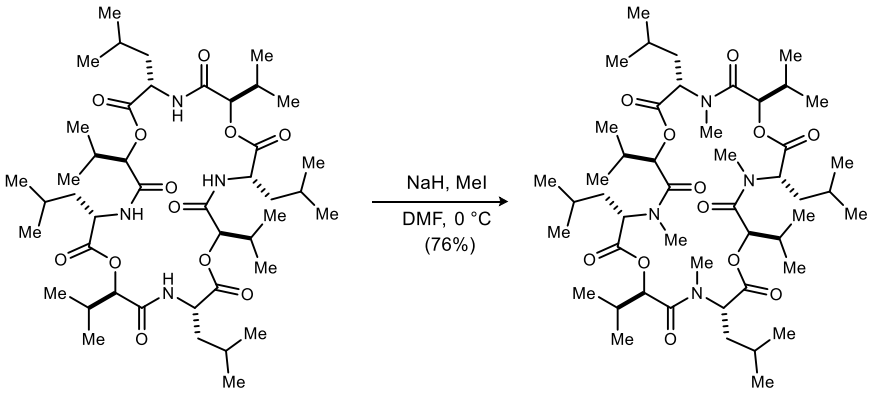

(–)-Bassianolide (*nat*-67). A flame-dried vial was charged with the *N*-H depsipeptide (7.0 mg, 8.2 μmol) and dry DMF (164 μL) at 0 °C. Methyl iodide (20.4 μL, 328 μmol) was added to the reaction mixture, and NaH (2.0 mg, 82 μmol in DMF (82 μL)) was then added dropwise. The reaction was allowed to stir at 0 °C for 25 m, and it was then quenched by the dropwise addition of satd aq NH_4Cl. The aqueous layer was extracted with EtOAc, and the combined organic layers were washed with satd aq $NaHCO_3$, satd aq $Na_2S_2O_3$, water and brine, and then dried and concentrated to afford a residue that was subjected to preparative HPLC (5-95% aqueous acetonitrile, 210 nm, flow rate: 8 mL/min, R_t = 25.0 min) to afford (-)-bassianolide (5.7 mg, 76%) as an amorphous solid. $[\alpha]_D^{20}$ -60 (*c* 0.11, $CHCl_3$);[14] R_f = 0.23 (10% acetone/$CHCl_3$); IR (film) 2957, 2922, 2852, 1738, 1669, 1460, 1375, 1261, 1203, 1091, 1019 cm^{-1}; HRMS (ESI): Exact mass calcd for $C_{48}H_{84}N_4NaO_{12}$ $[M+Na]^+$ 931.5983, found 931.5953.

Comparison of prepared (-)-bassianolide with literature values:

^{1}H δ Literature	Mult, *J* values	^{1}H δ Synthesis	Mult, *J* values
0.52	d, *J* = 7.0 Hz	0.55	d, *J* = 6.8 Hz
0.63	d, *J* = 7.0 Hz	0.67	d, *J* = 7.6 Hz
0.83-1.00	m	0.84-1.04	m
1.28	m	1.28-1.51	s of m
1.39	m		
1.51	m		
1.58	m	1.58	m
1.68-1.85	m	1.68-1.88	m
2.07	m	2.00-2.25	br m
2.15-2.22	m		
2.82	s	2.89	s
2.85	s	3.01	s
2.98	s	3.04	s
3.01	s	3.1	s
3.22	s	3.25	s
4.39	dd, *J* = 11.6, 4.0 Hz	4.43	dd, *J* = 10.6, 4.4 Hz
4.96	d, *J* = 2.3 Hz	4.99	d, *J* = 2.8 Hz
5.15	d, *J* = 7.7 Hz	5.16	br m
5.25	d, *J* = 6.9 Hz	5.28	d, *J* = 6.8 Hz
5.41	d, *J* = 7.9 Hz	5.45	d, *J* = 8.0 Hz
5.41	dd, *J* = 12.1, 4.2 Hz	5.45	dd, *J* = 11.8, 4.3 Hz
5.48	d, *J* = 2.2 Hz	5.5	d, *J* = 2.0 Hz
5.59	dd, *J* = 12.2, 4.6 Hz	5.62	dd, *J* = 12.3, 4.4 Hz
5.62	dd, *J* = 12.2, 4.3 Hz	5.65	dd, *J* = 12.3, 4.2 Hz

^{13}C Literature values	^{13}C Synthesis values	Difference	^{13}C Literature values	^{13}C Synthesis values	Difference
14.7	14.7	0	30.5	30.5	0
15.7	15.7	0	30.7	30.8	0.1
17.8	17.9	0.1	30.9	30.9	0
18.1	18	0.1	31	31.2	0.2
18.2	18.2	0	31.6	31.6	0
18.4	18.4	0	36.7	36.74	0.04
18.5	18.44	0.06	36.7	36.78	0.08
18.6	18.6	0	37.6	37.6	0
18.7	18.7	0	37.9	37.9	0
20.2	20.1	0.1	38.5	38.5	0
20.6	20.6	0	53.3	53.2	0.1
20.8	20.7	0.1	54.2	54.2	0
20.8	20.8	0	54.3	54.23	0.07
21	21	0	57.5	57.5	0
21.3	21.2	0.1	74.2	74.2	0
23.4	23.3	0.1	74.3	74.3	0
23.5	23.4	0.1	75.2	75.2	0
23.5	23.5	0	76.8	76.8	0
23.6	23.6	0	168.7	168.6	0.1
23.7	23.7	0	169.1	169.1	0
24.7	24.7	0	169.4	169.4	0
24.9	24.8	0.1	170.2	170.2	0
24.9	24.9	0	170.3	170.24	0.06
25.2	25.2	0	170.5	170.5	0
25.4	25.4	0	170.8	170.8	0
28.2	28.2	0	171	171	0
29.6	29.55	0.05	171.4	171.3	0.1
29.7	29.58	0.12	171.5	171.5	0
30.2	30.2	0			

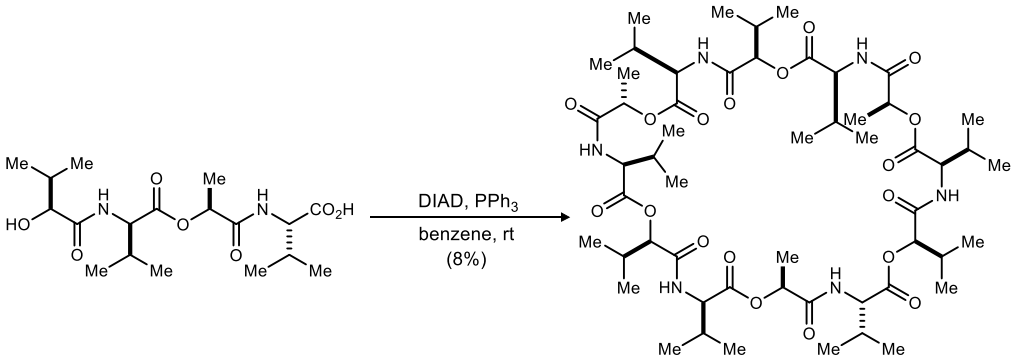

(+)-Valinomycin (*nat*-68). Following the Tetradepsipeptide MCO general procedure, *seco*-acid **122** (15.0 mg, 39.0 μmol) was stirred for 24 h at ambient temperature to afford a pale yellow oil. Preparative HPLC (5-95% aqueous acetonitrile, 210 nm, flow rate: 8 mL/min, R_t = 26.2 m) provided the 36-membered macrocycle, (+)-

[14] Lit: $[\alpha]_D^{22}$ -73 (*c* 3.3, $CHCl_3$) Kanaoka, M.; Isogai, A.; Murakoshi, S.; Ichinoe, M.; Suzuki, A.; Tamura, S. *Agric. Biol. Chem.* **1978**, *42*, 629.

valinomycin, (1.2 mg, 8%) as a white solid. $[\alpha]_D^{25}$ +18 (*c* 0.34, $CHCl_3$);[15] R_f = 0.36 (5% MeOH/DCM); IR (film) 3300, 2967, 2877, 1760, 1660, 1538, 1468, 1372, 1301, 1183, 1125, 1098, 1008 cm^{-1}; ^1H NMR (400 MHz, $CDCl_3$) δ 7.85 (d, *J* = 8.4 Hz, 1H), 7.76 (d, *J* = 5.8 Hz, 1H), 5.32 (q, *J* = 6.9 Hz, 1H), 5.02 (d, *J* = 3.1 Hz, 1H), 4.13 (dd, *J* = 9.7, 8.1 Hz, 1H), 3.99 (dd, *J* = 10.5, 6.2 Hz, 1H) 2.39-2.20 (m, 3H), 1.45 (d, *J* = 6.8 Hz, 3H), 1.08 (d, *J* = 6.6 Hz, 3H), 1.05 (d, *J* = 6.7 Hz, 3H), 0.99 (d, *J* = 7.0 Hz, 3H), 0.97 (d, *J* = 6.9 Hz, 3H), 0.96 (d, *J* = 6.6 Hz, 6H); ^{13}C NMR (150 MHz, DMSO-*d*$_6$) ppm; HRMS (ESI): Exact mass calcd for $C_{54}H_{90}N_6NaO_{18}$ $[M+Na]^+$ 1133.6204, found 1133.6209.

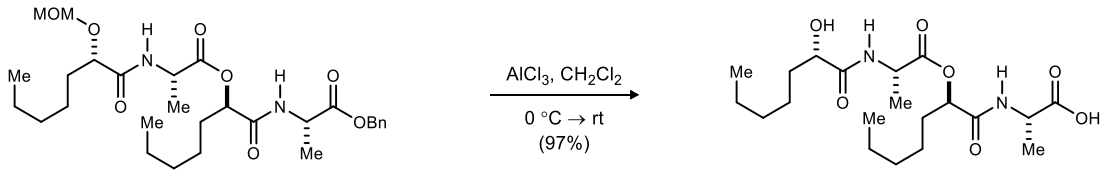

((*R*)-2-((((*S*)-2-Hydroxyheptanoyl)-*L*-alanyl)oxy)heptanoyl)-*L*-alanine (70). A flame-dried round-bottomed flask under inert atmosphere was charged with $AlCl_3$ (169 mg, 1.27 mmol) and CH_2Cl_2 (1.3 mL) at 0 °C. The MOM and benzyl-protected depsipeptide (70.0 mg, 127 μmol) was dissolved in CH_2Cl_2 (500 μL) and added dropwise to the stirring solution. The reaction was allowed to slowly warm to ambient temperature and stir for 15 m, and then poured into ice water. The aqueous layer was extracted with EtOAc, and the combined organic layers were washed with water and brine, dried, and concentrated to a yellow residue that was subjected to preparative HPLC (5-95% aqueous acetonitrile, 210 nm, flow rate: 8 mL/min, R_t = 17.5 m) to afford the *seco*-acid (51.3 mg, 97%) as a colorless foam. $[\alpha]_D^{20}$ +6 (*c* 0.10, $CHCl_3$); R_f = 0.16 (10% MeOH/DCM); IR (film) 3316, 2956, 2929, 2859, 1746, 1655, 1537, 1457, 1379, 1304, 1210, 1155, 1062 cm^{-1}; ^1H NMR (400 MHz, $CDCl_3$) δ 7.41 (br d, *J* = 6.0 Hz, 1H), 7.06 (br s, 1H), 5.21 (dd, *J* = 7.9, 4.0 Hz, 1H), 4.53 (dq, *J* = 7.2, 7.2 Hz, 1H), 4.45 (br dq, *J* = 6.9, 6.9 Hz, 1H), 4.15 (dd, *J* = 7.8, 3.7 Hz, 1H), 1.97-1.77 (series of m, 3H), 1.68-1.58 (m, 1H), 1.49 (d, *J* = 7.2 Hz, 3H), 1.47 (d, *J* = 7.3 Hz, 3H), 1.42-1.15 (br m, 12H), 0.91-0.86 (m, 6H), COO*H* and O*H* not observed; ^{13}C NMR (125 MHz, $CDCl_3$) ppm 174.3, 173.8, 173.2, 172.3, 74.6, 72.0, 48.47, 48.42, 34.4, 31.4 (2C), 31.2, 24.5, 24.4, 22.5, 22.4, 17.0 (2C), 13.97, 13.92; HRMS (ESI): Exact mass calcd for $C_{20}H_{36}N_2NaO_7$ $[M+Na]^+$ 439.2420, found 439.2440.

((*S*)-2-((((*R*)-2-Hydroxyheptanoyl)-*D*-alanyl)oxy)heptanoyl)-*D*-alanine (*ent*-70) was prepared following an identical procedure, but from *ent*-12. Preparative HPLC (5-95% aqueous acetonitrile, 210 nm, flow rate: 8 mL/min, R_t = 17.5 m) afforded the *seco*-acid with spectroscopic data identical to its enantiomer, except $[\alpha]_D^{20}$ -7 (*c* 0.10, $CHCl_3$).

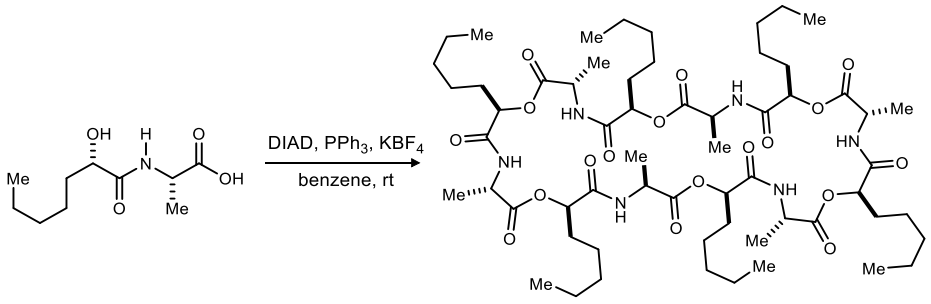

[15] Literature value: $[\alpha]_D^{25}$ +16 (*c* 0.35, $CHCl_3$) Pettit, G. R.; Tan, R.; Melody, N.; Kielty, J. M.; Pettit, R. K.; Herald, D. L.; Tucker, B. E.; Mallavia, L. P.; Doubek, D. L.; Schmidt, J. M. *Bioorg. Med. Chem.* **1999**, *7*, 895.

(3*S*,6*R*,9*S*,12*R*,15*S*,18*R*,21*S*,24*R*,27*S*,30*R*,33*S*,36*R*)-3,9,15,21,27,33-Hexamethyl-6,12,18,24,30,36-hexapentyl-1,7,13,19,25,31-hexaoxa-4,10,16,22,28,34-hexaazacyclohexatriacontan-2,5,8,11,14,17,20,23,26,29,32,35-dodecaone (72). Following the Didepsipeptide MCO general procedure, *seco*-acid **74** (15.0 mg, 69.0 μmol) with KBF_4 (21.8 mg, 173 μmol) were stirred at ambient temperature for 24 h to afford a pale yellow oil. Preparative HPLC (5-95% aqueous acetonitrile, 210 nm, flow rate: 8 mL/min, R_t = 23.8 m) provided the 36-membered macrocycle (6.0 mg, 44%) as an opaque film. $[\alpha]_D^{20}$ -12 (*c* 0.10, $CHCl_3$); R_f = 0.10 (4% MeOH/DCM); IR (film) 3286, 2955, 2925, 2856, 1748, 1656, 1542, 1454, 1376, 1260, 1189, 1158, 1115, 1062, 1018 cm^{-1}; ^1H NMR (400 MHz, $CDCl_3$) δ 6.95 (br d, *J* = 7.8 Hz, 1H), 5.13 (dd, *J* = 7.6, 4.7 Hz, 1H), 4.59 (dq, *J* = 7.3, 7.3 Hz, 1H), 1.92-1.76 (m, 2H), 1.47 (d, *J* = 7.1 Hz, 3H), 1.40-1.25 (br m, 6H), 0.88 (t, *J* = 6.7 Hz, 3H); ^{13}C NMR (125 MHz, $CDCl_3$) ppm 171.4, 169.4, 74.8, 48.4, 31.3, 31.2, 24.4, 22.4, 17.3, 13.9; HRMS (ESI): Exact mass calcd for $C_{60}H_{101}N_6Na_2O_{18}$ $[M-H+2Na]^+$ 1239.6968, found 1239.6981.

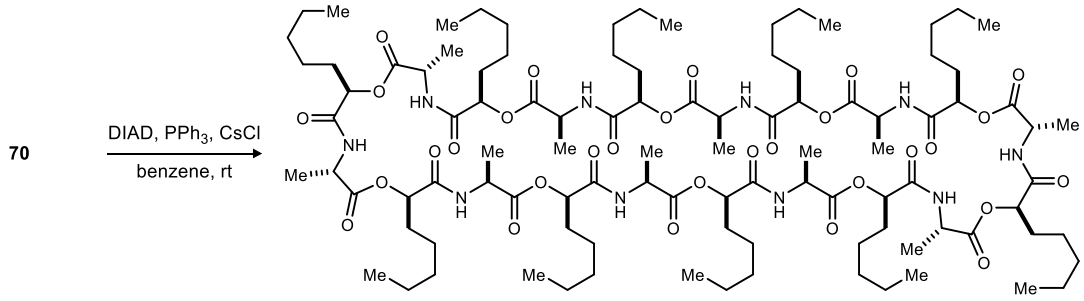

(3*S*,6*R*,9*S*,12*R*,15*S*,18*R*,21*S*,24*R*,27*S*,30*R*,33*S*,36*R*,39*S*,42*R*,45*S*,48*R*,51*S*,54*R*,57*S*,60*R*)-3,9,15,21,27,33,39,45,51,57-Decamethyl-6,12,18,24,30,36,42,48,54,60-decapentyl-1,7,13,19,25,31,37,43,49,55-decaoxa-4,10,16,22,28,34,40,46,52,58-decaazacyclohexacontan-2,5,8,11,14,17,20,23,26,29,32,35,38,41,44,47,50,53,56,59-icosaone (73). Following the Tetradepsipeptide MCO general procedure, *seco*-acid **70** (18.0 mg, 43.0 μmol) with CsCl (36.2 mg, 215 μmol) was stirred for 24 h at ambient temperature to afford a pale yellow oil. Preparative HPLC (5-95% aqueous acetonitrile, 210 nm, flow rate: 8 mL/min, R_t = 36.0 m) provided the 60-membered macrocycle (2.5 mg, 15%) as a colorless oil. $[\alpha]_D^{20}$ +33 (*c* 0.11, $CHCl_3$); R_f = 0.27 (4% MeOH/DCM); IR (film) 3312, 2957, 2925, 2855, 1750, 1658, 1545, 1456, 1381, 1261, 1195, 1157, 1064, 1020, 803 cm^{-1}; ^1H NMR (400 MHz, $CDCl_3$) δ 7.09 (br d, *J* = 6.8 Hz, 1H), 5.10 (dd, *J* = 8.4, 4.2 Hz, 1H), 4.49 (dq, *J* = 7.2, 7.2 Hz, 1H), 1.95-1.86 (m, 1H), 1.80-1.71 (m, 1H), 1.45 (d, *J* = 7.2 Hz, 3H), 1.39-1.25 (br m, 6H), 0.88 (t, *J* = 6.5 Hz, 3H); ^{13}C NMR (125 MHz, $CDCl_3$) ppm 171.9, 170.2, 74.2, 48.5, 31.3, 31.2, 24.5, 22.3, 16.9, 13.9; HRMS (ESI): Exact mass calcd for $C_{100}H_{170}N_{10}NaO_{30}$ $[M+Na]^+$ 2015.2014, found 2015.2047.

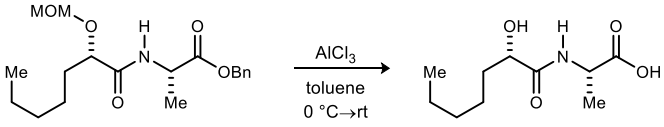

((*S*)-2-Hydroxyheptanoyl)-*L*-alanine (74). Following the Global Deprotection general procedure, the amide (215 mg, 699 μmol) stirred at ambient temperature for 25 m to afford a yellow residue. Preparative HPLC (5-95% aqueous acetonitrile, 210 nm, flow rate: 8 mL/min, R_t = 12.2 m) provided the *seco*-acid (114 mg, 75%) as a tan crystalline solid. Mp = 70-72 °C; $[\alpha]_D^{20}$ -14 (*c* 0.17, $CHCl_3$); R_f = 0.28 (20% MeOH/DCM); IR (film) 3386, 2925, 2855, 1729, 1649, 1535, 1459, 1378, 1300, 1220, 1154 cm^{-1}; ^1H NMR (400 MHz, DMSO-d_6) δ 7.76 (br d, *J* = 7.3 Hz, 1H), 5.45 (br s, 1H), 4.21 (br dq, *J* = 7.2, 7.2 Hz, 1H), 3.84 (dd, *J* = 7.3, 4.0 Hz, 1H), 1.65-1.57 (m, 1H), 1.49-1.40 (m, 1H), 1.36-1.30 (m, 2H), 1.28 (d, *J* = 7.1 Hz, 3H), 1.25-1.19 (br m, 4H), 0.85 (t, *J* = 6.8 Hz,

3H), COO*H* not observed; ^{13}C NMR (100 MHz, DMSO-d_6) ppm 173.9, 173.5, 70.7, 47.1, 34.2, 31.1, 24.1, 22.0, 17.6, 13.9; HRMS (CI): Exact mass calcd for $C_{10}H_{18}NO_3$ [M-OH] 200.1281, found 200.1282.

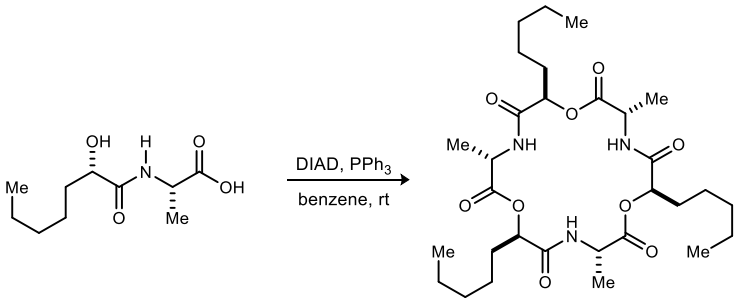

(3*S*,6*R*,9*S*,12*R*,15*S*,18*R*)-3,9,15-Trimethyl-6,12,18-tripentyl-1,7,13-trioxa-4,10,16-triazacyclooctadecane-2,5,8,11,14,17-hexaone (75). Following the Didepsipeptide MCO general procedure, *seco*-acid **74** (15.0 mg, 69.0 μmol) without a salt additive was stirred at ambient temperature for 24 h to afford a pale yellow oil. Preparative HPLC (5-95% aqueous acetonitrile, 210 nm, flow rate: 8 mL/min, R_t = 23.8 m) provided the 18-membered macrocycle (1.2 mg, 9%) as a colorless oil. $[\alpha]_D^{20}$ -23 (*c* 0.10, $CHCl_3$); R_f = 0.27 (4% MeOH/DCM); IR (film) 3209, 2922, 2853, 1756, 1696, 1556, 1457, 1380, 1260, 1211, 1171, 1106 cm^{-1}; ^{1}H NMR (400 MHz, $CDCl_3$) δ 6.96 (br d, *J* = 8.4 Hz, 1H), 5.12 (dd, *J* = 7.8, 4.8 Hz, 1H), 4.59 (dq, *J* = 7.4, 7.2 Hz, 1H), 1.91-1.77 (m, 2H), 1.47 (d, *J* = 7.2 Hz, 3H), 1.37-1.29 (br m, 6H), 0.88 (t, *J* = 6.4 Hz, 3H); ^{13}C NMR (150 MHz, $CDCl_3$) ppm 171.5, 169.5, 74.9, 48.5, 31.4, 31.3, 24.5, 22.4, 17.4, 14.0; HRMS (ESI): Exact mass calcd for $C_{30}H_{51}N_3NaO_9$ $[M+Na]^+$ 620.3523, found 620.3516.

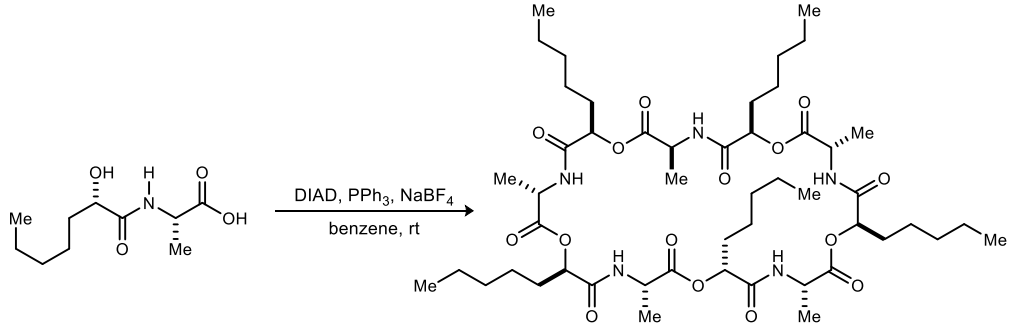

(3*S*,6*R*,9*S*,12*R*,15*S*,18*R*,21*S*,24*R*,27*S*,30*R*)-3,9,15,21,27-Pentamethyl-6,12,18,24,30-pentapentyl-1,7,13,19,25-pentaoxa-4,10,16,22,28-pentaazacyclotriacontane-2,5,8,11,14,17,20,23,26,29-decaone (76). Following the Didepsipeptide MCO general procedure, *seco*-acid **74** (15.0 mg, 69.0 μmol) with $NaBF_4$ (19.0 mg, 173 μmol) were stirred at ambient temperature for 24 h to afford a pale yellow oil. Preparative HPLC (5-95% aqueous acetonitrile, 210 nm, flow rate: 8 mL/min, R_t = 35.5 m) provided the 30-membered macrocycle (2.60 mg, 19%) as a colorless oil. $[\alpha]_D^{20}$ +3.3 (*c* 0.30, $CHCl_3$); R_f = 0.25 (3% MeOH/DCM); IR (film) 3315, 2957, 2924, 2854, 1747, 1664, 1547, 1458, 1380, 1261, 1200, 1117 cm^{-1}; ^{1}H NMR (400 MHz, $CDCl_3$) δ 7.12 (br d, *J* = 3.2 Hz, 1H), 5.09 (dd, *J* = 7.8, 4.4 Hz, 1H), 4.50 (dq, *J* = 7.2, 6.4 Hz, 1H), 1.91-1.86 (m, 1H), 1.80-1.71 (m, 1H), 1.45 (d, *J* = 7.2 Hz, 3H), 1.39-1.28 (br m, 6H), 0.88 (t, *J* = 6.4 Hz, 3H); ^{13}C NMR (150 MHz, $CDCl_3$) ppm 172.1, 170.2, 74.3, 48.5, 31.4, 31.3, 24.6, 22.4, 17.0, 13.9; HRMS (ESI): Exact mass calcd for $C_{50}H_{85}N_5NaO_{15}$ $[M+Na]^+$ 1018.5940, found 1018.5908.

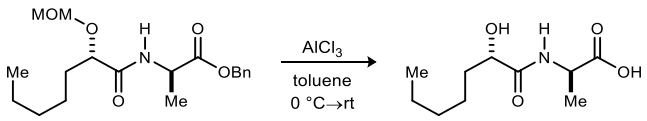

((*S*)-2-Hydroxyheptanoyl)-*D*-alanine (77). Following the global deprotection general procedure, amide ***epi*-45** (202 mg, 575 μmol) was stirred at ambient temperature for 25 m to afford a yellow residue. Preparative HPLC (5-95% aqueous acetonitrile, 210 nm, flow rate: 8 mL/min, R_t = 12.7 m) provided the *seco*-acid (93.7 mg, 75%) as a tan solid. Mp = 85-87 °C; $[\alpha]_D^{20}$ -25 (*c* 0.40, $CHCl_3$); R_f = 0.40 (20% MeOH/DCM); IR (film) 3315, 2923, 2854, 1732, 1626, 1537, 1457, 1292, 1258, 1210, 1158, 1128, 1080, 1020 cm^{-1}; ^1H NMR (400 MHz, DMSO-d_6) δ 7.75 (br d, *J* = 7.0 Hz, 1H), 5.46 (br s, 1H), 4.14 (br dq, *J* = 7.7, 6.6 Hz, 1H), 3.84 (dd, *J* = 7.3, 4.0 Hz, 1H), 1.64-1.56 (m, 1H), 1.49-1.40 (m, 1H), 1.36-1.30 (m, 2H), 1.27 (d, *J* = 7.1 Hz, 3H), 1.25-1.19 (br m, 4H), 0.85 (t, *J* = 6.9 Hz, 3H), COO*H* not observed; ^{13}C NMR (125 MHz, DMSO-d_6) ppm 173.9, 173.5, 70.8, 47.3, 34.2, 31.1, 24.1, 22.0, 17.7, 13.9; HRMS (ESI): Exact mass calcd for $C_{10}H_{18}NO_4$ $[M-H]^-$ 216.1236, found 216.1246.

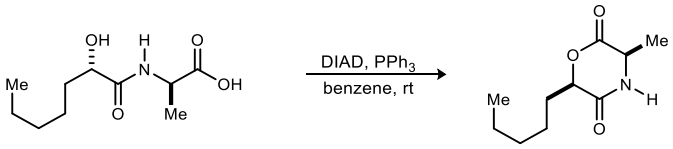

(3*R*,6*R*)-3-Methyl-6-pentylmorpholine-2,5-dione (78). Following the Didepsipeptide MCO general procedure, *seco*-acid **77** (20.0 mg, 92.0 μmol) without a salt additive was stirred at ambient temperature for 24 h to afford a pale yellow oil. Preparative HPLC (5-95% aqueous acetonitrile, 210 nm, flow rate: 8 mL/min, R_t = 15.5 min) provided the 6-membered macrocycle (6.1 mg, 33%) as a viscous oil. $[\alpha]_D^{20}$ +6.1 (*c* 0.28, $CHCl_3$); R_f = 0.17 (2% MeOH/DCM); IR (film) 3376, 2923, 2855, 1730, 1651, 1531, 1458, 1260, 1153, 1120 cm^{-1}; ^1H NMR (400 MHz, $CDCl_3$) δ 6.17 (br s, 1H), 4.78 (dd, *J* = 7.9, 4.0 Hz, 1H), 4.25 (q, *J* = 6.8 Hz, 1H), 2.12-2.03 (m, 1H), 1.94-1.85 (m, 1H), 1.49 (d, *J* = 6.7 Hz, 3H), 1.61-1.53 (m, 1H), 1.50-1.43 (m, 1H), 1.37-1.32 (br m, 4H), 0.90 (t, *J* = 7.1 Hz, 3H); ^{13}C NMR (100 MHz, $CDCl_3$) ppm 168.4, 168.1, 78.2, 49.3, 31.3, 30.3, 24.2, 22.3, 17.5, 13.9; HRMS (CI): Exact mass calcd for $C_{10}H_{18}NNaO_3$ $[M+H]^+$ 200.1281, found 200.1279.

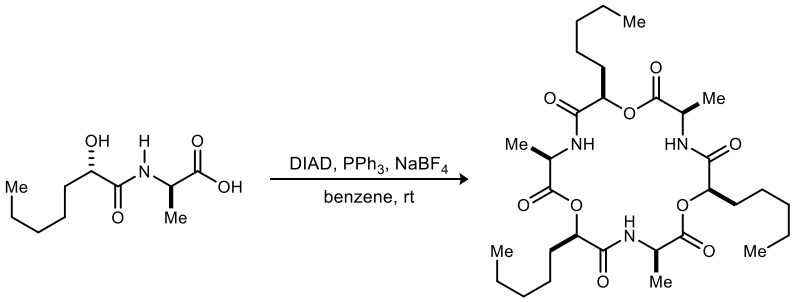

(3*R*,6*R*,9*R*,12*R*,15*R*,18*R*)-3,9,15-Trimethyl-6,12,18-tripentyl-1,7,13-trioxa-4,10,16-triazacyclooctadecane-2,5,8,11,14,17-hexaone (79). Following the Didepsipeptide MCO general procedure, *seco*-acid **77** (20.0 mg, 92.0 μmol) with $NaBF_4$ (25.1 mg, 230 μmol) were stirred at ambient temperature for 24 h to afford a pale yellow oil. Preparative HPLC (5-95% aqueous acetonitrile, 210 nm, flow rate: 8 mL/min, R_t = 24.8 min) provided the 18-membered macrocycle (5.3 mg, 29%) as an opaque film. $[\alpha]_D^{20}$ +26 (*c* 0.25, $CHCl_3$); R_f = 0.30 (3% MeOH/DCM); IR (film) 3277, 2952, 2853, 1753, 1663, 1542, 1456, 1218 cm^{-1}; ^1H NMR (400 MHz, $CDCl_3$) δ 6.89 (br d, *J* = 5.2 Hz, 1H), 5.19 (dd, *J* = 5.5, 4.6 Hz, 1H), 4.63 (dq, *J* = 7.1, 7.1 Hz, 1H), 1.96-1.81 (m, 2H), 1.49 (d, *J* = 7.1 Hz,

3H), 1.39-1.26 (br m, 6H), 0.89 (t, *J* = 6.4 Hz, 3H); ^{13}C NMR (150 MHz, $CDCl_3$) ppm 169.8, 169.6, 74.3, 48.9, 31.6, 31.3, 24.6, 22.4, 17.5, 13.9; HRMS (ESI): Exact mass calcd for $C_{30}H_{51}N_3NaO_9$ $[M+Na]^+$ 620.3523, found 620.3547.

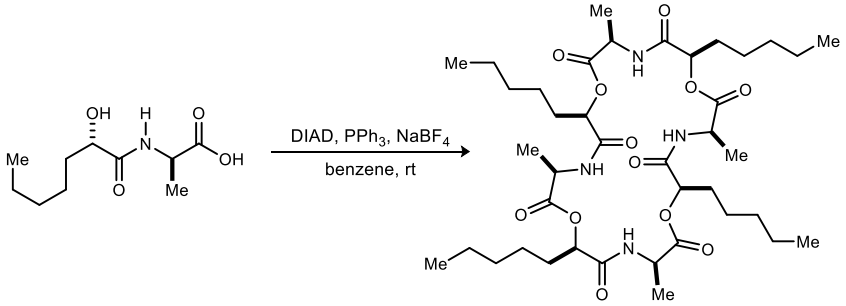

(3*R*,6*R*,9*R*,12*R*,15*R*,18*R*,21*R*,24*R*)-3,9,15,21-Tetramethyl-6,12,18,24-tetrapentyl-1,7,13,19-tetraoxa-4,10,16,22-tetraazacyclotetracosan-2,5,8,11,14,17,20,23-octaone (80). Following the Didepsipeptide MCO general procedure, *seco*-acid **77** (20.0 mg, 92.0 μmol) and $NaBF_4$ (25.1 mg, 230 μmol) were stirred at ambient temperature for 24 h to afford a pale yellow oil. Preparative HPLC (5-95% aqueous acetonitrile, 210 nm, flow rate: 8 mL/min, R_t = 28.2 min) provided the 24-membered macrocycle as a white solid (5.0 mg, 27%). Mp = 173-175 °C; $[\alpha]_D^{20}$ +32 (*c* 0.13 $CHCl_3$); R_f = 0.26 (3% MeOH/DCM); IR (film) 3281, 2924, 2854, 1750, 1655, 1543, 1458, 1260, 1060 cm^{-1}; ^{1}H NMR (600 MHz, $CDCl_3$) δ 6.79 (br m, 1H), 5.13 (br dd, *J* = 6.5, 5.5 Hz, 1H), 4.66 (br dq, *J* = 6.9, 6.7 Hz, 1H), 1.94-1.88 (m, 1H), 1.83-1.77 (m, 1H), 1.51 (d, *J* = 7.2 Hz, 3H), 1.35-1.25 (br m, 6H), 0.88 (t, *J* = 6.6 Hz, 3H); ^{13}C NMR (150 MHz, $CDCl_3$) ppm 170.7, 169.6, 74.9, 48.4, 31.3, 31.1, 24.4, 22.4, 17.5, 13.9; HRMS (ESI): Exact mass calcd for $C_{40}H_{68}N_4NaO_{12}$[M+Na]$^+$ 819.4731, found 819.4739.

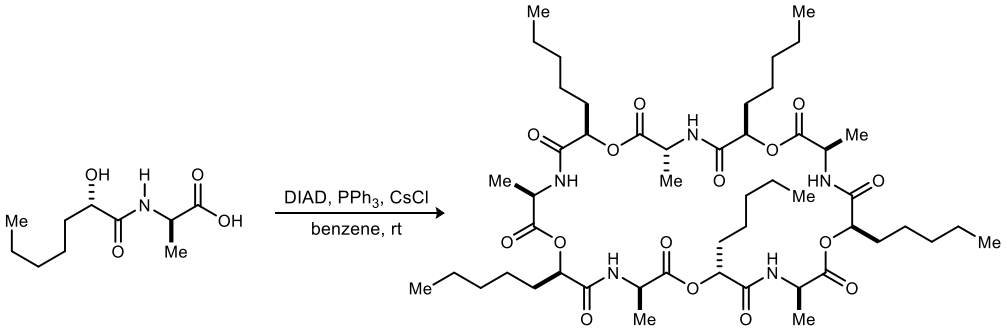

(3*R*,6*R*,9*R*,12*R*,15*R*,18*R*,21*R*,24*R*,27*R*,30*R*)-3,9,15,21,27-Pentamethyl-6,12,18,24,30-pentapentyl-1,7,13,19,25-pentaoxa-4,10,16,22,28-pentaazacyclotriacontane-2,5,8,11,14,17,20,23,26,29-decaone (81). Following the Didepsipeptide MCO general procedure, the *seco*-acid (15.0 mg, 69.0 μmol) with CsCl (29.1 mg, 173 μmol) were stirred at ambient temperature for 24 h to afford a pale yellow oil. Preparative HPLC (5-95% aqueous acetonitrile, 210 nm, flow rate: 8 mL/min, R_t = 36.8 min) provided the 30-membered macrocycle (3.7 mg, 27%) as an opaque film. $[\alpha]_D^{20}$ +6.0 (*c* 0.10, $CHCl_3$); R_f = 0.37 (3% MeOH/DCM); IR (film) 3298, 2924, 2853, 1749, 1656, 1544, 1458, 1378, 1261 cm^{-1}; ^{1}H NMR (400 MHz, $CDCl_3$) δ 7.03 (br d, *J* = 6.8 Hz, 1H), 5.19 (dd, *J* = 8.4, 4.1 Hz, 1H), 4.42 (dq, *J* = 6.8, 6.7 Hz, 1H), 1.96-1.89 (m, 1H), 1.78-1.69 (m, 1H), 1.52 (d, *J* = 7.2 Hz, 3H), 1.39-1.28 (br m, 6H), 0.88 (t, *J* = 6.8 Hz, 3H); ^{13}C NMR (150 MHz, $CDCl_3$) ppm 171.9, 170.3, 74.5, 49.0, 31.7, 31.3, 24.6, 22.4, 17.3, 13.9; HRMS (ESI): Exact mass calcd for $C_{50}H_{85}N_5NaO_{15}$[M+Na]$^+$ 1018.5940, found 1018.5942.

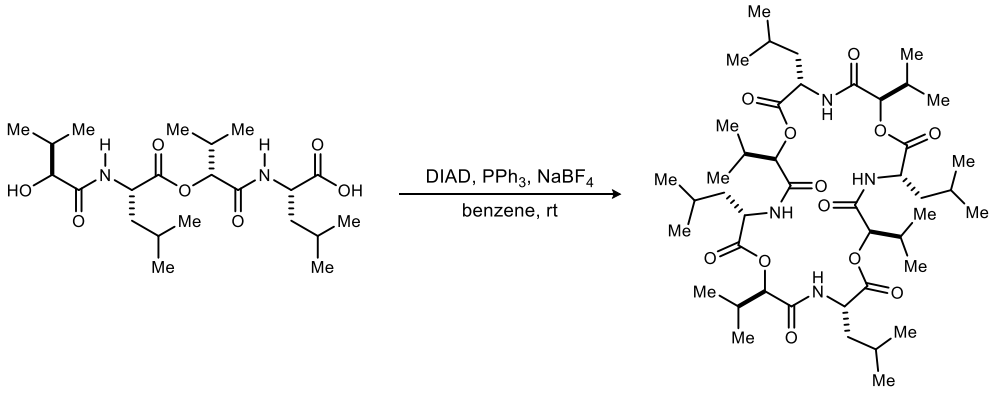

(3*S*,6*R*,9*S*,12*R*,15*S*,18*R*,21*S*,24*R*)-3,9,15,21-Tetraisobutyl-6,12,18,24-tetraisopropyl-1,7,13,19-tetraoxa-4,10,16,22-tetraazacyclotetracosan-2,5,8,11,14,17,20,23-octaone (91). Following the Tetradepsipeptide MCO general procedure, the *seco*-acid (20.0 mg, 45.0 μmol) with $NaBF_4$ (24.7 mg, 225 μmol) was stirred for 18 h at ambient temperature to afford a chunky white solid. Preparative HPLC (5-95% aqueous acetonitrile, 210 nm, flow rate: 8 mL/min, R_t = 26.2 m) provided the 24-membered macrocycle (6.0 mg, 31%) as a white powder. $[\alpha]_D^{20}$ -21 (*c* 0.11, MeOH); R_f = 0.1 (3% MeOH/DCM); IR (film) 3353, 2958, 2922, 2852, 1736, 1654, 1557, 1459, 1261, 1099, 1157, 1020, 800 cm^{-1}; ^1H NMR (400 MHz, DMSO-d_6) δ 9.06 (d, *J* = 9.6 Hz, 1H), 4.69 (d, *J* = 5.6 Hz, 1H), 4.66 (ddd, *J* = 12.3, 9.6, 2.7 Hz, 1H), 2.31 (ddd, *J* = 12.7, 12.7, 2.6 Hz, 1H), 2.06 (br qqd, *J* = 6.7 Hz, 1H), 1.50-1.42 (br m, 1H), 1.39-1.36 (ddd, 12.7, 12.7, 2.6 Hz, 1H), 0.98 (d, *J* = 6.7 Hz, 3H), 0.93 (d, *J* = 6.8 Hz, 3H), 0.81 (d, *J* = 6.5 Hz, 3H), 0.77 (d, *J* = 6.3 Hz, 3H); ^{13}C NMR (125 MHz, DMSO-d_6) ppm 171.9, 168.4, 79.4, 49.2, 40.7, 29.9, 23.10, 23.07, 20.2, 18.5, 18.2; HRMS (ESI): Exact mass calcd for $C_{44}H_{76}N_4NaO_{12}$ $[M+Na]^+$ 875.5357, found 875.5361.

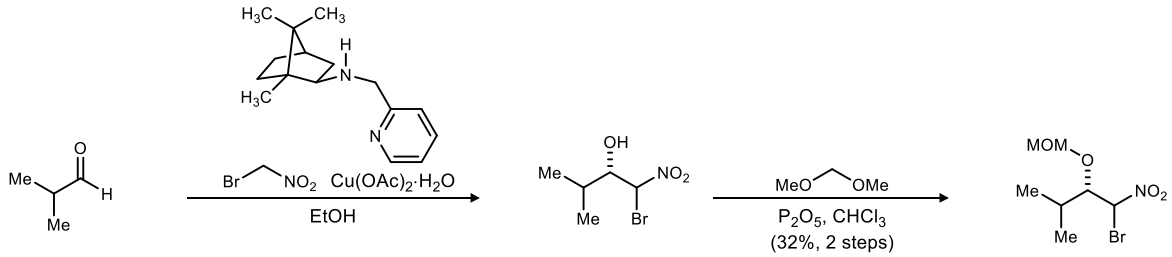

(2*S*)-1-Bromo-2-(methoxymethoxy)-3-methyl-1-butane (92). Following the Blay[3] enantioselective Henry procedure, isobutyraldehyde (595 μL, 6.51 mmol) and bromonitromethane (4.54 mL, 65.1 mmol) were stirred for 5 days at -20 °C. The reaction was quenched dropwise at -20 °C with 1 N HCl and the aqueous layer was extracted with CH_2Cl_2. Following drying and concentration under reduced pressure, the crude alcohol was dissolved in $CHCl_3$ (33 mL), treated with P_2O_5 (9.24 g, 65.1 mmol) and dimethoxymethane (11.5 mL, 76.1 mmol), and stirred at ambient temperature overnight. The reaction was cooled to 0 °C, quenched slowly with satd aq $NaHCO_3$, and then poured into CH_2Cl_2. The aqueous layer was extracted with CH_2Cl_2. The organic layers were dried and concentrated to an oil that was subjected to flash column chromatography (SiO_2, 1-3% diethyl ether in hexanes) to afford the title compound in 2:1 dr as a pale yellow oil (534 mg, 32%, 2 steps). The diastereomers were determined to be 81/84% ee by chiral HPLC analysis. R_f = 0.52 (10% EtOAc/hexanes) R_f = 0.50 (10% Et_2O/hexanes); IR (film) 2968, 1571, 1471, 1356, 1156, 1137, 1105, 1088, 1027, 972, 924, 712 cm^{-1}; ^1H NMR (400 MHz, $CDCl_3$)[16] δ 6.10 (d, *J* = 3.6 Hz, 1H), 5.82 (d, *J* = 9.0 Hz, 1H), 4.69 (d, *J* =7.0 Hz, 1H), 4.66 (d, *J* = 7.0 Hz, 1H), 4.62 (d, *J* = 6.8 Hz, 1H), 4.59 (d, *J* = 6.8 Hz, 1H), 4.07 (dd, *J* = 9.1, 2.5 Hz, 1H), 3.94 (dd, *J* = 7.0, 3.6

[16] Characterized as a mixture of diastereomers

Hz, 1H), 3.38 (s, 3H), 3.35 (s, 3H), 2.29 (qqd, *J* = 6.9, 2.5 Hz, 1H), 1.95 (qqd, *J* = 6.8, 6.8 Hz, 1H), 1.07 (d, *J* = 6.3 Hz, 3H), 1.05 (d, *J* = 6.7 Hz, 3H), 1.02 (d, *J* = 6.8 Hz, 3H), 0.93 (d, *J* = 6.8 Hz, 3H); ^{13}C NMR (100 MHz, $CDCl_3$) ppm 99.0, 98.5, 84.9, 84.7 (2C), 84.6, 56.8, 56.7, 31.8, 29.1, 19.7, 19.0, 17.9, 15.1; HRMS (CI): Exact mass calcd for $C_7H_{18}BrN_2O_4$ $[M+NH_4]^+$ 273.0444, found 273.0443.

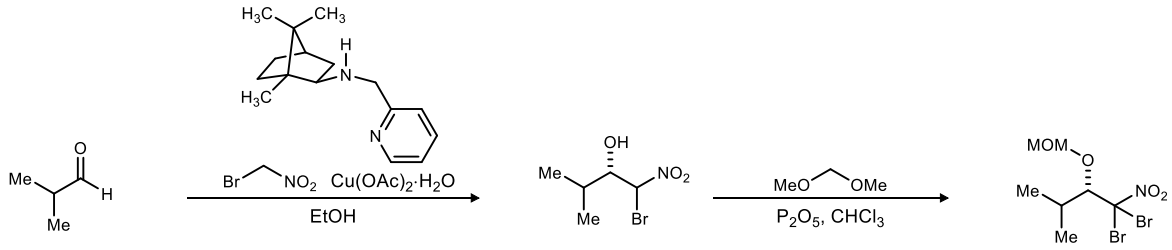

(*S*)-1,1-dibromo-2-(methoxymethoxy)-3-methyl-1-nitrobutane (93). This dibromonitroalkane is isolated as a side product from the Henry and MOM protection sequence as a pale yellow oil. R_f = 0.46 (10% Et_2O/hexanes); IR (film) 3397, 2965, 2932, 1576, 1327, 1158, 1094, 1025, 972, 827 cm^{-1}; ^{1}H NMR (500 MHz, $CDCl_3$) δ 4.69 (d, *J* = 7.1 Hz, 1H), 4.67 (d, *J* = 7.1 Hz, 1H), 4.33 (d, *J* = 2.1 Hz, 1H), 3.40 (s, 3H), 2.33 (qqd, *J* = 7.0, 2.1 Hz, 1H), 1.18 (d, *J* = 7.0 Hz, 3H), 1.14 (d, *J* = 6.8 Hz, 3H); ^{13}C NMR (100 MHz, $CDCl_3$) ppm 99.0, 93.5, 88.7, 57.1, 31.1, 23.1, 17.4; HRMS (CI): Exact mass calcd for $C_7H_{12}N^{79}Br^{81}Br$ $[M-H]^+$ 333.9107, found 333.9105.

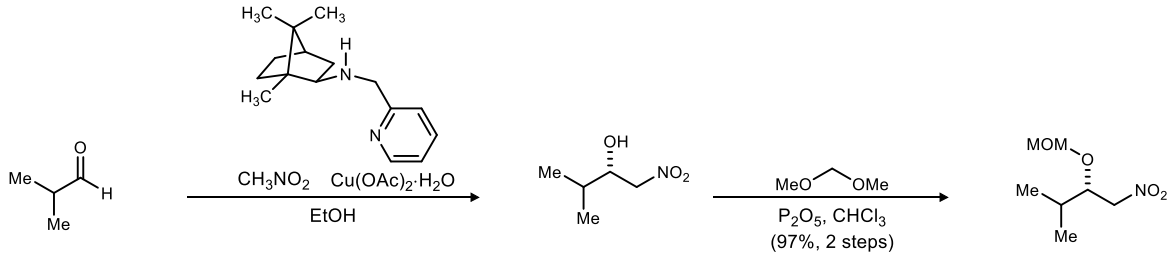

(*S*)-2-(Methoxymethoxy)-3-methyl-1-nitrobutane (95). Following the Blay enantioselective Henry procedure, isobutanal (50.0 µL, 548 µmol) and nitromethane (295 µL, 5.48 mmol) were stirred for 3 days at 0 °C. The reaction was quenched dropwise at 0 °C with 1 N HCl and the aqueous layer was extracted with CH_2Cl_2. The organic layers were dried and concentrated under reduced pressure. The crude alcohol was dissolved in $CHCl_3$ (2.74mL), treated with P_2O_5 (778 mg, 5.48 mmol) and dimethoxymethane (970 µL, 11.0 mmol), and stirred at ambient temperature overnight. The reaction was cooled to 0 °C, quenched slowly with satd aq $NaHCO_3$, and then poured into CH_2Cl_2. The aqueous layer was extracted with CH_2Cl_2. The organic layers were dried and concentrated to an oil that was subjected to flash column chromatography (SiO_2, 3-10% diethyl ether in hexanes) to afford the title compound as a colorless oil (94 mg, 97%, 2 steps). The enantiopurity was determined to be 87% ee by chiral HPLC analysis (Chiralcel OD-H, 2% ^{i}PrOH /hexanes, 0.4 mL/min, t_r(e_1, major) = 26.8 min, t_r(e_2, minor) = 28.8 min). R_f = 0.26 (10% Et_2O/hexanes); IR (film) 2965, 1558, 1387, 1369, 1156, 1103, 1034, 914, 745 cm^{-1}; ^{1}H NMR (400 MHz, $CDCl_3$) δ 4.67 (d, *J* = 7.0 Hz, 1H), 4.65 (d, *J* = 7.0 Hz, 1H), 4.50 (dd, *J* = 12.4, 8.6 Hz, 1H), 4.42 (dd, *J* = 12.4, 3.4 Hz, 1H), 4.13 (ddd, *J* = 8.6, 4.7, 3.5 Hz, 1H), 3.35 (s, 3H), 2.02 (qqd, *J* = 6.9, 4.7 Hz, 1H), 0.98 (d, *J* = 6.9 Hz, 6H); ^{13}C NMR (100 MHz, $CDCl_3$) ppm 96.8, 79.8, 77.1, 56.0, 30.5, 17.9, 17.4; HRMS (CI): Exact mass calcd for $C_7H_{16}NO_4$ $[M+H]^+$ 178.1074, found 178.1079.

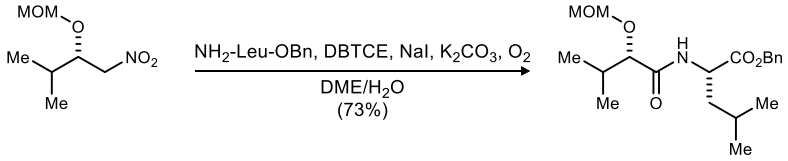

Benzyl ((*S*)-2-(methoxymethoxy)-3-methylbutanoyl)-L-leucinate (97). Following the One-Pot UmAS General Procedure, nitroalkane (30.0 mg, 169 µmol) and amine (45.0 mg, 203 mmol) afforded an orange oil. The residue was subjected to preparative HPLC (5-95% aqueous acetonitrile, 210 nm, flow rate: 8 mL/min, R_t = 26.7 min) to afford the major diastereomer (45.0 mg, 73%) as a waxy yellow solid. Mp = 56-58 °C; $[\alpha]_D^{25}$ -69 (*c* 0.21, $CHCl_3$); R_f = 0.22 (15% EtOAc/hexanes); IR (film) 3297, 2954, 1735, 1653, 1533, 1454, 1273, 1212, 1155, 1132, 1031, 978, 753 cm^{-1}; ^1H NMR (400 MHz, $CDCl_3$) δ 7.37-7.29 (m, 5H), 6.85 (br d, *J* = 8.9 Hz, 1H), 5.17 (d, *J* = 12.2 Hz, 1H), 5.13 (d, *J* = 12.2 Hz, 1H), 4.73 (ddd, *J* = 9.0, 9.0, 5.0 Hz, 1H), 4.65 (d, *J* = 6.6 Hz, 1H), 4.62 (d, *J* = 6.6 Hz, 1H), 3.89 (d, *J* = 4.0 Hz, 1H), 3.38 (s, 3H), 2.14 (qqd, *J* = 6.9, 4.1 Hz, 1H), 1.70-1.57 (m, 3H), 1.00 (d, *J* = 6.9 Hz, 3H), 0.92 (d, *J* = 6.6 Hz, 9H); ^{13}C NMR (100 MHz, $CDCl_3$) ppm 172.6, 171.7, 135.3, 128.5, 128.4, 128.2, 96.7, 82.3, 67.0, 56.3, 50.1, 41.5, 31.3, 24.8, 22.8, 21.6, 19.0, 16.9; HRMS (ESI): Exact mass calcd for $C_{20}H_{31}NNaO_5$ $[M+Na]^+$ 388.2100, found 388.2084.

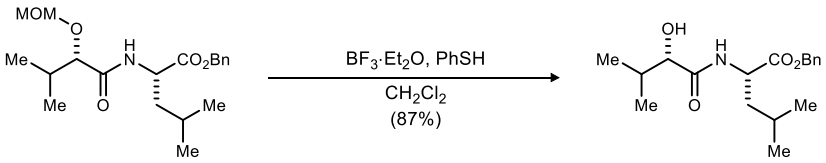

Benzyl ((*S*)-2-hydroxy-3-methylbutanoyl)-*L*-leucinate (99). Following general MOM Deprotection procedure I, the amide (160 mg, 438 µmol) afforded a yellow oil. Flash column chromatography (SiO_2, 10-25% ethyl acetate in hexanes) provided the alcohol (118 mg, 87%) as a pale yellow oil. $[\alpha]_D^{25}$ -48 (*c* 0.19, $CHCl_3$); R_f = 0.19 (25% EtOAc/hexanes); IR (film) 3387, 2960, 2932, 2873, 1741, 1654, 1523, 1459, 1385, 1368, 1339, 1273, 1192, 1152, 1022 cm^{-1}; ^1H NMR (400 MHz, $CDCl_3$) δ 7.39-7.31 (m, 5H), 6.74 (br d, *J* = 7.5 Hz, 1H), 5.18 (d, *J* = 13.0 Hz, 1H), 5.14 (d, *J* = 13.0 Hz, 1H), 4.71 (ddd, *J* = 8.6, 8.6, 5.0 Hz, 1H), 4.01 (dd, *J* = 5.4, 3.3 Hz, 1H), 2.41 (d, *J* = 5.3 Hz, 1H), 2.17 (qqd, *J* = 6.8, 3.2 Hz, 1H), 1.71-1.56 (m, 3H), 1.03 (d, *J* = 7.0 Hz, 3H), 0.92 (d, *J* = 6.2 Hz, 6H), 0.86 (d, *J* = 6.8 Hz, 3H); ^{13}C NMR (125 MHz, $CDCl_3$) ppm 172.9, 172.7, 135.3, 128.6, 128.4, 128.2, 76.3, 67.1, 50.4, 41.4, 31.9, 24.9, 22.8, 21.7, 19.1, 15.5; HRMS (ESI): Exact mass calcd for $C_{18}H_{27}NNaO_4$ $[M+Na]^+$ 344.1838, found 344.1829.

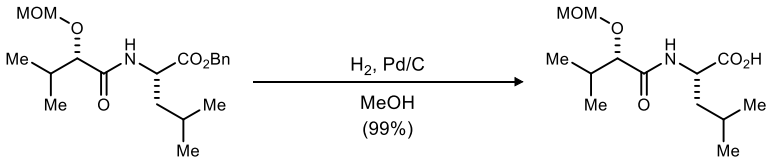

((*S*)-2-(Methoxymethoxy)-3-methylbutanoyl)-*L*-leucine (100). Following general benzyl-deprotection procedure I, the amide (160 mg, 438 µmol) afforded the acid (121 mg, 99%) as an analytically pure pale yellow oil. $[\alpha]_D^{25}$ -83 (*c* 0.10, $CHCl_3$); R_f = 0.31 (10% MeOH/DCM); IR (film) 3409, 3302, 2960, 2931, 2874, 1733, 1656, 1524, 1471, 1387, 1369, 1264, 1213, 1156, 1103, 1088, 1034 cm^{-1}; ^1H NMR (400 MHz, $CDCl_3$) δ 6.84 (br d, *J* = 7.0 Hz, 1H), 4.72 (d, *J* = 6.4 Hz, 1H), 4.67 (d, *J* = 6.4 Hz, 1H), 4.61 (br m, 1H), 3.91 (d, *J* = 3.7 Hz, 1H), 3.42 (s, 3H), 2.15 (br m, 1H), 1.78-1.61 (m, 3H), 1.01 (d, *J* = 6.8 Hz, 3H), 0.97 (d, *J* = 6.0 Hz, 3H), 0.94 (d, *J* =

7.0 Hz, 3H), 0.93 (d, *J* = 7.0 Hz, 3H), COO*H* not observed; ^{13}C NMR (125 MHz, $CDCl_3$) ppm 176.1, 172.8, 97.0, 82.5, 56.4, 50.4, 40.8, 31.4, 24.9, 22.9, 21.5, 19.0, 16.9; HRMS (ESI): Exact mass calcd for $C_{13}H_{25}NNaO_5$ $[M+Na]^+$ 298.1630, found 298.1625.

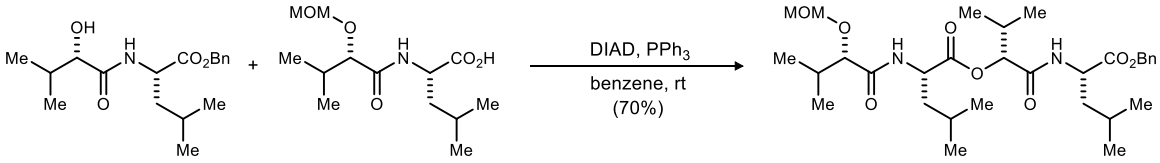

Benzyl ((*R*)-2-((((*S*)-2-(methoxymethoxy)-3-methylbutanoyl)-*L*-leucyl)oxy)-3-methylbutanoyl)-*L*-leucinate (101). Following the Mitsunobu general procedure, alcohol (216 mg, 672 μmol) and acid (235 mg, 853 μmol) at ambient temperature for 24 h afforded a crude brown oil. Flash column chromatography (SiO_2, 10-25% ethyl acetate in hexanes) followed by preperative HPLC (5-95% aqueous acetonitrile, 210 nm, flow rate: 8 mL/min, R_t = 28.5 min) provided the didepsipeptide (273 mg, 70%) as a pale yellow oil. $[\alpha]_D^{25}$ -37 (*c* 0.13, $CHCl_3$); R_f = 0.31 (25% EtOAc/hexanes); IR (film) 3315, 2961, 2874, 1747, 1653, 1536, 1470, 1387, 1369, 1340, 1153, 1130, 1108, 1034 cm^{-1}; ^{1}H NMR (400 MHz, $CDCl_3$) δ 7.35-7.31 (m, 5H), 7.15 (br d, *J* = 8.4 Hz, 1H), 6.83 (br d, *J* = 5.8 Hz, 1H), 5.18 (d, *J* = 12.4 Hz, 1H), 5.12 (d, *J* = 12.4 Hz, 1H), 5.11 (d, *J* = 3.2 Hz, 1H), 4.68 (m, 1H), 4.68 (d, *J* = 6.6 Hz, 1H), 4.65 (d, *J* = 6.6 Hz, 1H), 4.43 (br ddd, *J* = 13.6, 6.5 Hz, 1H), 3.82 (d, *J* = 3.9 Hz, 1H), 3.42 (s, 3H), 2.43 (qqd, *J* = 6.8, 3.0 Hz, 1H), 2.12 (qqd, *J* = 6.9, 4.1 Hz, 1H), 1.76-1.58 (m, 6H), 1.02 (d, *J* = 6.0 Hz, 3H), 0.99 (d, *J* = 7.1 Hz, 3H), 0.97 (d, *J* = 6.8 Hz, 3H), 0.95 (d, *J* = 7.4 Hz, 3H), 0.93 (d, *J* = 7.1 Hz, 3H), 0.92 (d, *J* = 6.8 Hz, 3H), 0.89 (d, *J* = 6.4 Hz, 3H), 0.87 (d, *J* = 6.4 Hz, 3H);^{13}C NMR (125 MHz, $CDCl_3$) ppm 172.63, 172.60, 172.5, 169.1, 135.7, 128.5 (2C), 128.2, 97.1, 82.4, 78.6, 66.8, 56.4, 51.4, 50.6, 40.3, 40.2, 31.3, 30.4, 24.9, 24.6, 22.9, 22.5, 22.1, 21.5, 19.1, 18.8, 17.0, 16.2; HRMS (ESI): Exact mass calcd for $C_{31}H_{50}N_2NaO_8$ $[M+Na]^+$ 601.3465, found 601.3436

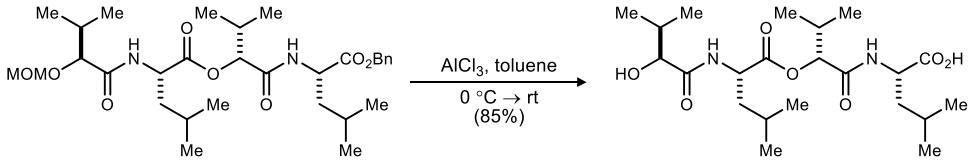

((*R*)-2-((((*S*)-2-Hydroxy-3-methylbutanoyl)-*L*-leucyl)oxy)-3-methylbutanoyl)-*L*-leucine (102). Following the Global Deprotection general procedure, the amide (263 mg, 455 μmol) stirred at ambient temperature for 25 m to afford a yellow residue. Preparative HPLC (5-95% aqueous acetonitrile, 210 nm, flow rate: 8 mL/min, R_t = 18.3 min) provided the *seco*-acid (170 mg, 85%) as a pale yellow oil. $[\alpha]_D^{25}$ -30 (*c* 0.13, $CHCl_3$); R_f = 0.19 (10% MeOH/DCM); IR (film) 3314, 2961, 2931, 2874, 1740, 1656, 1545, 1469, 1369, 1237, 1155, 1022 cm^{-1}; ^{1}H NMR (400 MHz, DMSO-d_6) δ 8.07 (d, *J* = 8.1 Hz, 1H), 7.98 (d, *J* = 8.4 Hz, 1H), 5.56 (br s, 1H), 4.76 (d, *J* = 4.0 Hz, 1H), 4.44 (ddd, *J* = 10.2, 8.0, 5.0 Hz, 1H), 4.28 (ddd, *J* = 11.0, 8.5, 4.1 Hz, 1H), 3.76 (d, *J* = 3.4 Hz, 1H), 2.14 (qqd, *J* = 6.8, 4.0 Hz, 1H), 2.02 (qqd, *J* = 6.8, 3.5 Hz, 1H), 1.80 (ddd, *J* = 13.0, 10.3, 4.7 Hz, 1H), 1.66-1.45 (m, 5H), 0.93-0.84 (m, 18H), 0.79 (d, *J* = 6.2 Hz, 3H), 0.77 (d, *J* = 6.8 Hz, 3H), COO*H* not observed; ^{13}C NMR (125 MHz, DMSO-d_6) ppm 173.8, 173.6, 171.9, 168.6, 77.9, 75.1, 50.1, 49.7, 39.7, 39.5, 31.2, 30.0, 24.2, 24.0, 22.9, 22.8, 21.2, 20.8, 19.1, 18.8, 16.5, 16.0; HRMS (ESI): Exact mass calcd for $C_{22}H_{40}N_2NaO_7$ $[M+Na]^+$ 467.2733, found 467.2714.

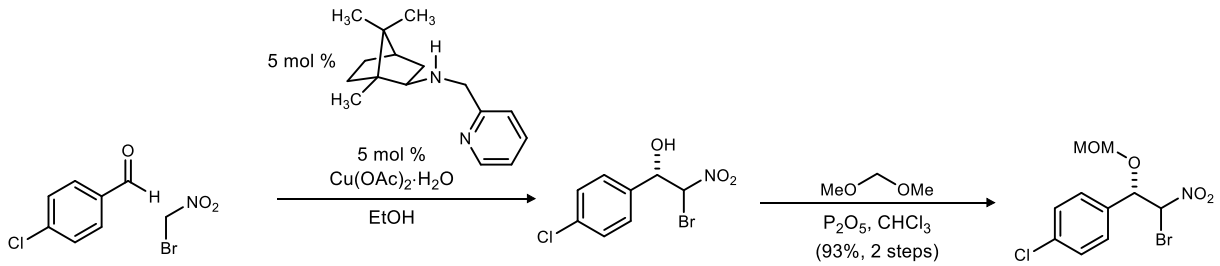

1-((1*S*)-2-Bromo-1-(methoxymethoxy)-2-nitroethyl)-4-chlorobenzene (106). Following the Blay[3] enantioselective Henry procedure, Blay ligand (87.0 mg, 356 µmol) and $Cu(OAc)_2$•H_2O (71.1 mg, 356 µmol) were stirred at ambient temperature in EtOH (29 mL) for 1 h. The royal blue solution was then cooled to -20 °C and 4-chlorobenzaldehyde (1.00 g, 7.11 mmol) was added and allowed to stir for 10 m before bromonitromethane (4.96 mL, 71.1 mmol) addition. After stirring for 3 days at -20 °C, the reaction was quenched dropwise at -20 °C with pre-chilled 1 N HCl and the aqueous layer was extracted with CH_2Cl_2. Following drying and concentration under reduced pressure, the crude alcohol was dissolved in $CHCl_3$ (36 mL), treated with P_2O_5 (10.1 g, 71.1 mmol) and dimethoxymethane (12.6 mL, 142 mmol), and stirred at ambient temperature overnight. The reaction was cooled to 0 °C, quenched slowly with satd aq $NaHCO_3$, and then poured into CH_2Cl_2. The aqueous layer was extracted with CH_2Cl_2. The organic layers were dried and concentrated to an oil that was subjected to flash column chromatography (SiO_2, 4-8% diethyl ether in hexanes) to afford the title compound in 2:1 d.r. as a pale yellow solid (2.15 g, 93%, 2 steps). The diastereomers were determined to be 84% ee by chiral HPLC analysis. Recrystallization from hexane afforded 1.35 g (62% recovery) of white crystals. The crystals were determined to be 99% ee by chiral HPLC analysis (Chiralpak AD-H, 3% EtOH /hexanes, 0.8 mL/min, t_r(d_1e_1, major) = 11.6 min, t_r(d_1e_2, minor) = 13.7 min, t_r(d_2e_1, minor) = 19.1 min, t_r(d_2e_2, major) = 26.9 min). Characterization data is identical to that previously reported for this bromonitroalkane.[17]

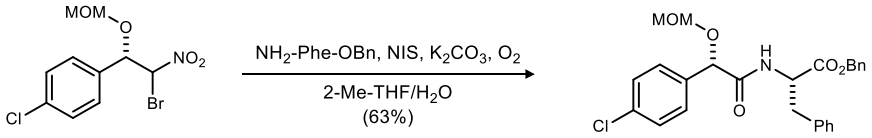

Benzyl ((*S*)-2-(4-chlorophenyl)-2-(methoxymethoxy)acetyl)-*L*-phenylalaninate (108). Following the UmAS general procedure, bromonitroalkane (750 mg, 2.31 mmol) and amine (707 mg, 2.77 mmol) afforded a mahogany colored oil. The residue was subjected to flash column chromatography (SiO_2, 10-25% ethyl acetate in hexanes) to afford the amide as a waxy yellow solid (680 mg, 63%). Mp = 82-85 °C; $[\alpha]_D^{20}$ +42 (*c* 0.76, $CHCl_3$); R_f = 0.33 (30% EtOAc/hexanes); IR (film) 3338, 3065, 2920, 2851, 1740, 1660, 1595, 1528, 1493, 1456, 1408, 1262, 1225, 1152, 1098, 1098, 1037 cm^{-1}; ^1H NMR (400 MHz, $CDCl_3$) δ 7.40-7.35 (m, 3H), 7.34-7.31 (m, 2H), 7.30-7.27 (m, 2H), 7.23-7.14 (m, 6H), 6.90-6.88 (m, 2H), 5.22 (d, *J* = 12.1 Hz, 1H), 5.13 (d, *J* = 12.1 Hz, 1H), 5.01 (s, 1H), 4.94 (ddd, *J* = 8.3, 6.0, 6.0 Hz, 1H), 4.61 (d, *J* = 6.7 Hz, 1H), 4.56 (d, *J* = 6.7 Hz, 1H), 3.26 (s, 3H), 3.16 (dd, *J* = 13.9, 5.7 Hz, 1H), 3.05 (dd, *J* = 13.9, 6.4 Hz, 1H); ^{13}C NMR (150 MHz, $CDCl_3$) ppm 171.1, 169.7, 135.4, 135.3, 135.0, 134.3, 129.3, 128.7 (2C), 128.6 (2C), 128.52, 128.48, 127.0, 94.5, 76.9, 67.4, 56.0, 52.5, 37.7; HRMS (ESI): Exact mass calcd for $C_{26}H_{26}ClNNaO_5$ $[M+Na]^+$ 490.1397, found 490.1407.

[17] Leighty, M. W.; Shen, B.; Johnston, J. N. *J. Am. Chem. Soc.* **2012**, *134*, 15233.

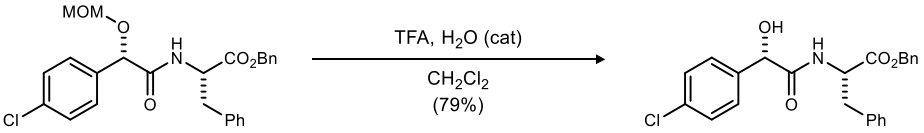

Benzyl ((*S*)-2-(4-chlorophenyl)-2-hydroxyacetyl)-*L*-phenylalaninate (109). Following general MOM deprotection procedure II, the amide (435 mg, 930 µmol) afforded a crude pale yellow oil. Flash column chromatography (SiO_2, 20-45% ethyl acetate in hexanes) afforded the alcohol (312 mg, 79%) as a pale yellow oil. $[\alpha]_D^{20}$ +24 (*c* 0.28, $CHCl_3$); R_f = 0.16 (35% EtOAc/hexanes); IR (film) 3387, 3064, 3032, 2920, 1740, 1662, 1596, 1522, 1494, 1493, 1454, 1385, 1351, 1263, 1192, 1119, 1084, 1015 cm^{-1}; ^1H NMR (400 MHz, $CDCl_3$) δ 7.39-7.36 (m, 3H), 7.30-7.27 (m, 4H), 7.23-7.16 (m, 5H), 6.91-6.89 (m, 2H), 6.69 (br d, *J* = 8.0 Hz, 1H), 5.17 (d, *J* = 12.1 Hz, 1H), 5.11 (d, *J* = 12.1 Hz, 1H), 5.02 (d, *J* = 3.7 Hz, 1H), 4.88 (ddd, *J* = 7.9, 6.0, 6.0 Hz, 1H), 3.20 (d, *J* = 3.8 Hz, 1H), 3.16 (dd, *J* = 13.9, 5.7 Hz, 1H), 3.05 (dd, *J* = 13.9, 6.3 Hz, 1H); ^{13}C NMR (100 MHz, $CDCl_3$) ppm 171.1, 170.9, 137.2, 135.3, 134.9, 134.5, 129.2, 128.9, 128.66, 128.64, 128.61, 128.58, 128.0, 127.1, 73.5, 67.5, 53.0, 37.6; HRMS (ESI): Exact mass calcd for $C_{24}H_{22}ClNNaO_4$ $[M+Na]^+$ 446.1135, found 446.1133.

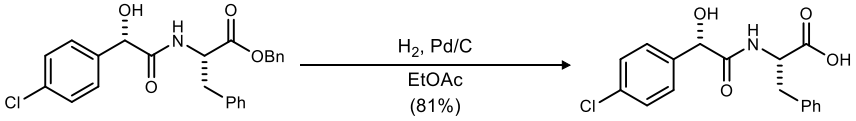

((*S*)-2-(4-Chlorophenyl)-2-hydroxyacetyl)-*L*-phenylalanine (110). Following general Benzyl Deprotection procedure II, the amide (309 mg, 729 µmol) afforded a crude tan solid. Preparative HPLC (5-95% aqueous acetonitrile, 210 nm, flow rate: 20 mL/min, R_t = 3.68 m) purification provided the *seco*-acid (196 mg, 81%) as a white solid. Mp = 181-184 °C; $[\alpha]_D^{20}$ +34 (*c* 0.93, MeOH); R_f = 0.14 (20% MeOH/DCM); IR (film) 3357, 3198, 3039, 3927, 1720, 1620, 1527, 1407, 1262, 1176, 1069 cm^{-1}; ^1H NMR (400 MHz, DMSO-*d*$_6$) δ 7.94 (d, *J* = 8.2 Hz, 1H), 5.45 (br s, 1H), 7.33-7.30 (m, 2H), 7.22-7.19 (m, 5H), 7.09-7.07 (m, 2H), 6.39 (d, *J* = 4.8 Hz, 1H), 4.90 (d, *J* = 4.8 Hz, 1H), 4.50 (ddd, *J* = 8.3, 8.3, 5.0 Hz, 1H), 3.07 (dd, 13.7, 5.0 Hz, 1H), 3.01 (dd, *J* = 13.7, 8.4 Hz, 1H), COO*H* not observed; ^{13}C NMR (150 MHz, DMSO-*d*$_6$) ppm 172.6, 171.3, 139.9, 137.2, 131.9, 129.2, 128.5, 128.1, 127.8, 126.3, 72.5, 52.5, 36.3; HRMS (ESI): Exact mass calcd for $C_{17}H_{16}ClNNaO_4$ $[M+Na]^+$ 356.0666, found 356.0681.

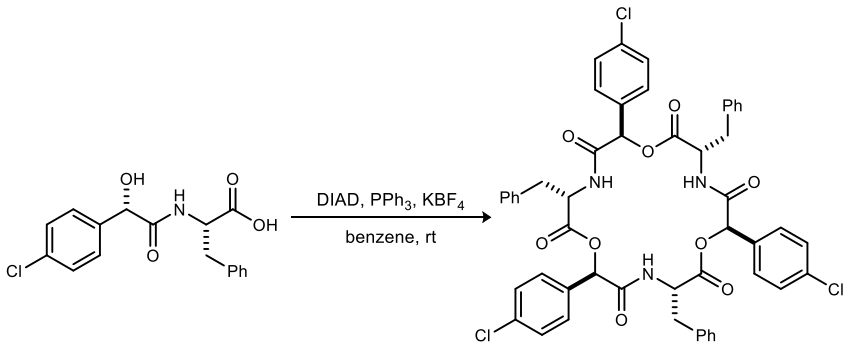

(3*S*,6*R*,9*S*,12*R*,15*S*,18*R*)-3,9,15-Tribenzyl-6,12,18-tris(4-chlorophenyl)-1,7,13-trioxa-4,10,16-triazacyclooctadecane-2,5,8,11,14,17-hexaone (111). Following the Didepsipeptide MCO General Procedure, the *seco*-acid (25.0 mg, 75.0 µmol) and KBF_4 (23.5 mg, 187 µmol) were stirred at ambient temperature for 24 h to afford a yellow solid. Preparative HPLC (5-95% aqueous acetonitrile, 210 nm, flow rate: 8 mL/min, R_t = 26.8 m) provided the 18-membered macrocycle (5.3 mg, 22%) as a yellow viscous oil. $[\alpha]_D^{20}$ -3.2 (*c* 0.44, $CHCl_3$); R_f

= 0.42 (5% MeOH/DCM); IR (film) 3268, 3065, 2930, 1748, 1672, 1555, 1493, 1453, 1377, 1202, 1130, 1094, 1015 cm^{-1}; ^1H NMR (400 MHz, DMSO-d_6) δ 9.39 (br d, J = 5.5 Hz, 1H), 8.94 (br d, J = 8.2 Hz, 1H), 7.94 (d, J = 9.2 Hz, 1H), 7.39 (d, J = 8.6 Hz, 2H), 7.36 (d, J = 8.6 Hz, 2H), 7.30 (d, J = 8.7 Hz, 2H), 7.27 (d, J = 8.7 Hz, 2H), 7.25-7.21 (m, 5H), 7.17-7.06 (m, 12H), 6.66 (d, J = 8.5 Hz, 2H), 6.17 (s, 1H), 5.93 (s, 1H), 5.67 (s, 1H), 4.81 (ddd, J = 11.8, 9.2, 4.5 Hz, 1H), 4.48 (br ddd, J = 8.9, 8.9, 5.7 Hz, 1H), 4.33 (br ddd, J = 8.0, 8.0, 5.7 Hz, 1H), 3.55 (dd, J = 13.9, 4.0 Hz, 1H), 2.14-2.96 (m, 5H); ^{13}C NMR (150 MHz, CD_3CN[18]) ppm 171.43, 171.36, 170.4, 169.2, 169.1, 168.9, 137.8 (2C), 137.2, 135.3, 135.26, 135.24, 134.3 (2C), 134.1, 130.2 (2C), 130.15, 130.12, 129.79, 129.77, 129.6 (2C), 129.51, 129.49, 129.46, 129.3, 127.9, 127.8, 127.7, 76.6, 76.1, 75.5, 55.8, 55.0, 54.3, 37.1 (2C), 36.8; HRMS (ESI): Exact mass calcd for $C_{51}H_{42}Cl_3N_3NaO_9$ $[M+Na]^+$ 968.1884, found 968.1891.

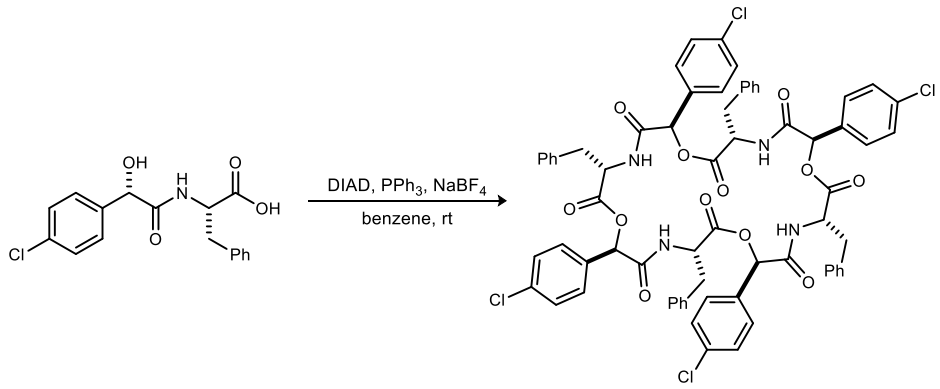

(3*S*,6*R*,9*S*,12*R*,15*S*,18*R*,21*S*,24*R*)-3,9,15,21-Tetrabenzyl-6,12,18,24-tetrakis(4-chlorophenyl)-1,7,13,19-tetraoxa-4,10,16,22-tetraazacyclotetracosan-2,5,8,11,14,17,20,23-octaone (112). Following the Didepsipeptide MCO General Procedure, the *seco*-acid (25.0 mg, 75.0 μmol) and $NaBF_4$ (20.5 mg, 187 μmol) were stirred at ambient temperature for 24 h to afford a yellow solid. Preparative HPLC (5-95% aqueous acetonitrile, 210 nm, flow rate: 8 mL/min, R_t = 28.3 m) provided the 24-membered macrocycle (7.0 mg, 30%) as a white solid. Mp = 208-210 °C; $[\alpha]_D^{20}$ -19 (c 0.26, $CHCl_3$); R_f = 0.57 (5% MeOH/DCM); IR (film) 3292, 3064, 3030, 2925, 2855, 1743, 1666, 1596, 1554, 1528, 1491, 1454, 1382, 1345, 1264, 1209, 1182, 1092, 1014 cm^{-1}; ^1H NMR (400 MHz, DMSO-d_6) δ 8.81 (br d, J = 8.2 Hz, 1H), 7.20 (br d, J = 8.4 Hz, 2H), 7.15-7.14 (m, 3H), 7.09-7.04 (br m, 4H), 5.99 (br s, 1H), 4.68-4.62 (br m, 1H), 3.15-3.11 (br m, 1H), 3.07-3.02 (br m, 1H); ^{13}C NMR (150 MHz, DMSO-d_6) ppm 169.8, 167.5, 136.7, 133.6, 133.5, 129.6, 129.0, 128.3, 128.1, 126.4, 74.4, 53.5, 36.7; HRMS (ESI): Exact mass calcd for $C_{68}H_{56}{}^{35}Cl_3{}^{37}ClN_4NaO_{12}$ $[M+Na]^+$ 1285.2517, found 1285.2533.

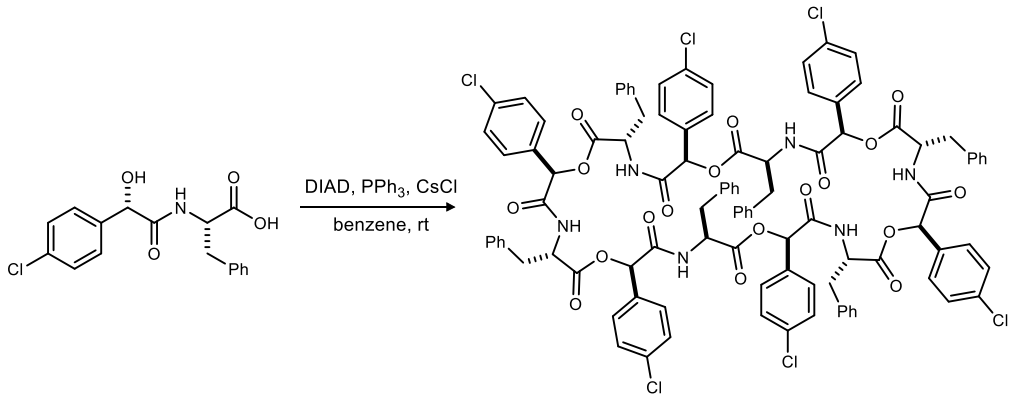

[18] The resolution of carbonyl carbon peaks was extremely poor in DMSO-d_6, so CD_3CN was used instead. However, the ^1H spectrum was too broad in CD_3CN to report a reliable line listing, so the ^1H spectrum in DMSO-d_6 was used to provide clearer characterization data.

(3*S*,6*R*,9*S*,12*R*,15*S*,18*R*,21*S*,24*R*,27*S*,30*R*,33*S*,36*R*)-3,9,15,21,27,33-Hexabenzyl-6,12,18,24,30,36-hexakis(4-chlorophenyl)-1,7,13,19,25,31-hexaoxa-4,10,16,22,28,34-hexaazacyclohexatriacontan-2,5,8,11,14,17,20,23,26,29,32,35-dodecaone (113). Following the Didepsipeptide MCO General Procedure, the *seco*-acid (25.0 mg, 75.0 μmol) and CsCl (31.4 mg, 187 μmol) were stirred at ambient temperature for 24 h to afford a yellow solid. Preparative HPLC (5-95% aqueous acetonitrile, 210 nm, flow rate: 8 mL/min, R_t = 25.6 m) provided the 36-membered macrocycle (6.4 mg, 27%) as a yellow solid. Mp = 146-148 °C; $[\alpha]_D^{20}$ -41 (*c* 0.35, $CHCl_3$); R_f = 0.71 (5% MeOH/DCM); IR (film) 3287, 3031, 2933, 1753, 1666, 1598, 1532, 1494, 1453, 1375, 1215, 1180, 1094, 1016 cm^{-1}; ^1H NMR (400 MHz, DMSO-d_6) δ 8.91 (br d, *J* = 7.5 Hz, 1H), 7.25 (d, *J* = 8.5 Hz, 2H), 7.21-7.17 (m, 5H), 7.07 (d, *J* = 8.5 Hz, 2H), 6.01 (s, 1H), 4.62 (br ddd, *J* = 8.8, 6.4 Hz, 1H), 3.11 (dd, *J* = 13.7, 6.0 Hz, 1H), 3.03 (dd, *J* = 13.6, 9.4 Hz, 1H); ^{13}C NMR (150 MHz, DMSO-d_6) ppm 169.9, 166.9, 136.7, 134.0, 133.0, 129.2, 128.6, 128.20, 128.14, 126.6, 74.1, 53.3, 36.3; HRMS (ESI): Exact mass calcd for $C_{102}H_{84}Cl_6N_6NaO_{18}$ $[M+Na]^+$ 1913.3871, found 1913.3885.

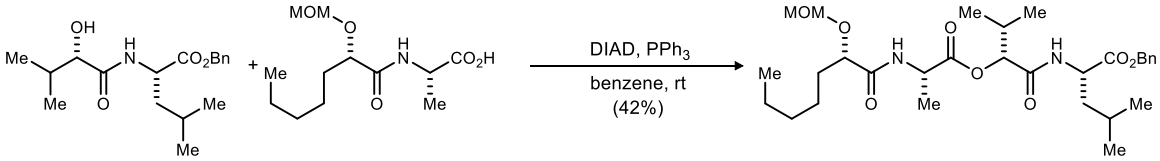

Benzyl ((*R*)-2-((((*S*)-2-(Methoxymethoxy)heptanoyl)-*L*-alanyl)oxy)-3-methylbutanoyl)-*L*-leucinate (115). Following the Mitsunobu general procedure, alcohol (48.0 mg, 149 μmol) and acid (50.0 mg, 191 μmol) at ambient temperature for 24 h afforded a crude brown oil. Flash column chromatography (SiO_2, 15-35% ethyl acetate in hexanes) followed by preparative HPLC (5-95% aqueous acetonitrile, 210 nm, flow rate: 8 mL/min, R_t = 27.8 min) provided the didepsipeptide (35 mg, 42%) as a white viscous oil. $[\alpha]_D^{20}$ -23 (*c* 0.20, $CHCl_3$); R_f = 0.27 (30% EtOAc/hexanes); IR (film) 3297, 2958, 2919, 2851, 1748, 1655, 1542, 1459, 1371, 1195, 1154, 1130, 1018 cm^{-1}; ^1H NMR (400 MHz, $CDCl_3$) δ 7.37-7.31 (m, 5H), 6.99 (br d, *J* = 6.0 Hz, 1H), 6.94 (br d, *J* = 7.1 Hz, 1H), 5.19 (d, *J* = 12.4 Hz, 1H), 5.12 (d, *J* = 12.4 Hz, 1H), 5.11 (d, *J* = 3.4 Hz, 1H), 4.70-4.64 (m, 3H), 4.45 (dq, *J* = 6.9, 6.9 Hz, 1H), 4.02 (dd, *J* = 6.5, 4.5 Hz, 1H), 3.41 (s, 3H), 2.42 (qqd, *J* = 6.9, 6.9, 3.4 Hz, 1H) 1.81-1.60 (m, 5H), 1.48 (d, *J* =7.1 Hz, 3H), 1.43-1.28 (m, 6H), 0.95 (d, *J* = 7.0 Hz, 3H), 0.93 (d, *J* = 7.1 Hz, 3H), 0.89 (d, *J* = 6.2 Hz, 3H), 0.88 (d, *J* = 6.2 Hz, 3H), 0.87 (t, *J* = 6.4 Hz, 3H); ^{13}C NMR (150 MHz, $CDCl_3$) ppm 173.0, 172.47, 172.45, 169.0, 135.6, 128.5, 128.2, 128.1, 96.3, 78.6, 77.5, 66.8, 56.2, 50.6, 48.5, 40.4, 32.6, 31.5, 30.4, 24.7, 24.3, 22.9, 22.5, 21.5, 18.9, 17.4, 16.2, 14.0; HRMS (ESI): Exact mass calcd for $C_{30}H_{48}N_2NaO_8$ $[M+Na]^+$ 587.3308, found 587.3306.

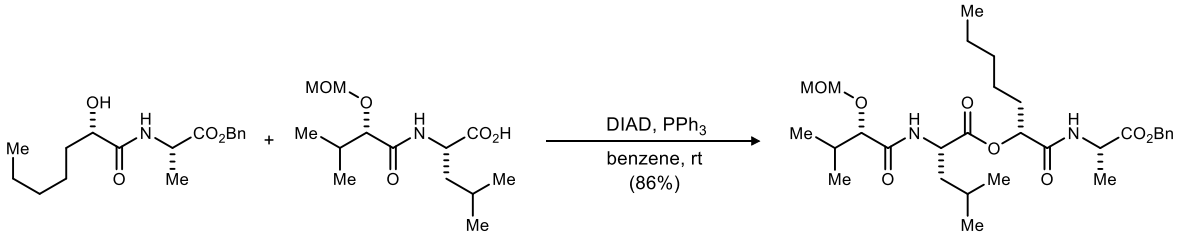

(*R*)-1-(((*S*)-1-(Benzyloxy)-1-oxopropan-2-yl)amino)-1-oxoheptan-2-yl ((*S*)-2-(methoxymethoxy)-3-methylbutanoyl)-L-leucinate (116). Following the Mitsunobu general procedure, alcohol (51.0 mg, 166 μmol) and acid (60.0 mg, 218 μmol) at ambient temperature for 24 h afforded a crude brown oil. Flash column chromatography (SiO_2, 15-20% ethyl acetate in hexanes) followed by preparative HPLC (5-95% aqueous acetonitrile, 210 nm, flow rate: 8 mL/min, R_t = 28.3 min) provided the didepsipeptide (80 mg, 86%) as a white viscous oil. $[\alpha]_D^{20}$ -19 (*c* 0.10, $CHCl_3$); R_f = 0.31 (30% EtOAc/hexanes); IR (film) 3312, 2958, 2931, 2873, 1749, 1658, 1534, 1458, 1383, 1261, 1155, 1034 cm^{-1}; ^1H NMR (600 MHz, $CDCl_3$) δ 7.37-7.30 (m, 5H), 7.29 (br d, *J*

= 7.3 Hz, 1H), 6.82 (br d, *J* = 6.4 Hz, 1H), 5.21 (d, *J* = 12.4 Hz, 1H), 5.18 (dd, *J* = 8.4, 3.9 Hz, 1H), 5.12 (d, *J* = 12.4 Hz, 1H), 4.68 (d, *J* = 6.6 Hz, 1H), 4.65 (d, *J* = 6.6 Hz, 1H), 4.59 (dq, *J* = 7.3, 7.3 Hz, 1H), 4.42 (ddd, *J* = 7.9, 6.8, 6.8 Hz, 1H), 3.82 (d, *J* = 4.0 Hz, 1H), 3.42 (s, 3H), 2.42 (qqd, *J* = 6.9, 6.9, 4.0 Hz, 1H) 1.94-1.88 (m, 1H), 1.86-1.79 (m, 1H), 1.73-1.60 (m, 3H), 1.43 (d, *J* =7.1 Hz, 3H), 1.38-1.23 (m, 6H), 1.00 (d, *J* = 6.1 Hz, 3H), 0.98 (d, *J* = 6.9 Hz, 3H), 0.96 (d, *J* = 6.2 Hz, 3H), 0.92 (d, *J* = 6.9 Hz, 3H), 0.87 (t, *J* = 6.8 Hz, 3H); ^{13}C NMR (150 MHz, $CDCl_3$) ppm 172.7, 172.5, 172.4, 169.5, 135.7, 128.5, 128.2, 128.1, 97.0, 82.4, 74.6, 66.8, 56.5, 51.4, 48.1, 40.2, 31.6, 31.4, 31.2, 25.0, 24.6, 22.5, 22.4, 22.1, 18.8, 17.2, 17.1, 13.9; HRMS (ESI): Exact mass calcd for $C_{30}H_{48}N_2NaO_8$ $[M+Na]^+$ 587.3308, found 587.3334.

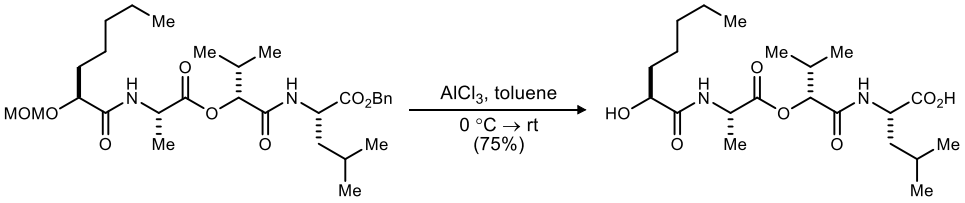

((*R*)-2-((((*S*)-2-Hydroxyheptanoyl)-*L*-alanyl)oxy)-3-methylbutanoyl)-*L*-leucine (117). Following the Global Deprotection General Procedure, the amide (30.0 mg, 53.0 μmol) was stirred at ambient temperature for 25 m to afford an orange residue. Preparative HPLC (5-95% aqueous acetonitrile, 210 nm, flow rate: 8 mL/min, R_t = 18.5 m) provided the *seco*-acid (17 mg, 75%) as a viscous colorless oil. $[\alpha]_D^{20}$ -15 (*c* 0.35, $CHCl_3$); R_f = 0.70 (20% MeOH/DCM); IR (film) 3326, 2959, 2928, 2871, 1746, 1653, 1542, 1461, 1203, 1155 cm^{-1}; ^{1}H NMR (400 MHz, DMSO-d_6) δ 8.21 (d, *J* = 7.1 Hz, 1H), 7.94 (d, *J* = 8.2 Hz, 1H), 4.76 (d, *J* = 3.8 Hz, 1H), 4.37 (dq, *J* = 7.2, 7.2 Hz, 1H), 4.26 (ddd, *J* = 10.7, 8.2, 4.1 Hz, 1H), 3.86 (dd, *J* = 7.8, 3.8 Hz, 1H), 2.17 (qqd, *J* = 6.9, 6.9, 3.8 Hz, 1H), 1.71-1.44 (series of m, 5H), 1.35 (d, *J* = 7.2 Hz, 3H), 1.34-1.20 (m, 6H), 0.89 (d, *J* = 6.8 Hz, 3H), 0.88 (d, *J* = 6.9 Hz, 3H), 0.851 (d, *J* = 6.3 Hz, 3H), 0.849 (t, *J* = 6.6 Hz, 3H), 0.80 (d, *J* = 6.3 Hz, 3H), COO*H* and O*H* not observed; ^{13}C NMR (100 MHz, DMSO-d_6) ppm 174.4, 173.8, 172.0, 168.6, 77.8, 70.7, 49.8, 47.7, 39.5, 34.2, 31.1, 30.1, 24.3, 24.1, 22.9, 22.0, 21.0, 18.7, 17.1, 16.3, 13.9; HRMS (ESI): Exact mass calcd for $C_{21}H_{38}N_2NaO_7$ $[M+Na]^+$ 453.2577, found 453.2576.

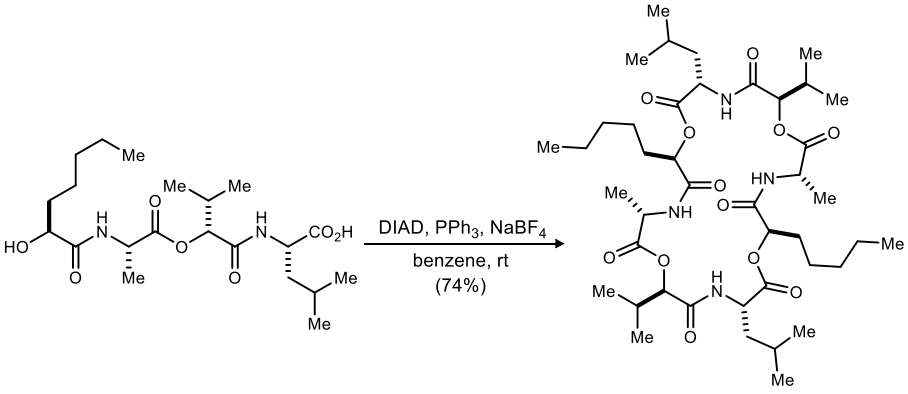

(3*S*,6*R*,9*S*,12*R*,15*S*,18*R*,21*S*,24*R*)-3,15-Diisobutyl-6,18-diisopropyl-9,21-dimethyl-12,24-dipentyl-1,7,13,19-tetraoxa-4,10,16,22-tetraazacyclotetracosan-2,5,8,11,14,17,20,23-octaone (118). Following the Tetradepsipeptide MCO general procedure, *seco*-acid **117** (10.0 mg, 23.0 μmol) with $NaBF_4$ (12.6 mg, 115 μmol) was stirred at ambient temperature for 24 h to afford a pale yellow oil. Preparative HPLC (5-95% aqueous acetonitrile, 210 nm, flow rate: 8 mL/min, R_t = 24.3 m) provided the 24-membered macrocycle (7.0 mg, 74%) as a white solid. Mp = 180 °C (dec); $[\alpha]_D^{20}$ -20 (*c* 0.11, $CHCl_3$); R_f = 0.28 (4% MeOH/DCM); IR (film) 3268, 2924, 2854, 1740, 1677, 1648, 1556, 1451, 1247, 1156, 1094, 1023 cm^{-1}; ^{1}H NMR (400 MHz, $CDCl_3$) δ 7.07 (br d, *J* = 7.3 Hz, 1H), 6.95 (br d, *J* = 7.4 Hz, 1H), 5.19 (dd, *J* = 7.7, 5.2 Hz, 1H), 4.86 (d, *J* = 5.1 Hz, 1H), 4.43 (dq, *J* = 7.2,

7.2 Hz, 1H), 4.18 (br ddd, *J* = 14.4, 7.4 Hz, 1H), 2.25 (br qqd, *J* = 6.7, 5.8 Hz, 1H), 1.94-1.88 (m, 1H), 1.80-1.77 (m, 2H), 1.72-1.62 (m, 2H), 1.46 (d, *J* = 7.1 Hz, 3H), 1.33-1.25 (br m, 6H), 0.98 (d, *J* = 7.3 Hz, 6H), 0.95 (d, *J* = 6.6 Hz, 6H), 0.87 (t, *J* = 6.8 Hz, 3H); ^{13}C NMR (150 MHz, $CDCl_3$) ppm 171.3, 170.9, 170.2, 169.9, 79.2, 73.7, 51.5, 48.4, 39.6, 31.4, 31.3, 30.4, 24.9, 24.7, 22.9, 22.4, 21.5, 18.5, 17.5, 16.5, 13.9; HRMS (ESI): Exact mass calcd for $C_{42}H_{72}N_4NaO_{12}$ $[M+Na]^+$ 847.5044, found 847.5043.

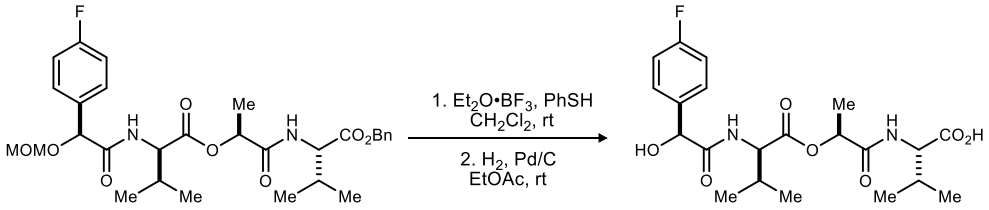

((*S*)-2-((((*S*)-2-(4-Fluorophenyl)-2-hydroxyacetyl)-D-valyl)oxy)propanoyl)-L-valine (122). Following the general MOM deprotection I and benzyl deprotection II procedures, the amide (113 mg, 197 µmol) afforded a crude tan solid. Preparative HPLC (5-95% aqueous acetonitrile, 210 nm, flow rate: 20 mL/min, R_t = 2.74 m) provided the *seco*-acid (54 mg, 63%, 2 steps) as a fluffy white solid. $[\alpha]_D^{20}$ +16 (*c* 0.17, MeOH); R_f = 0.29 (20% MeOH/DCM); IR (film) 3336, 3086, 2965, 2925, 1744, 1723, 1666, 1623, 1539, 1511, 1465, 1393, 1373, 1303, 1269, 1217, 1148, 1070, 1041 cm^{-1}; ^{1}H NMR (400 MHz, DMSO-d_6) δ 8.13 (d, *J* = 8.6 Hz, 1H), 7.99 (d, *J* = 8.7 Hz, 1H), 7.47 (dd, *J* = 8.6, 5.7 Hz, 2H), 7.13 (dd, *J* = 8.9, 8.9 Hz, 2H), 6.25 (d, *J* = 4.8 Hz, 1H), 5.07 (s, 1H), 5.05 (q, *J* = 6.8 Hz, 1H), 4.24 (dd, *J* = 8.7, 5.9 Hz, 1H), 4.14 (dd, *J* = 8.6, 5.9 Hz, 1H), 2.13 (qqd, *J* = 6.7, 6.7, 6.3 Hz, 1H), 2.07 (qqd, *J* = 6.6, 6.6, 6.3 Hz, 1H), 1.27 (d, *J* = 6.8 Hz, 3H), 0.88 (d, *J* = 6.8 Hz, 6H), 0.85 (d, *J* = 6.8 Hz, 3H), 0.82 (d, *J* = 6.8 Hz, 3H), COO*H* not observed; ^{13}C NMR (150 MHz, DMSO-d_6) ppm 172.7, 172.1, 170.3, 169.7, 161.5 (d, $^1J_{CF}$ = 243 Hz), 137.3, 128.6 (d, $^3J_{CF}$ = 8.1 Hz), 114.6 (d, $^2J_{CF}$ = 21 Hz), 72.3, 69.9, 56.9, 56.7, 30.1, 29.9, 19.0, 18.8, 17.9, 17.8, 17.4; ^{19}F NMR (376 Hz, DMSO-d_6) δ -115.3; HRMS (ESI): Exact mass calcd for $C_{21}H_{29}FN_2NaO_7$ $[M+Na]^+$ 463.1856, found 463.1843.

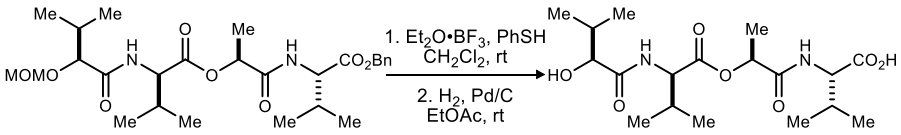

((*S*)-2-((((*S*)-2-Hydroxy-3-methylbutanoyl)-D-valyl)oxy)propanoyl)-L-valine (123). Following the general MOM deprotection I and benzyl deprotection II procedures, the amide (76 mg, 145 µmol) afforded a crude tan solid. Preparative HPLC (5-95% aqueous acetonitrile, 210 nm, flow rate: 20 mL/min, R_t = 2.33 m) provided the *seco*-acid (31 mg, 58%, 2 steps) as a fluffy white solid. $[\alpha]_D^{20}$ -13 (*c* 0.21, MeOH); R_f = 0.36 (20% MeOH/DCM); IR (film) 3323, 2966, 2934, 2878, 1740, 1662, 1533, 1466, 1374, 1204, 1148, 1092, 1025 cm^{-1}; ^{1}H NMR (600 MHz, DMSO-d_6) δ 8.12 (d, *J* = 8.5 Hz, 1H), 7.61 (d, *J* = 8.6 Hz, 1H), 5.46 (d, *J* = 5.8 Hz, 1H), 5.08 (q, *J* = 6.8 Hz, 1H), 4.25 (dd, *J* = 8.6, 5.9 Hz, 1H), 4.14 (dd, *J* = 8.6, 5.8 Hz, 1H), 3.77 (dd, *J* = 5.6, 3.8 Hz, 1H), 2.12 (qqd, *J* = 6.8, 6.8, 6.4 Hz, 1H), 2.07 (qqd, *J* = 6.7, 6.7, 6.4 Hz, 1H), 1.97 (m, 1H), 1.31 (d, *J* = 6.8 Hz, 3H), 0.91-0.87 (m, 15H), 0.76 (d, *J* = 6.8 Hz, 3H), COO*H* not observed; ^{13}C NMR (150 MHz, DMSO-d_6) ppm 173.6, 172.7, 170.4, 169.8, 75.1, 69.9, 57.0, 56.7, 31.4, 30.0, 29.9, 19.2, 19.0, 18.9, 17.94, 17.9, 17.4, 16.0; HRMS (ESI): Exact mass calcd for $C_{18}H_{32}N_2NaO_7$ $[M+Na]^+$ 411.2102, found 411.2105.

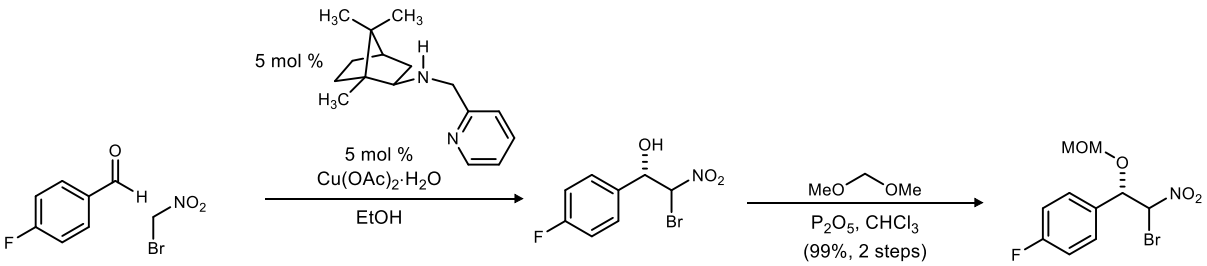

1-((1*S*)-2-Bromo-1-(methoxymethoxy)-2-nitroethyl)-4-fluorobenzene (129). Following the Blay[3] enantioselective Henry procedure, Blay ligand (79.7 mg, 326 µmol) and $Cu(OAc)_2$•H_2O (65.1 mg, 326 µmol) were stirred at ambient temperature in EtOH (26 mL) for 1 h. The royal blue solution was then cooled to -20 °C and 4-fluorobenzaldehyde (698 µL, 6.51 mmol) was added and allowed to stir for 10 m before bromonitromethane (4.54 mL, 65.1 mmol) addition. After stirring for 3 days at -20 °C, the reaction was quenched dropwise at -20 °C with pre-chilled 1 N HCl and the aqueous layer was extracted with CH_2Cl_2. Following drying and concentration under reduced pressure, the crude alcohol was dissolved in $CHCl_3$ (33 mL), treated with P_2O_5 (9.30 g, 65.1 mmol) and dimethoxymethane (11.5 mL, 131 mmol), and stirred at ambient temperature overnight. The reaction was cooled to 0 °C, quenched slowly with satd aq $NaHCO_3$, and then poured into CH_2Cl_2. The aqueous layer was extracted with CH_2Cl_2. The organic layers were dried and concentrated to an oil that was subjected to flash column chromatography (SiO_2, 4-8% diethyl ether in hexanes) to afford the title compound in 2:1 d.r. as a pale yellow solid (2.00 g, 99%, 2 steps). The diastereomers were determined to be 80/79% ee by chiral HPLC analysis. Recrystallization from hexanes afforded 1.69 g (85% recovery) of white crystals. The crystals were determined to be 99% ee (each diastereomer) by chiral HPLC analysis (Chiralpak AD-H, 3% EtOH /hexanes, 0.8 mL/min, $t_r(d_1e_1$, major) = 10.0 min, $t_r(d_1e_2$, minor) = 13.1 min, $t_r(d_2e_1$, minor) = 14.9 min, $t_r(d_2e_2$, major) = 29.3 min). Characterization data is identical to that previously reported for this bromonitroalkane.[19]

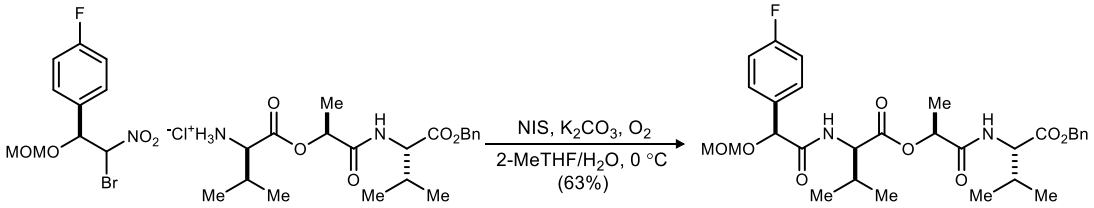

Benzyl ((*S*)-2-((((*S*)-2-(4-Fluorophenyl)-2-(methoxymethoxy)acetyl)-D-valyl)oxy)propanoyl)-L-valinate (130). Following the UmAS general procedure, bromonitroalkane (311 mg, 1.01 mmol) and amine (350 mg, 844 µmol) afforded an orange oil. The residue was subjected to flash column chromatography (SiO_2, 20-45% ethyl acetate in hexanes) to afford the amide as a colorless oil (313 mg, 65%). $[\alpha]_D^{20}$ +20 (*c* 1.3, $CHCl_3$); R_f = 0.38 (50% EtOAc/hexanes); IR (film) 3321, 3068, 2964, 2933, 1742, 1673, 1512, 1264, 1375, 1306, 1262, 1223, 1192, 1151, 1095, 1037cm^{-1}; ^{1}H NMR (600 MHz, $CDCl_3$) δ 7.39 (dd, *J* = 8.6, 5.3 Hz, 2H), 7.36-7.29 (m, 5H), 7.29 (d, *J* = 8.6 Hz, 1H), 7.01 (dd, *J* = 8.7, 8.7 Hz, 2H), 6.65 (d, *J* = 8.5 Hz, 1H), 5.25 (q, *J* = 6.8 Hz, 1H), 5.14 (d, *J* = 12 Hz, 1H), 5.10 (s, 1H), 5.08 (d, *J* = 12 Hz, 1H), 4.69 (d, *J* = 6.6 Hz, 1H), 4.63 (d, *J* = 6.6 Hz, 1H), 4.51 (dd, *J* = 8.3, 5.3 Hz, 1H), 4.48 (dd, *J* = 8.5, 5.2 Hz, 1H), 3.38 (s, 3H), 2.29 (m, 1H), 2.13 (m, 1H), 1.46 (d, *J* = 6.8 Hz, 3H), 1.02 (d, *J* = 6.8 Hz, 3H), 1.01 (d, *J* = 6.7 Hz, 3H), 0.87 (d, *J* = 6.8 Hz, 3H), 0.84 (d, *J* = 6.9 Hz, 3H); ^{13}C NMR (150 MHz, $CDCl_3$) ppm 171.2, 170.44, 170.42, 169.6, 162.9 (d, $^1J_{CF}$ = 247 Hz), 135.3, 132.4 (d, $^4J_{CF}$ =2.9 Hz), 129.5 (d, $^3J_{CF}$ = 8.4 Hz), 128.6, 128.4, 128.3, 115.5 (d, $^2J_{CF}$ = 22 Hz), 94.3, 77.0, 71.3, 67.0, 57.2, 57.1, 56.0, 31.0, 30.9, 18.94, 18.88, 18.0, 17.8, 17.7; ^{19}F NMR (376 Hz, $CDCl_3$) δ -113.3; HRMS (ESI): Exact mass calcd for $C_{30}H_{39}FN_2NaO_8$ $[M+Na]^+$ 597.2588, found 597.2590.

[19] Leighty, M. W.; Shen, B.; Johnston, J. N. *J. Am. Chem. Soc.* **2012**, *134*, 15233.

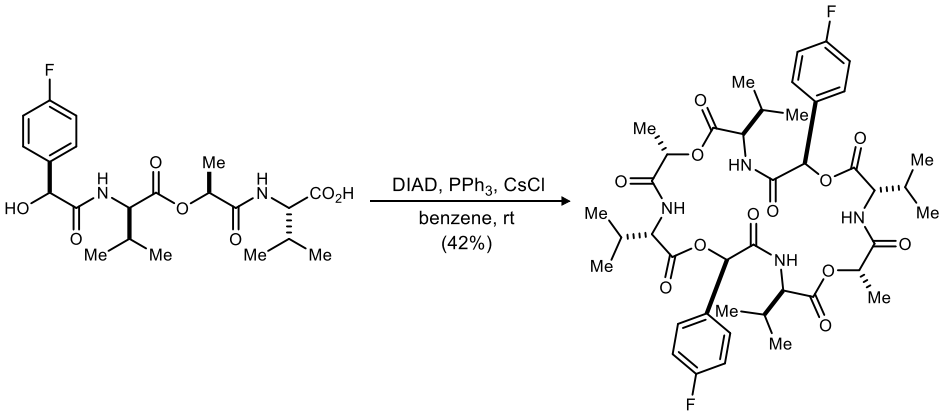

(3*R*,6*R*,9*S*,12S,15*R*,18*R*,21*S*,24*S*)-6,18-bis(4-Fluorophenyl)-3,9,15,21-tetraisopropyl-12,24-dimethyl-1,7,13,19-tetraoxa-4,10,16,22-tetraazacyclotetracosan-2,5,8,11,14,17,20,23-octaone (131). Following the Tetradepsipeptide MCO general procedure, *seco*-acid **122** (15.0 mg, 34.0 μmol) with CsCl (28.6 mg, 170 μmol) was stirred for 24 h at ambient temperature to afford a pale yellow oil. Preparative HPLC (5-95% aqueous acetonitrile, 210 nm, flow rate: 8 mL/min, R_t = 25.7 m) provided the 24-membered macrocycle (6.0 mg, 42%) as a white solid. $[\alpha]_D^{20}$ -2.6 (*c* 0.53, $CHCl_3$); R_f = 0.77 (5% MeOH/DCM); IR (film) 3312, 3053, 2967, 2934, 2877, 1752, 1669, 1537, 1512, 1373, 1263, 1229, 1184, 1143, 1094 cm^{-1}; ^1H NMR (600 MHz, DMSO-d_6) δ 8.38 (s,1H), 7.99 (d, *J* = 7.0 Hz, 1H), 7.37 (dd, *J* = 8.6, 5.5 Hz, 2H), 6.88 (dd, *J* = 8.4, 8.4 Hz, 2H), 6.14 (s, 1H), 5.08 (q, *J* = 6.8 Hz, 1H), 4.16 (dd, *J* = 7.7, 7.7 Hz, 1H), 4.09 (dd, *J* = 7.1, 6.3 Hz, 1H), 2.21-2.15 (m, 2H), 1.31 (d, *J* = 7.0 Hz, 3H), 1.01 (d, *J* = 6.7 Hz, 3H), 0.93 (d, *J* = 6.7 Hz, 3H), 0.92 (d, *J* = 6.6 Hz, 3H), 0.86 (d, *J* = 6.7 Hz, 3H); ^{13}C NMR (150 MHz, DMSO-d_6) ppm 170.3, 169.8 (2C), 168.3, 161.9 (d, $^1J_{CF}$ = 244 Hz), 131.4, 129.2 (d, $^3J_{CF}$ = 8.3 Hz), 114.9 (d, $^2J_{CF}$ = 21 Hz), 73.0, 68.6, 58.8, 58.2, 29.0 (2C), 18.9 (2C), 18.64, 18.58, 17.4; ^{19}F NMR (376 Hz, $CDCl_3$) δ -114.0; HRMS (ESI): Exact mass calcd for $C_{42}H_{54}F_2N_4NaO_{12}$ $[M+Na]^+$ 867.3604, found 867.3611.

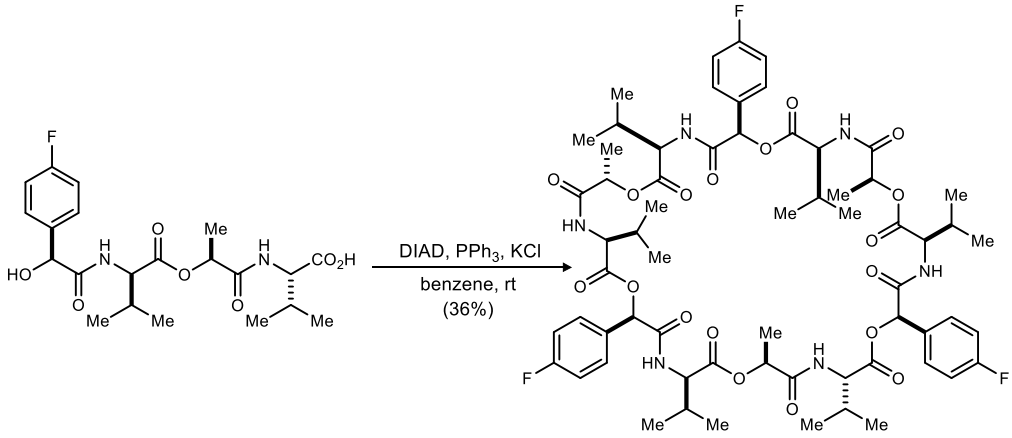

(3*R*,6*R*,9*S*,12S,15*R*,18*R*,21*S*,24*S*,27*R*,30*R*,33*S*,36*S*)-6,18,30-tris(4-Fluorophenyl)-3,9,15,21,27,33-hexaisopropyl-12,24,36-trimethyl-1,7,13,19,25,31-hexaoxa-4,10,16,22,28,34-hexaazacyclohexatriacontan-2,5,8,11,14,17,20,23,26,29,32,35-dodecaone (132). Following the Tetradepsipeptide MCO general procedure, *seco*-acid **122** (11.0 mg, 25.0 μmol) with KCl (9.30 mg, 125 μmol) was stirred for 24 h at ambient temperature to afford a pale yellow oil. Preparative HPLC (5-95% aqueous acetonitrile, 210 nm, flow rate: 8 mL/min, R_t = 31.8 m) provided the symmetric conformer of the 36-membered macrocycle (3.8 mg, 36%) as a white solid. $[\alpha]_D^{20}$ +1.7 (*c* 0.26, MeOH); R_f = 0.32 (5% MeOH/DCM); IR (film) 3271, 3051, 2923, 2853, 1743, 1656, 1554, 1518, 1459, 1377, 1305, 1260, 1196, 1154, 1043 cm^{-1}; ^1H NMR (600 MHz, DMSO-d_6) δ 8.40 (d, *J* = 7.9 Hz, 1H), 8.22 (d, *J* = 8.4 Hz, 1H), 7.48 (dd, *J* = 8.8, 5.4 Hz, 2H), 7.17 (dd, *J* = 8.9, 8.9 Hz, 2H), 5.97 (s, 1H), 4.99 (q, *J* = 6.8 Hz,

1H), 4.51 (dd, *J* = 8.3, 6.2 Hz, 1H), 4.13 (dd, *J* = 7.6, 7.6 Hz, 1H), 2.15 (qqd, *J* = 6.8, 6.8, 6.8 Hz, 2H), 1.23 (d, *J* = 6.9 Hz, 3H), 0.90 (d, *J* = 6.7 Hz, 3H), 0.87 (d, *J* = 6.6 Hz, 3H), 0.84 (d, *J* = 6.8 Hz, 3H), 0.80 (d, *J* = 6.8 Hz, 3H); ^{13}C NMR (150 MHz, DMSO-d_6) ppm 170.2, 170.1, 169.9, 168.0, 162.1 (d, $^{1}J_{CF}$ = 248 Hz), 131.8, 129.6 (d, $^{3}J_{CF}$ = 8.4 Hz), 115.2 (d, $^{2}J_{CF}$ = 22 Hz), 74.4, 69.7, 58.0, 56.9, 29.9, 29.4, 18.8, 18.7, 18.5, 17.7, 17.2; ^{19}F NMR (376 Hz, DMSO-d_6) δ -113.2; HRMS (ESI): Exact mass calcd for $C_{63}H_{81}F_3N_6NaO_{18}$ [M+Na]$^+$ 1289.5457, found 1289.5414.

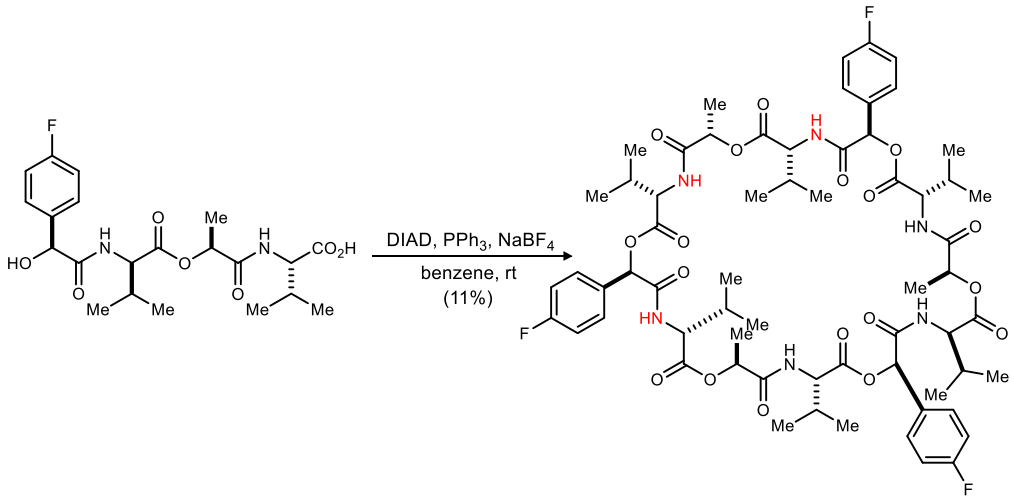

(3*R*,6*R*,9*S*,12S,15*R*,18*R*,21*S*,24*S*,27*R*,30*R*,33*S*,36*S*)-6,18,30-tris(4-Fluorophenyl)-3,9,15,21,27,33-hexaisopropyl-12,24,36-trimethyl-1,7,13,19,25,31-hexaoxa-4,10,16,22,28,34-hexaazacyclohexatriacontan-2,5,8,11,14,17,20,23,26,29,32,35-dodecaone (133). Following the Tetradepsipeptide MCO general procedure, *seco*-acid **122** (15.0 mg, 34.0 µmol) with $NaBF_4$ (18.7 mg, 170 µmol) was stirred for 24 h at ambient temperature to afford a pale yellow oil. Preparative HPLC (5-95% aqueous acetonitrile, 210 nm, flow rate: 8 mL/min, R_t = 28.7 m) provided the asymmetric conformer of the 36-membered macrocycle (1.6 mg, 11%) as an opaque film. $[\alpha]_D^{20}$ -1.3 (*c* 0.13, MeOH); R_f = 0.64 (5% MeOH/DCM); IR (film) 3308, 2923, 2854, 1750, 1665, 1536, 1462, 1375, 1228, 1184, 1146, 1095 cm^{-1}; ^{1}H NMR (900 MHz, DMSO-d_6) δ 8.60 (d, *J* = 8.6 Hz, 1H), 8.48 (d, *J* = 7.3 Hz, 1H), 8.41 (d, *J* = 7.8 Hz, 1H), 8.34 (d, *J* = 6.9 Hz, 1H), 8.17 (d, *J* = 8.2 Hz, 1H), 8.12 (d, *J* = 7.8 Hz, 1H), 7.58 (dd, *J* = 8.6, 5.5 Hz, 2H), 7.54 (dd, *J* = 8.0, 5.5 Hz, 2H), 7.49 (dd, *J* = 8.8, 5.1 Hz, 2H), 7.23 (dd, *J* = 8.8, 8.8 Hz, 2H), 7.21-7.19 (m, 4H), 6.08 (s, 1H), 6.03 (s, 1H), 6.00 (s, 1H), 4.99 (q, *J* = 6.8 Hz, 1H), 4.98 (q, *J* = 6.4 Hz, 1H), 4.97 (q, *J* = 6.9 Hz, 1H), 4.44 (dd, *J* = 8.7, 5.8 Hz, 1H), 4.42 (dd, *J* = 8.0, 6.6 Hz, 1H), 4.24 (dd, *J* = 7.0, 5.9 Hz, 1H), 4.23 (dd, *J* = 7.4, 7.4 Hz, 1H), 4.15 (dd, *J* = 7.7, 5.5 Hz, 1H), 4.11 (dd, *J* = 7.4, 7.4 Hz, 1H), 2.23-2.11 (m, 5H), 2.01 (m, 1H), 1.30 (d, *J* = 6.8 Hz, 3H), 1.27 (d, *J* = 6.8 Hz, 3H), 1.21 (d, *J* = 6.8 Hz, 3H), 1.00 (d, *J* = 6.8 Hz, 3H), 0.96 (d, *J* = 6.8 Hz, 3H), 0.93 (d, *J* = 6.7 Hz, 3H), 0.89 (d, *J* = 6.7 Hz, 3H), 0.88 (d, *J* = 7.5 Hz, 3H), 0.87 (d, *J* = 7.0 Hz, 3H), 0.859 (d, *J* = 6.8 Hz, 3H), 0.856 (d, *J* = 6.8 Hz, 3H), 0.84 (d, *J* = 6.7 Hz, 3H), 0.82 (d, *J* = 6.8 Hz, 3H), 0.76 (d, *J* = 6.8 Hz, 3H), 0.63 (d, *J* = 6.8 Hz, 3H); ^{13}C NMR (225 MHz, DMSO-d_6) ppm 170.6, 170.4, 170.24, 170.19, 170.15, 170.1, 169.9, 169.83, 169.81, 168.3, 167.9, 167.8, 162.17 (d, $^{1}J_{CF}$ = 247 Hz), 162.16 (d, $^{1}J_{CF}$ = 245 Hz), 162.14 (d, $^{1}J_{CF}$ = 246 Hz), 132.0, 131.9, 131.6, 129.8 (d, $^{3}J_{CF}$ = 9.3 Hz), 129.5 (d, $^{3}J_{CF}$ = 9.0 Hz), 129.3 (d, $^{3}J_{CF}$ = 8.1 Hz), 115.28 (d, $^{2}J_{CF}$ = 23 Hz) (2C), 115.26 (d, $^{2}J_{CF}$ = 22 Hz), 74.5, 74.28, 74.26, 69.7 (2C), 69.6, 58.3, 57.8, 57.4, 57.2, 57.1, 57.0, 30.2, 29.87, 29.85, 29.8, 29.5, 29.3, 18.82, 18.79 (2C), 18.76, 18.7, 18.64, 18.60, 18.4, 18.2, 17.9, 17.7 (2C), 17.4, 17.3, 17.2; ^{19}F NMR (376 Hz, DMSO-d_6) δ -113.21, -113.22, -113.27; HRMS (ESI): $C_{63}H_{81}F_3N_6NaO_{18}$ [M+Na]$^+$ 1289.5457, found 1289.5414.

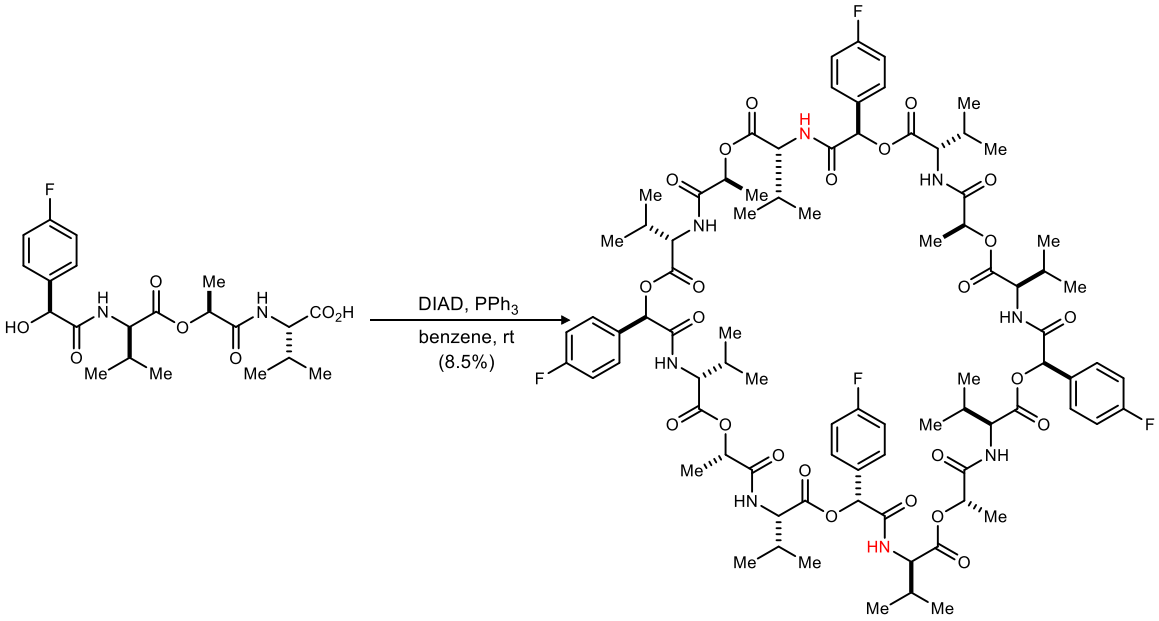

(3*R*,6*R*,9*S*,12S,15*R*,18*R*,21*S*,24*S*,27*R*,30*R*,33*S*,36*S*,39*R*,42*R*,45*S*,48*S*)-6,18,30,42-tetrakis(4-Fluorophenyl)-3,9,15,21,27,33,39,45-octaisopropyl-12,24,36,48-tetramethyl-1,7,13,19,25,31,37,43-octaoxa-4,10,16,22,28,34,40,46-octaazacyclooctatetracontan-2,5,8,11,14,17,20,23,26,29,32,35,38,41,44,47-hexadecaone (134). Following the Tetradepsipeptide MCO general procedure, *seco*-acid **122** (20.0 mg, 45.0 µmol) was stirred for 24 h at ambient temperature to afford a pale yellow oil. Preparative HPLC (5-95% aqueous acetonitrile, 210 nm, flow rate: 8 mL/min, R_t = 23.9 m) provided the 48-membered macrocycle (1.6 mg, 8.5%) as an opaque film. $[\alpha]_D^{20}$ -4.5 (*c* 0.16, MeOH); R_f = 0.85 (5% MeOH/DCM); IR (film) 3308, 2924, 2854, 1745, 1675, 1513, 1462, 1377, 1185, 1146 cm^{-1}; ^1H NMR (800 MHz, DMSO-d_6) δ 8.52 (d, *J* = 3.8 Hz, 1H), 8.36 (d, *J* = 4.2 Hz, 1H), 7.87 (d, *J* = 7.8 Hz, 1H), 7.85 (d, *J* = 8.6 Hz, 1H), 7.47 (dd, *J* = 8.6, 5.4 Hz, 2H), 7.44 (dd, *J* = 8.7, 5.5 Hz, 2H), 7.23 (dd, *J* = 8.8, 8.8 Hz, 2H), 7.21 (dd, *J* = 8.9, 8.9 Hz, 2H), 6.20 (s, 1H), 6.01 (s, 1H), 5.16 (q, *J* = 7.0 Hz, 1H), 4.94 (q, *J* = 6.9 Hz, 1H), 4.20 (dd, *J* = 8.5, 8.5 Hz, 1H), 4.87 (dd, *J* = 4.9, 4.9 Hz, 1H), 4.00 (dd, *J* = 7.9, 5.0 Hz, 1H), 3.92 (dd, *J* = 8.3, 8.3 Hz, 1H), 2.30 (m, 1H), 2.22 (m, 1H), 2.13 (m, 1H), 2.00 (m, 1H), 1.39 (d, *J* = 7.0 Hz, 3H), 1.37 (d, *J* = 7.0 Hz, 3H), 1.01 (d, *J* = 6.6 Hz, 3H), 0.96 (d, *J* = 6.9 Hz, 3H), 0.94 (d, *J* = 6.7 Hz, 3H), 0.92 (d, *J* = 6.9 Hz, 3H), 0.90 (d, *J* = 6.7 Hz, 3H), 0.89 (d, *J* = 6.6 Hz, 3H), 0.82 (d, *J* = 6.8 Hz, 3H), 0.76 (d, *J* = 6.7 Hz, 3H); ^{13}C NMR (200 MHz, DMSO-d_6) ppm 172.4, 170.7, 170.5, 169.9, 169.8, 169.5, 168.2, 167.7, 162.3 (d, $^1J_{CF}$ = 245 Hz), 162.1 (d, $^1J_{CF}$ = 245 Hz), 132.14 (d, $^4J_{CF}$ = 2.5 Hz), 132.10 (d, $^4J_{CF}$ = 2.3 Hz), 130.1 (d, $^3J_{CF}$ = 8.3 Hz), 130.0 (d, $^3J_{CF}$ = 8.3 Hz), 115.3 (d, $^2J_{CF}$ = 22 Hz), 115.2 (d, $^2J_{CF}$ = 22 Hz), 74.6, 73.3, 68.9, 68.5, 59.4, 59.0, 58.9, 57.7, 29.5, 29.4, 29.3, 28.9, 19.11, 19.06 (2C), 19.0, 18.9, 18.43, 18.41, 18.3, 17.84, 17.81; ^{19}F NMR (376 Hz, DMSO-d_6) δ -112.8, -113.2; (HRMS (ESI): Exact mass calcd for $C_{84}H_{109}F_4N_8O_{24}$ $[M+H]^+$ 1689.7490, found 1689.7427.

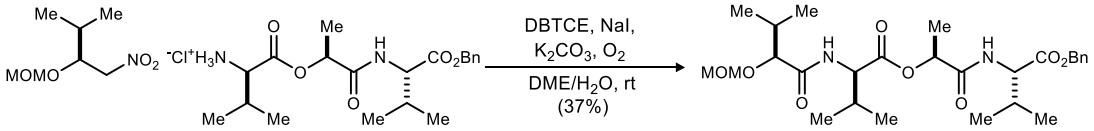

Benzyl ((*S*)-2-((((*S*)-2-(Methoxymethoxy)-3-methylbutanoyl)-D-valyl)oxy)propanoyl)-L-valinate (135). Following the One-Pot UmAS General Procedure, nitroalkane (100 mg, 564 µmol) and amine (281 mg, 677 mmol) afforded an orange oil. The residue was subjected to flash column chromatography (SiO_2, 20-45% ethyl acetate in hexanes), and then preparative HPLC (5-95% aqueous acetonitrile, 210 nm, flow rate: 8 mL/min, R_t =

23.3 min) to afford the major diastereomer (104 mg, 37%) as a colorless oil. $[\alpha]_D^{20}$ -7.3 (*c* 0.27, $CHCl_3$); R_f = 0.18 (30% EtOAc/hexanes); IR (film) 3313, 3065, 2965, 3879, 2827, 1743, 1667, 1522, 1461, 1374, 1306, 1262, 1188, 1151, 1091cm^{-1}; ^{1}H NMR (600 MHz, $CDCl_3$) δ 7.38-7.30 (m, 5H), 6.97 (br d, *J* = 8.0 Hz, 1H), 6.81 (br d, *J* = 8.4 Hz, 1H), 5.29 (q, *J* = 6.8 Hz, 1H), 5.19 (d, *J* = 12 Hz, 1H), 5.13 (d, *J* = 12 Hz, 1H), 4.71 (d, *J* = 6.5 Hz, 1H), 4.66 (d, *J* = 6.4 Hz, 1H), 4.52 (dd, *J* = 8.5, 5.3 Hz, 1H), 4.48 (dd, *J* = 8.0, 5.7 Hz, 1H), 3.92 (d, *J* = 3.7 Hz, 1H), 3.43 (s, 3H), 2.27-2.13 (m, 3H), 1.50 (d, *J* = 6.8 Hz, 3H), 1.01 (d, *J* = 6.8 Hz, 3H), 1.00 (d, *J* = 6.5 Hz, 3H), 0.99 (d, *J* = 6.5 Hz, 3H), 0.93 (d, *J* = 6.9 Hz, 3H), 0.92 (d, *J* = 7.0 Hz, 3H), 0.90 (d, *J* = 7.0 Hz, 3H); ^{13}C NMR (150 MHz, $CDCl_3$) ppm 172.3, 171.3, 170.5, 169.8, 135.3, 128.6, 128.4, 128.3, 97.1, 82.9, 71.1, 67.0, 57.3, 57.2, 56.3, 31.5, 31.0, 30.7, 19.1, 18.9 (2C), 18.1, 17.9, 17.7, 16.6; HRMS (ESI): Exact mass calcd for $C_{27}H_{43}N_2O_8$ $[M+H]^+$ 523.3014, found 523.3012.

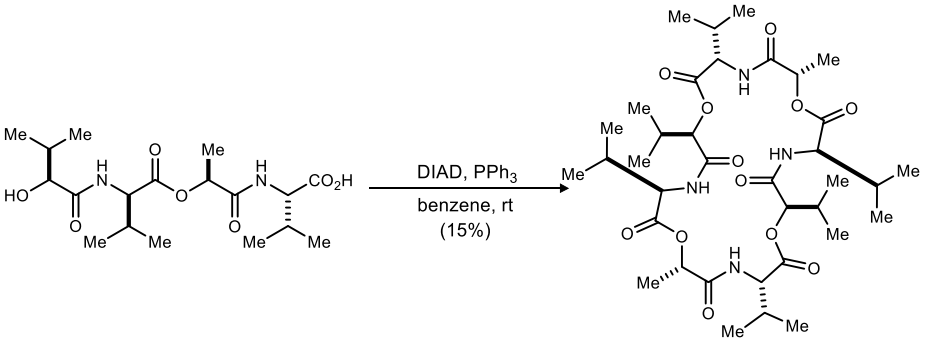

(+)-Montanastatin (*nat*-136). Following the Tetradepsipeptide MCO general procedure, *seco*-acid **122** (15.0 mg, 39.0 μmol) was stirred for 24 h at ambient temperature to afford a pale yellow oil. Preparative HPLC (5-95% aqueous acetonitrile, 210 nm, flow rate: 8 mL/min, R_t = 28.6 m) provided the 24-membered macrocycle, (+)-montanastatin, (2.1 mg, 15%) as a white solid. $[\alpha]_D^{25}$ +11.6 (*c* 0.14, $CHCl_3$);[20] R_f = 0.80 (5% MeOH/DCM); IR (film) 3316, 2964, 2923, 2854, 1752, 1668, 1536, 1465, 1373, 1296, 1261, 1186, 1142, 1095, 1014 cm^{-1}; ^{1}H NMR (600 MHz, $CDCl_3$) δ 7.11 (d, *J* = 8.9 Hz, 1H), 7.08 (d, *J* = 9.2 Hz, 1H), 5.10 (q, *J* = 6.8 Hz, 1H), 5.07 (d, *J* = 3.7 Hz, 1H), 4.29 (dd, *J* = 9.2, 9.2 Hz, 1H), 4.24 (dd, *J* = 9.5, 9.5 Hz, 1H), 2.31-2.22 (m, 3H), 1.47 (d, *J* = 6.9 Hz, 3H), 1.01 (d, *J* = 6.7 Hz, 3H), 1.00 (d, *J* = 6.7 Hz, 3H), 0.984 (d, *J* = 6.8 Hz, 6H), 0.981 (d, *J* = 6.6 Hz, 3H), 0.96 (d, *J* = 6.9 Hz, 3H); ^{13}C NMR (150 MHz, $CDCl_3$) ppm 172.7, 171.0, 170.4, 169.9, 78.7, 71.5, 58.1, 57.6, 30.5, 28.46, 28.43, 19.7, 19.5, 18.9, 18.1, 18.6, 18.3, 16.9; HRMS (ESI): Exact mass calcd for $C_{36}H_{60}N_4NaO_{12}$ $[M+Na]^+$ 763.4100, found 763.4102.

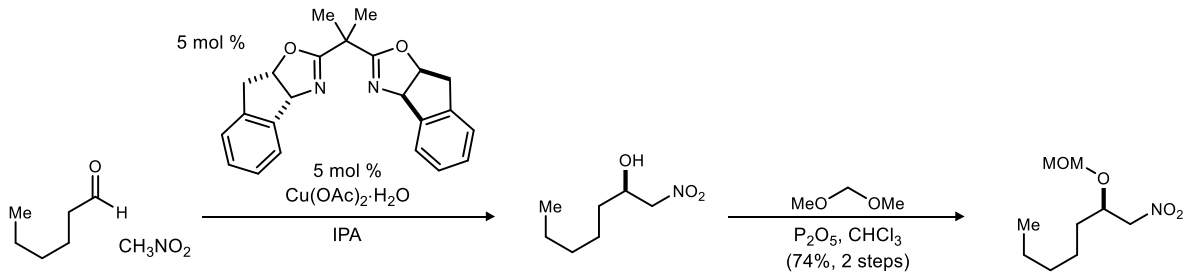

(*R*)-2-(Methoxymethoxy)-1-nitroheptane (137). Following the Evans[21] enantioselective Henry procedure, IndaBOX (117 mg, 326 μmol) and $Cu(OAc)_2$•H_2O (65.0 mg, 326 μmol) stirred at ambient temperature in IPA (13 mL) for 1 h. The cerulean blue solution was then cooled to 0 °C and hexanal (800 μL, 6.51 mmol) was added

[20] Literature value: $[\alpha]_D^{25}$ +11.6 (*c* 0.14, $CHCl_3$); Pettit, G. R.; Tan, R.; Melody, N.; Kielty, J. M.; Pettit, R. K.; Herald, D. L.; Tucker, B. E.; Mallavia, L. P.; Doubek, D. L.; Schmidt, J. M. *Bioorg. Med. Chem.* **1999**, *7*, 895.

[21] Evans, D. A.; Seidel, D.; Rueping, M.; Lam, H. W.; Shaw, J. T.; Downey, C. W. *J. Am. Chem. Soc.* **2003**, *125*, 12692.

and allowed to stir for 10 m before nitromethane (3.50 mL, 65.1 mmol) addition. After stirring for 4 days at 0 °C, the reaction was quenched dropwise at 0 °C with pre-chilled 1 N HCl and the aqueous layer was extracted with CH_2Cl_2. Following drying and concentration under reduced pressure, the crude alcohol was dissolved in $CHCl_3$ (32.6 mL), treated with P_2O_5 (9.24 g, 65.1 mmol) and dimethoxymethane (11.5 mL, 130 mmol), and stirred at ambient temperature overnight. The reaction was cooled to 0 °C, quenched slowly with satd aq $NaHCO_3$, and then poured into CH_2Cl_2. The aqueous layer was extracted with CH_2Cl_2. The organic layers were dried and concentrated to an oil that was subjected to flash column chromatography (SiO_2, 3-6% diethyl ether in hexanes) to afford the title compound as a pale yellow oil (990 mg, 74%, 2 steps). The enantiopurity was determined to be 96% ee by chiral HPLC analysis (Chiralcel OD-H, 2% ^{i}PrOH /hexanes, 0.4 mL/min, $t_r(e_1$, major) = 16.4 min, $t_r(e_2$, minor) = 18.9 min). $[\alpha]_D^{20}$ -10 (c 0.60, $CHCl_3$); R_f = 0.16 (6% Et_2O/hexanes); IR (film) 2932, 2861, 1558, 1463, 1385, 1156, 1138, 1105, 1032, 919 cm^{-1}; ^{1}H NMR (400 MHz, $CDCl_3$) δ 4.67 (d, J = 7.1 Hz, 1H), 4.65 (d, J = 7.1 Hz, 1H), 4.50 (dd, J = 12.4, 8.1 Hz, 1H), 4.42 (dd, J = 12.4, 3.9 Hz, 1H), 4.27 (dddd, J = 8.1, 6.1, 6.1, 3.9 Hz, 1H), 3.35 (s, 3H), 1.71-1.56 (m, 2H), 1.38-1.29 (br m, 6H), 0.90 (t, J = 6.8 Hz, 3H); ^{13}C NMR (100 MHz, $CDCl_3$) ppm 96.2, 79.1, 74.9, 55.9, 32.3, 31.6, 24.5, 22.5, 13.9; HRMS (CI): Exact mass calcd for $C_9H_{19}N_1O_4Na$ $[M+Na]^+$ 228.1212, found 228.1207.

Appendix 7.2 Isothermal Titration Calorimetry (ITC)

7.2.1 ITC instrument/experiment instructions

General Information: ITC measurements were performed using a Microcal PEAQ-ITC instrument (MicroCal Inc., Northampton, MA). All experiments were performed at 25 °C *in anhydrous methanol*. Optimal instrument settings for consistent results *in methanol* include: reference power set to 5 µcal/mol, stir speed set to 1000 rpm, and instrument feedback set to low. These settings are extremely important when conducting experiments in methanol in order to avoid instrumental overcompensation for measured heats (resulting in oscillating raw heats).

Instrument Preparation & Sample Loading:
Prior to use, the injection syringe, sample cell, and reference cell were thoroughly rinsed with anhydrous methanol.
The reference cell was then loaded with 300 µL of anhydrous methanol. The loading syringe was used to gently tap the bottom of the reference cell to release any trapped bubbles, and finally remove any displaced methanol in the overflow area.
The sample cell was rinsed with 100 µL of macrocycle solution, and then filled with 300 µL of macrocycle solution. Once again, the loading syringe was used to gently tap the bottom of the sample cell to release any trapped bubbles, and finally remove any displaced sample solution from the cell overflow area.
Two 100 µL Eppendorf tubes were filled with 70 µL of alkali metal salt solution. The first tube was used to rinse the injection syringe with one purge-refill cycle, and then discarded. The second tube was then loaded into the injection syringe. Finally, excess salt solution was removed from the exterior of the syringe tip by gently rinsing/drying the outside of the syringe (manually) with anhydrous methanol.
After entering all appropriate experimental details into the run software, the injection syringe was placed into the sample cell, and run-equilibration was started. During equilibration, the syringe will spin at experimental rpm while the instrument calibrates to the programmed reference power setting. The equilibration period will last for up to 10 minutes. Note that valuable information about the quality of sample loading can be assessed during this time. An unstable baseline is indicative of trapped air bubbles in the sample cell, which if observed, can be remedied by halting the equilibration, repeating the degassing procedure, and then restarting the equilibration. After equilibration is completed, the programmed titration will automatically start.

Experimental Titration Details: Alkali metal salt solution (MeOH, 6.0-8.0 mM) in a 40 µL injection syringe was titrated into a macrocycle solution (MeOH, 300-400 µM) loaded in the sample cell of the calorimeter. One 0.4 µL, 0.8 s duration preliminary injection, and fifteen 2.6 µL, 5.6 s duration injections were made with 150 s of elapsed time between each injection. Data from the first injection were discarded due to diffusion between the syringe and the sample cell solution. Control experiments were performed under the same conditions by injection of the alkali metal salt solution into methanol alone.

Data Analysis: The integrated binding isotherms were fitted using the non-linear, one-site model software provided by Microcal. For most experiments, the titration curves revealed a 1:1 ion to macrocycle binding stoichiometry. A few of the titrations exhibited 2:1 binding stoichiometry. However, the resulting isotherm was still in the shape of a single-site binding curve, which indicates that the macrocycle is cooperatively binding two ions in one site, or two identical binding sites.[22] Using the one-site model with an N-value greater than 1 will fit the isotherm reasonably accurately for this purpose.[23] Additionally, some experiments resulted in atypical s-shaped curves, which are characteristic of aggregate formation at the beginning of the titration.[23] In these cases,

[22] Clavería-Gimeno, R.; Velazquez-Campoy, A.; Pey, A. L. *Arch. Biochem. Biophys.* **2017**, *636*, 17.
[23] Darby, S. J.; Platts, L.; Daniel, M. S.; Cowieson, A. J.; Falconer, R. J. *J. Therm. Anal. Calorim.* **2016**, *127*, 1201.

the binding affinity of curve post-aggregation was measured.[23] At the end of each titration experiment, the resulting heats resembled those that were generated in the control experiment. To account for this background dissociation isotherm, a regression of the last three heats of the raw binding isotherm was subtracted from the data.[24] [25]

7.2.2 ITC thermograms

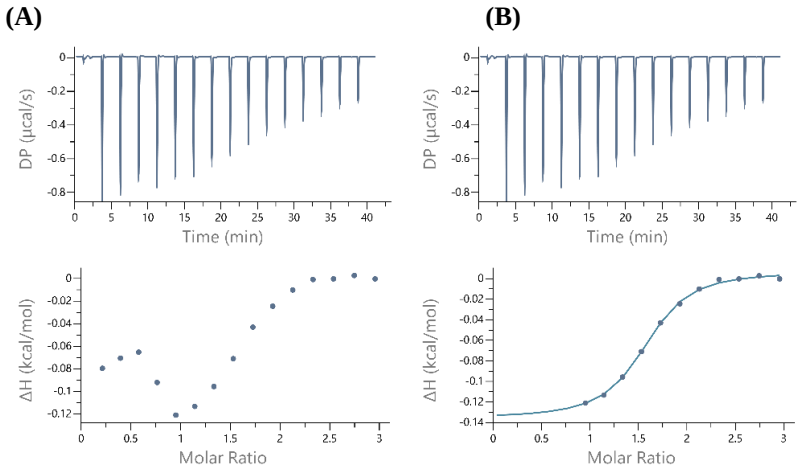

Figure 1. (A) Raw ITC isotherm and (B) processed ITC isotherm for the titration of $NaPF_6$ (5.00 mM) into 75 (360 µM) in MeOH at 25 °C.

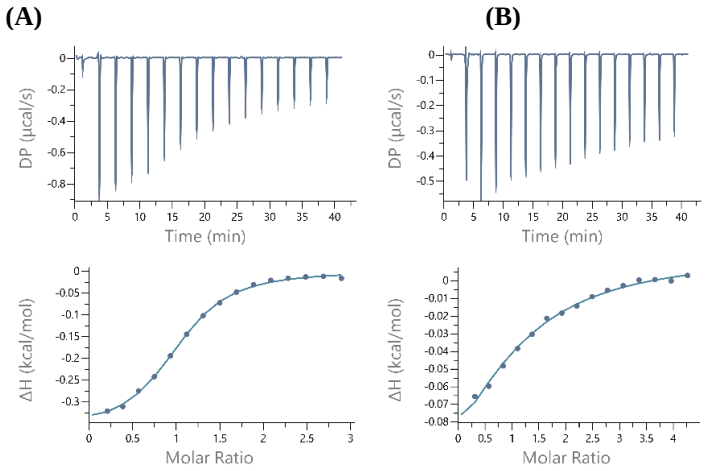

Figure 2. ITC isotherms for the titration of (A) $NaPF_6$ (4.10 mM) and (B) KCl (6.00 mM) into 53 (300 µM) in MeOH at 25 °C.

[24] Hallen, D. *Pure & Appl. Chem.* **1993**, *65*, 1527.
[25] Holdgate, G. A. In *BioTechniques*; EATON PUBLISHING CO: 2001; Vol. 31, p 164.

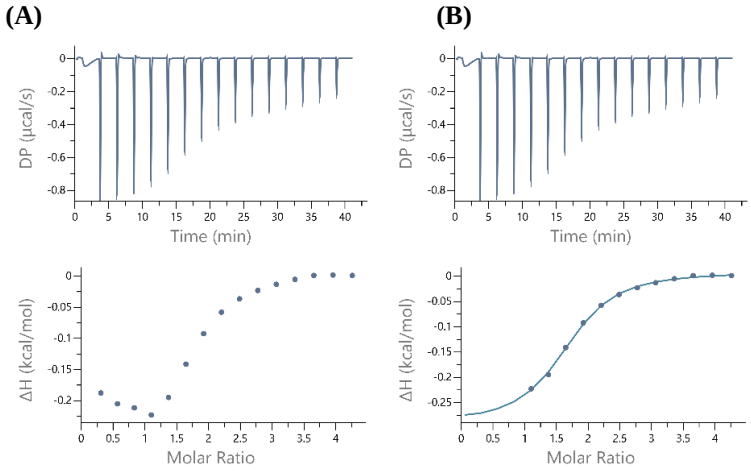

Figure 3. (A) Raw ITC isotherm and (B) processed ITC isotherm for the titration of $NaPF_6$ (6.00 mM) into 76 (300 µM) in MeOH at 25 °C.

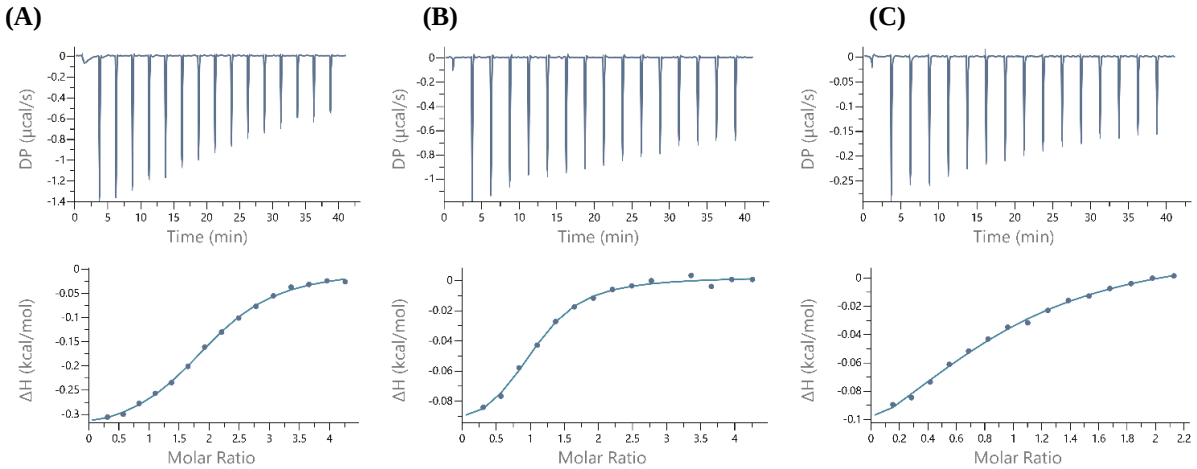

Figure 4. ITC isotherms for the titration of (A) $NaPF_6$ (6.00 mM), (B) KCl (6.00 mM), and (C) CsCl (3.00 mM) into 72 (300 µM) in MeOH at 25 °C.

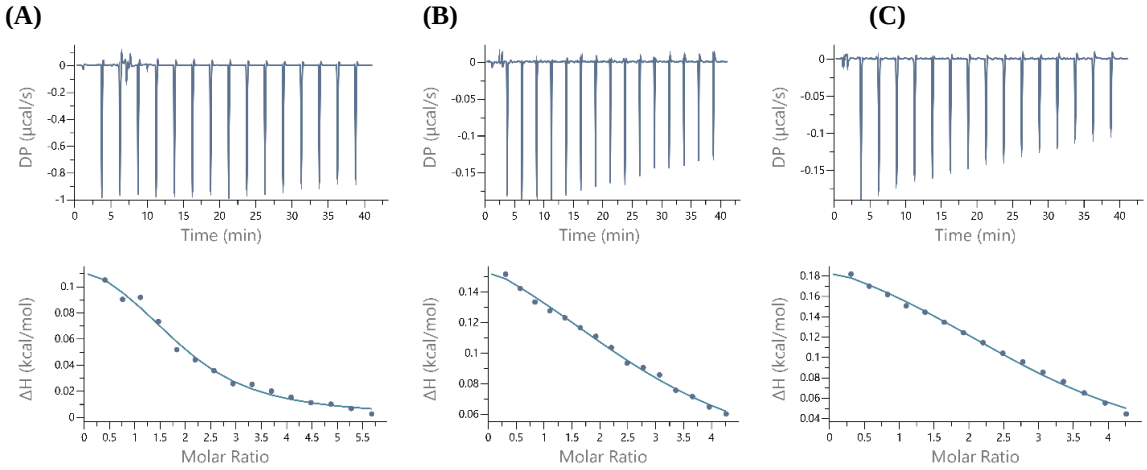

Figure 5. ITC isotherms for the titration of (A) $NaPF_6$ (8.00 mM), (B) KCl (6.00 mM), and (C) CsCl (6.00 mM) into 73 (300 µM) in MeOH at 25 °C.

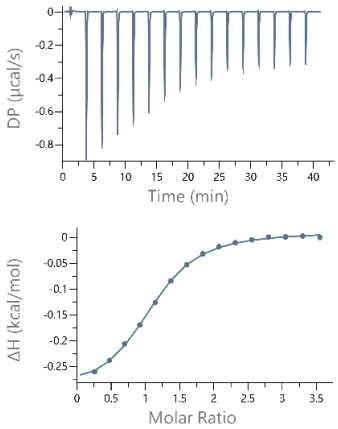

Figure 6. ITC isotherm for the titration of $NaPF_6$ (5.00 mM) into 79 (300 µM) in MeOH at 25 °C.

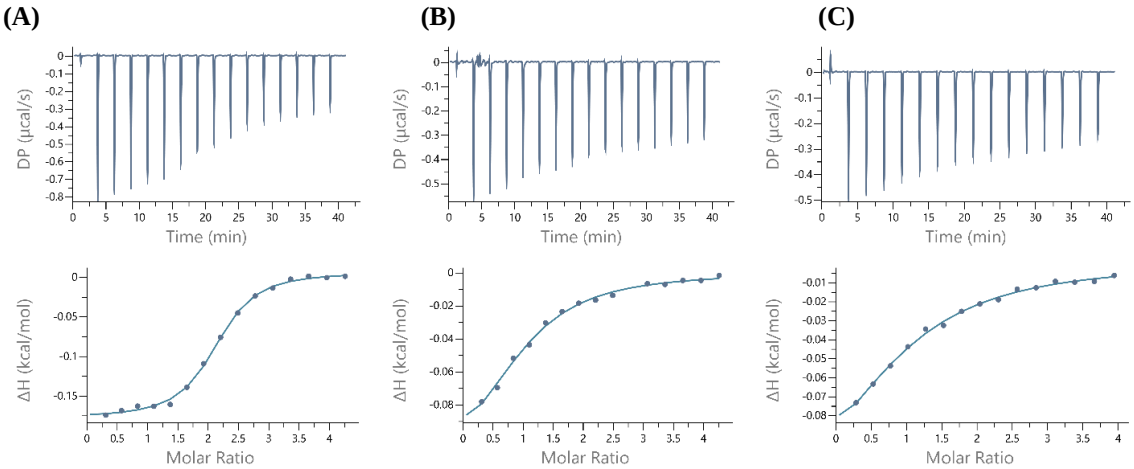

Figure 7. ITC isotherms for the titration of (A) $NaPF_6$ (5.00 mM), (B) KSCN (5.00 mM), and (C) CsCl (5.00 mM) into 80 (250, 250, 270 µM respectively) in MeOH at 25 °C.

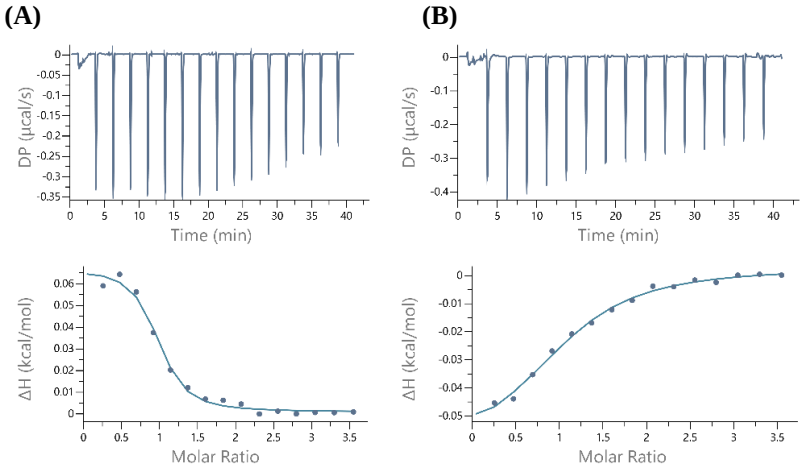

Figure 8. ITC isotherms for the titration of (A) $NaPF_6$ (5.00 mM) and (B) CsCl (5.00 mM) into 81 (300 µM) in MeOH at 25 °C.

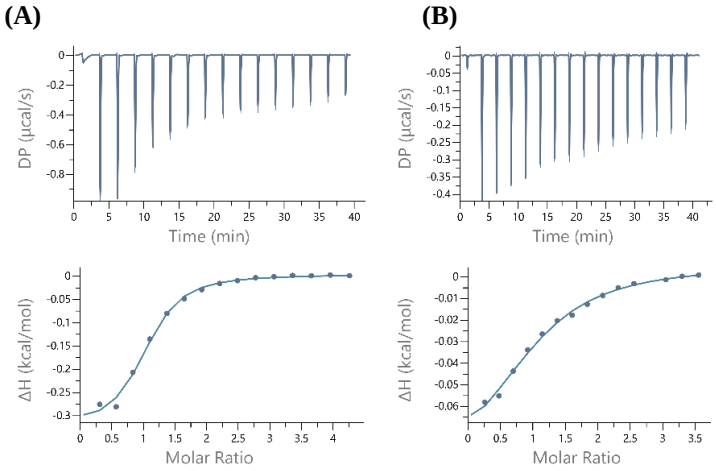

Figure 9. ITC isotherms for the titration of (A) $NaPF_6$ (6.00 mM) and (B) KSCN (5.00 mM) into 111 (300 µM) in MeOH at 25 °C.

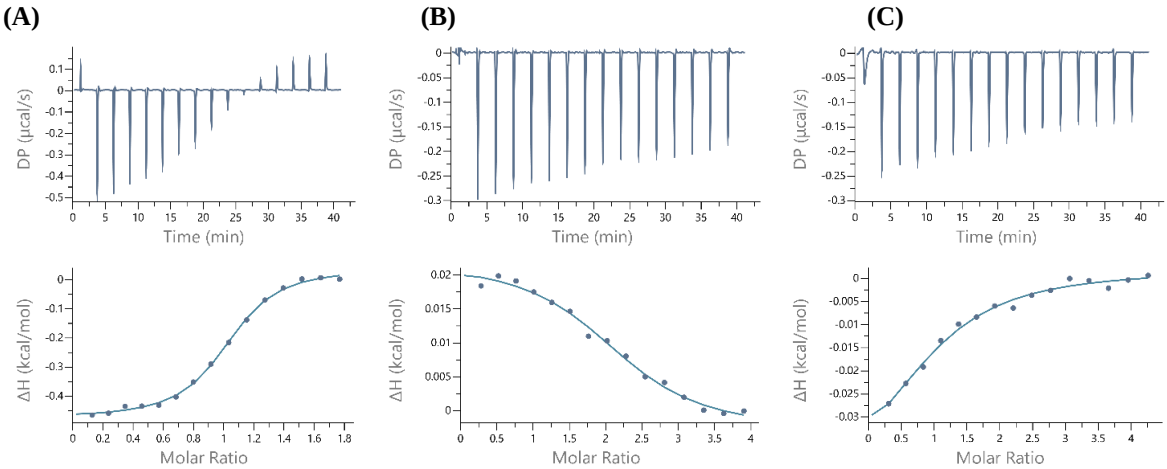

Figure 10. ITC isotherms for the titration of (A) $NaPF_6$ (2.50 mM), (B) KSCN (5.50 mM), and (C) CsCl (6.00 mM) into 112 (300 µM respectively) in MeOH at 25 °C.

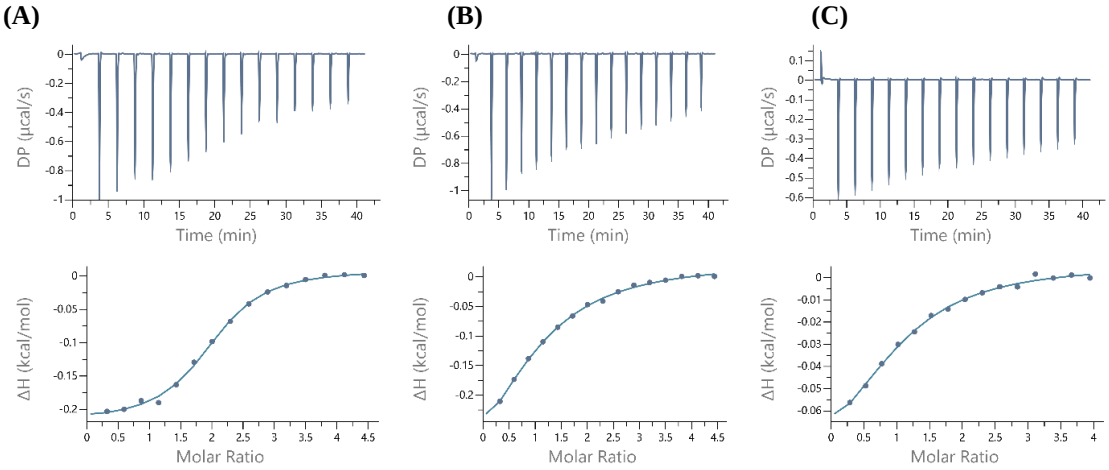

Figure 11. ITC isotherms for the titration of (A) $NaPF_6$ (5.00 mM), (B) KSCN (5.00 mM), and (C) CsCl (5.00 mM) into 113 (240, 240, 270 µM respectively) in MeOH at 25 °C.

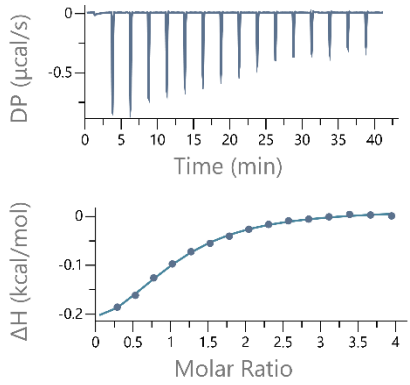

Figure 12. ITC isotherm for the titration of KSCN (5.00 mM) into 132 (270 µM) in MeOH at 25 °C.

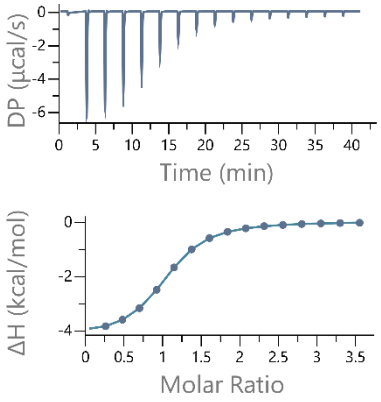

Figure 13. ITC isotherm for the titration of KSCN into *nat*-valinomycin 68 (300 µM) in MeOH at 25 °C.

Appendix 7.3 Ion mobility data summary for compounds 131-134

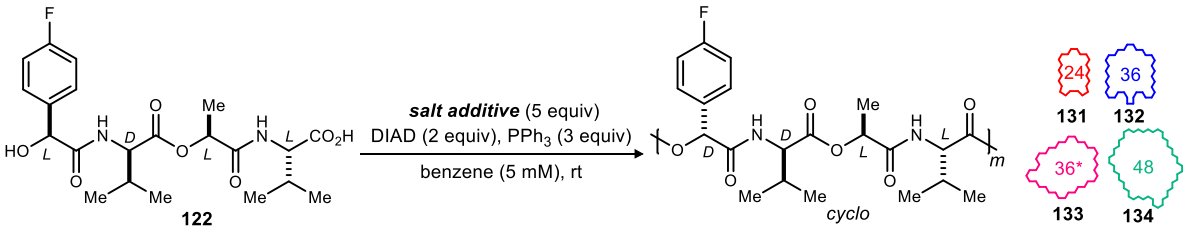

Two of the products of the above reaction (**133** and **134**) were in question because of their unexpectedly unsymmetrical ^{1}H NMR spectra, and masses that originally matched **131** and **132**. In order to definitively elucidate their structures, we worked with the Center for Innovative Technology to obtain ion-mobility and MS/MS analysis on each of the compounds. The results of the ion mobility experiments are shown below:

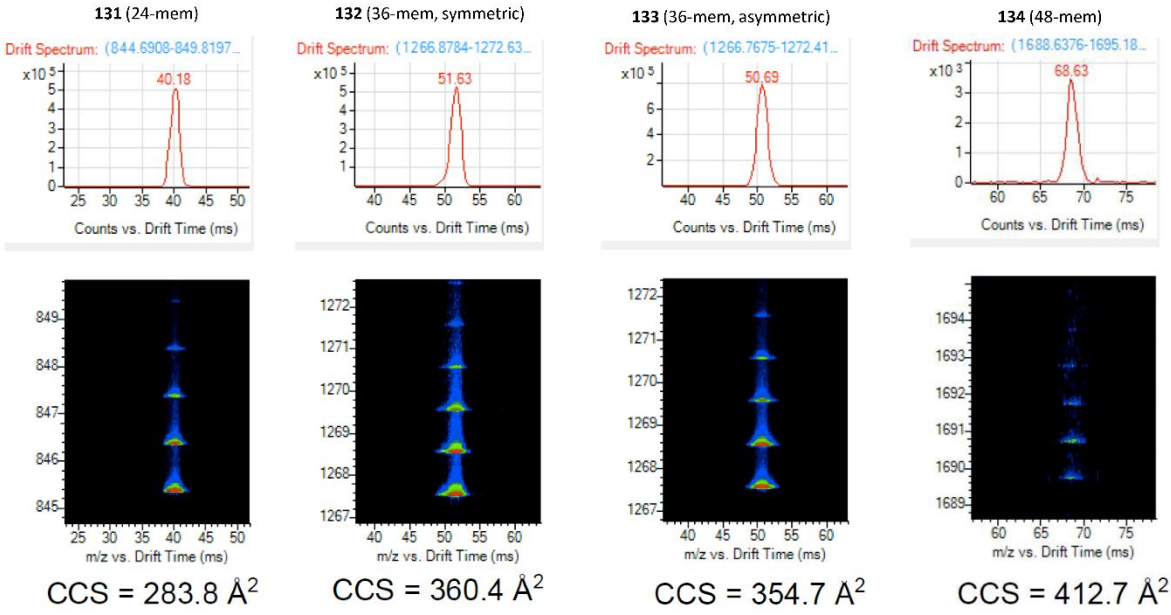

A parent ion peak for **134** was observed at 1688, whereas by standard HRMS methods its half mass (844) was observed instead. Cleavage to half mass is not uncommon with these oligodepsipeptides because their numerous ester linkages make them much more susceptible to hydrolysis under typical ionization conditions. The collision cross section for **134** parent peak fits with the trend of larger cross section and later retention time for larger macrocycles. We also observed its half-mass fragment with the same CCS and retention time as **131**, which confirms that **134** is, indeed, a macrocycle double the size of **131**. As for **133**, its CCS is statistically different from that of **132**, even though they have the same mass and nearly identical retention times. This is indicative that that **133** is the same size as **132**, but structurally distinct. However, MS/MS analysis comparison of **133** to **132** revealed identical fragmentation patterns at identical voltages. This indicates that **133** is the same type of macrocyclic structure as **132**. From these results we can deduce that **132** and **133** are essentially the same compound, but in distinct, separable conformations. This phenomenon is not unprecedented for macrocyclic structures, especially those with aryl rings and peptidic structures (discussed in more detail in Chapter 4). MS/MS on all four compounds showed similar fragmentation patterns, which supports assignment of macrocyclic structure for each. We also collected MS/MS on **123** as a linear peptide control. In comparison to **123**, all four macrocycles needed much more voltage to completely fragment. Linear peptide **123** was fragmented at only 40 V, whereas compounds **131**, **132**, **133**, **134** needed 80 V to completely fragment.

Appendix 7.4 Biological methods

7.4.1 Isolation of ventricular myocytes

The use of animals was approved by the Animal Care and Use Committee of Vanderbilt University, USA (animal protocol #M1600090-00) and performed in accordance with NIH guidelines. Ventricular myocytes from 12 to 16 week old C57BL/6 wild type or calsequestrin 2 knockout ($CASQ2^{-/-}$) mice were isolated from the heart by collagenase digestion as previously described.[26] Cells were then washed twice by gravity sedimentation for 20 minutes at room temperature in standard Tyrode solution with 0.2 mM $CaCl_2$. The final suspension contained 0.6 mM Ca^{2+} and the cells were immediately used for Ca^{2+} sparks or intact intracellular Ca^{2+} measurements.

7.4.2 Spark measurements in permeabilized myocytes

Isolated ventricular myocytes were plated onto laminin-coated glass cover slips and allowed to attach for 10 minutes at room temperature (22 - 24 °C). The attached cells were permeabilized with saponin (40 µg/mL) for 40 seconds and then bathed for 15 minutes in a freshly-made internal solution (pH = 7.2) containing (mM): K-aspartate (120), KCl (15), K_2HPO_4 (5), $MgCl_2$ (5.6), HEPES (10), dextran (4% w/v), MgATP (5), Phosphocreatine-Na_2 (10), creatine phosphokinase (10 U/mL), reduced L-glutathione (10), EGTA (0.5), $CaCl_2$ (0.12), calmodulin (100 nM), and Fluo-4 (0.03). The internal solution contained dimethyl sulfoxide (DMSO) at 0.03% as control or *nat*-**1**, **7**, **8**, or their respective enantiomers (*ent*-) in 0.03% DMSO. Confocal imaging was performed on a Zeiss LSM 510 inverted laser scanning confocal microscope equipped with a 40X / 1.30 NA planar oil immersion objective. Fluo-4 was excited by an argon laser at 488 nm and the fluorescence emission was passed through a 505 nm long pass filter to photomultiplier tube detectors. Cell sparks were imaged in line-scan mode in those cells that had characteristic brick-shape morphology. Lines were positioned longitudinally near the center of the cell, avoiding nuclei. SR Ca^{2+} load was measured as the Ca^{2+} transient amplitude induced by application of 10 mM caffeine. Image analysis was performed in ImageJ with the SparkMaster plugin[27] using a background setting of 5 and criteria of 3.8. Spark mass was calculated from the equation: spark mass = 1.206 * Amplitude * FWHM^3. Leak was calculated from the equation: leak = frequency * mass.

7.4.3 Free Ca^{2+} measurements

Calcium standards from ThermoFisher (Calcium Calibration Kit #1, catalog #C3008MP) were used to generate a standard curve of the free Ca^{2+} concentration from 0 to 1.35 µM, according to the provided protocol. DMSO or *nat*-**1**, **7**, **8**, or their respective enantiomers (25 µM) were incubated for 10 minutes in sparks solution assay conditions. Fluorescence measurements were recorded at 25 °C using a GloMax Discover 96-well plate reader (Promega) equipped with a 475 nm excitation and a 500 – 550 nm emission filter. Background fluorescence was measured from the signal emitted in the absence of Fluo-4 and subtracted from all other fluorescence measurements.

7.4.4 Intracellular Ca^{2+} measurements in intact myocytes

Cardiomyocytes were pre-incubated for 2.5 hours with DMSO or *ent*-**1**. Myocytes were then loaded with Fura-2 acetoxymethyl ester (Fura-2 AM; Invitrogen) as described previously.[28] Briefly, isolated single ventricular

[26] Knollmann, B. C.; Chopra, N.; Hlaing, T.; Akin, B.; Yang, T.; Ettensohn, K.; Knollmann, B. E.; Horton, K. D.; Weissman, N. J.; Holinstat, I.; Zhang, W.; Roden, D. M.; Jones, L. R.; Franzini-Armstrong, C.; Pfeifer, K. *J. Clin. Invest.* **2006**, *116*, 2510.
[27] Picht, E.; Zima, A. V.; Blatter, L. A.; Bers, D. M. *Am. J. Physiol. Cell Physiol.* **2007**, *293*, C1073.
[28] Hwang, H. S.; Hasdemir, C.; Laver, D.; Mehra, D.; Turhan, K.; Faggioni, M.; Yin, H.; Knollmann, B. C. *Circ. Arrhythm. Electrophysiol.* **2011**, *4*, 128.

myocytes were incubated with 2 µM Fura-2 AM for 6 minutes, washed 2 x 10 minutes with normal Tyrode's (NT) solution containing 250 µM probenecid (all solutions retained DMSO or *ent*-**1**). The composition of NT used for Fura-2 loading and washing was (in mM): 134 NaCl, 5.4 KCl, 1.2 $CaCl_2$, 1 $MgCl_2$, 10 glucose, and 10 HEPES (pH adjusted to 7.4 with NaOH). After Fura-2 loading, experiments were conducted in NT solution containing 1 µM isoproterenol and 2 mM $CaCl_2$. Fura-2 AM-loaded Myocytes were electrically paced at 3 Hz field stimulation for 20 seconds, followed by no electrical stimulation for 40 seconds, and then perfused with 10 mM caffeine for 5 seconds to estimate total SR Ca^{2+}. Intracellular Ca^{2+} transients were recorded using a dual-beam excitation fluorescence photometry setup (IonOptix Corp.). All experiments were conducted at room temperature. Spontaneous Ca^{2+} waves and triggered beats were quantified during the 40-second period following cessation of the pacing train. The amplitude of the caffeine-induced Ca^{2+} transient was used as an estimate of total SR Ca^{2+} content. Ca^{2+} transients were analyzed using IonWizard data analysis software (Milton, MA).

7.4.5 Electrocardiogram (ECG) recordings in CASQ2-/- mice

11 – 19 week old CASQ2-/- mice were manually restrained by scruffing, injected intraperitoneally (i.p.) with 30 mg/kg (compound/body weight) *nat*-(-)-verticilide, *ent*-(+)-verticilide, or DMSO (of equivalent volume), and returned to their cage. After 30 minutes, mice were anesthetized with inhaled isoflurane titrated to the lowest possible level to maintain anesthesia (assessed by lack of toe-pinch reflex) and four subcutaneous limb electrodes were placed. Baseline ECG was recorded for approximately 2 minutes (until stable heart rate was achieved); there were no differences in baseline respiration or heart rate between groups. Isoproterenol (3.0 mg/kg i.p.) was administered to induce CPVT and ECG recordings were continued until the cessation of ectopic beats for at least one minute. An individual blinded to the treatment group performed ECG analysis using LabChart v7.3.8 (ADInstruments) and quantified ectopic beats and episodes of non-sustained ventricular tachycardia (defined as greater than two consecutive ectopic beats). Median QRS duration and PR interval were measured from a ≥ 10 s strip during baseline using the automated "ECG Analysis" plugin available with LabChart. There were no observed changes in behavior or pain and distress following single-dose injection of *nat*-**1** or *ent*-**1** over a period of four weeks and the mortality rate was zero.

7.4.6 [^{3}H]ryanodine binding assay

Isolation of SR vesicles from porcine *longissimus dorsi* muscle and cardiac ventricle was carried out exactly as previously described.[29] Cardiac and skeletal SR membranes (3 mg/mL and 2 mg/mL, respectively) were incubated with 20 mM PIPES (pH 7.0), 150 mM KCl, 5 mM GSH, 2 mM DTT, 1 µg/mL aprotinin/leupeptin, 0.1 mg/mL BSA, 5 mM ATP, 0.1 µM calmodulin, 65 µM CaCl2 (30 nM free Ca^{2+}, as determined by MaxChelator), and 10 nM [3H]ryanodine for 3 hours at 37 °C. Solutions included DMSO, *nat*-**1**, *ent*-**1**, or tetracaine at various concentrations. Samples were filtered through grade GF/B Glass Microfiber filters (Brandel Inc., Gaithersburg, MD) using a 96-sample Brandel Harvester in 4 ml of Ecolite scintillation mixture (MP Biomedicals, Solon, OH). The [^{3}H] retained on the filter was measured using a Beckman LS6000 scintillation counter.

7.4.7 Statistical Analyses

Statistical analysis was performed using Prism v6.01 (GraphPad Software, Inc.). Appropriate statistical tests were used as noted and reported in the figure legends. A *p* value of 0.05 was used as the threshold to reject the null hypothesis.

[29] Rebbeck, R. T.; Nitu, F. R.; Rohde, D.; Most, P.; Bers, D. M.; Thomas, D. D.; Cornea, R. L. *J. Biol. Chem.* **2016**, *291*, 15896.

Appendix 7.5: NMR Spectra

Appendix 7.5-X

Figure 1. ^{1}H NMR (400 MHz, $CDCl_3$) of ***nat*-21**

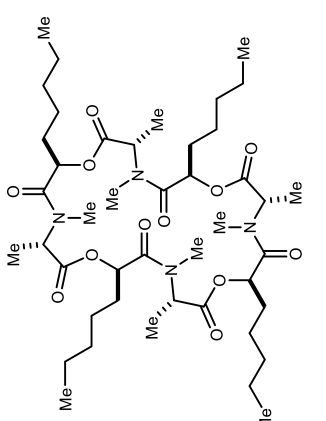

^{1}H δ Literature	Mult, *J* values	^{1}H δ Synthesis	Mult, *J* values
0.88	m	0.82-0.89	br m
1.30	m	1.06-1.31	br m
1.31	m		
1.38	d, *J* = 7.2 Hz	1.38	d, *J* = 7.2 Hz
1.39	d, *J* = 7.4 Hz	1.39	d, *J* = 7.5 Hz
1.41	d, *J* = 7.4 Hz	1.41	d, *J* = 7.3 Hz
1.45	d, *J* = 7.3 Hz	1.45	d, *J* = 7.4 Hz
1.59	d, *J* = 7.3 Hz	1.59	d, *J* = 7.0 Hz
1.78	m	1.73-1.90	br m
2.89	s	2.89	s
2.91	s	2.91	s
2.96	s	2.96	s
3.01	s	3.01	s
3.18	s	3.18	s
4.56	q, *J* = 7.3 Hz	4.56	q, *J* = 7.3 Hz
5.11	dd, *J* = 10.6, 2.5 Hz	5.11	dd, *J* = 11.0, 2.4 Hz
5.30	q, *J* = 7.4 Hz	5.3	q, *J* = 7.3 Hz
5.32	dd, *J* = 10.1, 3.3 Hz	5.32	dd, *J* = 9.9, 3.3 Hz
5.36	dd, *J* = 9.0, 5.3 Hz	5.36	dd, *J* = 8.5, 5.0 Hz
5.40	q, *J* = 7.2 Hz	5.4	q, *J* = 7.2 Hz
5.42	m	5.42	m (overlapping)
5.45	dd, *J* = 8.4, 5.3 Hz	5.45	dd, *J* = 8.4, 5.4 Hz
5.53	q, *J* = 7.3 Hz	5.53	q, *J* = 7.3 Hz
5.54	q, *J* = 7.4 Hz	5.54	q, *J* = 7.5 Hz

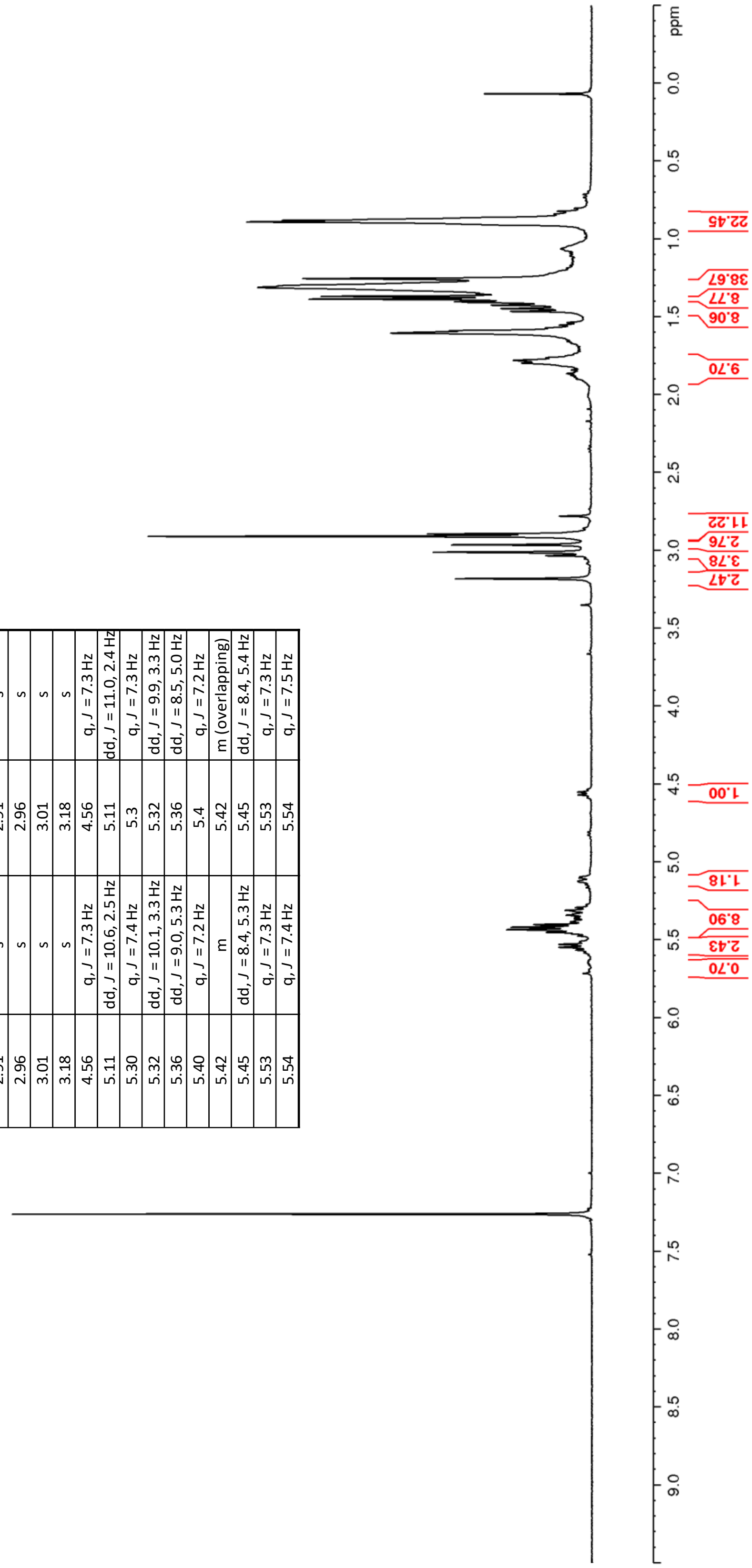

Figure 2. ^{13}C NMR (150 MHz, $CDCl_3$) of ***nat*-21**

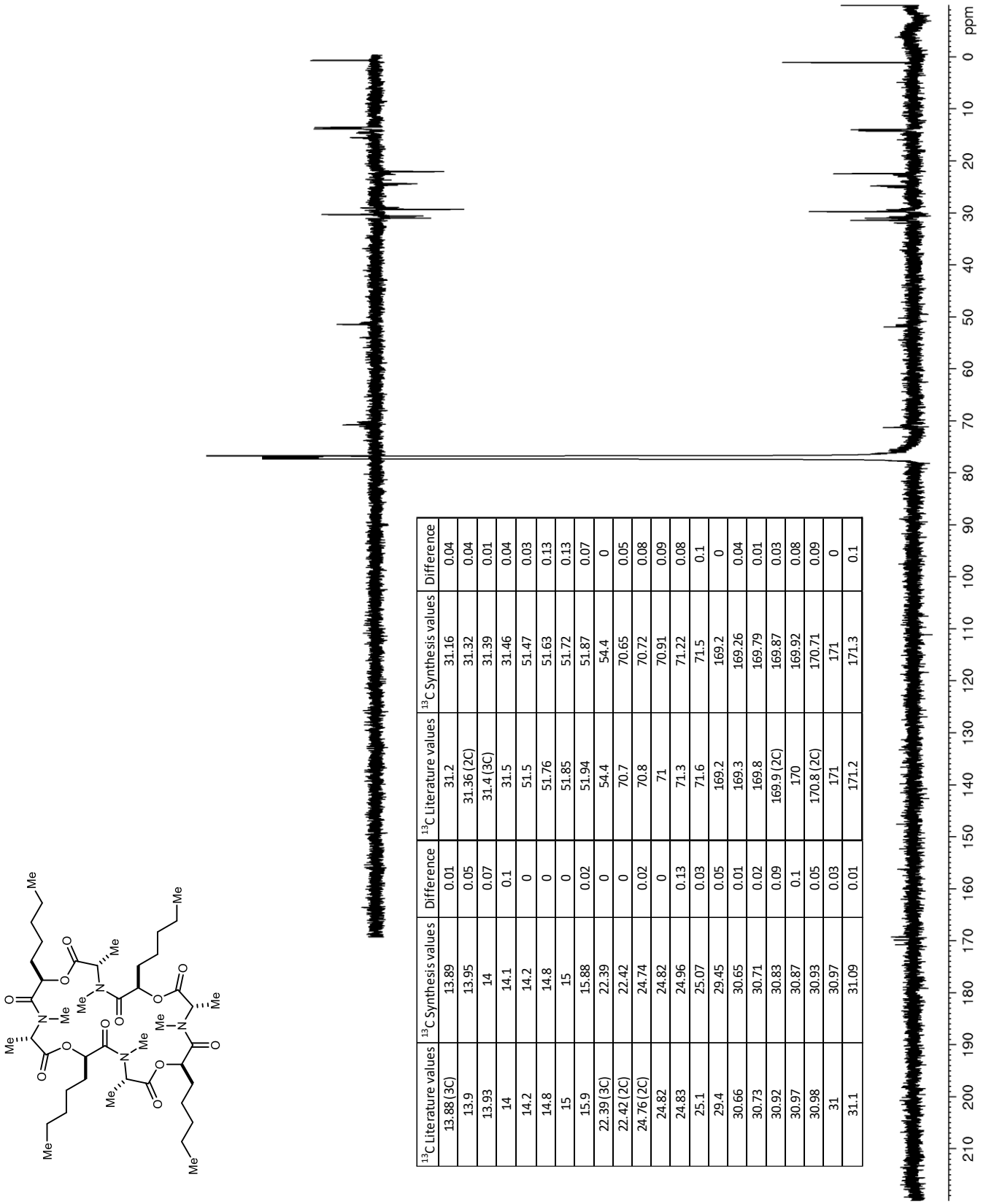

^{13}C Literature values	^{13}C Synthesis values	Difference	^{13}C Literature values	^{13}C Synthesis values	Difference
13.88 (3C)	13.89	0.01	31.2	31.16	0.04
13.9	13.95	0.05	31.36 (2C)	31.32	0.04
13.93	14	0.07	31.4 (3C)	31.39	0.01
14	14.1	0.1	31.5	31.46	0.04
14.2	14.2	0	51.5	51.47	0.03
14.8	14.8	0	51.76	51.63	0.13
15	15	0	51.85	51.72	0.13
15.9	15.88	0.02	51.94	51.87	0.07
22.39 (3C)	22.39	0	54.4	54.4	0
22.42 (2C)	22.42	0	70.7	70.65	0.05
24.76 (2C)	24.74	0.02	70.8	70.72	0.08
24.82	24.82	0	71	70.91	0.09
24.83	24.96	0.13	71.3	71.22	0.08
25.1	25.07	0.03	71.6	71.5	0.1
29.4	29.45	0.05	169.2	169.2	0
30.66	30.65	0.01	169.3	169.26	0.04
30.73	30.71	0.02	169.8	169.79	0.01
30.92	30.83	0.09	169.9 (2C)	169.87	0.03
30.97	30.87	0.1	170	169.92	0.08
30.98	30.93	0.05	170.8 (2C)	170.71	0.09
31	30.97	0.03	171	171	0
31.1	31.09	0.01	171.2	171.3	0.1

Figure 3. ^{1}H NMR (600 MHz, $CDCl_3$) of **28**

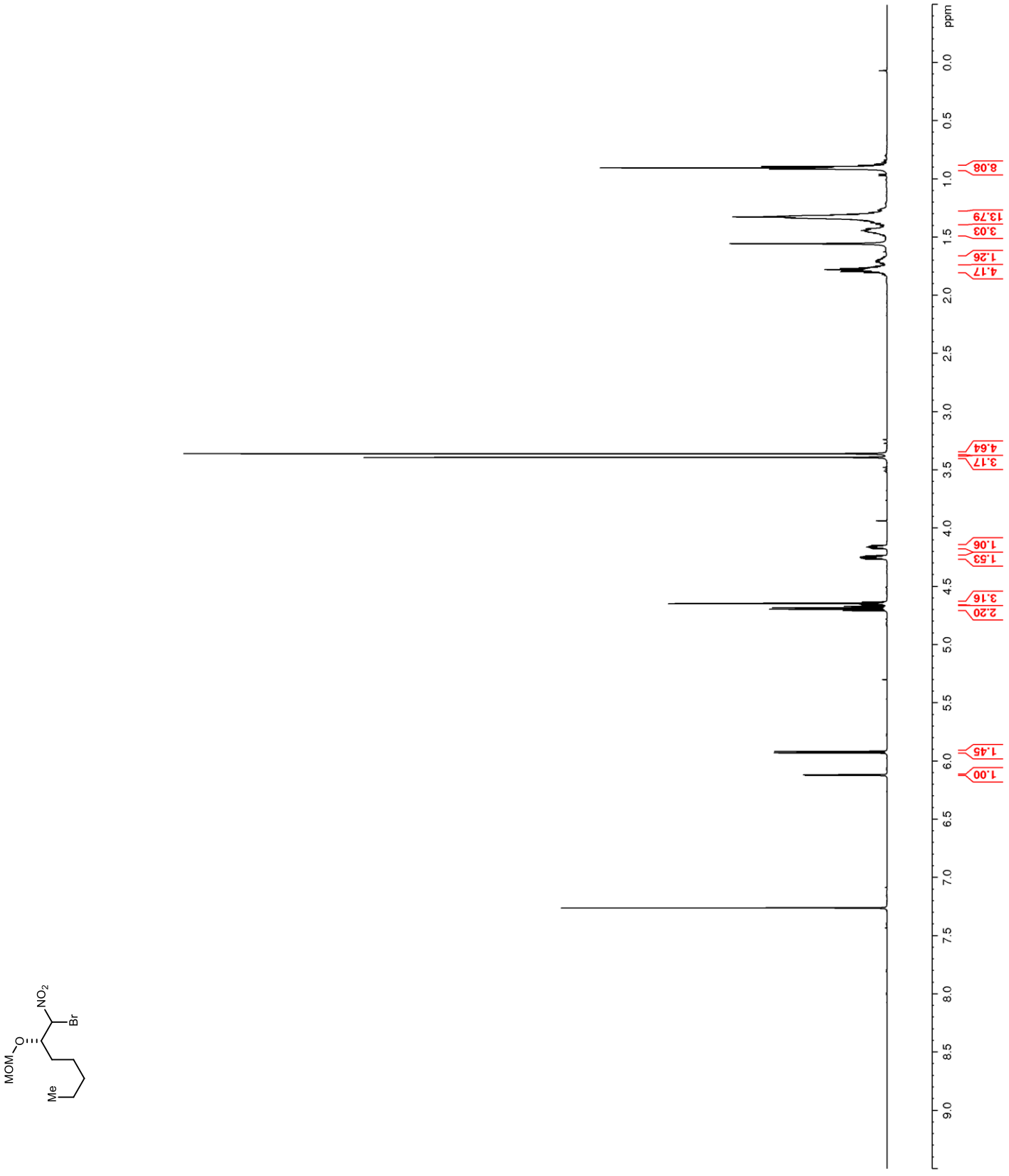

Figure 4. ^{13}C NMR (150 MHz, $CDCl_3$) of **28**

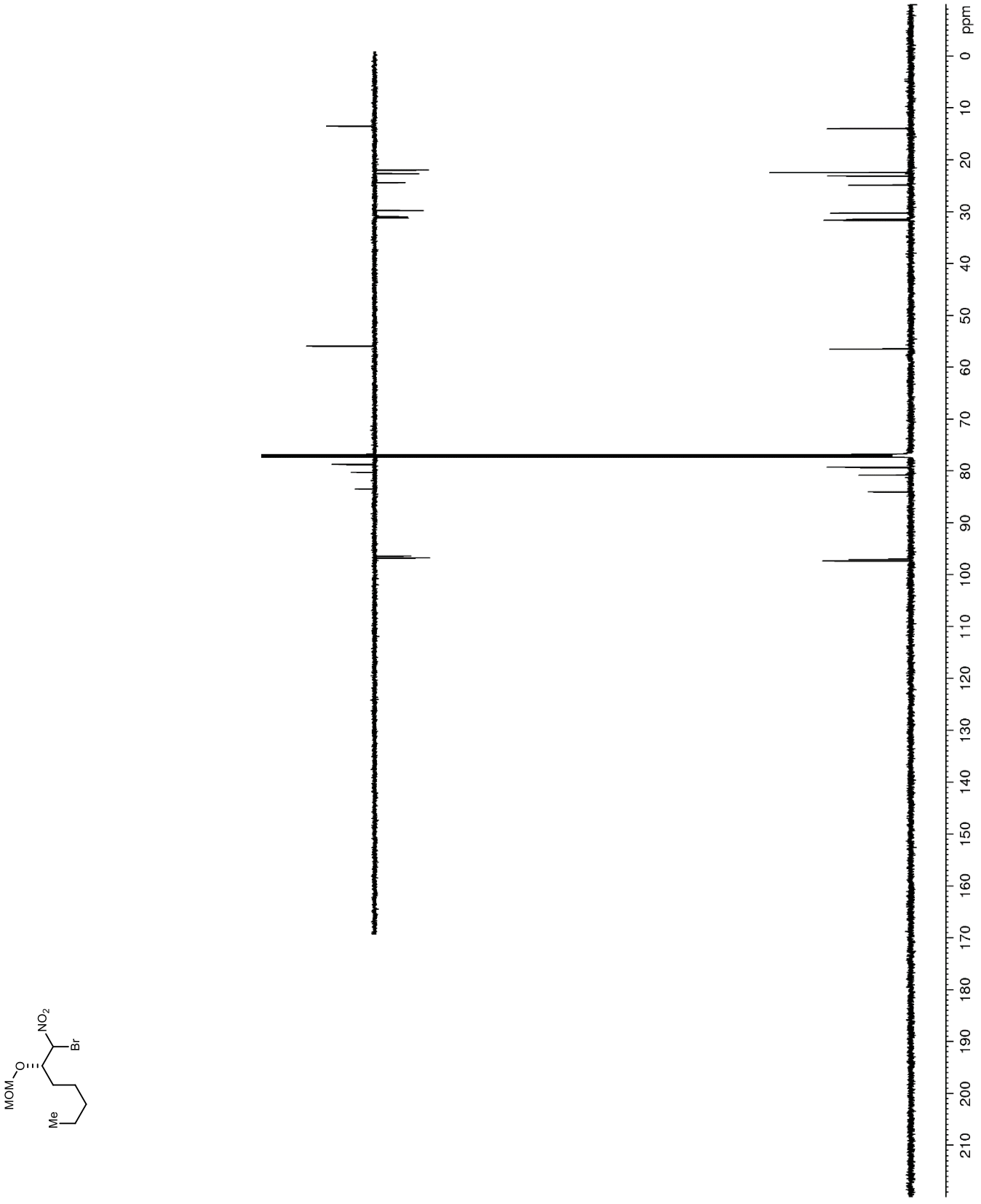

Figure 5. ^{1}H NMR (600 MHz, $CDCl_3$) of **29**

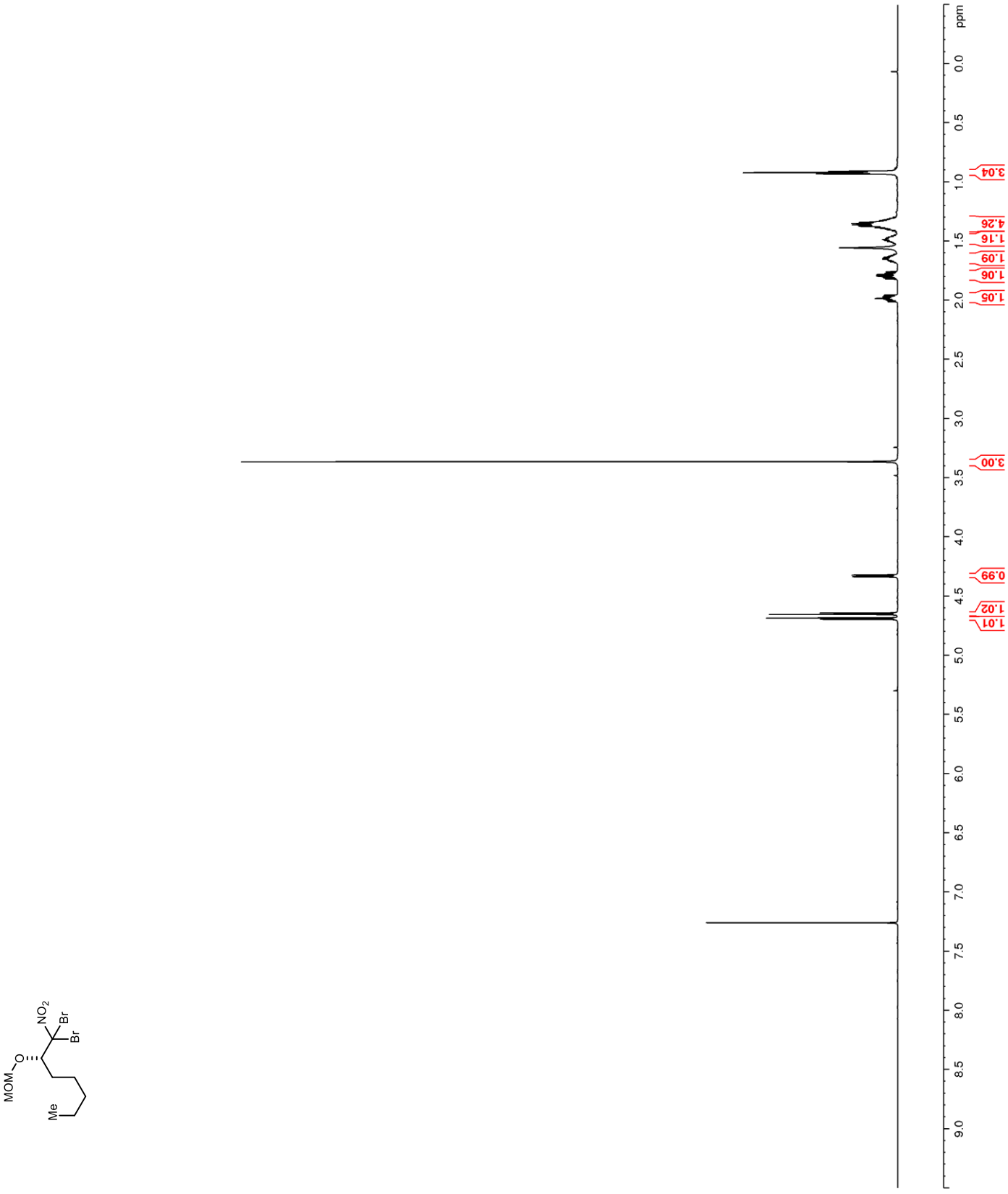

Figure 6. ^{13}C NMR (150 MHz, $CDCl_3$) of **29**

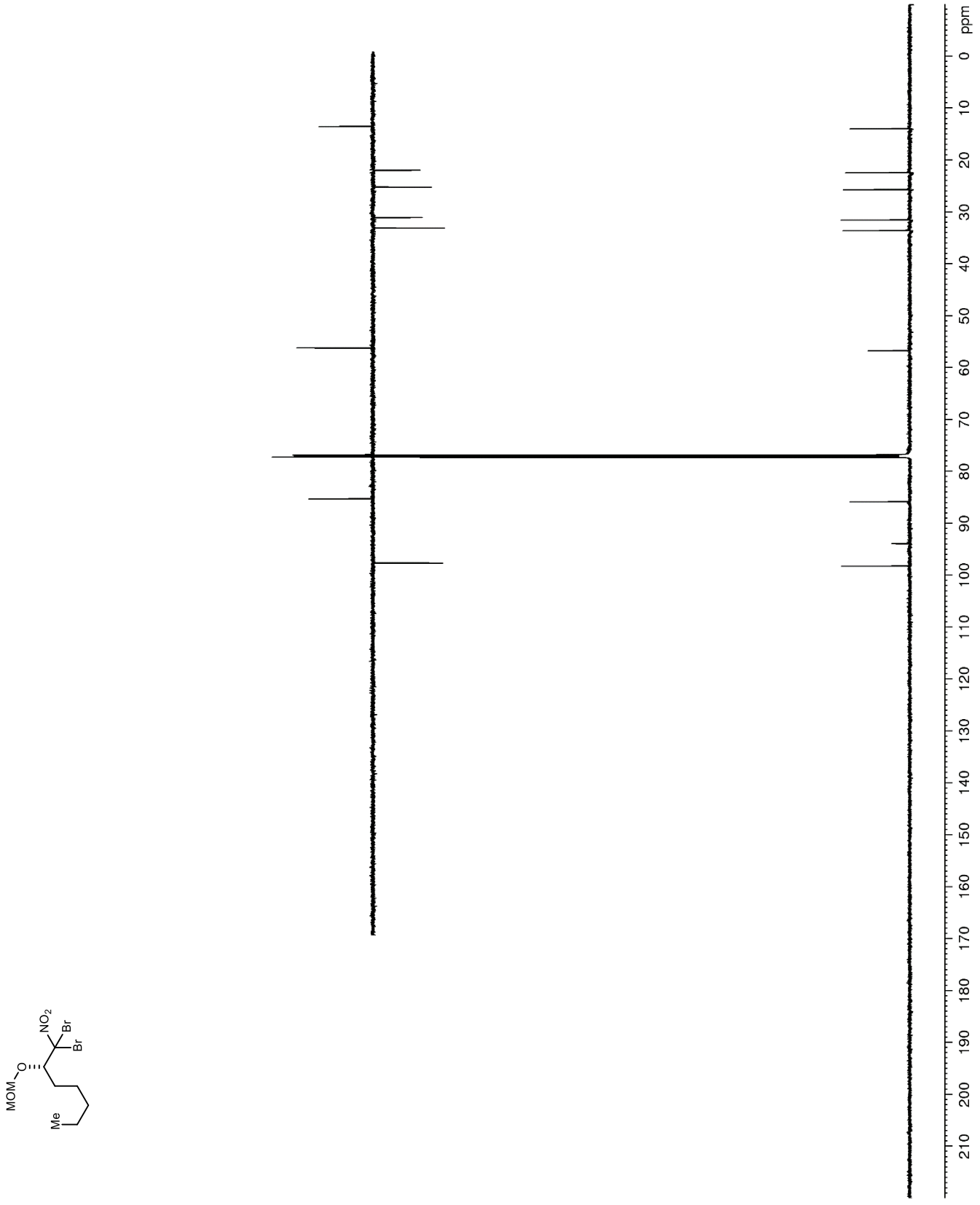

Figure 7. ^{1}H NMR (600 MHz, $CDCl_3$) of **31**

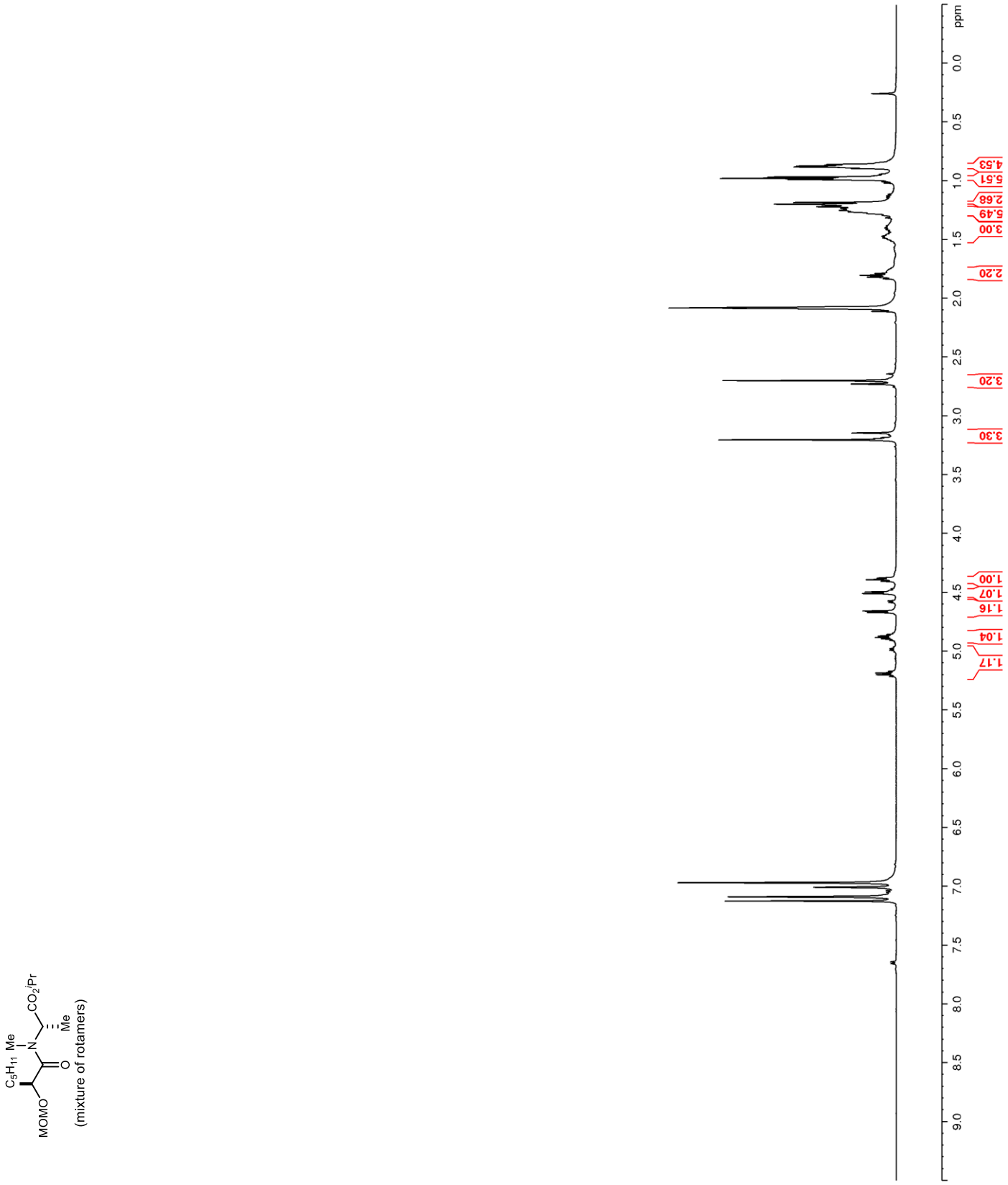

Figure 8. ^{13}C NMR (150 MHz, $CDCl_3$) of **31**

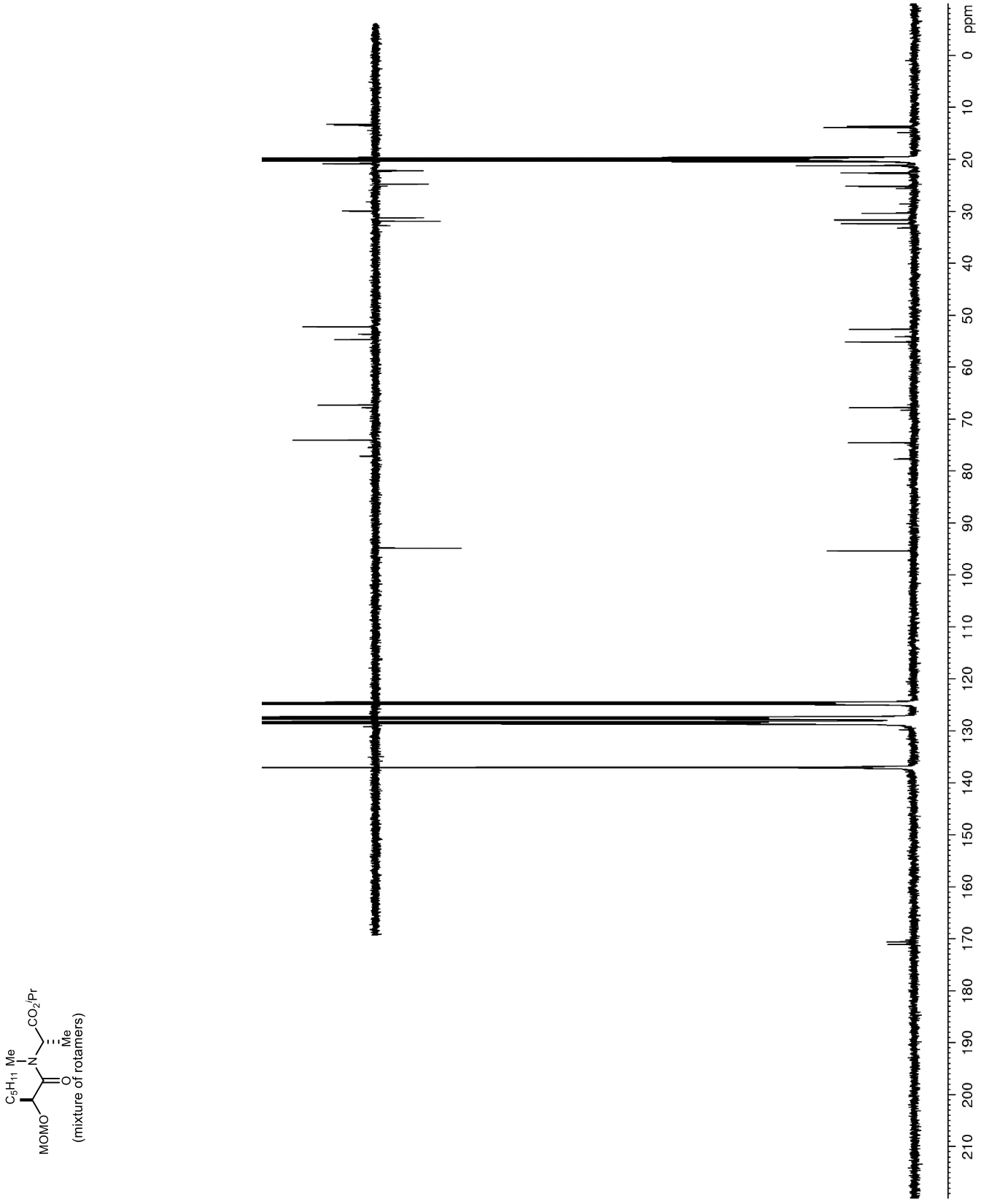

Figure 9. ^{1}H NMR (600 MHz, $CDCl_3$) of **33**

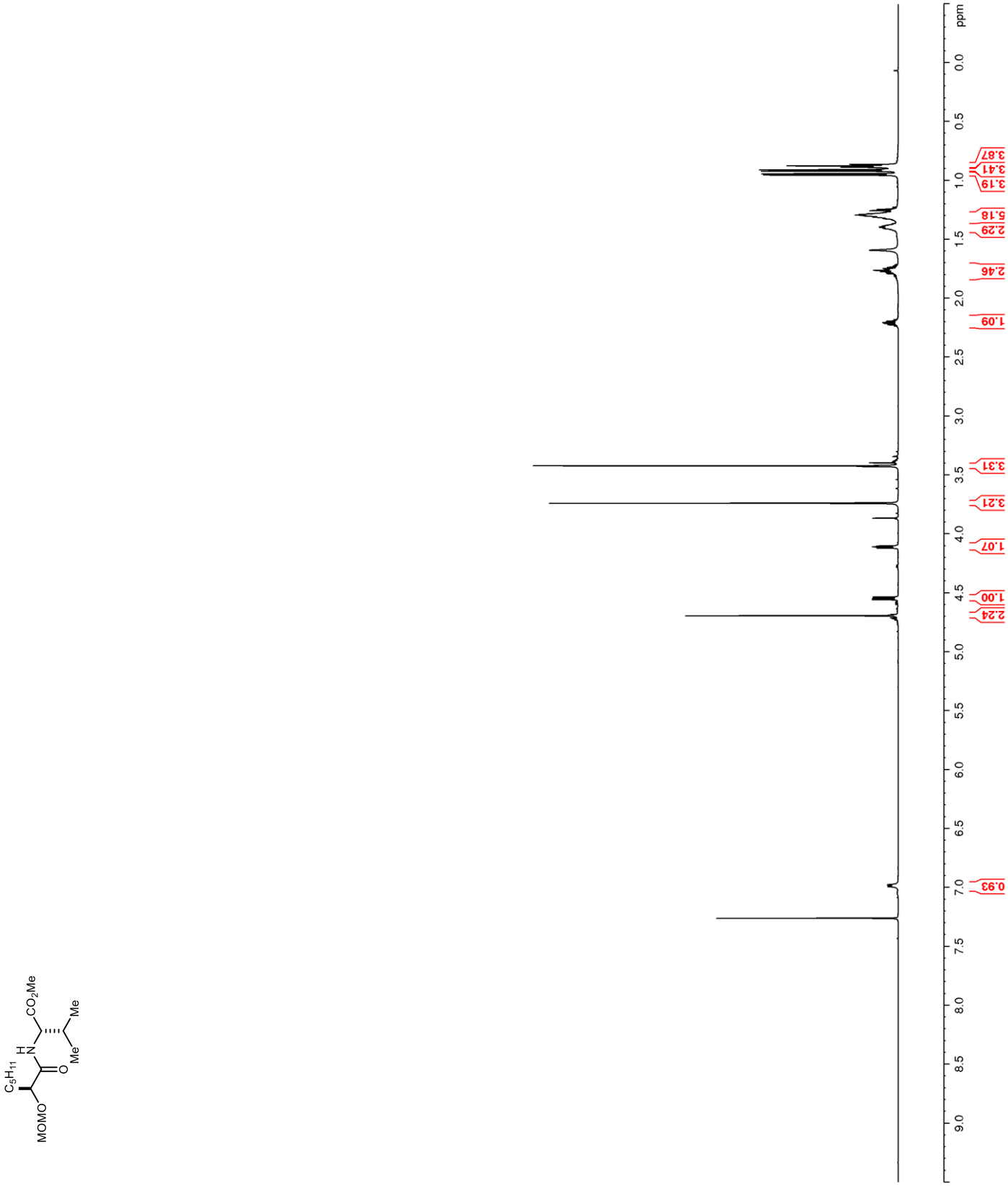

Figure 10. ^{13}C NMR (150 MHz, $CDCl_3$) of **33**

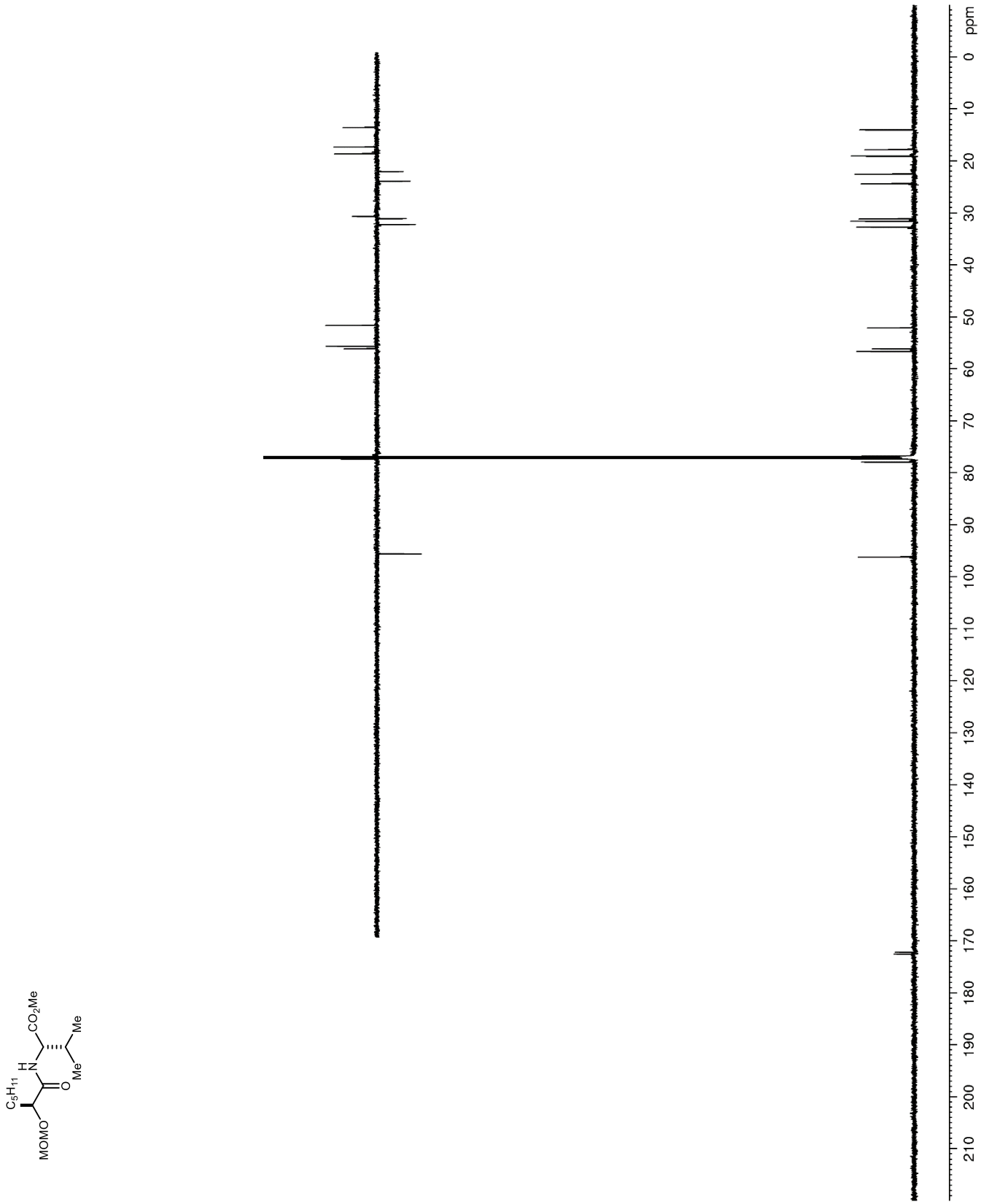

Figure 11. ^{1}H NMR (500 MHz, $CDCl_3$) of **36**

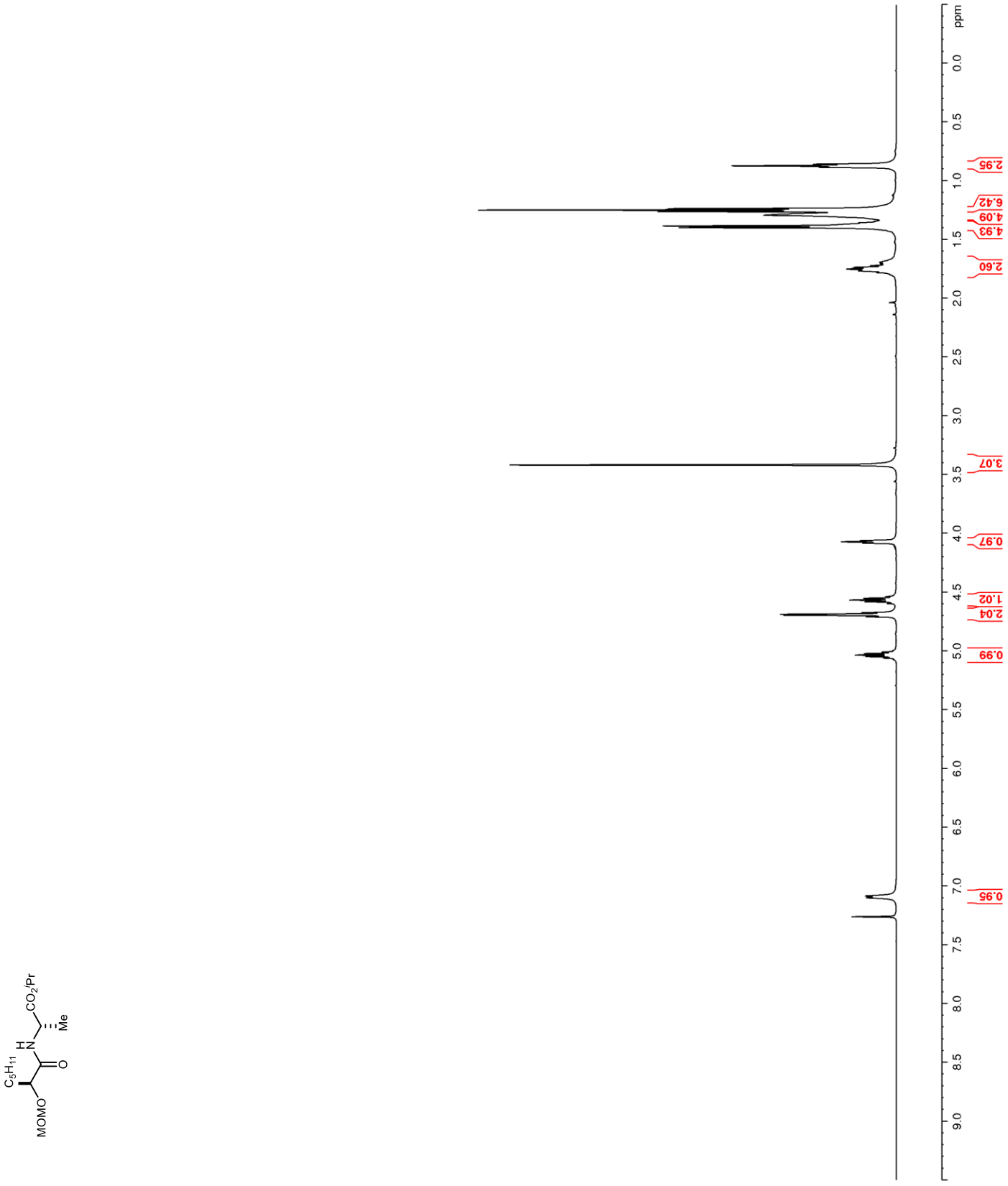

Figure 12. ^{13}C NMR (125 MHz, $CDCl_3$) of **36**

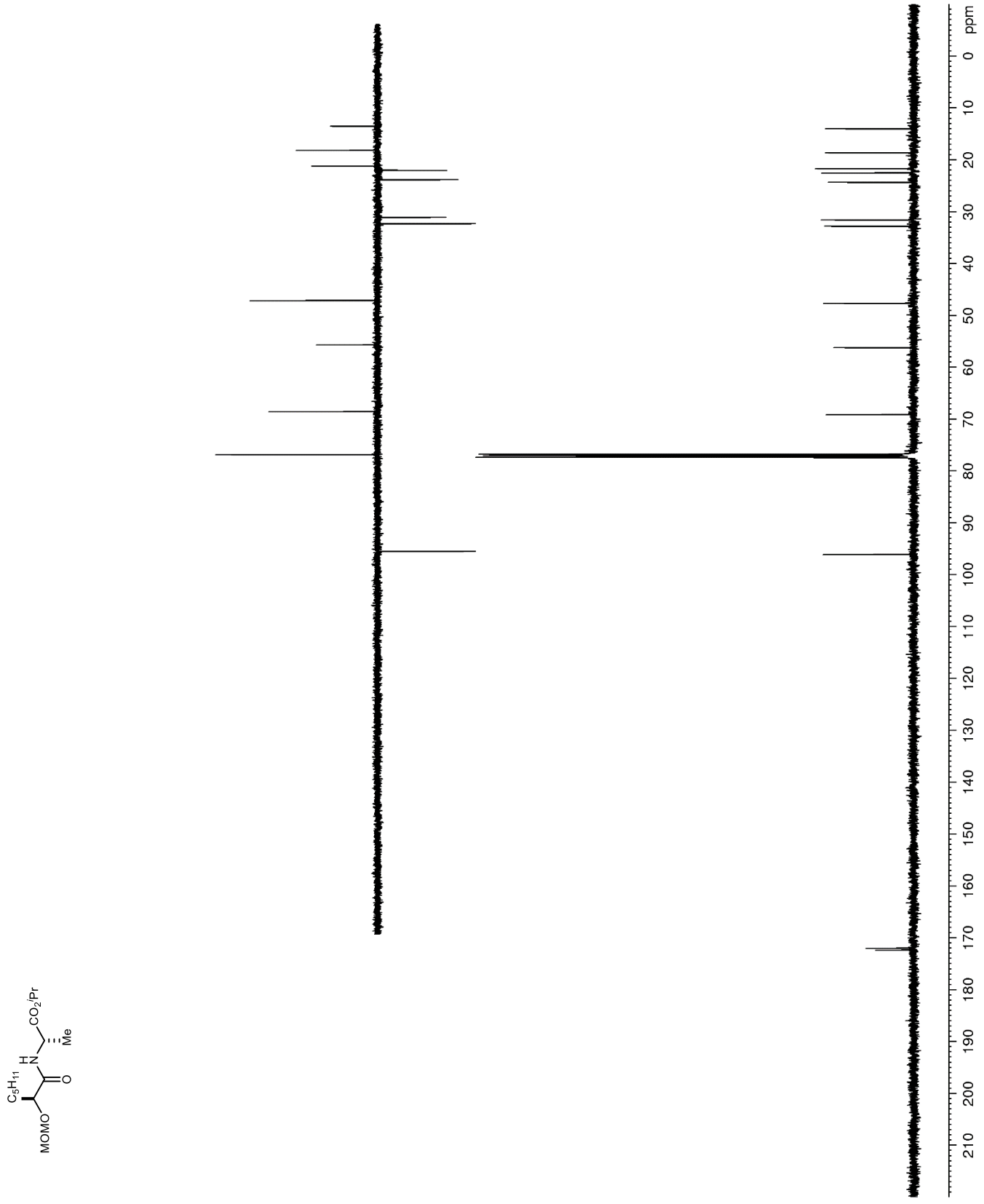

Figure 13. ^{1}H NMR (600 MHz, $CDCl_3$) of **37**

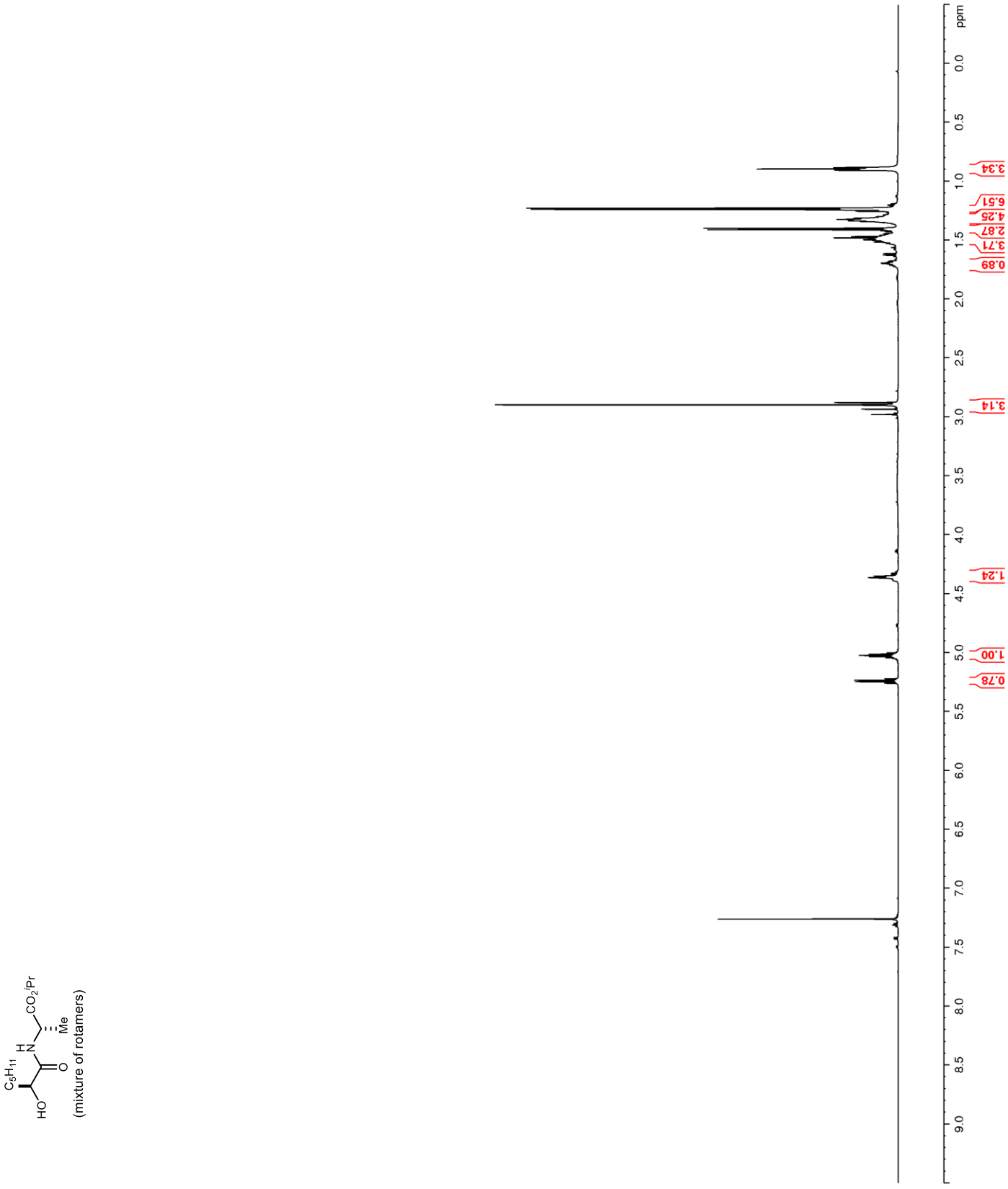

Figure 14. ^{13}C NMR (150 MHz, $CDCl_3$) of **37**

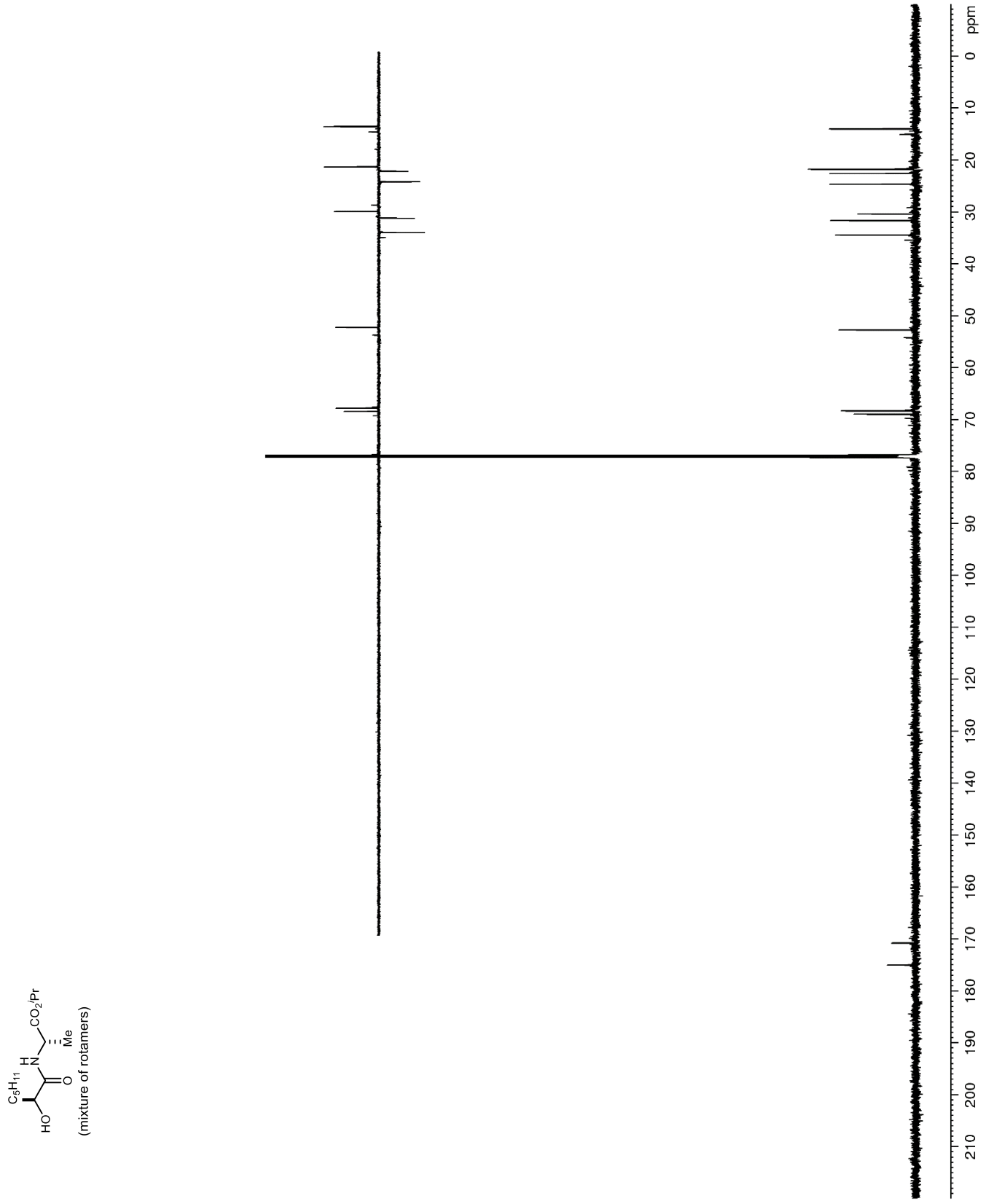

Figure 15. ^{1}H NMR (600 MHz, $CDCl_3$) of **38**

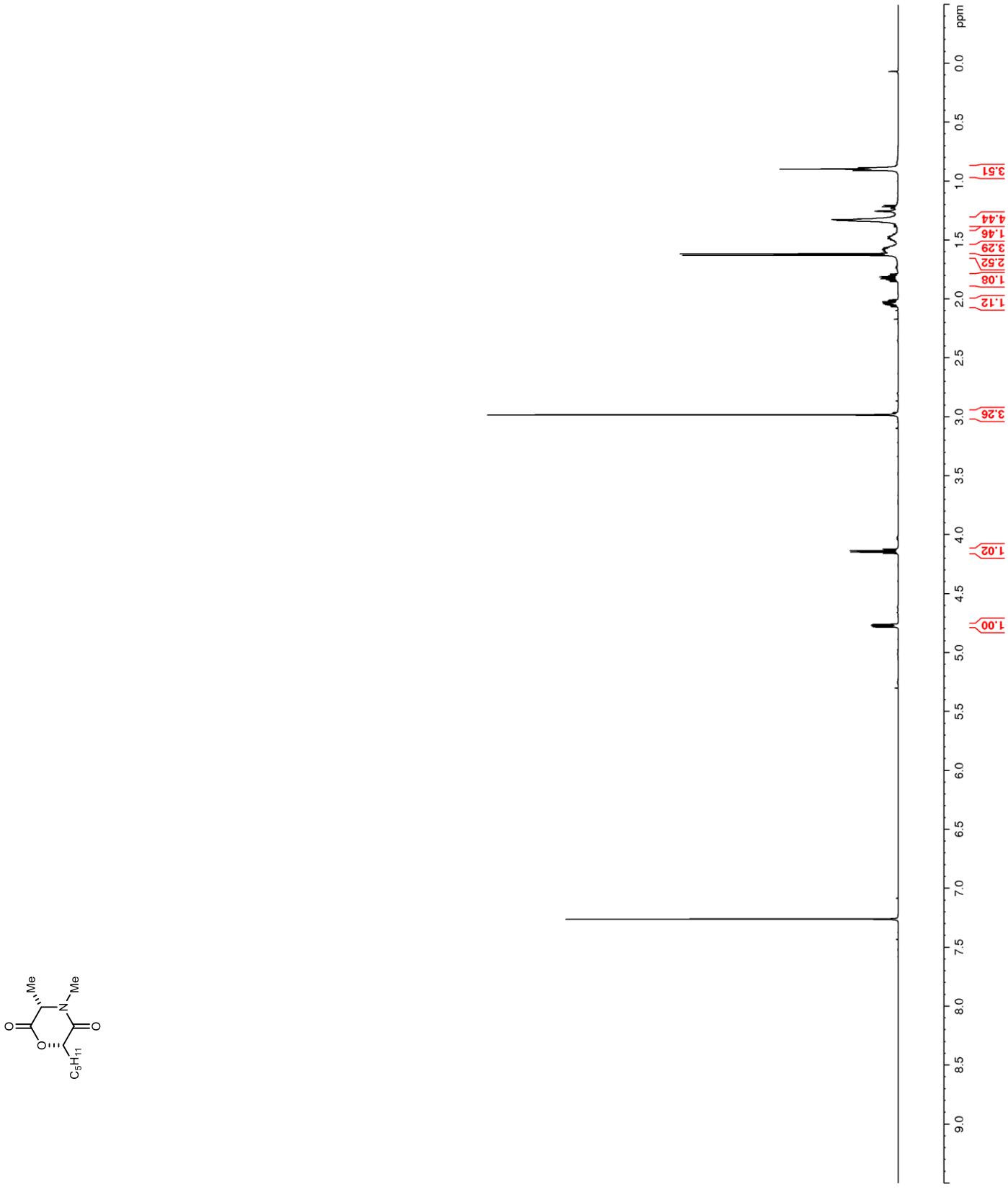

Figure 16. ^{13}C NMR (150 MHz, $CDCl_3$) of **38**

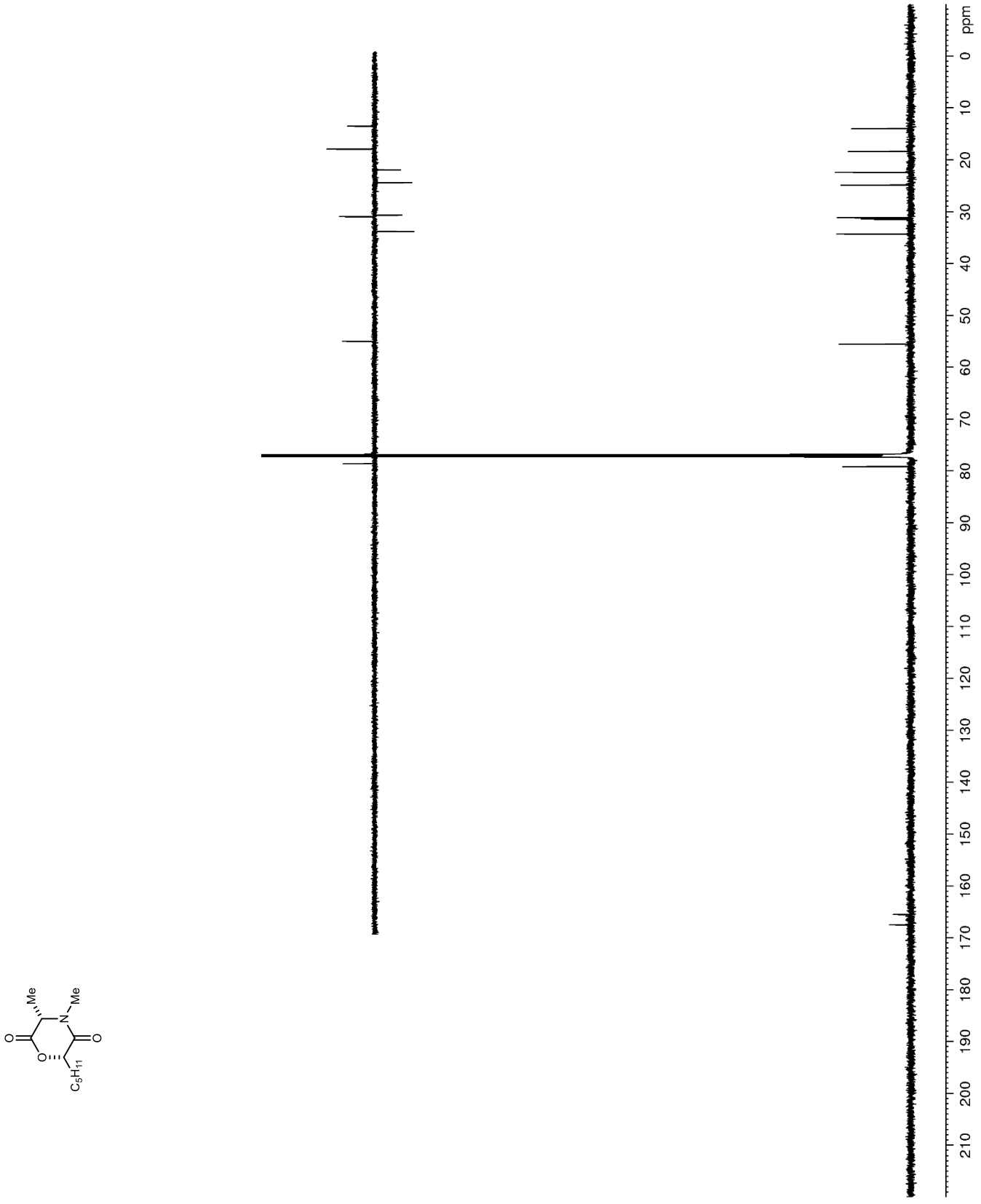

Figure 17. ^{1}H NMR (600 MHz, $CDCl_3$) of **39**

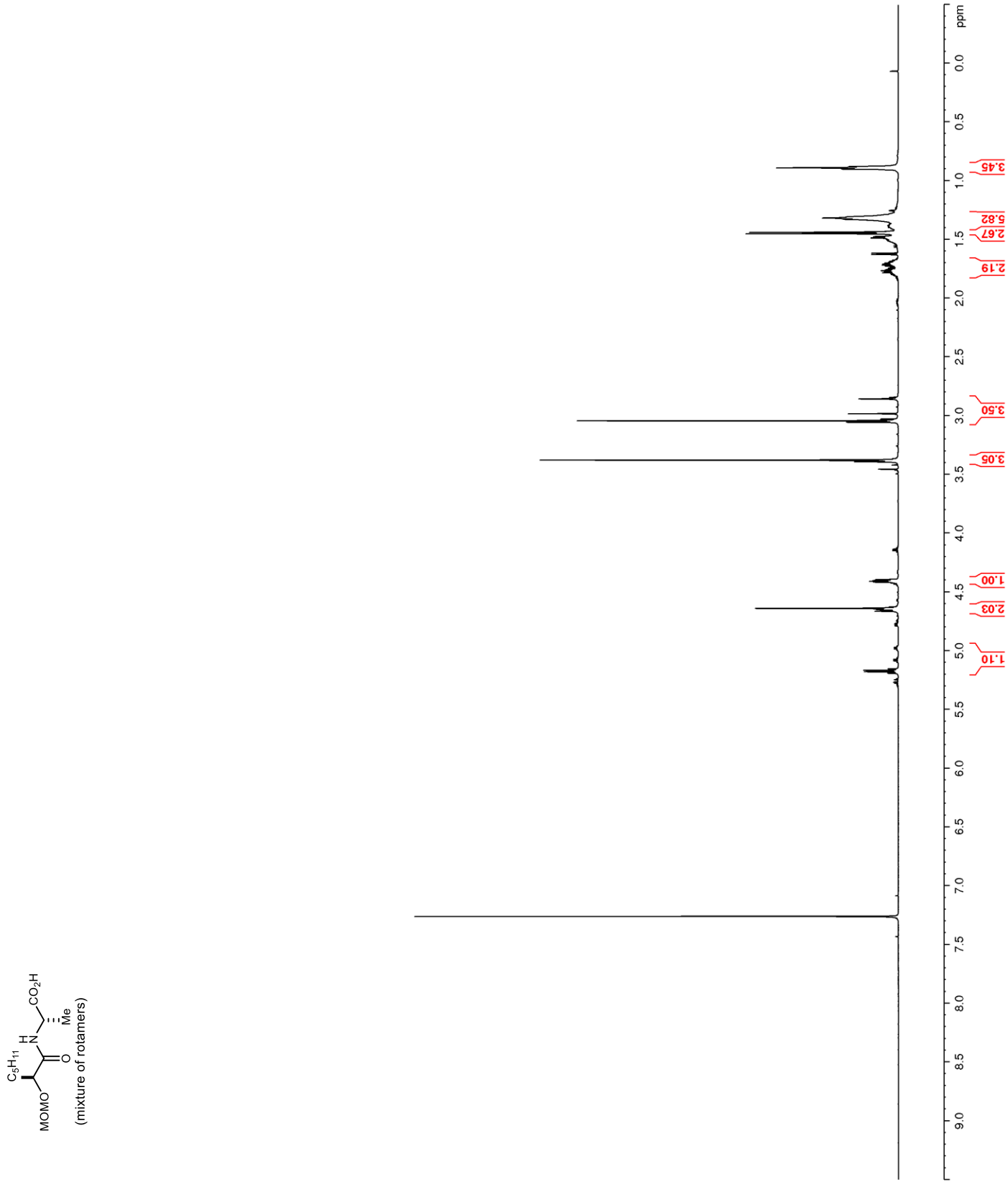

Figure 18. ^{13}C NMR (150 MHz, $CDCl_3$) of **39**

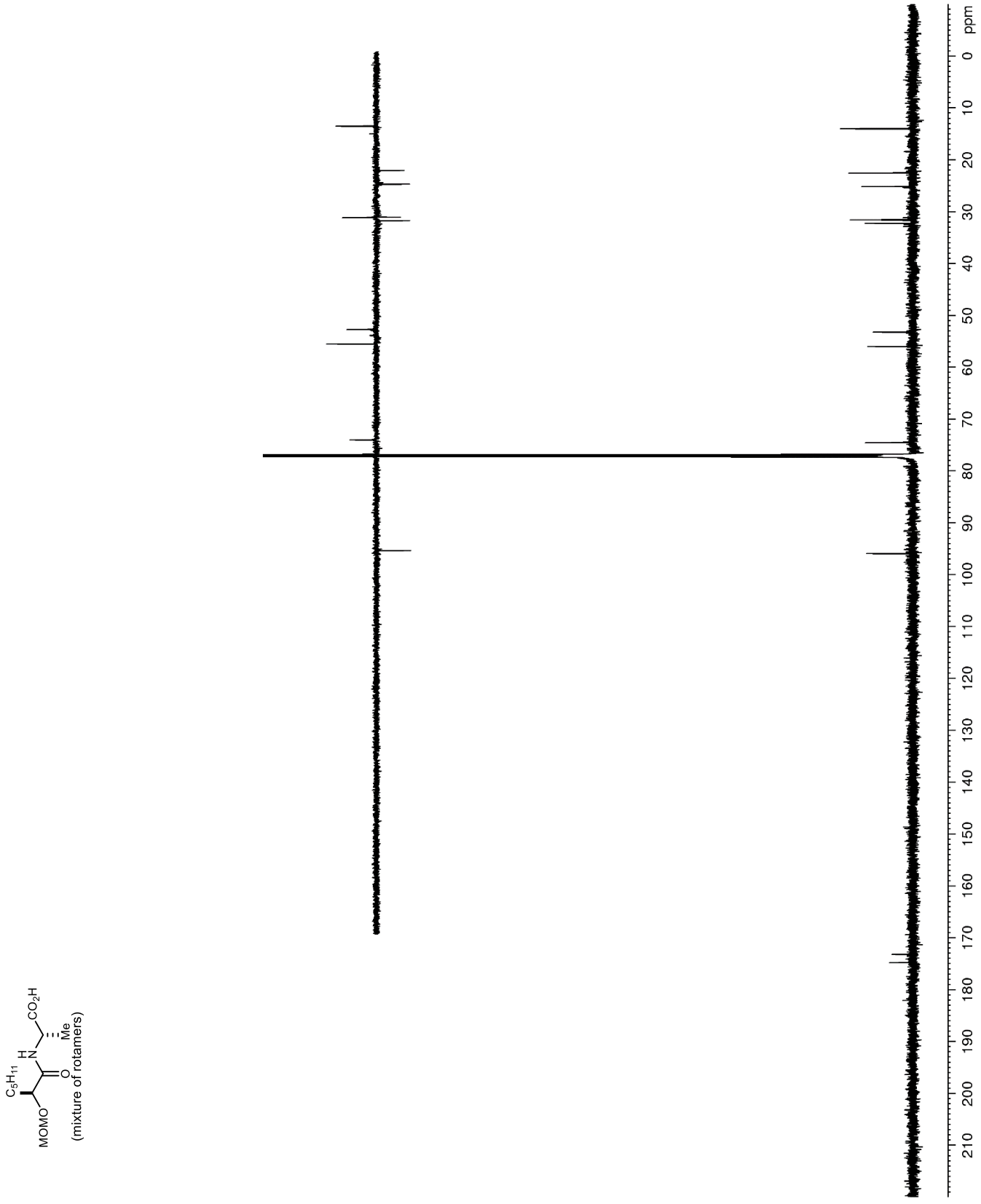

Figure 19. ^{1}H NMR (600 MHz, $CDCl_3$) of **40**

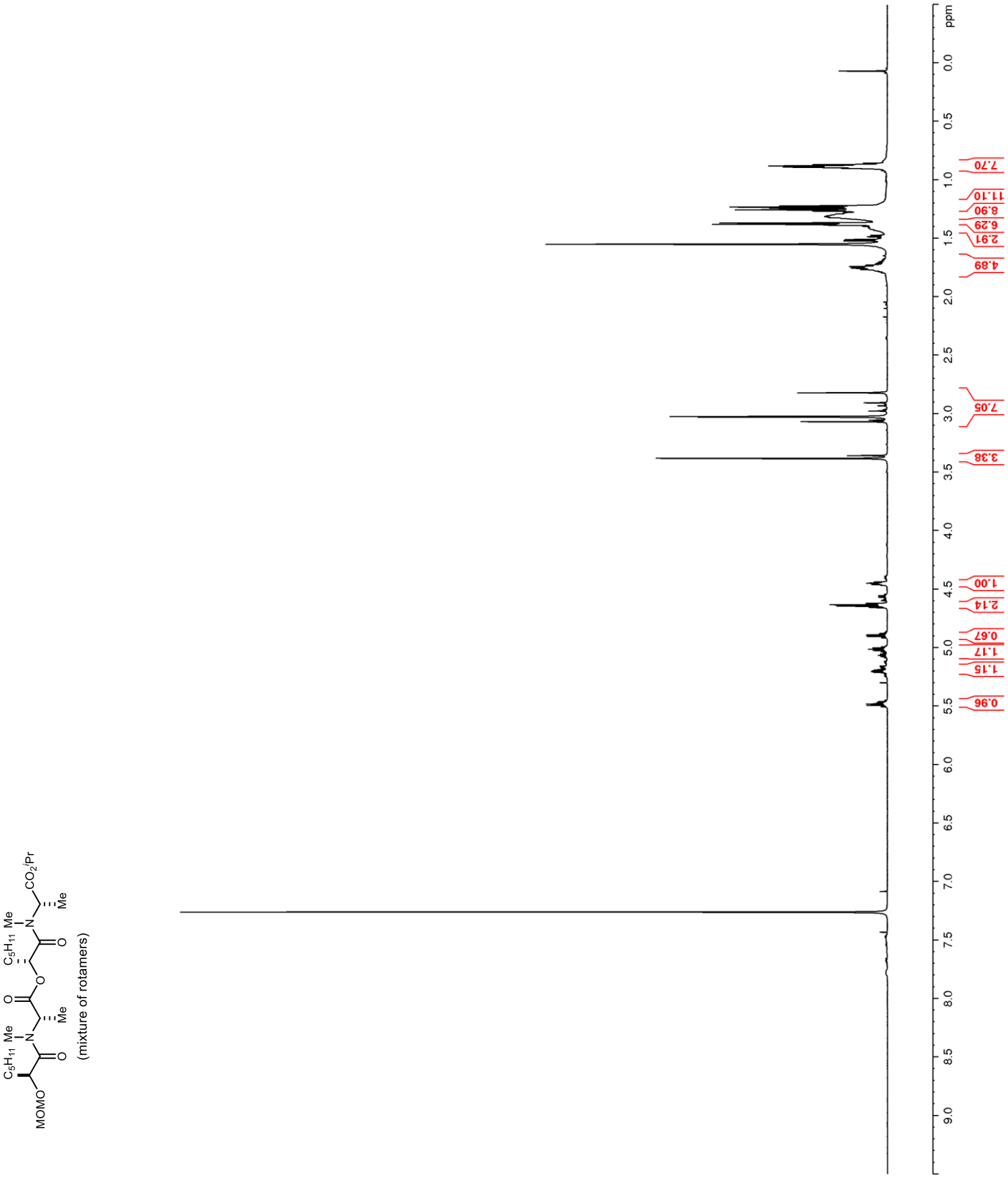

Figure 20. ^{13}C NMR (150 MHz, $CDCl_3$) of **40**

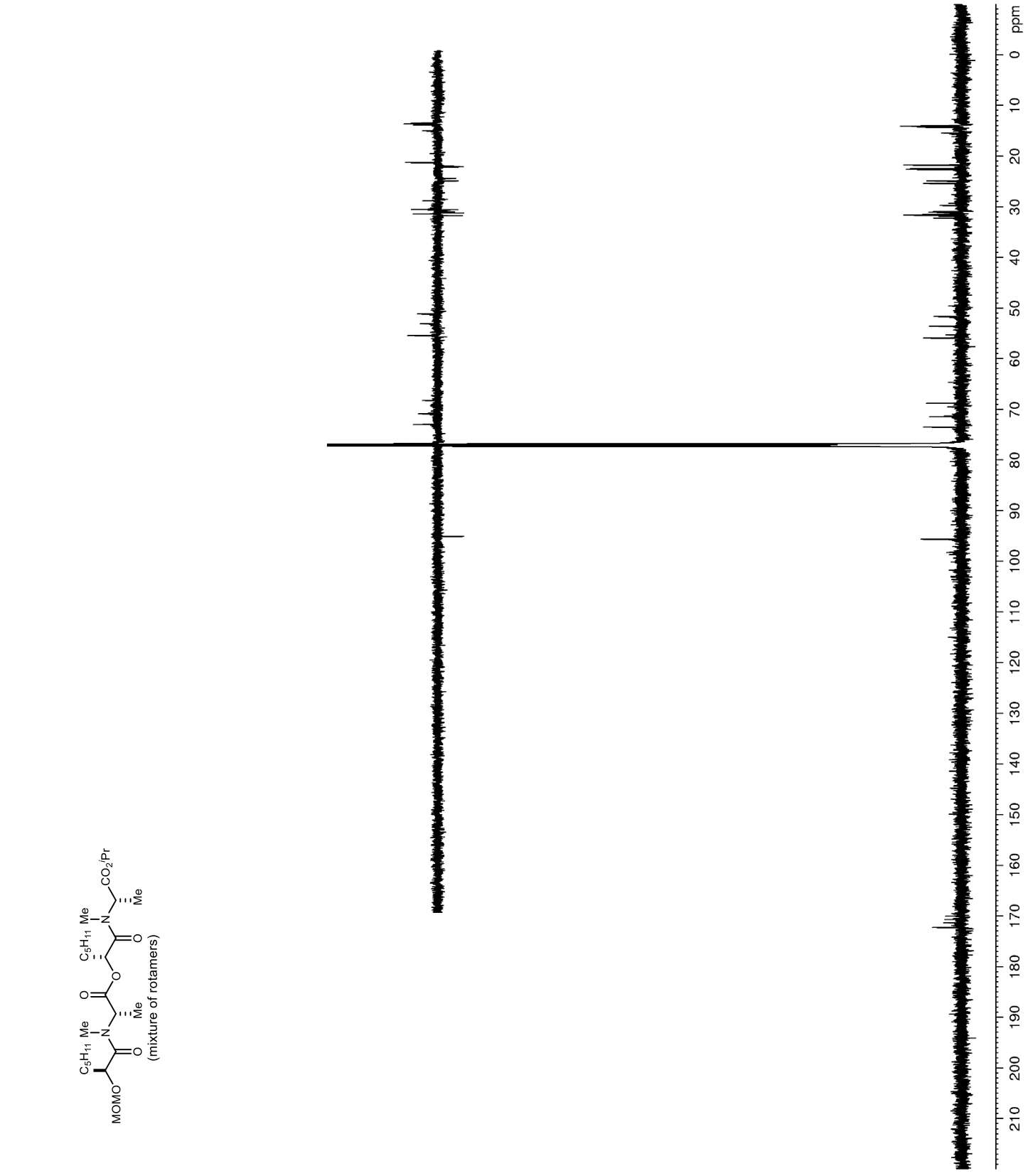

Figure 21. ^{1}H NMR (400 MHz, $CDCl_3$) of **45**

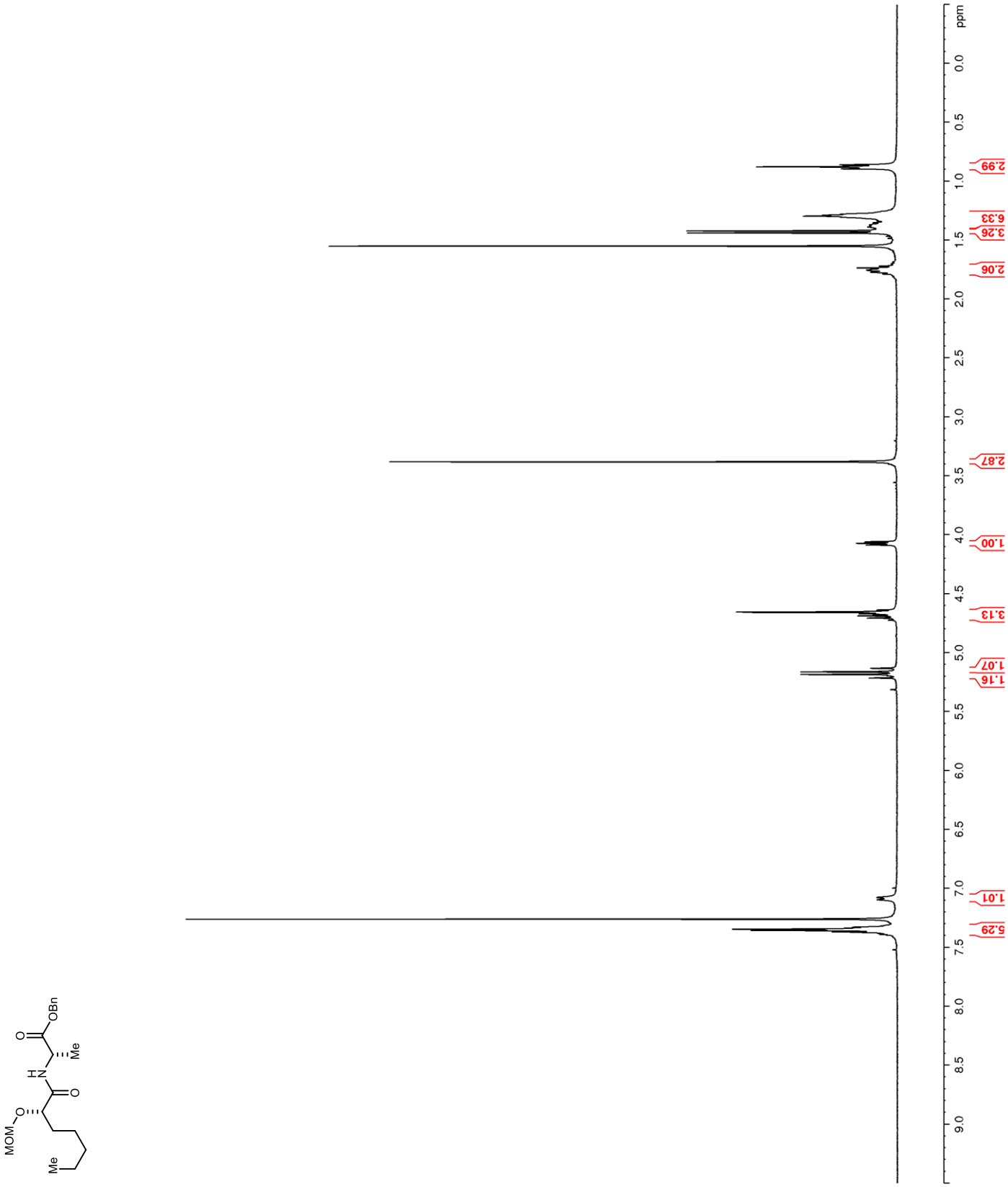

Figure 22. ^{13}C NMR (150 MHz, $CDCl_3$) of **45**

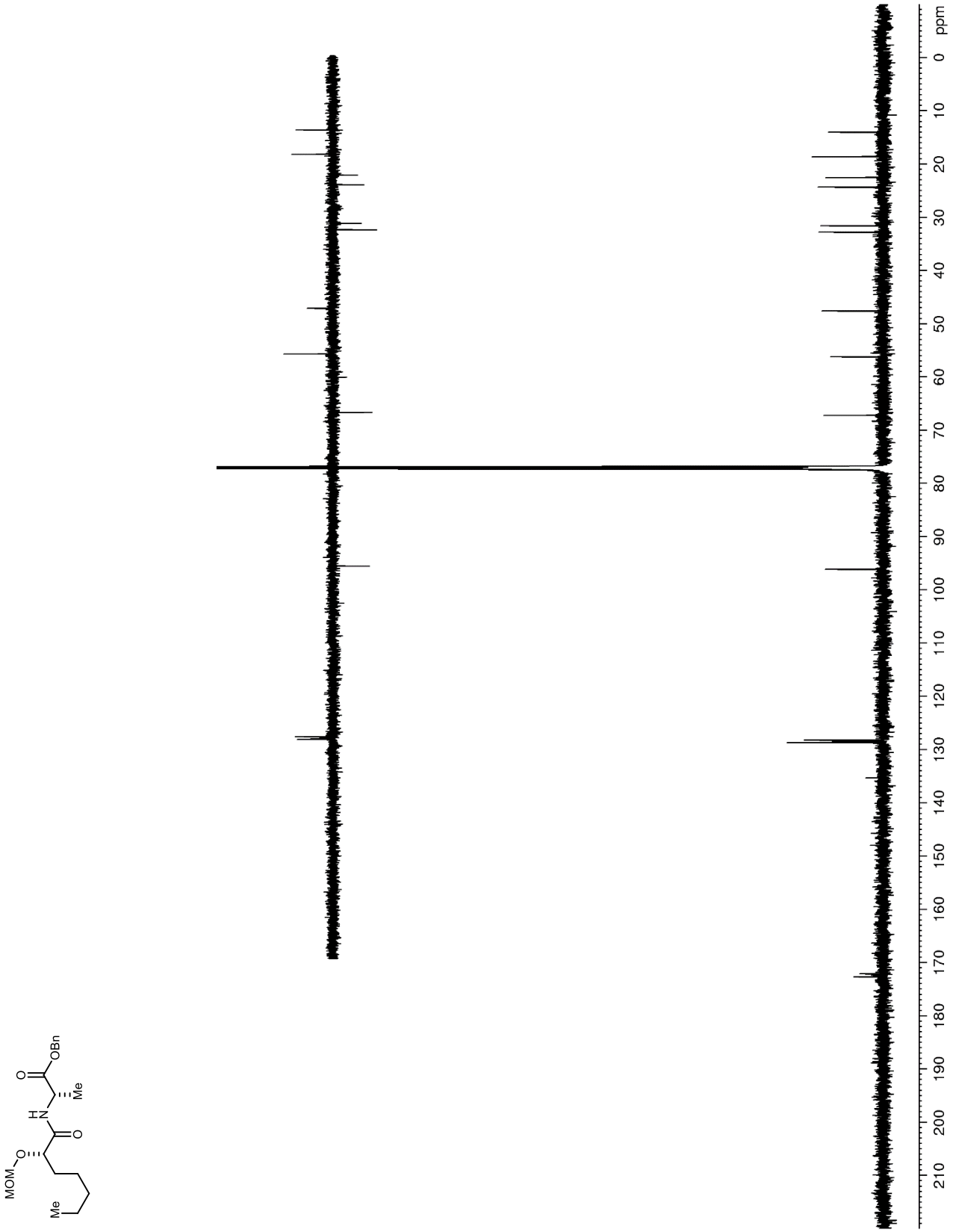

Figure 23. ^{1}H NMR (400 MHz, $CDCl_3$) of **46**

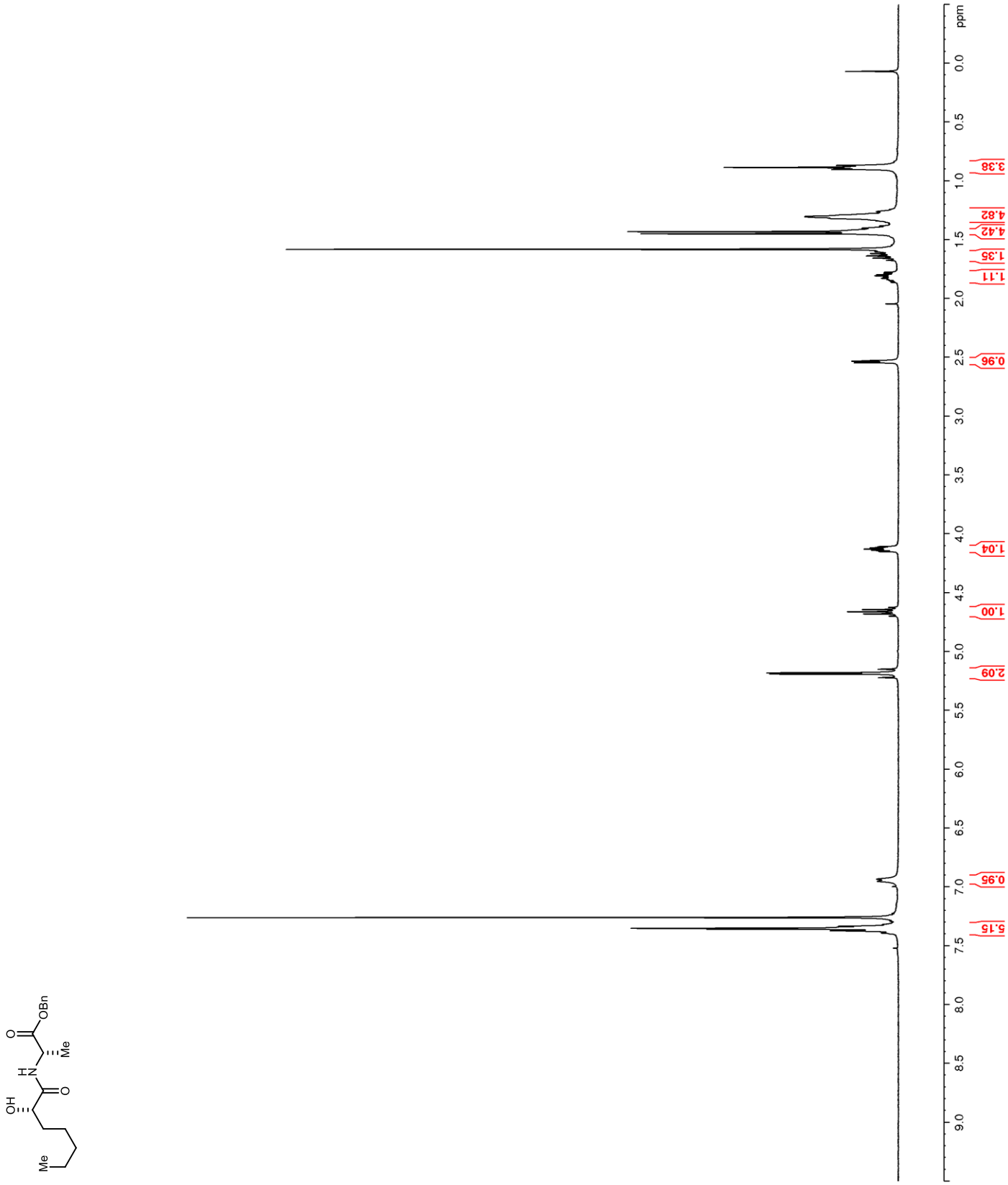

Figure 24. ^{13}C NMR (125 MHz, $CDCl_3$) of **46**

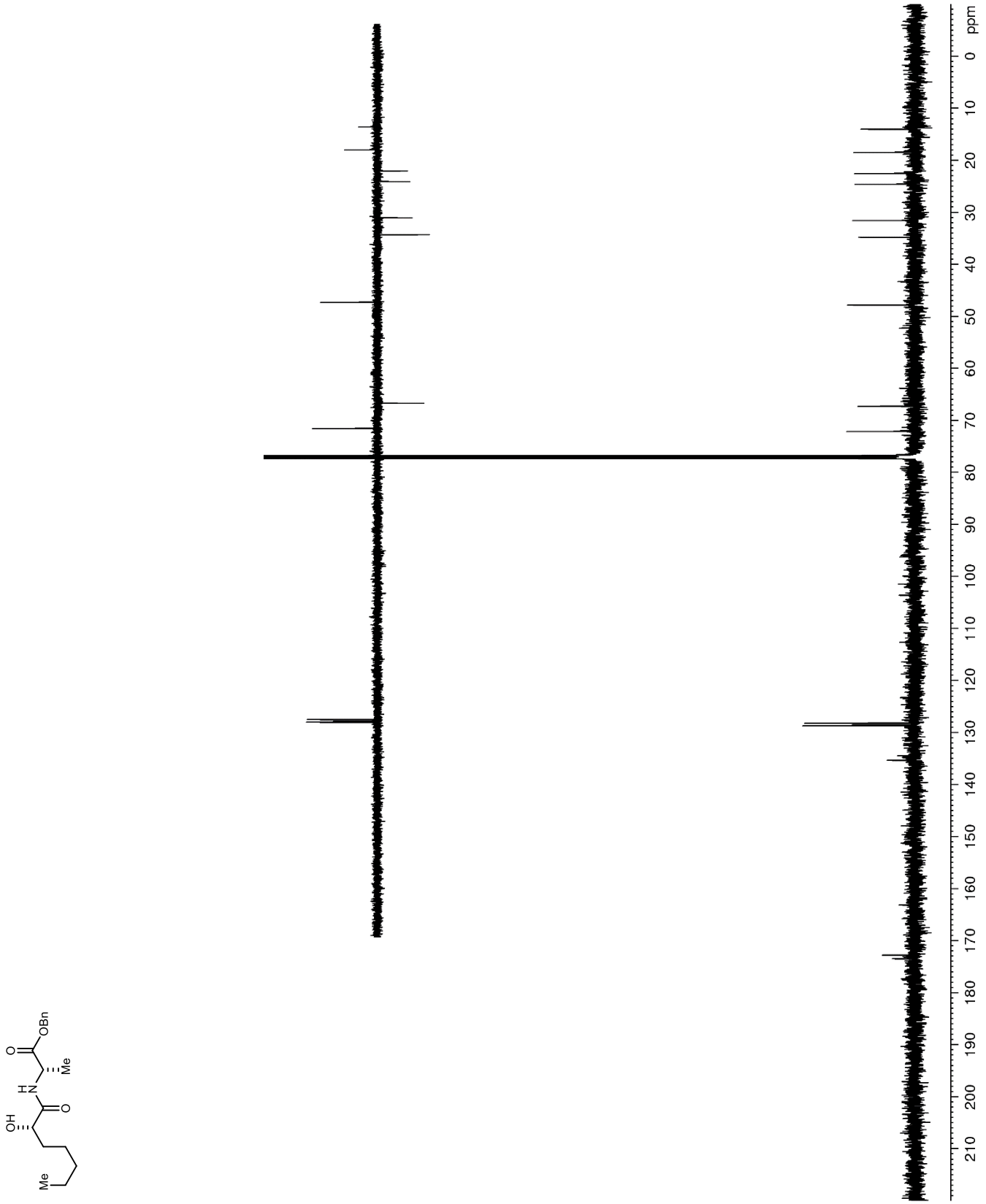

Figure 25. ^{1}H NMR (400 MHz, $CDCl_3$) of **47**

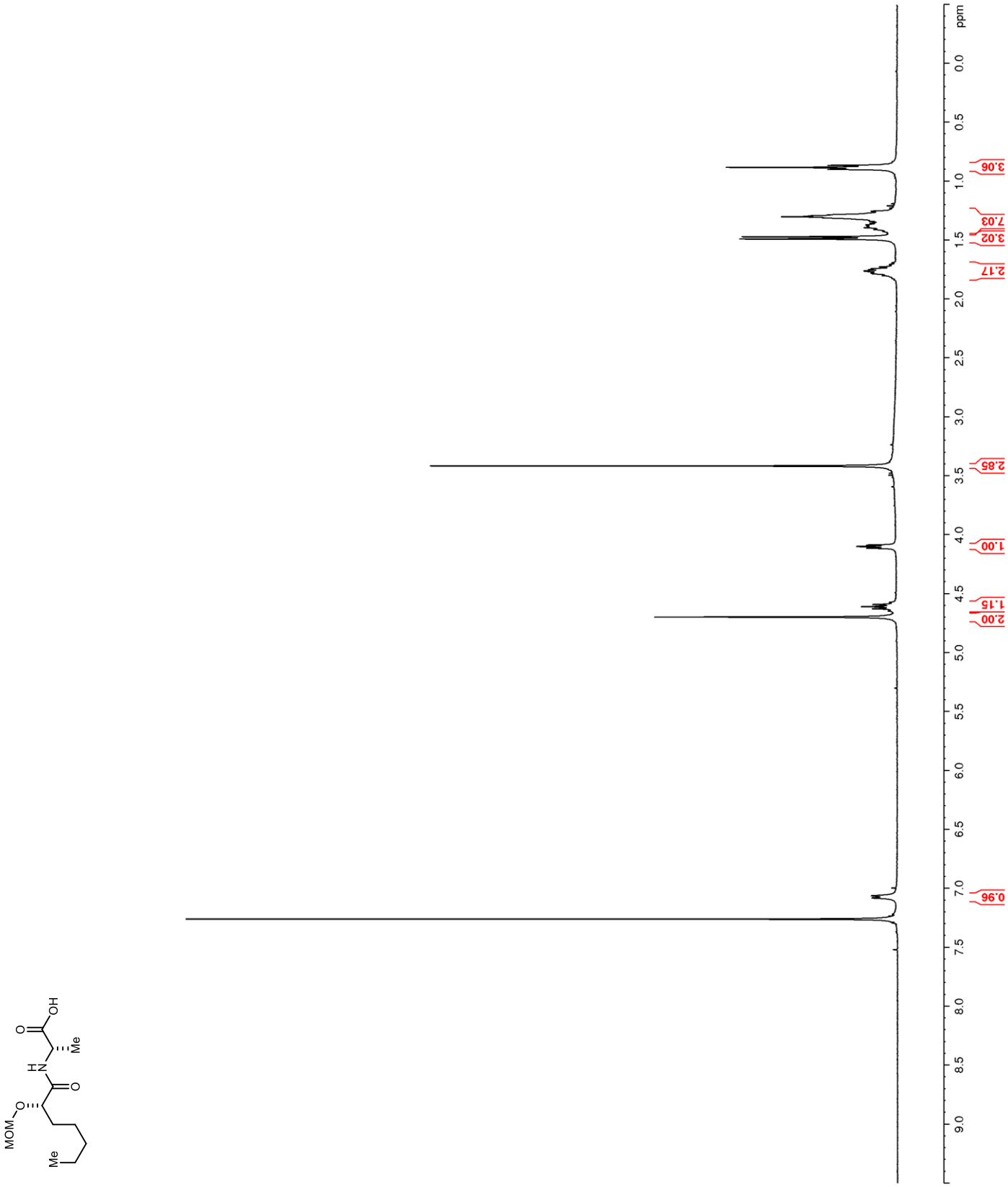

Figure 26. ^{13}C NMR (125 MHz, $CDCl_3$) of **47**

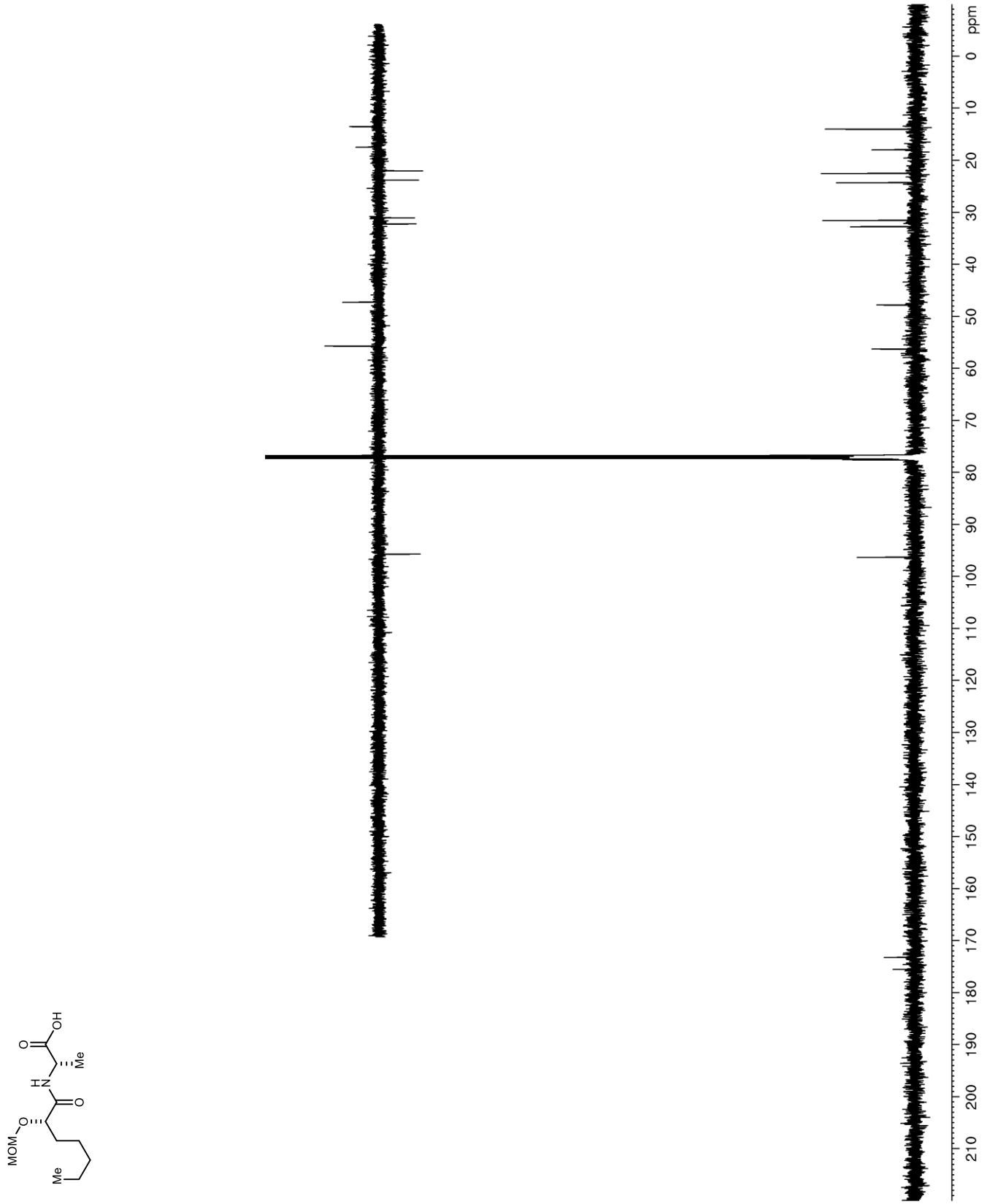

Figure 27. ^{1}H NMR (400 MHz, $CDCl_3$) of **48**

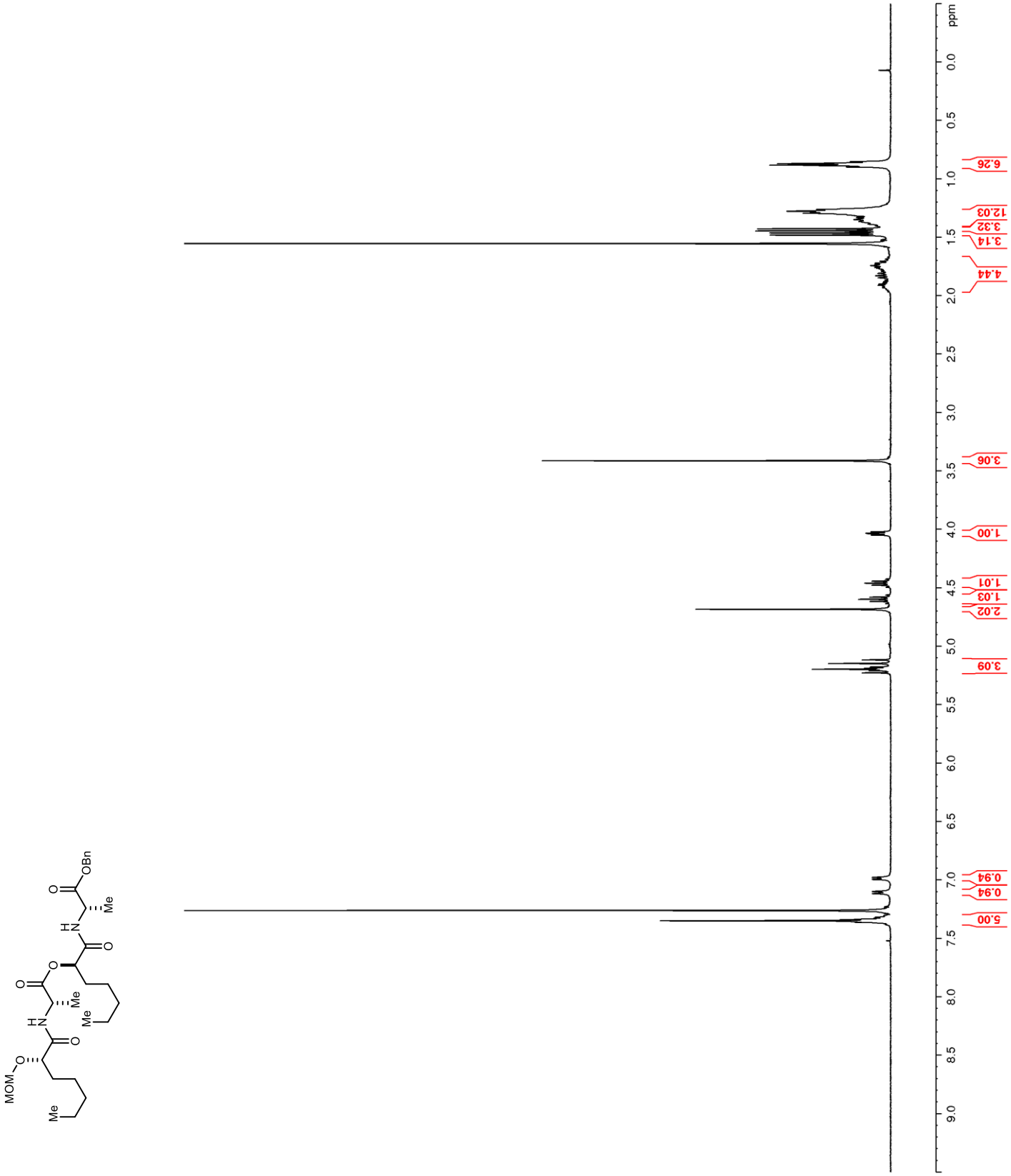

Figure 28. ^{13}C NMR (125 MHz, $CDCl_3$) of **48**

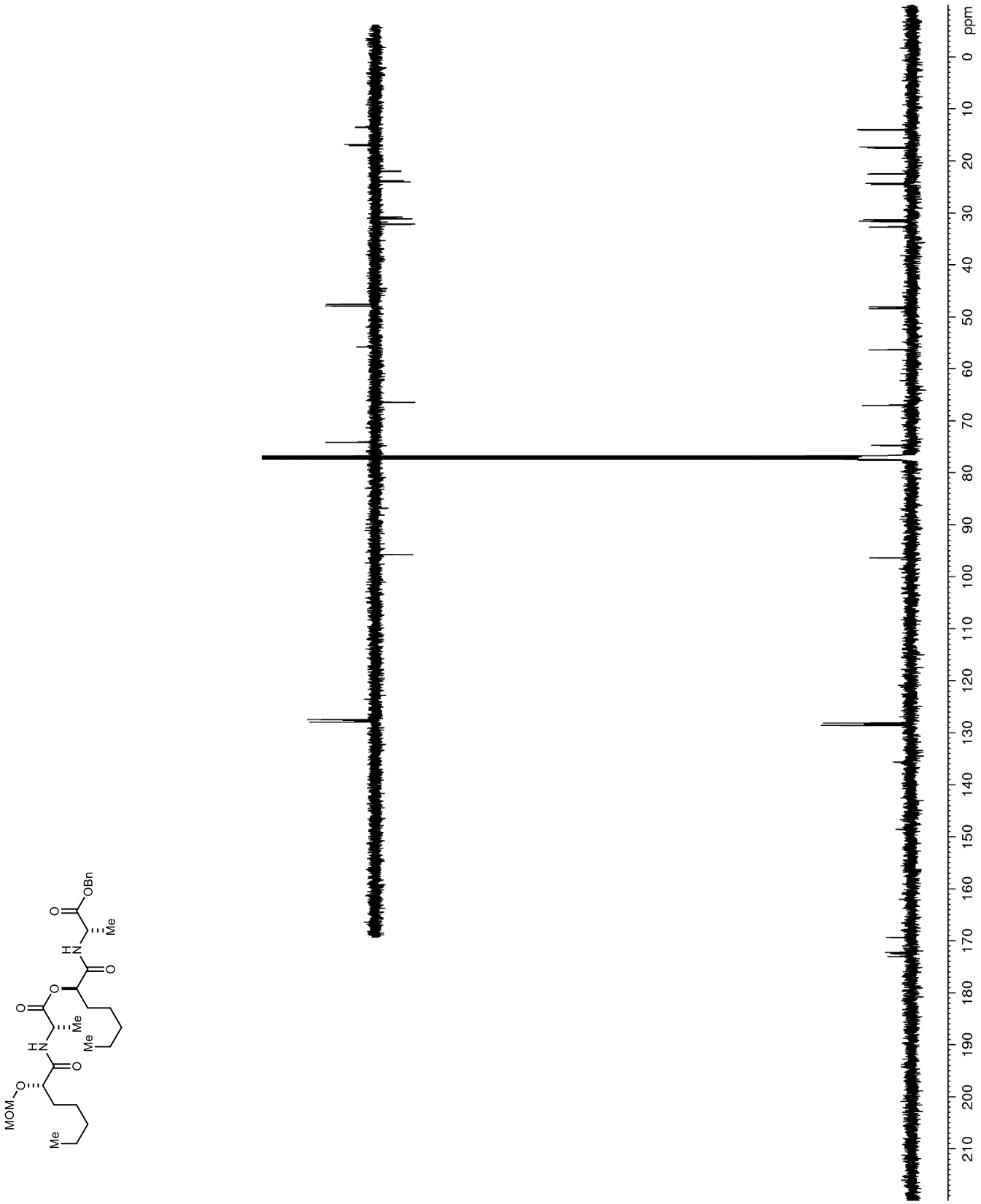

Figure 29. ^{1}H NMR (400 MHz, $CDCl_3$) of **49**

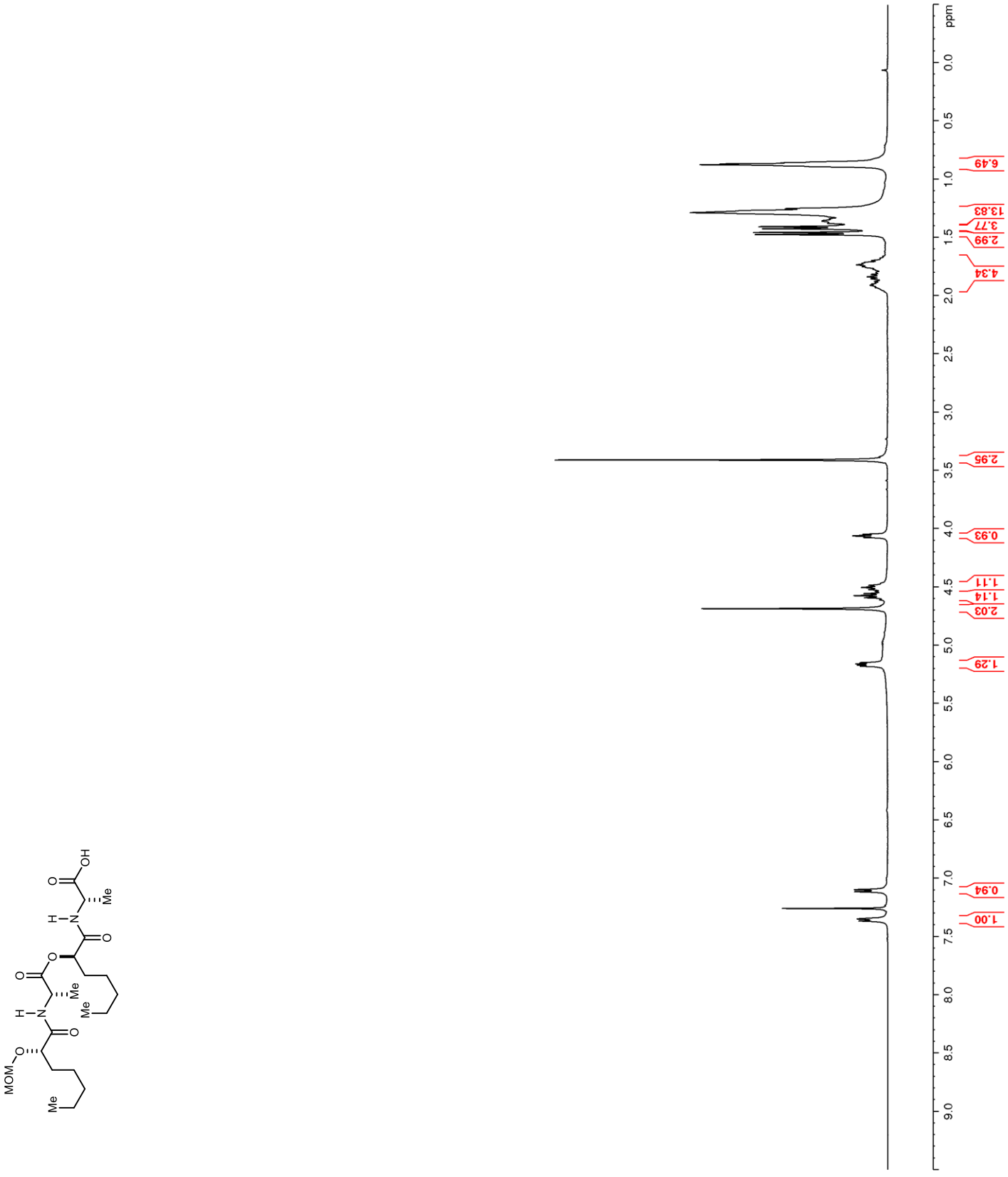

Figure 30. ^{13}C NMR (125 MHz, $CDCl_3$) of **49**

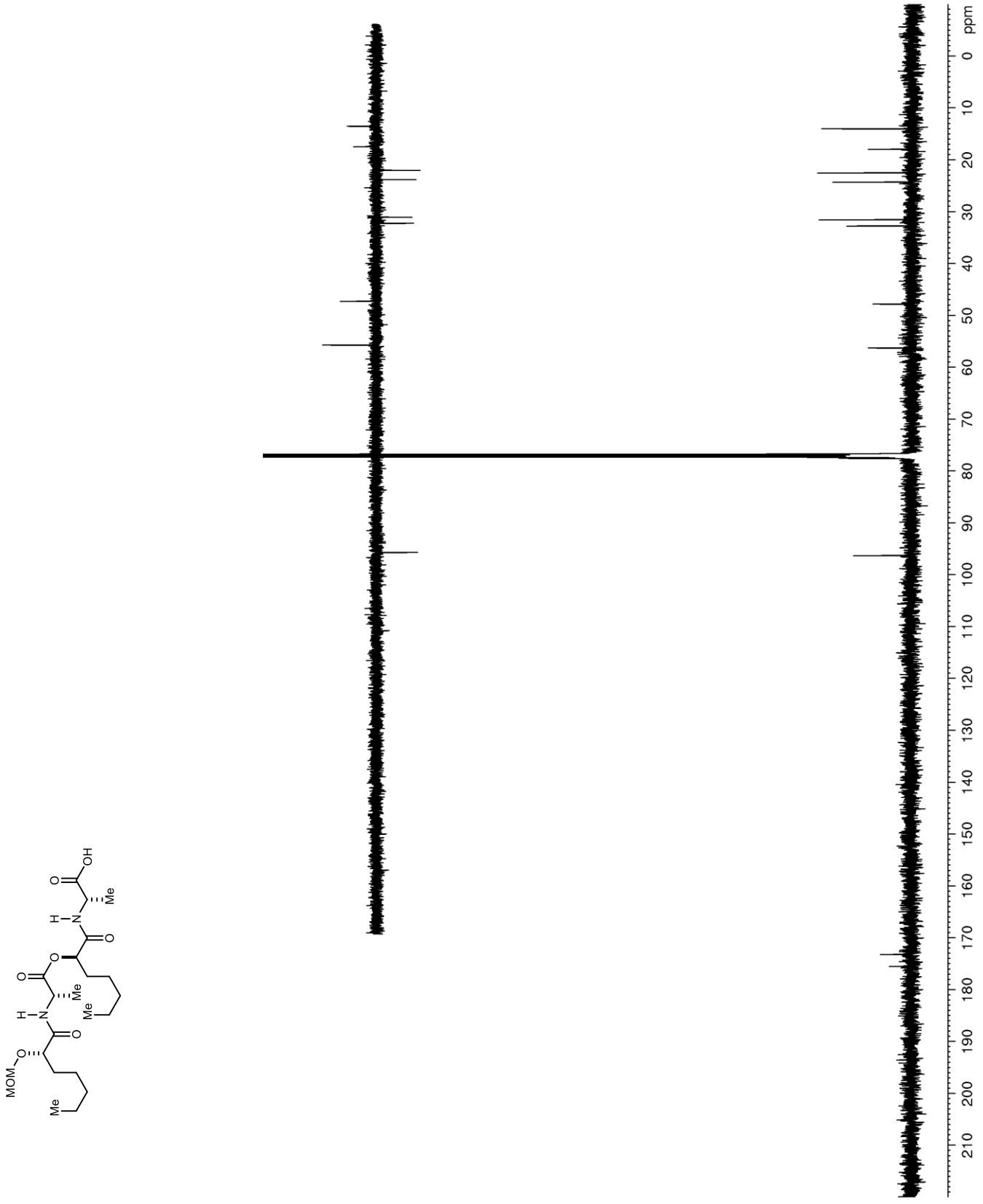

Figure 31. ^{1}H NMR (400 MHz, $CDCl_3$) of **50**

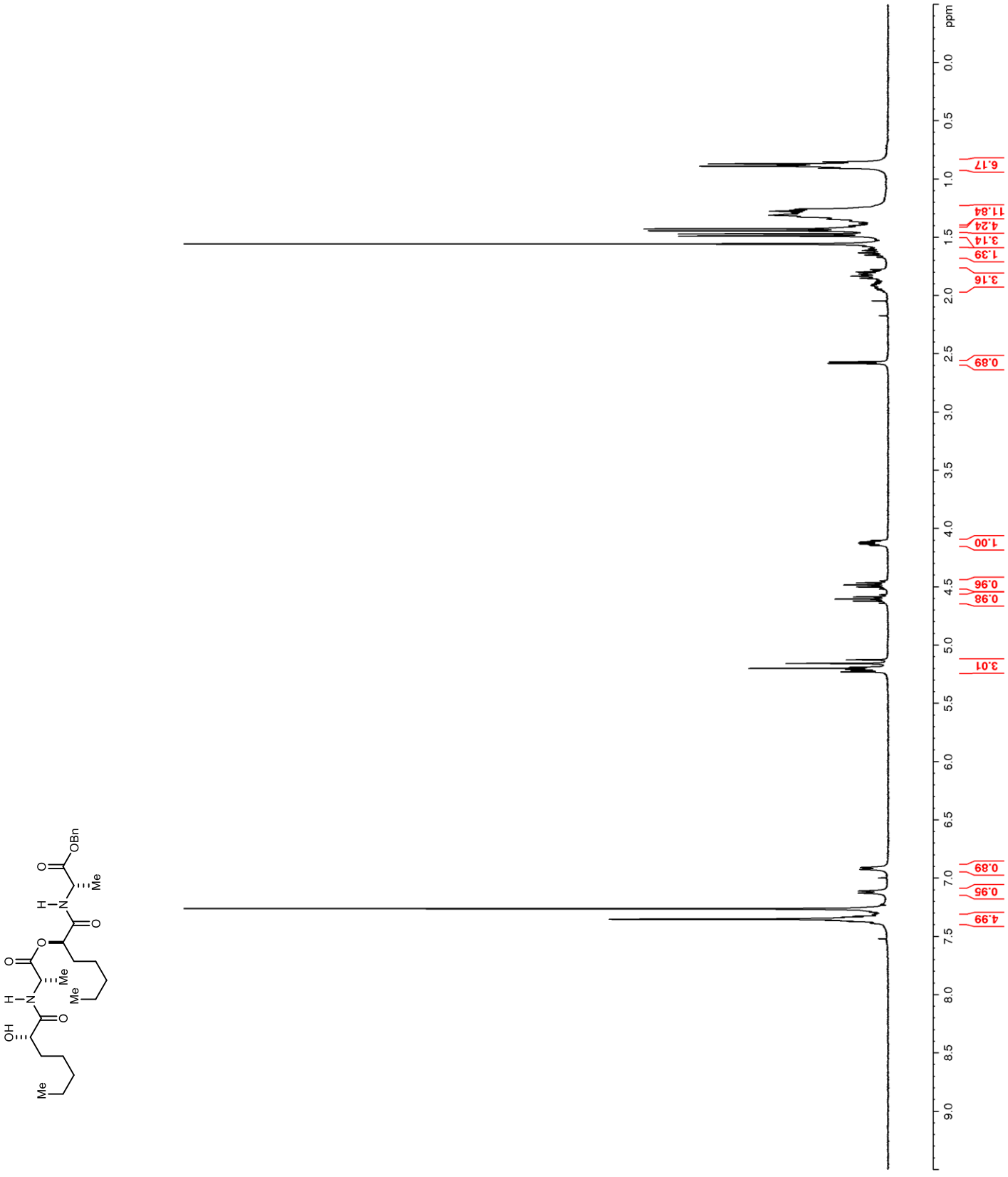

Figure 32. ^{13}C NMR (125 MHz, $CDCl_3$) of **50**

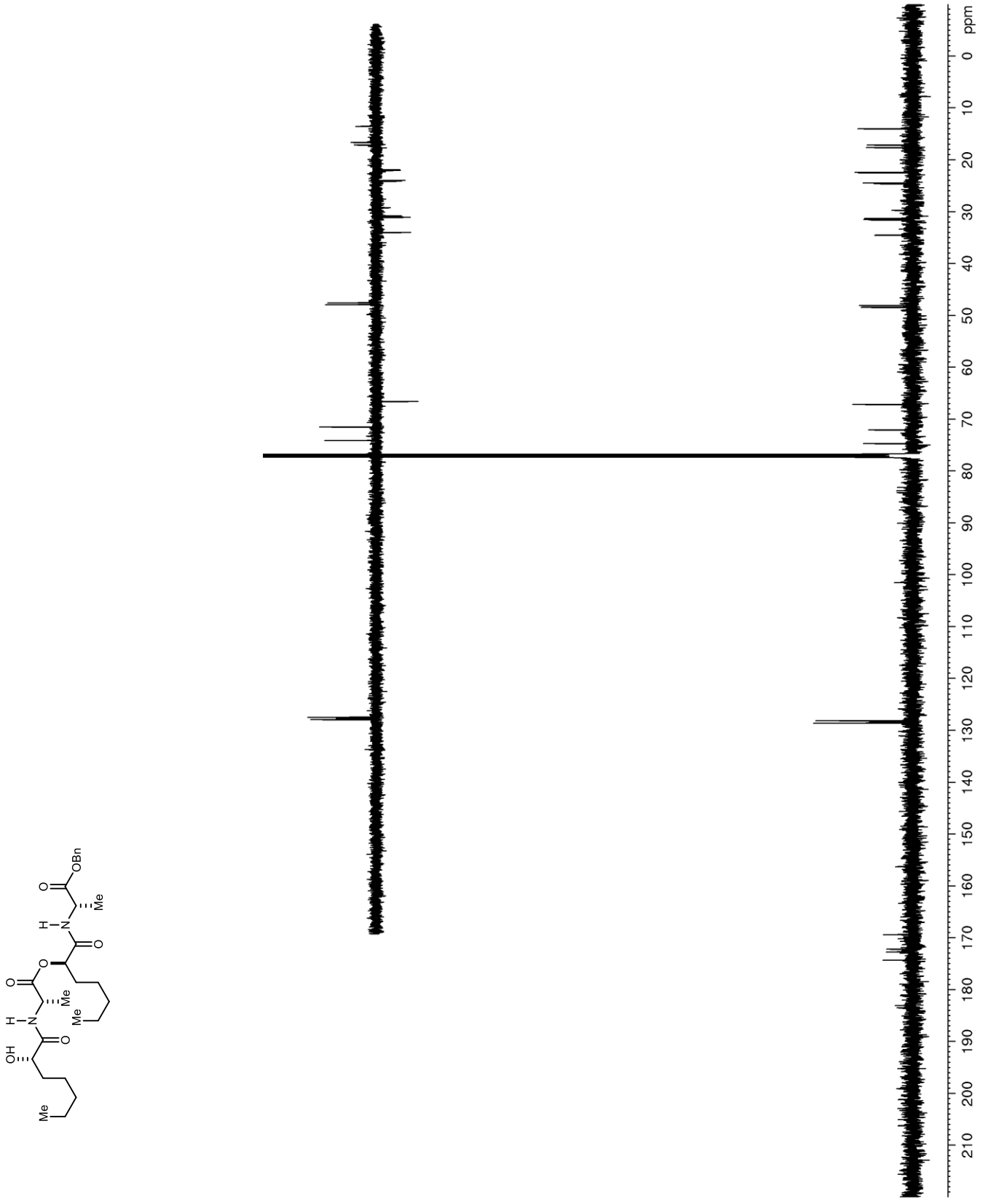

Figure 33. ^{1}H NMR (400 MHz, $CDCl_3$) of **51**

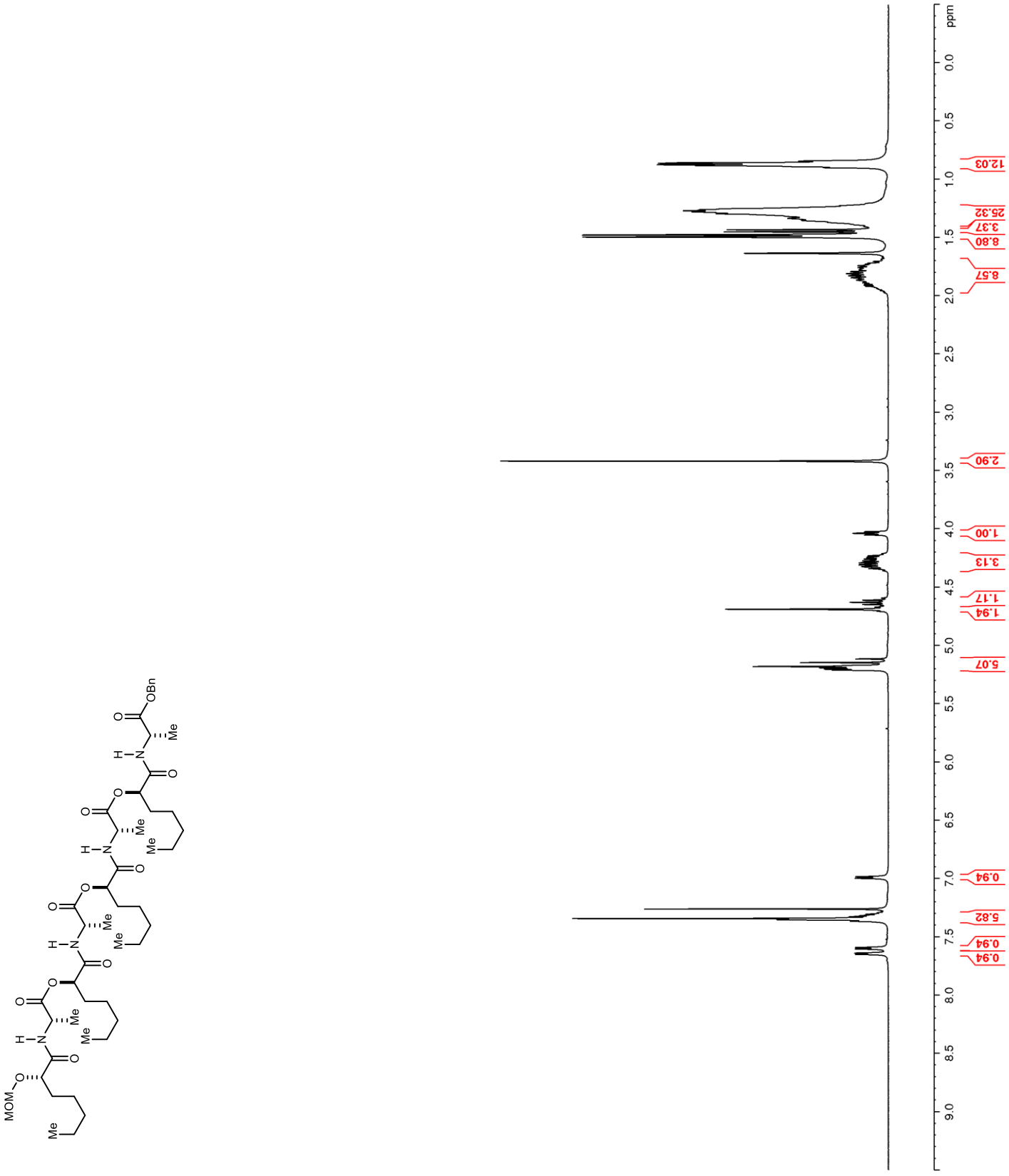

Figure 34. ^{13}C NMR (125 MHz, $CDCl_3$) of **51**

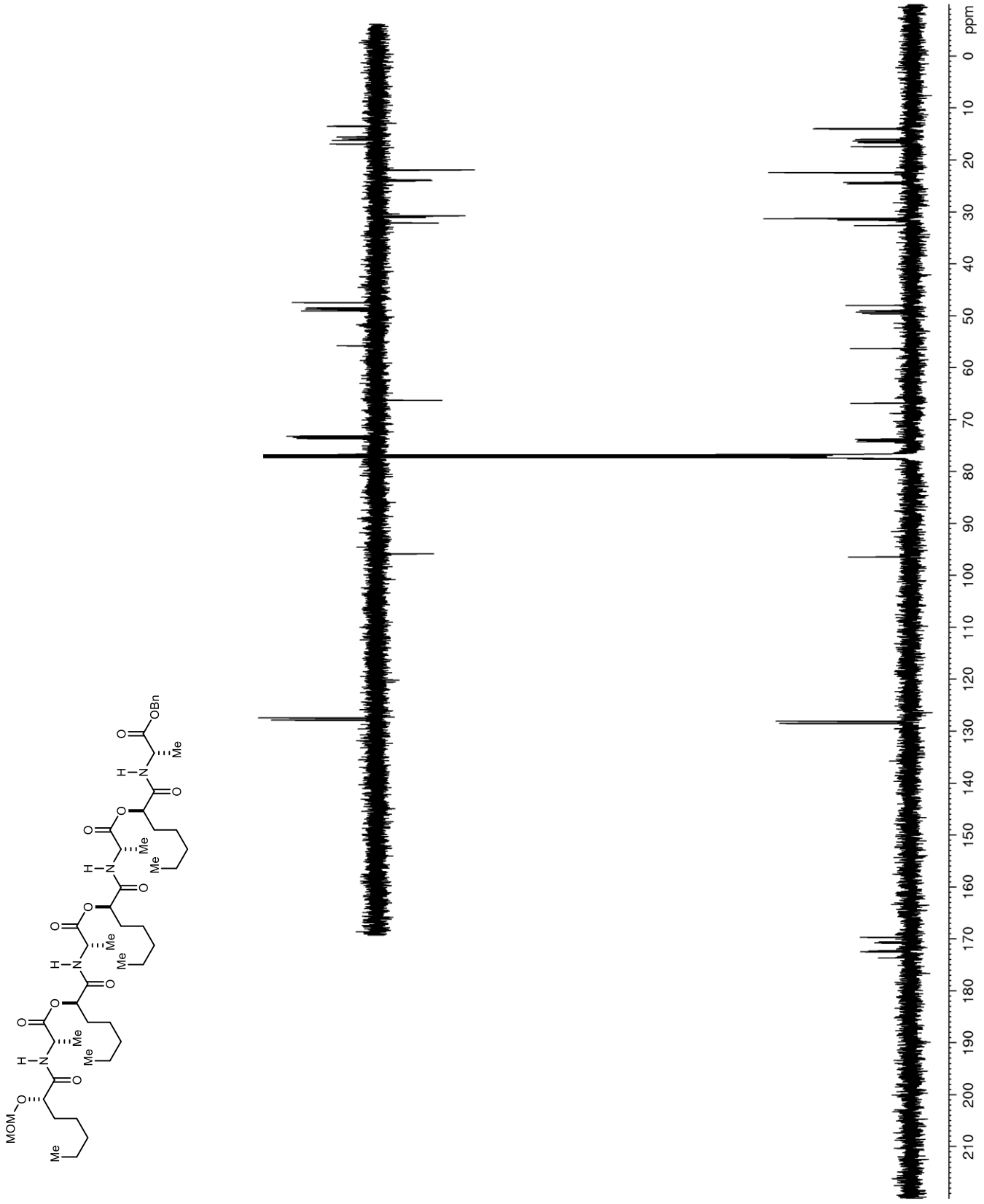

Figure 35. ^{1}H NMR (400 MHz, $CDCl_3$) of **52**

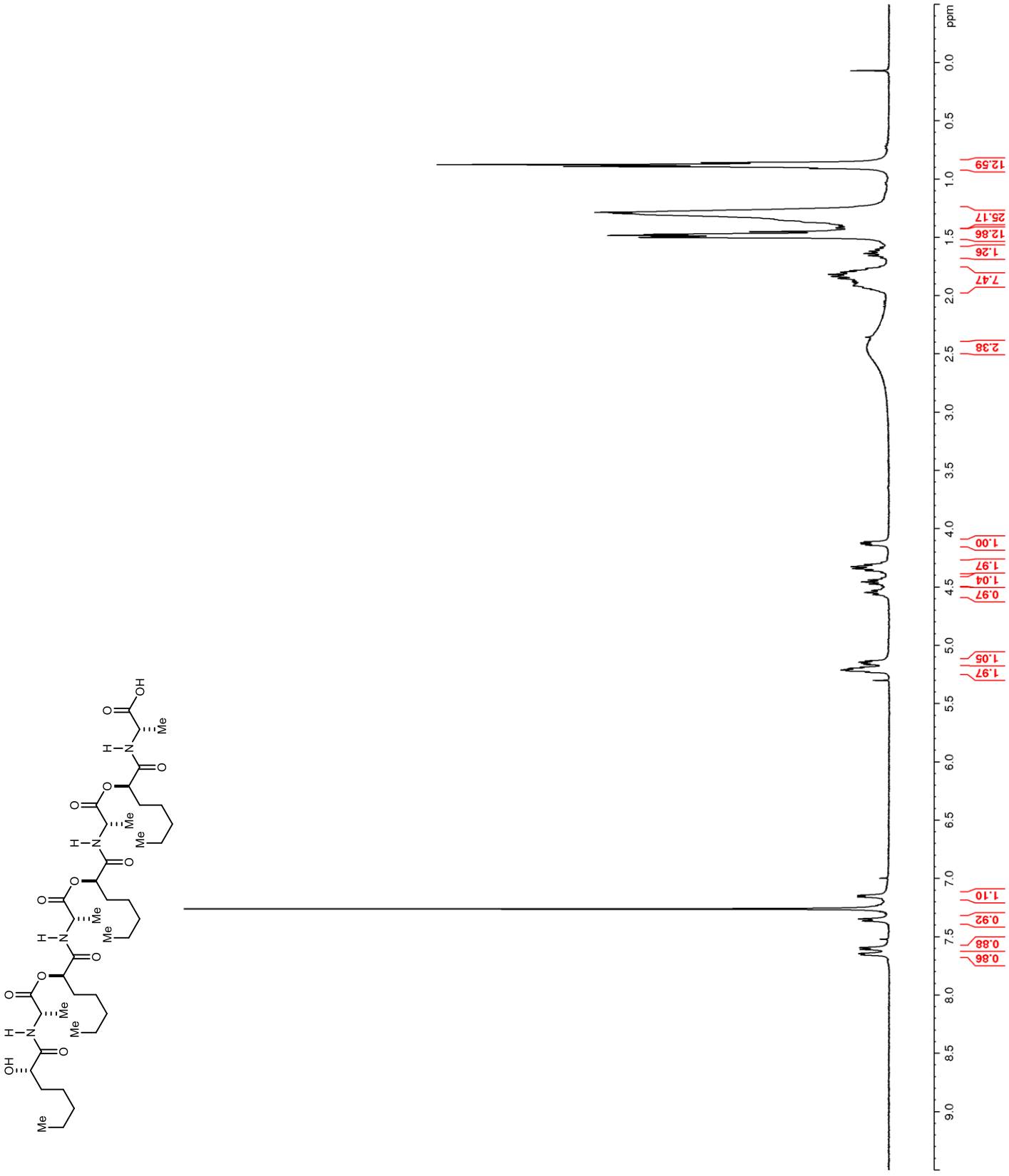

Figure 36. ^{13}C NMR (125 MHz, $CDCl_3$) of **52**

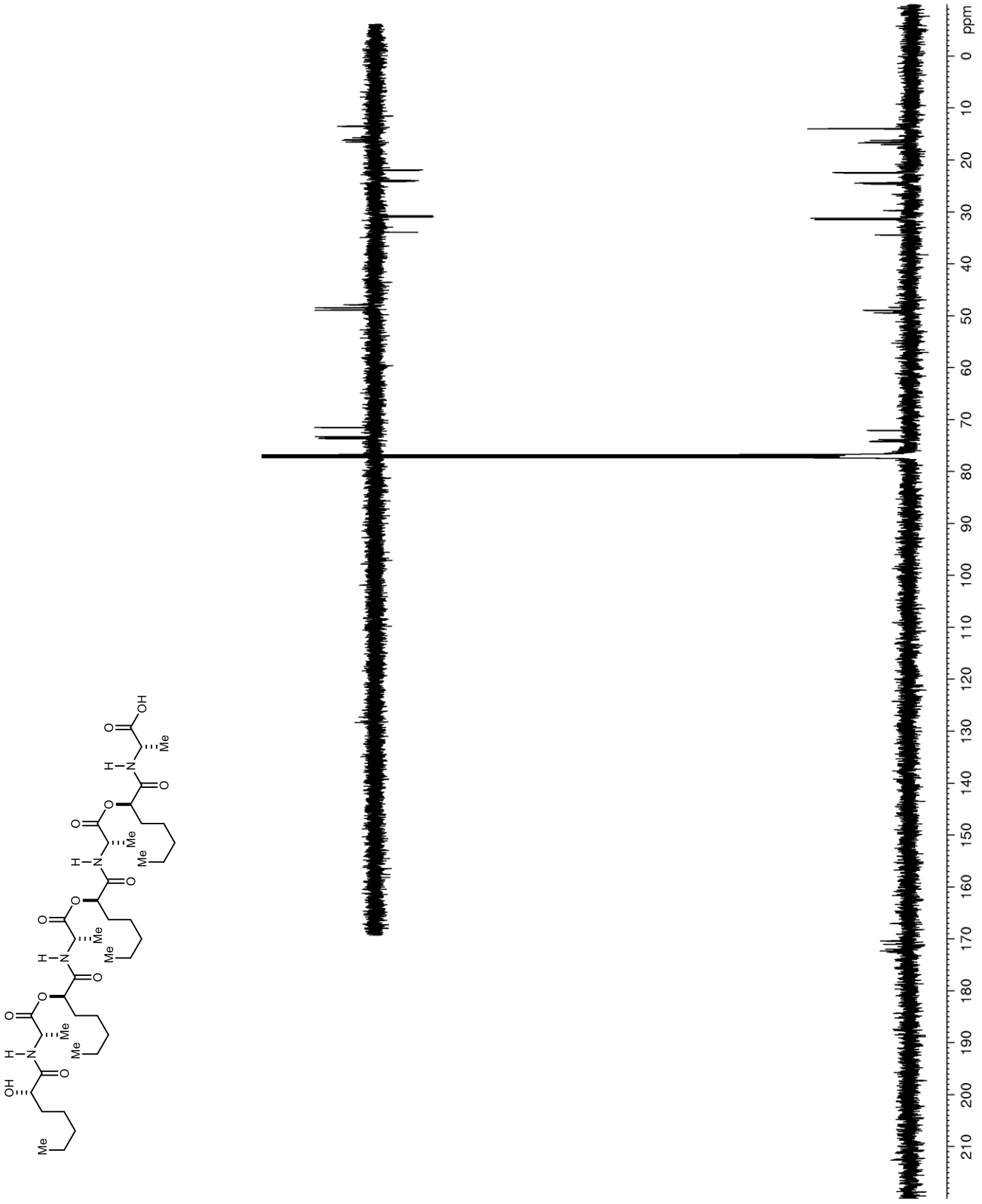

Figure 37. ^{1}H NMR (400 MHz, $CDCl_3$) of **53**

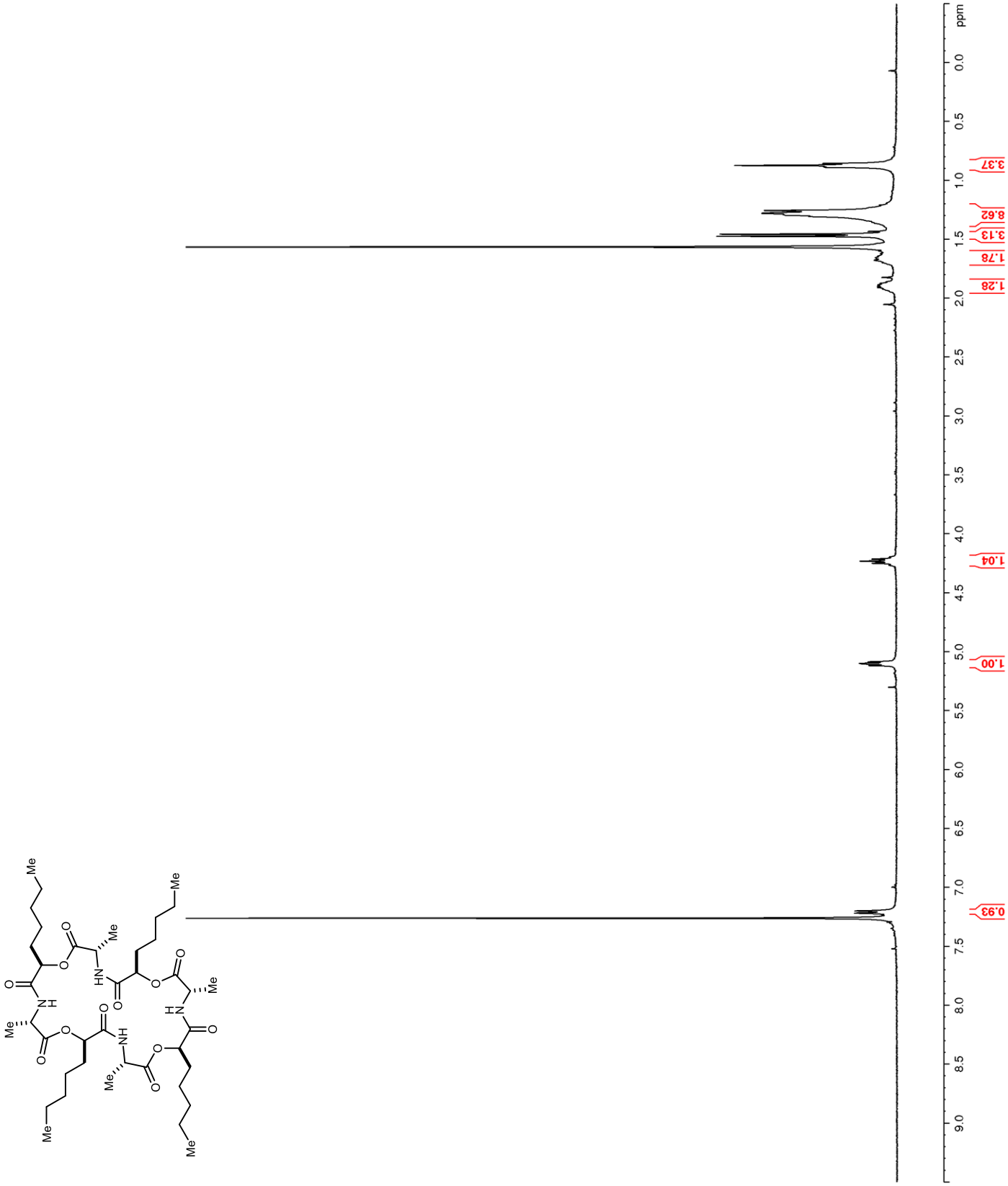

Figure 38. ^{13}C NMR (125 MHz, $CDCl_3$) of **53**

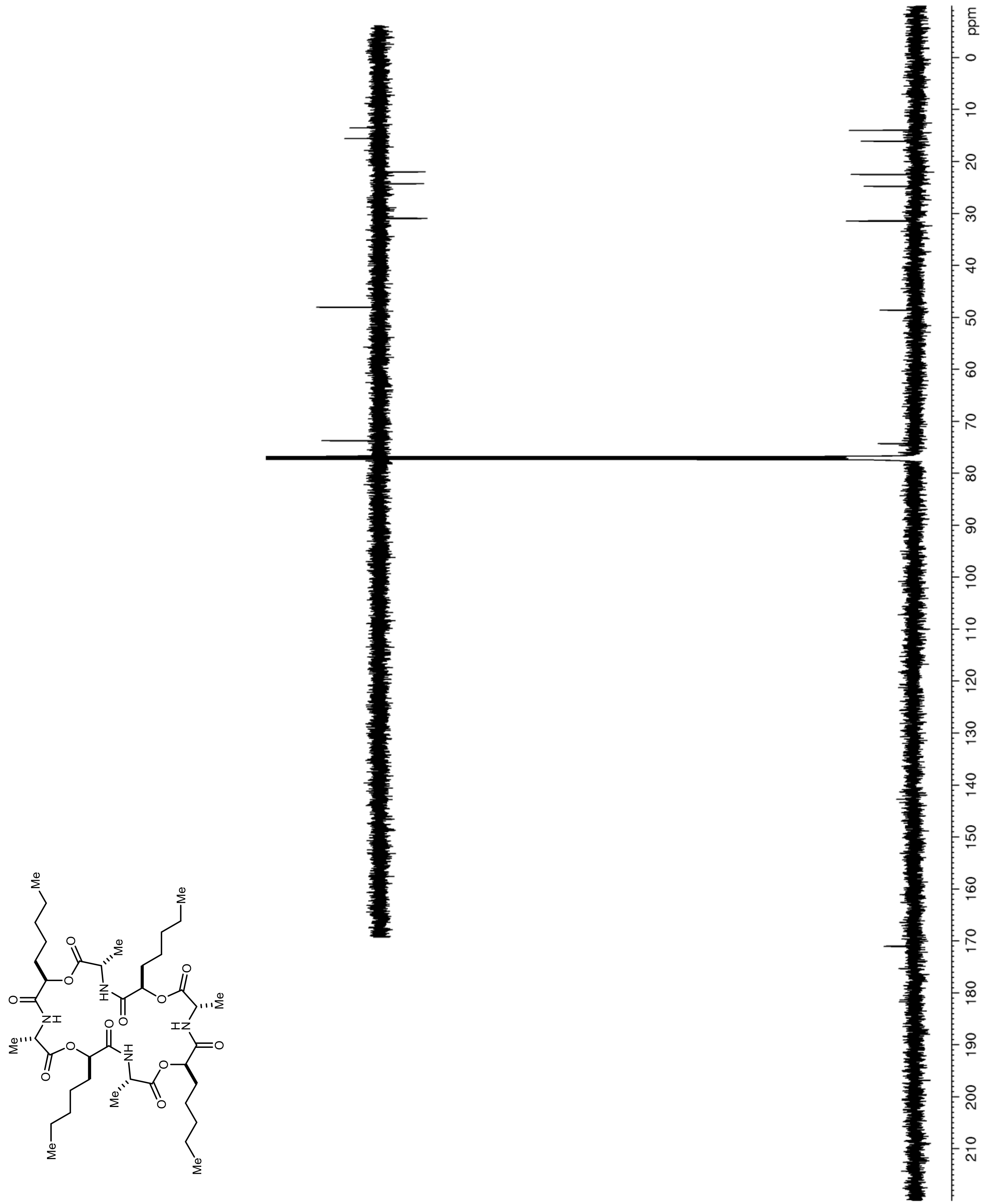

Figure 39. ^{1}H NMR (400 MHz, $CDCl_3$) of *epi*-**53**

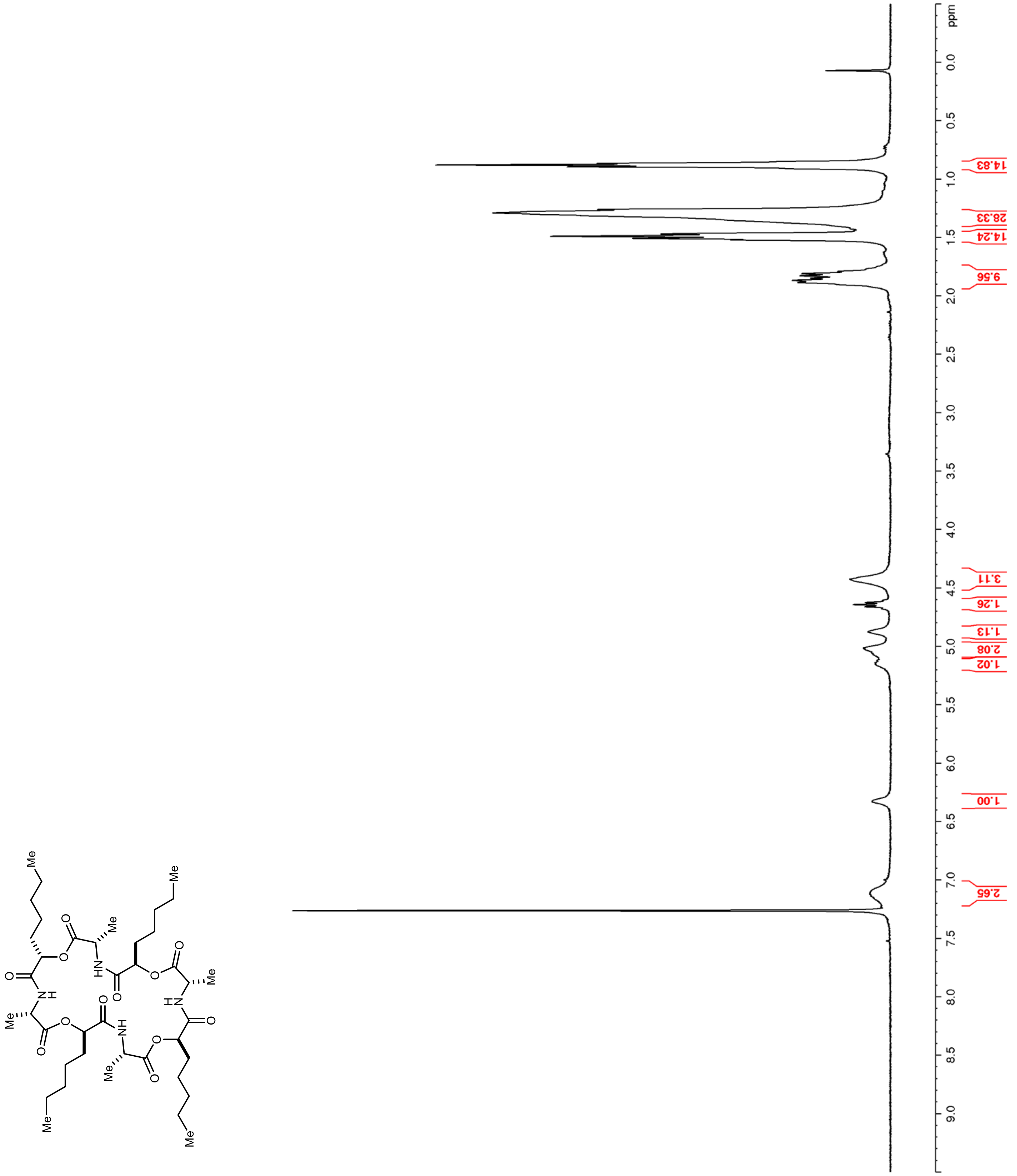

Figure 40. ^{13}C NMR (125 MHz, $CDCl_3$) of *epi*-**53**

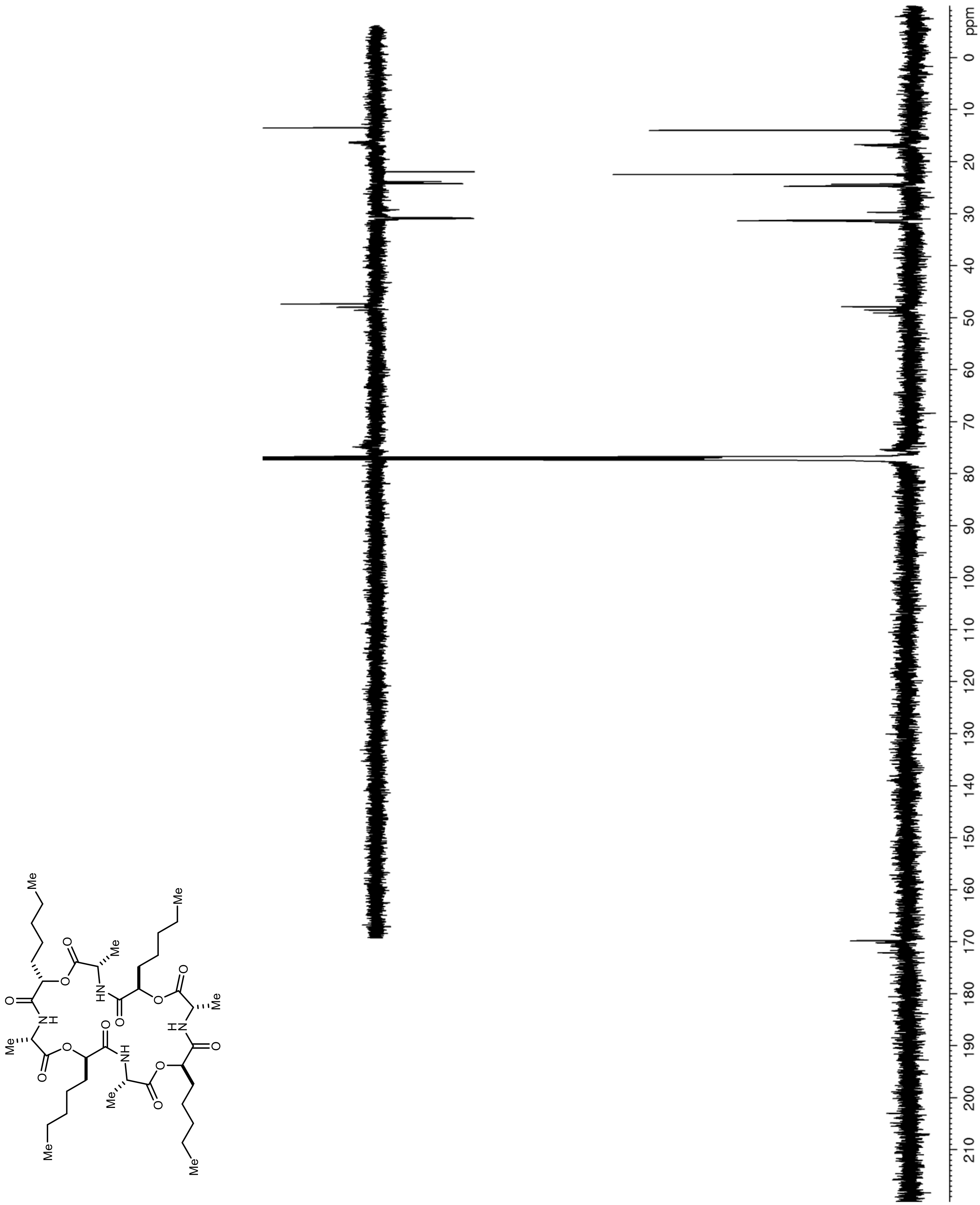

Figure 41. ^{1}H NMR (500 MHz, $CDCl_3$) of **62**

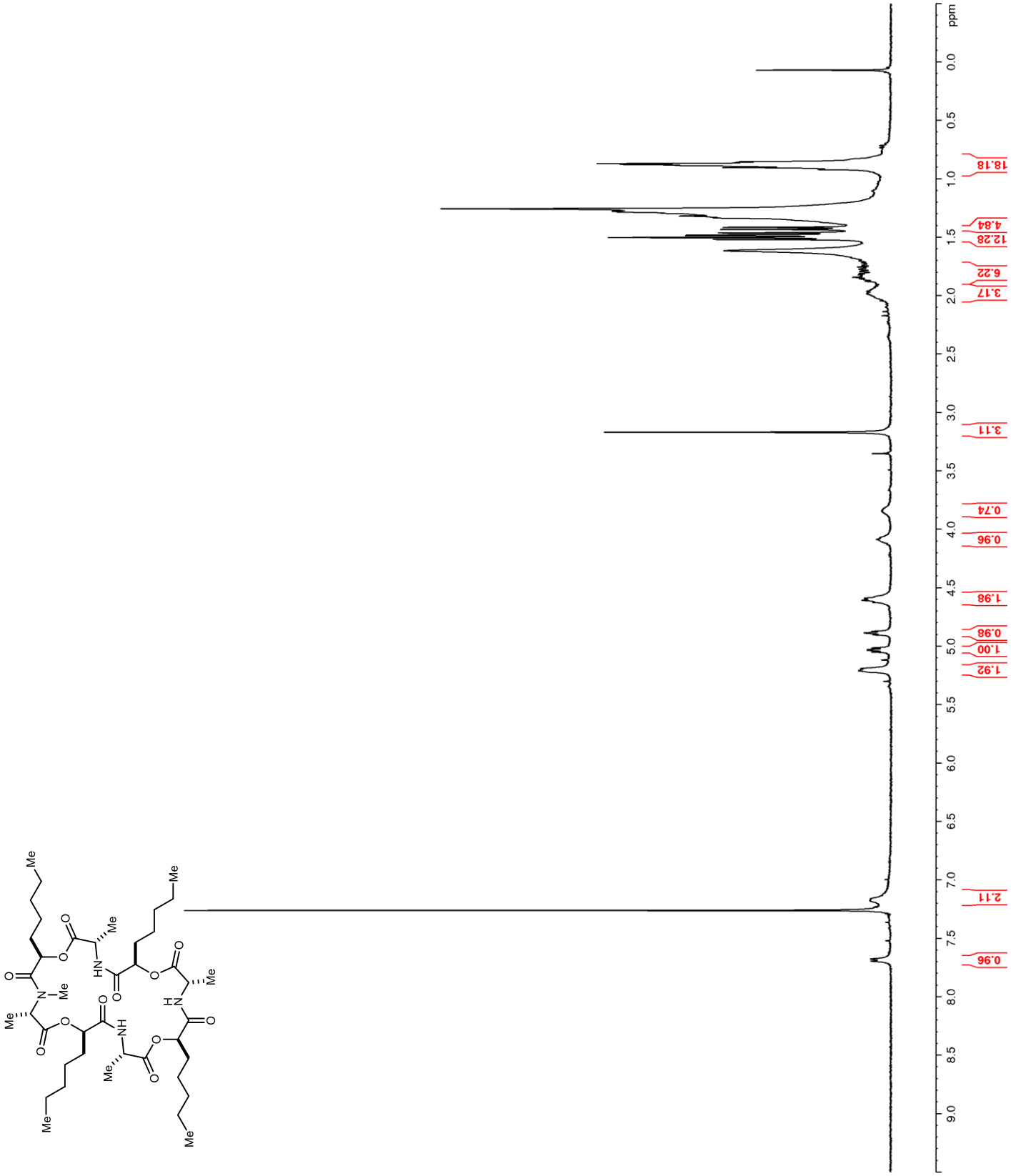

Figure 42. ^{13}C NMR (125 MHz, $CDCl_3$) of **62**

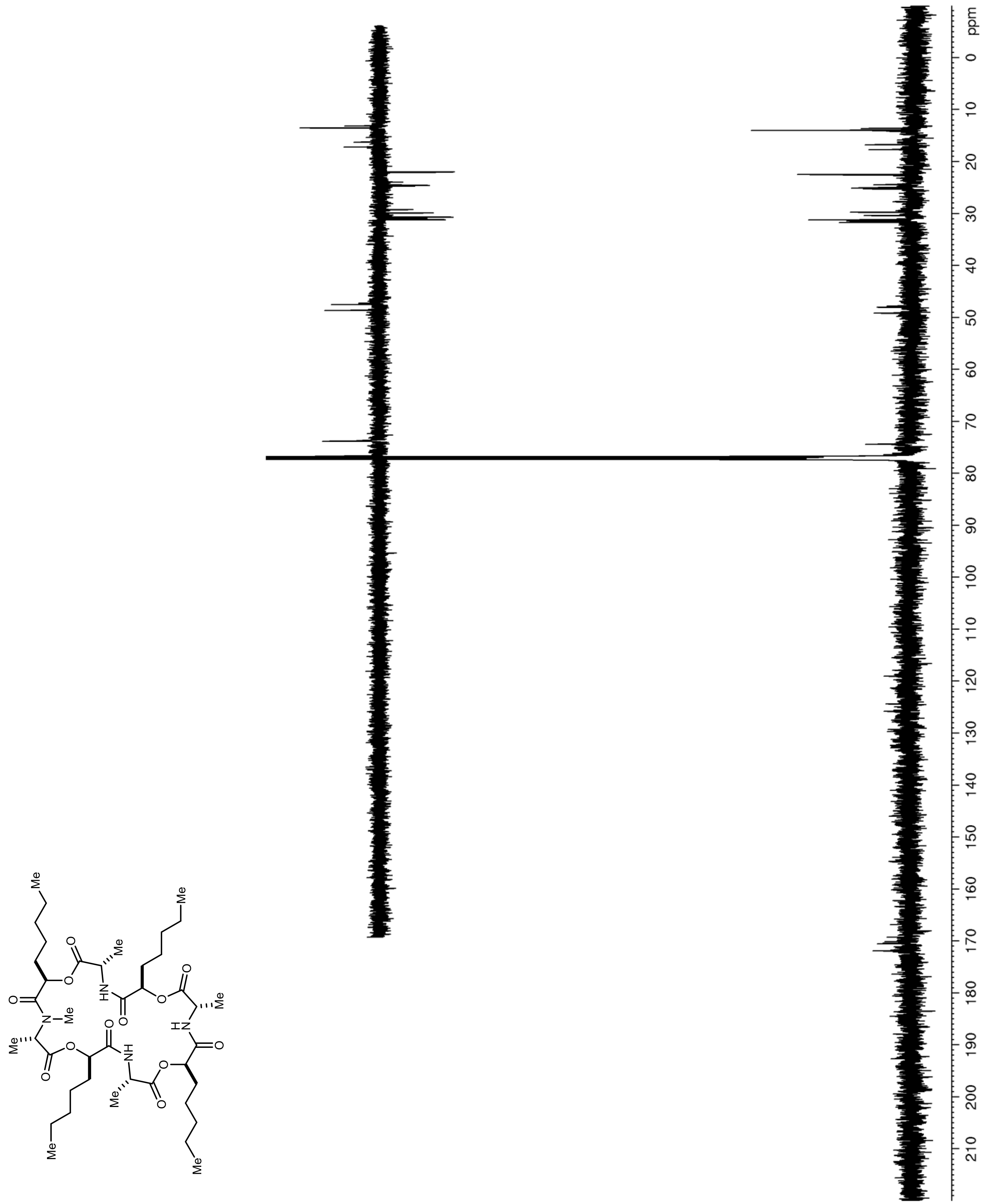

Figure 43. ^{1}H NMR (400 MHz, $CDCl_3$) of **63**

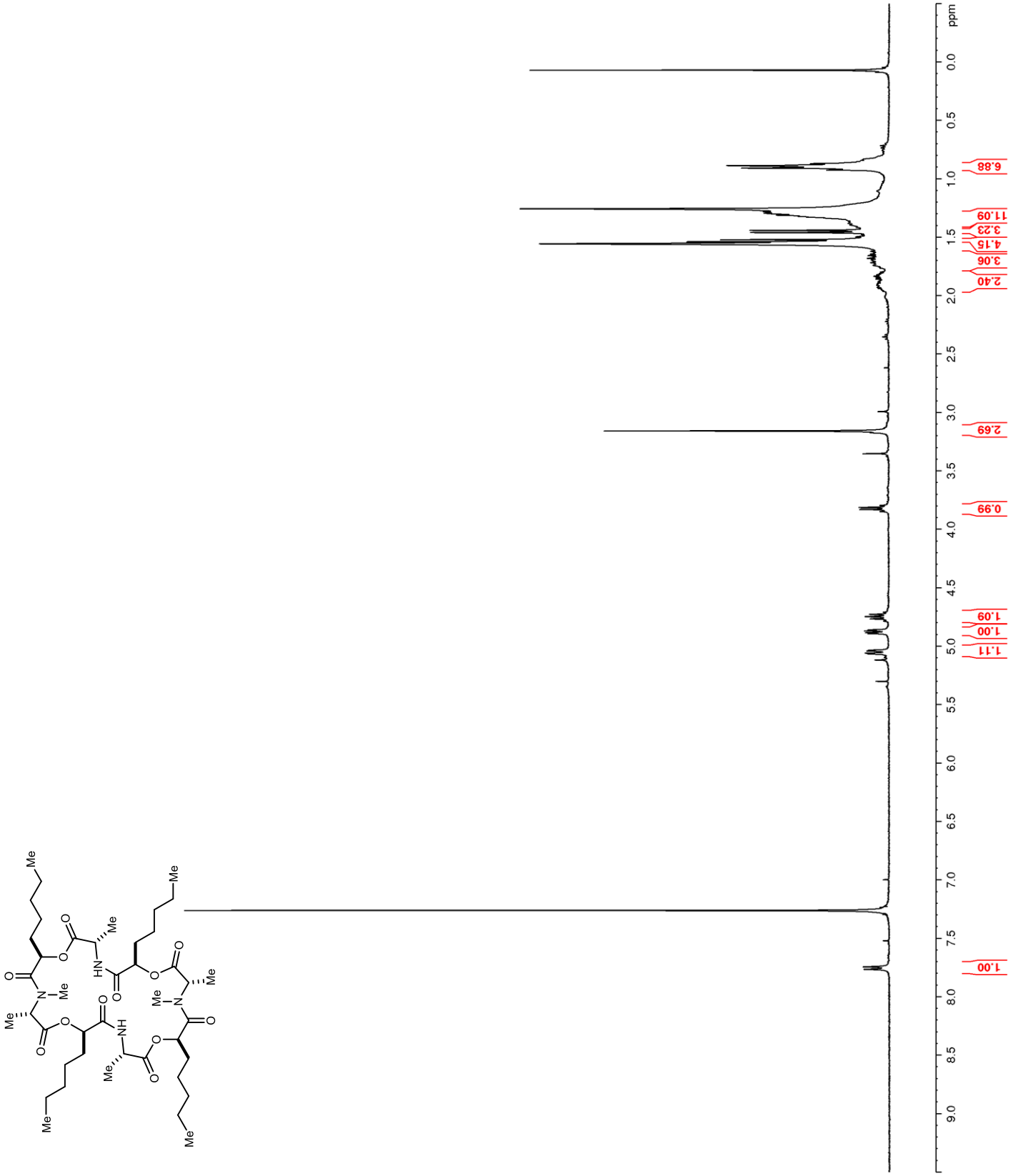

Figure 44. ^{13}C NMR (125 MHz, $CDCl_3$) of **63**

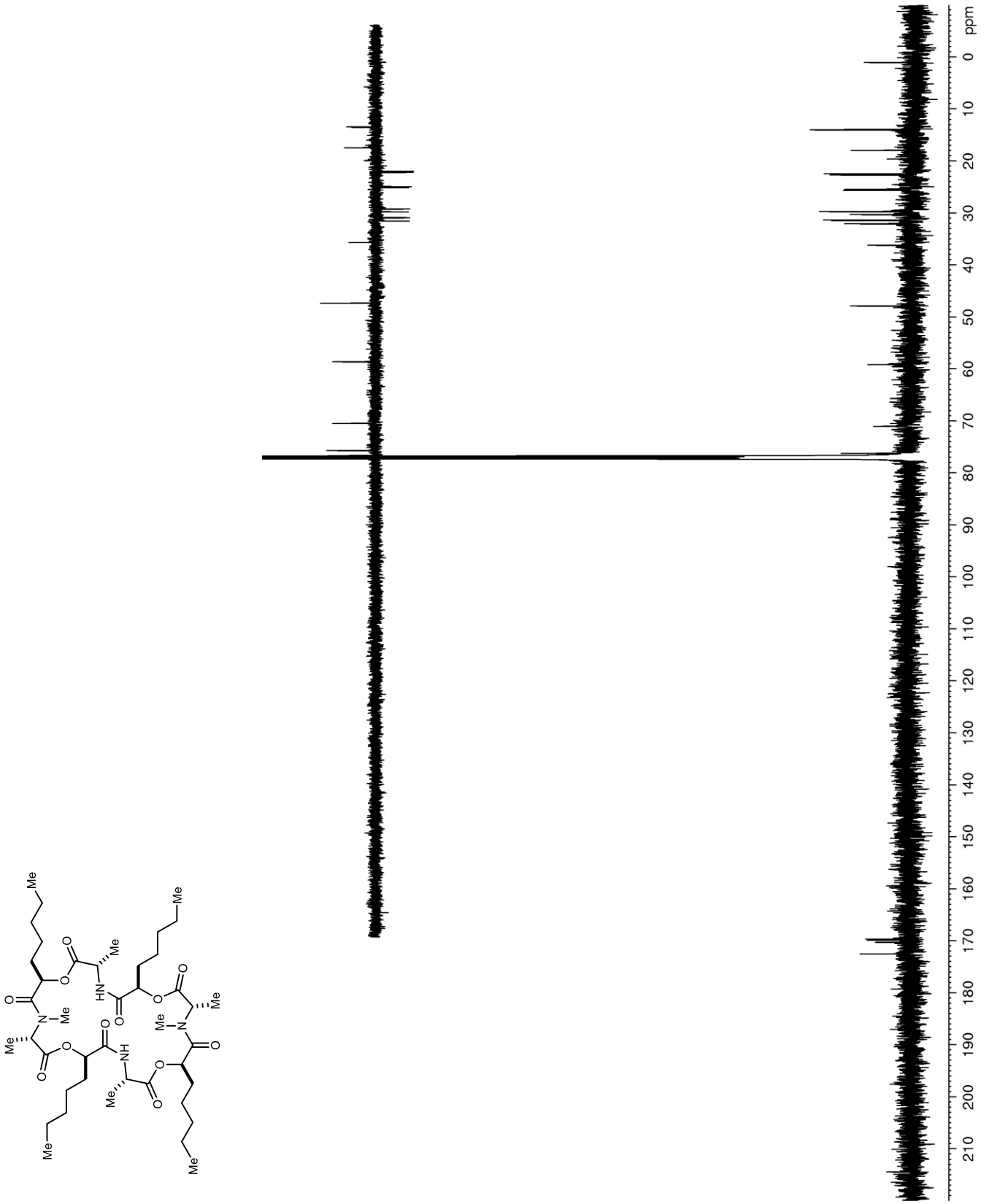

Figure 45. ^{1}H NMR (400 MHz, $CDCl_3$) of ***nat*-67**

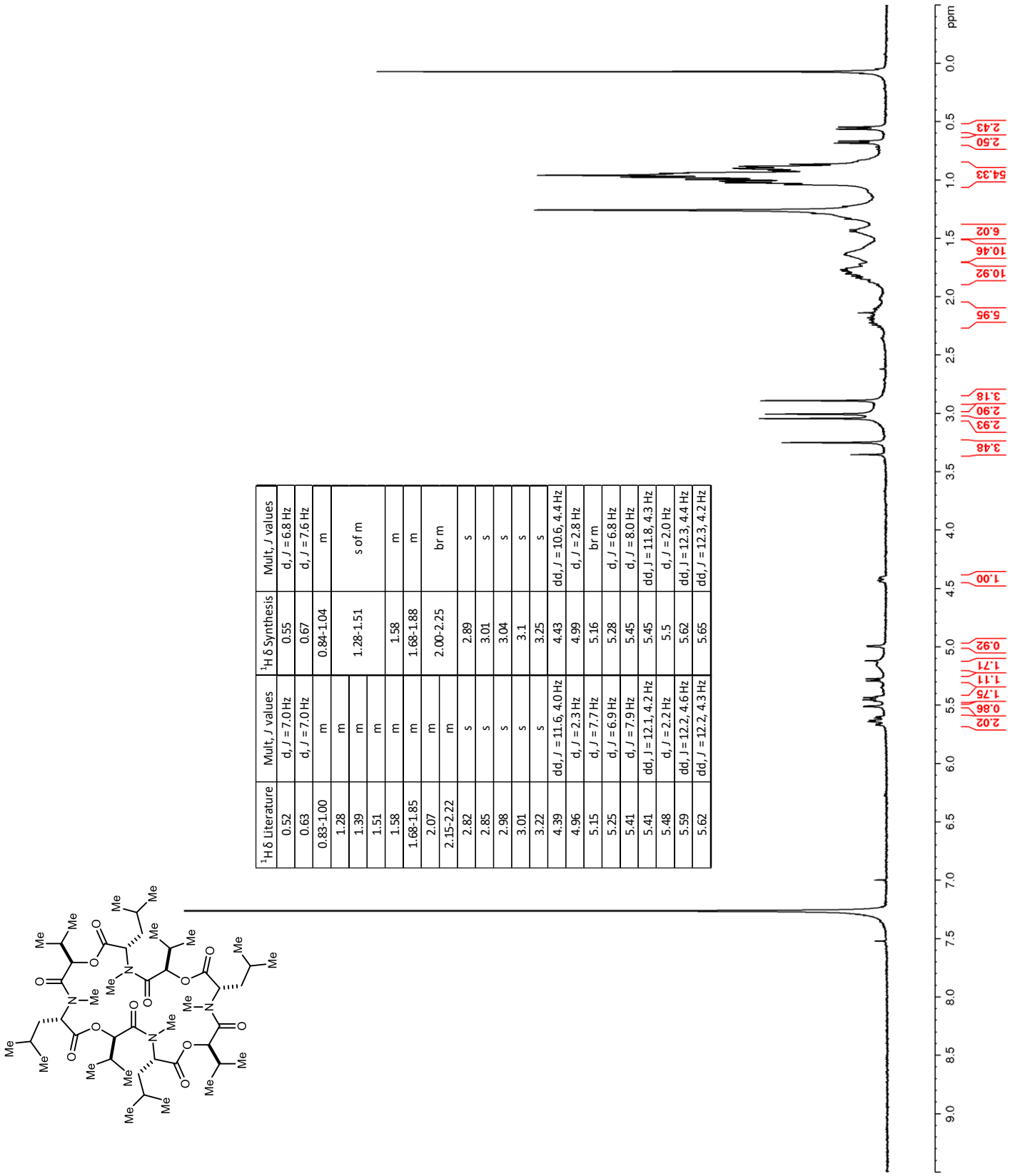

^{1}H δ Literature	Mult, *J* values	^{1}H δ Synthesis	Mult, *J* values
0.52	d, *J* = 7.0 Hz	0.55	d, *J* = 6.8 Hz
0.63	d, *J* = 7.0 Hz	0.67	d, *J* = 7.6 Hz
0.83-1.00	m	0.84-1.04	m
1.28	m	1.28-1.51	s of m
1.39	m		
1.51	m		
1.58	m	1.58	m
1.68-1.85	m	1.68-1.88	m
2.07	m	2.00-2.25	br m
2.15-2.22	m		
2.82	s	2.89	s
2.85	s	3.01	s
2.98	s	3.04	s
3.01	s	3.1	s
3.22	s	3.25	s
4.39	dd, *J* = 11.6, 4.0 Hz	4.43	dd, *J* = 10.6, 4.4 Hz
4.96	d, *J* = 2.3 Hz	4.99	d, *J* = 2.8 Hz
5.15	d, *J* = 7.7 Hz	5.16	br m
5.25	d, *J* = 6.9 Hz	5.28	d, *J* = 6.8 Hz
5.41	d, *J* = 7.9 Hz	5.45	d, *J* = 8.0 Hz
5.41	dd, *J* = 12.1, 4.2 Hz	5.45	dd, *J* = 11.8, 4.3 Hz
5.48	d, *J* = 2.2 Hz	5.5	d, *J* = 2.0 Hz
5.59	dd, *J* = 12.2, 4.6 Hz	5.62	dd, *J* = 12.3, 4.4 Hz
5.62	dd, *J* = 12.2, 4.3 Hz	5.65	dd, *J* = 12.3, 4.2 Hz

Figure 46. ^{13}C NMR (150 MHz, $CDCl_3$) of ***nat*-67**

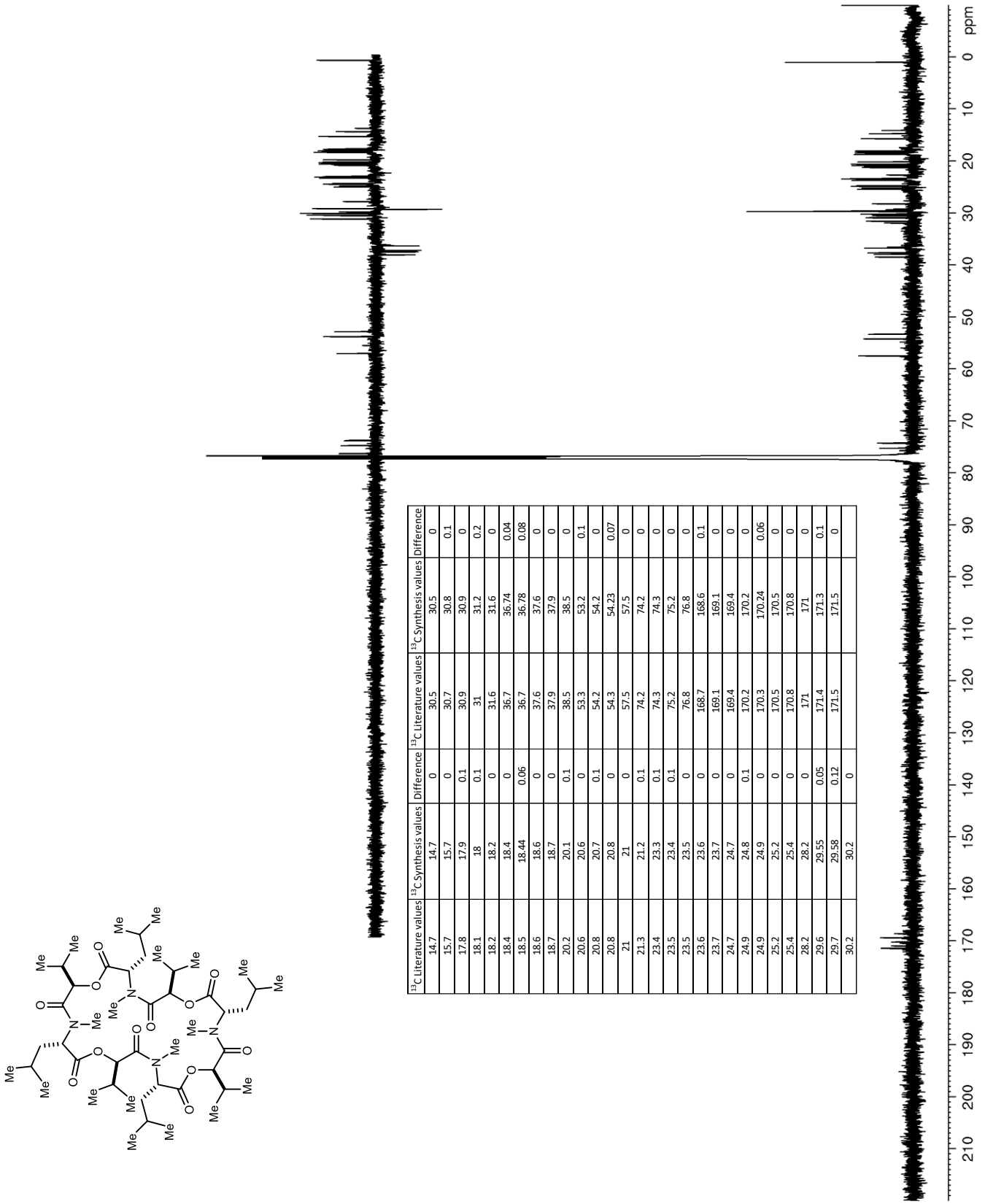

^{13}C Literature values	^{13}C Synthesis values	Difference	^{13}C Literature values	^{13}C Synthesis values	Difference
14.7	14.7	0	30.5	30.5	0
15.7	15.7	0	30.7	30.8	0.1
17.8	17.9	0.1	30.9	30.9	0
18.1	18	0.1	31	31.2	0.2
18.2	18.2	0	31.6	31.6	0
18.4	18.4	0	35.7	36.74	0.04
18.5	18.44	0.06	36.7	36.78	0.08
18.6	18.6	0	37.6	37.6	0
18.7	18.7	0	37.9	37.9	0
20.2	20.1	0.1	38.5	38.5	0
20.6	20.6	0	53.3	53.2	0.1
20.8	20.7	0.1	54.2	54.2	0
20.8	20.8	0	54.3	54.23	0.07
21	21	0	57.5	57.5	0
21.3	21.2	0.1	74.2	74.2	0
23.4	23.3	0.1	74.3	74.3	0
23.5	23.4	0.1	75.2	75.2	0
23.5	23.5	0	76.8	76.8	0
23.6	23.6	0	168.7	168.6	0.1
23.7	23.7	0	169.1	169.1	0
24.7	24.7	0	169.4	169.4	0
24.9	24.8	0.1	170.2	170.2	0
24.9	24.9	0	170.3	170.24	0.06
25.2	25.2	0	170.5	170.5	0
25.4	25.4	0	170.8	170.8	0
28.2	28.2	0	171	171	0
29.6	29.55	0.05	171.4	171.3	0.1
29.7	29.58	0.12	171.5	171.5	0
30.2	30.2	0			

Figure 47. ^{1}H NMR (400 MHz, $CDCl_3$) of ***nat*-68**

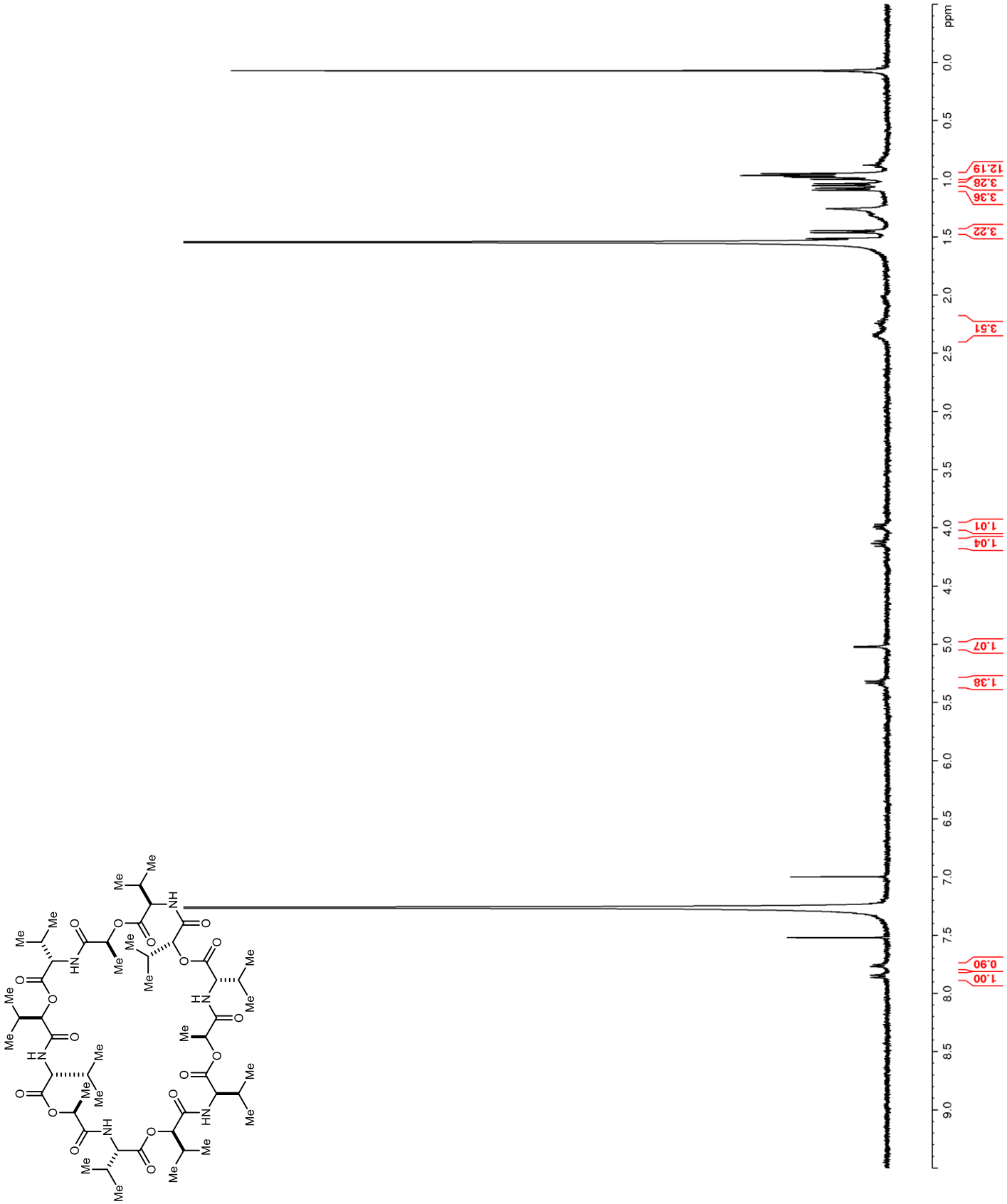

Figure 48. ^{1}H NMR (400 MHz, $CDCl_3$) of **70**

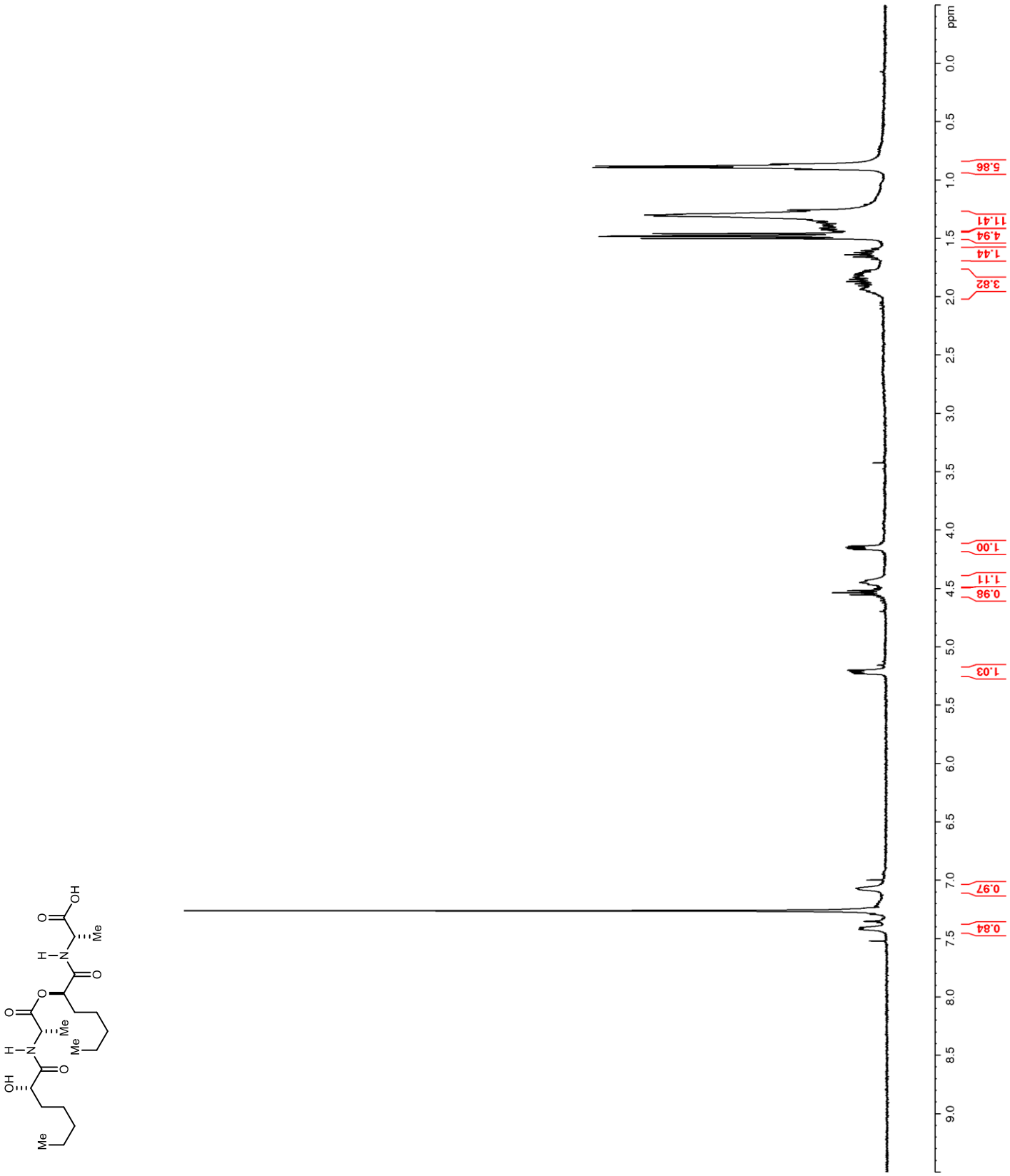

Figure 49. ^{13}C NMR (125 MHz, $CDCl_3$) of **70**

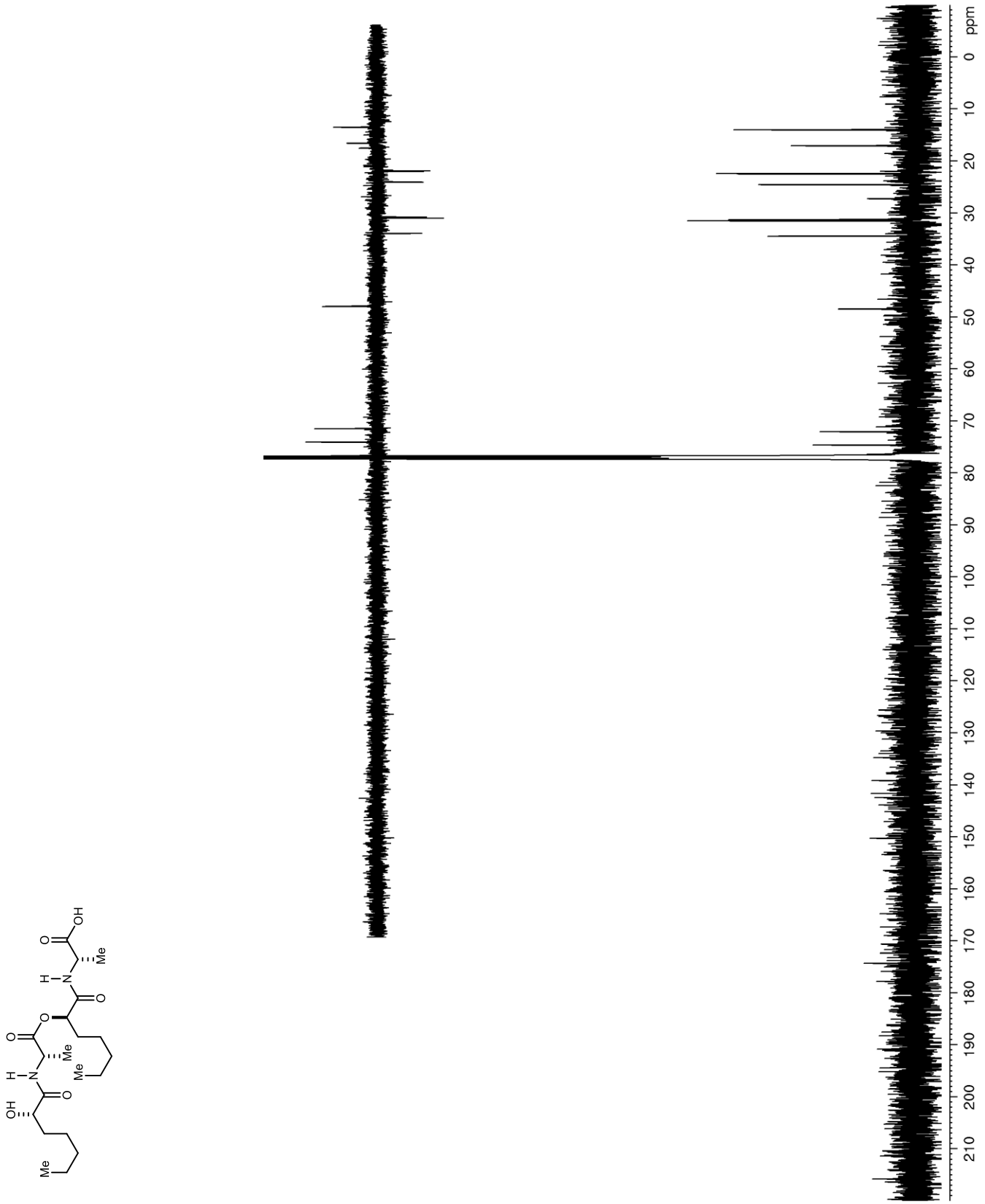

Figure 50. ^{1}H NMR (400 MHz, $CDCl_3$) of **72**

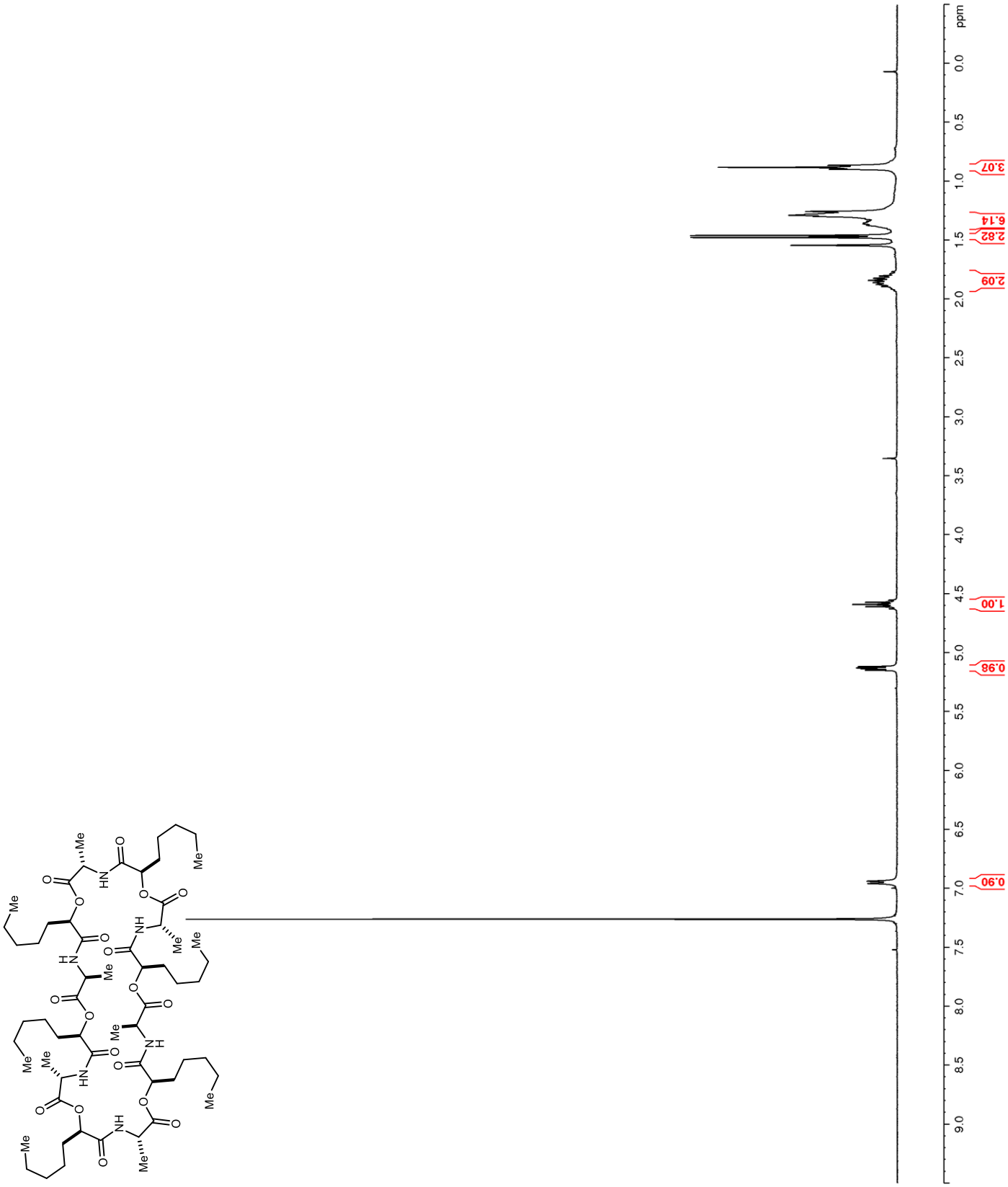

Figure 51. ^{13}C NMR (125 MHz, $CDCl_3$) of **72**

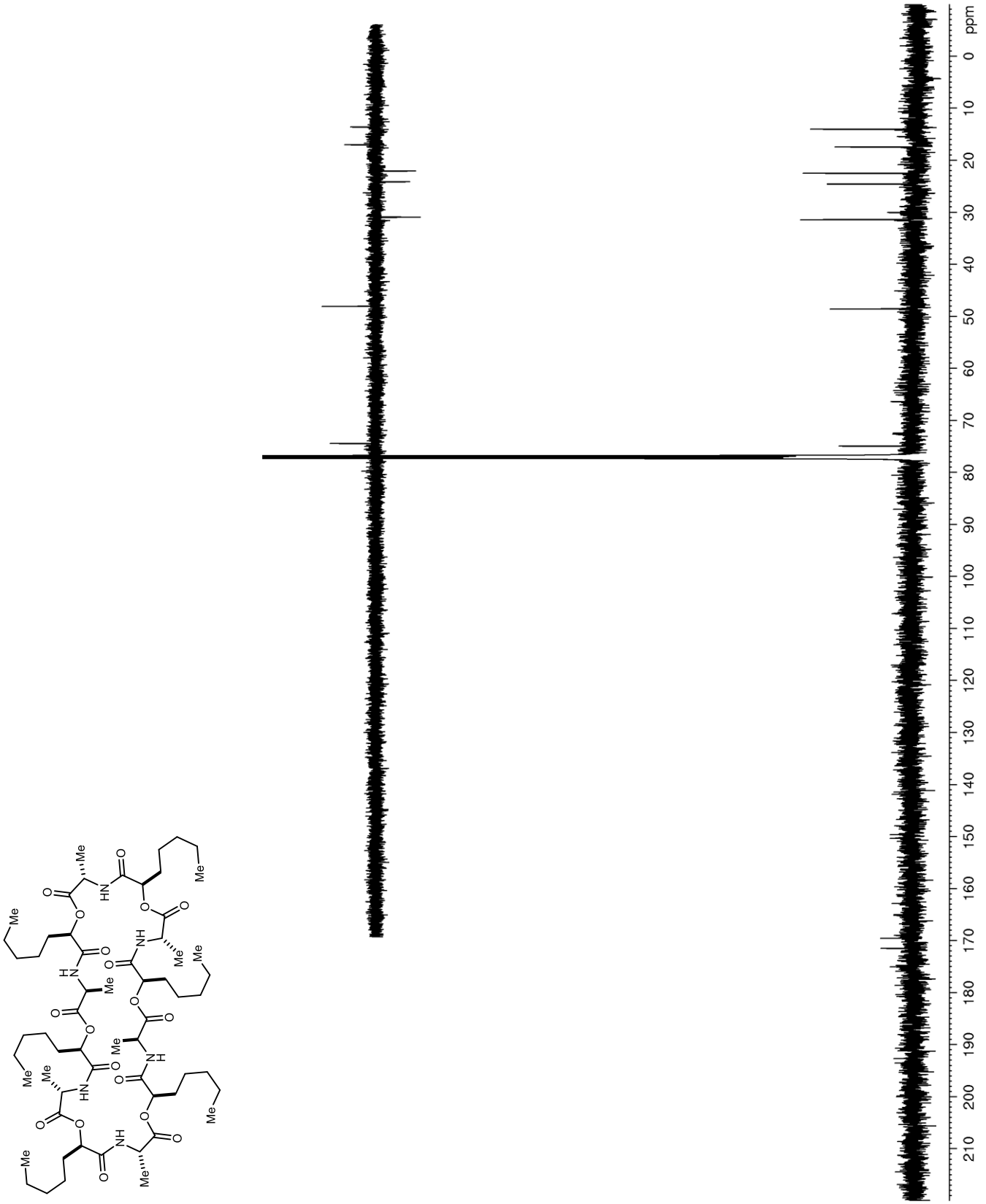

Figure 52. ^{1}H NMR (400 MHz, $CDCl_3$) of **73**

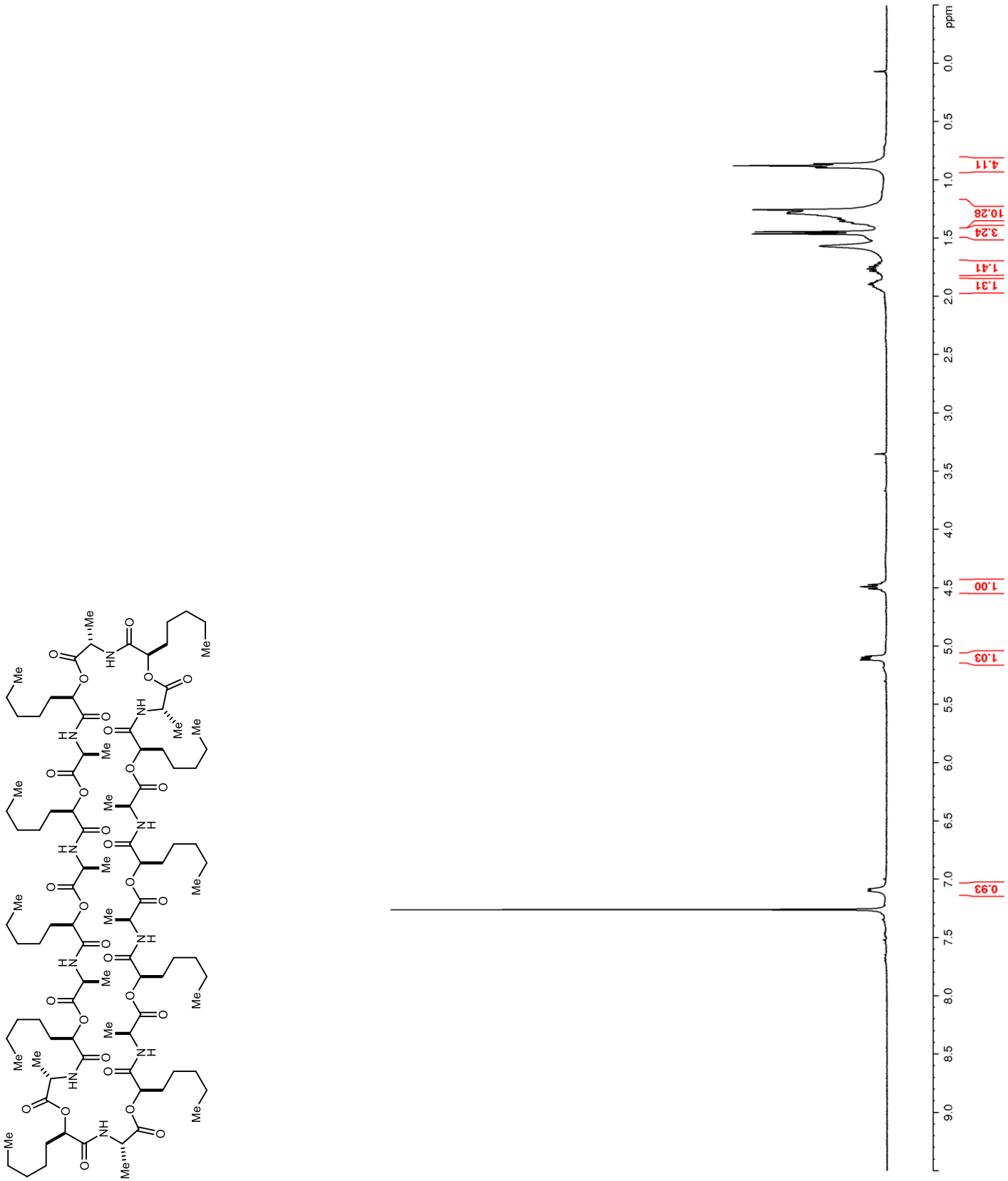

Figure 53. ^{13}C NMR (125 MHz, $CDCl_3$) of **73**

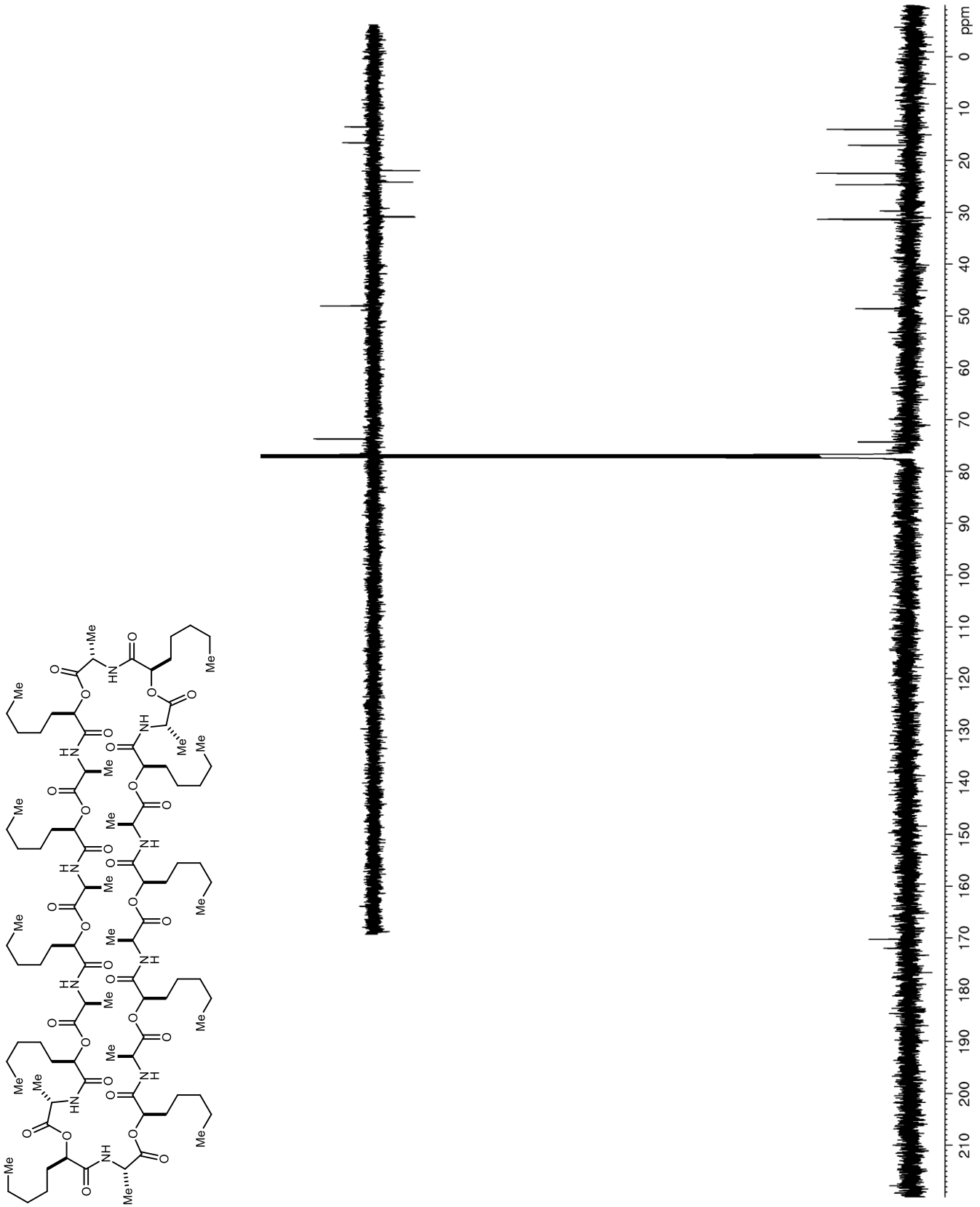

Figure 54. ^{1}H NMR (400 MHz, DMSO-d_6) of **74**

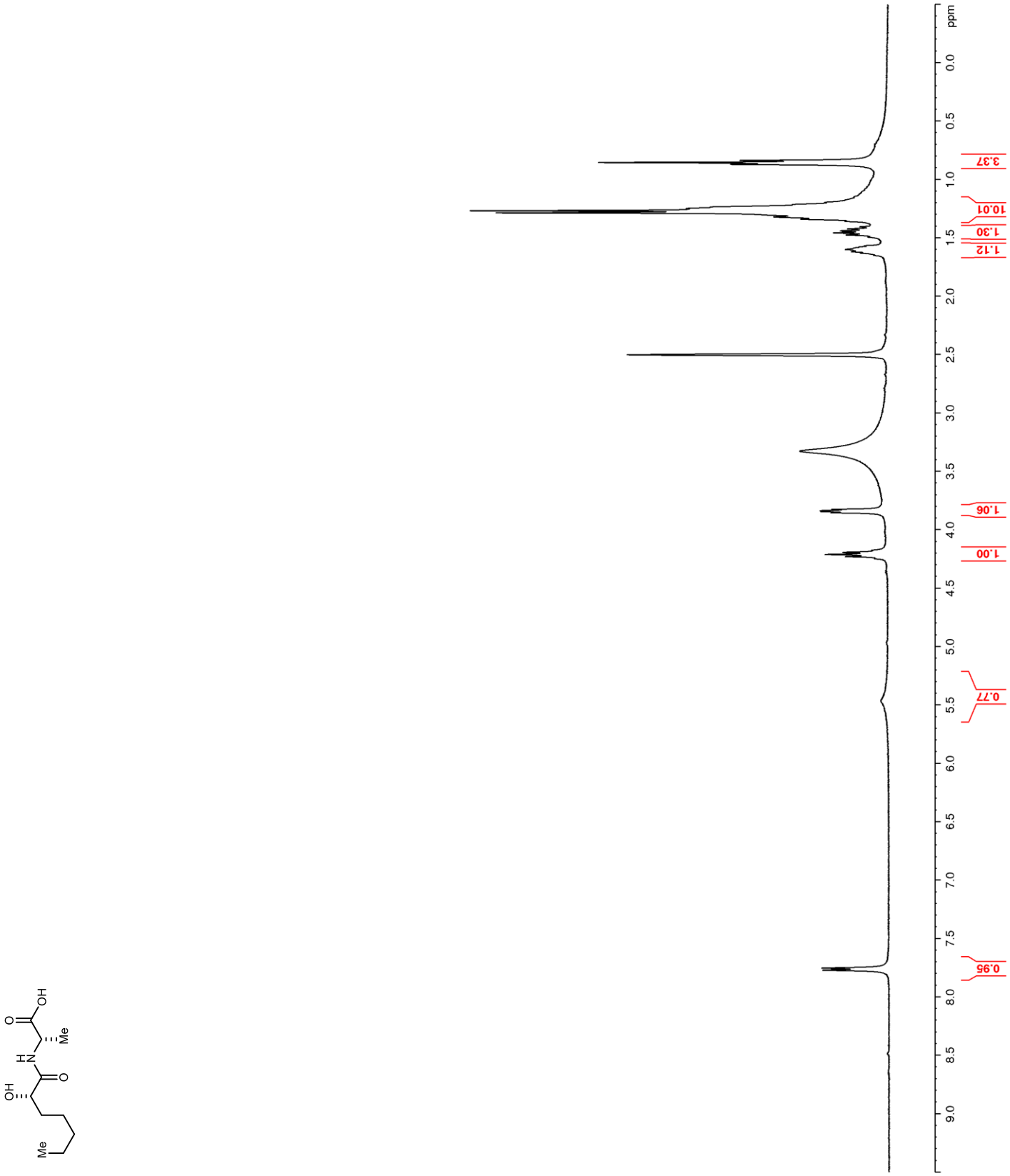

Figure 55. ^{13}C NMR (125 MHz, DMSO-d_6) of **74**

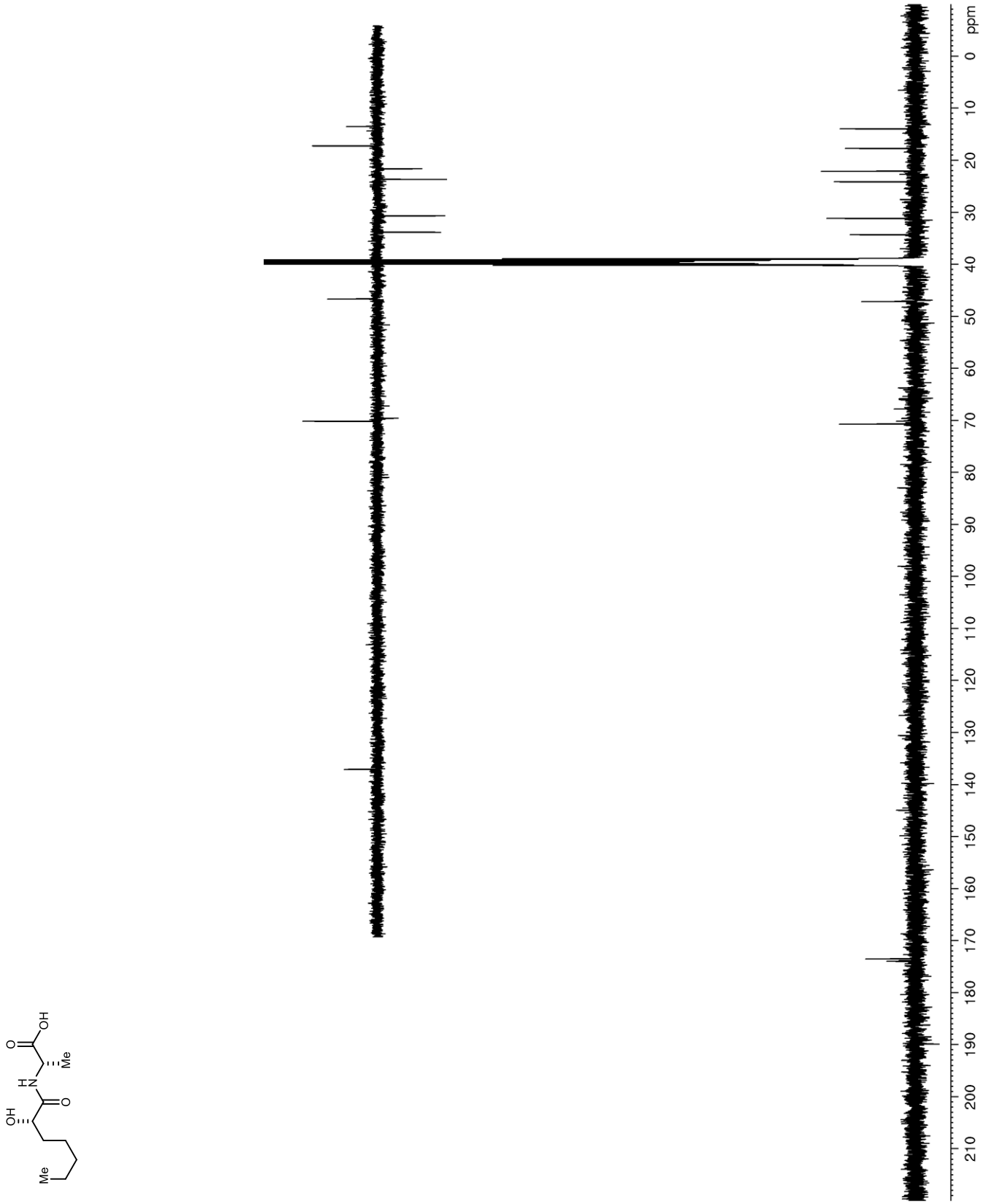

Figure 56. ^{1}H NMR (400 MHz, $CDCl_3$) of **75**

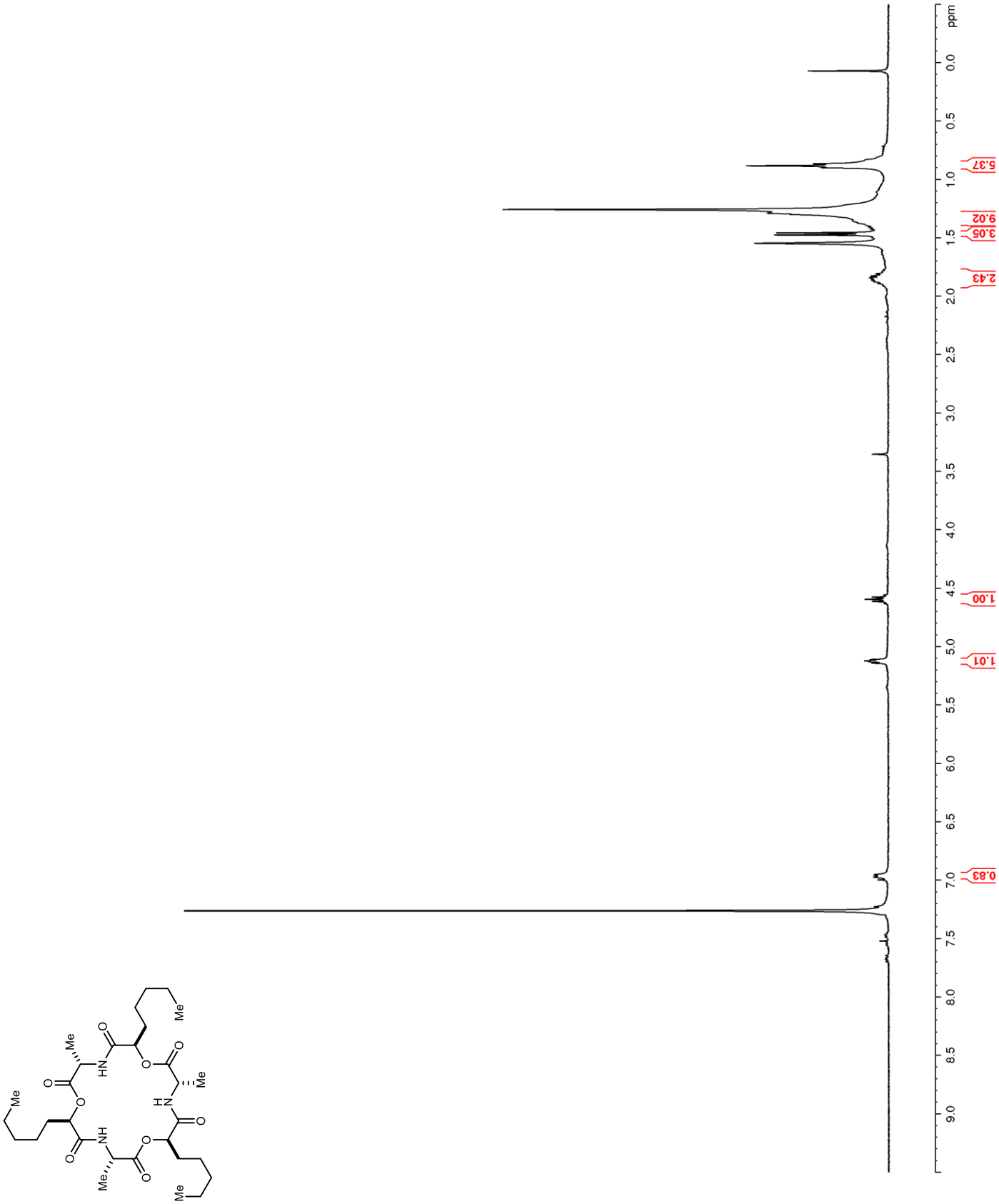

Figure 57. ^{13}C NMR (150 MHz, $CDCl_3$) of **75**

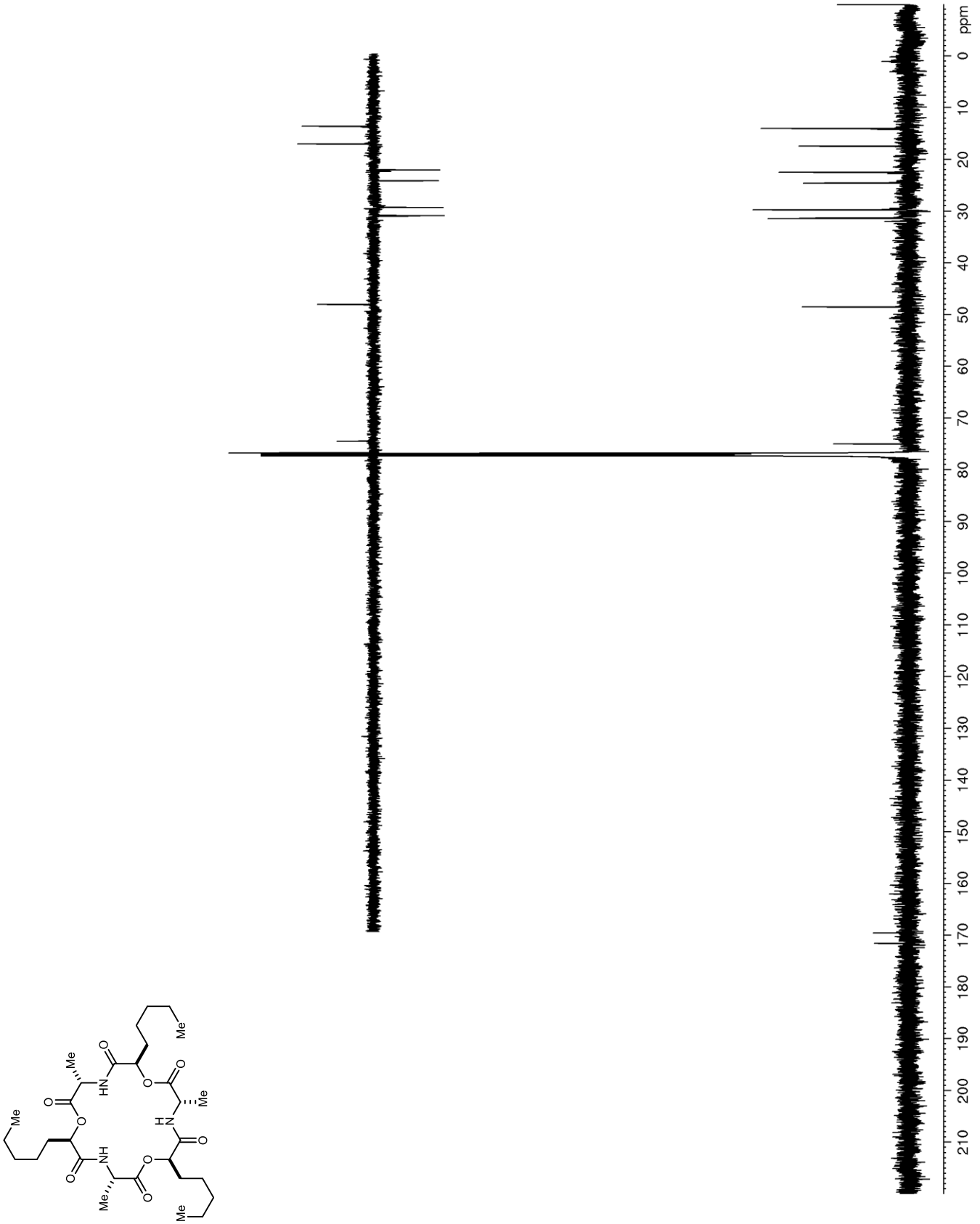

Figure 58. ^{1}H NMR (400 MHz, $CDCl_3$) of **76**

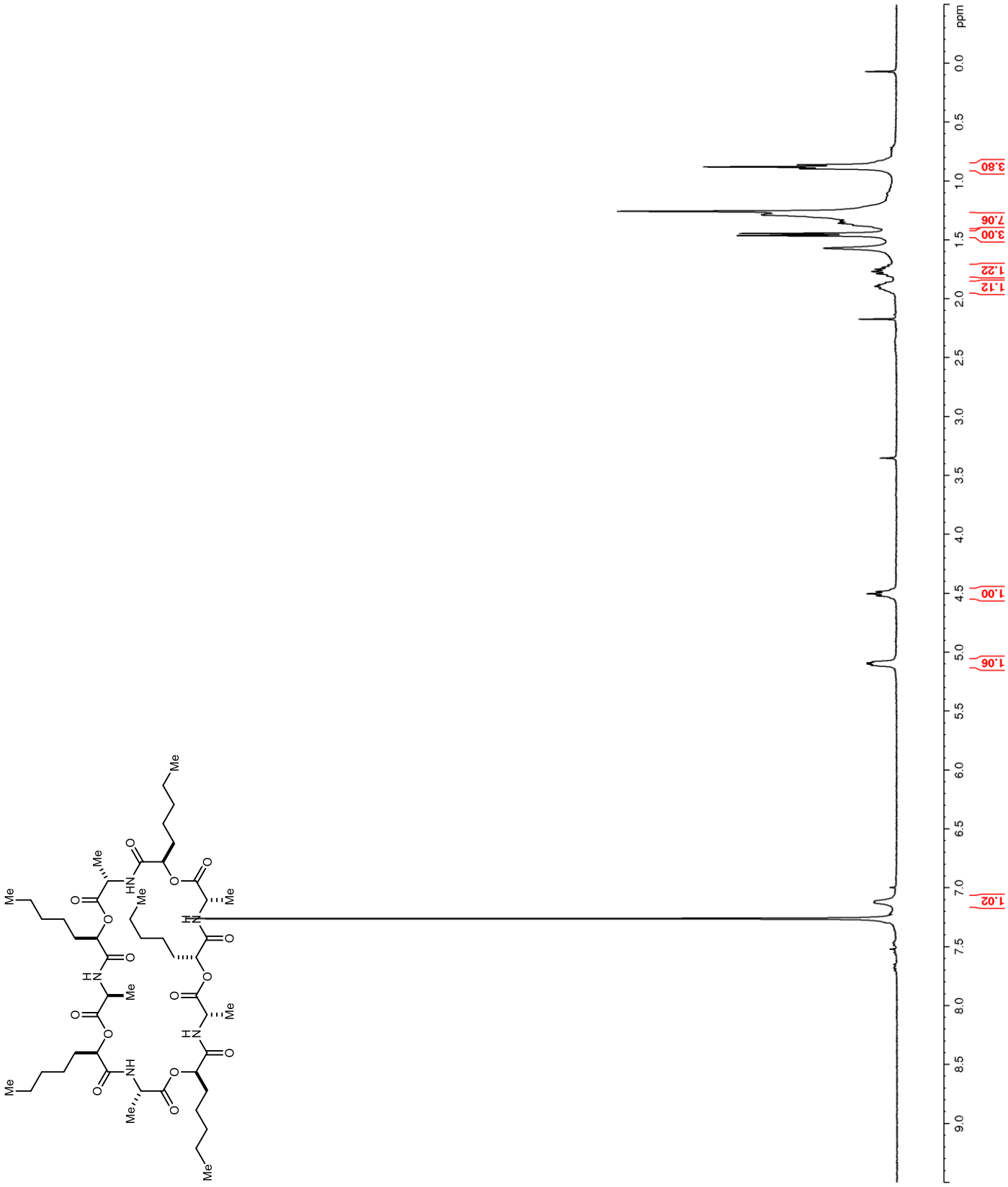

Figure 59. ^{13}C NMR (150 MHz, $CDCl_3$) of **76**

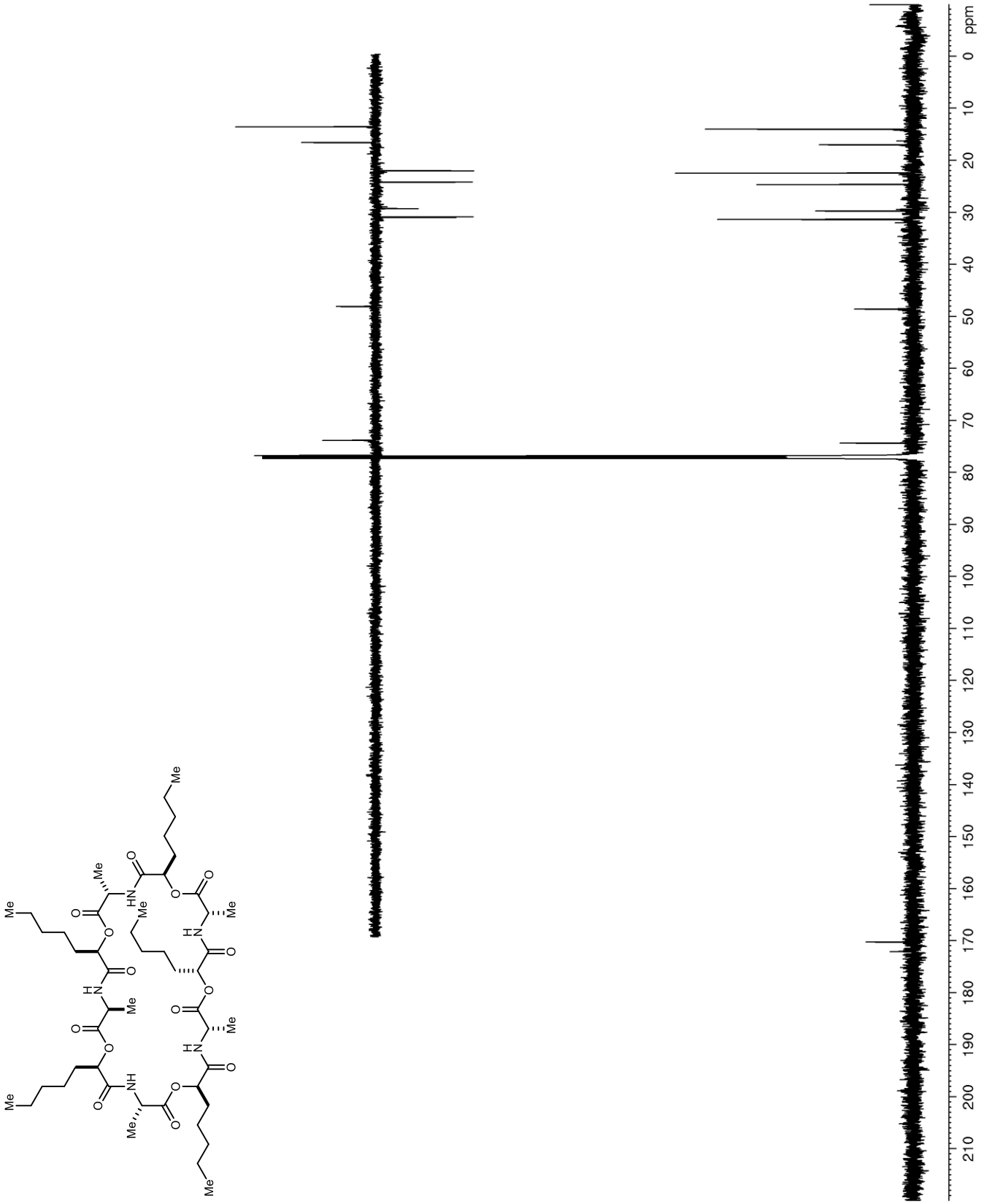

Figure 60. ^{1}H NMR (400 MHz, DMSO-d_6) of **77**

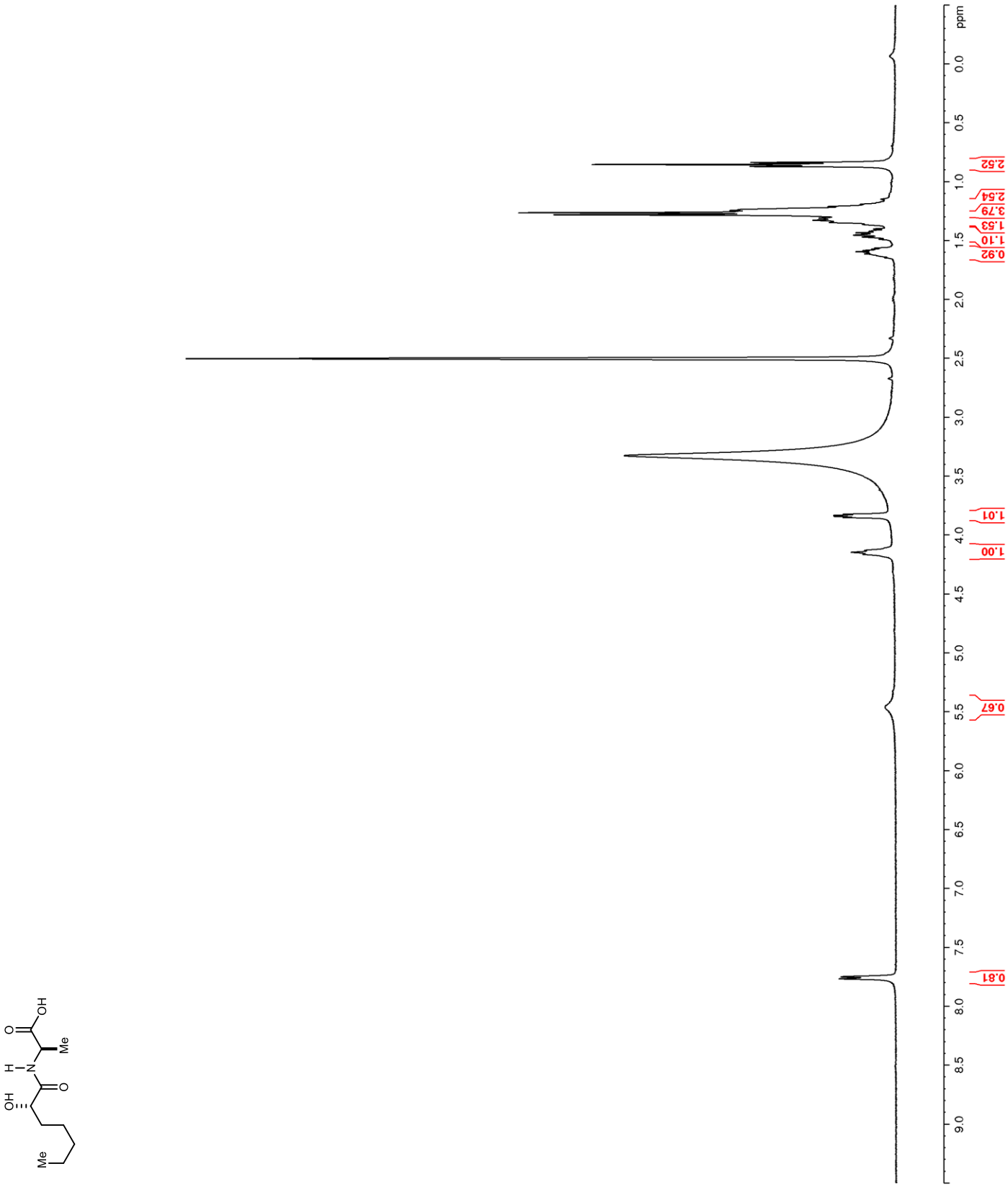

Figure 61. ^{13}C NMR (125 MHz, DMSO-d_6) of **77**

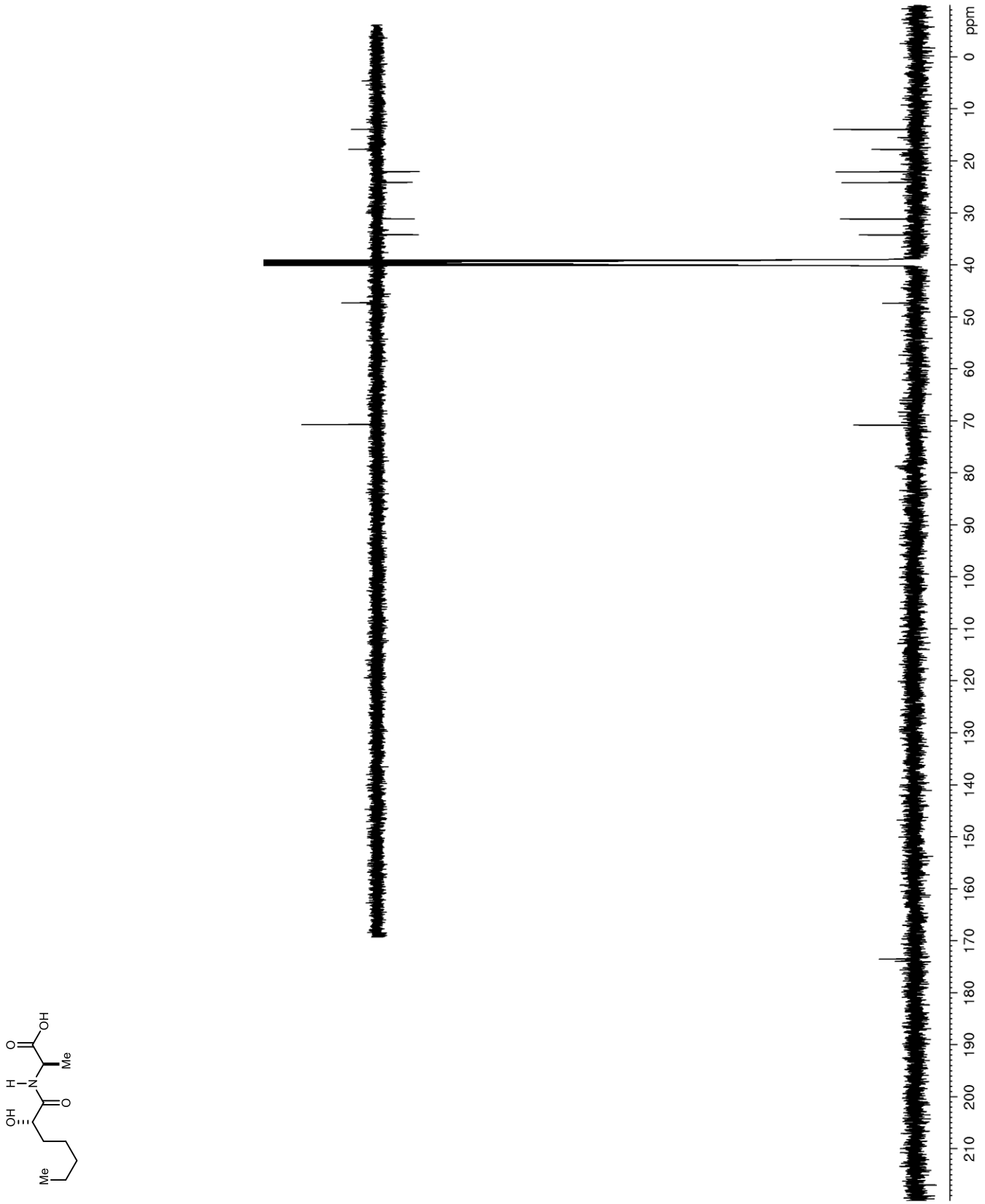

Figure 62. ^{1}H NMR (400 MHz, $CDCl_3$) of **78**

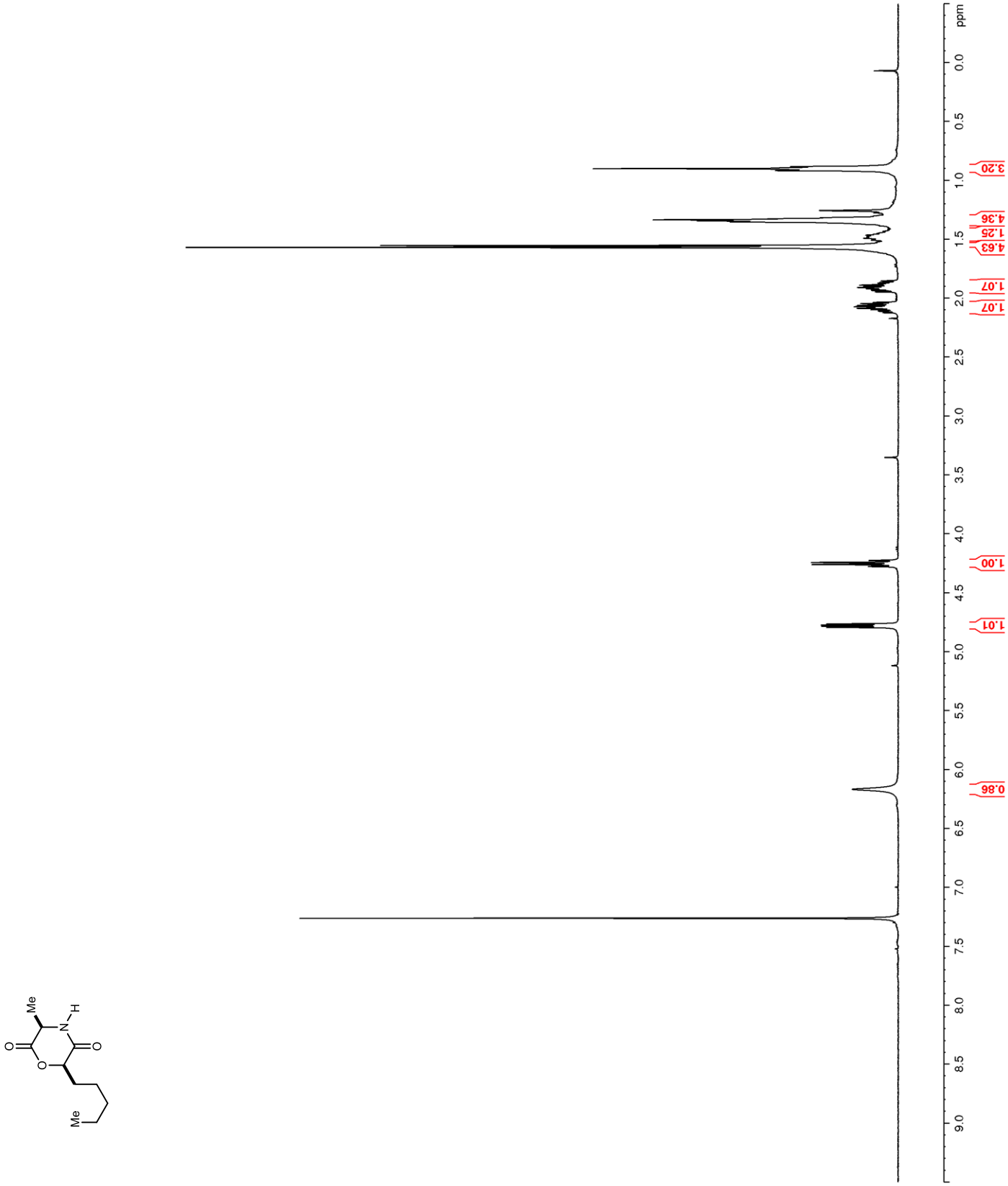

Figure 63. ^{13}C NMR (100 MHz, $CDCl_3$) of **78**

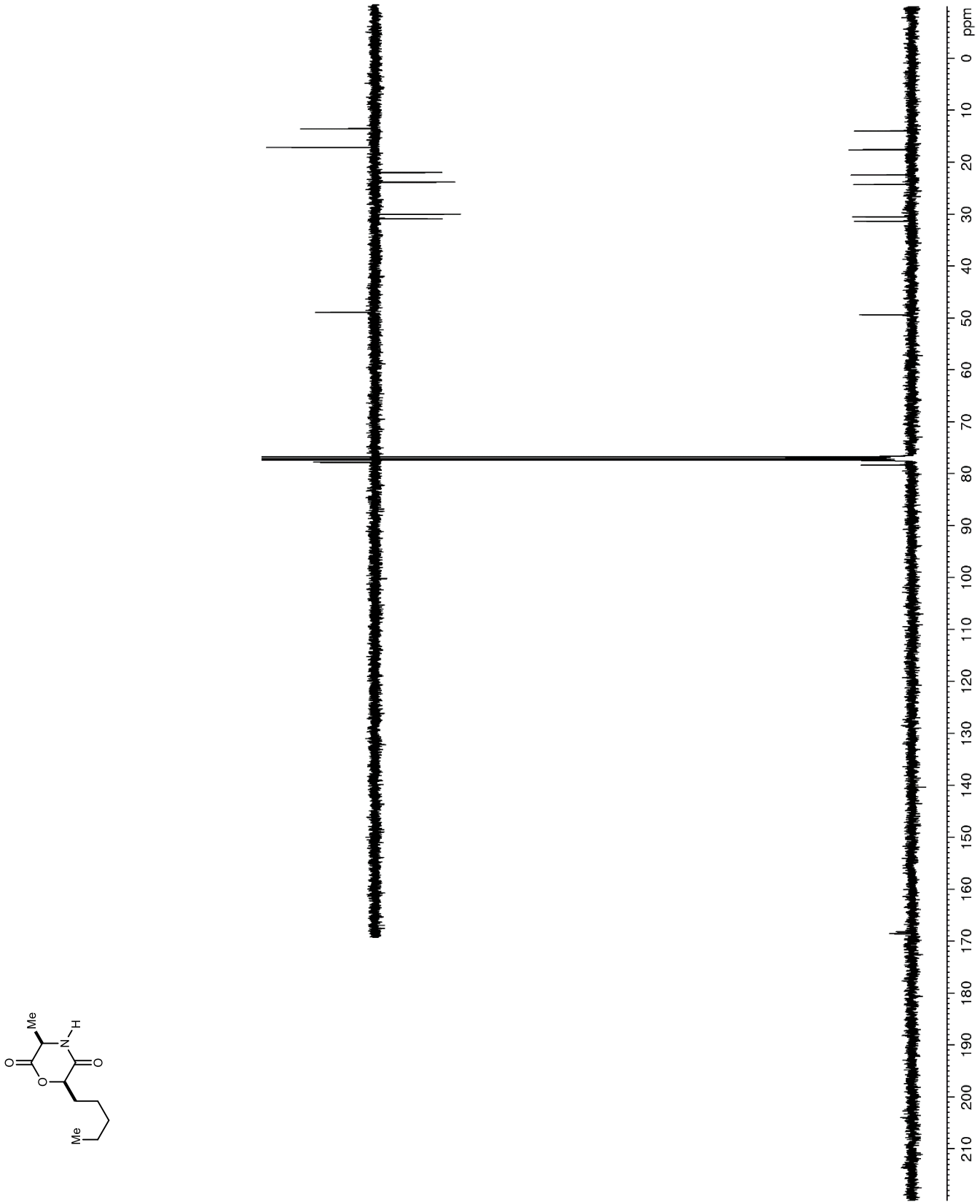

Figure 64. ^{1}H NMR (400 MHz, $CDCl_3$) of **79**

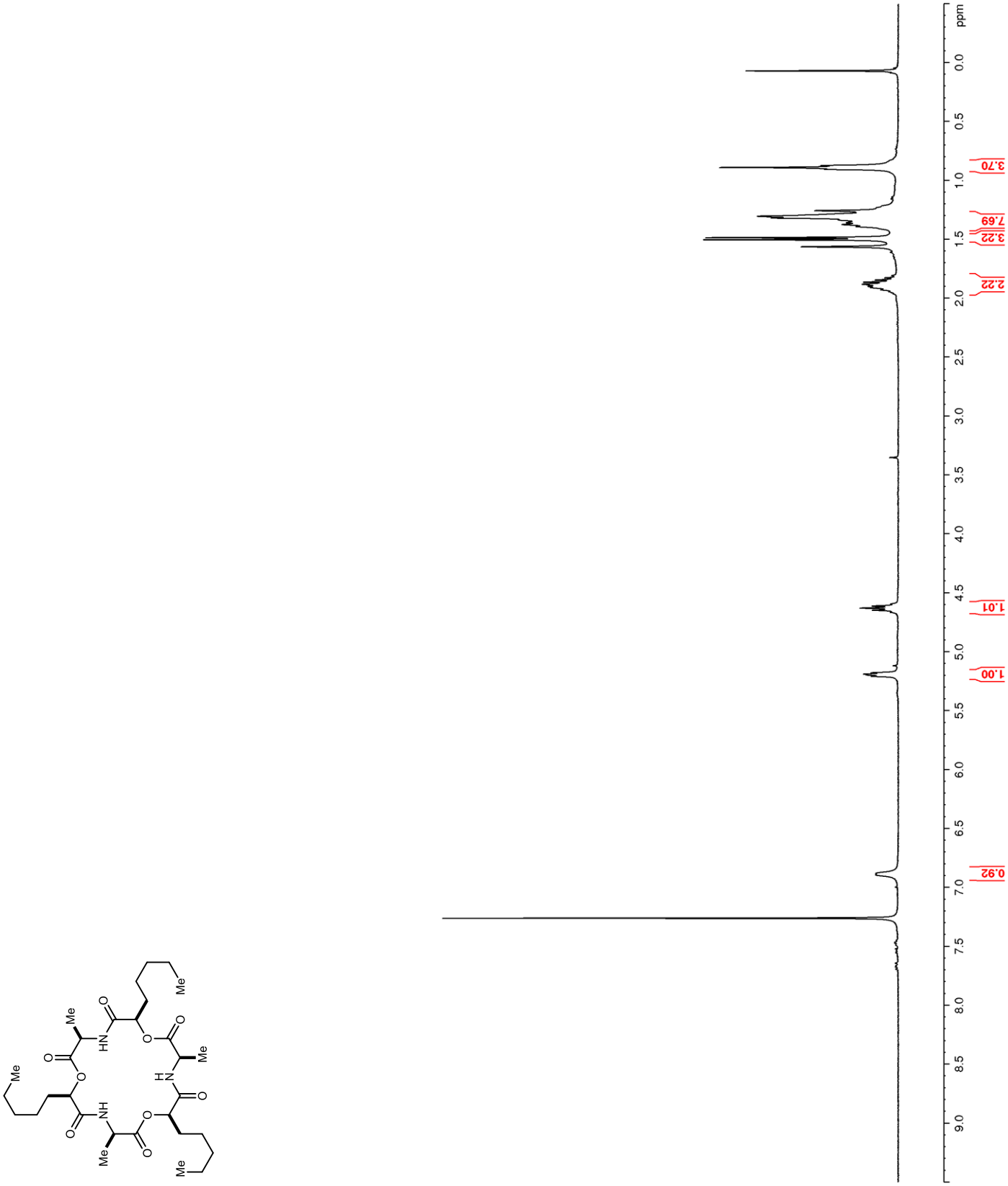

Figure 65. ^{13}C NMR (150 MHz, $CDCl_3$) of **79**

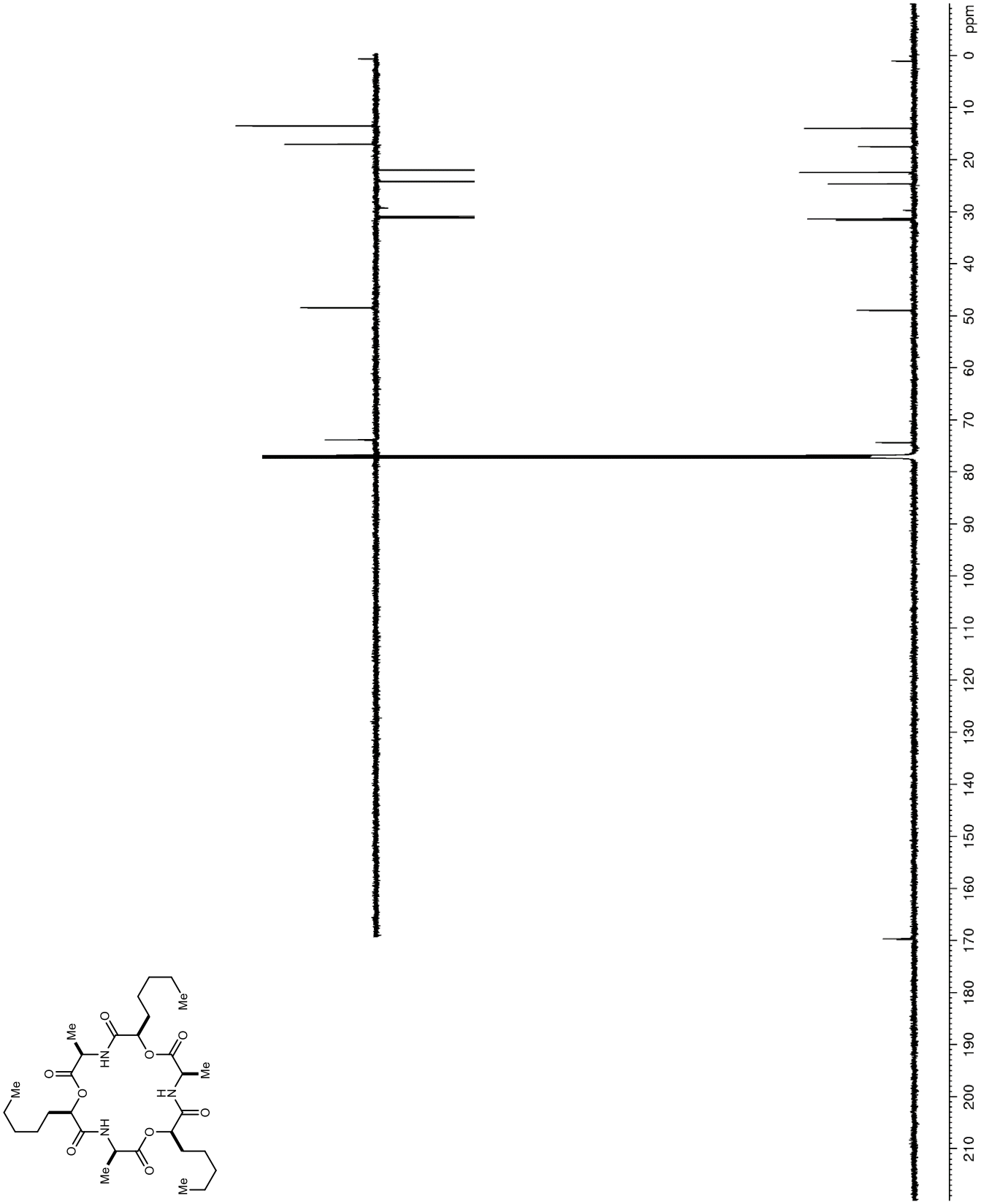

Figure 66. ^{1}H NMR (600 MHz, $CDCl_3$) of **80**

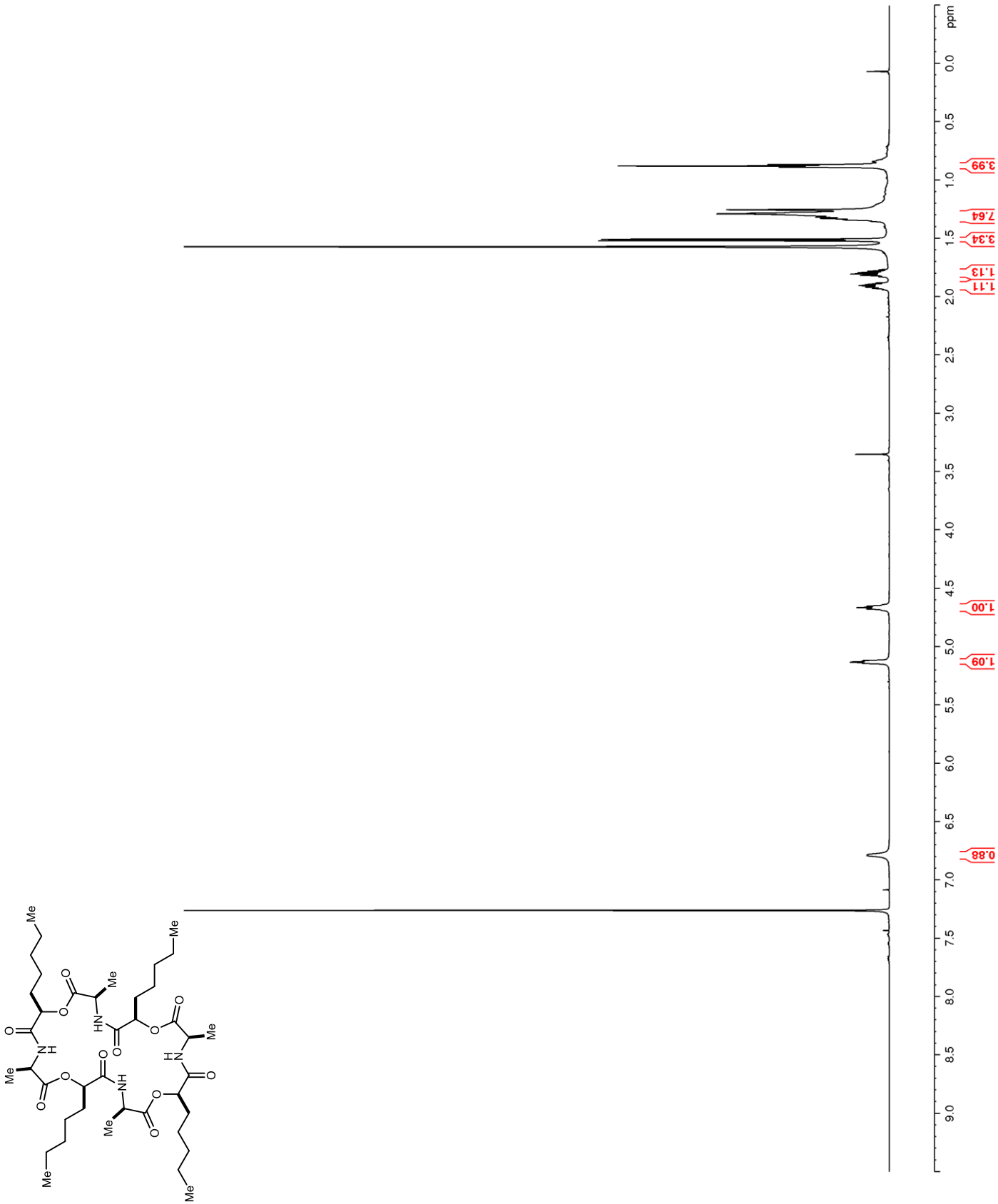

Figure 67. ^{13}C NMR (150 MHz, $CDCl_3$) of **80**

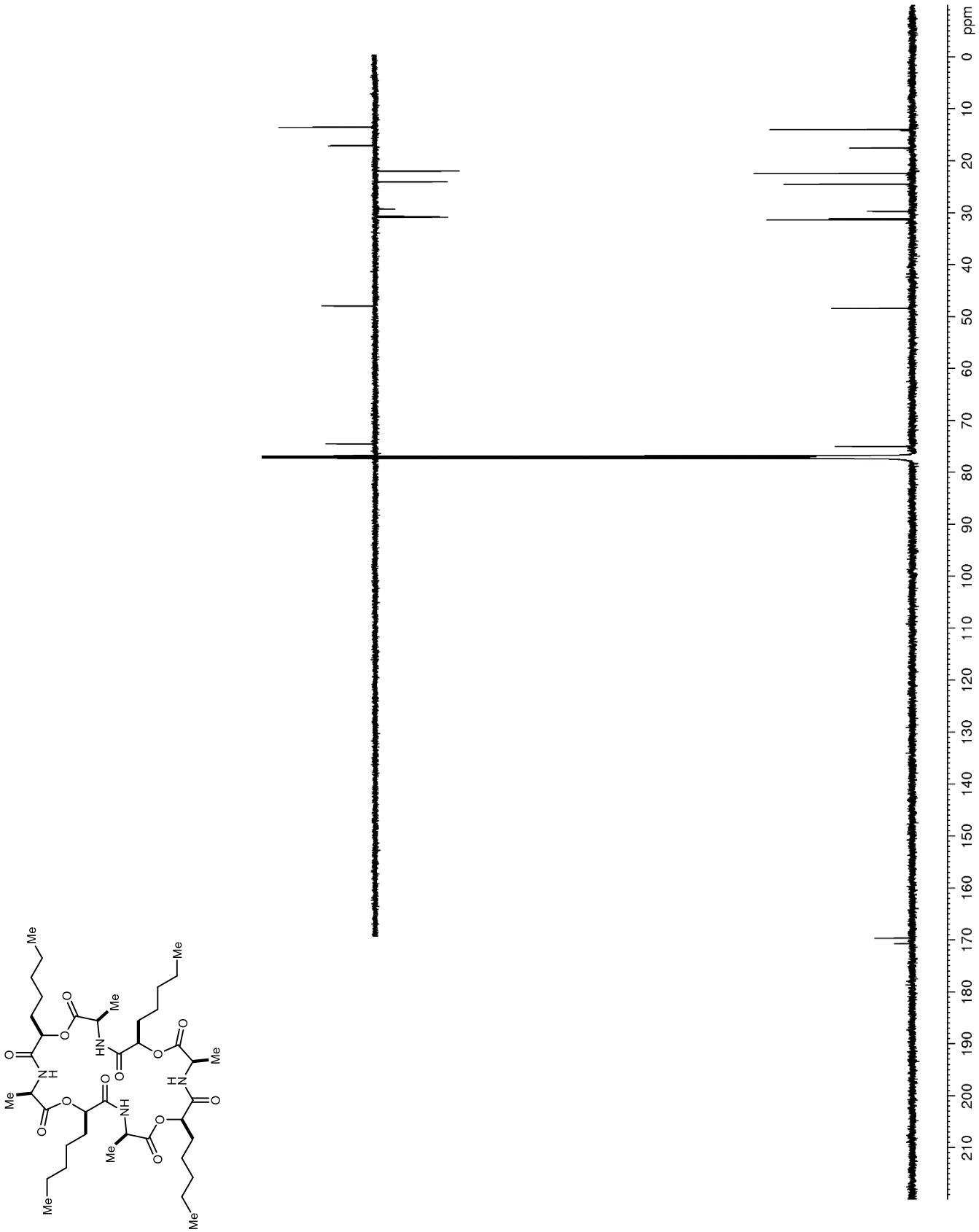

Figure 68. ^{1}H NMR (400 MHz, $CDCl_3$) of **81**

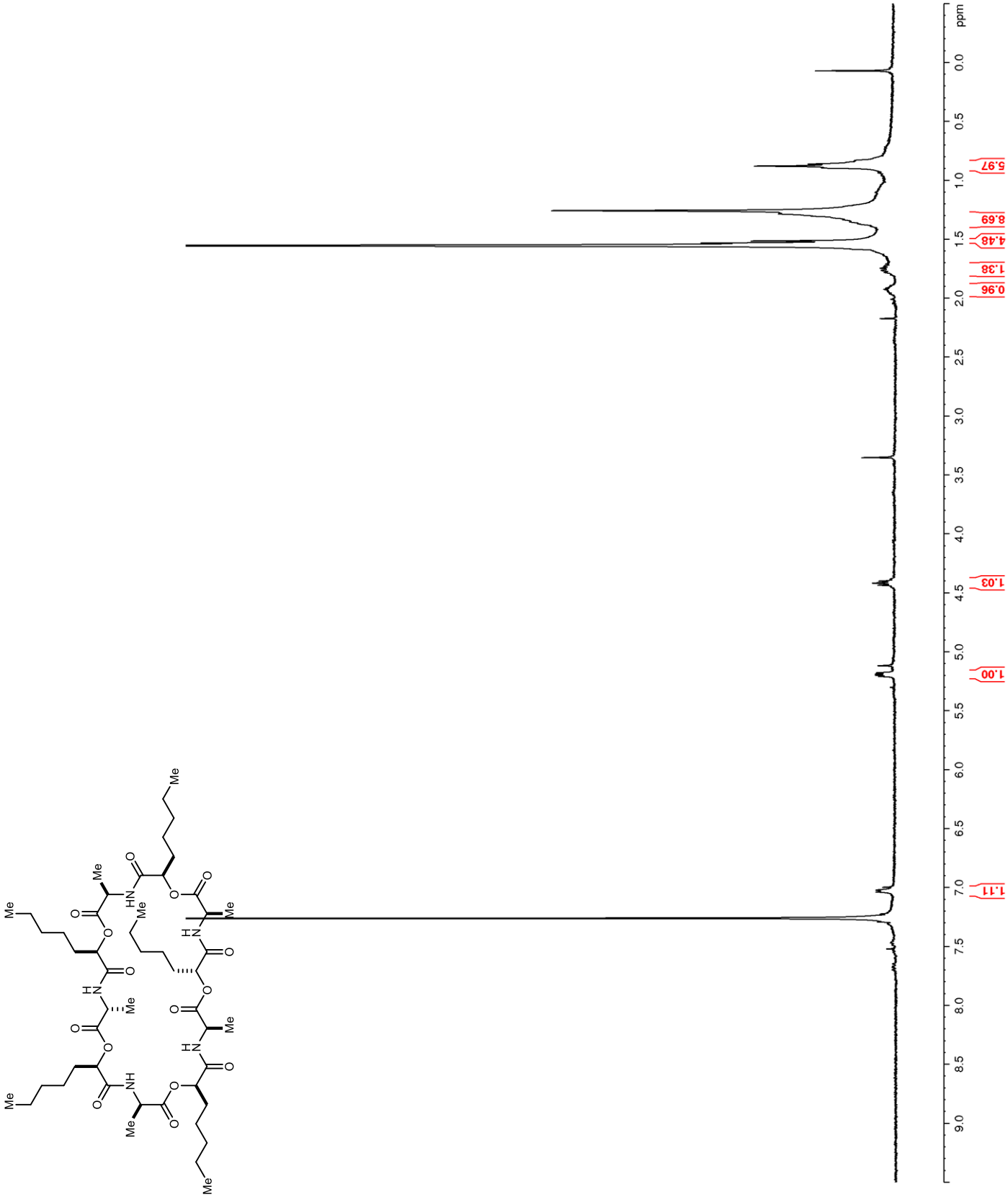

Figure 69. ^{13}C NMR (150 MHz, $CDCl_3$) of **81**

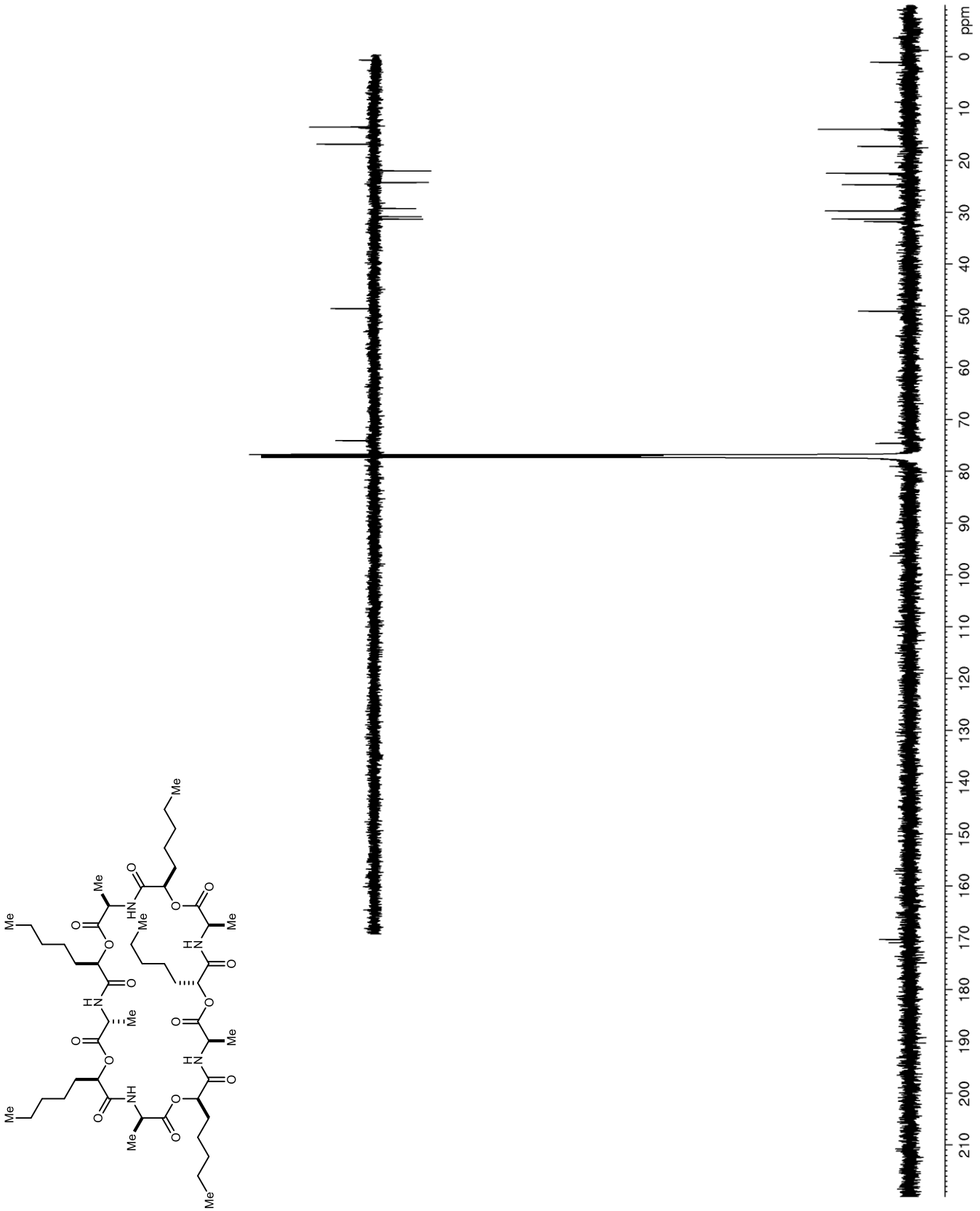

Figure 70. ^{1}H NMR (400 MHz, DMSO-d_6) of **91**

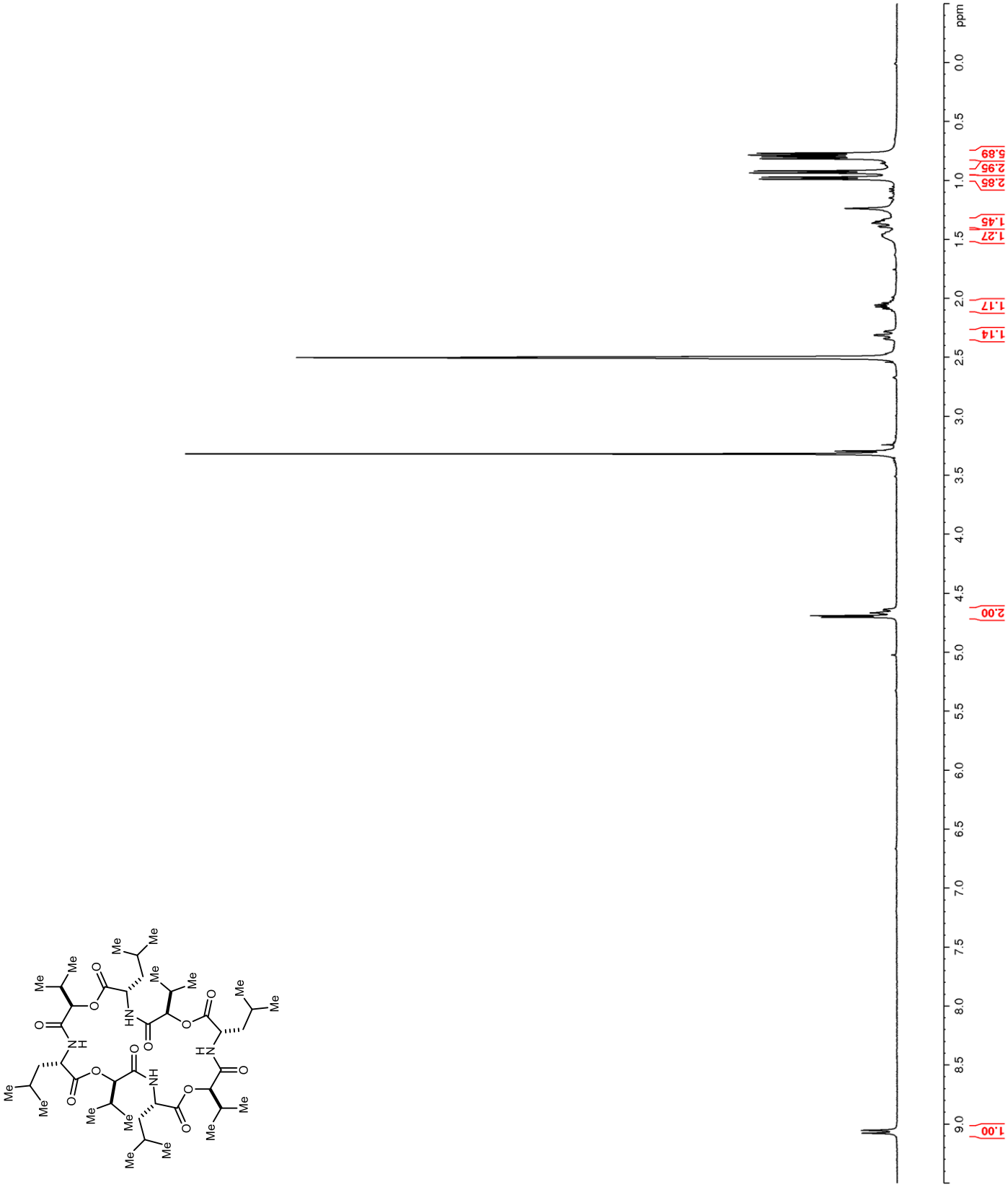

Figure 71. ^{13}C NMR (125 MHz, DMSO-d_6) of **91**

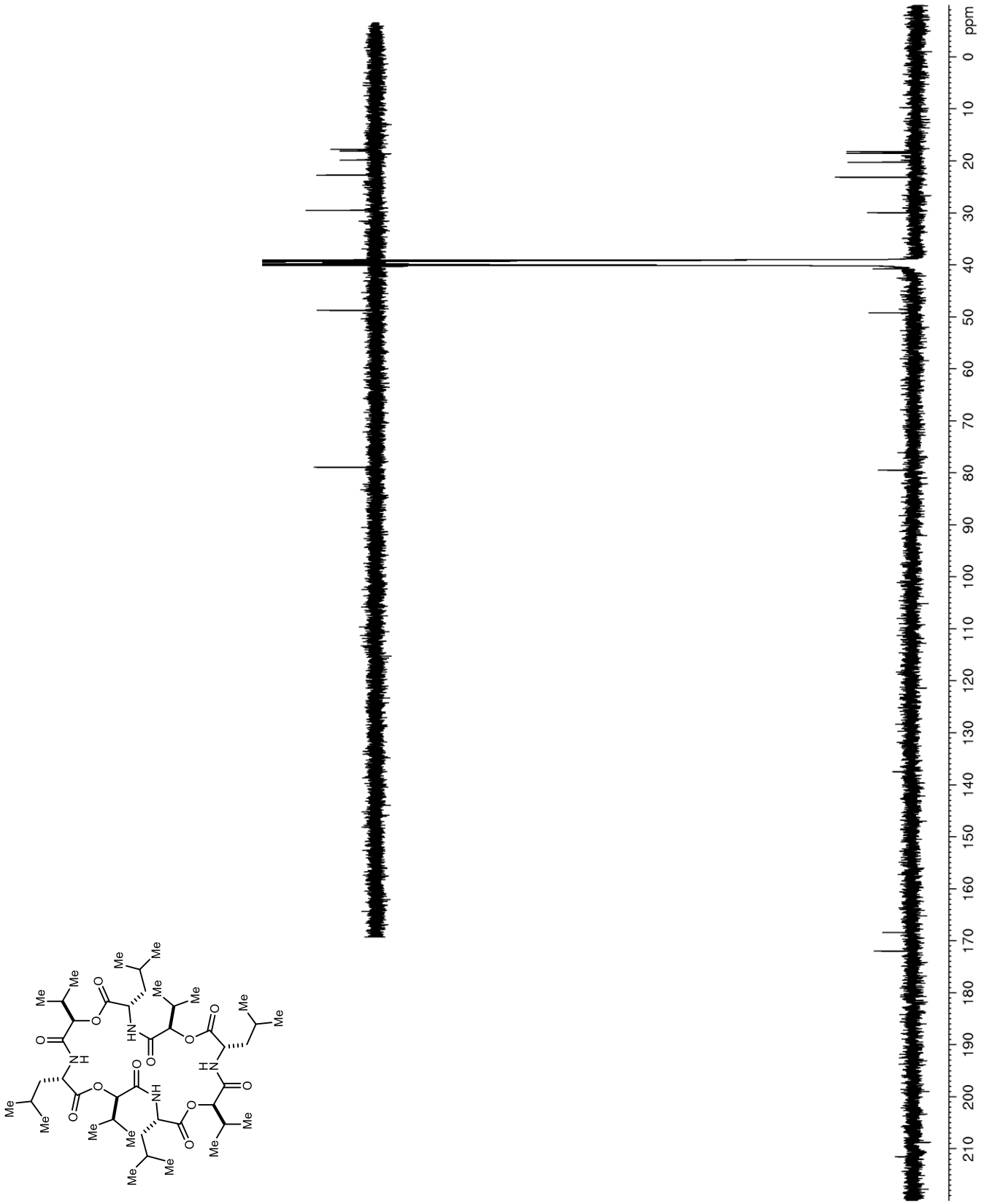

Figure 72. ^{1}H NMR (400 MHz, $CDCl_3$) of **92**

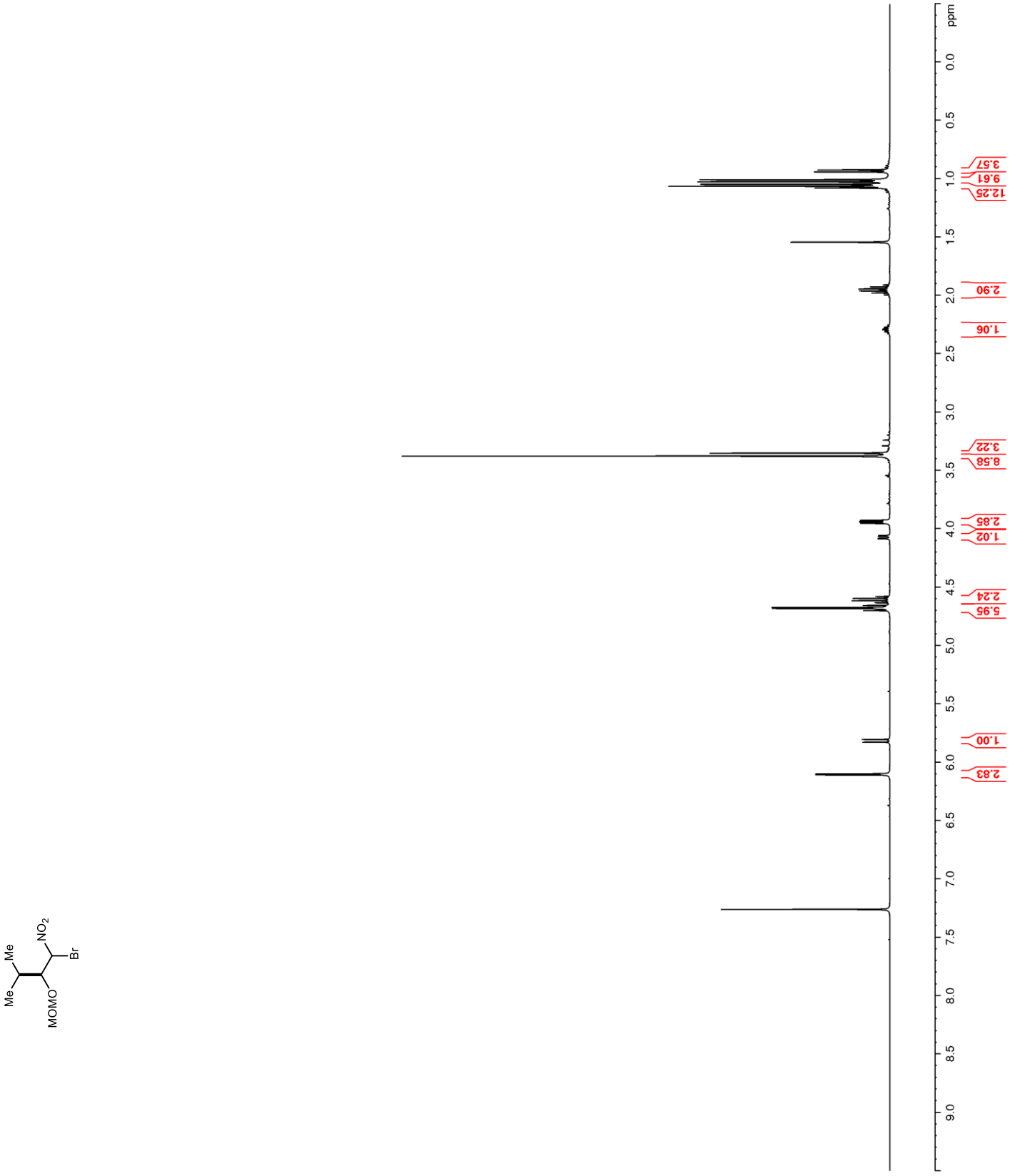

Figure 73. ^{13}C NMR (100 MHz, $CDCl_3$) of **92**

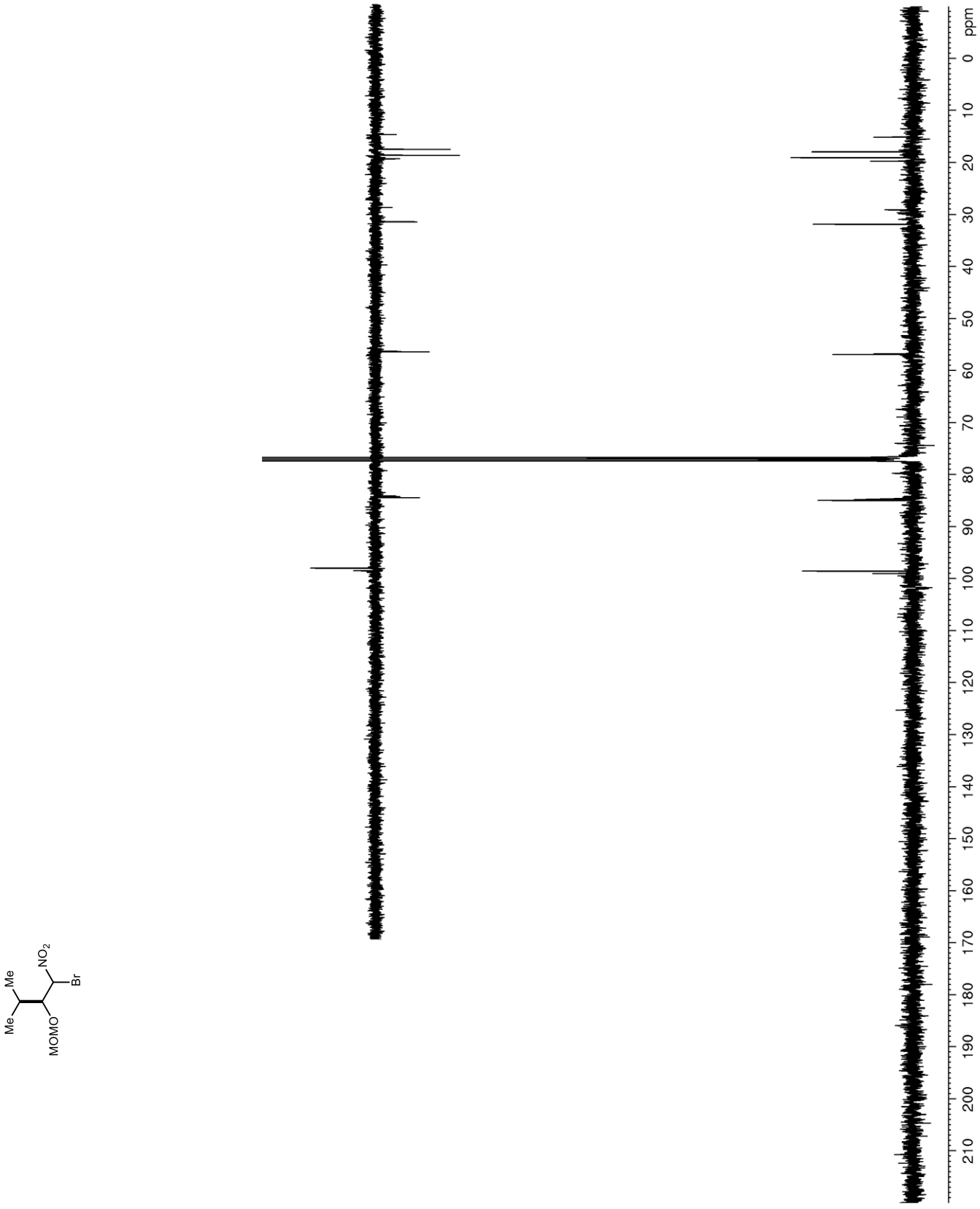

Figure 74. ^{1}H NMR (500 MHz, $CDCl_3$) of **93**

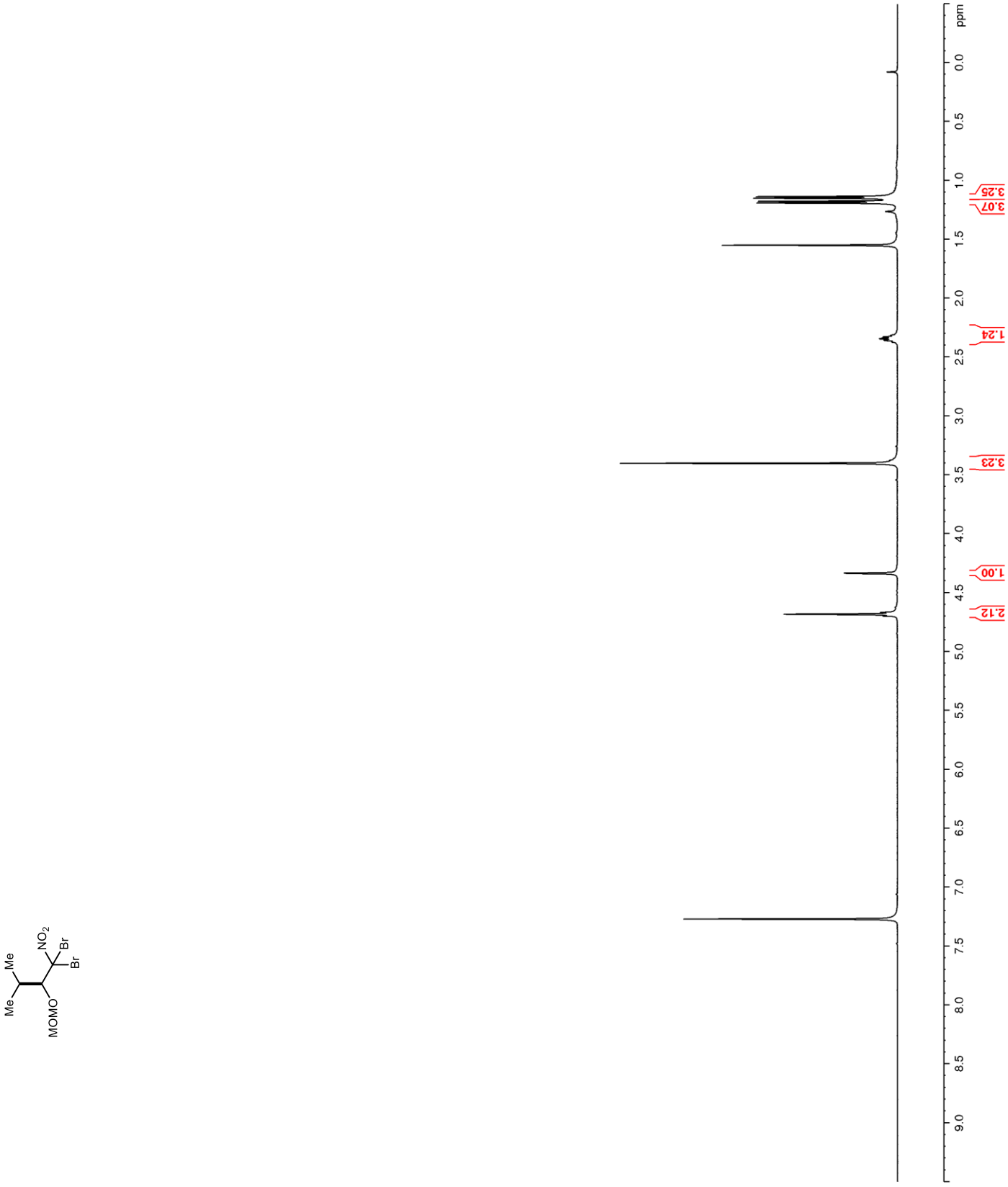

Figure 75. ^{13}C NMR (100 MHz, $CDCl_3$) of **93**

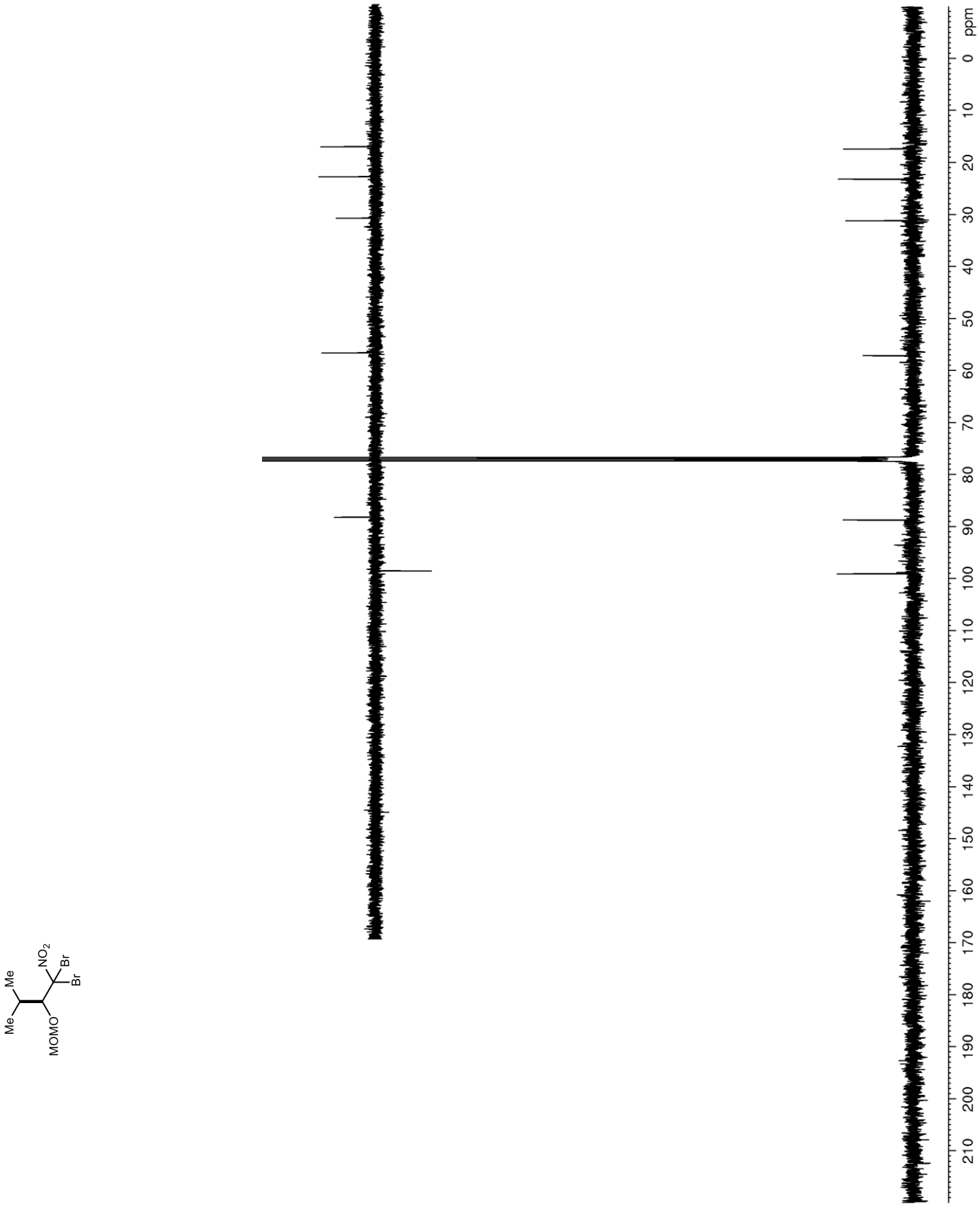

Figure 76. ^{1}H NMR (400 MHz, $CDCl_3$) of **95**

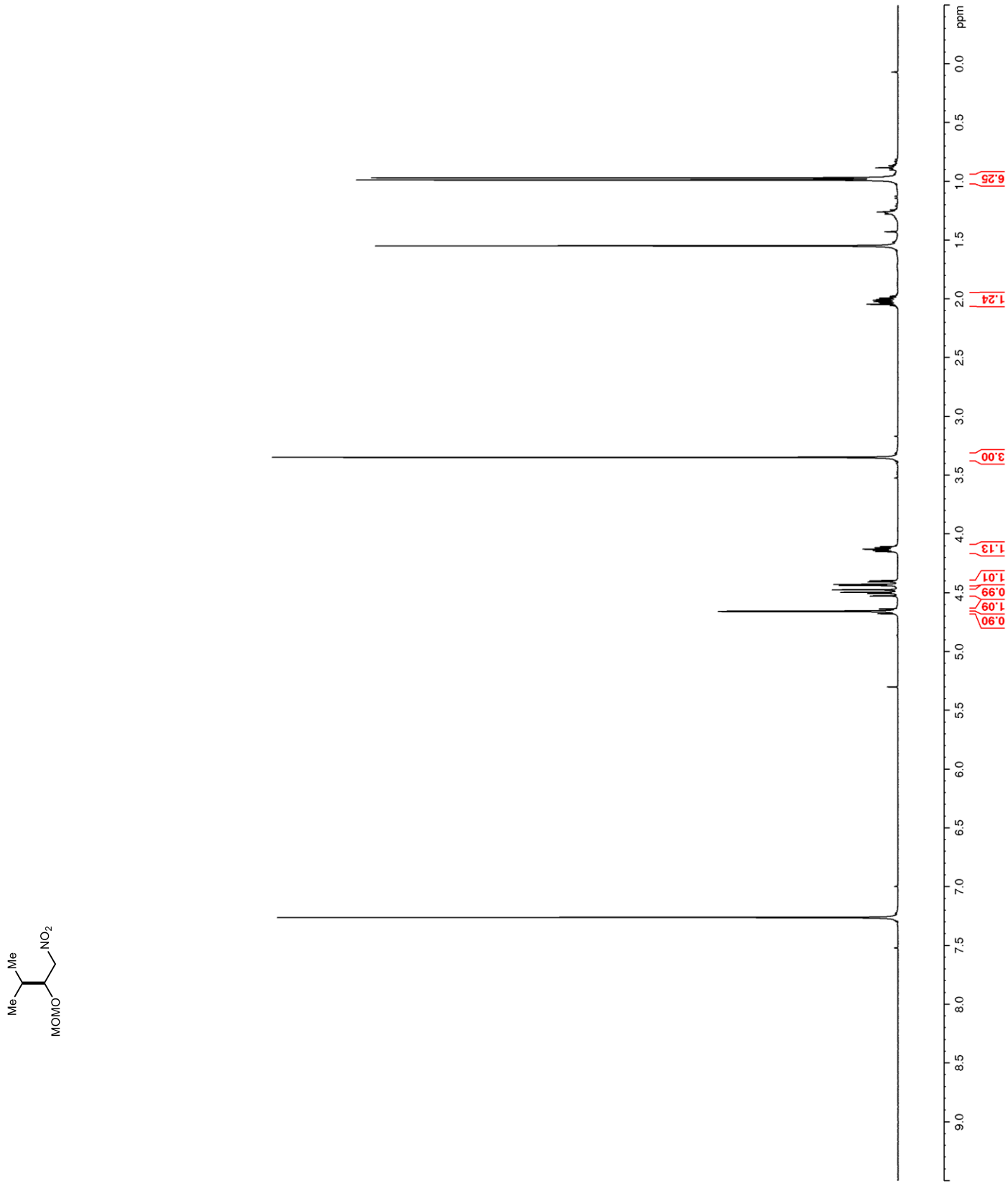

Figure 77. ^{13}C NMR (100 MHz, $CDCl_3$) of **95**

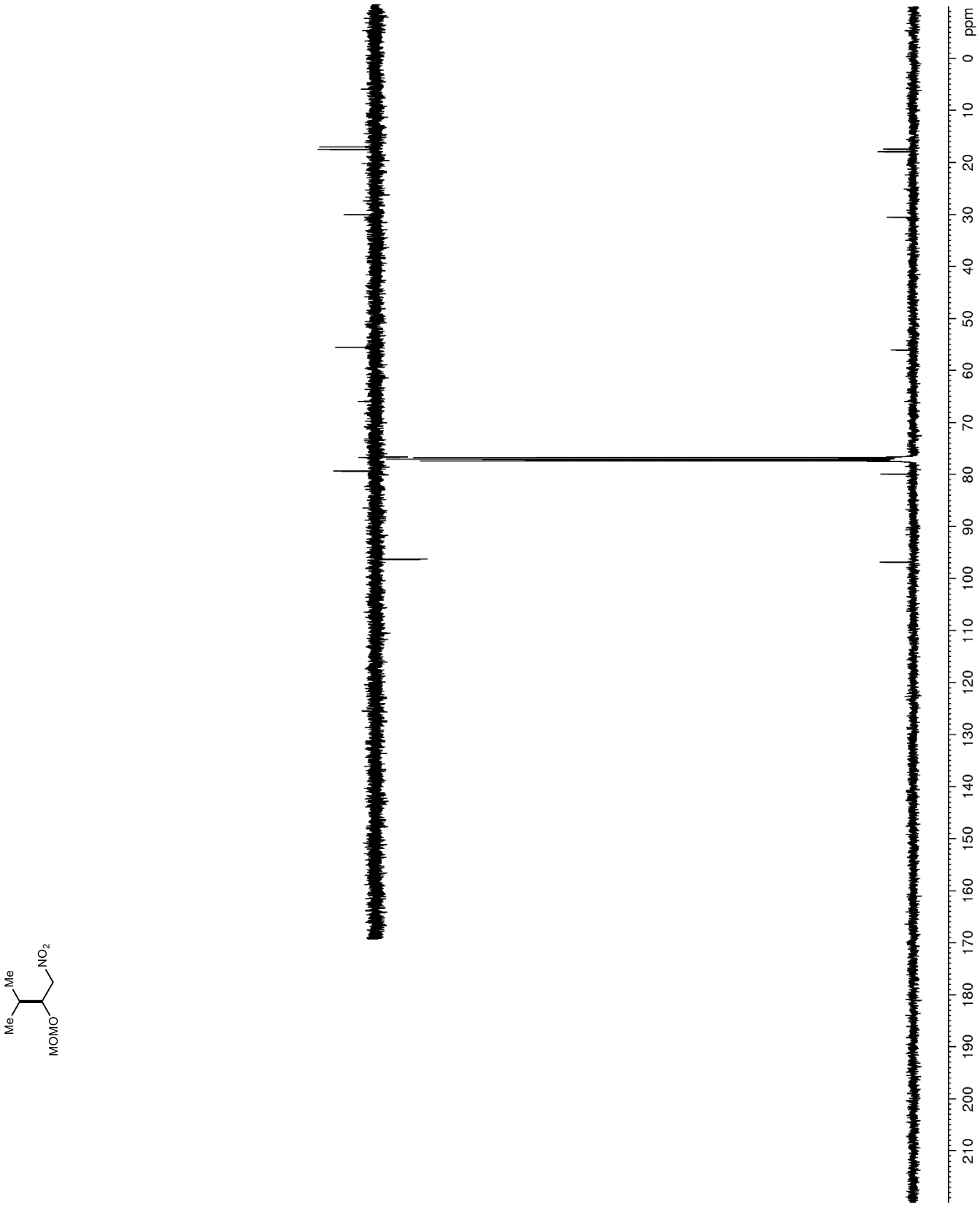

Figure 78. ^{1}H NMR (400 MHz, $CDCl_3$) of **97**

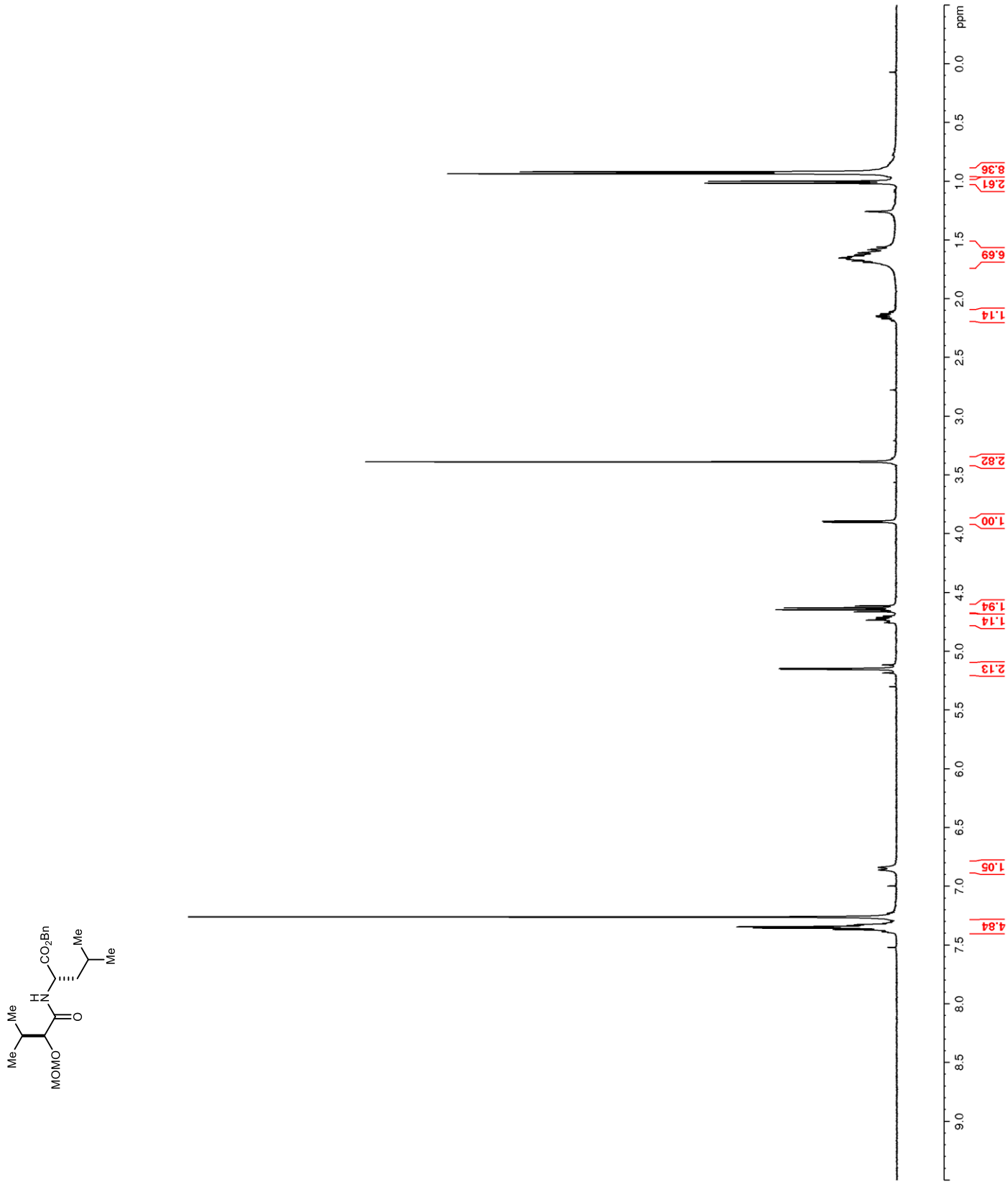

Figure 79. ^{13}C NMR (100 MHz, $CDCl_3$) of **97**

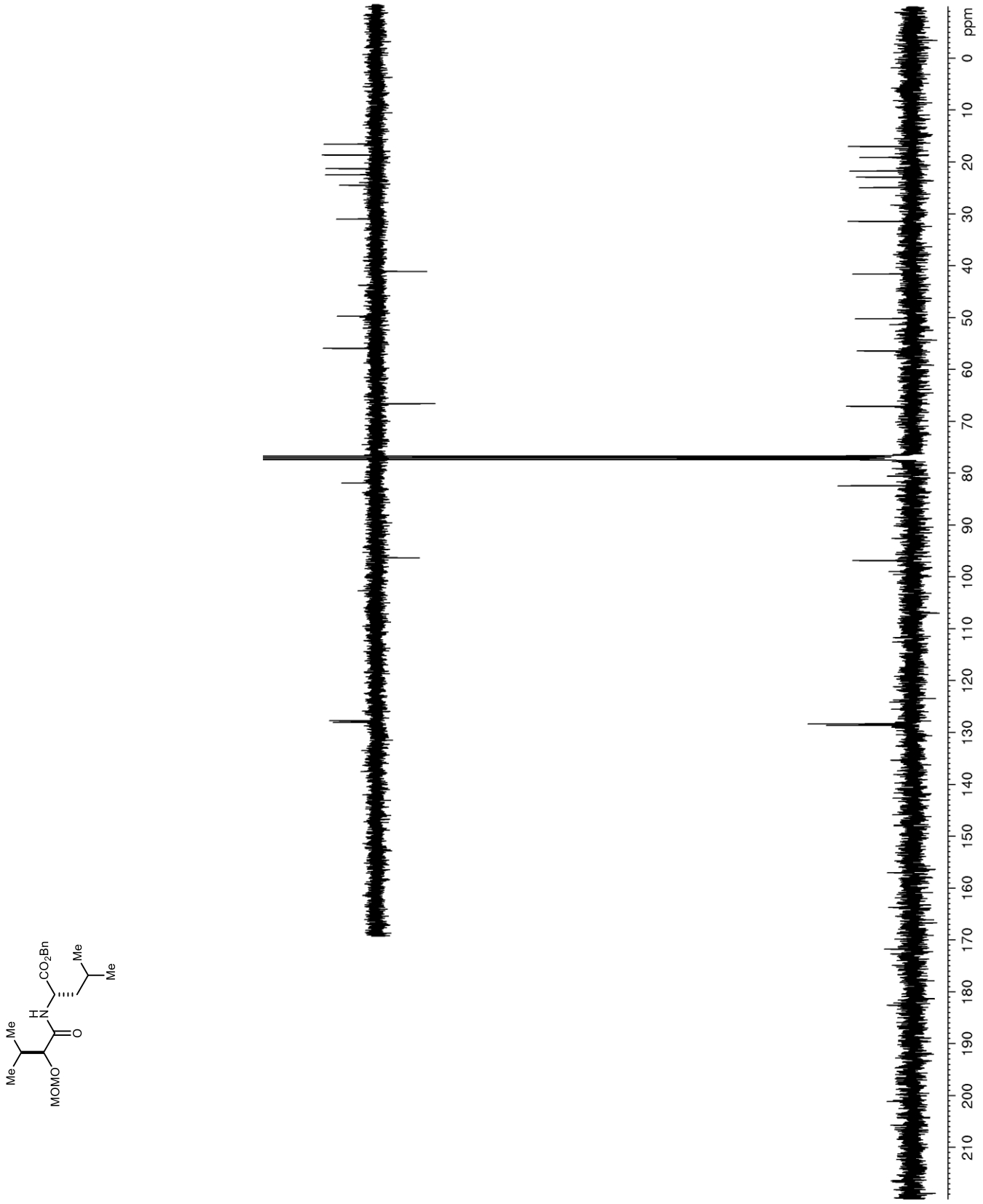

Figure 80. ^{1}H NMR (400 MHz, $CDCl_3$) of **99**

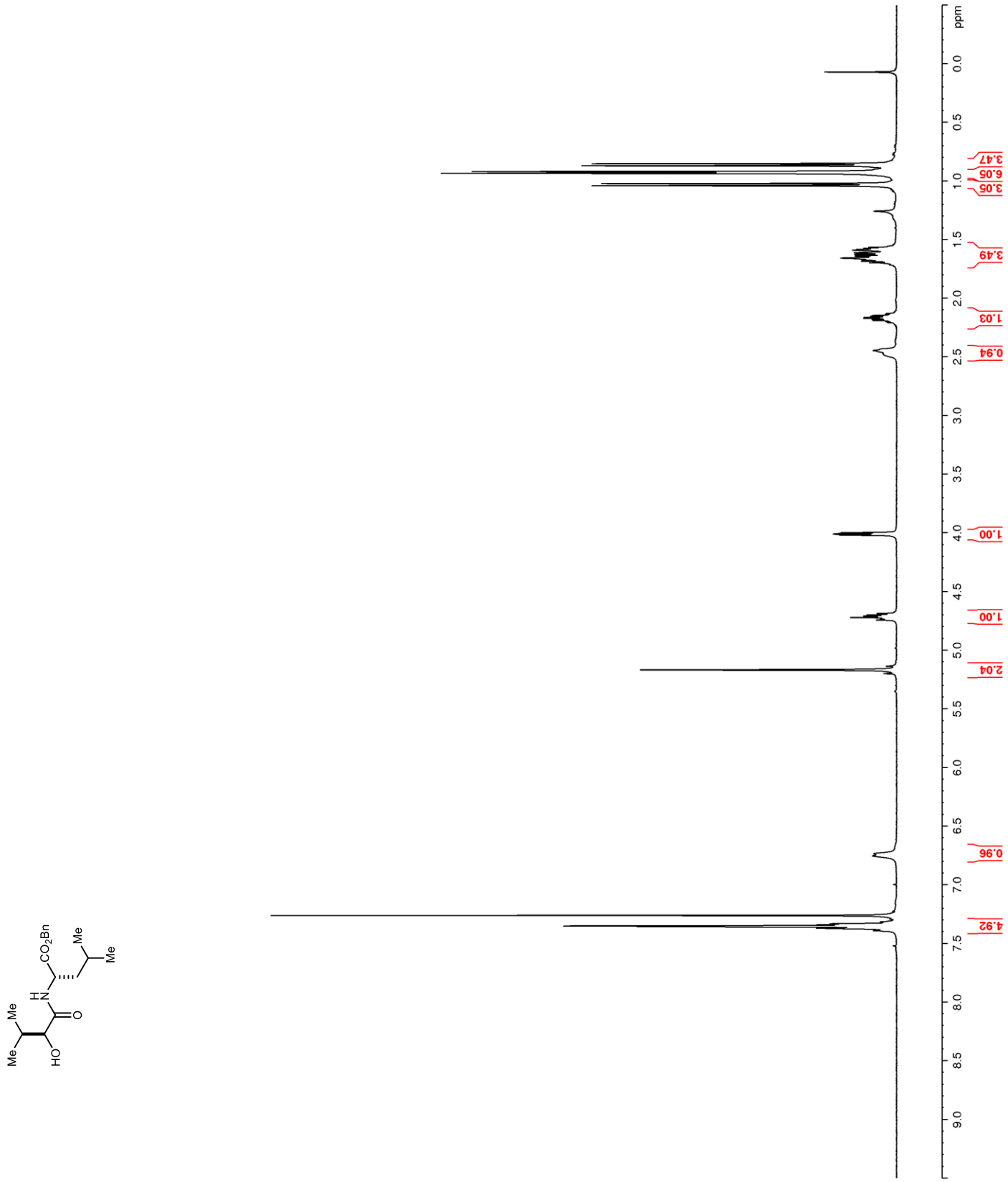

Figure 81. ^{13}C NMR (125 MHz, $CDCl_3$) of **99**

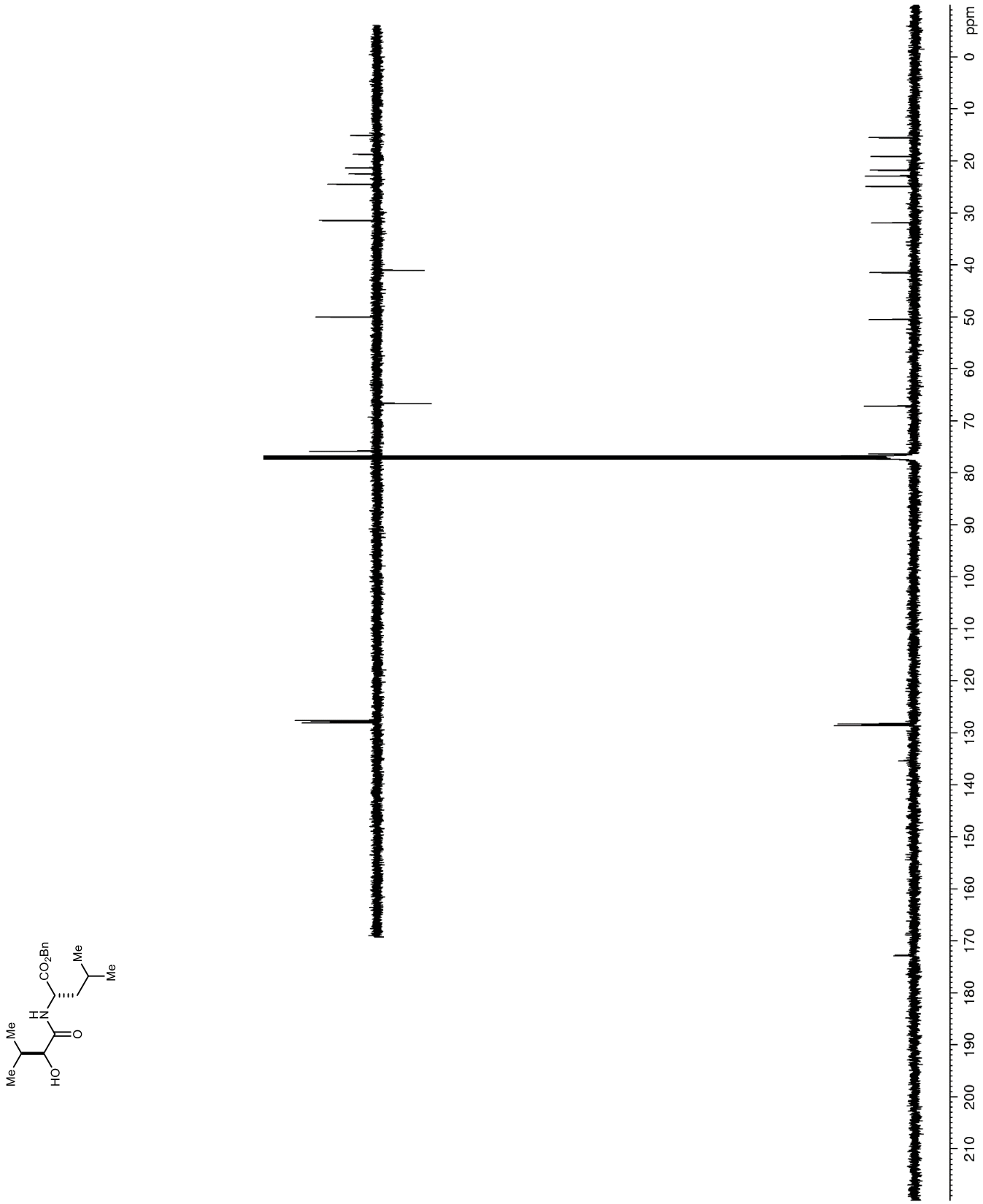

Figure 82. ^{1}H NMR (400 MHz, $CDCl_3$) of **100**

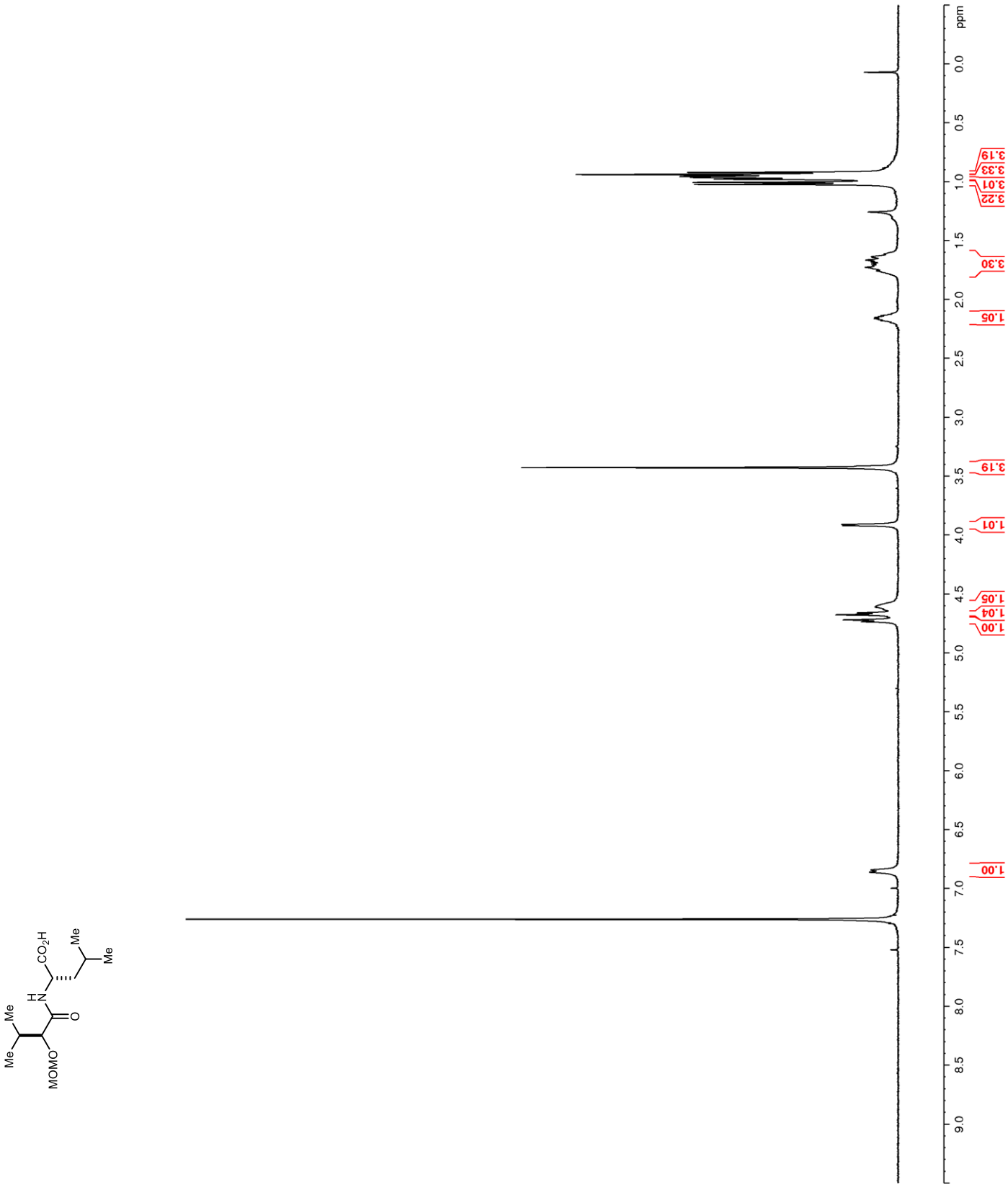

Figure 83. ^{13}C NMR (125 MHz, $CDCl_3$) of **100**

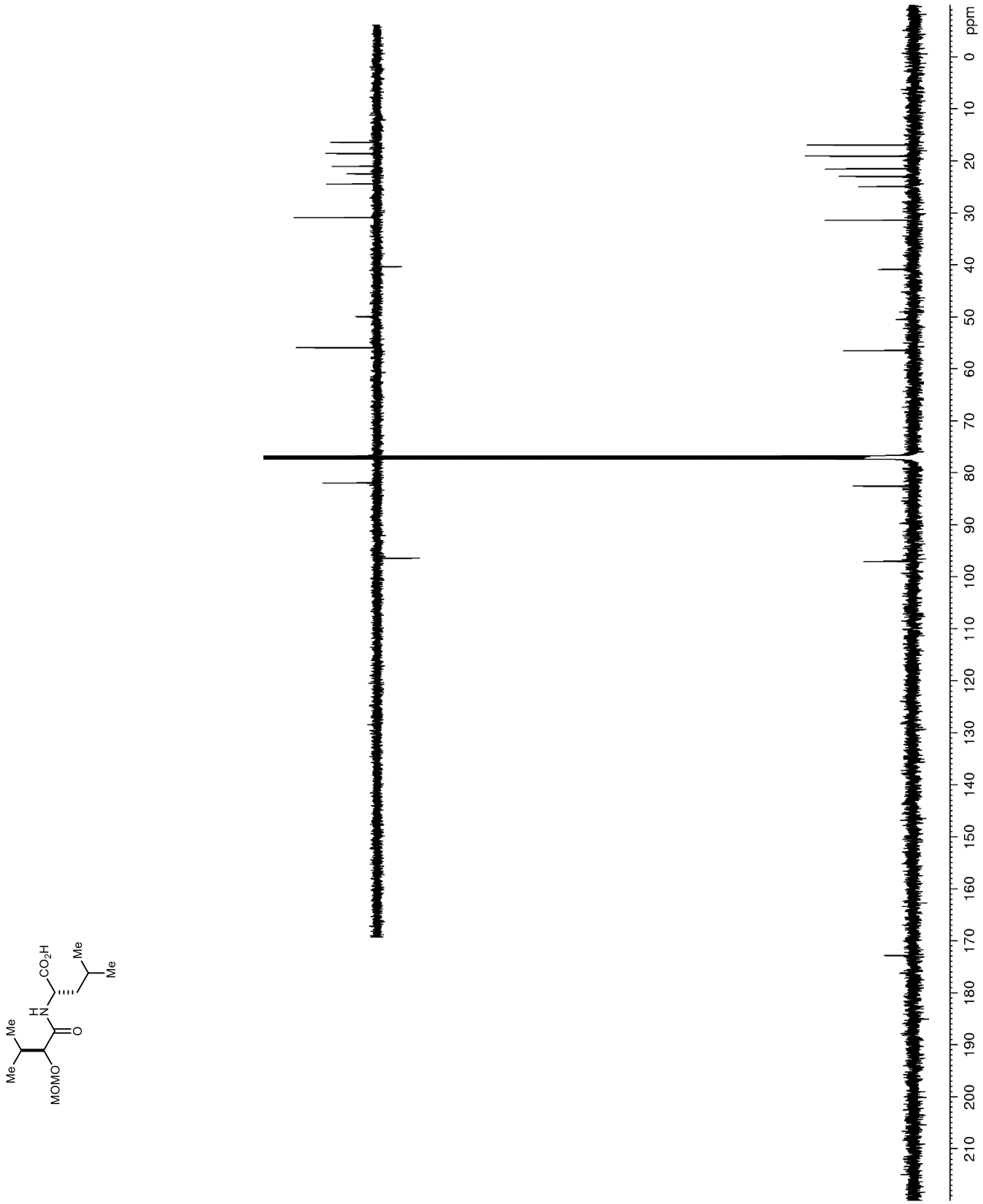

Figure 84. ^{1}H NMR (400 MHz, $CDCl_3$) of **101**

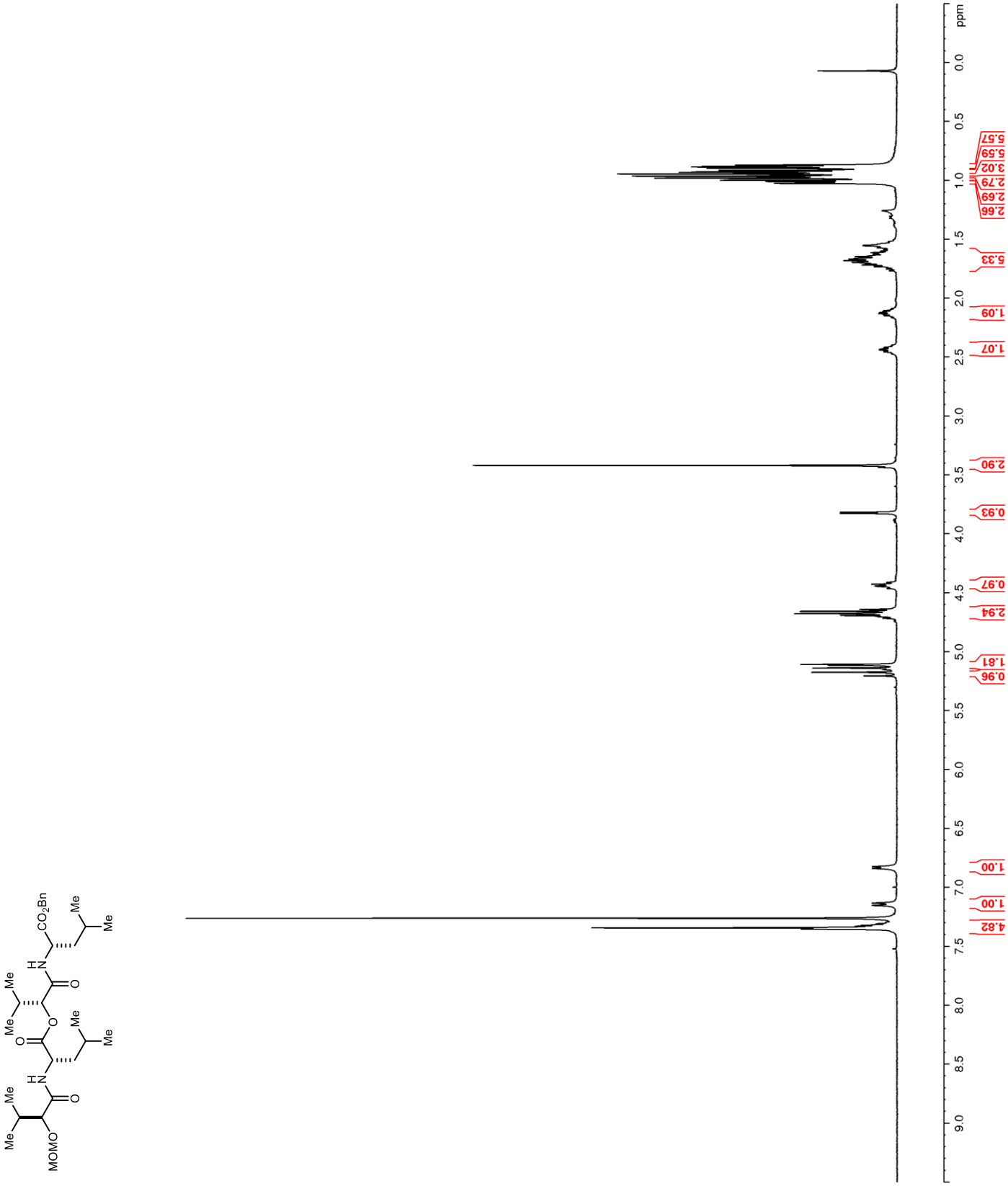

Figure 85. ^{13}C NMR (125 MHz, $CDCl_3$) of **101**

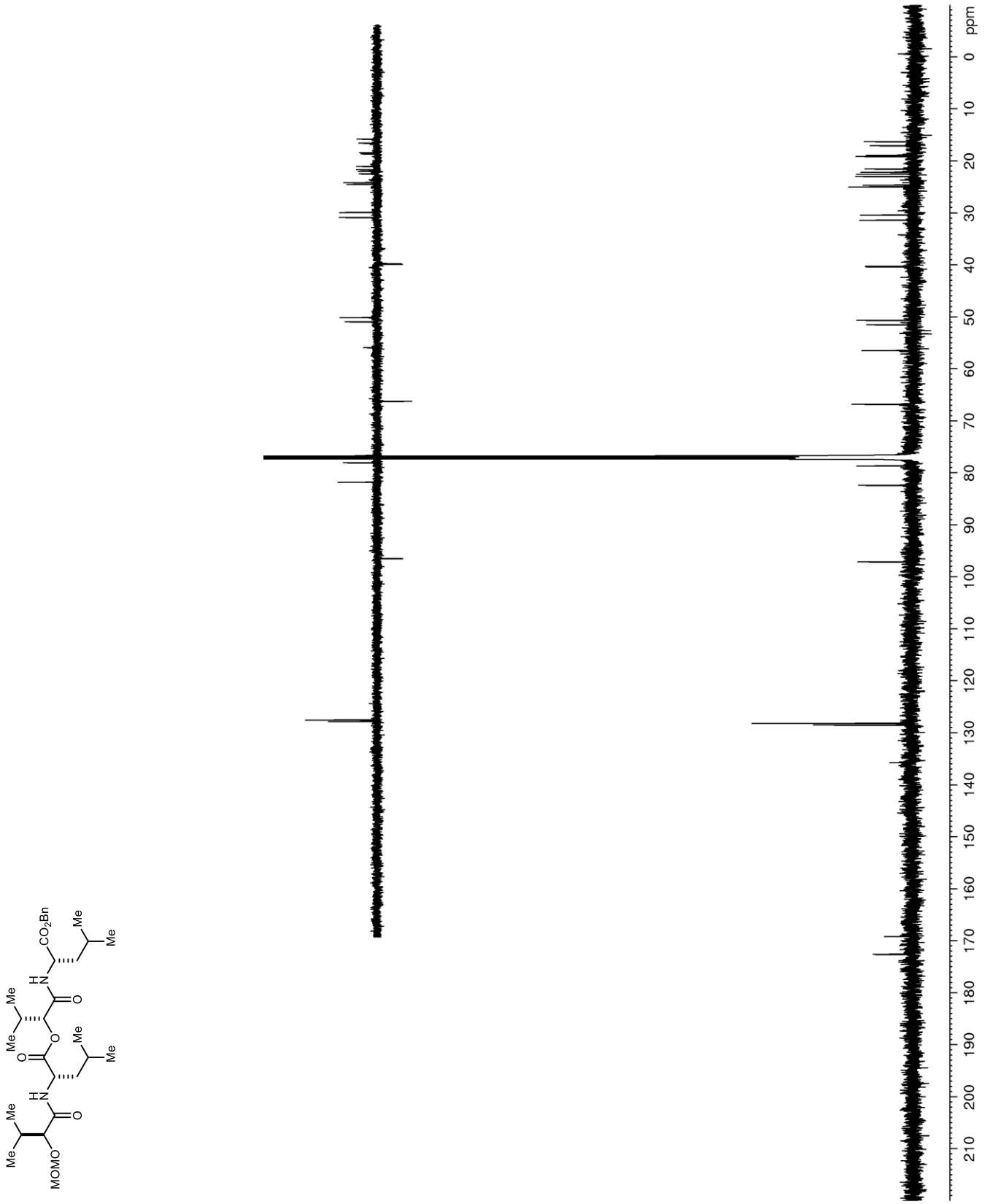

Figure 86. ^{1}H NMR (400 MHz, DMSO-d_6) of **102**

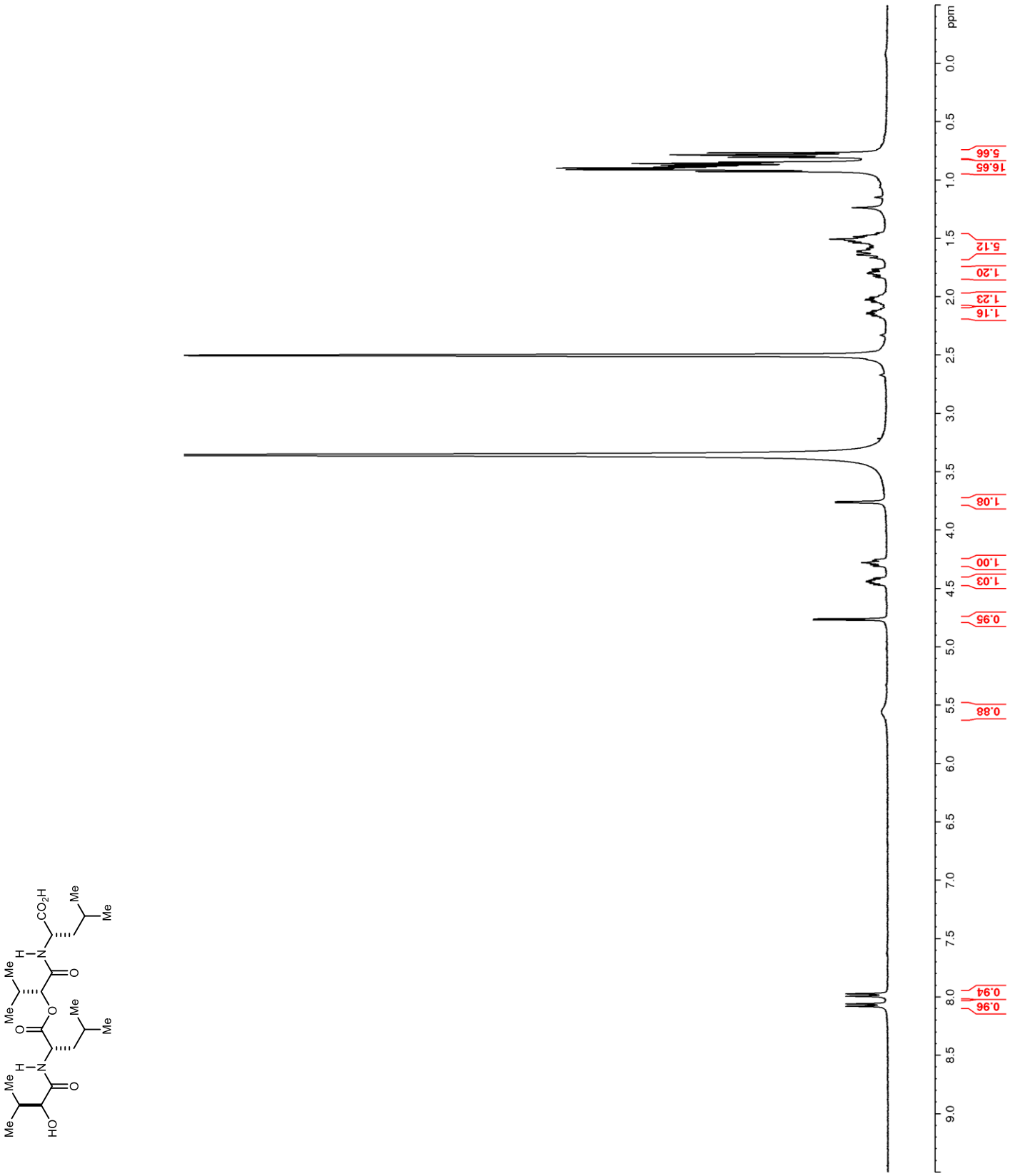

Figure 87. ^{13}C NMR (125 MHz, DMSO-d_6) of **20**

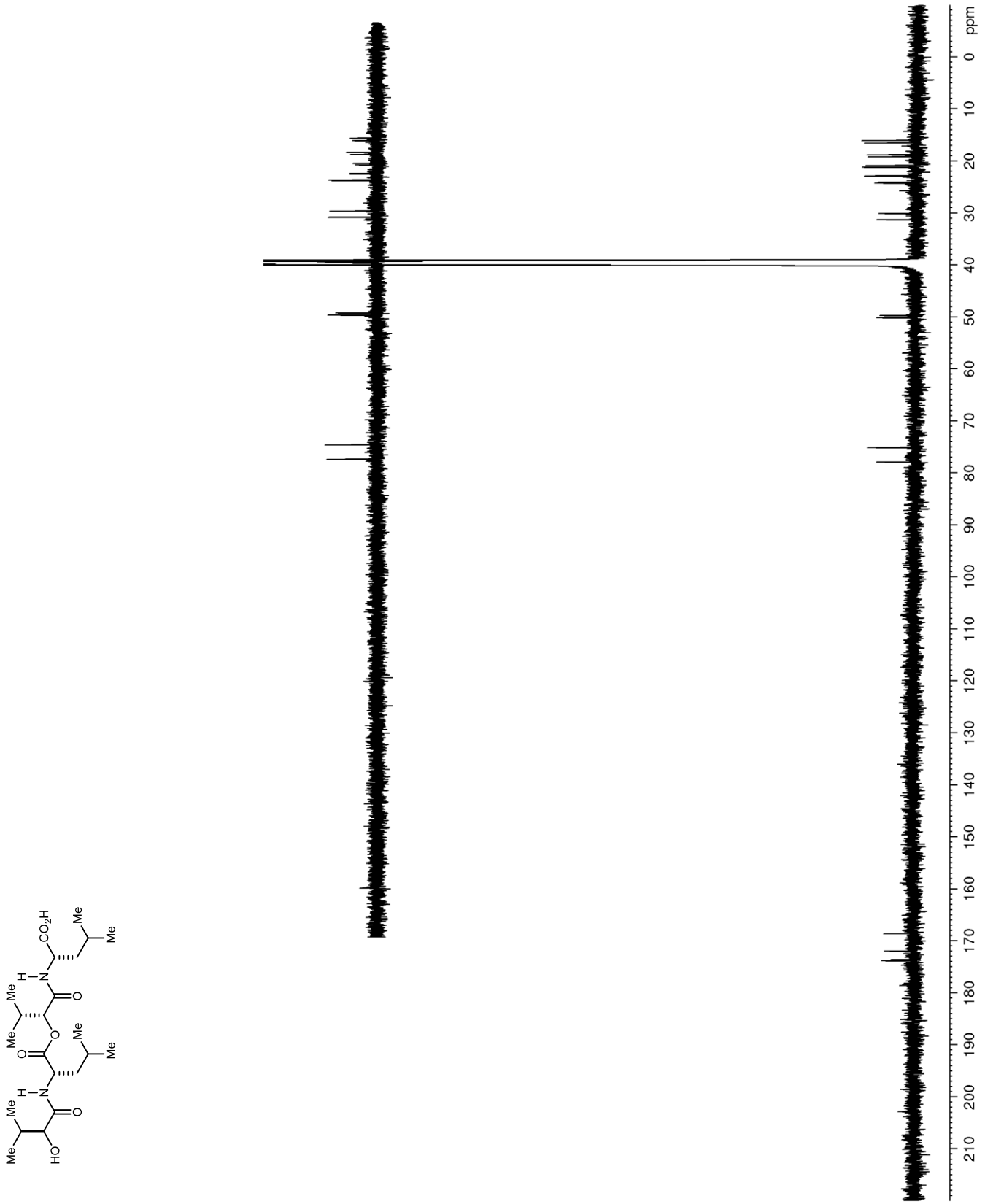

Figure 88. ^{1}H NMR (400 MHz, $CDCl_3$) of **108**

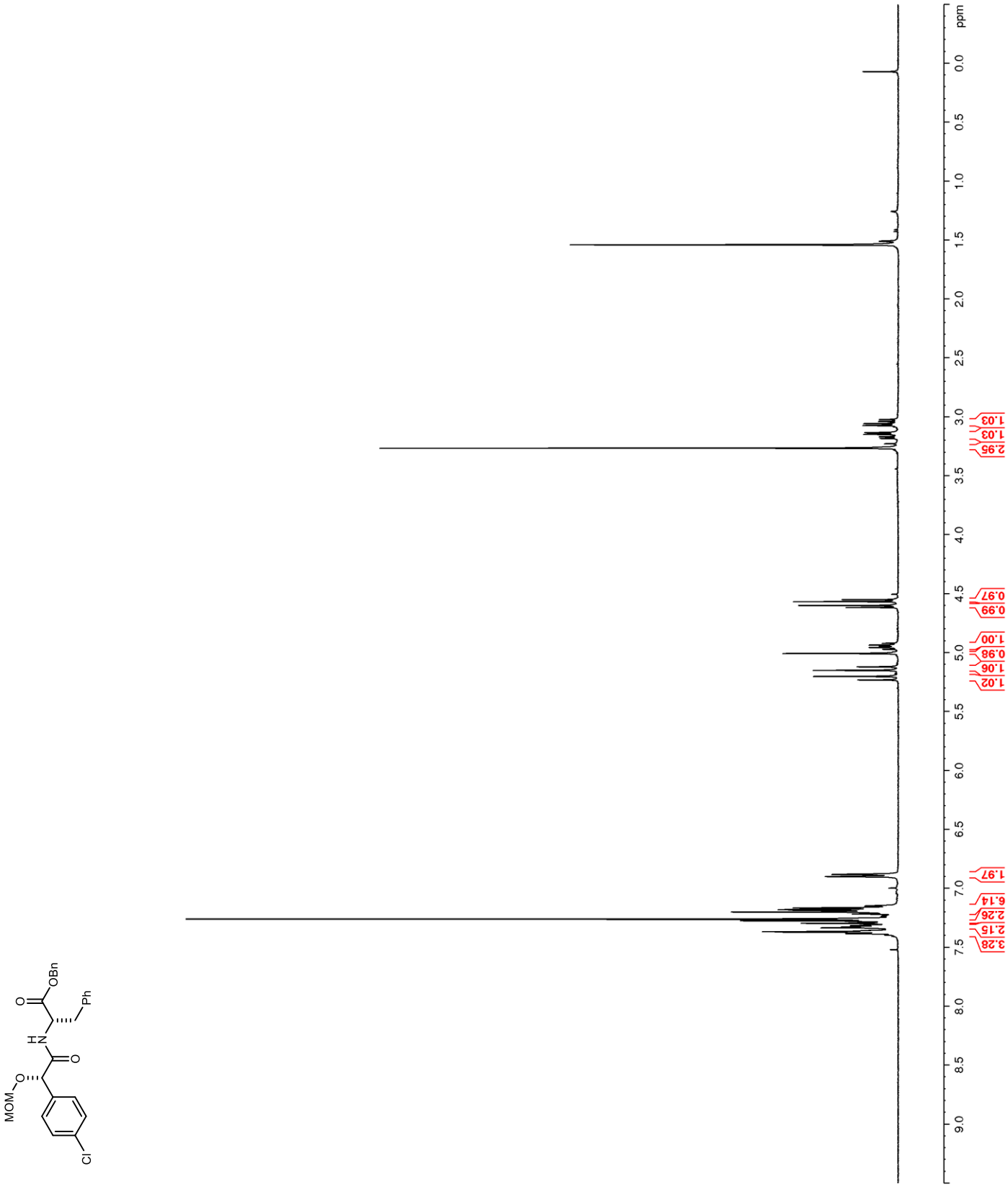

Figure 89. ^{13}C NMR (150 MHz, $CDCl_3$) of **108**

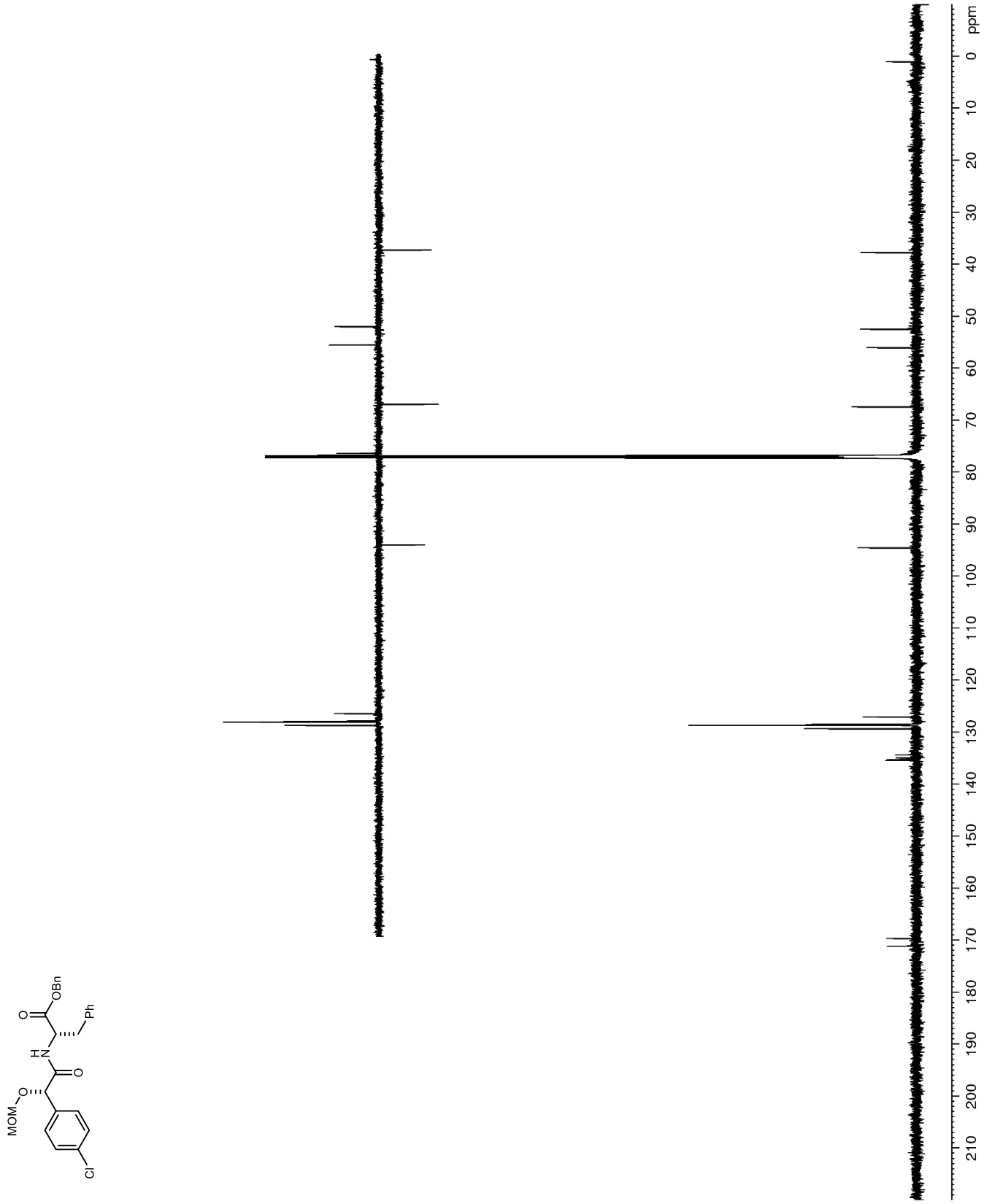

Figure 90. ^{1}H NMR (400 MHz, $CDCl_3$) of **109**

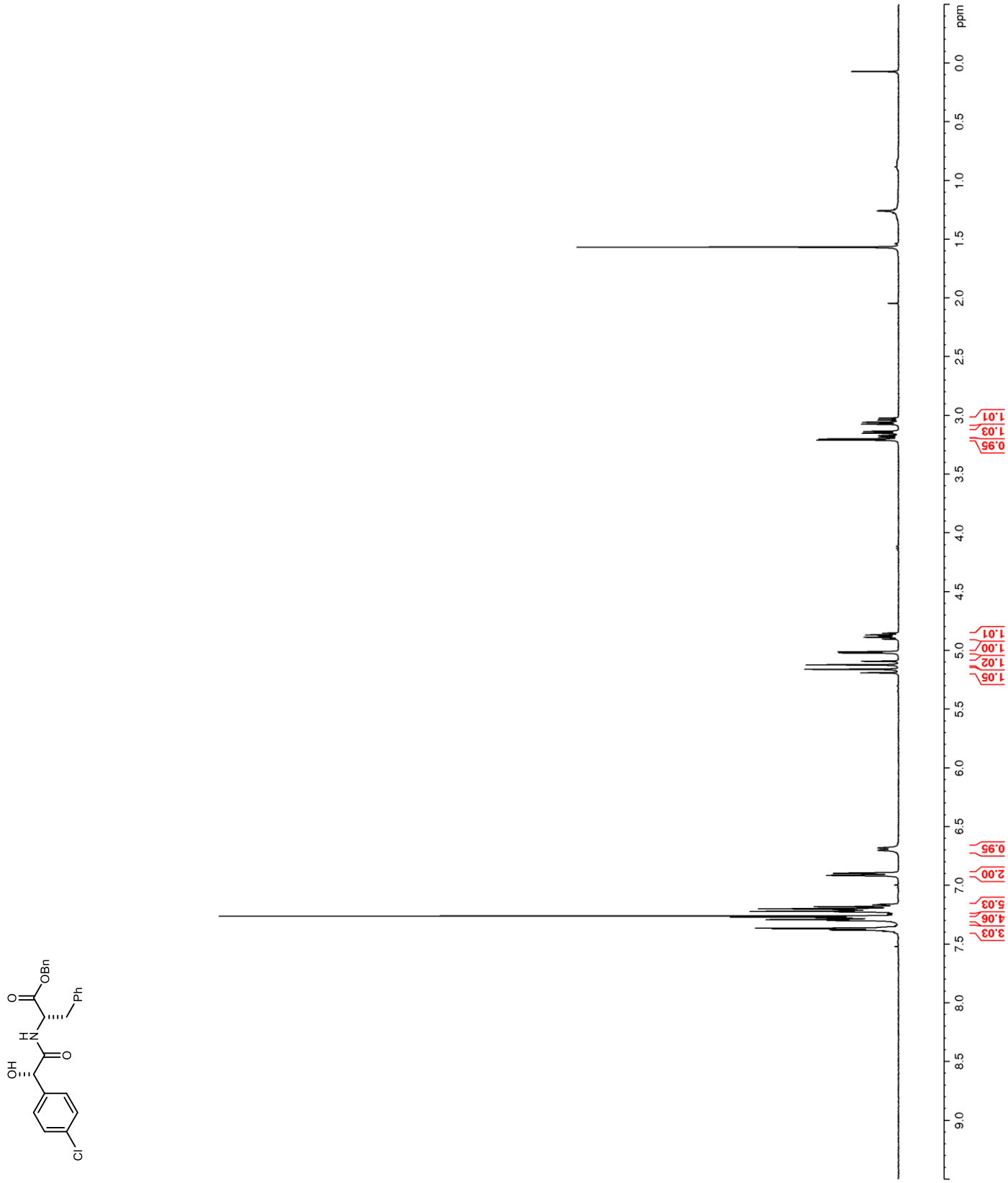

Figure 91. ^{13}C NMR (100 MHz, $CDCl_3$) of **109**

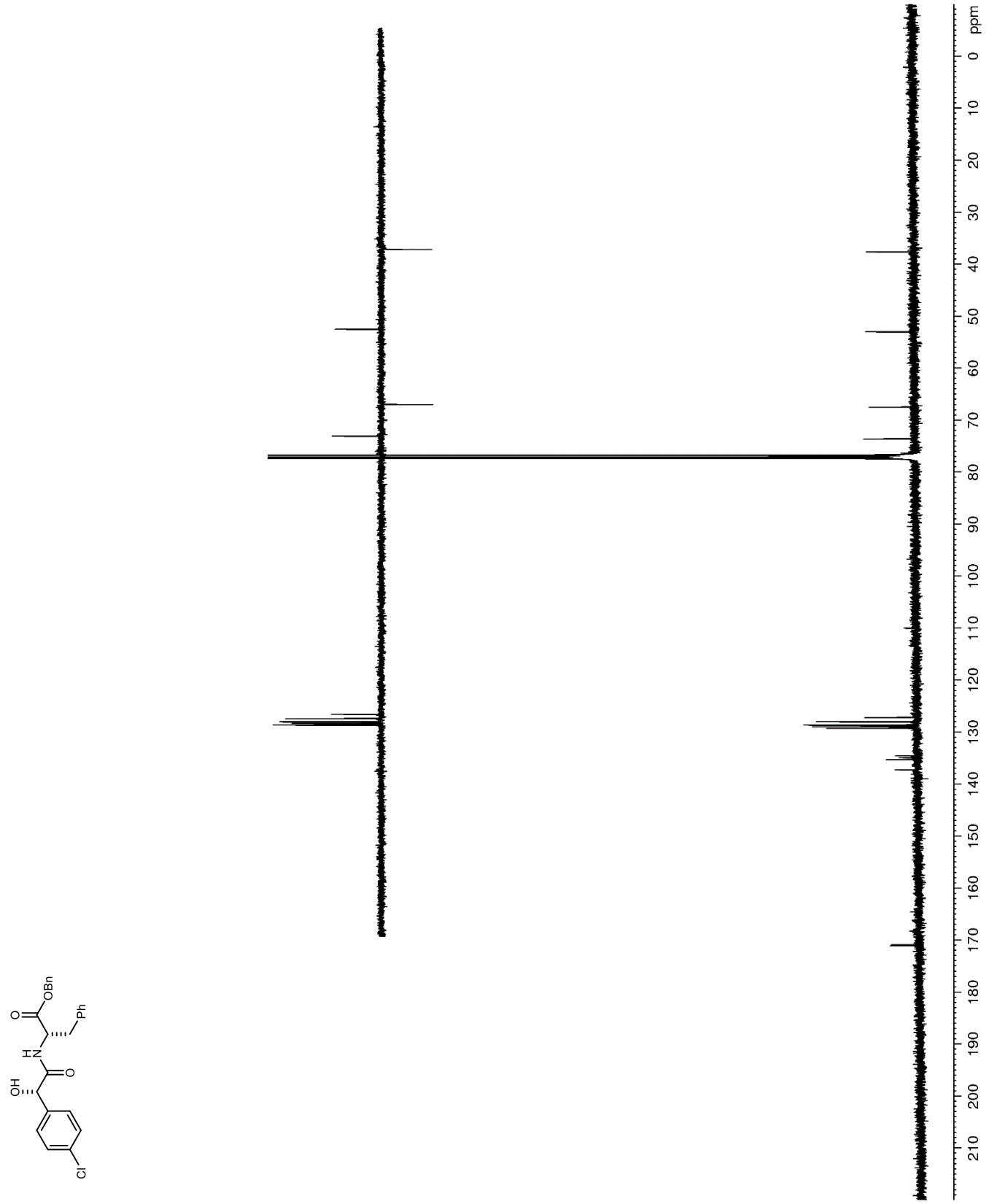

Figure 92. ^{1}H NMR (400 MHz, DMSO-d_6) of **110**

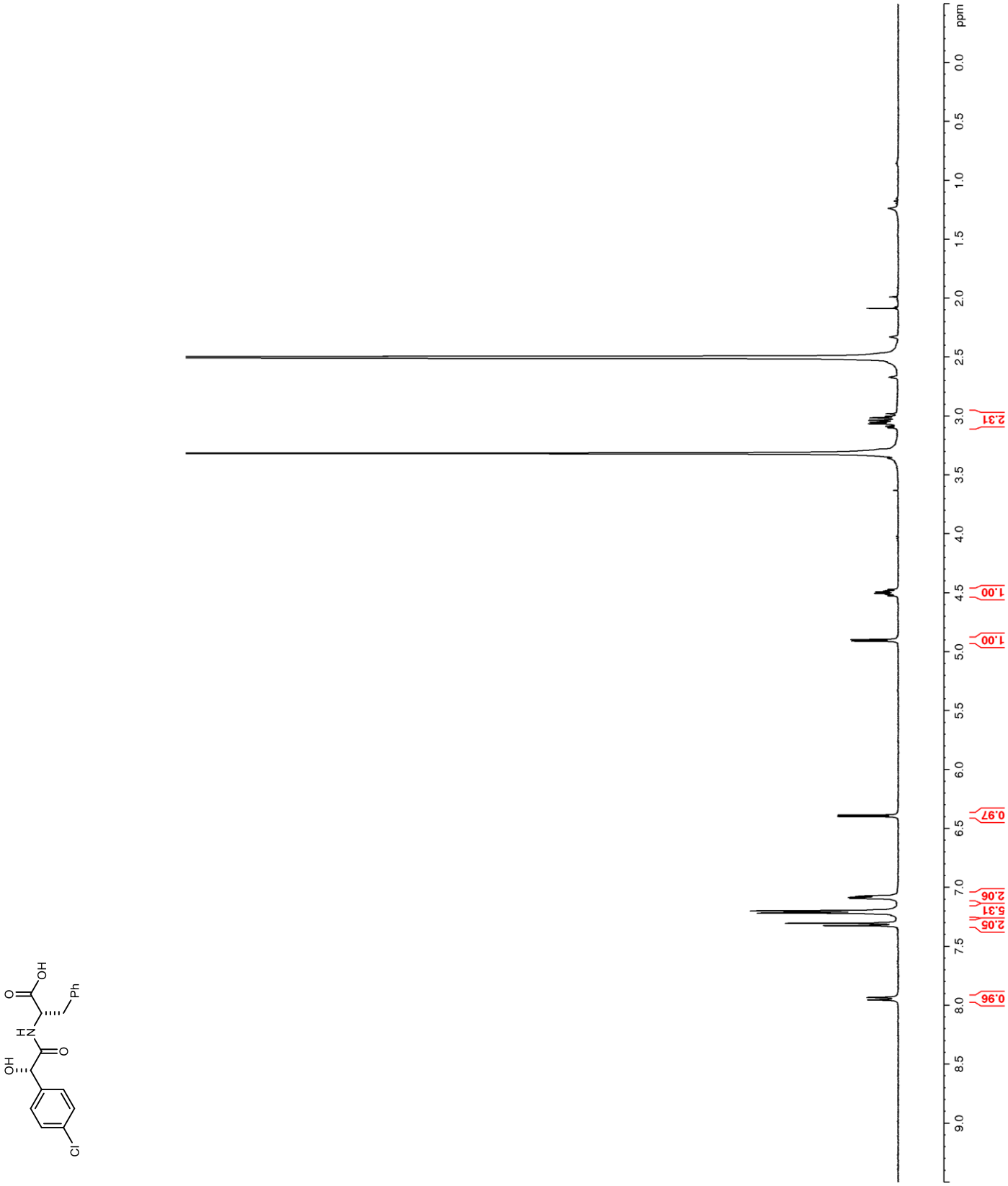

Figure 93. ^{13}C NMR (150 MHz, DMSO-d_6) of **110**

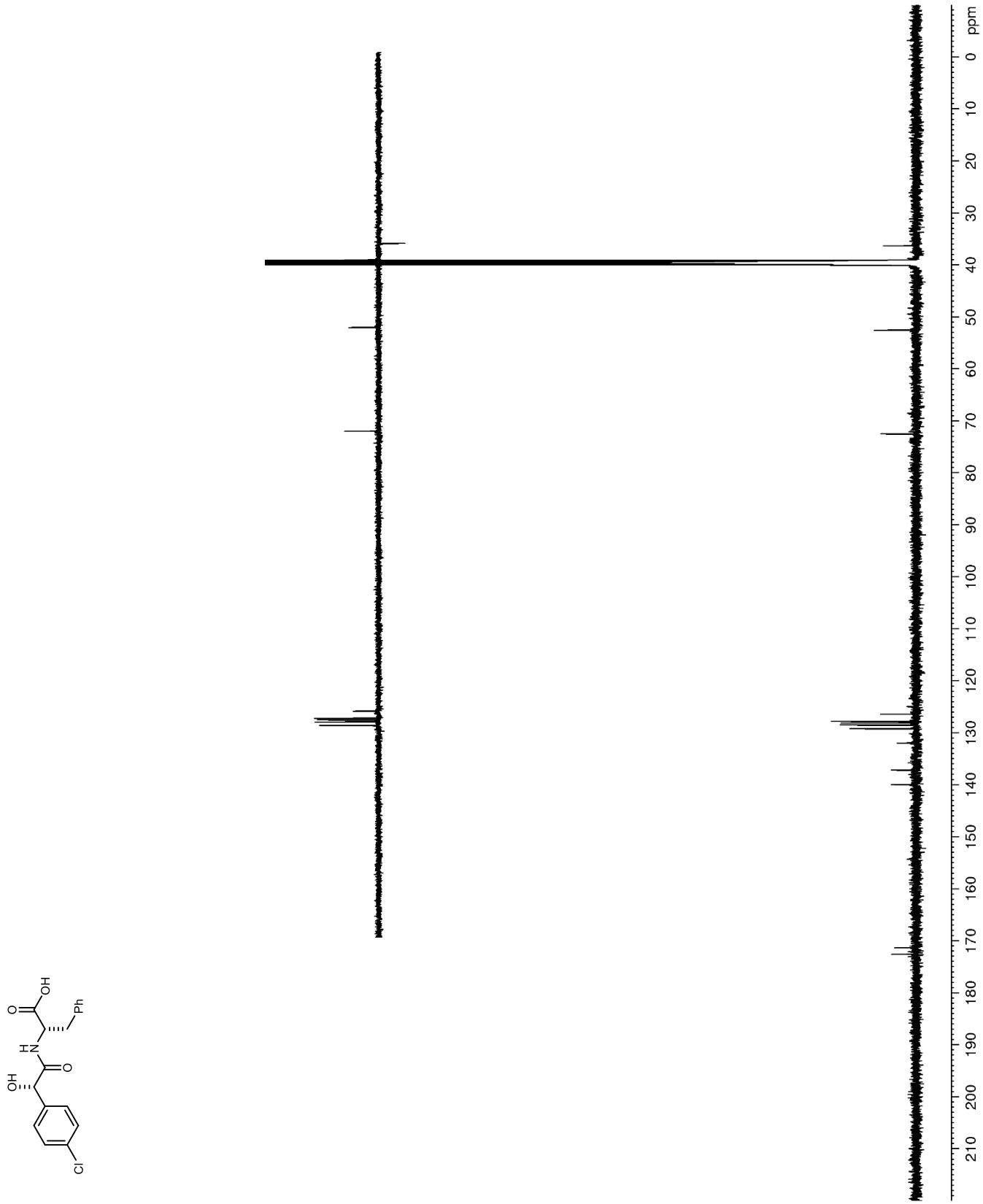

Figure 94. ^{1}H NMR (400 MHz, DMSO-d_6) of **111**

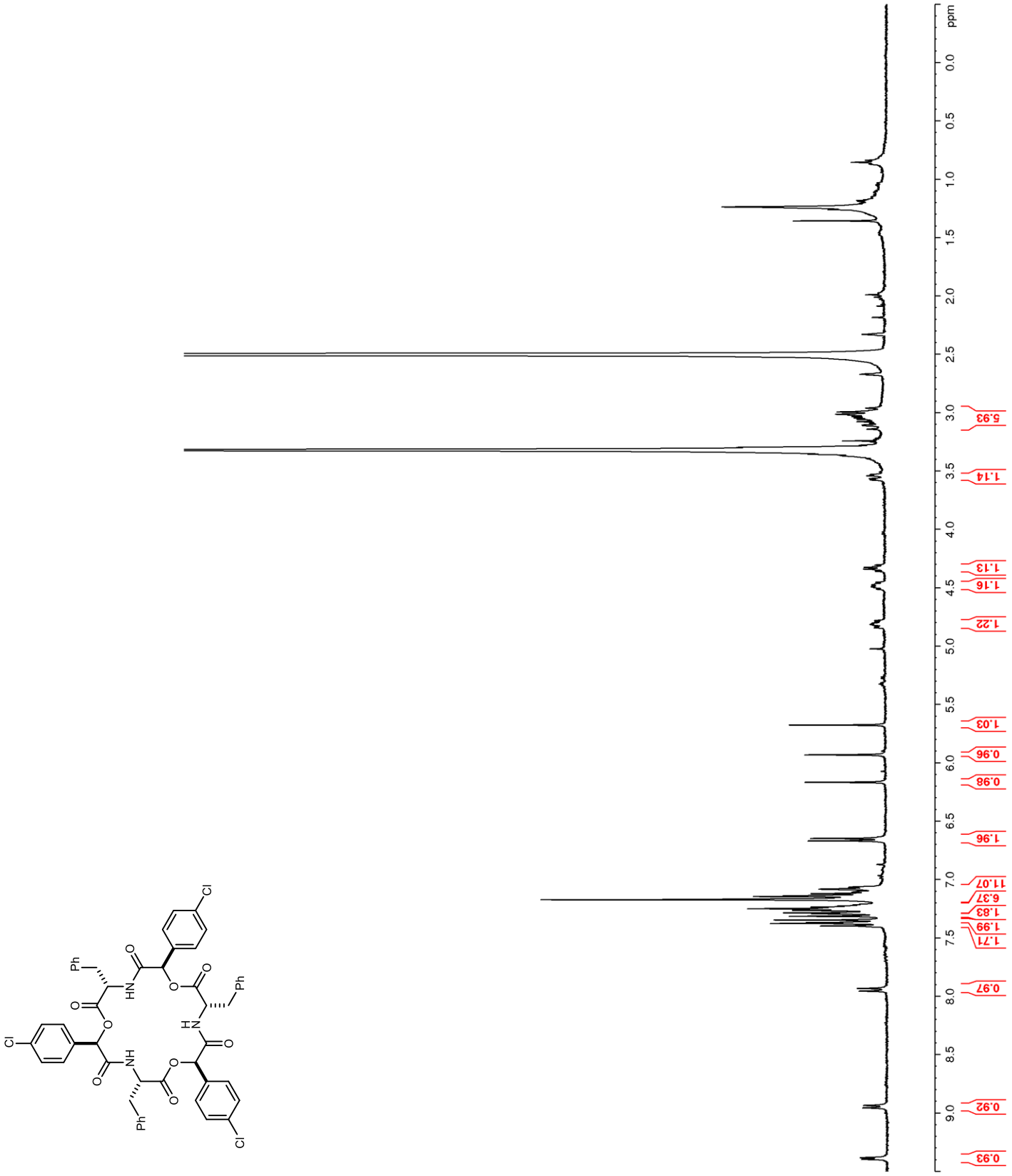

Figure 95. ^{13}C NMR (150 MHz, CD_3CN) of **111**

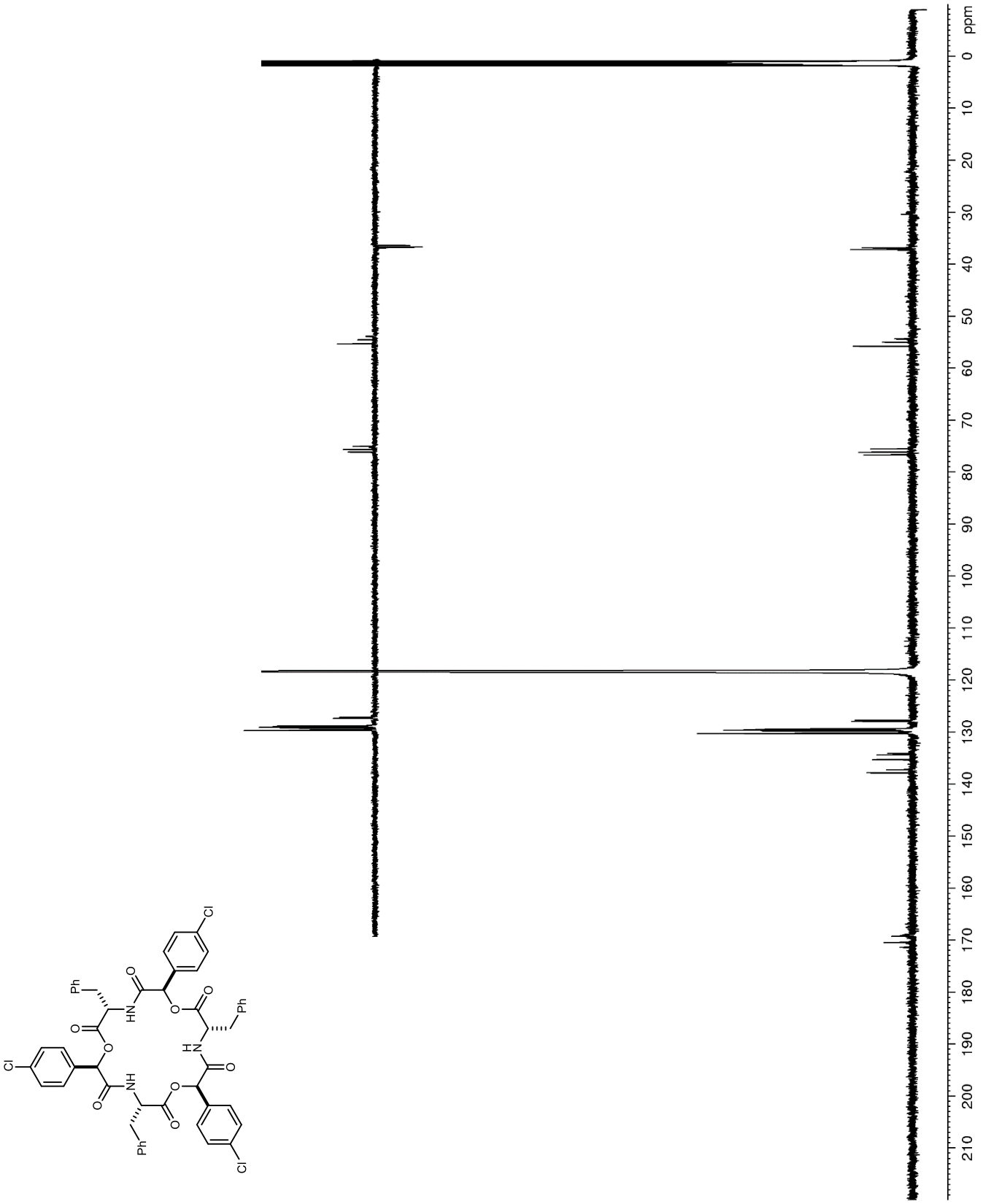

Figure 96. ^{1}H NMR (400 MHz, DMSO-d_6) of **112**

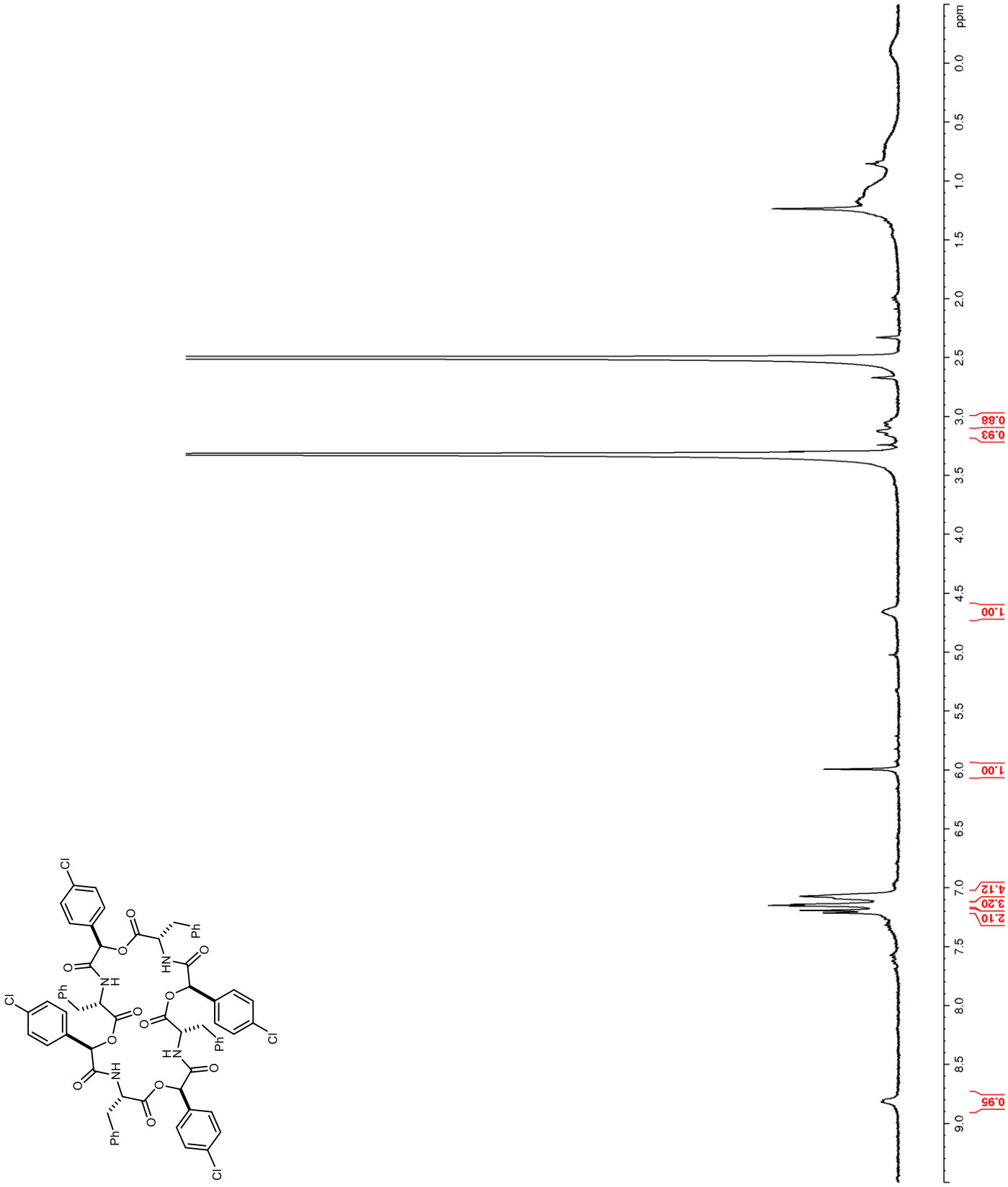

Figure 97. ^{13}C NMR (150 MHz, DMSO-d_6) of **112**

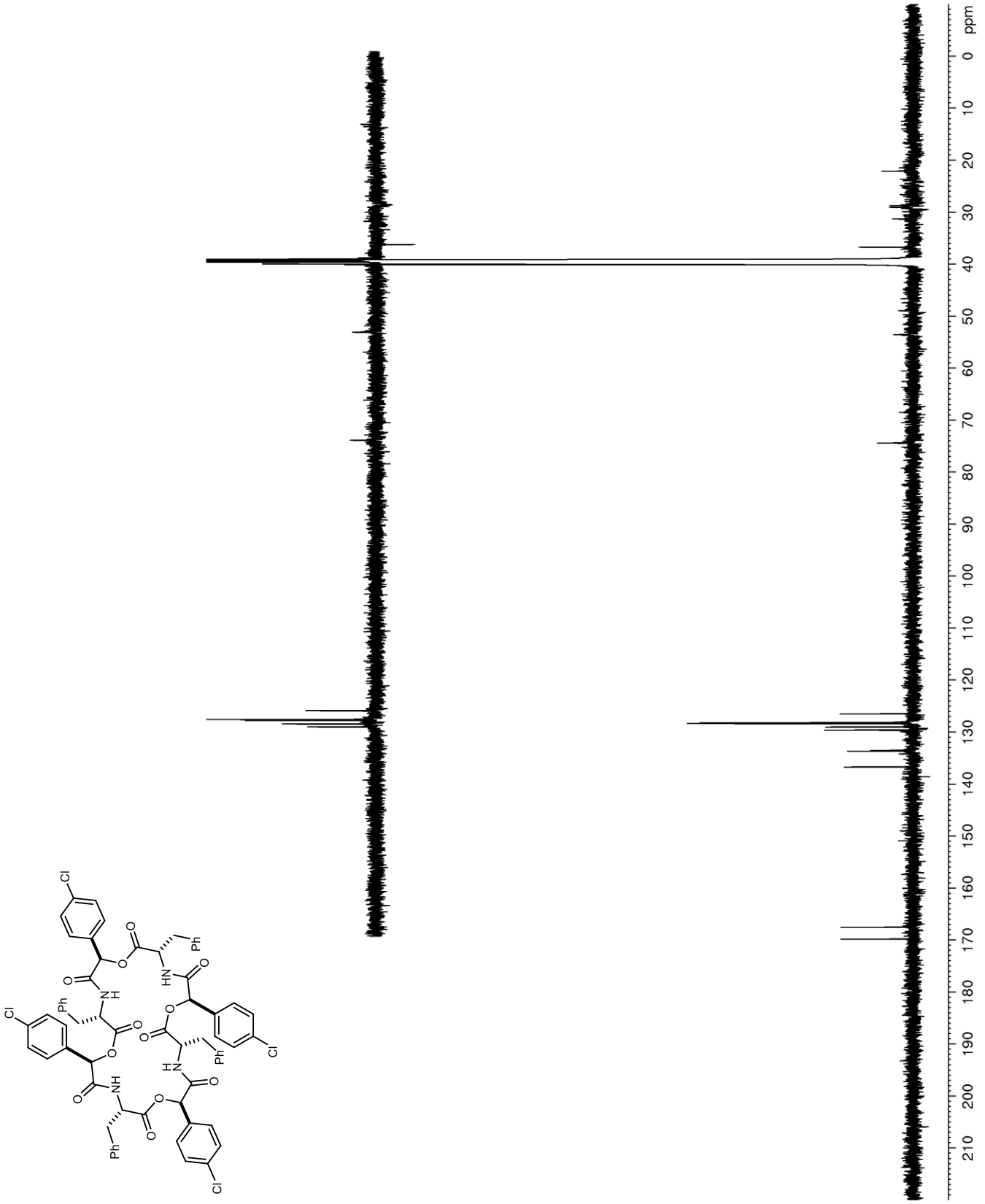

Figure 98. ^{1}H NMR (400 MHz, DMSO-d_6) of **113**

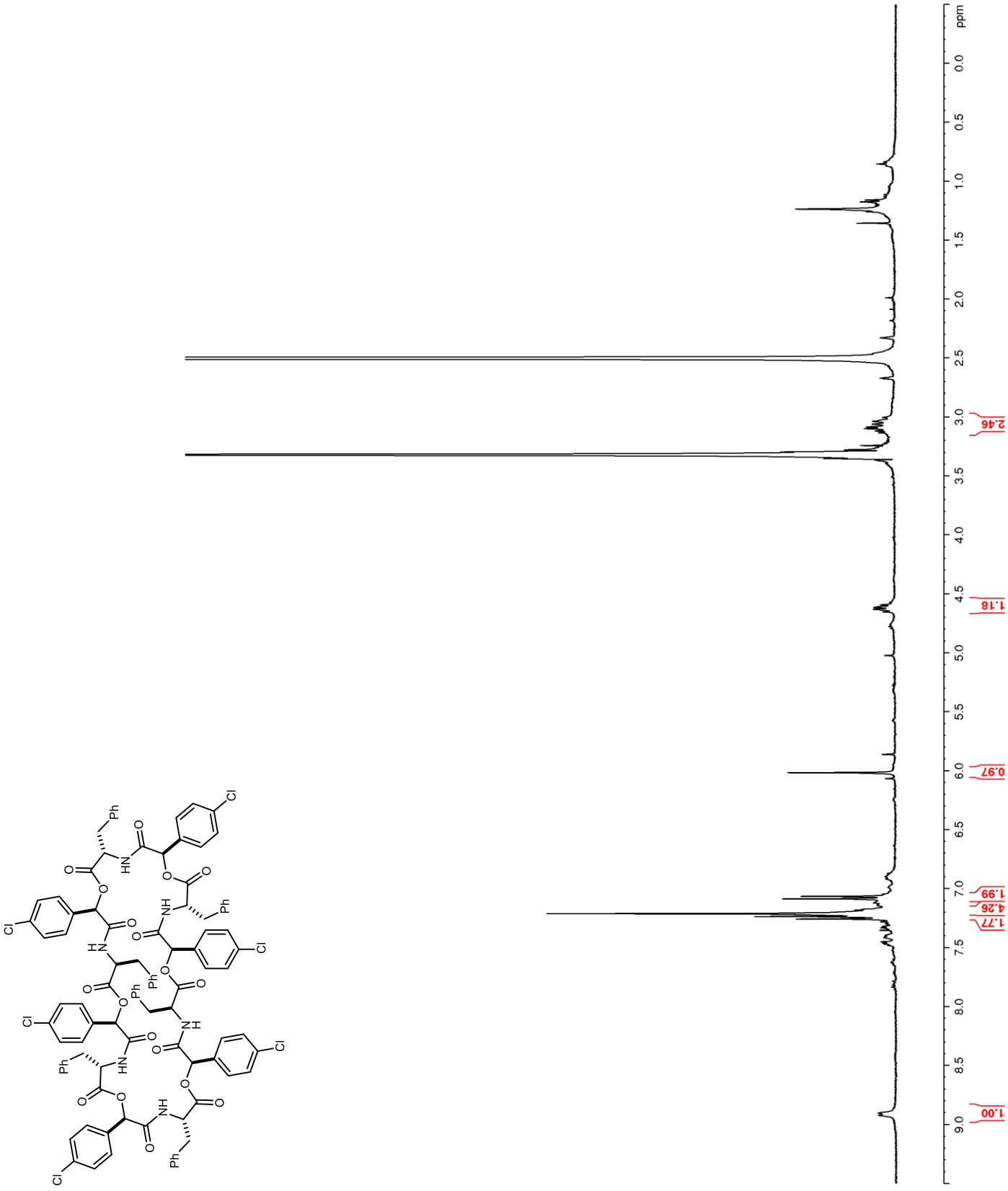

Figure 99. ^{13}C NMR (150 MHz, DMSO-d_6) of **113**

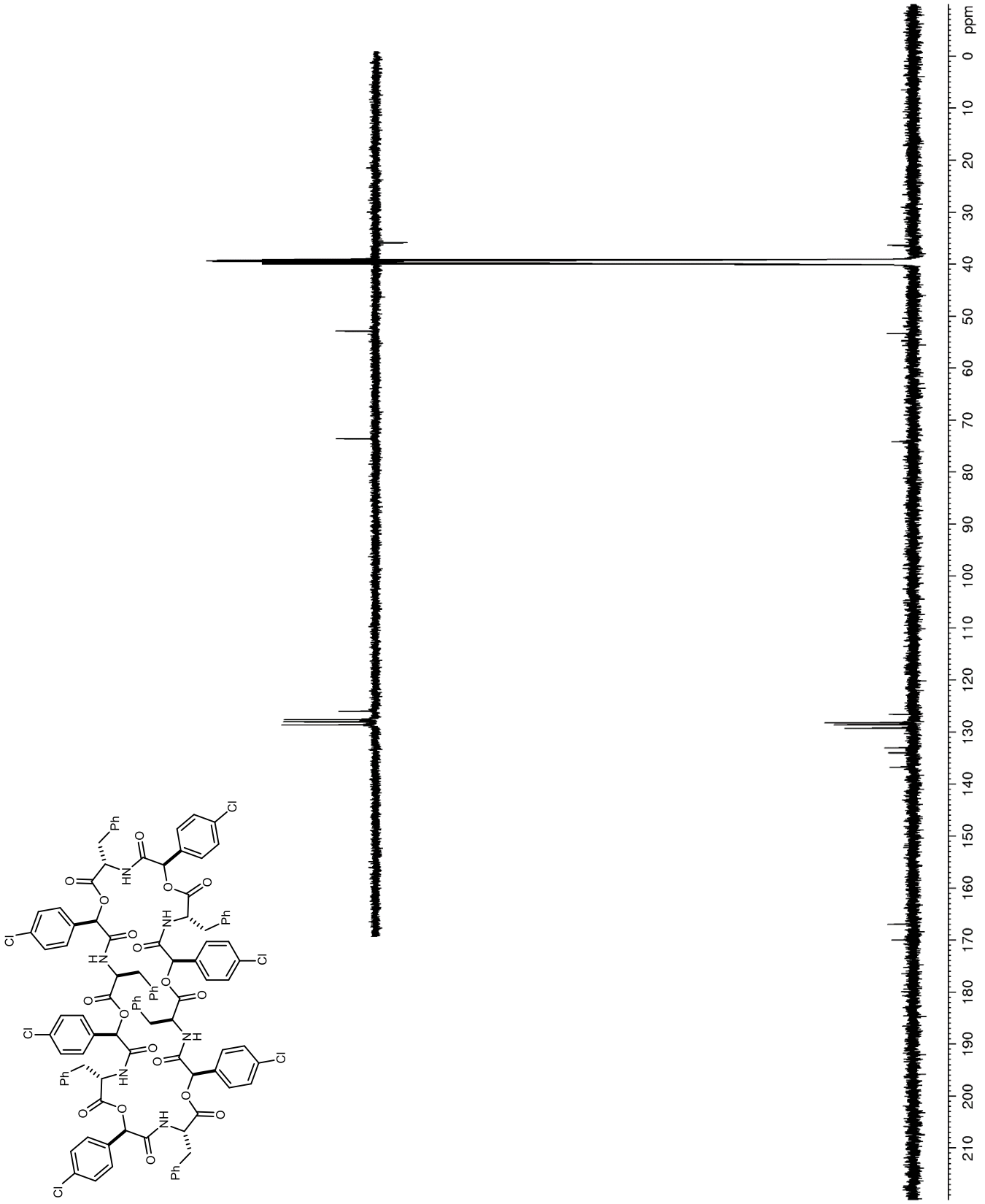

Figure 100. ^{1}H NMR (400 MHz, $CDCl_3$) of **115**

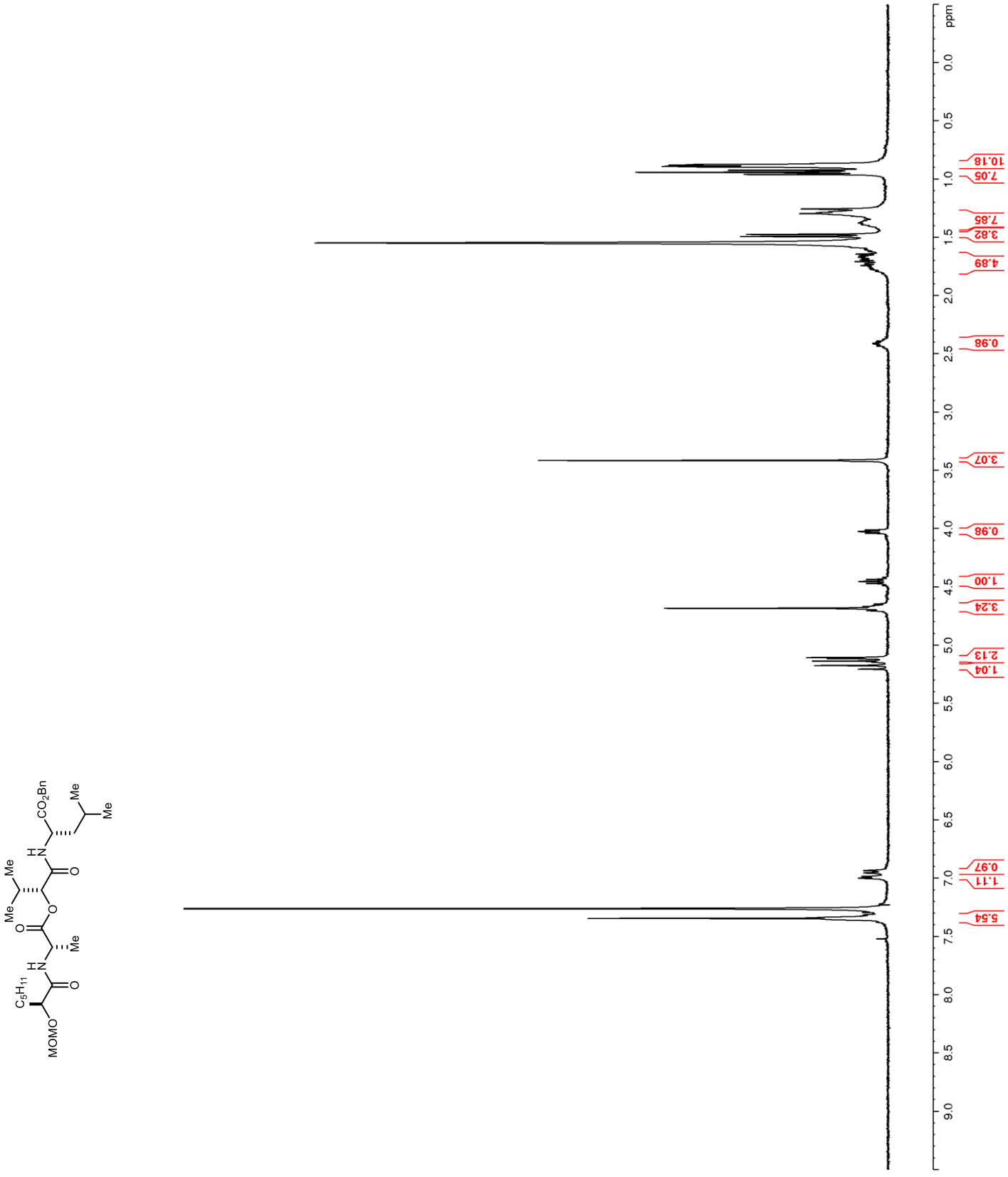

Figure 101. ^{13}C NMR (150 MHz, $CDCl_3$) of **115**

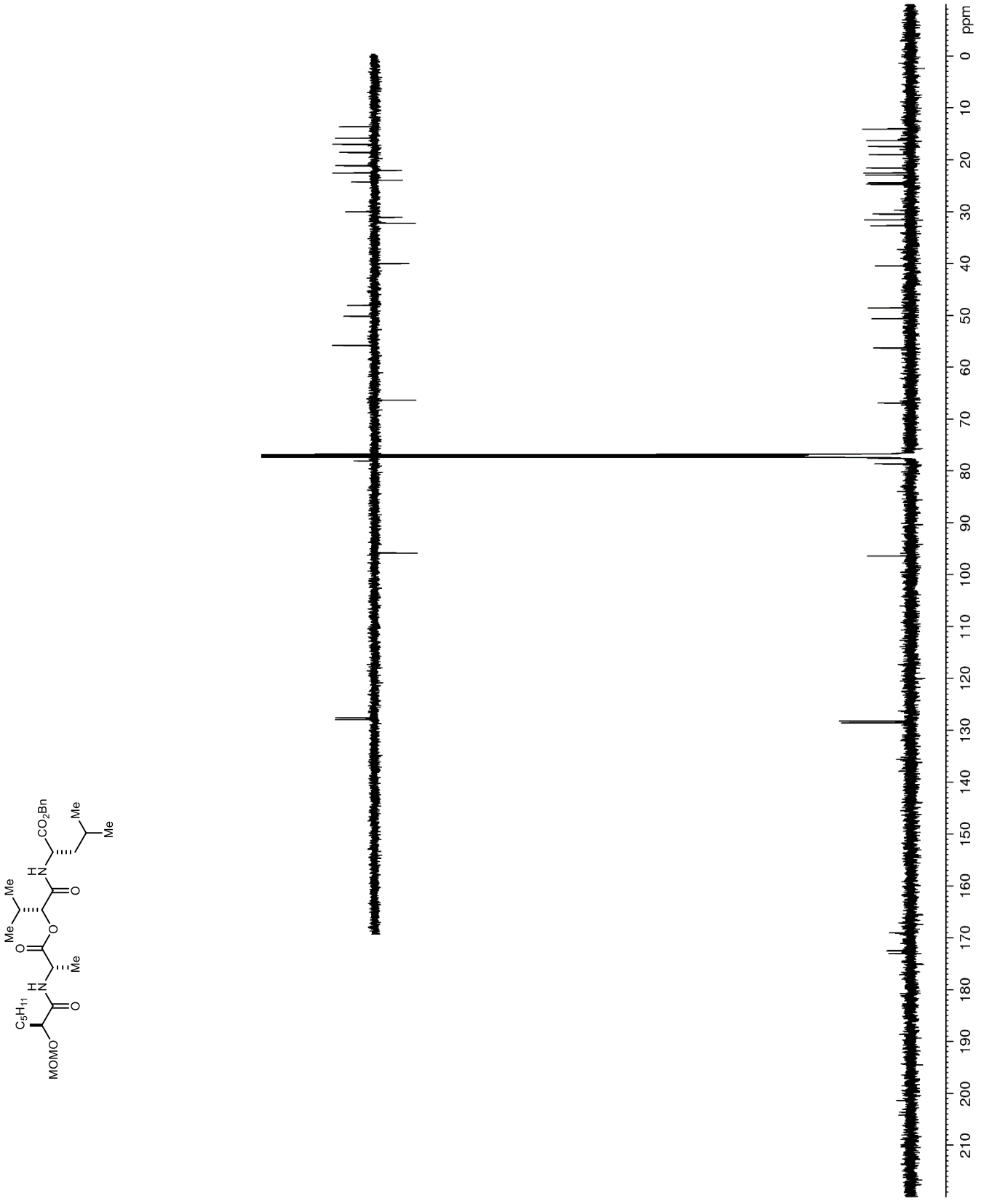

Figure 102. ^{1}H NMR (600 MHz, $CDCl_3$) of **116**

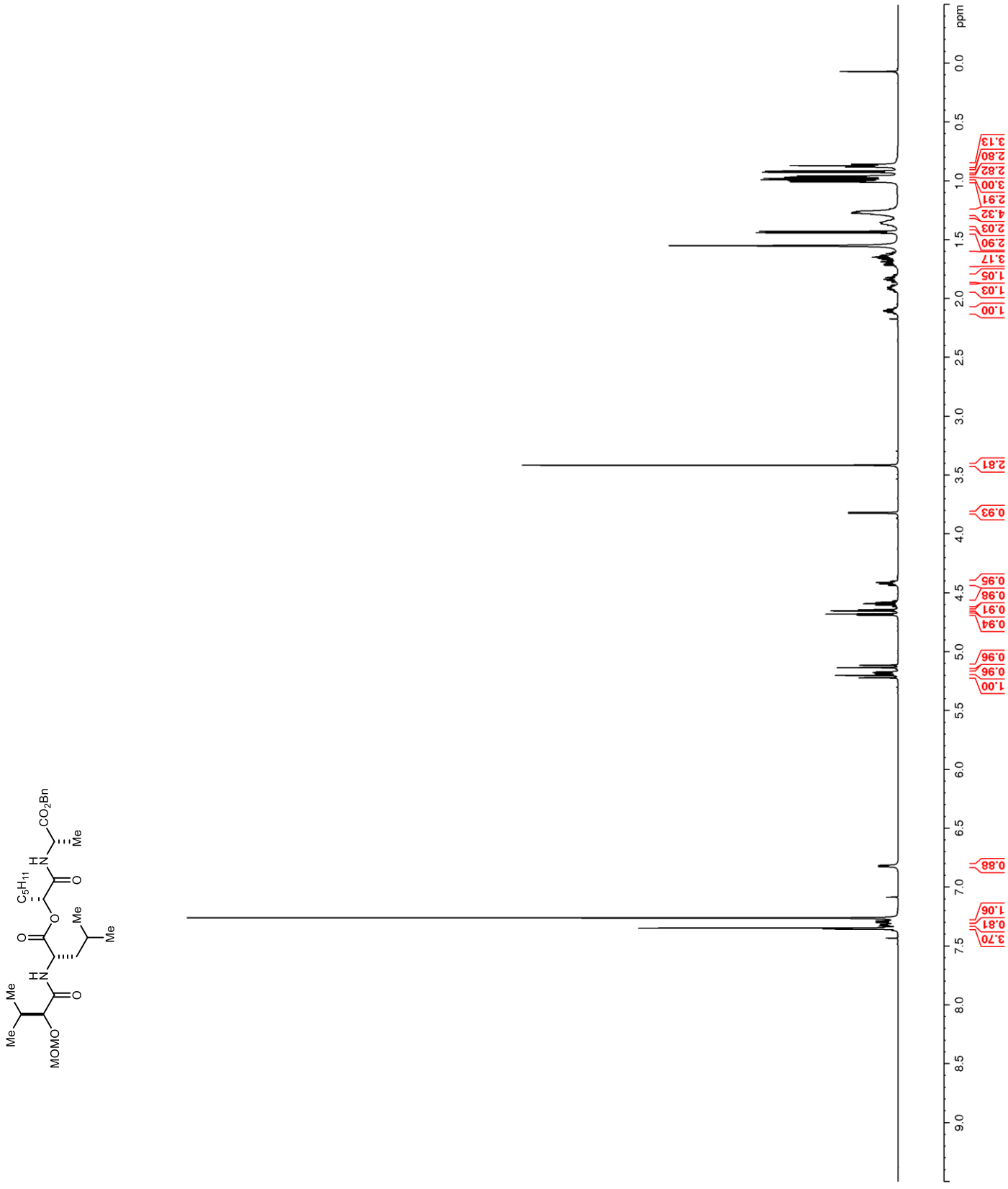

Figure 103. ^{13}C NMR (150 MHz, $CDCl_3$) of **116**

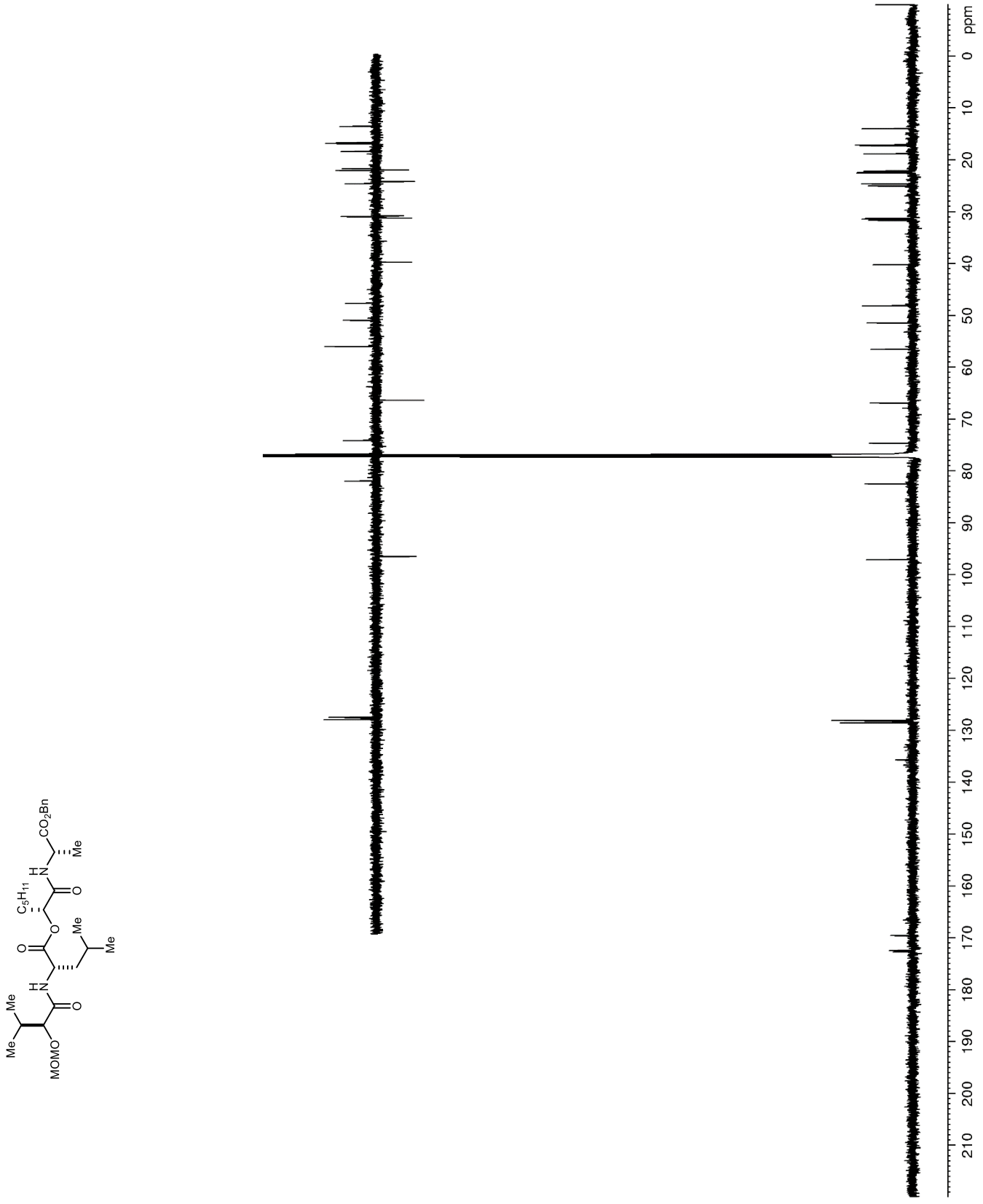

Figure 104. ^{1}H NMR (400 MHz, DMSO-d_6) of **117**

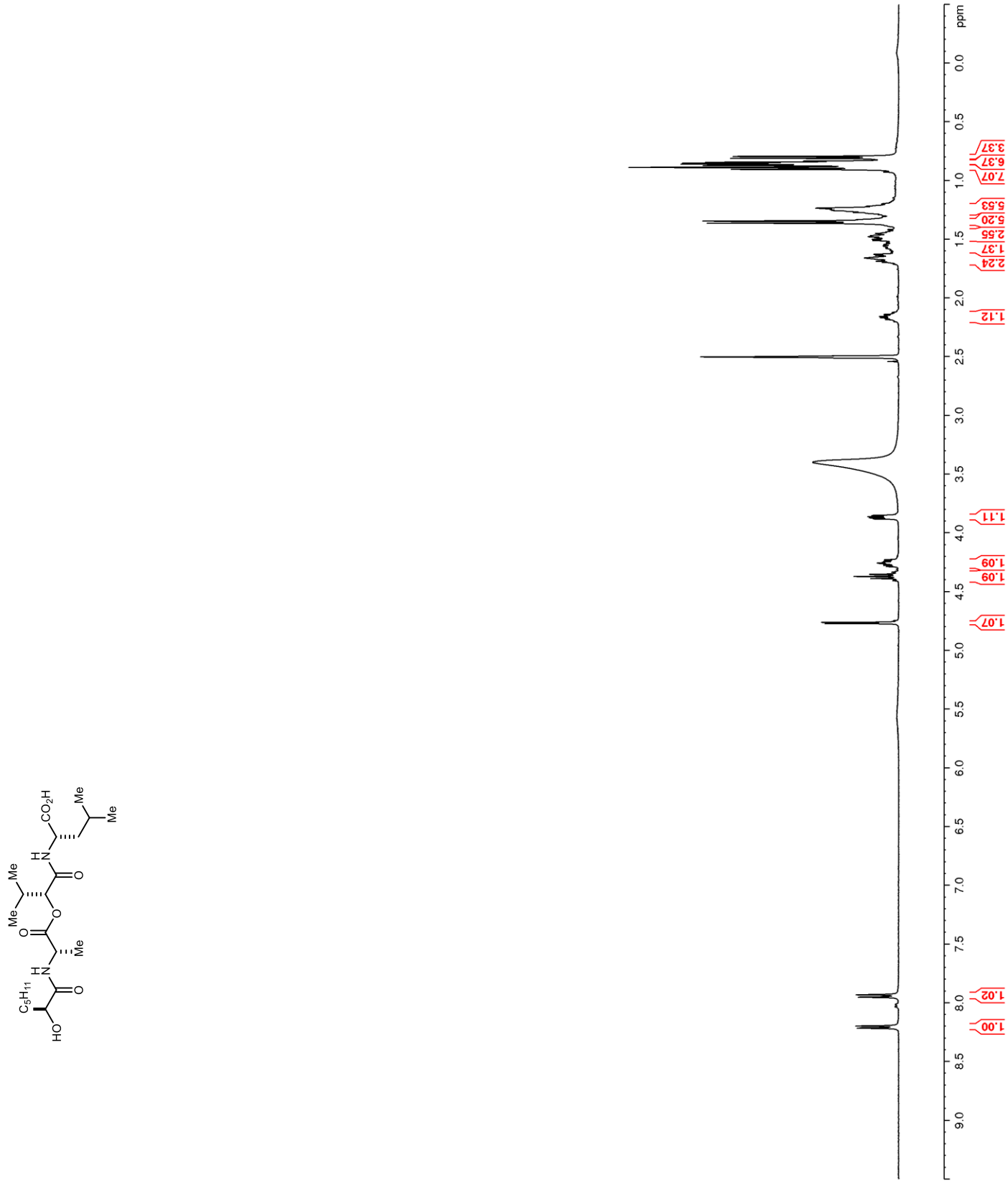

Figure 105. ^{13}C NMR (100 MHz, DMSO-d_6) of **117**

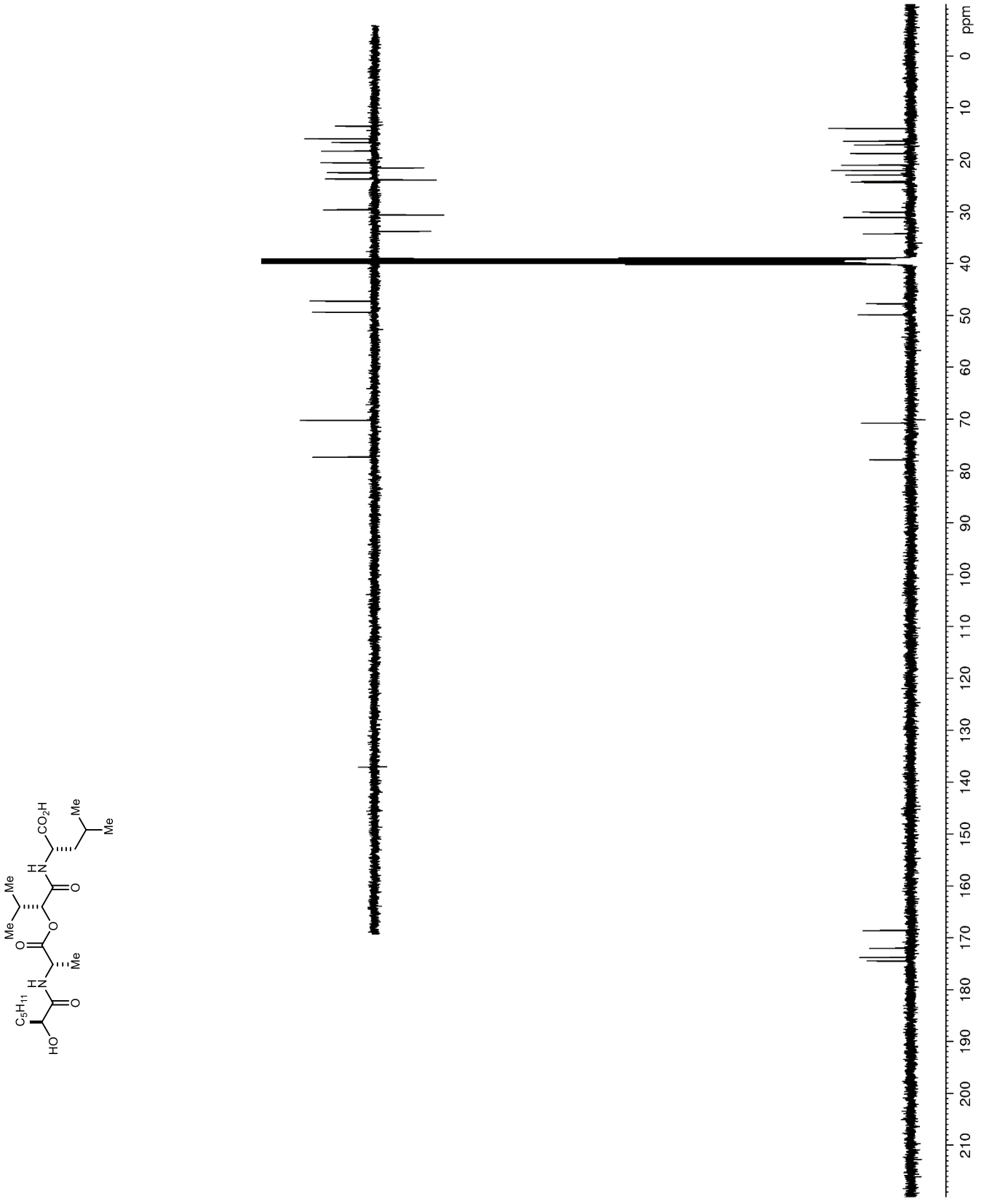

Figure 106. ^{1}H NMR (400 MHz, $CDCl_3$) of **118**

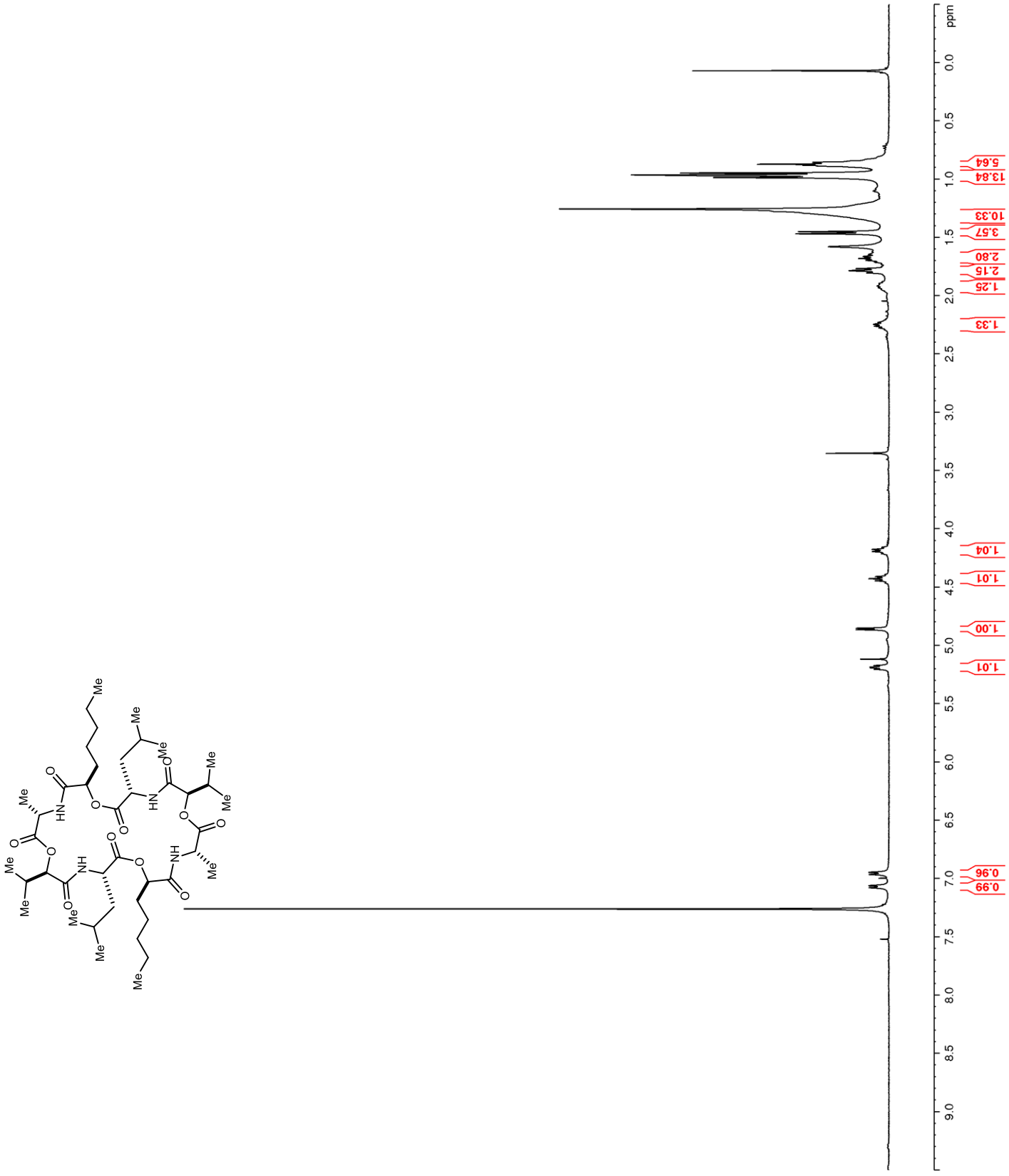

Figure 107. ^{13}C NMR (150 MHz, $CDCl_3$) of **118**

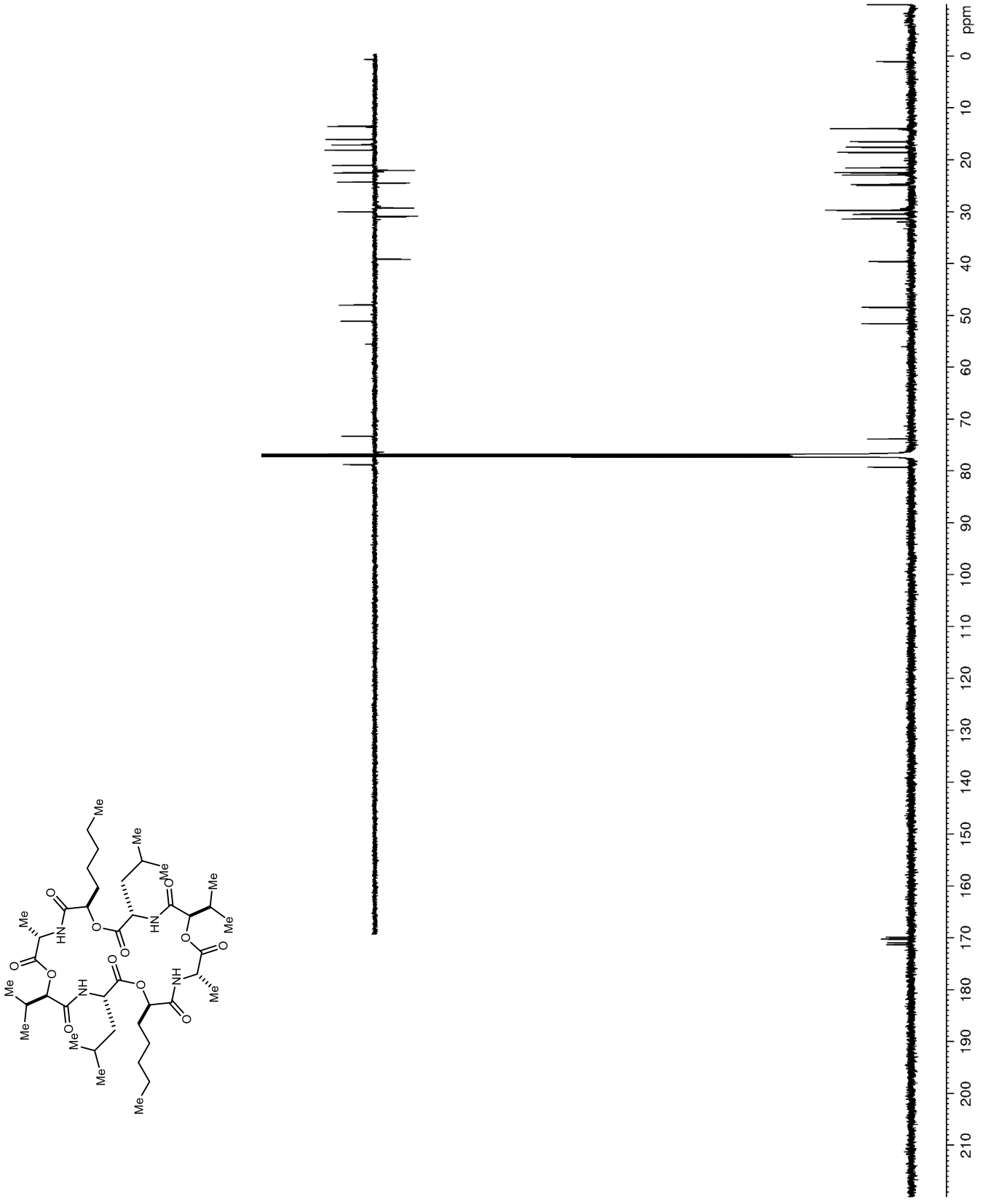

Figure 108. ^{1}H NMR (400 MHz, DMSO-d_6) of **122**

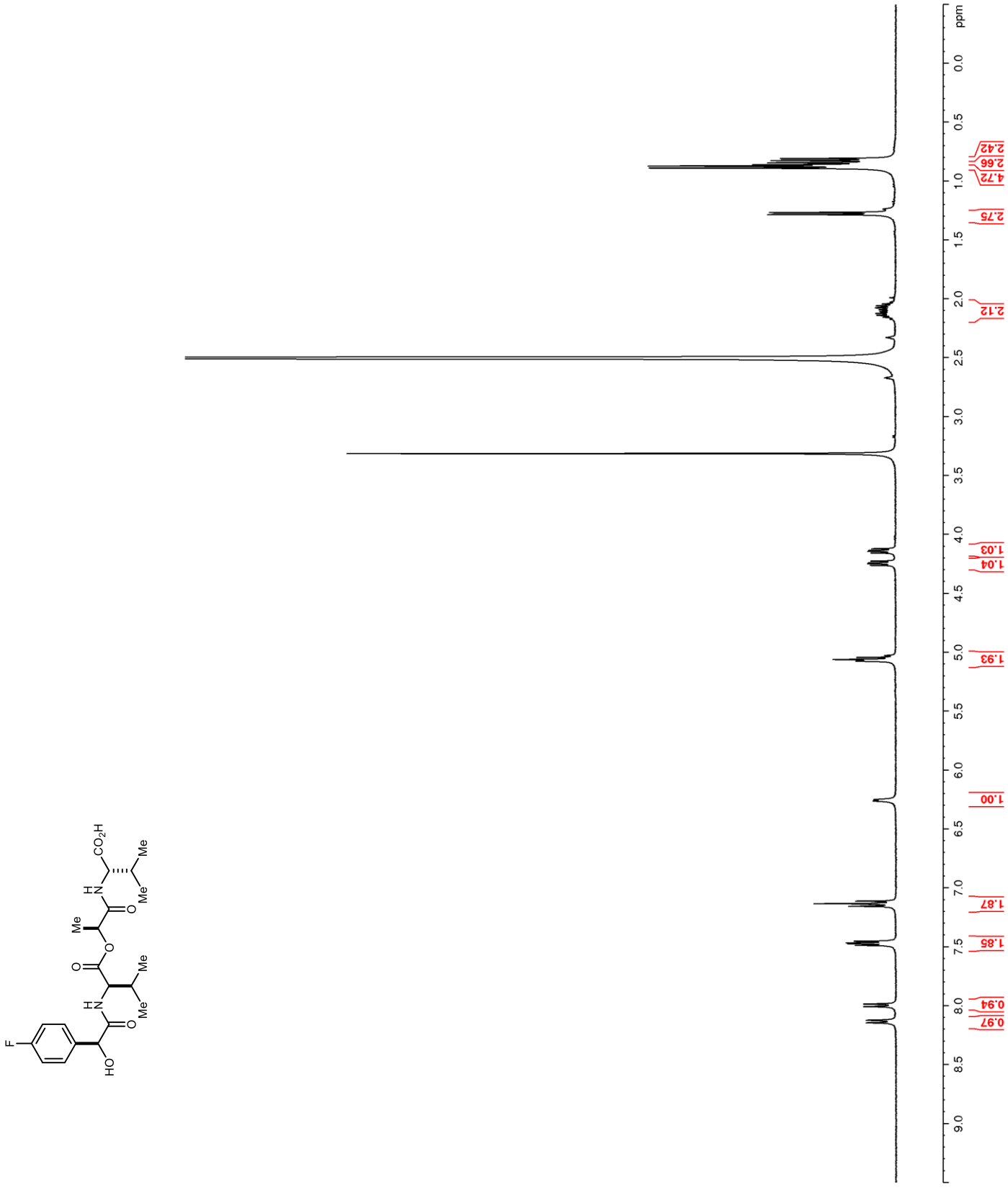

Figure 109. ^{13}C NMR (150 MHz, DMSO-d_6) of **122**

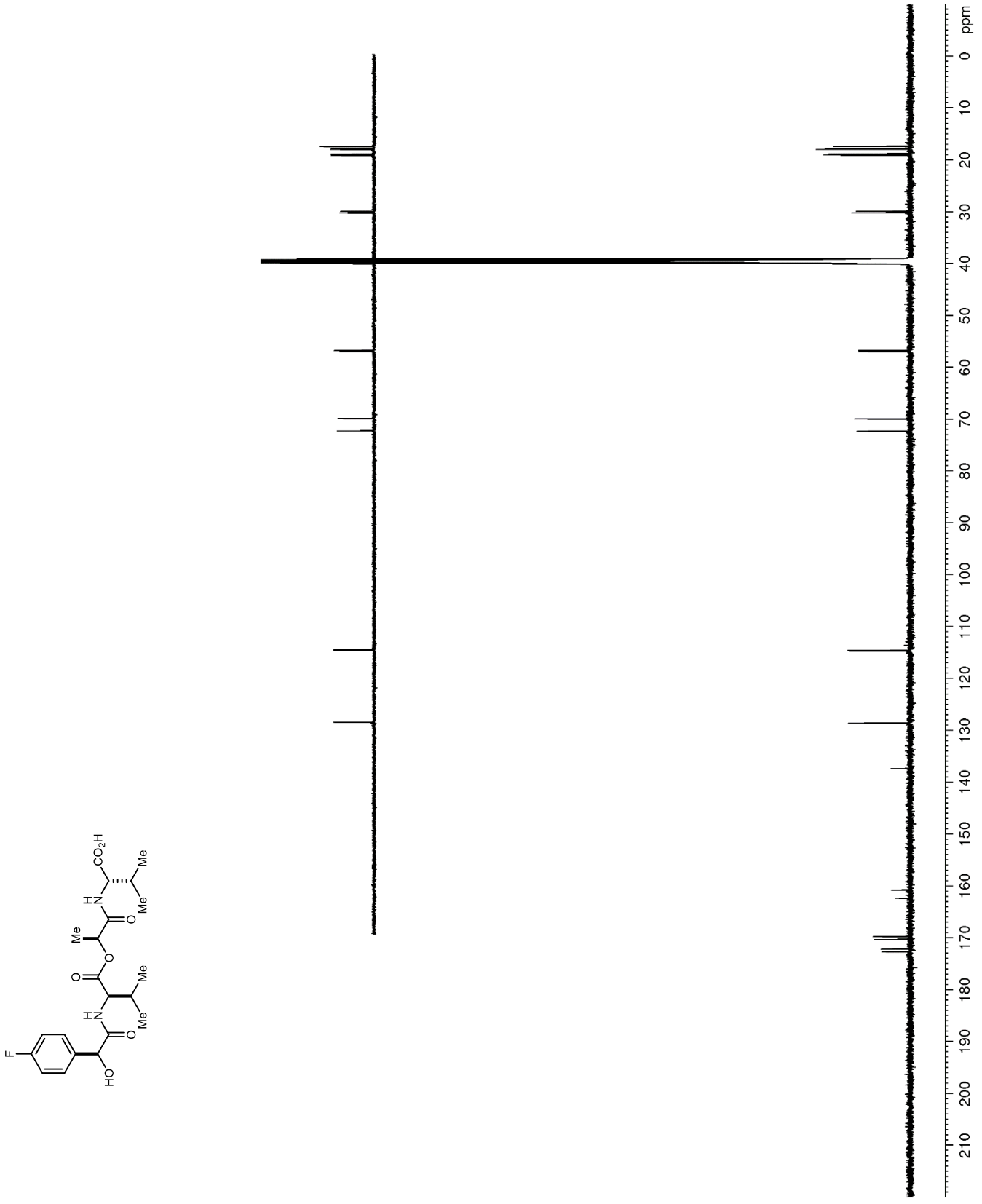

Figure 110. ^{1}H NMR (600 MHz, DMSO-d_6) of **123**

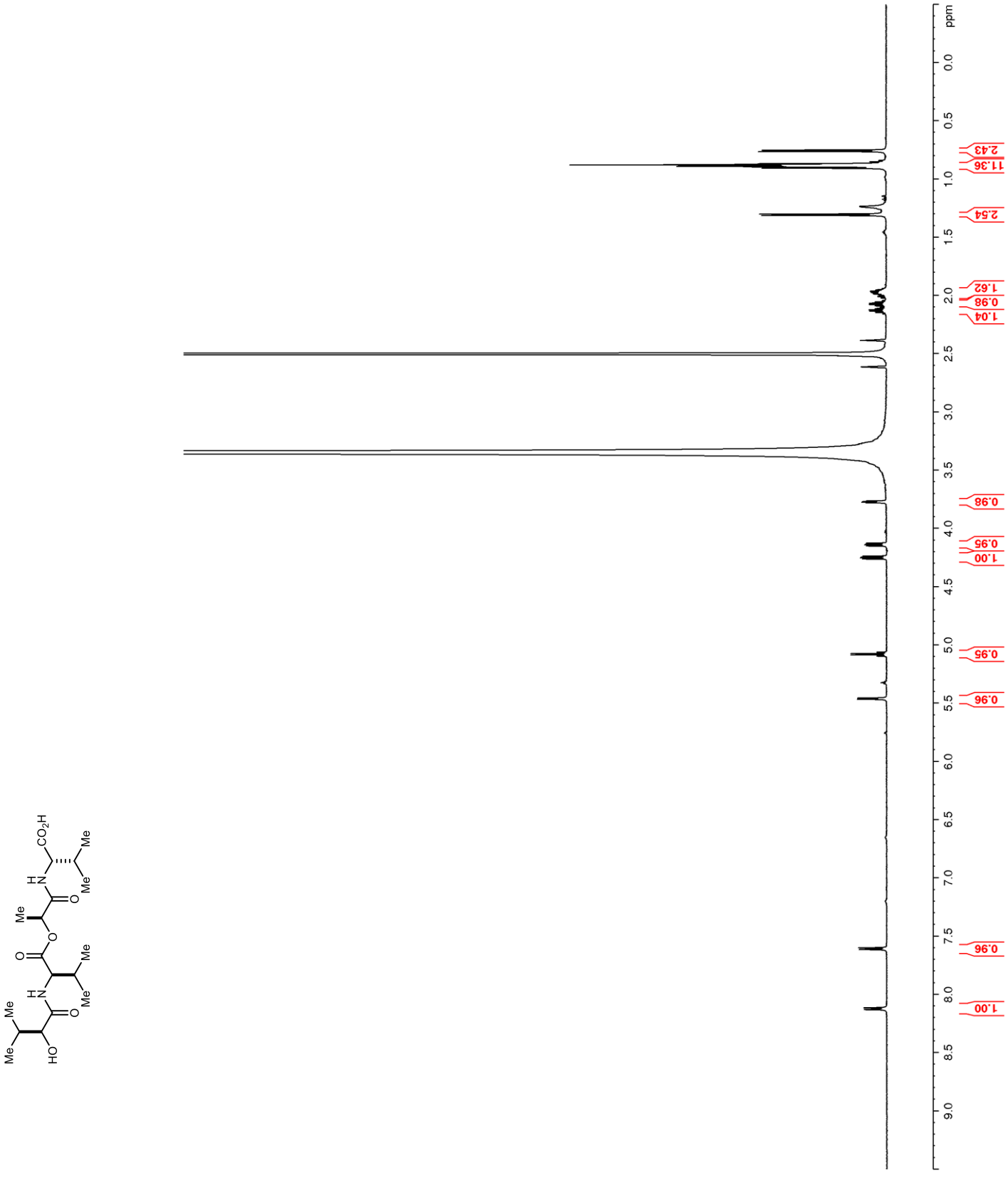

Figure 111. ^{13}C NMR (150 MHz, DMSO-d_6) of **123**

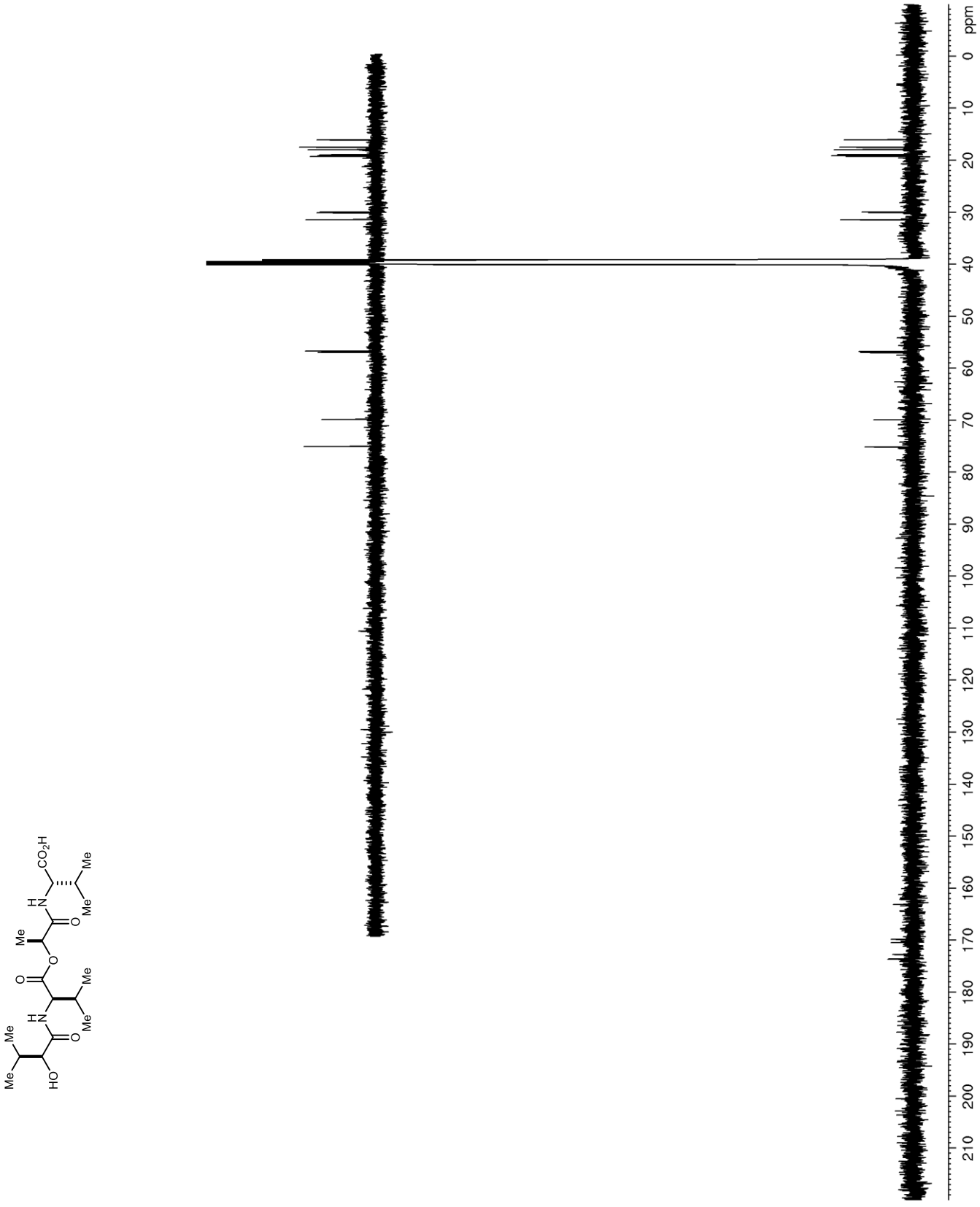

Figure 112. ^{1}H NMR (600 MHz, $CDCl_3$) of **130**

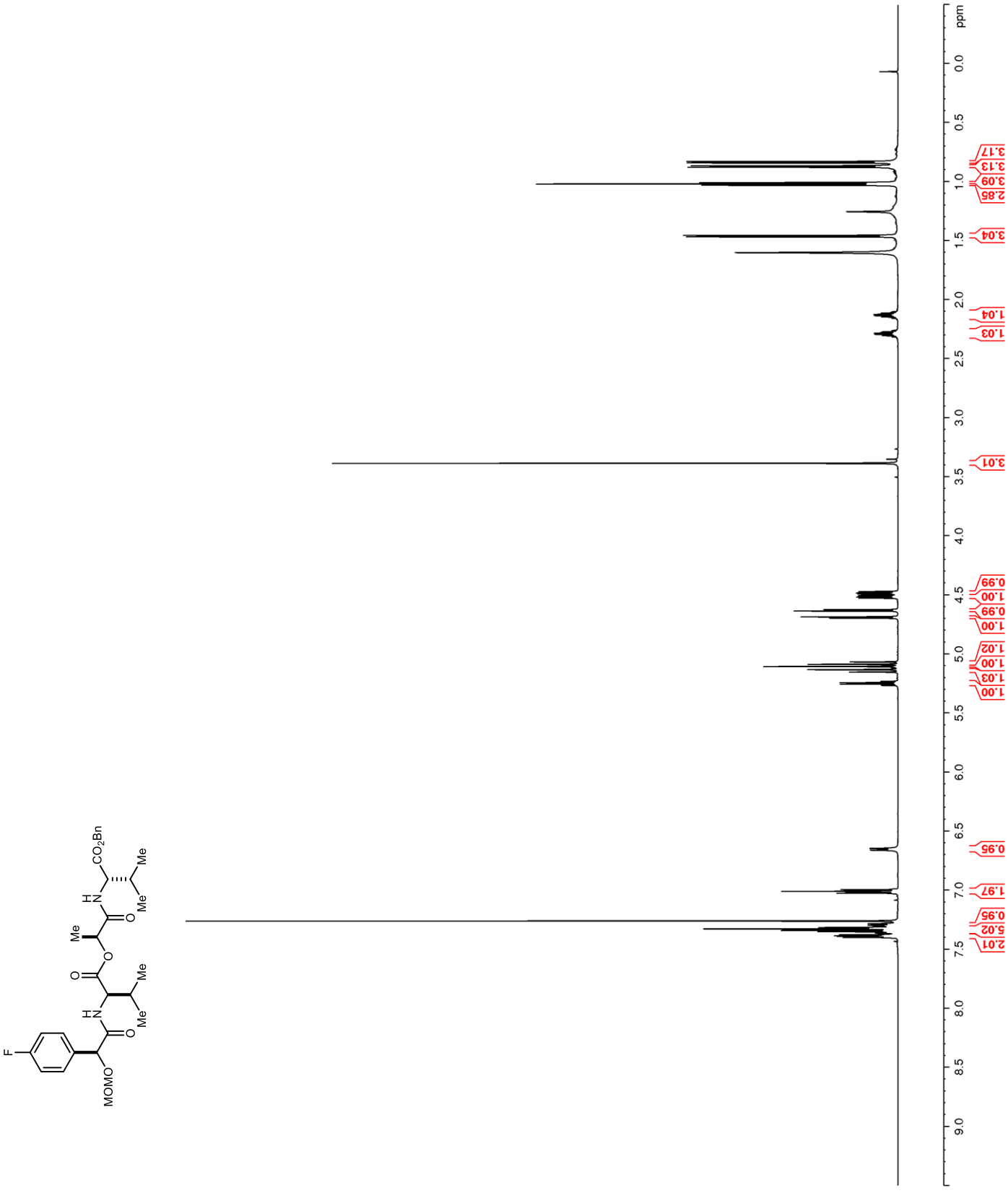

Figure 113. ^{13}C NMR (150 MHz, $CDCl_3$) of **130**

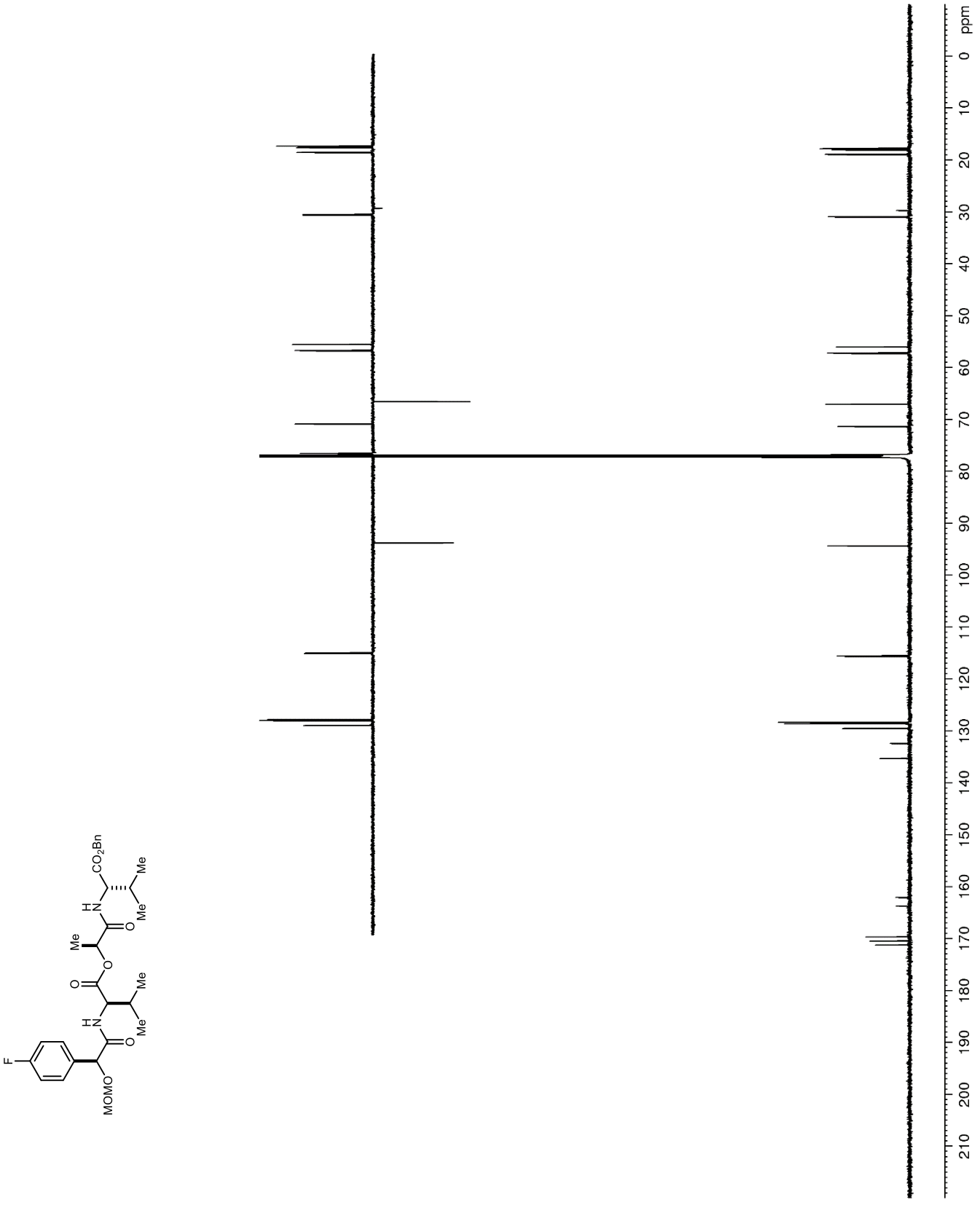

Figure 114. ^{1}H NMR (600 MHz, DMSO-d_6) of **131**

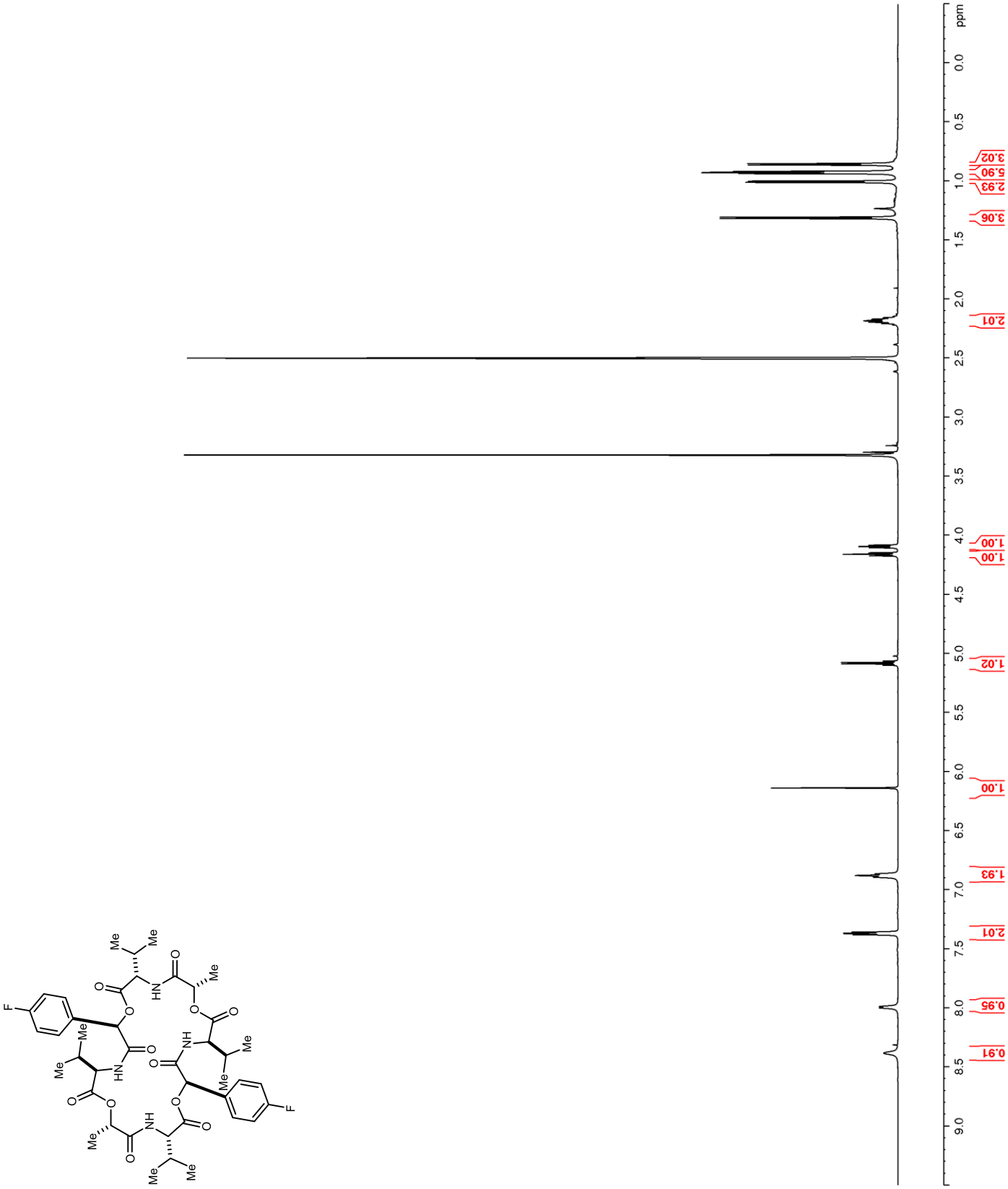

Figure 115. ^{13}C NMR (150 MHz, DMSO-d_6) of **131**

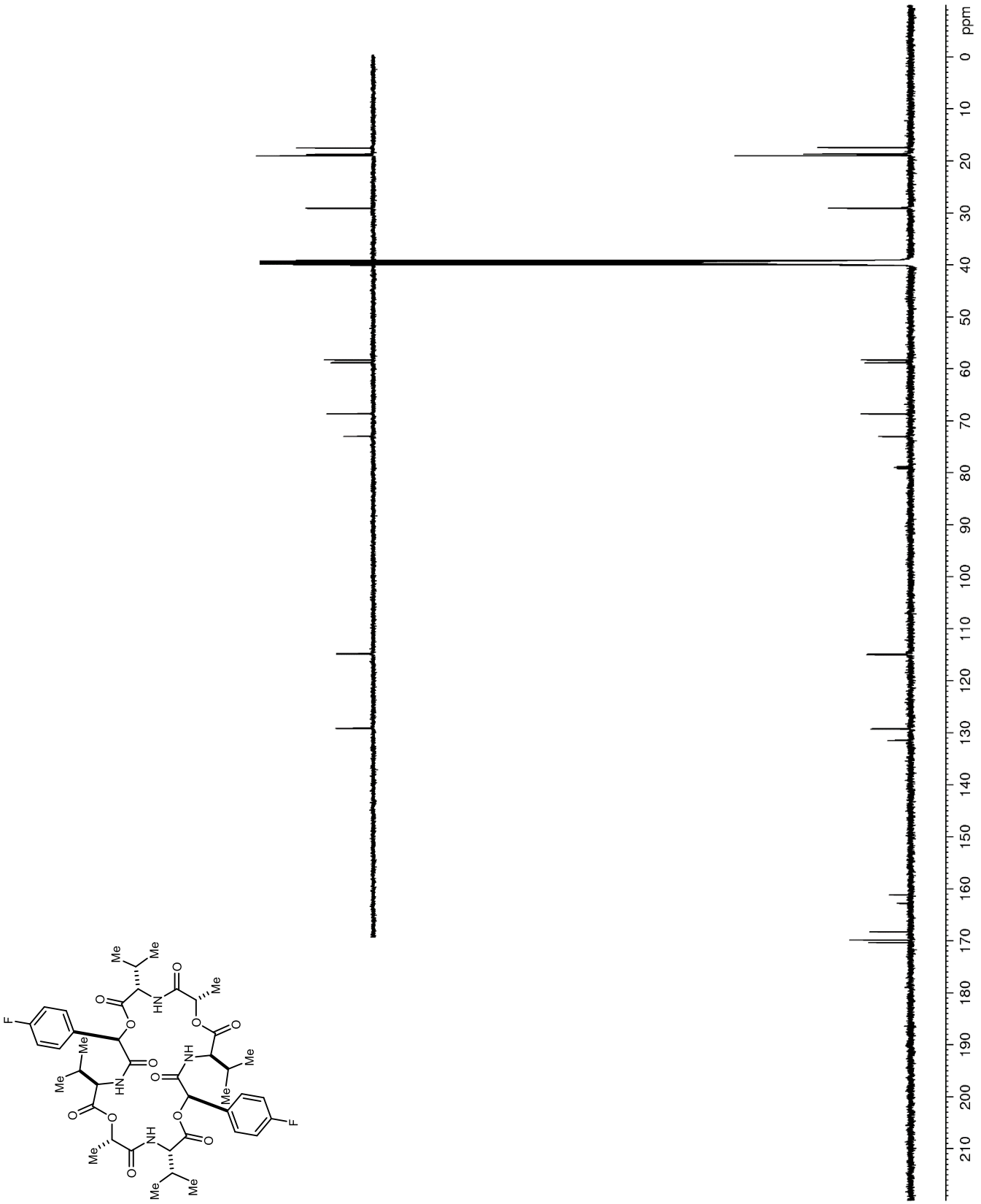

Figure 116. ^{1}H NMR (600 MHz, DMSO-d_6) of **132**

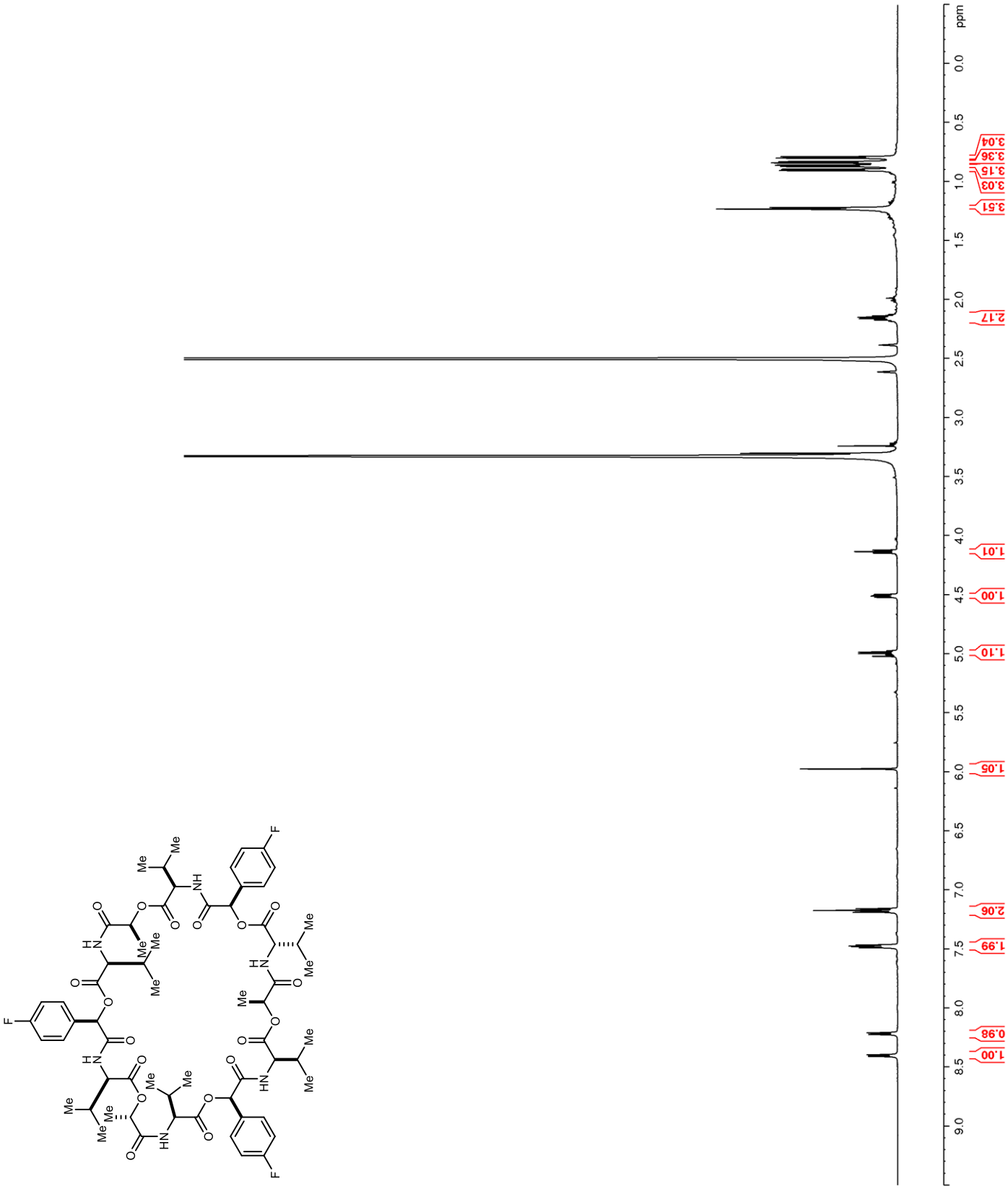

Figure 117. ^{13}C NMR (150 MHz, DMSO-d_6) of **132**

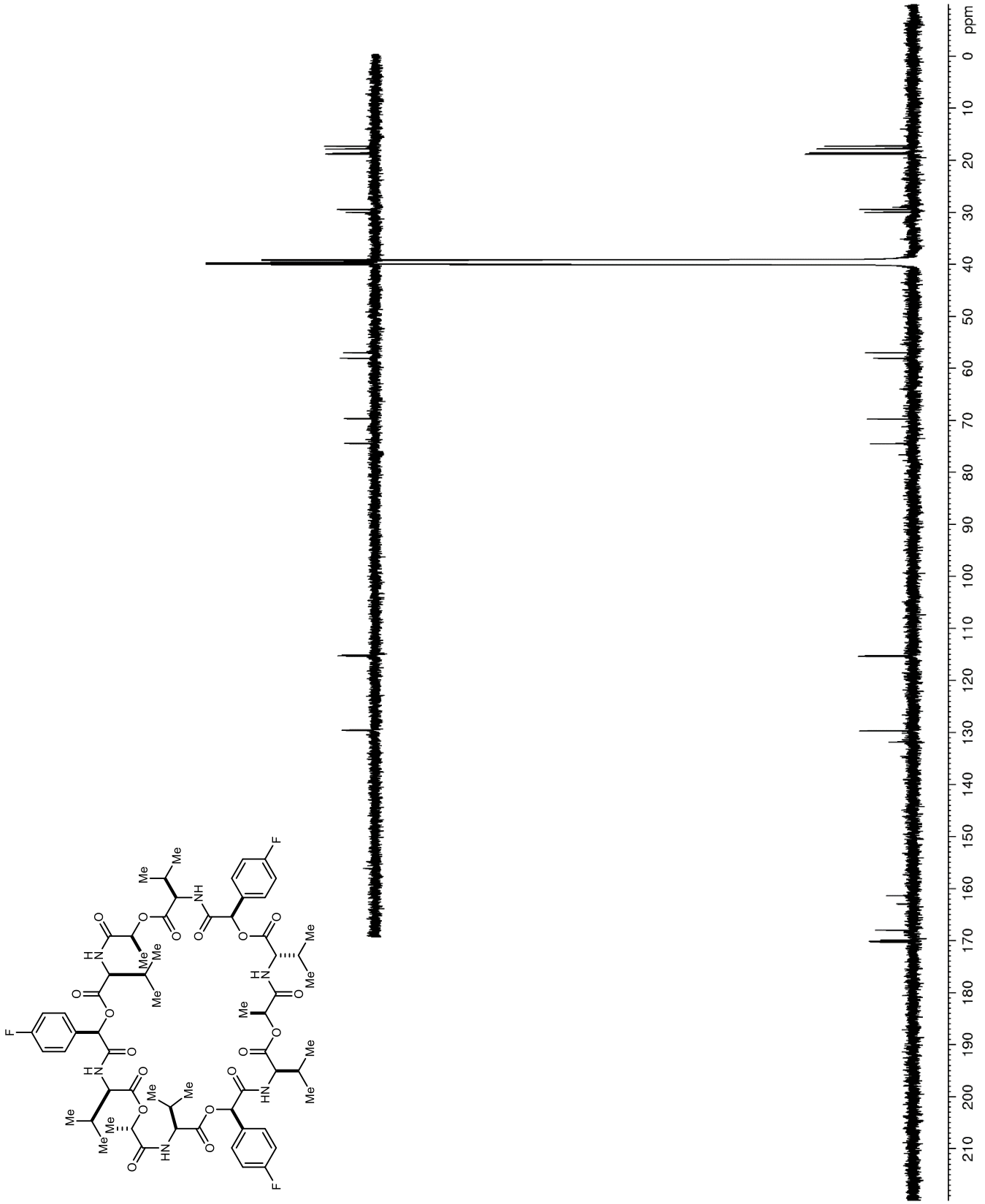

Figure 118. ^{1}H NMR (900 MHz, DMSO-d_6) of **133**

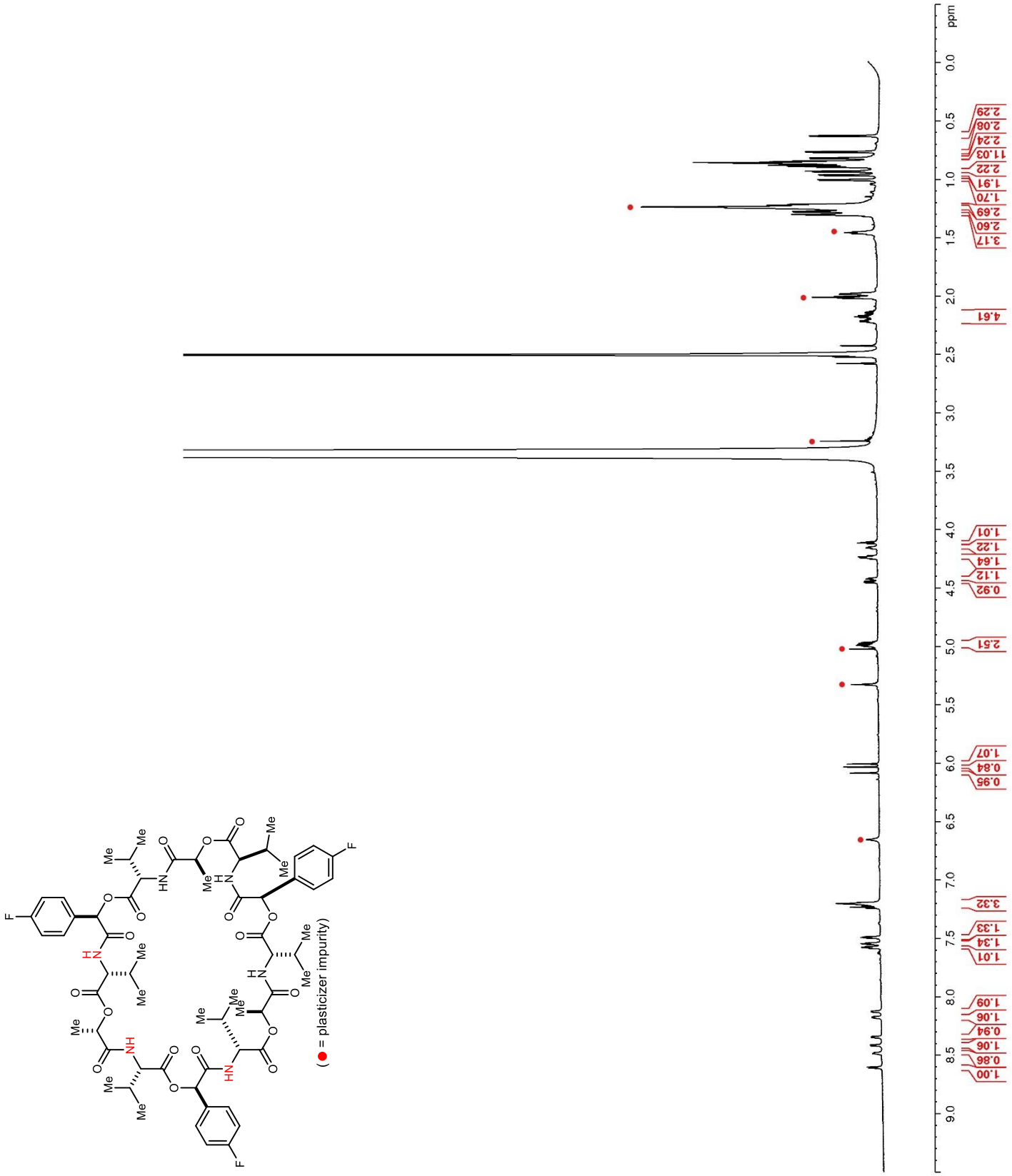

Figure 119. ^{13}C NMR (225 MHz, DMSO-d_6) of **133**

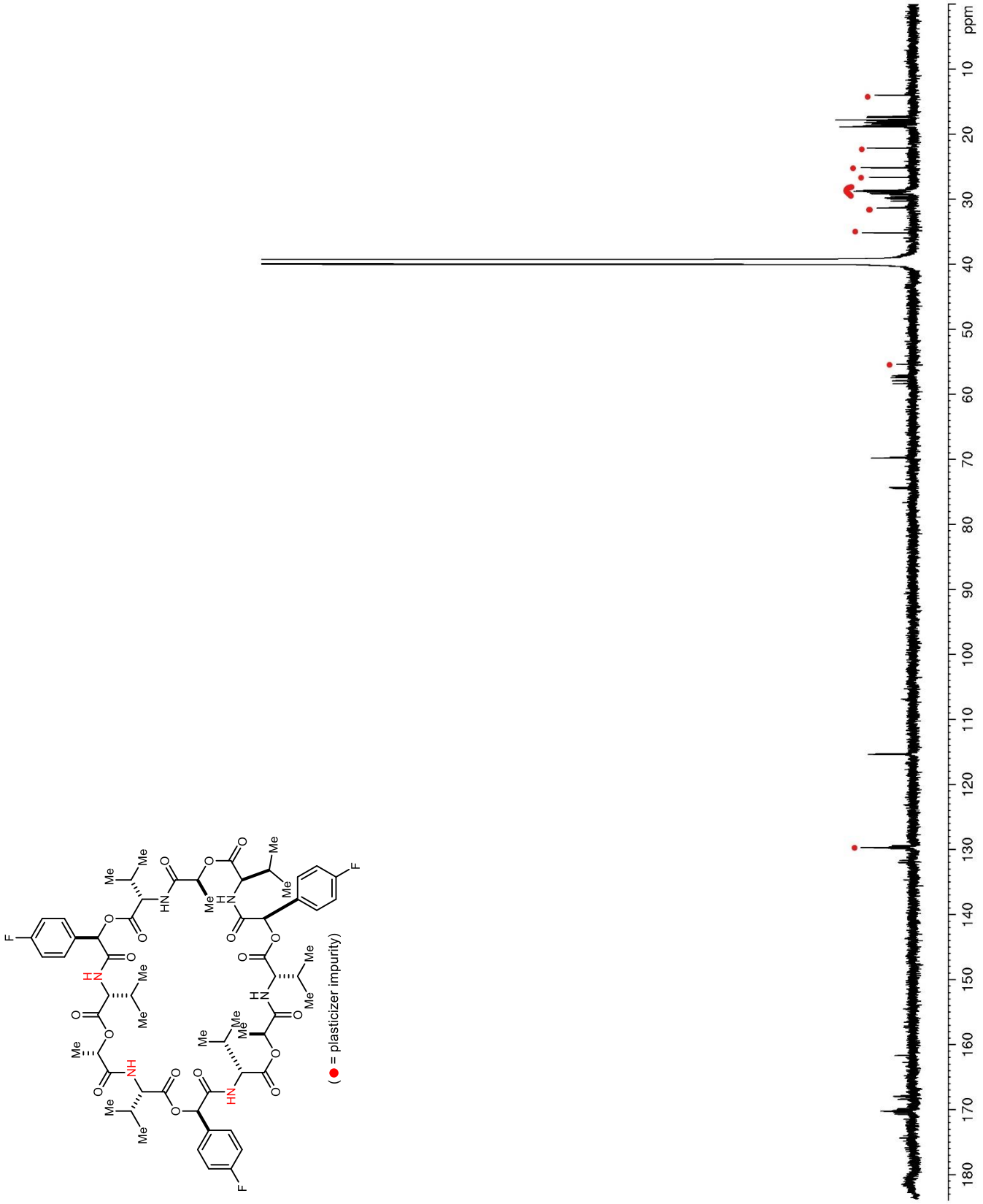

Figure 120. ^{1}H-^{13}C HSQC (225 MHz, DMSO-d_6) of **133**

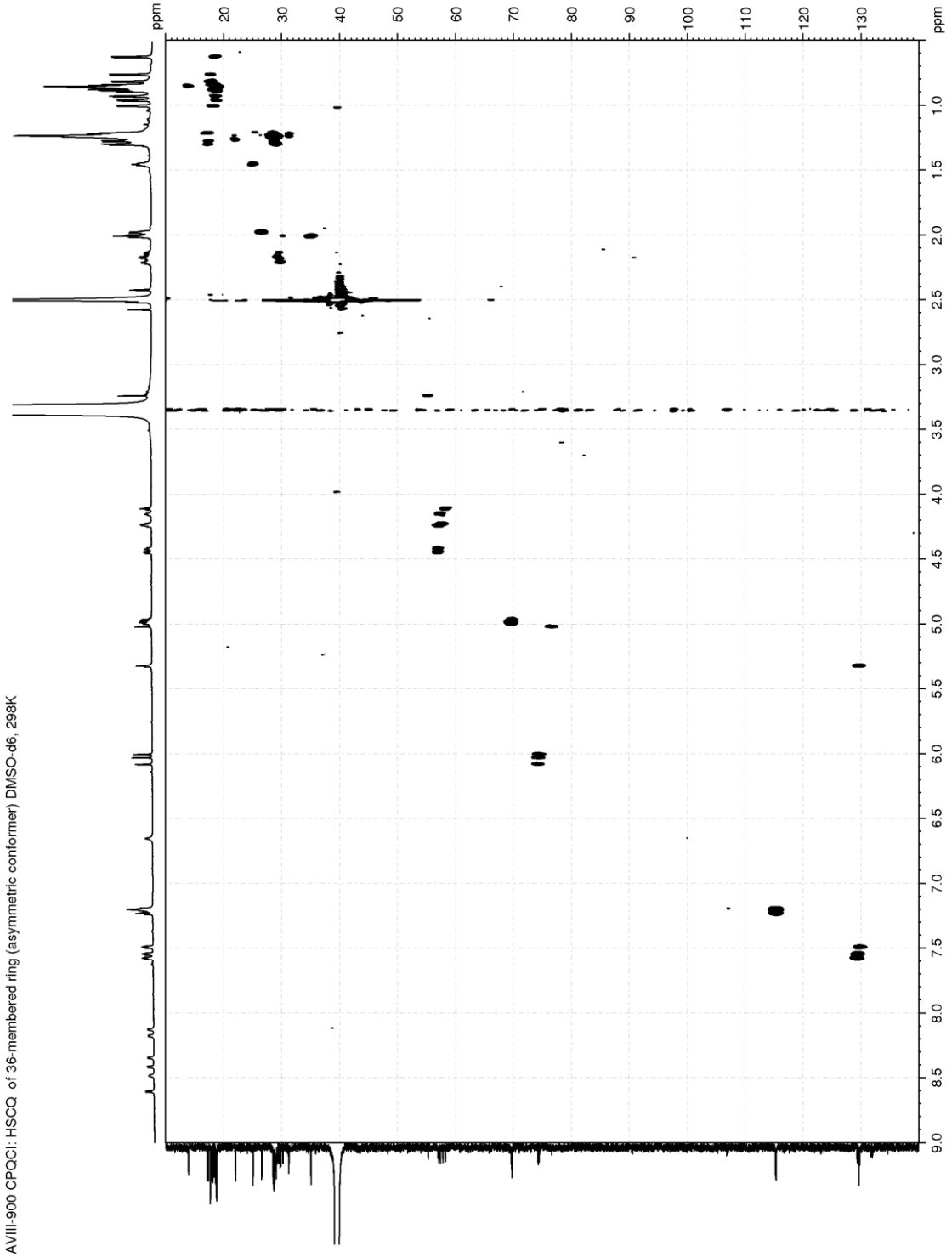

Figure 121. HMBC (225 MHz, DMSO-d_6) of **133**

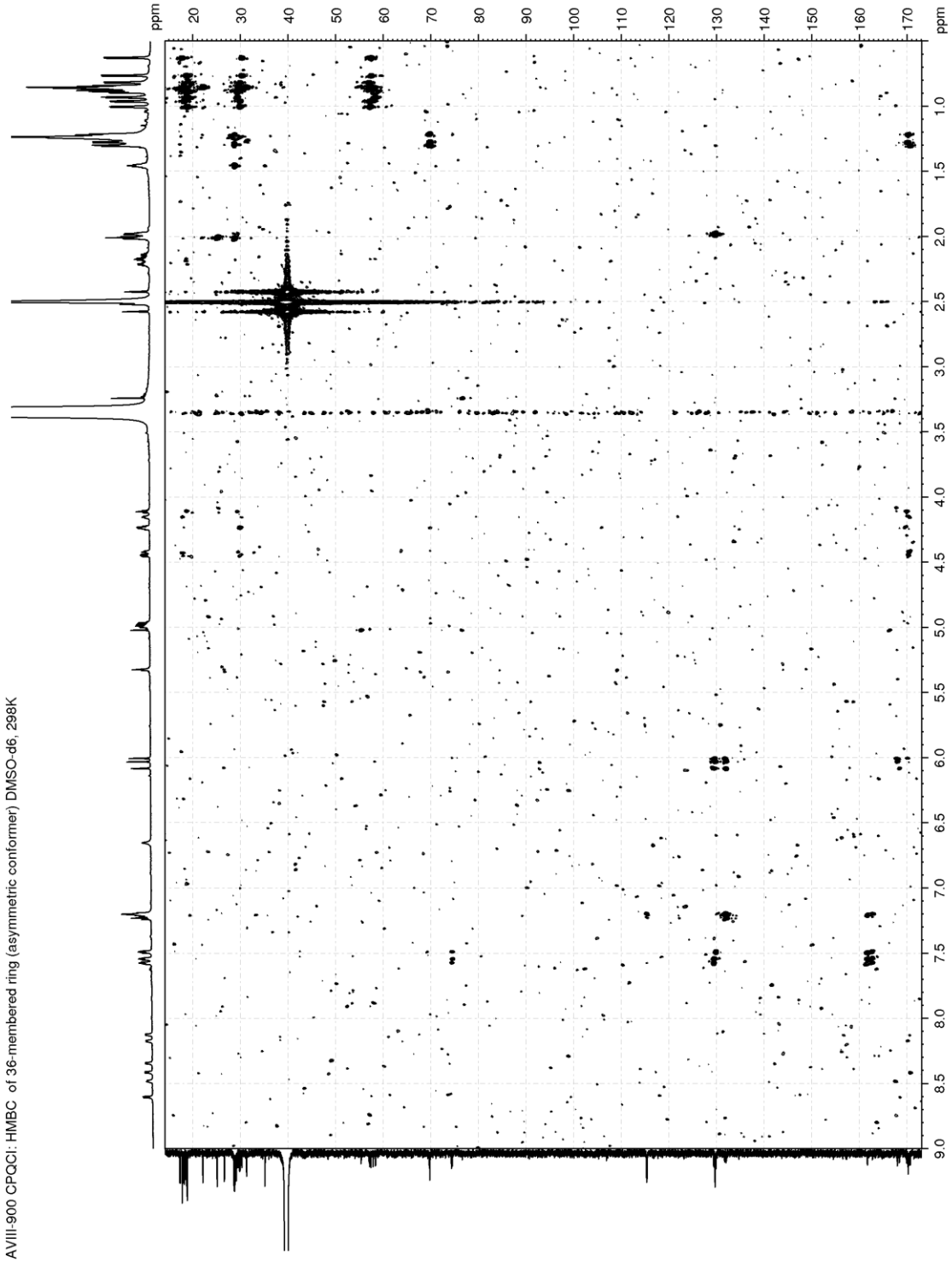

Figure 122. NOESY (900 MHz, DMSO-d_6) of **133**

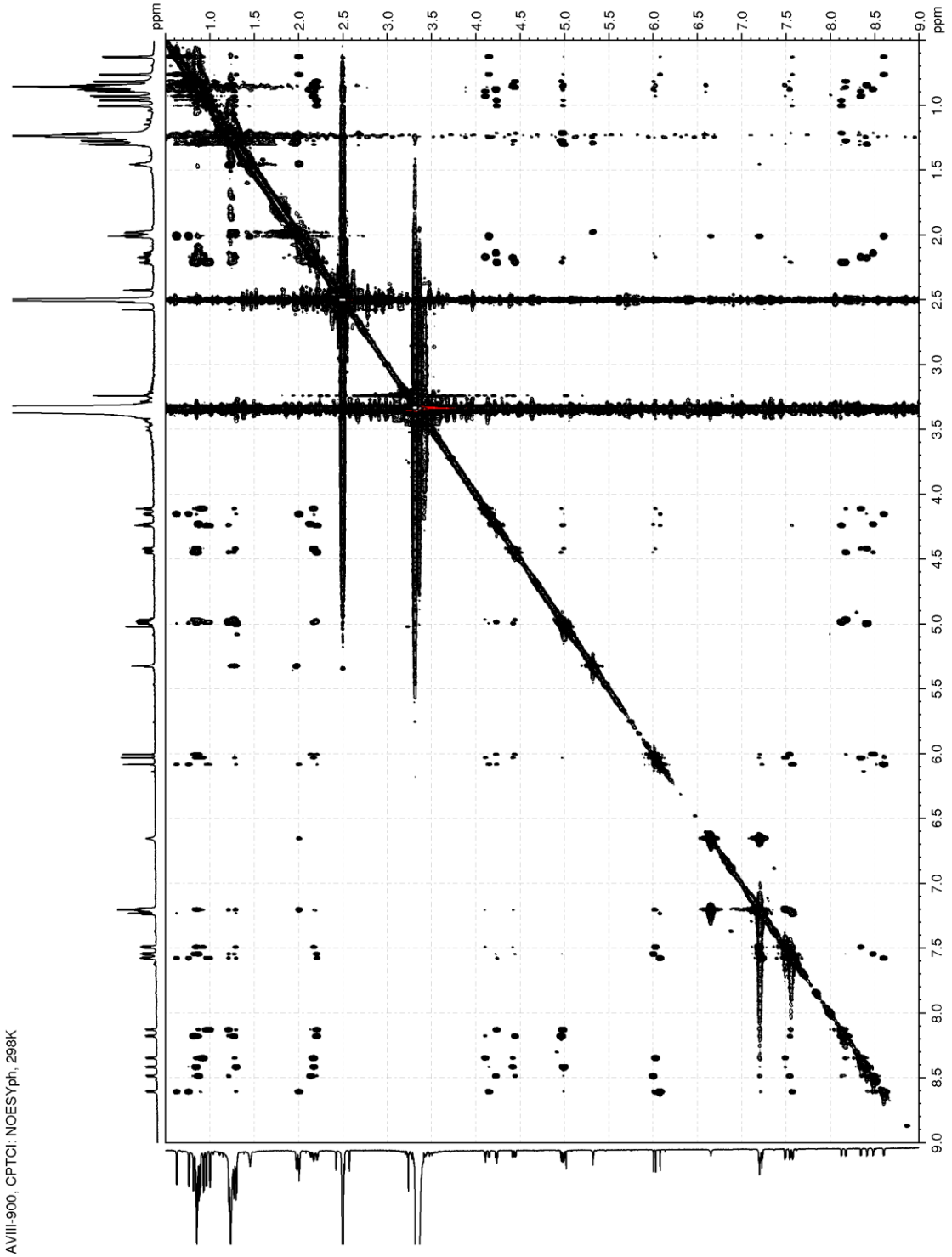

Figure 123. ^{1}H NMR (800 MHz, DMSO-d_6) of **134**

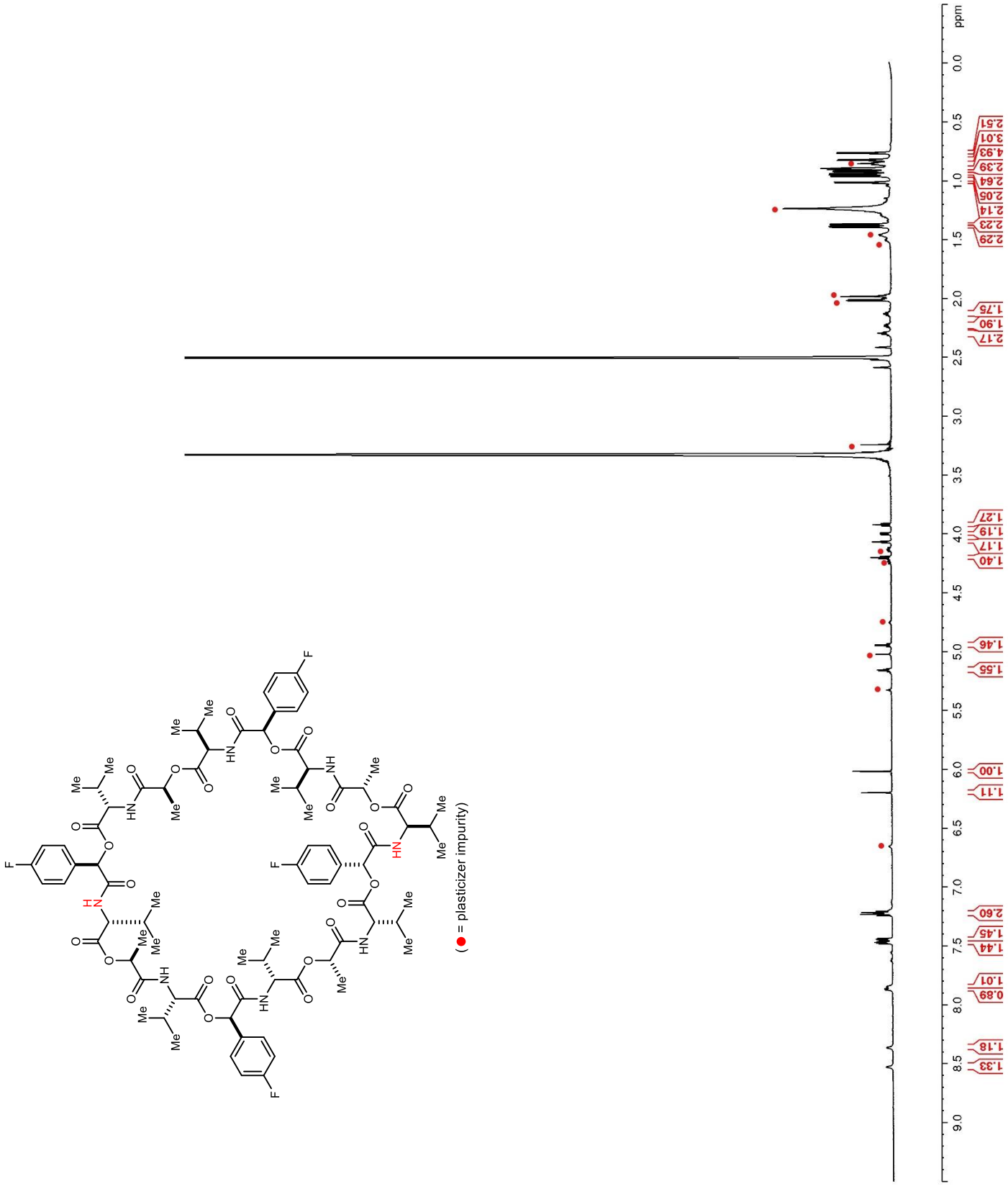

Figure 124. ^{13}C NMR (200 MHz, DMSO-d_6) of **134**

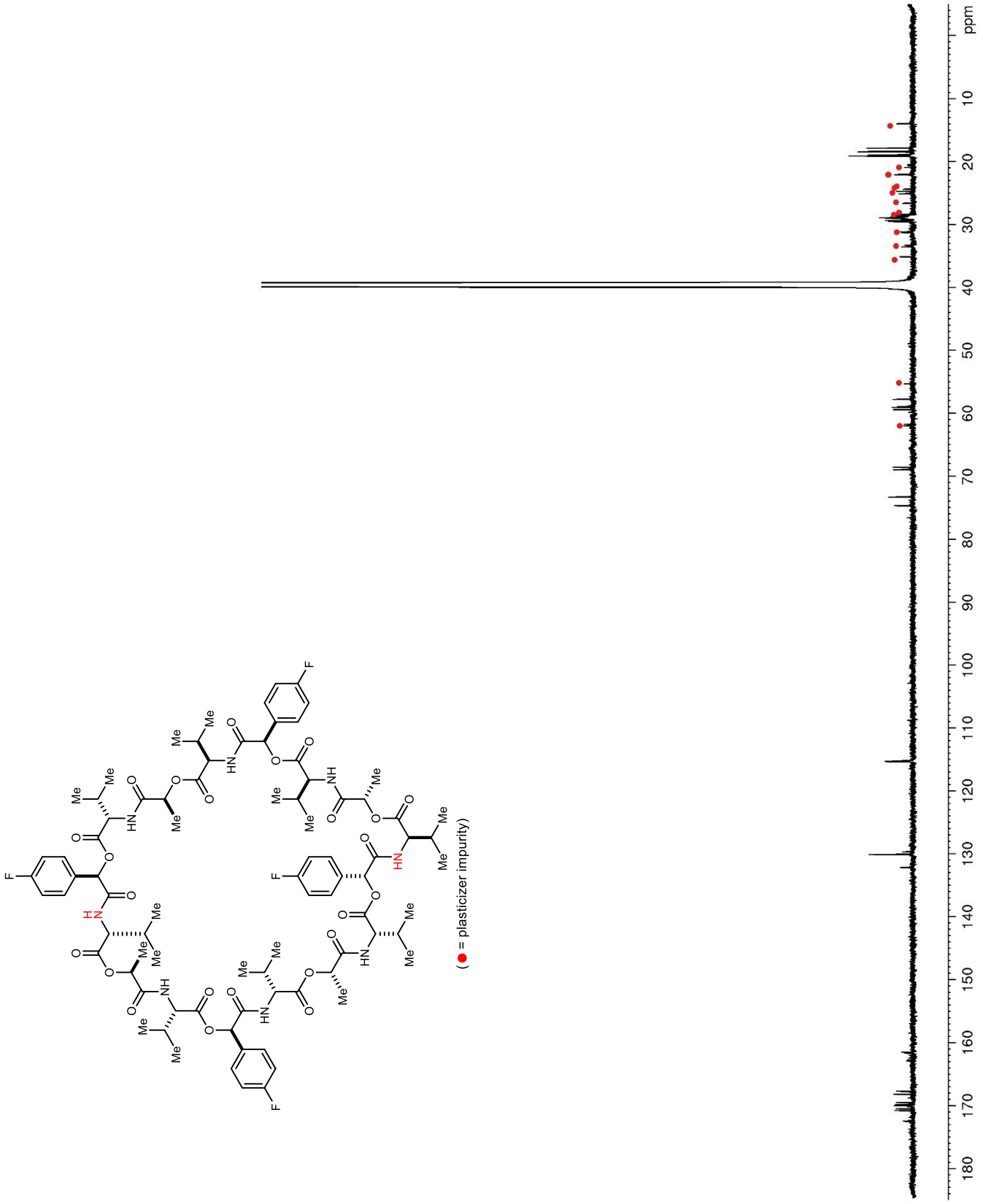

Figure 125. HSQC (200 MHz, DMSO-d_6) of **134**

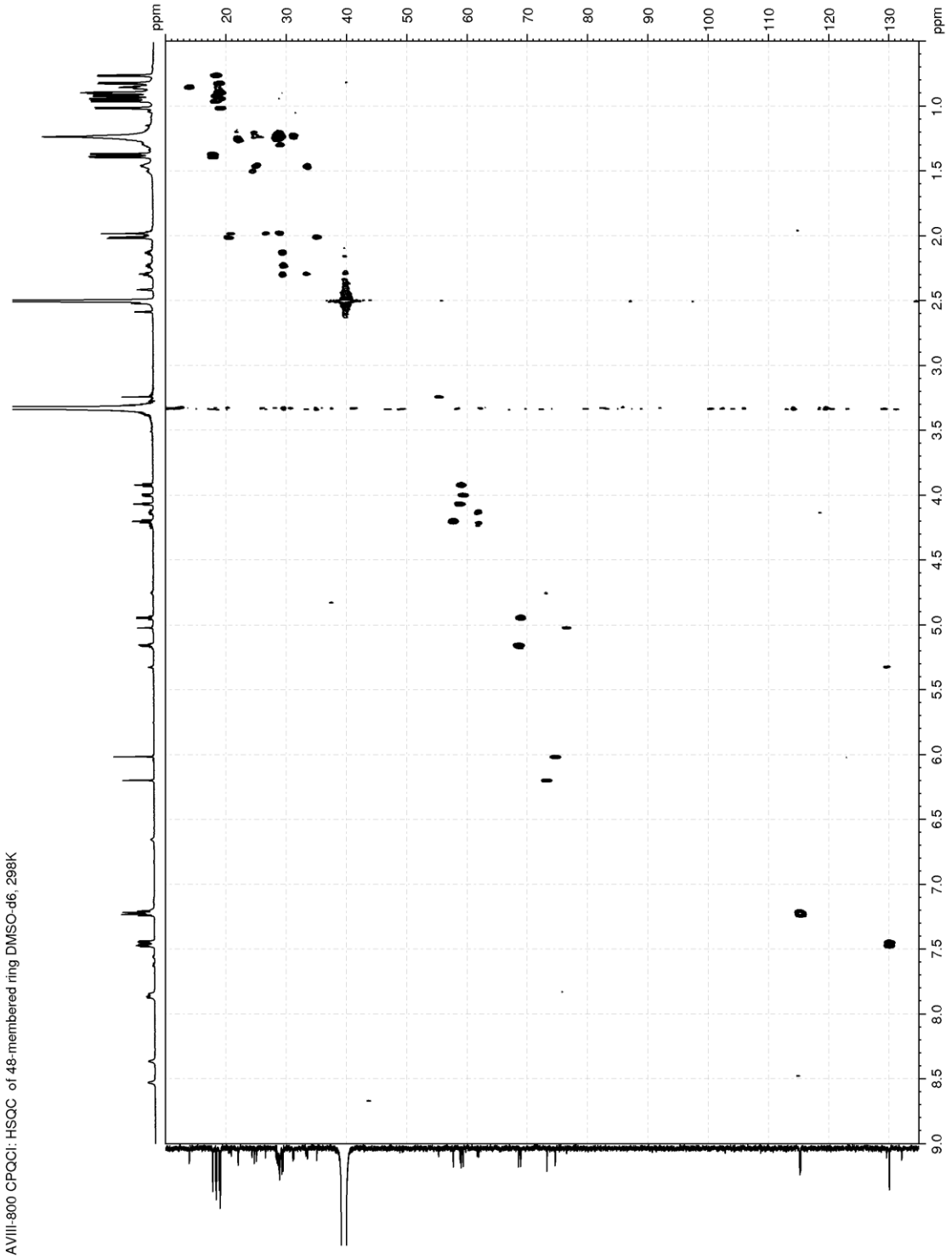

Figure 126. HMBC (200 MHz, DMSO-d_6) of **134**

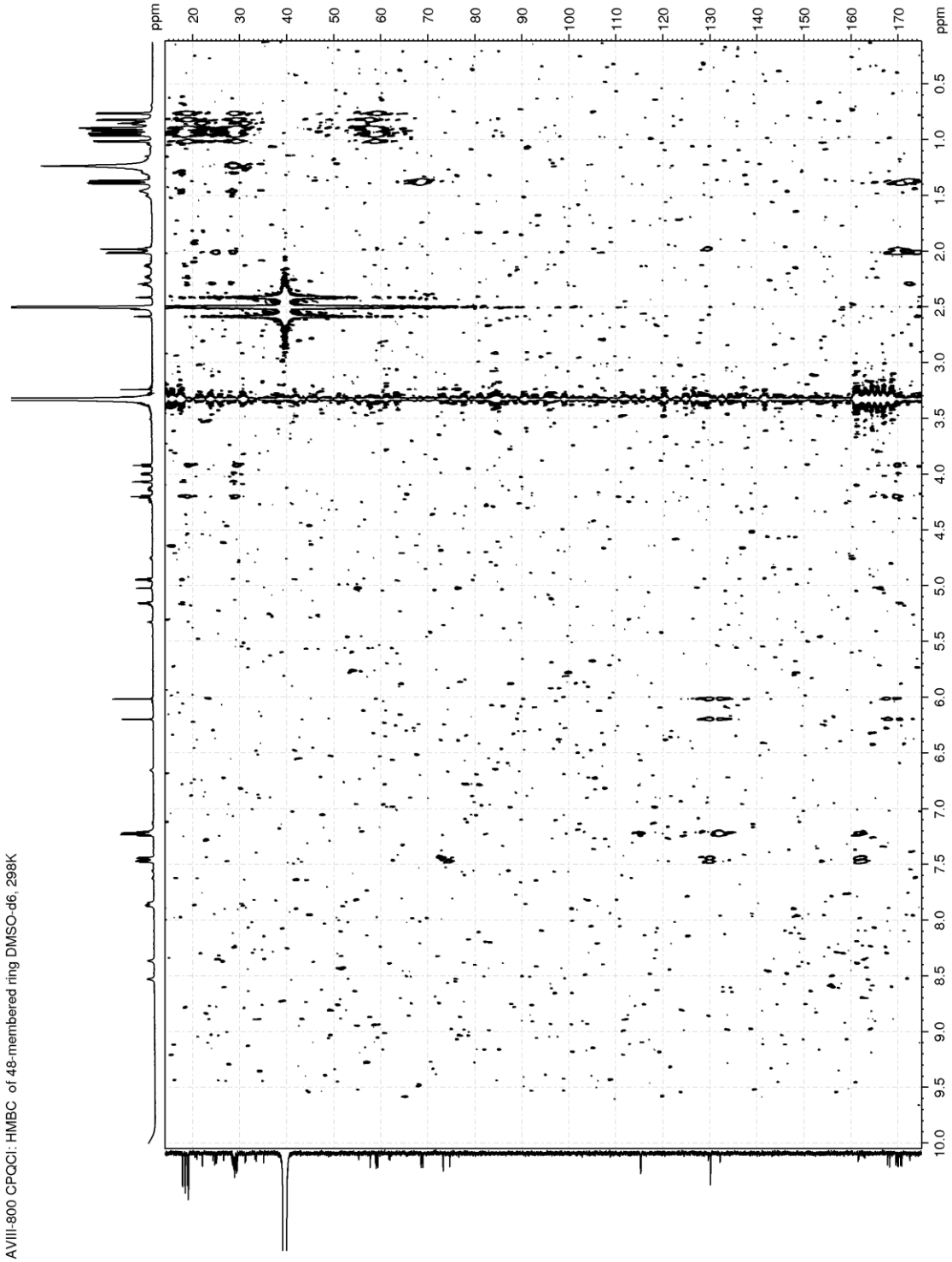

Figure 127. NOESY (800 MHz, DMSO-d_6) of **134**

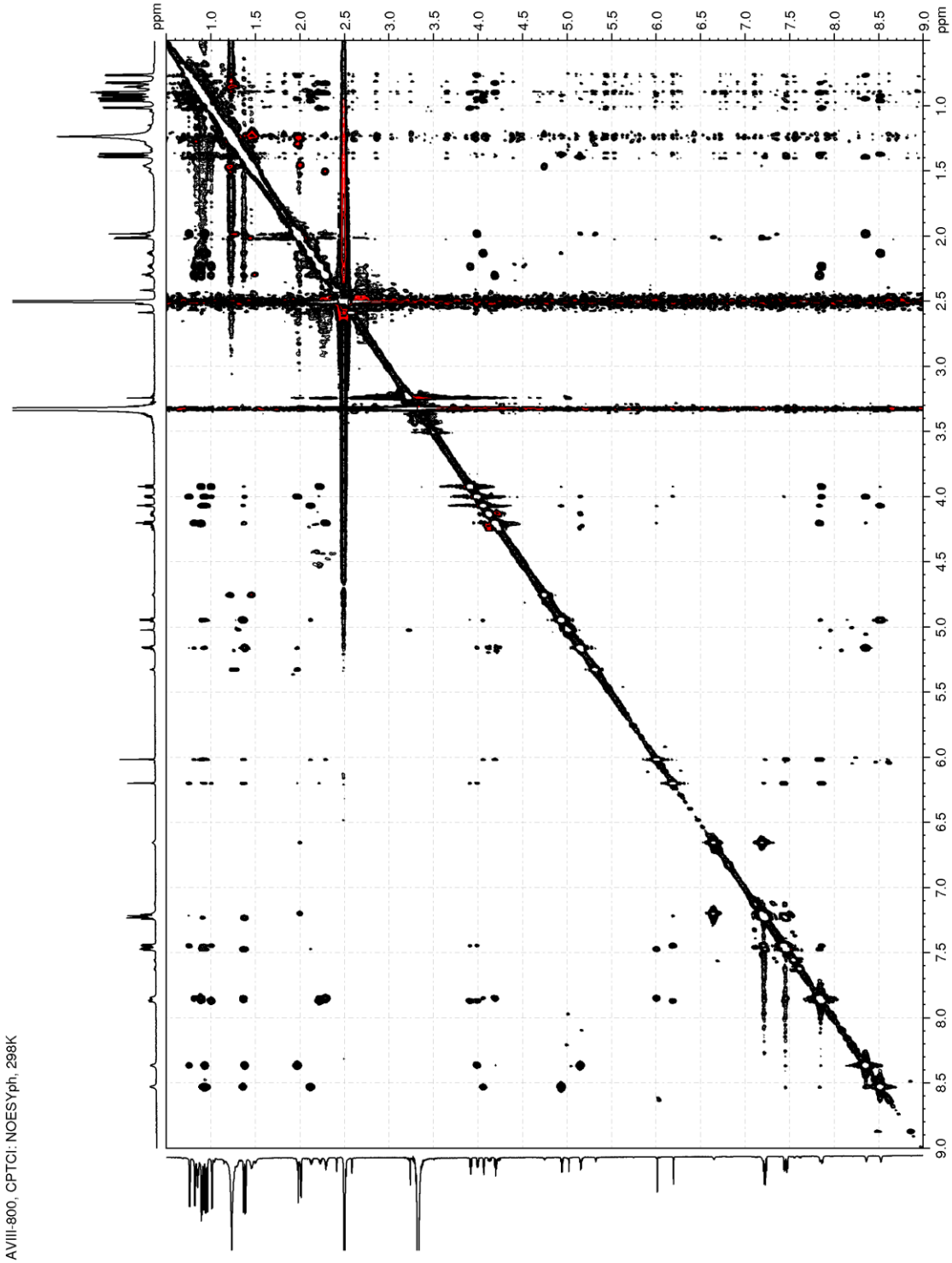

Figure 128. ^{1}H NMR (600 MHz, $CDCl_3$) of **135**

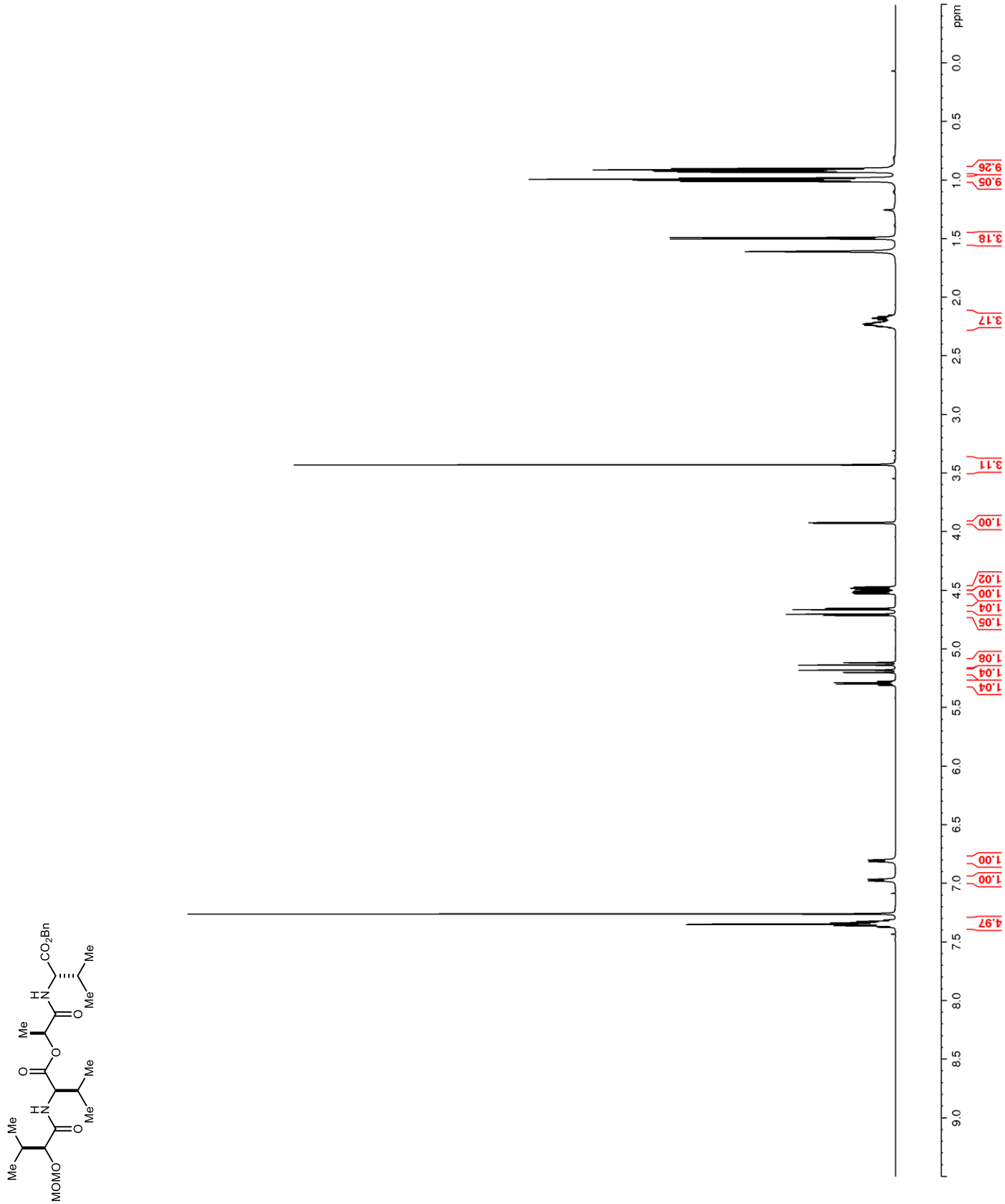

Figure 129. ^{13}C NMR (150 MHz, $CDCl_3$) of **135**

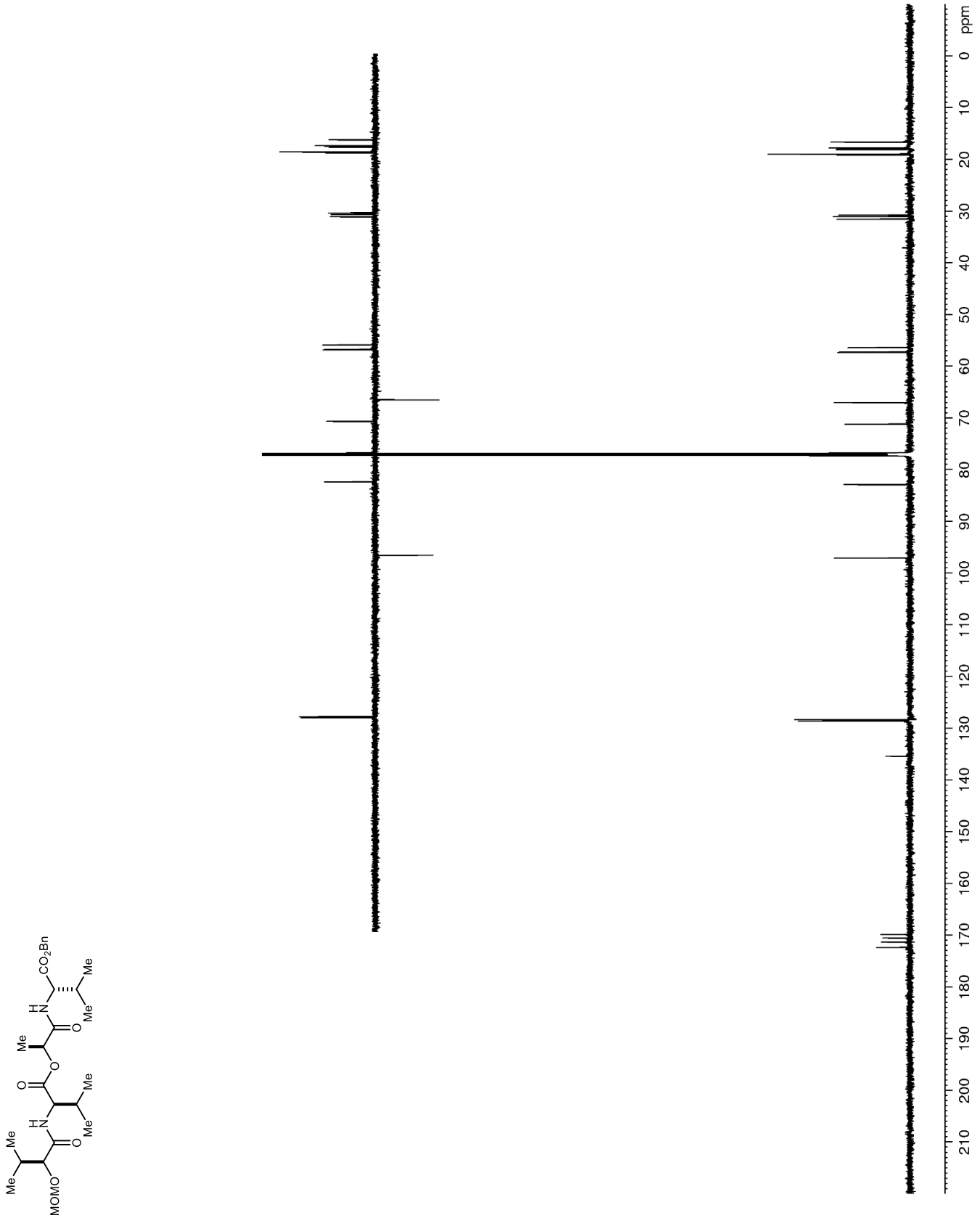

Figure 130. ^{1}H NMR (600 MHz, $CDCl_3$) of ***nat*-136**

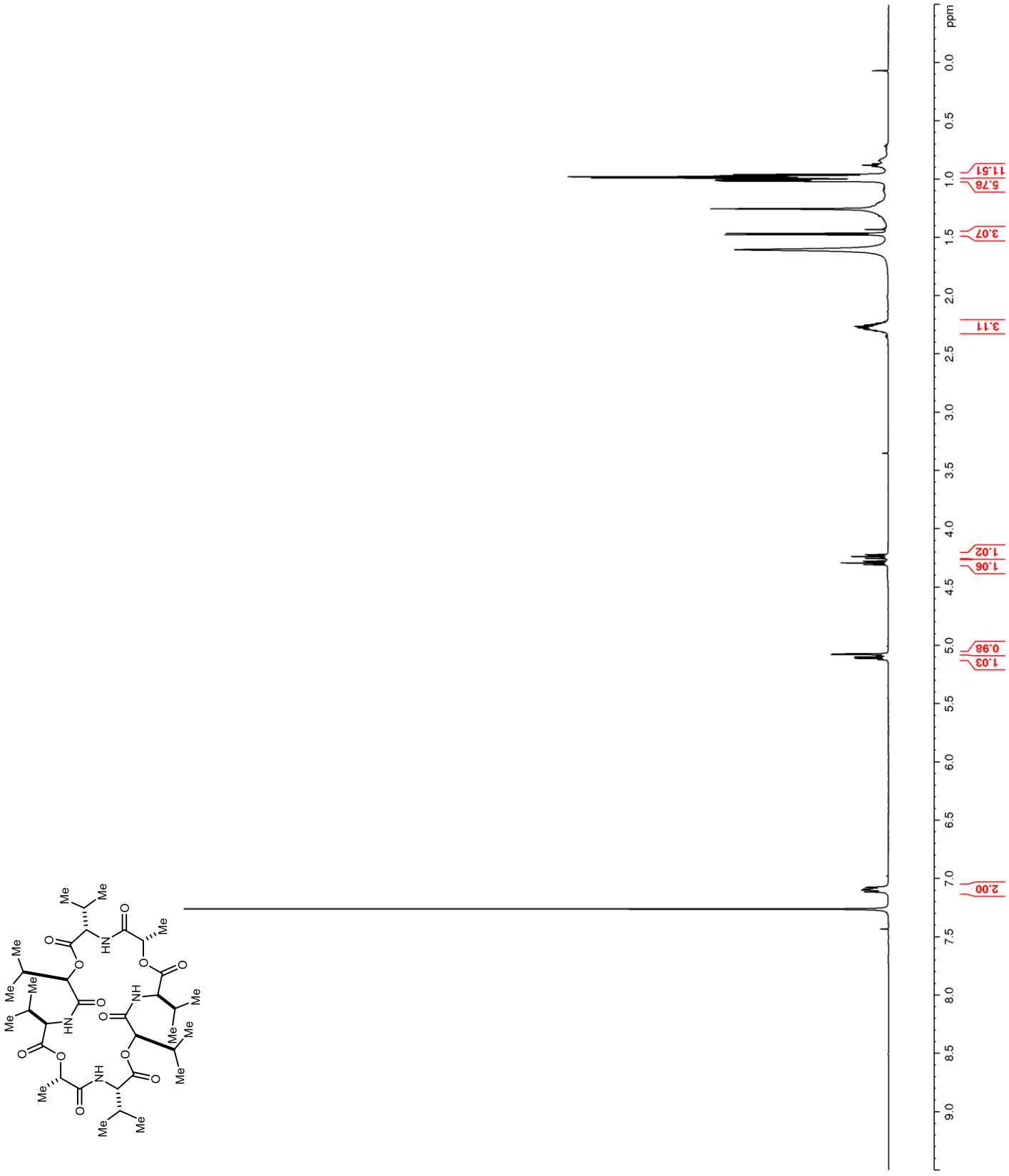

Figure 131. ^{13}C NMR (150 MHz, $CDCl_3$) of ***nat*-136**

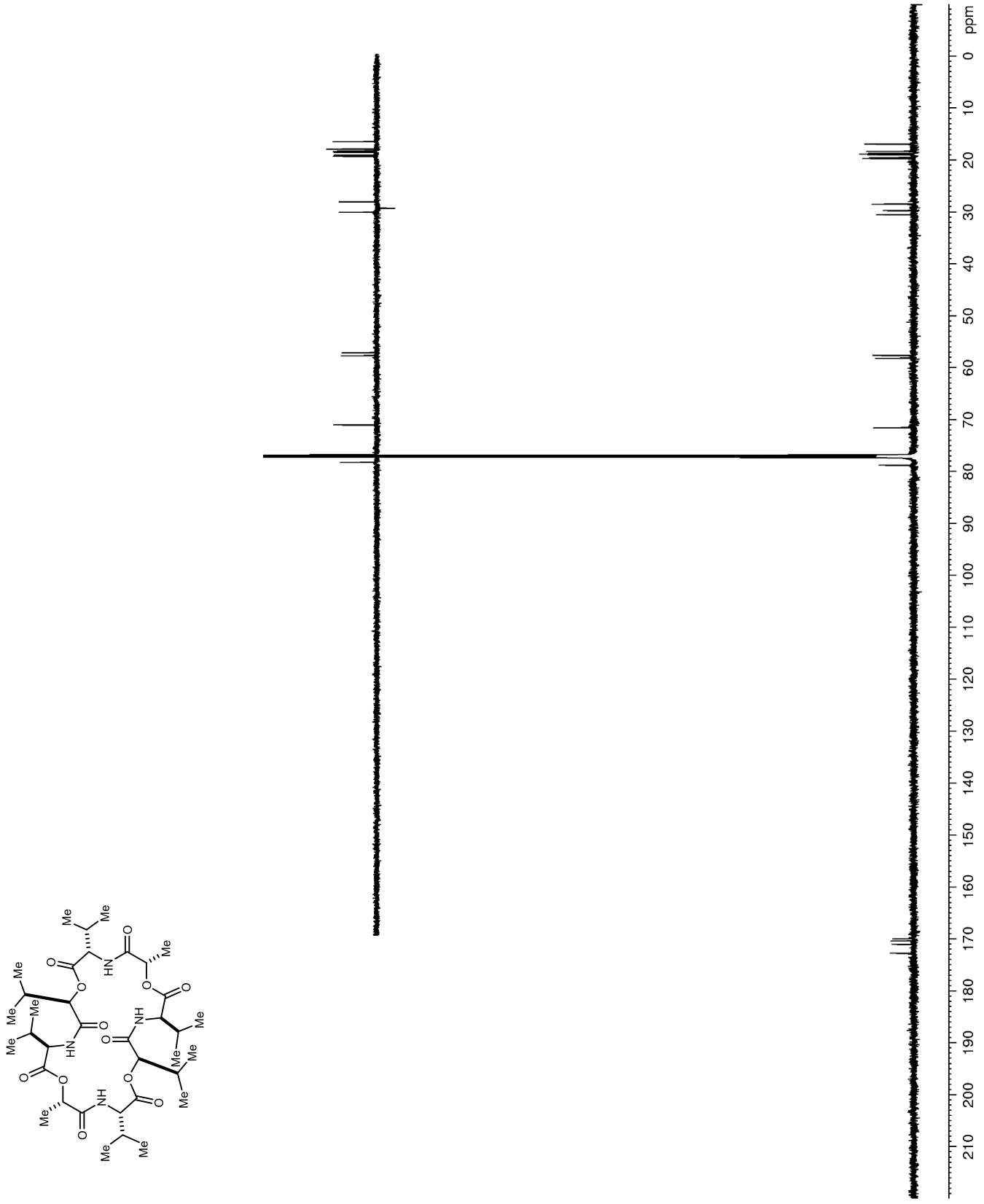

Figure 132. ^{1}H NMR (400 MHz, $CDCl_3$) of **137**

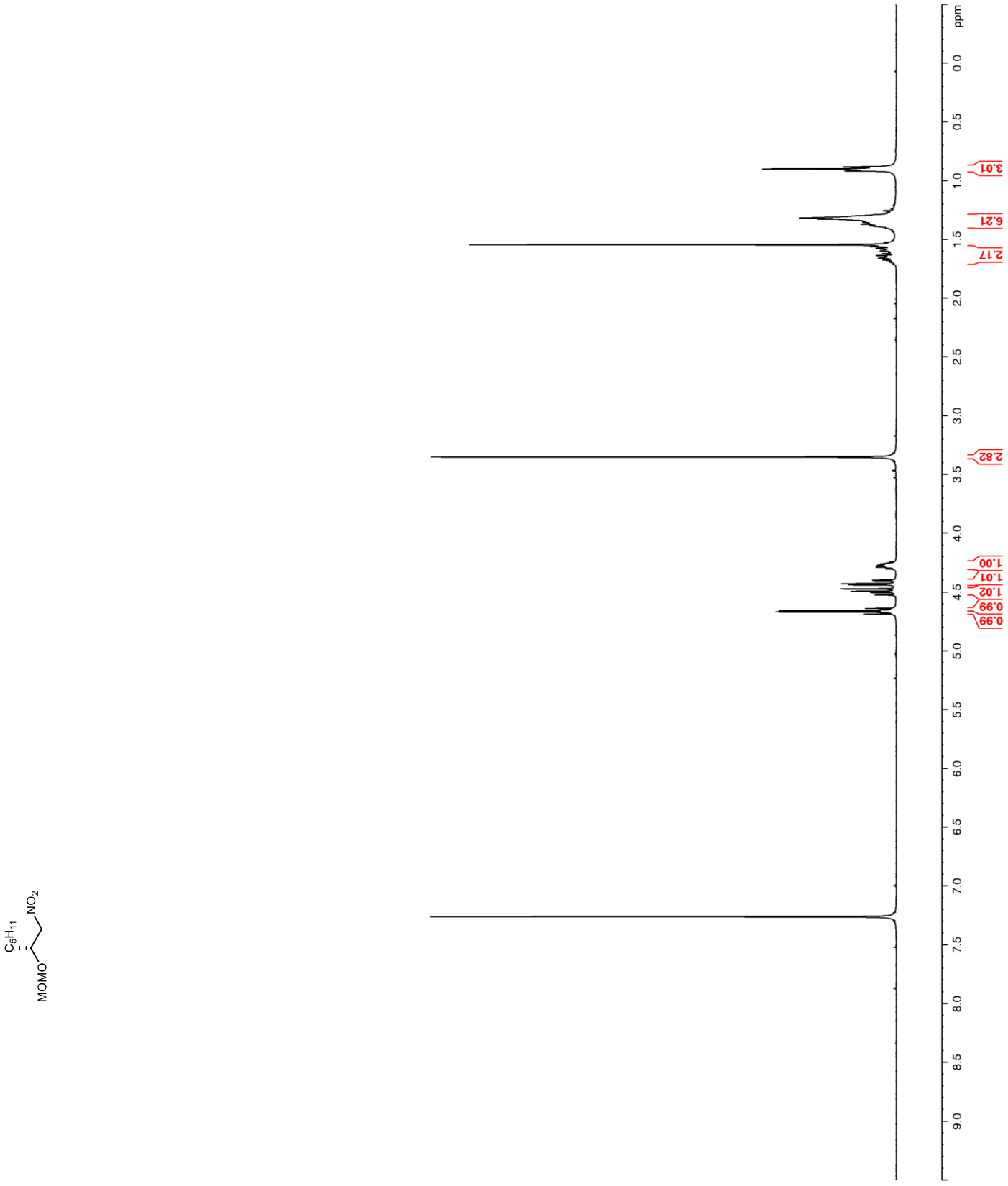

Figure 133. ^{13}C NMR (100 MHz, $CDCl_3$) of **137**